University of London

The Molecular Structure of Future Fuels

Paul R. Hellier

MEng Environmental Engineering

Submitted in partial fulfilment of the requirements
for the degree of Doctor of Philosophy
at University College London,
University of London.

March 2013

I, Paul Hellier confirm that the work presented in this thesis is my own. Where information has been derived from other sources, I confirm that this has been indicated in the thesis.

Dated:

Abstract

Future fuels will be developed from a variety of biomass and fossil sources, and must seek to address the adverse environmental impacts of current fossil fuel usage. To this end, understanding how the molecular structure of a fuel impacts on the processes of combustion and emissions production is critical in selecting suitable feed-stocks and conversion methods.

This work presents experimental studies carried out on a compression ignition engine equipped with a novel low volume fuel system. This system was designed and manufactured so as that several series of single-molecule fuels, and also binary fuel mixtures, could be tested to investigate the effect of fuel molecular structure on combustion and emissions. Features of fuel molecular structure that were studied include: alkyl chain length and degree of saturation, double bond position and isomerisation and the fatty acid ester alcohol moiety. The interactions between cyclic molecules and *n*-alkanes were also studied, as was the potential of carbonate esters and terpenes as future sustainable fuels; the latter produced from genetically modified micro-organisms.

The engine tests were carried out at constant injection timing and they were repeated at constant ignition timing and at constant ignition delay, the latter being achieved through the addition to the various fuels of small quantities of ignition improver (2-ethylhexyl nitrate). In tests conducted at constant injection and constant ignition timing the ignition delay of the molecule was found to be the primary driver of combustion phasing, the balance between premixed and diffusion-controlled combustion and, thereby, exhaust emissions. The various features of molecular structure were found to influence the duration of ignition delay, and an effect of interactions of binary fuel mixtures was also visible. Physical properties, such as viscosity, impacted on the production of exhaust emissions, and in extreme cases also influenced combustion phasing and heat release.

Acknowledgements

Firstly, I wish to acknowledge the contribution of Professor Nicos Ladommatos, whose vision, knowledge and experience, practical assistance and wise support as PhD supervisor guided this project from inception to successful completion.

The invaluable support of my industrial supervisor, Dr. Robert Allan, is also gratefully recognised, as is the financial contribution made by BP Global Fuels to this project. The insights and knowledge of Dr. John Rogerson, Dr. Sorin Filip, Dr. Marc Payne and Dr. Martin Gold have also been of great assistance in interpreting the combustion and emissions results generated. Many thanks go to Mr. Barry Cheeseman and Dr. Paul Richards of Innospec Ltd. for the thermo-gravimetric analysis of the fatty acid esters and the invitation to conduct this analysis at Ellesmere Port.

Collaborations with researchers from outside UCL's Department of Mechanical Engineering have added immensely to the value of this project, providing both inspiration and context for the work. As such, thanks are due to Dr. Saul Purton, Mrs. Lamya Al-Haj and Ms. Nancy Yanan Xu of UCL's Institute of Structural Molecular Biology, and also Mr. Marco Lizzul of UCL Civil and Environmental Engineering. Outside of UCL, thanks go to Dr. Talal Yusaf of the Faculty of Engineering and Surveying at the University of Southern Queensland for his collaboration in testing lipids from micro-algae.

Thanks are due to all of those with whom I have shared the Thermodynamics Laboratory within UCL's Department of Mechanical Engineering, but the following merit special mention: Dr. Alessandro Schönborn who gave me the keys to his lab and provided invaluable support in the early days of this project, Dr. Alan Todd for appreciating the merits of composting, Dr. Andreas Birgel for the trip to Japan and his frequent assistance, Dr. Priyesh Patel, also for Japan, and almost invariably feeling worse about his PhD project than me mine, Mr. Midhat Talibi for his assistance in running the spark ignition engine tests, Mr. Mart Magi for the binary mixture droplet sizing and Ms. Elina Kolvisto for tolerating my continued presence.

For their constant encouragement and support, I must express my gratitude to all of my friends and family, and in particular my parents, Mr. Robert and Mrs. Ann Hellier. Finally, special thanks are due to Vijayalakshmi Krishnan, for her infinite patience and support throughout.

Contents

List of Figures

List of Tables

Nomenclature

2 EHN	2 ethylhexyl nitrate
3,7-d-1-o	3, 7 dimethyl - 1 - octanol
C:H	carbon to hydrogen ratio
CAD	crank angle degree
Cda	citral dimethyl acetal
CFR	Cooperative Fuel Research
CID	constant ignition delay
CO	carbon monoxide
CO_2	carbon dioxide
COV	coefficient of variation
D1MPC	di-1-methyl propyl carbonate
D2MPC	di-2-methyl propyl carbonate
DAQ	data acquisition
dCAD	1^{st} derivative of crank angle position
DCN	derived cetane number
DEC	di-ethyl carbonate
dHRR	1st derivative of heat release rate
DMC	di-methyl carbonate
DME	di-methyl ether
DnBC	di-*n*-butyl carbonate
Dp	particle diameter
DTBC	di-tert-butyl carbonate
FABE	fatty acid butyl ester
Geranyl a.	Geranyl acetate
HRR	heat release rate

IMEP	indicated mean effective pressure
IQT	ignition quality testing
NO_x	nitrogen oxides
NTC	negative temperature coefficient
O_2	oxygen
PID	proportional integral derivative
PWM	pulse width modulation
SOC	start of combustion
SOC	start of combustion
SOC2	second point of combustion
SOI	Start of injection
TDC	top-dead-centre
TGA	thermo-gravimetric analysis
THC	total hydrocarbons
WOT	wide-open throttle

1. Introduction and background

There is consensus that the anthropogenic release of fossil bound CO_2 is resulting in global warming (Zecca and Chiari, 2010; Bach, 1979; Wuebbles and Jain, 2001) and potentially catastrophic climate change. This fact, coupled with fears regarding security of supply of traditional fossil fuels, is driving the move towards alternative liquid fuels. However, to mitigate the adverse impacts of continued fossil fuel combustion will require not only the substitution of such fuels with alternatives that demonstrate sustainability throughout their lifecycle, but are also fit for purpose within the existing energy infrastructure.

In 2010, 22 % (wt/wt) of global CO_2 emissions arose from the transport sector (second only to electricity generation), a total of ≈ 6.8 giga-tonnes of CO_2, of which ≈ 5 giga-tonnes were produced by road transported (International Energy Agency, 2012). Therefore, it can be seen that the development of alternative sustainable fuels for internal combustion engines could contribute substantially to reductions in anthropogenic emissions of fossil bound CO_2. While globally, light passenger vehicles are predominantly gasoline fuelled, recently in Europe sales of diesel fuelled light passenger vehicles have approached 50 % and are projected to increase globally in the coming decade (www.hybridcars.com, 2012). Furthermore, in the UK, buses, coaches and heavy goods vehicles were responsible for 21.5 % of greenhouse gas emissions from transport in 2009 (Transport Statistics, 2011). As such, displacing the use of fossil diesel with renewable alternatives is an increasingly important step in reducing the adverse environmental impacts of road transport.

In addition to the need to react to the potential dangers of climate change posed by anthropogenic release of CO_2, other damaging pollutants formed during combustion, such as nitrogen oxides and soot, are continuously subject to stricter controls which are designed to limit adverse environmental impacts (European Union, 2010). Legislation to control NO_x emissions exist as they have been shown to cause acid rain, which can lead to deforestation, pollution of waterways and damage to the built environment, and can contribute to photochemical smog which has health implications in major urban centres (Badr and Probert, 1993; Nevers, 1995). Particulate emissions, and in particular those from compression ignition combustion of diesel fuels, have been shown to result in both adverse health and environmental impacts (Betha and Balasubramanian, 2011), and in recent years smaller particles (of diameter less than 100 nm) have been especially implicated (Li et al., 2009). In

the case of compression ignition engines, reductions in exhaust emissions of nitrous oxides and soot to meet legislative requirements have primarily come from advances in engine technology and post combustion exhaust treatment. However, these can compromise efficiency, which is undesirable when seeking to reduce CO_2 emissions, and so design of fuels to limit pollutant emissions will become increasingly important as cleaner combustion is sought.

Vegetable oils were amongst the first widely considered alternatives to liquid fossil fuels, and the products of transesterification of such oils with alcohols are now widely used as bio-diesel. In the UK, the Renewable Transport Fuel Obligation ensures that all diesel sold will contain a minimum of 5 % bio-diesel as of April 2013 (Government, 2007). However, while bio-diesel from vegetable oils does reduce tailpipe emissions of fossil bound carbon, there are increasing concerns as to the sustainability of such bio-diesels when considering the entirety of the fuel lifecycle (European Commission, 2012). Investigations into alternative sources of natural oils that do not compete with food crops are gaining impetus, and for the example the use of algae in this manner has seen much interest of late. However, while the feedstock is renewable, the production of algal bio-diesel via lipid extraction and transesterification does not yet represent a low-carbon route to replace fossil fuels. It is also, at present, generally considered economically non-viable without either government subsidy or the a decline in global oil resources and a concurrent escalation in the price of crude fossil oil (Campbell et al., 2011; Gallagher, 2011; Lee, 2011).

Therefore, it can be seen that every aspect of a fuel's lifecycle, from sourcing of feed-stocks to eventual use, must come under increasing scrutiny to ensure long-term sustainability. While the fossil diesel utilised for the past hundred years has been a mixture of molecular components, defined by a range of physical properties, the fuels of tomorrow will have more distinct molecular structures, defined by the material from which they are drawn and the chemical and physical processes to which they are subjected. Therefore, understanding how specific features of molecular structure impact on energy release during combustion of a fuel, and formation of pollutants, is invaluable in aiding the design of future fuels. Furthermore, future fuels are likely to be a mixture of many compounds of dissimilar chemical structure, and so developing an understanding of how individual components interact to dictate combustion phasing and contribute to the production of emissions is also required. The investigations presented in this work were conducted in the hope that the knowledge gained

will aid the selection and processing of future fuels according to molecular structure, contributing to the need for new fuels that are compatible with current combustion equipment but which carry a significantly reduced environmental burden relative to traditional fossil fuels.

2. Literature review

This literature review presents an outline of the sources of current and possible sustainable fuels, followed by a more detailed description of the processes of compression ignition combustion and formation of nitrogen oxides (NO_x) and particulate matter. This includes discussion of the low temperature reaction kinetics of fuel molecules, and the impact of molecular structure on these pathways. Finally, where previous experimental studies have identified impacts of molecular structure on compression ignition combustion, these are also reviewed.

2.1. Potential sources of sustainable fuels

At present the vast majority of liquid fuels consumed for combustion are fossil fuels, obtained by the extraction of crude oil and subsequent processing to produce fuels which are largely defined by physical properties, such as boiling point or density. However, liquid fuels from biomass are of increasing importance, and so the potential sources and processing of biomass for fuels are reviewed as this is vital in understanding, and perhaps predicting, the composition of future fuels.

2.1.1. Fatty acid esters

In the context of bio-diesel production (as defined in Chapter 1), the term fatty acid refers to triglycerides, which are in fact three fatty acid alkyl chains which have esterified naturally to triacyglycerol. The fatty acid alkly chains present in the natural oils utilised for bio-diesel production are are predominantly between 16 and 18 carbon atoms long (Ma and Hanna, 1999), and range from being fully saturated to containing four double bonds between carbon atoms.

Figure 2.1 shows a typical transesterification reaction of a triglyceride with methanol, which results in the production of three fatty acid ester molecules and one of glycerol (Durrett et al., 2008; Ma and Hanna, 1999; Meher et al., 2006; Singh and Singh, 2010). As can be seen in Figure 2.1, this is achieved by substitution of the fatty acid chains with OH groups from an alcohol (to form glycerol), while the alkyl moiety of the alcohol bonds to the terminal oxygen of the fatty acid (to form a fatty acid ester). The displacement of all three fatty acid chains from the triglyceride may not occur simultaneously and intermediate products of diglycerides and monoglycerides are likely to be formed, and may already be present naturally

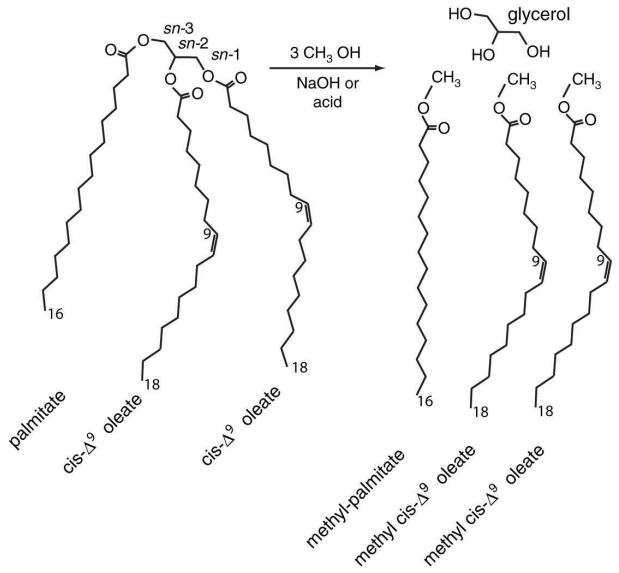

Figure 2.1: Typical transesterification reaction of a triglyceride with methanol (Durrett et al., 2008)

in the oil in very small volumes (Singh and Singh, 2010). Also sometimes present in small volumes within the oil are free fatty acids and water, both of reach can result in a reduced yield of esters (Meher et al., 2006).

Methods of transesterification vary according to the catalyst and reaction conditions employed, and have been the subject of several reviews (Meher et al., 2006; Vyas et al., 2010; Lam et al., 2010; Leung et al., 2010). Currently the most widespread method utilised in the industrial production of bio-diesel is the use of a homogenous alkali catalyst (where both reaction mixture and catalyst are in a liquid state), such as sodium hydroxide or potassium hydroxide (Borges and Diaz, 2012). Using a basic catalyst the reaction mixture must be stirred continuously for between 2 - 3 hours at elevated temperatures of 340 K at ambient pressure, with two resultant liquid phases containing esters and glycerol respectively. With pure vegetable oils near 100 % purity can be obtained with any base catalyst, however, the highest yields are obtained using alkalis such a sodium or potassium methoxide which contain a methyl group; in all cases recovery of a homogenous catalyst is complex where possible (Graboski and McCormick, 1998). Alkali catalysts are not suitable for oils containing free fatty acids in excess of 0.5 % (wt/wt), such as waste oils (Lam et al., 2010), as subsequent formation of soaps from the free fatty acids increases solubility of esters in glycerol, complicating product separation (Vyas

et al., 2010). Furthermore, the use of an alkali catalyst prevents the use of alcohols other than methanol; Meher et al. (2006) note that relative to methanol the use of ethanol sees the formation of emulsions of intermediates and products which are far more stable, thereby reducing reaction rates and increasing the complexity of product separation .

More suitable for impure oils are acid catalysed reactions where an acid, such as HCl or H_2SO_4, simultaneously catalyses both the esterification of free fatty acids to triglycerides and the subsequent transesterification of all triglycerides to esters (Lam et al., 2010; Leung et al., 2010). The use of homogenous catalysts involves high energy and resource use in the form large volumes of water for washing and recovery of the catalyst from the products for subsequent reuse; the wash water will then also require treatment (Geuens et al., 2008). Solid heterogeneous catalysts, both acidic and basic, have been suggested to remedy this issue and strong acid catalysts (such as sulfated tin oxides) have been found to be suitable for oils with high levels of impurities and seen conversion of triglycerides at yields in excess of 90 %, though elevated temperatures up to 500 K and reaction times of as much as 10 hours are required (Vyas et al., 2010; Borges and Diaz, 2012; Jothiramalingam and Wang, 2009).

Wahlen et al. (2008) show that longer chain alcohols than methanol (*n*-propanol, *n*-butanol and *iso*-butanol) are far superior in the acid catalysed conversion of mixed feedstock to alkyl esters, with yields 30 % greater than for methanol and ethanol. Wahlen et al. (2008) optimised the process for use with *n*-butanol at 80 °C, resulting in yields of up to 98 % in converting an oil of up to 80 % free fatty acids. It was suggested that the hydrophobic nature of the longer chained alcohols increases miscibility in oil and thus the level of reactant mixing. The higher boiling point of these alcohols also allows for the tranesterification to take place under higher temperatures, and thus with faster reaction times; Vyas et al. (2010) quote a reaction time of 69 hours with methanol which decreases with alcohol chain length to 3 hours when using butanol as the alcohol reactant.

An alternative method of catalysation without side reactions is the use of enzymes such as lipase, which have been found to be most successful when immobilised (also making for easy catalyst recovery). Lipase is sensitive to the presence of alcohol and excessive volumes can deactivate the enzymes; however, increasing the chain length or degree of branching of the alcohol reduces the degree of enzyme deactivation.

Temperatures of around 330 K and reaction durations of up to 48 hours are required; however the major obstacle to industrial use of the method at present is the cost of suitable enzymes (Vyas et al., 2010; Lam et al., 2010; Bajaj et al., 2010).

To avoid the use of a catalyst altogether, transesterification under supercritical conditions has been investigated and found to decrease reaction times to minutes. Under supercritical conditions all reactants are in a single homogenous phase, accelerating reaction times as no mass transfer is required, and no catalyst required as at such conditions the alcohol acts as an acid catalyst (Vyas et al., 2010). Geuens et al. (2008) describe the laboratory scale transesterification of refined rapeseed oil with 1-butanol without the use of a catalyst; long chain alcohols are more suitable for supercritical transesterification as they have higher boiling points. Passive silicon carbide elements were utilised to facilitate microwave heating to the organic mixtures and 91 % fatty acid butyl ester (FABE) conversion occurred at conditions confirmed by Geuens et al. (2008) as supercritical with both microwave and autoclave heating, though the autoclave method showed a decrease in FABE yield of 65 %, relative to the method of microwave heating. However, at present the high energy input required to achieve supercritical conditions prevents industrial uptake (Vyas et al., 2010).

Among the first primary crops to be considered for bio-diesel production were sunflower, rapeseed and soybean oil (Schwab et al., 1987) and these three now dominate crop production for bio-diesel in the European Union, with the largest land use for rapeseed, sunflower and a smaller proportion for soybean (European Biodiesel Board, 2010). Concerns over the strain on global food supplies due to the diversion of agricultural land for the production of biomass for fuels has lead to much investigation into new potential sources of fatty acids. Sources as diverse as coconuts and tobacco seeds have been considered, and many studies (Pinzi et al., 2000; Shay, 1993; Singh and Singh, 2010) have assessed the viability and sustainability of such feed-stocks. Such assessments are complex with global and local environmental and economic impacts needing to be considered. While fatty acids from differing sources will exhibit varying degrees of saturation and alkyl chain lengths, and this will impact on the properties of the resulting fuel, to characterise all the various sources of fatty acid is beyond the scope of this review.

However, one novel source of oils that that differs significantly in nature and has garnered particular interest of late are micro-organisms, such as micro-algae, which

naturally produce and accumulate triglycerides within cell membranes (Bastianoni et al., 2008). Methods for the extraction of lipids from microbial biomass generally involve a process of freeze drying and grinding followed by solvent extraction (Vicente et al., 2009).

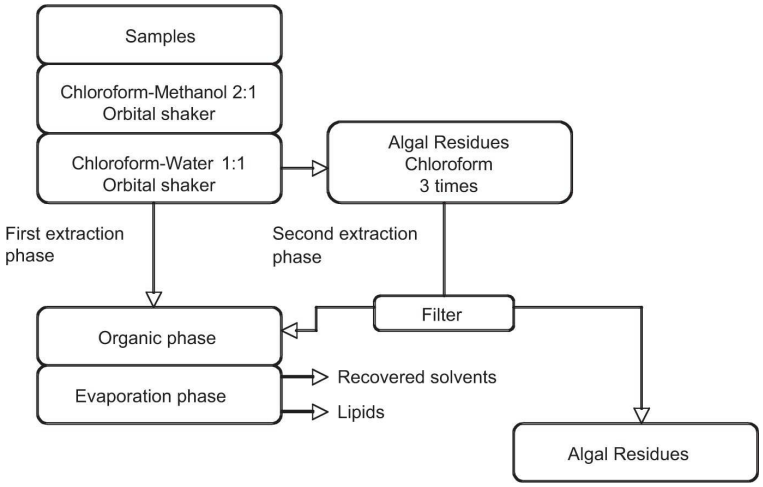

Figure 2.2: Laboratory lipid extraction (Bastianoni et al., 2008)

Figure 2.2 shows the Bligh and Dyer procedure which is commonly used for lipid extraction from algal biomass; utilsing a modified version of this method Ogawa et al. (2007) extracted oils from two species of micro-algae at rates between 1.87 and 2.40 mgg^{-1} fresh mass.

In addition to transesterification of lipids extracted from micro-organisms, the nature of microbial biomass makes it suitable for direct conversion to bio-diesel without the need for a separate lipid extraction process. Johnson and Wen (2009) compare a direct transesterification method to a two step method, in this instance with the micro-algae species *Schizochytrium limacinum*. In this study *S. limacinum* was grown heterotrophically in a medium of crude glycerol dissolved in artificial seawater, and transesterified either directly or with a lipid extraction stage. The two step method involved lipid extraction following the Bligh and Dyer procedure using chloroform and methanol solvent system with subsequent separation by centrifuge. Both methods were utilised with the reaction of freeze dried biomass and also wet biomass (80% w/w). No significant difference between the two methods in the yield of fatty acid esters was observed with dry biomass as the feedstock; however, the two stage process performed significantly better when utilising wet biomass.

Micro-algae has thus far seen more study than either yeast or fungi, however, the latter two have distinct advantages in that conventional microbe bioreactors can be utilised for their growth, resulting in higher yield and lower costs. Vicente et al. (2009) report on the use of oleaginous fungi (also making mention of interest in oleaginous yeast) as a source of lipids for subsequent conversion to bio-diesel, citing reports that indicate certain species of fungi may contain a maximum lipid content in dry biomass of between 57 and 86 %. In addition to the potential high lipid yield it is stated that these species have been grown in cultures of raw glycerol, itself a by-product of transesterification. Three solvent systems for the extraction of lipids from fungal biomass are: chloroform: methanol (2:1 volume ratio), chloroform: methanol: water (1:4:0.8 volume ratio) with the addition of water allowing a substantial decrease in the volume of solvent utilised, and *n*-hexane, all used in a manner similar to the Bligh and Dyer procedure. Of the three methods when utilised with the fungi *M. cirinelloides* the highest yield (19.9 wt %) with the lowest extraction losses (1.7 % (wt/wt)) was obtained with chloroform and methanol, addition of water to the solvent system resulted in mildly lower yields (-1 % (wt/wt)) and appreciably higher losses (4.5 % (wt/wt)), while use of *n*-hexane returned a lipid yield of 15.3 % with losses of 3.8 wt % (Vicente et al., 2009). Upon lipid extraction and analysis 86.15 % of the lipids obtained were either free fatty acids of saponifiable (containing at least one fatty acid ester linkage) and thus suitable for transesterification, unsuitable lipids obtained include carotenoids, sterols, tocopherols and retinoids . Of these lipids the 37 % (wt/wt) comprised of oleic acid (18:1), 20 % wt palmitic acid (16:1), 18.5 % wt linolenic acid (18:3) and 14.3 % wt linoleic acid (18:2). Later analysis of the same species but grown in a liquid medium as opposed to solid produced even higher levels of saponifiable lipids at 98 wt %, probably due to the absence of light. Such conditions also reduced the level of free fatty acids from 31.6 wt % to 3.6 wt % (Vicente et al., 2010), suggesting that a resultant bio-diesel would contain a greater proportion of more saturated species.

Vicente et al. (2009) also present a method in which *M. cirinelloides* is grown on a solid substrate is directly transesterfied via acid catalysation, with FAME yields compared to those obtained to a two step process of lipid extraction and subsequent transesterification. At reaction conditions of 65 °C and using a variety of acid catalysts (H_2SO_4, HCL and BF), an average fatty acid ester yield of 18 $\pm$ 1 % (wt/wt) was obtained by the one-step method, with an ester concentration of

greater than 99 % (wt/wt). Ester yield from previously extracted lipids reacted under the same conditions ranged between 91.5 - 98 wt % with non saponifiable lipids comprising the remainder, suggesting that the one step procedure to be a more efficient method of lipid extraction (Vicente et al., 2009). Vicente et al. (2010) later found a near identical result when growing *M. cirinelloides* in a liquid medium; growth on solid medium is considered unfeasible on an industrial scale.

2.1.2. Chemical and physical conversion of biomass

Several methods have been utilised, or attempted, in the conversion of lignocellulosic biomass to useful hydrocarbon products, and in general terms involve the physical and chemical transformation of the material by the application of heat or pressure in the presence of chemical reactants.

Gasification is the heating of biomass to temperatures of around 900 °C in the presence of a catalyst (or 1300 °C without) and reacting with air, oxygen or steam, and ideally results in the production of a gaseous mixture of carbon monoxide (CO), carbon dioxide (CO_2), hydrogen (H_2), methane (CH_4) and nitrogen (N_2). Undesired gaseous products include aromatics such as benzene, toluene and naphthalene, such contaminants are referred to as "tars" and typically require a multi-step scrubbing process before the gas stream is further utilised (Naik et al., 2010). Huber et al. (2006) report on "Solar gasification" where concentrated solar energy is used to heat biomass to 850 °C.

The products of gasification (CO, CO_2, H_2 and CH_4) are suitable feedstock for Fischer Tropsch processes whereby the gaseous mixture is reformed into complex hydrocarbons and water over a metal catalyst. Products from Fischer Tropsch processes are predominantly straight carbon chain hydrocarbons, with some branched molecules and primary alcohols also formed. Carbon chains length are in the range of 2 to 33, though polymerisation involved in the process tends to result in longer chained (waxy) hydrocarbons, which may then require further processing (Huber et al., 2006; Larson and Jin, 1999). At present production and subsequent cracking of long chain alkanes is normal practice, however coupling of a cobalt or iron catalyst with a zeolite catalyst has been shown to produce shorter chains and aromatics. Hydrogen and methanol are also commonly produced from syngas, by the water shift reaction and methanolysis respectively (Huber et al., 2006; Naik et al., 2010). An integrated process of converting biomass to liquid fuel is referred to as biomass

to liquid (BTL). Such a demonstration plant found yields of Fischer Tropsch diesel (120 L/T of biomass) to be lower than ethanol (320 L/T biomass) when producing from the same quantity of biomass, by gasification and then conversion of syngas by Fischer Tropsch and hydrolysis and fermentation respectively, though by the Fischer Tropsch process the potentially useful by-products of natural gas and electricity were also produced (Huber et al., 2006).

Liquefaction of biomass requires solvents, a catalyst and a reducing gas such as CO or H_2 with reaction conditions of 50 - 200 bar and 250 - 325 °C. The resulting hydrocarbons are a complex mixture of volatile organics which are highly viscous and thus require further addition of solvents, some of which are recoverable. Wu et al. (2009) found that direct deoxy - liquefaction at 350 °C of poplar tree leaves with subsequent distillation resulted in an oil of which 34 % was composed of alkanes in the range of C7 - C29. The quality and yield from liquefaction is considered lower than that of products from fast pyrolysis. Pyrolysis is the heating of biomass in the complete absence of oxygen to produce solid, liquid and gaseous hydrocarbon products at between 1 - 5 bar. Conventional pyrolysis is undertaken on large pieces of wood over several minutes and produces carbon rich solid residues (charcoal), whereas fast pyrolysis occurs in under 10 seconds on biomass particles (Dp $<$ 1 mm) and produces high yields of solid and liquid products. Flash pyrolysis operates at even lower residence times with even smaller particle sizes and gives high liquid yields. Bio-oil from fast pyrolysis contain a mixture of alphatic alcohols and aldehydes, aromatics such as furanoids and benzanoids, fatty acids, esters, ketones and high molecular mass compounds, which could potentially be used directly in a compression ignition engine (though as they are acidic in nature not suitable as a drop in replacement for fossil diesel), with solvent extraction of specific species possible. Bio - oil can be upgraded to remove less desirable compounds, by hydrogenation or use of a zeolite catalyst and steam reforming can be utilised to produce syngas from bio-oil (Huber et al., 2006; Naik et al., 2010).

Huber et al. (2006) suggest that the goal of chemical transformation of cellulosic biomass is to obtain a useful product via the production of monomer units, and such a transformation can be achieved at low temperatures with acid hydrolysis. When using ligoncellulose as a feedstock pre-treatment is required to decrease cellulose crystallinity, increase the biomass surface area available for subsequent reaction and remove hemicelluloses. This can be achieved via physical processes such as milling,

chemically with dilute acids or ammonia that require subsequent neutralisation, or thermally using high pressure steam at 200 °C without the need of a solvent. The goal of hydrolysis is to convert cellulose to sugars, i.e.

$$_{n}(C_6H_{10}O_5) + _{n}(H_2O) \rightarrow _{n}(C_6H_{12}O) \tag{2.1}$$

Using acid as a catalyst 70 % yields can be obtained with 5 hydroxymethylfurfal and levulinic acid as by-products. The final product of acid catalysation is levulinic acid and is produced in industry from cellulose feeds such as paper mill waste and agricultural residues. Hot water hydrolysis (210 °C) is suitable for the breakdown of hemicellulose (Huber et al., 2006).

Lignin accounts for between some 15 - 30 % of woody biomass, and is a major by product of wood pulping and currently utilised mainly for power generation and solvent recovery. Binder et al. (2009) report on the potential of lignin in the production of aromatic compounds, showing that phenols can be obtained via the cleavage of connecting alkyl and ether units. Figure 2.3 shows a generalised lignin structure.

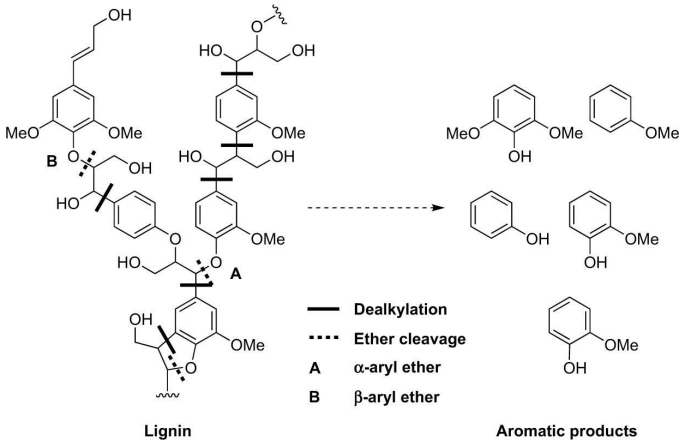

Figure 2.3: Generalised chemical structure of lignin and schematic for its conversion into monomeric aromatic products (Binder et al., 2009)

Metal based catalysts have also been used in lignin conversion; however Binder et al. (2009) prefer the use of acid catalysts as higher yields have been reported at lower reaction temperatures. Ionic liquids are attractive as unlike other organic solvents they readily dissolve lignin, though possess melting points as high as 100

°C and may start decomposing at 200 °C. The subsequent experimental procedures of Binder et al. (2009) fail to depolymerise lignin, but carbohydrates are receptive to the procedure and so the method may have some use in selective conversion of biomass .

A potential transformation of alcohols to fuel molecules of higher molecular weight is the production of carbonate esters. Such molecules (which consist of a carbonyl group connecting two alkyl groups) have most commonly been produced by the reaction of carbon monoxide (CO) with alcohols (most commonly methanol and ethanol to form di-methyl carbonate and di-ethyl carbonate respectively)(Dunn et al., 2001; Oyevaar et al., 2000; Pacheco and Marshall, 1997; Paret et al., 1996; Roh et al., 2003; Zhu et al., 2011). However, more recently, synthesis of carbonates from CO_2 has received interest(Keiski, 2009; Shaikh and Sivaram, 1996). Tian et al. (2007) describe a laboratory scale method for production of di-alkyl carbonates from a variety of alcohols and CO_2, via formation of propylene oxide and in the presence of a reusable inorganic base catalyst. Conversion yields of between 73 - 99 % were achieved with concurrent production of 1,2-propandiol. i. Fujita et al. (2001) produced di-methyl carbonate (DMC) from the reaction of CO_2 with methanol in the presence of potassium chloride. Variation of CO_2 pressure during the reaction shifted the balance between production of DMC and the other observed reactant product, di-methyl ether.

2.1.3. Micro-organisms

Micro-organisms have been employed in the conversion of biomass to liquid fuels for some time. Due to use as a substitute for gasoline, ethanol has been produced industrially from biomass since the early 20^{th} century by means of fermentation and distillation processes utilizing primarily agricultural feed-stocks (sugar cane in Brazil and corn in the USA) (Rosillo-Calle and Walter, 2006). Batch methods for the production of longer chain alcohols from biomass have also been utilized industrially, albeit to a lesser extent. Continuous *iso*-propanol, butanol and ethanol (IBE) fermentation has been successfully conducted by the immobilisation of the bacteria *Clostridium beijerinckii* in a substrate of glucose and yeast (Krouwel et al., 1983). However, at the time of the investigation several technical deficiencies of the reactor limited solvent production.

The anaerobic bacteria *Clostridium acetobutylicum* can also be used to convert biomass through combined acetone-butanol-ethanol (ABE) fermentation. Recent increased viability of butanol production by this process can be attributed to the development of new methods of continuous fermentation that do not result in the destruction of the bacteria on product recovery and leave immobilised cells in-situ: gas stripping, liquid to liquid extraction using a selective solvent, or pervaporation where butanol in vapour form is made to diffuse through a membrane (Ezeji et al., 2007). Recently large petroleum companies have invested in production of butanol from biomass and several butanol production facilities are under development (www.butamax.com, 2011; www.gevo.com, 2011).

Other reported means of producing alcohols (primarily ethanol) include separation of sugars from rice straw by enzymatic hydrolysis and subsequent fermentation by fungal strains (Abedinifar et al., 2009; Huber et al., 2006). Ethanol can be produced from syngas by reaction with anaerobic bacteria, with acetic acid formed as a by-product (Huber et al., 2006). Scholz et al. (2013) describe the production of ethanol by the yeast *Saccharomyces cerevisiae* from starch obtained from the hydrolysation of the microalgae *Chlamydomonas reinhardtii*.

Micro-organisms have also been observed to directly produce alkanes and alkenes. Fermentation of coconuts for 9 months, under storage conditions, by the bacteria *Chrysosporum Xerophilum* was observed by Kinderlerer et al. (1988) to produce a range of volatiles, including *n*-undecane, 1-nonene and 1-decene. Cyanobacteria, found in microbial soil crusts in deserts are known producers of alkanes. Dembitsky et al. (2001) found one such species, *M. Vaginatus* from the Negev desert, that when grown on dry agar produced the *n*-alkanes octane, tetradecane, heptadecane and octadecane in addition to a variety of branched alkanes in the range of C6 - C17 (Dembitsky et al., 2001). Other studies have observed cyanobacteria whose volatile production consisted of purely the four *n*-alkanes C8, C14, C17 and C18, with *n*-heptadecane by far the largest single component at 70 %.

An exciting development in recent years has been the advent of genetic modification techniques of various micro-organisms to enhance production of liquid hydrocarbons (Peralta-Yahya et al., 2012). These have the potential to not only alter the metabolic pathways of micro-organisms to preferentially produce specific hydrocarbon species (Ducat et al., 2011), but also introduce systems that see the desired molecules excreted from the micro-organism and greatly simplify product harvest-

ing (Dunlop et al., 2011). Of the photosynthetic micro-organisms to which such methods could be applied, Ruffing (2011) state that cyanobacteria are preferable to micro-algae as they are more resilient to environmental stresses, such as extreme light and temperature conditions, and possess a simpler genetic make-up that can be more easily engineered.

2.2. Compression ignition combustion

In recent years, understanding the processes of combustion and emissions formation in compression ignition engines has been aided by the conceptual model of compression ignition combustion first proposed by Dec (1997), who utilised laser diagnostic methods to make direct, quantitative and accurate measurements of the events occurring during combustion. Previous attempts to model compression ignition combustion were based on steady spray combustion in furnaces and gas turbines, only considering the quasi-steady portion of compression ignition combustion after the initial premixed phase and before the end of fuel injection with wall interactions not included. It was, therefore, considered very difficult to quantify the relationships between fuel spray behaviour, flame structure and fuel burning rate (Heywood, 1988).

An early attempt at understanding the compression ignition combustion process was made by Faeth (1977), who described the steady state of compression ignition combustion as a fuel rich cold centred diffusion flame, with combustion occurring as a sheath where the air and (liquid and vapour) fuel mixture reaches an appropriate equivalence ratio. It was not possible to understand whether combustion occurred as one large sheath flame around the fuel jet, or as many smaller diffusion flames encompassing single droplets; however, the basic model fitted the limited data sets available at the time. The following sections describe the now better understood stages of compression ignition combustion, drawing heavily on the work of Dec (1997).

2.2.1. Ignition delay

The ignition delay period is generally considered that between the start of fuel injection (SOI) and the start of combustion (SOC) .

The physical processes occurring during ignition delay are described as follows in the conceptual model of diesel combustion proposed by Dec (1997). As the injection starts all fuel emerging from the injector is liquid, downstream air is then entrained into the fuel jet leading to fuel vaporisation. Imaging of fuel injection showed that the jet length of the fuel is limited by evaporation due to entrainment of hot air within the cylinder. Injector hole size and temperature at top-dead-centre (TDC) impacted on the jet length, while injection pressure appeared not to. Following this, a distinct vapour fuel region along the periphery of fuel jet begins to develop beyond the extent of liquid fuel droplets. The maximum point of liquid penetration is then reached. However, the vapour jet continues to penetrate with a head vortex developing, and in the leading portion a relatively uniform air fuel mixture is formed with an equivalence ratio of between two to four. Rayleigh scatter images showing this progression also indicated that there is no pure fuel core within the jet, instead throughout there is a uniform, but fuel rich, combustible mixture with a well defined boundary with the surrounding air and that there is only a very narrow band of stoichiometric mixture at this edge.

During this time chemical breakdown of the fuel commences and temperatures increase to a critical level at which autoignition can occur; this is discussed in detail in Section 2.3. Autoignition was investigated by Dec (1997) using chemiluminescence imaging to detect the commencement of heat release. Chemiluminescence is first observed in the vapour fuel regions near the injector tip and progresses down the conical fuel jet, until the highest levels of chemiluminescence is emitted by the pure vapour zone. Furthermore, the observed chemiluminescence was never limited purely to specific regions, suggesting simultaneous ignition at multiple points volumetrically throughout the leading edge of the air and fuel mixture. As such, identifying the start of combustion is difficult, in general it is determined from a change in gradient in the in cylinder pressure data. This point is considered well defined in direct injection, but for in-direct, and also presumably homogenous charge compression ignition (HCCI), is more difficult to pin-point accurately (Katrasnik et al., 2006; Heywood, 1988).

2.2.2. Premixed phase

Following autoignition of the fuel air mixture two distinct phases of combustion are observed. The first of which encompasses autoignition and flame propagation

is the combustion of fuel and air mixed to combustible proportions during the ignition delay. After autoignition, the flame develops along contours of fuel and air stoichiometry of equivalence ration between 1-1.5. In addition, separate sites of autoignition may occur spontaneously and the flame is spread by turbulent mixing, with the entire spray quickly enveloped by flame. In-cylinder gas sampling indicates high levels of CO within the flame enveloped spray suggesting that the mixture at this point is still fuel rich (Heywood, 1988). According to the conceptual model of Dec (Dec, 1997), as the heat release curve initially moves upwards little evidence of fuel breakdown is apparent, however, shortly afterwards polyaromatic hydrocarbons (PAH) are evident across the leading section of the fuel jet, suggesting that the premixed burn phase occurs volumetrically throughout the mixture cone. The rapid spike observed in heat release at this point therefore indicated that the premixed burn phase is primarily comprised of the combustion of fuel rich mixture, and is in agreement with concurrent high in-cylinder levels of CO.

2.2.3. Diffusion flame (mixing rate controlled) and combustion tail

Subsequent to the premixed burn phase, combustion completes during the diffusion flame, or mixing rate controlled, phase. Combustion by this mode proceeds at the rate at which new fuel air mixture is formed and so rates of burning are lower than during the premixed burn phase. Heywood (1988) provides examples where these two phases are clearly visible in derivations of heat release rate obtained from the measurement of in-cylinder pressure. Dec (1997) found that as the premixed burn phase continues, temperatures and radical concentrations become high enough for a diffusion flame to develop at the interface of the excess fuel zone and surrounding air. Observation of diffusion combustion was achieved by the detection of OH radicals. No OH radicals were observed during the premixed burn phase due to the richness of the mixture (equivalence ratio of 2 - 4), and high OH concentrations are thought to only arise from a diffusion flame where combustion is near stoichiometric. OH radicals were first observed in small regions to the side and on the periphery of the fuel jet and then encompass the leading front of the flame back to a point just downstream of the injector tip. The combustion tail is considered to be the period following the end of injection, during which the the remaining liquid fuel quickly evaporates and the fuel rich zone moves outwards from the injector towards the chamber wall (Heywood, 1988).

2.3. Low temperature reaction kinetics

The influence of fuel molecular structure on the low temperature (T < 900 K) kinetics of ignition delay has been described in some detail by Westbrook (2000). From the description of Westbrook (2000), autoignition occurs at a critical temperature range of between 900 - 1000 K at which accumulated H_2O_2 (hydrogen peroxide) rapidly decomposes to OH radicals. Therefore, ignoring physical mixing processes, ignition delay can be considered a function of the rate at which this critical temperature is reached. This is determined by the low temperature kinetic mechanisms that occur after the start of injection (SOI). As the temperature rises towards 900-1000 K, hydrogen atoms are abstracted from the fuel molecule and replaced by O_2:

$$C_xH_y \rightarrow C_xH_{y\text{-}1} + H^* \tag{2.2}$$

$$R + O_2 \rightarrow RO_2 \tag{2.3}$$

These molecules then isomerise, during which no atoms are added or removed, but the structure of the molecule is rearranged, i.e.

$$R + O_2 \rightarrow QOOH \tag{2.4}$$

Isomerisation rates are determined partly by the structure of the alkyl chain, and also the number of atoms involved (ring size). During isomerisation, a C - H bond is broken and therefore, the strength of the C - H bond is important in determining the rates of isomerisation reactions. The strongest C - H bond in an alkyl chain is that of a primary carbon atom (a carbon atom with only one adjacent bonded carbon atom), followed by that of a secondary carbon atom (a carbon atom bonded to two adjacent carbon atoms) and weaker still is that of a tertiary carbon atom (a carbon atom with three adjacent and bonded carbon atoms). Following the initial

isomerisation, a molecule can accept another oxygen molecule (O_2) and undergo a second isomerisation reaction. This can be represented by:

$$QOOH + O_2 \rightarrow O_2QOOH \tag{2.5}$$

$$O_2QOOH + O_2 \rightarrow HOOPOOH \tag{2.6}$$

This molecule is then stable to around 800 K, by which point it will break down as follows to produce at least three radical species from the initial consumption of just one (Equation 2.3):

$$HOOPOOH \rightarrow OPOOH + OH \tag{2.7}$$

$$OPOOH \rightarrow \geq 2 \text{ radical species} \tag{2.8}$$

Therefore, increasing the straight carbon chain length of a molecule, and thus the number of weak secondary carbon to carbon bonds, speeds up isomerisation reactions, and the critical temperature for H_2O_2 decomposition is reached more quickly.

While Westbrook (2000) describes the low temperature reactions of alkyl chains, the uptake of oxygenated fuels, such as fatty acid esters, has seen interest in the low temperature behaviour of fuel molecules containing oxygen. The possible routes of decomposition of oxygenates of the general formula $ROC^{\bullet}=O$ at low temperatures (Buchholz et al., 2004; Glaude et al., 2005) are:

$$ROC^{\bullet}=O \leftrightarrow R^{\bullet} + CO_2 \tag{2.9}$$

$$ROC^{\bullet}{=}O \leftrightarrow RO^{\bullet} + CO \tag{2.10}$$

The route of decomposition in which CO_2 is produced (Equation 2.9) is undesirable from the perspective of utilising oxygenated molecules to control soot emissions (Glaude et al., 2005), as the entire oxygen content of the molecules is consumed in addition to a single carbon atom (the effects of fuel bound oxygen on particulate emissions are discussed in Section 2.4.4).

2.4. Emissions formation in compression ignition combustion

Concurrent to the release of energy during compression ignition combustion is the production of both gaseous and particulate emissions, and the following sections describe the formation of both.

2.4.1. NO_x

Nitrogen oxides form either from nitrogen within a fuel or atmospheric nitrogen present during the combustion reaction. Formation of NO_x from the latter source was first described by Zeldovich et al. (1947). From this work the production of NO_x by the "thermal" or "Zeldovich" mechanism was defined as the the oxidation of atmospheric nitrogen (Bowman, 1975), i.e.

$$O + N_2 \leftrightarrow NO + N \tag{2.11}$$

$$N + O_2 \leftrightarrow NO + O \tag{2.12}$$

In 1970 the following reaction of atmospheric nitrogen with OH radicals was proposed by Lavoie et al. (1970), and suggested to contribute especially in near to stoichiometric and rich mixtures.

$$N + OH \leftrightarrow NO + H \tag{2.13}$$

These three reactions are collectively referred to as the extended Zeldovich mechanism (Miller and Bowman, 1989), and the forward steps of the above equilibrium reactions require large activation energies (Heywood, 1988), hence formation of NO_x by these reactions is highly temperature dependent and conditions of high temperature and high O_2 concentrations will result in high NO_x formation rates (Bowman, 1975). Therefore, production in post flame gases dominates that of production during combustion in the flame front as the high and rising pressure during combustion gases have a very short residence time in the flame front while gases formed at the start of combustion will be at a considerable higher temperature by the end of combustion (Heywood, 1988).

On first describing the above mechanism, Zeldovich suggested that the formation of NO_x can be decoupled from the fuel oxidation reactions as these proceed much more quickly (Zeldovich et al., 1947). However, O and OH radicals are also important in fuel oxidation and comparison of a coupled and decoupled model by Miller and Bowman (1989) shows that the non-equilibrium conditions produced by the fuel oxidation and low temperature reactions does result in slightly higher initial formation of NO_x, though this effect is small and reduces further with increasing temperatures as combustion reactions advance. Modelling NO_x formation decoupled from fuel oxidation allows for the impact of temperature and fuel:air equivalence ratio to be observed. Numerical modelling in this manner shows an increase in NO_x formation with rising temperature and decreasing equivalence ratio, as rates of reaction increase and more oxygen is available (for oxidation of nitrogen). However, if individual combustion reactions can be considered as being adiabatic and at constant pressure, it is seen that NO_x formation will peak at a stoichiometric fuel:air composition (Heywood, 1988).

When no nitrogen is present within a fuel then formation by the thermal mechanism is considered to be the largest contributor to NO_x emissions (Miller and Bowman, 1989). Several studies have seen experimental NO_x concentrations that can be explained entirely by the Zeldovich mechanism, while others found significantly higher than expected levels of NO_x, especially for fuel rich mixtures (Bowman, 1975). In the early 1970's several theories were put forward for the discrepancy observed (Bowman, 1975), and the mechanism believed to be most significant is that of "prompt" formation suggested by Fenimore in 1971. By comparing the predicted rates of NO_x production purely by the thermal mechanism with results of sampling both adia-

batic and non-adiabatic flames of methane and ethylene, it was found that while in all cases post-combustion the equilibrium equations for the thermal production of NO_x dominated, there is some NO_x production in the fuel rich primary reaction. The mechanism for this "prompt" formation was not identified, however, as the rate of formation is much greater than the anticipated post combustion thermal production, a mechanism involving degradation of N_2 by reaction with hydrocarbons appeared possible. Fenimore (1971) suggested this as a probable mechanism as the alternative (high concentrations of O_2 required for the thermal mechanism) appears far more improbable in the fuel rich primary reaction zone.

Since first suggested the prompt mechanism has in some cases found to occur due to super-equilibrium concentrations of O and OH, but is primarily driven by the reaction of hydrocarbon species with molecular nitrogen (Miller and Bowman, 1989). This was later confirmed by assessing the necessary activation energies for various possible short chain hydrocarbon radicals and subsequent rates of reaction, Miller and Bowman (1989) found that the most likely formation path is that first suggested by Fenimore (1971), i.e.

$$CH + N_2 \leftrightarrow HCN + N \tag{2.14}$$

Experimental studies show that for any given pressure the reaction rate of the reaction shown in Equation 2.14 decreases with increasing temperature (Miller and Bowman, 1989). Another reaction suggested as important in prompt formation is the is the direct action of molecular nitrogen and carbon, i.e.

$$C + N_2 \leftrightarrow C + N \tag{2.15}$$

This reaction is highly endothermic and so the contribution to overall levels of prompt NO_x increases with temperature. Important in predicting prompt NO_x formation is establishing CH concentrations (which are fuel dependent), rates of nitrogen fixation and the rates of inter-conversion between different nitrogen fragments. Miller and Bowman (1989) propose that thermal NO_x formation is only dominant in an equivalence ratio between $\Phi = 0.8$ to 1, with prompt formation more important in richer conditions.

Fuel bound nitrogen can also contribute to NO_x formation and will be of most importance when combustion occurs under rich conditions. Of the fossil fuels this is most apparent with coal (and coal derived fuels), as coal comprises of between 0.5 - 2 % nitrogen (Miller and Bowman, 1989). Laboratory scale burner experiments suggest that the yield of NO_x from fuel bound nitrogen is independent of the form the nitrogen takes, whether an intrinsic part of the fuel molecule or an additive to the fuel stream such NH_3, and almost entirely dependent on the local combustion conditions (Fenimore, 1972). Initial reactions of fuel bound nitrogen are the conversion to hydrogen cyanide when held in an aromatic ring and ammonia when the nitrogen is present as an amine. Subsequent oxidation of hydrogen cyanide releases molecular nitrogen for equilibrium reaction with O_2 and NO. Miller and Bowman (1989) discuss in depth this reaction and also the reverse for the purpose of post-combustion NO_x removal.

NO_x refers to both nitrogen oxide (NO) and nitrogen dioxide (NO_2), and when discussing NO_x emissions from an internal combustion engine both are present. Heywood (1988) reports that based on chemical equilibrium for post combustion gases at typical flame temperatures, the percentage of NO_2 as the total NO_x should be negligible, however in compression engine exhaust emissions NO_2 has been seen to comprise between 10 - 30 % of total NO_x. Bowman (1975) suggested that NO_2 formation and subsequent decomposition back to NO could occur via the following mechanism in the flame front:

$$NO + HO_2 \leftrightarrow NO_2 + OH \tag{2.16}$$

$$NO_2 + O \leftrightarrow NO + O_2 \tag{2.17}$$

In compression ignition combustion the step of conversion from NO_2 back to NO is quenched by cooler regions of gas in the cylinder due to the non-homogenous nature of diesel combustion. Following peak in cylinder pressure and the commencement of the expansion stroke NO, chemistry freezes as gas temperatures fall below the activation level due to the expanding volume and the turbulent mixing of high temperature gases with those at lower temperatures (Heywood, 1988). Bowman

(1975) gives values to the rate of reaction constant describing NO_2 formations and destruction and it can be seen that NO_2 decomposition back to NO will proceed around five times as quickly as its formation from NO.

Optical measurements of diesel combustion in a heavy duty diesel engine by Dec (1997) showed the initial stages of fuel rich combustion to not be conductive to NO_x formation by either thermal or prompt mechanisms, due to the low presence of oxygen and low adiabatic flame temperatures. Furthermore most NO production was observed to occur on the lean side of the diffusion flame.

Verbiezen et al. (2007) took in-cylinder measurements of NO in a heavy duty diesel engine using laser induced fluorescence (LIF) at a variety of start of injection (SOI) timings at constant indicated mean effective pressure (IMEP) . These were complimented by modelling of NO formation, by only the extended Zeldovich mechanism, during the mixing controlled burn phase. The results showed a clear trend of increasing NO exhaust and in-cylinder concentrations with advanced SOI and constant IMEP. Measurements of peak in-cylinder temperature by CO_2 and O_2 absorption remain constant and independent of SOI while average in cylinder temperatures increase with advanced SOI, highlighting the temperature sensitivity of NO formation. This agrees with the highly documented observation that increasing the cetane number of a fuel, or retarding the SOI , results in a reduction in NO_x emissions (Graboski and McCormick, 1998; Heywood, 1988). Szybist et al. (2007) found that the time of maximum global temperature to be the dominant variable in NO_x production, as a later time of maximum temperature will allow less time for the formation of NO_x before temperatures fall below the required level for the reaction to proceed and nitrogen reaction kinetics freeze (Heywood, 1988).

While no direct evidence of any prompt NO formation was found by Verbiezen et al. (2007), the results did not exclude the possibility that NO could be forming by this route during the premixed phase (during which imaging techniques used to measure the equivalence ratio found the fuel air mixture too fuel rich for the production of thermal NO). The LIF probe was positioned too far away from the premixed burn phase to detect any prompt NO, but it was suggested that the first detection of NO by the LIF probe occurred long enough after the start of the premixed burn phase for prompt NO formed during this combustion stage to have travelled by convection to the probe position. However, the first NO detection also coincides with the start of the diffusion controlled burn phase, (as implied by the first

detection of soot luminosity, and as suggested by Dec (1997)) so it is also possible that the first NO detected was formed locally by the thermal mechanism. Modelling of NO production using only the thermal mechanism, at the same conditions as those used for the engine experiments of Verbiezen et al. (2007), found that rates of thermal NO production were fast enough to account for the vast majority of the experimentally recorded levels of NO. However, there was a consistently negative offset in the NO emissions predicted by the model, relative to the measured NO concentrations, and so it is possible that this was due to prompt NO formed earlier during the premixed combustion phase.

2.4.2. Carbon monoxide

Carbon monoxide arises when fuel combustion is incomplete, i.e. oxidation of fuel bound carbon is incomplete, in general due to insufficient air (the mixture is fuel rich). Heywood (1988) considers that emissions of CO from diesel engines are low enough to be unimportant and direct investigation into CO production is uncommon. General observations have been made, such as increasing the temperature of the in-cylinder mixture (for example with a glow plug) tends to decrease levels of CO in exhaust emissions (Arregle et al., 2006). Bowman (1975), however, does discuss in some detail the formation of CO from combustion systems. From comparison of exhaust level measurements of CO to those taken in-cylinder (which found to be higher) he concludes that CO formation and destruction is kinetically controlled. It is suggested that the initial step of CO formation may occur during the initial oxidation of a fuel molecule, i.e.

$$\mathrm{RH} \leftrightarrow \mathrm{R} \leftrightarrow \mathrm{RO_2} \leftrightarrow \mathrm{RCO} \leftrightarrow \mathrm{CO} \tag{2.18}$$

Oxidation of the CO to CO_2 is then thought to occur primarily by oxidation by OH radicals, however, the rate of this reaction is slow in comparison to reaction by which CO forms. Oxidation of the CO by HO_2 and O_2 radicals is also possible, though the latter is thought unlikely due to an extremely low rate of reaction (Bowman, 1975).

2.4.3. Un-burnt hydrocarbons

There are several plausible reasons for the presence of un-burnt hydrocarbons in the exhaust of compression ignition engines, and these are reviewed by Heywood (1988) who describes two primary paths by which fuel can avoid being involved in the process of combustion (or do so only partially). Both a very lean or very rich mixture will see a flame fail to sustain, and thus fuel oxidation will take place only by thermal reaction during the expansion stroke and much fuel is left unconsumed. Wall temperature is important, suggesting that quenching of fuel air mixture is significant; emissions of un-burnt hydrocarbons decrease significantly with an increase in oil temperature. Over-lean areas of fuel and air mixture will exist on the very edge of the injected fuel jet (ie. fuel first injected) and some of this will be of an equivalence ratio too far below stoichiometric too auto-ignite. Thus increased ignition delay will correlate with increased emissions of un-burnt hydrocarbons. The opposite problem, under-mixing of fuel with air, can occur when the fuel contained in the nozzle sac volume enters the cylinder at low velocity. Under-mixing can also occur due to injection of excess fuel, and will again result in hydrocarbons remaining un-burnt.

2.4.4. Particulates

Soot from compression ignition engines is a solid comprising of carbon and hydrogen in a ratio of approximately 8:1 (Tree and Svensson, 2007). In developing his conceptual model of diesel combustion many detailed observations on soot formation were made by Dec (1997). Initially, soot particles formed in the pre-mixed phase were very small. However, half a crank angle degree later larger soot particles were definitely observed in the centre of the jet and also in much greater numbers on the periphery, suggesting a separate formation mechanism at the two locations. Soot levels and distribution continue to increase onwards through the cross section of the leading edge of the jet, with the largest concentration remaining at the periphery. Soot formation during the first part of mixing controlled burn (diffusion flame) is initially very similar to that at the end of the premixed phase. However, a pattern of higher concentrations of soot at the head vortex and lower concentrations upstream, nearer the injector tip, become apparent. Upstream soot continues to form across the entire cross-section of the fuel jet, even after the premixed phase is complete. Much larger particles are present at the periphery of the head vortex and continue to increase in size throughout the combustion event, while those upstream remain of

a similar smaller size throughout. This suggests that initial small particle formation occurs upstream, with additional formation and an increase in size occurring as the particles move downstream to the head vortex.

Following the end of injection a change is apparent in the soot distribution pattern, with a higher soot concentration now occurring in the upstream portion of the jet and larger particles also present. Dec (1997) hypothesises that this may be due to be throttling of fuel flow as the injector closes resulting in poor atomisation and mixing, producing higher soot formation along the fuel jet axis. Pockets of soot are still visible near the end of heat release and Dec (1997) suggests that soot avoids oxidation either as the exhaust valve opens before the process is complete, or that areas of flame and reaction mixture on the periphery of the event are extinguished.

Drawing heavily on the observations of Dec (1997), Tree and Svensson (2007) set out the fundamental sequence of five processes whereby conversion of liquid or solid phase hydrocarbons results in solid particles (soot), as is shown in Figure 2.4 and described in the following paragraph.

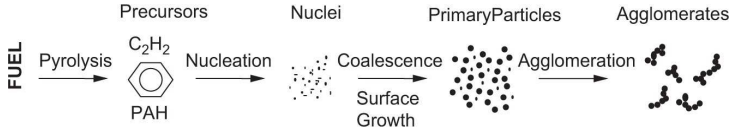

Figure 2.4: Schematic diagram of the steps in the soot formation process (Tree and Svensson, 2007)

The process of soot formation shown in Figure 2.4 initiates with the breakdown of fuel molecules. Such pyrolysis reactions are endothermic, requiring high temperatures upon and producing unsaturated hydrocarbons, polyacetylenes and PAH, and radicals such as hydrogen are important accelerants of pyrolysis. Following pyrolysis, nucleation is the forming of the initial solid particles (Dp 1.5 to 2 nm) from gas phase hydrocarbons. Nucleation requires high temperatures (1300 to 1600 K) and high radical concentrations to facilitate the addition of small aliphatic molecules to larger aromatic structures. Subsequent nuclei are not a major contributor to total soot mass but are crucial in that they provide active sites for further soot growth. This is termed surface growth and is the addition of gas phase hydrocarbons (primarily acetylene) to reactive radical sites on the nuclei; addition slows with increasing particle size and a decrease in the number of radical sites available. Surface growth is less dependent on temperature and radical concentrations than initial nucleation

and so occurs outside the primary reaction zone. This process maintains the total number of soot particles but greatly increases the total mass of soot. Coalescence (coagulation) and agglomeration follow which increase particle size, hold total soot mass constant and reduce the number of particles. Coagulations sees two spherical particles combing to form one spherical primary particle, while in agglomeration primary particles stick together while maintaining their individual shape resulting in chains or clumps of particles. Primary particle size has been observed as highly dependent on the combustion strategy but are in general between 20 - 70 nm. Subsequent agglomerates forming after combustion are of 100 nm in size and greater.

A sixth process, concurrent with all others and important in determining ultimate soot levels, is that of soot oxidation, the conversion of solid hydrocarbon back to a gaseous phase as CO, CO_2, H_2 or H_2O. Soot oxidation has been observed to commence at temperatures of 1300 K and is considered a two stage process: initial absorption of an oxygen species onto the particle with the subsequent desorption with a fuel component now attached. Under rich and stoichiometric conditions OH oxidation dominates, while for lean conditions O_2 oxidation also takes place. Rates of soot formation increase with temperature but less so than oxidation and thus if oxygen is present, as in the case of a premixed flames, increased temperature can result in lower soot production. In diffusion flames where no oxygen is present in the pyrolysis region soot levels increase with temperature.

Tree and Svensson (2007) also give an overview of the impact of physical factors affecting soot production, with temperature identified as the primary driver and peak soot formation occurring between 1500 - 1700 K. The in-cylinder pressure experienced a by a flame affects a wide range of variables during the combustion event and so to isolate the effects of pressure on soot formation is difficult, though higher in-cylinder pressure are likely to increase rates of reaction due to a higher number of radical collisions. The influence of mixture stoichiometry is also complex, and while either fuel bound oxygen or increased mixing tends to decrease soot levels this is not universally observed. The complex impact of oxygen arises due to the interdependency of temperature and oxygen concentration and the separate effects of the two are difficult to isolate. Initial increases in soot with increased oxygen concentration have been observed in counter-flow diffusion flames, levels reach a peak as increased oxygen availability can increase fuel breakdown and the availability of soot precursors (dependent on fuel composition) and also results in an increase

in temperature. When oxygen levels increase further (equivalence ratio of 2 to 10), oxidation rates become faster than the rate of temperature increase and soot production falls. Tree and Svensson (2007) suggest that fuel molecular structure is only of significant importance in determining soot levels in diffusion flames, and that for all flames an increased number of C-C bonds will produce greater soot levels.

Lin and Wang (2004) and Cantrell et al. (2008) studied of the impact of flame lift off length (LOL) indicate a strong relationship between conditions within the premixed burn phase and final soot exhaust emissions. Longer LOL results in a premixed phase in which more oxygen has been entrained and a greater portion of the fuel is burnt and thus lower soot emissions occur.

2.5. Effects of fuel molecular structure on compression ignition combustion and emissions formation

2.5.1. Acyclic non-oxygenates

For many years consideration of how the molecular structure of a fuel impacts on combustion phasing and emissions has been by the measurement of the cetane number (Heywood, 1988). In addition to the many measurements of the cetane number of non oxygenated hydrocarbons including *n*-alkanes (Murphy et al., 2004), the cetane index utilises *n*-hexadecane as the baseline for a cetane number equal to 100 and tetra - methyl - pentane as the zero value, implying that straight long chained alkanes are most suitable for compression ignition combustion and shorter chained, methyl branched alkanes less so.

The effect of straight carbon chain length on ignition quality has been found to be linear by Knothe et al. (2006) who, by means of ignition quality testing (IQT) determination, found that *n*-hexadecane (C16) has a higher cetane number than *n*-dodecane (C12), and in engine tests found levels of CO and total hydrocarbons (THC) to be greater for *n*-hexadecane than *n*-dodecane, while both produced identical levels of NO_x and PM. Roy (2005) in low load tests in a common rail direct injection engine found *n*-heptane (C7) to exhibit a longer ignition delay than the reference diesel tested while *n*-decane (C10) possessed an equivalent ignition delay duration to that of the reference diesel. In a work primarily intended to identify the cause of exhaust odour in diesel engines, Aaronson and Matula (1971) combusted pure *n*-hexadecane in a Cooperative Fuel Research (CFR) cetane rating engine at

a speed of 1000 rpm and compression ratio of 1:14. Through gas chromatography Aaronson and Matula (1971) identified many differing species of aldehydes, alcohols, acids and aromatic compounds in the exhaust gas. Further spray burner experiments and use of non-aromatic lubricating oil during engine experiments suggested that the hydrocarbon species found in the exhaust gas had formed from *n*-hexadecane during the combustion process and were not pyrolysis products of lubricating oil.

Shen et al. (2009) experimentally investigated the ignition delay times of *n*-heptane, *n*-decane, *n*-dodecane and *n*-tetradecane in a shock tube at temperature conditions of between 786 - 1396 K and found no discernable influence of straight carbon chain length on the duration of ignition delay. Mixtures of the vaporised alkanes were permitted to premix with air for between 15 minutes to three hours before transfer to the heated shock tube (the temperature of which varied from room temperature for heptane to 160 °C for tetradecane). Ignition delay times were measured by observation of OH emissions and in-tube pressure measurement. The results showed that for all of the alkanes studied, and for all equivalence ratios, as temperature and pressure increase so the ignition delay decreases, with clear indication of a negative temperature coefficient (NTC) region at lower temperatures. A comparison was then made of the relative reactivity of the alkanes studied, and it is concluded that any difference in ignition time due to alkane structure is slight and well within the margins of error. Furthermore, Shen et al. (2009) also report several other shock tube and rapid compression machine studies that are in agreement with this result and therefore suggest that at C7 and greater the rates of low temperature isomerisation of fuel molecules is less dependent on the straight carbon chain length than at shorter carbon chain lengths. The detailed chemical kinetic reaction mechanisms for *n*-alkanes developed by Westbrook et al. (2008), also suggest that between C8 - 16, ignition qualities of *n*-alkanes are similar enough to be exchanged for each other in simulations and in creating fuel surrogates.

Measurements of the cetane numbers of linear alkenes, compiled by Murphy et al. (2004), have shown, that in comparison to linear *n*-alkanes, the presence of a double bond reduces the ignition quality of the fuel. For example, *n*-heptane has a cetane number of 54 while 1-heptene has a cetane number of 32, and *n*-hexadecane a cetane number of 100 while 1-hexadecene was found to possess a cetane number of 87.

In addition, several studies utilising rapid compression machines have identified differences in reactivity between *n*-alkanes and un-branched alkenes of identical car-

bon chain length, and furthermore the importance of the position of the double bond within the alkene (Minetti et al., 1999; Tanaka et al., 2003; Vanhove et al., 2005). Minetti et al. (1999) discuss the pre-ignition kinetics of *n*-pentane and 1-pentene based on experimental results of premixed stoichiometric fuel and air mixtures in a rapid compression machine of compression ratio 9.4 : 1. They find that 1-pentene has a lower reactivity than *n*-pentane and suggest that this is due to competing reaction pathways in the oxidation of 1-pentene and a reduction in the availability of radical species. While the low temperature kinetics of 1-pentene follow the same general reaction steps of oxidation and isomerisation as *n*-alkanes (described in Section 2.3), the presence of double bonds, to which radicals such as OH and HO_2 can add directly, creates reaction pathways specific to alkenes.

When considering the production of particulates, the presence of a double bond in a straight carbon chain has been observed as an influence outside of impacts on combustion phasing. Ladommatos et al. (1996) found that when considering the sooting tendencies of pure hydrocarbon species in a laminar diffusion flame (in which the fuels had been pre-vaporised) that the presence of a double bond within the carbon chain increases the sooting tendency.

The first comparative study of olefin double bond position, and also *cis* versus *trans* isomerisation, was conducted in the late 1960's by Salooja (1968) who investigated the combustion properties of 1-butene and also *trans*- and *cis*-2-butene. In both flow reactor and variable compression engine experiments (the latter conducted to determine knocking tendencies), 1-butene was found to be the most reactive, followed respectively by *cis*-2-butene and *trans*-2-butene. The cool flame combustion of pentene isomers was studied by Hughes and Prodhan (1973) in the early 1970's. They found 1-pentene to possess the shortest ignition delay, but no difference between that of *cis*- and *trans*-2-pentene. More recently, the low temperature oxidation of 1-pentene was investigated by Prabhu et al. (1996) in a pressurized flow reactor. Sampling of the reaction mixture and identification of the species present revealed that the abstraction of hydrogen atoms from the saturated portion of the alkene was far more prevalent than radical addition to the double bond. Tanaka et al. (2003) and Vanhove et al. (2005) studied the premixed stoichiometric combustion in rapid compression machines of heptene and hexene *trans* isomers respectively. In both instances, moving the position of the double bond progressively towards the centre of the molecule consistently resulted in an increased duration of ignition delay.

Furthermore, in addition to possessing the longest ignition delay, in both studies the isomer with the double bond in the three position showed only single stage ignition in contrast to the other isomers studied which showed two stage ignition.

Mehl et al. (2011, 2008) and Bounaceur et al. (2009) utilised the experimental data of Tanaka et al. (2003) and Vanhove et al. (2005) to develop detailed chemical models that sought to better understand the changes in olefin reactivity with varying double bond position. Highlighted was the importance of the carbon chain length of the saturated portions of the alkenes studied (Hughes and Prodhan, 1973; Mehl et al., 2008; Salooja, 1968; Vanhove et al., 2005) and how the properties of the C-H bonds present in these chains influence the well understood mechanisms of low temperature *n*-alkane oxidation (Westbrook, 2000). In addition, as the chain length of the residual saturated alkyl chains decreases, reactions involving the double bond are of increasing importance (Mehl et al., 2008; Vanhove et al., 2005). The kinetic modelling of Bounaceur et al. (2009) found that for 1, *trans*-2 and *trans*-3 hexene the total rate of reactant consumption by reactions with an inhibiting influence on ignition was found to be 34 %, 49 % and 66 % respectively.

2.5.2. Fatty acid esters

While the advantages of fatty acid esters over the unprocessed vegetable oils first became apparent in the 1980's, investigating the merits of such fuels continues to be attract interest (Benjumea et al., 2010; Fisher et al., 2011). While the majority of such studies have primarily focused on the combustion and emissions characteristics of fatty acid esters relative to fossil diesels, in many cases such studies also cast light on the impacts of ester molecular structure.

A review by Graboski and McCormick (1998) describes many of the results of comparative studies between esters and fossil diesel fuel and gives a general overview as to the effects of ester molecular structure on combustion and emissions. Comprising 10-12 % wt/wt O_2 ester based fuels have a lower energy density but a higher flashpoint than fossil fuel diesel. Despite the lower fuel energy content economy is unaffected though torque is seen to decrease, however in comparison to fossil diesel esters have poor cold flow properties and higher viscosity results in poor atomisation. Esters also possess an iodine number greater than 115 resulting in excessive carbon deposits. Cetane number also increases with saturation and carbon chain length, but decreases with the number of double bonds present and the move-

ment of these double bonds and carbonyl groups towards the centre of the molecule. Considering exhaust emissions, NO_x levels were most often found to increase relative to fossil diesels, while particulates, CO and THC decreased. Levels of poly-aromatic hydrocarbons (PAH) in the exhaust gas also decrease, but the mutagenicity of such species increases.

The observed increase in NO_x emissions of esters, relative to fossil diesel, has been the focus of many studies. One of the more recent, by Mueller et al. (2009) differentiates the cause of this increase into combustion effects due to the differing fuel composition and engine calibration effects. Such engine calibration effects include adjusting for the differing bulk modulus of esterified fuels and thus can be removed with proper engine optimisation. Following the Dec (1997) model of combustion, the contribution of prompt NO_x is presumed to be minimal and only the thermal mechanism was considered. It is suggested that differing combustion phasing, adiabatic flame temperature, and lower radiative heat transfer (due to the reduced presence of soot in oxygenated fuels) may all be contributing to higher in-cylinder temperatures and thus NO_x production by the thermal mechanism. Mueller et al. (2009) set out to test these hypotheses by investigating the heat release and emissions from two ester fuels derived from soy bean (primarily comprising of C18:1 and C18:2 esters), one of which was doped with phenanthrene to increase sooting. In addition, two binary pure alkane reference fuels comprising of hexadecane and heptamethylnonane, blended in proportions to give a reference fuel of cetane number 45 and one of 70, were also tested.

The investigations of Mueller et al. (2009) were carried out in an optically accessible heavy duty diesel engine, at 800 rpm, with single injection to give SOC at approximately TDC, and several operating points of constant IMEP (Indicated mean effective pressure). At all operating conditions, the bio-diesel blends were seen to produce increased NO_x levels relative to the alkane reference fuels, and when comparing just the two bio-diesel blends, the blend exhibiting the highest radiative heat transfer, as measured by spatially integrated natural luminosity (SINL), did consistently produce lower NO_x emissions. However, the pure alkane fuel of cetane number 45 had a level of radiative heat transfer between that of the two bio-diesel blends but produced significantly lower NO_x emissions for all operating conditions. Thus while the experiment did show that radiative heat transfer is an important factor in determining in-cylinder temperatures (and thus thermal NO_x production), it could

not be isolated from other the variables under investigation and thus the importance of radiative heat transfer could not be quantified. At lower loads the maximum in-cylinder temperature (as calculated from the in-cylinder pressure measurements) was observed to be of greater magnitude and occur earlier in the combustion cycle for the bio-diesel blends and thus the longer residence time of combustion products at a higher temperature could account for the increased NO_x production. However, at higher load the maximum in-cylinder temperature appears of the same magnitude and at the same point for all fuels; were this factor the major contributor to NO_x formation emissions levels would be expected to be the same for all fuels at these conditions and this was not the case.

Combustion phasing for the ester blends was observed to proceed more quickly, the start of combustion (SOC) and ignition delay was nearly constant for all fuels, but the end of premixed burn (EOPMB) occurred earlier and the rates of combustion were found to be faster for the fatty acid ester fuels. Faster combustion in any phase would again lead to longer residence times at higher temperatures for combustion products, and the earlier combustion phasing is most noticeable at lower loads where the largest emissions of NO_x from the bio-diesel relative to the alkanes was observed.

Equivalence ratios at the lift off length (LOL) were also determined by optical methods. The ester blends were observed to be closer to stoichiometric, as would be expected with the presence of fuel bound oxygen. This led to the observation that mixture stoichiometry correlates with NO_x emissions, however the authors noted that it is impossible with the fuels tested to separate this observation from the fact that the bio-diesel blends contain oxygen. There is also a correlation between mixture stoichiometry and in-cylinder temperatures, products of combustion at nearer stoichiometric levels will see higher temperatures and higher oxygen concentrations. In addition adiabatic flame temperature was calculated for all fuels, while both bio-diesel blends do possess a higher adiabatic flame temperature than the pure alkanes, however, a clear correlation between the adiabatic flame temperature and NO_x emissions was not found.

In summary Mueller et al. (2009) concluded that all of the observed mechanisms play a role but that the relative importance of each varies with load and combustion phasing (low load being premixed dominated and high load being mixing controlled dominated) and cannot be estimated from the work presented. A conceptual explanation was offered for stoichiometry being the primary driver in NO_x productions,

mixtures closer to stoichiometric will see combustion products created more quickly at higher temperatures, and with longer residence times, leading to greater NO_x output by the thermal mechanism. For the mixtures further from stoichiometric the inverse can be seen to be true, a small pre-mixed fraction and slower combustion event with a fuel rich core will see lower temperatures.

A numerical investigation into the same phenomena of increased NO_x emissions from esterified fuels (relative to fossil diesel fuel) was made by Ban-Weiss et al. (2007). They start by considering the inverse relationship between cetane number and NO_x emissions (that a higher cetane number corresponds to a shorter ignition delay and subsequent lower NO_x emissions) observed by previous studies. However, the authors observe that cetane number is not the sole driver of NO_x emissions, as a bio-diesel of identical cetane number to a fossil diesel has been reported to exhibit higher NO_x emissions. It was suggested that the NO_x increase observed with fatty acid esters is not driven solely by the thermal mechanism but that the presence of double bonds leads to the formation of more hydrocarbon radical precursors to the prompt mechanism. Ban-Weiss et al. (2007) also postulated that the unsaturated nature of many of the esters resulted in the overall blend possessing a higher adiabatic flame temperature than fossil diesel and that the observed increased in NO_x could therefore also potentially be attributed to greater levels of formation by the thermal mechanism.

Combustion and subsequent NO_x formation simulations by Ban-Weiss et al. (2007) were undertook based on the idea of a "well-mixed balloon", where mass flows into the system but the mass flow out is zero (this was considered to be representative of the continued mixing of the fuel jet with air in compression ignition combustion). Long chain molecules were considered too complex to model (and the alkyl chain length deemed relatively insignificant relative to the presence of double bonds) and so shorter chain molecules highlighting the presence of a double bond in an *n*-alkane and a fatty acid ester were chosen. For both molecule types, the presence of a double bond coincided with a higher peak temperature and increase in NO_x production relative to the fully saturated form of the molecule. By removing in turn the governing equations for thermal and prompt NO_x production, it was found that the thermal mechanism was the primary formation route responsible for some 92 % of the total emission, whereas removal of the prompt reaction routes saw a reduction of in total NO_x emissions of 13 %.

Schönborn et al. (2009b) also investigated the increase in NO_x emissions when combusting esterified fatty acids by studying the combustion and emissions of single component ester fuels in a single cylinder direct injection common rail diesel engine at low loads. The fuel molecules were chosen to highlight the effect of straight carbon chain length and degree of unsaturation in the fatty acid moiety of a fatty acid ester, and also the straight carbon chain length in the alcohol moiety. By initially running the experiments at two timings of constant injection and constant point of ignition, the effect of ignition delay (and thus cetane number of the esters) was observed for constant physical conditions at the start of injection and repeated for constant physical conditions at the start of combustion. It was found at both conditions that increasing the fatty acid chain length reduced the level of NO_x emissions and also reduced the duration of ignition delay. Peak heat release rates were found to be lowest for molecules with the longest fatty acid chain length, thus the reduction in NO_x levels could be attributed to lower in-cylinder temperature and thus less thermal NO_x production. Reducing the number of double bonds in the fatty acid moiety increased the ignition quality of the ester and led to a similar reduction in thermal NO_x emissions, however calculated adiabatic flame temperatures of the esters also reduced with an increasing degree of saturation. Increasing the alcohol chain length from one to two saw a small increase in ignition quality and a lower peak heat release that coincided with a slightly lower emission of NO_x.

The ignition quality (and thus length of ignition delay) was then removed as a variable in the investigation by Schönborn et al. (2009b) by using varying quantities of the ignition quality improving additive 2 ethylhexyl nitrate (2 EHN) . Results of these subsequent engine experiments, for which both the start of injection and start of combustion occurred at the same timing and thus physical conditions (and patterns of heat release) were constant, found that the shortest fatty acid chained esters required the largest dose of 2 EHN, suggesting formation of NO_x from fuel bound nitrogen to be of little importance. Increasing un-saturation continued to result in increased NO_x emissions under the conditions of constant ignition delay, as did reducing the length of the carbon chain in the alcohol moiety.

The emission of particulates was also measured for all of the experiments conducted by Schönborn et al. (2009b) and described above. It was found that the number of nucleation mode particles ($Dp < 50$ nm) decreased with increasing ignition delay. By considering also results at constant ignition delay in the fatty acid esters ob-

served it was found that the number of nucleation mode particles increased in close correlation with increasing boiling point of the molecules tested. Thus it was suggested that the large number of nucleation mode particles emitted by fuels of high boiling point were in fact liquid droplets of re-condensed un-burnt fuel. The total mass of particulates emitted was found to correlate strongly with ignition delay, and, in the experiments where ignition delay was removed as a variable, increasing the number of double bonds in the fatty acid moiety was found to increase the total mass of particulates, as was a very long fatty acid carbon chain length of 22. From the results of these experiments, Schönborn et al. were able to qualitatively assess the importance of the various routes by which NO_x production from esters occurs. Firstly, length of ignition delay was found to be the dominant factor in shaping the combustion event, and emissions of NO_x and particulates were found to correspond to the changes in in-cylinder temperature brought about by the changing extent of the premixed burn fraction. Secondly, with ignition delays (and thus premixed burn fractions) equalised for esters of differing degrees of saturation and fatty acid carbon chain length the adiabatic flame temperature determines the level of NO_x emissions. Finally, the effect of soot radiative heat transfer in determining NO_x levels was thought to be small.

While the influence of the fatty acid moiety of fatty acid esters on compression ignition combustion has received significant interest, the impact of increasing the alcohol moiety has been less well understood. Knothe et al. (1997) reported on the cetane numbers of esters of varying alcohol moiety carbon chain length and fatty acid moiety saturation. The cetane numbers of methyl, ethyl, propyl and butyl esters of stearic (C18:0), oleic (C18:1), linoleic (C18:2) and linolenic (C18:3) acid, and also the pure acids, were determined by Ignition Quality Testing (IQT), with all components possessing a stated purity in excess of 99 %. The relationship between cetane number and carbon chain length in the alcohol moiety was, however, not linear in most cases. For example, the methyl esters of linoleic acid exhibited a higher cetane number than both the ethyl and propyl esters of linoleic acid. Serdari et al. (1999) similarly measured blended cetane numbers of methyl to butyl esters of various fatty acids, oleic (C18:1), palmitate (C16:0), myristate (C14:0) and laurate (C12:0). While for all the fatty acids butyl esters consistently possessed a higher blended cetane number than those prepared with shorter chain alcohols, again there was no linear trend between cetane number and alcohol carbon chain length.

In engine drive cycle tests, Makareviciene and Janulis (2003) compared emissions from pure rapeseed methyl ester to those from rapeseed ethyl ester, and found the ethyl ester to produce lower emissions of NO_x and CO, but an increased level of unburnt hydrocarbon emissions relative to the methyl ester of identical fatty acid moiety. During engine tests, Lapuerta et al. (2008) found no discernable difference in the ignition delay of methyl and ethyl esters prepared from waste cooking oil. A slight decrease in NO_x levels with the increased alcohol moiety chain length was detected and suggested by the authors to be either attributable to the reduced oxygen content or an unseen higher ignition quality of the ethyl ester. More significant were observed reductions in the level of un-burnt hydrocarbons emitted by the ethyl ester relative to the methyl, and lower smoke opacity, particulate mass and mean particle size produced by the methyl ester relative to the ethyl. These emissions characteristics were found to correlate well, but not exclusively, with fuel oxygen content.

Schönborn et al. (2009b), while investiging the combustion and emissions of single component fatty acid ester fuels, observed that increasing the alcohol chain length from one to two resulted in a small increase in ignition quality and a lower peak heat release rate. With ignition delay removed as a variable the ethyl ester produced lower emissions of NO_x but an increased total mass of particulates compared to the methyl ester. It was suggested that atomization of the ethyl ester suffered due to an elevated melting point relative to the methyl ester, and this contributed to the increase in the total mass of particulates. The lower oxygen content of the ethyl ester and soot formation pathways specific to the ethyl alcohol moiety were also mooted as possible causes of the increase.

Zhang et al. investigated, in two studies (2010; 2009), the influence of fatty acid ester molecular structure on ignition kinetics in a motored CFR engine at very low loads with constant equivalence ratio. Firstly the influence on double bond position within the fatty acid chain length and an increase in alcohol moiety chain length with constant fatty acid carbon chain length was studied by considering four esters with fatty acid chain length of 9 (methyl nonanoate, methyl 2-nonenoate, methyl 3-nonenoate and ethyl nonanoate). Secondly, the effect of alcohol chain length where the overall carbon number of the ester was kept constant was also studied (methyl heptanoate and ethyl hexanoate). The effect of introducing a double bond into the fatty acid chain length was found to greatly reduce the onset and magnitude of

the low temperature heat release relative to the fully saturated esters. Moving the double bond towards the centre of the fatty acid chain length further delayed the onset of the low temperature heat release rate and decreased its magnitude. The movement of the double bond towards the centre of fatty acid moiety was suggested to be an increasingly inhibiting influence due to the limitations that the position of the double bond placed on the formation of six and seven membered transition rings. Such transition rings are necessary for the isomerisation of alkyl peroxy radicals to peroxy alkyl structures, which is a key stage in the branching reactions that produce radicals necessary for autoignition (Westbrook, 2000; Zhang et al., 2009).

Zhang and Boehman (2010) found that increasing the alcohol chain length while keeping the fatty acid chain length constant (methyl nonanoate to ethyl nonanoate) increased the low temperature reactivity of the ester. This was attributed to a combination of an increase in the number of easily abstracted secondary C-H bonds when increasing the alcohol chain length, and the suggested potential of ethyl esters to undergo a six centred uni-molecular elimination reaction, which has relatively low activation energy. The proposed six centred uni-molecular elimination reaction of ethyl esters sees their pyrolysis, via an intermediate cyclic structure, without the need for any radical addition or external hydrogen abstraction. When the total number of carbon atoms in the ester was held constant and the alcohol chain length increased (methyl heptanoate to ethyl hexanoate) low temperate heat release magnitude reduced and onset commenced later. This highlights the importance of the fatty acid chain length relative to the alcohol moiety chain length, and it can be seen that increasing the alcohol chain length from one to two (which was seen increase low temperature reactivity when fatty acid chain length was held constant at 9) does not compensate for a decrease in the fatty acid chain length from seven to six.

In addition, Zhang and Boehman (2010) compared the heat release of methyl heptonate to that of *n*-heptane at identical conditions. *N*-heptane exhibited greater low temperature reactivity, which, given that both *n*-heptane and methyl heptonate possess alkyl chains of identical length, suggests that the presence of the ester suppress the low temperature reaction kinetics of the alkyl chain. This is attributed to a reduction in the ease with which internal hydrogen transfers can take place when the ester moiety is present; internal hydrogen transfer and isomerisation are important stages of low temperature chain branching reactions of alkyl chains, as discussed in Section 2.3. Furthermore, the potential of easy internal hydrogen transfer is fur-

ther reduced when increasing the carbon chain length of the alcohol moiety with a constant total carbon number, as is the case with ethyl hexanoate compared to methyl heptanoate. In both studies, to better understand the low temperature reaction pathways of the various molecules, exhaust sampling and gas chromatography identification of the species therein conducted. From the intermediates observed it was concluded that esters with fully saturated fatty acid components followed very similar reaction pathways to *n*-alkanes, while those containing a double bond in the fatty acid component appeared to be reacting along the same routes as olefins under similar conditions.

Kinoshita (2011) investigated the physical properties of palm oil fatty acid esters prepared with alcohols ranging from methanol to octanol. Pour points of methyl, ethyl, propyl and butyl esters were found to decrease with increasing alcohol moiety carbon chain length. When the alcohol moiety carbon number exceeded four, pour points were found to increase with an increase in the length of the alcohol moiety. Methyl, ethyl, *n*-propyl and *n*-butyl palm oil esters were also combusted in a single cylinder diesel engine with combustion and emissions characterized. No differences in either ignition delay or heat release were detected between the fuels, but the propyl and butyl esters did show elevated THC, CO and smoke emissions relative to the shorter alcohol chain esters. Kinoshita (2011) suggested this to be an effect of the lower oxygen content but higher kinematic viscosity and boiling point of the longer alcohol moiety esters, with all three properties impeding fuel and air mixing.

The use of branched alcohols in the production of fatty acid esters has received very little attention. Knothe et al. (2003) expanded their study of cetane numbers of fatty acid esters to include the effect of branching in the alcohol component of an ester. The authors predicted that, as with alkanes, branching of the carbon chain would reduce cetane number. However, results from the IQT measurements of ignition delay showed this not to be the case, with cetane numbers either increasing or remaining constant when introducing branching to the alcohol component and maintaining a constant number of carbon atoms. Kinoshita (2011) included an ester produced from iso-butanol in their study of palm oil esters with varying alcohol moiety. They found the peak heat release rate of the *iso*-butyl ester to be slightly higher than that of the esters with straight alcohol moieties and attributed this to a slightly longer ignition delay of the *iso*-butyl ester (0.1 CAD). Emissions of THC and

CO were similar to those of the *n*-propyl and *n*-butyl esters, with smoke emissions closest to those of the *n*-butyl ester.

2.5.3. Carbonate esters

The use of carbonates to displaces fossil fuels was originally investigated in the context of spark ignition combustion (Pacheco and Marshall, 1997), however, the potential for reduction of soot emissions via the use of oxygenated fuels led to the study of carbonates as an additive to fossil diesel (Arteconi et al., 2011). Zhang et al. (2005) investigated the heat release and emissions of blends of DMC with a fossil diesel, up to a maximum carbonate content of 15 % (vol/vol). Examination of the heat release traces revealed that addition of DMC to fossil diesel increasingly resulted in a longer ignition delay relative to the fossil diesel, and that the rate of combustion increased and the overall duration of combustion decreased. Reduced emissions of particulate matter with the presence of DMC were observed and attributed to the introduction of oxygen to the centre of the fuel rich spray, a reduction in the level of aromatics present in the fuel blend and the low carbon to hydrogen (C/H) ratio of DMC.

Cheung et al. (2011) also investigated the effect of blending DMC with fossil diesel in varying proportions, up to 18.6 % (vol/vol), on the levels of both gaseous and particulate emissions from a direct injection compression ignition engine. In addition to the longer ignition delay and shorter duration of combustion with increasing DMC content observed by Zhang et al. (2005), it was also observed that the extent of the premixed combustion phase increased, as did the brake specific fuel consumption (BSFC) and emissions of CO (Cheung et al., 2011). The increased BSFC was attributed to the lower calorific value of DMC relative to fossil diesel. The high latent heat of evaporation of DMC and the subsequent localized cooling this could induce, was identified as the cause of increased CO emissions via a greater degree of incomplete combustion. A decrease in the emission of particulate matter with increasing DMC content was again observed, and this was ascribed to the absence of carbon to carbon bonds within DMC, better atomization of DMC relative to fossil diesel and the greater extent of the premixed burn fraction. The improved atomization of DMC relative to fossil diesel has been observed in spray imaging (Wu et al., 2006; Xiaolu et al., 2006), with DMC found to possess a smaller droplet size which was attributed to the lower viscosity of the carbonate.

The functional group of carbonate esters differs from that of fatty acid esters only by the presence of a single oxygen; however, while esters have seen much study and are now mandatorily blended with fossil diesel, carbonates have received little attention as single component fuels. The investigation of DMC as a single component compression ignition engine fuel was conducted by Xiaolu et al. (2006) in a single cylinder two stroke engine with internal exhaust gas recirculation. Prior to injection of the carbonate, a pilot injection of fossil diesel was employed to raise in-cylinder temperatures and 1 % castor oil was added to the DMC to improve lubricity. Following the pilot injection of fossil diesel, combustion of the DMC was short and mostly premixed. Emissions of particulate matter appeared close to zero. However, relative to combustion of fossil diesel under the same conditions, emissions of un-burnt hydrocarbons increased and were attributed to the high latent heat of vaporization of DMC.

Combustion testing of carbonates, formed from longer alkyl chain alcohols, has to date been limited, although blending of di-ethyl (DEC) carbonate with fossil diesel has received some attention in the context of achieving reductions in soot emissions, similar to those reported in the use of DMC (Cheung et al., 2011; Zhang et al., 2005). Ren et al. (2007) measured the physical properties of both DEC and DMC blends with a fossil diesel. The density of the blends was found to increase with increasing carbonate content, while the viscosity decreased; the change in both properties for a given carbonate content was consistently greater in the case of DMC than DEC. In a later study, Ren et al. (2008) investigated the combustion and emissions characteristics of binary mixtures of DEC and DMC with fossil diesel in a direct injection compression ignition engine. The results of the tests were considered with regards to fuel blend oxygen content, and thus the performance of DEC relative to DMC is not readily apparent. An increase in ignition delay with oxygen content was observed regardless of the carbonate present. The duration of combustion and the emission of particulate matter were both observed to decrease with oxygen content, as did emissions of CO and THC under the conditions of the tests, these trends were attributed to oxygen enrichment of fuel rich areas. Bruno et al. (2009) investigated the distillation curves of fossil diesel blends containing between 10 to 30 % of either DMC or DEC. It was found that introduction of either carbonate resulted in a decrease in the initial boiling point of the blend, with the largest decrease observed in the case of those blends containing DMC.

2.5.4. Ethers

By far the most commonly considered ether for combustion in compression ignition engines is the simplest, di-methyl ether (DME) . In reviewing the use of DME as a fuel in diesel engines, Arcoumanis et al. (2008) highlights clearly the general advantages and disadvantages of DME. From a physical handling perspective DME is non-toxic but does have a very low boiling point ($\approx$ 25 °C) and thus requires special storage measures. This extremely low boiling point and the low carbon to hydrogen ratio of the molecule drastically reduces soot production in comparison to fossil diesel fuel. In addition to the low temperature oxidation and isomerisation observed in other hydrocarbons (Section 2.3), low temperature branching in ethers can also be achieved by pyrolysis of the ether, i.e.

$$CH_3OCH_3 \rightarrow CH_3O + CH_3 \tag{2.19}$$

Breaking of the C-O bond is easier than the abstraction of hydrogen atoms and thus ignition delays are shorter, and measurements of DME cetane number are generally somewhat higher than that for fossil diesel, at 78 for DME relative to $\approx$ 50 for a typical fossil diesel (Murphy et al., 2004). This shorter ignition delay results in a lower premixed fraction and therefore lower temperature and lower production of thermal NO_x. Near zero production of soot arises from the low carbon to hydrogen ratio and oxygen content of the molecule, reducing initial soot formation and increasing subsequent soot oxidation. Disadvantages of ethers in general arise from the molecules physical properties; lower calorific values require longer injection durations, low viscosity increases mechanical wear and a low modulus of elasticity means than more pumping work is required and injector needle lift is slower.

Numerical models have found DME to possess a shorter ignition delay than *n*-heptane in simulated direct injection engine studies (Hoffman and Abraham, 2009). Yu et al. (2009) validated such a simulation against engine experiments, with a fossil diesel fuel substituted for *n*-heptane, and found good agreement between the two approaches. The simulation was performed assuming a constant mass of fuel injected for a given injection duration, and so, as could be expected given the lower calorific value of DME relative to *n*-heptane, DME exhibited a lower peak pressure and temperature. More interesting are the observations regarding the mixing of

DME on injection into the cylinder. Comparative to *n*-heptane the much lower boiling point resulted in much quicker fuel evaporation and also a much shorter spray penetration. This results in a very narrow region of high temperatures near the injector, with the presence of oxygen in the fuel molecule dictating that this region is on the fuel side of the mixture interface. In the fuel region, also relative to *n*-heptane, DME generates a much higher hydrogen distribution which reduces soot formation and coupled with later soot oxidation results in the near zero levels of soot production.

Considering ethers other than DME, Schönborn et al. (2009a) compared di-ethyl ether (DEE) and di-isopropyl ether (DIPE) to DME when using a homogenous charge compression ignition (HCCI) strategy, while also comparing DME to fossil diesel in direct injection diffusion combustion. In direct injection experiments, the injection duration was adjusted so that the engine produced a constant power output from each fuel (which due to the much lower calorific value of DME resulted in a 50 % longer injection duration relative to the fossil diesel fuel) and while DME exhibited a shorter ignition delay and a greater proportion of mixing controlled combustion it also exhibited a higher peak pressure in the initial premixed stage of combustion. This was tentatively explained by the probable higher rate of fuel and air mixing for DME following injection, and the oxygen content of the DME resulting in far fewer intermediate species of incomplete combustion, which in the case of the fossil diesel fuel possibly burnt in the diffusion burn out phase very near the end of combustion.

Emissions of nitrogen oxides for DME were observed by Schönborn et al. (2009a) to be higher than those from the fossil diesel fuel and attributed to the higher peak temperatures reached with DME; adiabatic flame temperatures were calculated but found to be lower for DME. Other studies have, with the use of high EGR rates, produced ultralow NO_x emissions when direct injecting DME (Song et al., 2009). Schönborn et al. (2009a) found that DME produced much lower soot levels than the fossil diesel fuel and suggested that the presence of soot in the combustion gases of the fossil diesel fuel resulted in radiative heat transfer and contributed to the lower levels of NO_x found relative to DME. Near zero levels of NO_x were found when combusting DME in a HCCI regime, but with higher levels of particulates than when running the engine in direct injection diffusion controlled mode. The molecular structures of the three ethers tested under HCCI conditions was found to have a significant impact on ignition delay, increasing the length of the alkyl chains

from DME to DEE was found to reduce ignition delay, while introducing methyl branches to the alkyl chains, DME to DIPE, severely reduced the ignition quality and increased the duration of ignition delay. Furthermore, Schönborn et al. (2009a) found by injecting binary mixtures of two of the ethers it was possible, by altering the proportion of each component present, to control the start of combustion.

2.5.5. Alcohols

Due to their low cetane number (Murphy et al., 2004), short chained alcohols such as ethanol, propanol, iso-propanol and butanol have not been considered as single component fuels for compression ignition engines. However, they have been in utilised in engine studies as blends with either fossil diesel fuel or biodiesel (Lapuerta et al., 2009; Sayin, 2010), and considered as single component fuels in the context of understanding low temperature kinetics. While reporting measurements of ignition delay for *n*-butanol in shock tubes, Black et al. (2010) also model the chemical kinetics of low temperature combustion. They find that when considering *n*-butanol the weakest bond is the C-C bond adjacent to the OH group and that low temperature pyrolysis reactions are likely to occur. Such pyrolysis reactions often result in complex fission, the molecule splits and the alkyl chain can form an alkene. This may help explain the lower cetane number observed for alcohols relative equivalent *n*-alkanes (Murphy et al., 2004).

By comparison of *n*-butanol to *n*-ethanol, Black et al. (2010) also find that bond strengths of carbon to hydrogen atoms at the carbon atom adjacent to the OH group, and the bond between this carbon atom and OH group, are independent of the straight carbon chain length of the alcohol. This may be of significance when considering the ignition quality of differing carbon chain length alcohols. Kinetic modelling of the combustion of *n*-propanol and *iso*-propanol (Frassoldati et al., 2010) shows the lower reactivity of *iso*-propanol at low temperature conditions to be due to the dominance of molecular dehydration reactions for this molecule. Thus, at these conditions iso-propanol is reduced and produce H_2O, while in *n*-propanol radical producing pathways dominate.

2.5.6. Aromatics

Aromatic hydrocarbons make up a significant fraction of fossil fuels, and most commonly studied in the context of combustion is toluene. Such investigations have,

in general, focused on identifying the autoignition properties of binary mixtures of toluene with an alkane (such as *n*-heptane) so as to further understanding of fuel effects on the phenomena of knock in SI engines and the rate of combustion in HCCI engines. One such means of doing so has been the rapid pressurisation of fuel and air mixtures in high pressure shock tubes. Herzler et al. (2007) studied the ignition delay times of a mixture comprising 65 % toluene and 35 % *n*-heptane (by volume) at compression pressures of 10, 30 and 50 bar. While increasing the pressure consistently reduced ignition delay times, the effect of doing so became less important at higher pressures. For example, increasing the pressure from 10 to 30 bar resulted in a larger decrease in ignition delay than the same magnitude of pressure increase from 30 to 50 bar. Comparison of the data for the 65 % toluene blend to that of pure *n*-heptane from a previous study (Ciezki and Adomeit, 1993) showed reduced negative temperature coefficient (NTC) reactivity for the toluene containing mixture. Hartmann et al. (2011) investigated the behaviour of toluene and *n*-heptane blends containing up to 40 % (volume) toluene in a high pressure shock tube at 40 bar and a temperature range of 700 - 1200 K. Above 20 % toluene, further addition of toluene retarded the point of ignition and reduced the NTC region. Kinetic modelling suggested that the inhibiting effect of toluene on ignition of the mixtures to be highly temperature dependent and of greatest influence at 850 K for the conditions studied.

In studying HCCI in a rapid compression machine (RCM) with a peak compression ratio pressure of 4 bar, Tanaka et al. (2003) observed the significantly longer ignition delay of a fully premixed blend comprising 74 % toluene and 26 % *n*-heptane compared to that of pure *n*-heptane. Andrae et al. (2005) considered the autoignition of two toluene and *n*-heptane blends in a HCCI engine, both experimentally and through simulation. In engine tests, the blend containing a higher proportion of toluene exhibited longer ignition delays and initially the numerical simulation only accurately predicted these results when co-oxidation of the reactants was included. In addition to reactions involving the shared pool of radicals created by the oxidation of toluene and *n*-heptane, it was suggested that reactions between the resulting benzyl and heptyl radicals were also important. However, a later refinement of the model (Andrae et al., 2007), utilising more accurate rate constants for the experimental conditions studied, found such reactions to be of less significance than originally considered.

In a more recent RCM study, Di Sante (2012) investigated the ignition delay times of a range of toluene and *n*-heptane mixtures in differing proportions and final compression temperatures. It was found that increasing the percentage of toluene present in the blend increased both the 1st and 2nd stage ignition delay times, though the influence of toluene addition diminished with increasing temperature.

Vanhove et al. (2006) conducted a series of RCM experiments with a range of binary mixtures, including a 1/1 (% mols) toluene and *n*-heptane blend, at a range of temperatures between 650 - 900 K and a compression pressure of 3 - 5 bar. Analysis of the reaction mixtures during the ignition delay period revealed that in addition to *n*-heptane, toluene also underwent oxidation prior to autoignition. A similar mixture of benzene and *n*-heptane produced a similar profile of ignition delay with temperature, but sampling of the reaction mixture revealed that benzene had not reacted, suggesting that the inhibiting effect of toluene may not be chemical. Further mixtures of iso-octane and toluene did show a decrease in reactivity relative to pure iso-octane that was attributable to competition for radicals between the fuel components. This was attributed to the lesser reactivity of iso-octane relative to *n*-heptane, thus placing greater demand on the available radicals.

Xiao et al. (2000) investigated the combustion and emissions production of binary mixtures of *n*-heptane and up to 20 % (wt/wt) toluene in a Cooperative Fuel Research (CFR) indirect injection compression ignition engine. Increasing the percentage of toluene present in the blends increased the duration of ignition delay and also the levels of NO_x, THC and smoke emitted. An ignition improver (2 EHN) was subsequently added to the blend containing 20 % toluene in increasing quantities until the blend displayed the same duration of ignition delay as pure *n*-heptane. With the effect of ignition delay removed, the presence of toluene did not see a significant increase in NO_x or THC levels, though an increase in smoke emissions remained. It was concluded that while the increase in NO_x and THC emissions with increasing toluene content could be attributed to the change in combustion phasing with increasing ignition delay, the increase in smoke emissions was independent of ignition delay and likely the result of the increasing blend aromatic ring content.

2.6. Conclusions

Considering the potential sources of future fuels, the following conclusions can be drawn:

- Methods of fatty acid transesterification, such as acid catalysation or the use of supercritical reactions conditions, are under development that will extend the range of both fatty acid and alcohol feedstocks that can be utilised. Use of waste oils with high free fatty acid content and oils produced by micro-organisms, or longer chained alcohols than methanol, may render the future production fatty acid ester fuels more sustainable than the current reliance on base catalysation and methanol.

- Chemical and physical methods of converting biomass to liquid fuels can produce a wide range of potential fuel molecules. Such methods are, however, energy intensive and highly sensitive to the properties of the feedstock utilised.

- The direct conversion of biomass by micro-organisms has a long history of use in an industrial context, though with limitations on both feedstock and the range of molecules produced. However, in recent years methods of genetic engineering have been developed to boost the production of select hydrocarbon species and reduce the energy cost of subsequent harvesting.

The following points can be made to summarise the current understanding of the processes of compression ignition combustion and emissions formation:

- Direct injection compression ignition combustion can be characterised as the overlapping sequential occurrence of the following events: fuel jet formation and vaporisation, multiple site autoignition, combustion of fuel and air mixed prior to autoignition, and diffusion rate controlled combustion of remaining fuel.

- During the ignition delay period, fuel breakdown follows routes of low temperature reaction kinetics and concurrent temperature escalation towards autoignition is dependent of the the branching of radical species. Factors affecting the rate of branching reactions are the ease with which H atoms may be abstracted from the molecules and the potential of the remainder fuel molecule to undergo internal isomerisation.

- Formation of NO_x during compression ignition combustion is dominated by the thermal oxidation of atmospheric N_2. Rates of NO_x formation are temperature

dependent and increase with both increasing in-cylinder temperatures and increasing duration of gases at such conditions.

- Soot production in compression ignition combustion commences with fuel breakdown and the formation of nuclei to which subsequent radical addition occurs, followed by coagulation and agglomeration which increase particle size. Subsequent soot oxidation, rates of which increase with temperature, reduce levels of soot in exhaust gases.

Regarding previous studies that have considered the impact of the fuel molecular structure, the following may be concluded:

- Reducing alkyl chain length and the introduction of branching, by definition of cetane number, reduces the ignition quality of fuels for compression ignition engines. Increasing the degree of unsaturation in alkyl chains also reduce ignition quality, as does movement of double bonds to the centre of an alkyl chain.

- The reactivity of fatty acid esters is dominated by the fatty acid alkyl moiety. Levels of NO_x emitted by fatty acids are determined by the ignition quality of the ester (and subsequent impacts on combustion phasing), effects of fuel bound oxygen are stoichiometry and adiabatic flame temperatures.

- Other short chain alkyl chain oxygenates, such as carbonate esters and ethers, have been observed to significantly reduce exhaust soot levels. The nature of the oxygen bearing functional group is important in determining the ignition quality of such molecules.

- Aromatic molecules, such as toluene, have been observed to inhibit the low temperature reactivity of alkanes when present in fuel mixtures.

Therefore, it can be seen that the molecular structure of fuels has a significant impact on the efficiency of energy release and the formation of emissions during compression ignition combustion. Furthermore, new processes for the production of liquid fuels from sustainable sources will possess a variety of distinct molecular structures. There is, therefore, a need to increase understanding of the impact of fuel molecular structure on end-use so as to better select and guide the production of alternative fuels and expand the range of feedstocks that may be utilised.

The experimental studies presented in this work aim to achieve this through the combustion and emissions assessment of single and multi-component fuels of known molecular composition.

3. Experimental methodology

The present chapter describes the experimental apparatus utilised in the engine combustion studies. At the commencement of the project the engine facility was already in existence and a detailed description of all the apparatus present at that time can be found in the PhD thesis of Alessandro Schönborn (2009). However, numerous improvements and additions were made to the facility in order to conduct the experiments described herein (with continual maintenance of the engine and analysers also required) and such developments were a substantial component of this project. Most important was design, manufacture and debugging of a new fuel system for direct injection of very low volumes of a fuel (100 ml) at pressures up to 1600 bar.

3.1. Laboratory

All engine experiments presented in this work were conducted in the Thermodynamics Laboratory within the Department of Mechanical Engineering at University College London. The laboratory utilised was specifically designed for engine-dyno test bed experimentation and consisted of three areas: an engine test cell, an engine control room and a service corridor.

Figure 3.1 shows the laboratory layout (Schönborn, 2009). The engine test cell temperature was maintained with a wall-mounted air heater and both forced and natural ventilation. Control of the engine and data acquisition systems was conducted from the engine control room, with an armoured glass window between the control room and test cell allowing continual observation of the experiments. The adjacent service corridor housed the exhaust gas analysers and included a ventilated cupboard for storage of pressurised gas bottles.

3.2. Engine

Installed within the engine test cell for the duration of the project was a custom built 4 - stroke direct injection single cylinder compression ignition engine. This consisted of components taken from a production 2.0 litre 4 cylinder-turbo charged automotive diesel engine (Ford Duratorq 2.0 CD132 130PS) mounted onto a single cylinder crank case (Ricardo Hydra). The production cylinder head, injector, piston,

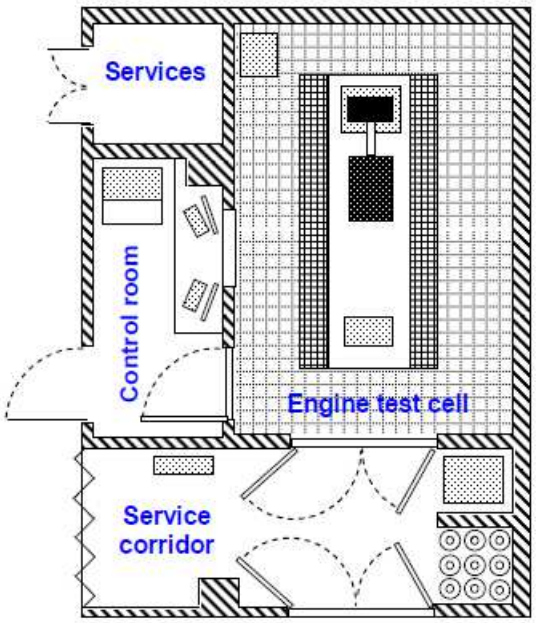

Figure 3.1: Laboratory layout (Schönborn, 2009)

connecting rod and cylinder liner were retained to preserve realistic combustion geometry. The engine geometry was measured and the geometric compression ratio determined as 15.8:1. In place of the glow-plug normally fitted in the production engine head, an adaptor of identical dimensions was fitted and housed a piezoelectric pressure transducer. Motoring of the engine at a constant speed up to a maximum of 5000 rpm was performed by a David McClure dynamometer to which the engine was coupled directly. The dynamometer was driven by a thyristor power unit and controlled by a Cussons test-bed console. Table 3.1 gives details of the engine geometry, while Figure 3.2 shows the engine test bed and dynamometer installation.

The engine was normally aspirated; the engine intake air was inducted from the test cell atmosphere, passing through a filter, a positive displacement air flow meter (Romet G40) and a plenum chamber. From the chamber, air in passed via flexible hosing of diameter 52 mm to an inline air heater (Secomak 571) and then into the intake manifold. The 2 kW heater was held at constant temperature by a proportional integral derivative (PID) temperature controller (CAL 9900); a maximum intake air temperature of 150 °C was achievable at an engine speed of 1200 rpm. The intake manifold had been adapted to include mounting of a piezoresistive pressure transducer and multiple thermocouples.

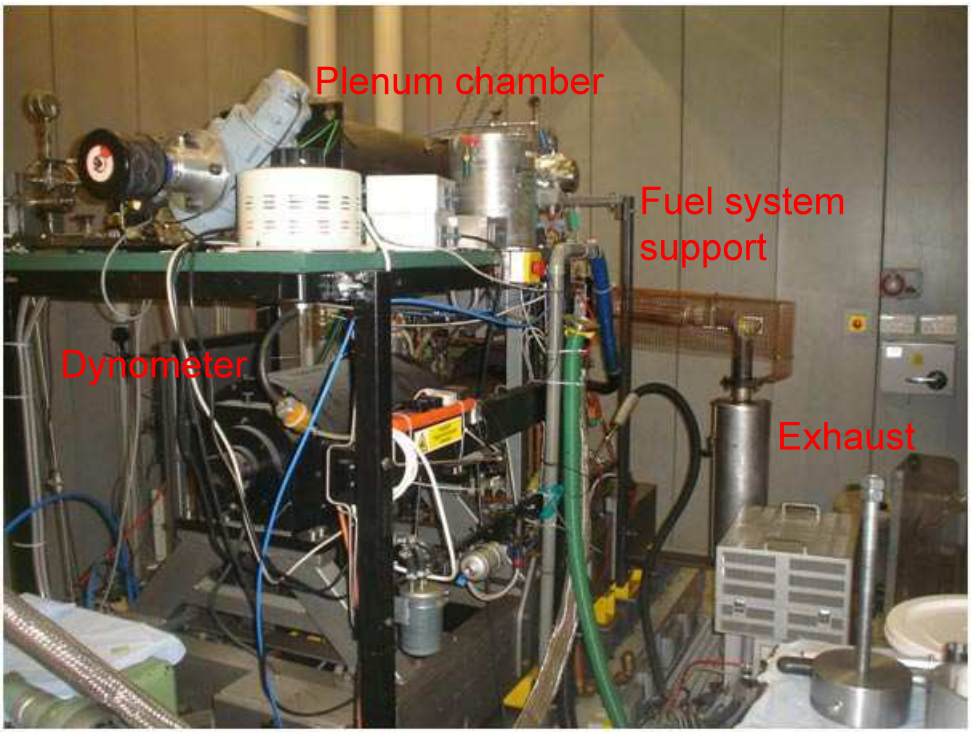

Figure 3.2: Engine test bed

As the air heater was maintained at constant temperature by a PID pulse-width modulator (PWM) controller, the air heating system was characterised to determine whether the PID controller introduced any engine cycle to cycle variation in the air temperature at the inlet manifold. Utilising a bare wire thermocouple and a slower response sheathed thermocouple, it was found that the thermal inertia of the system was great enough to prevent any such influence; the details of this investigation are available in Appendix A.

Exhaust gases from the engine exited via the exhaust port and were conveyed through 53 mm diameter steel tubing to a silencer from which they were evacuated by the laboratory exhaust extraction system. Exhaust gas sampling ports were present 180 mm downstream of the exhaust port with measurement of exhaust pressure and temperature also taking place at this point. Figure 3.3 shows, in the form of a schematic, the gas flows in and out of the engine.

Lubricating engine oil was pumped through the engine head and crankcase at a pressure of 4 bar by an external pump, and was kept at a constant temperature of 80 ± 2.5 °C. Constant oil temperature was maintained by heating with two heating elements within the oil sump and moderating with a closed-loop wax valve system

Table 3.1: Compression ignition engine specification

Engine head model	Ford Duratorq
Engine bottom end model	Ricardo Hydra
Number of cylinders	1
Cylinder bore	86 mm
Crankshaft stroke	86 mm
Swept volume	499.56 cc
Compression ratio	15.8 : 1
Maximum cylinder pressure	150 bar
Peak motoring pressure at test conditions	36 bar
Piston design	Central ω - bowl in piston

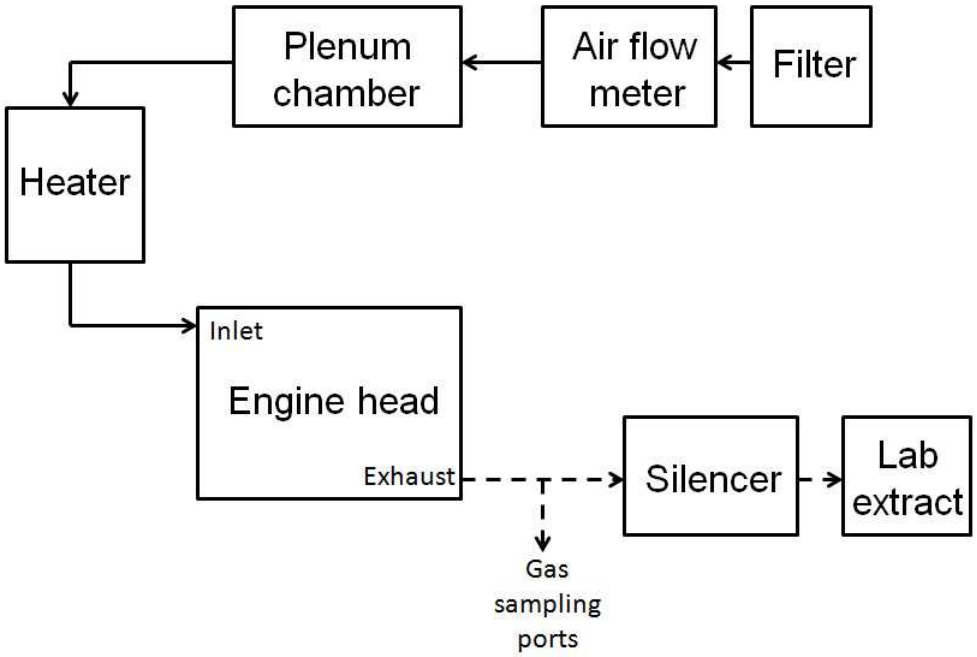

Figure 3.3: Schematic of engine gas flows

which controlled flow of chilled water to a heat exchanger through which the oil passes. A similar system was used to circulate and maintain the temperature of the engine coolant water at 80 ± 2.5 °C; though in this case a single external heater was

utilised and the system was not pressurised. Figure 3.4 shows the arrangement of both the lubricating oil and coolant system.

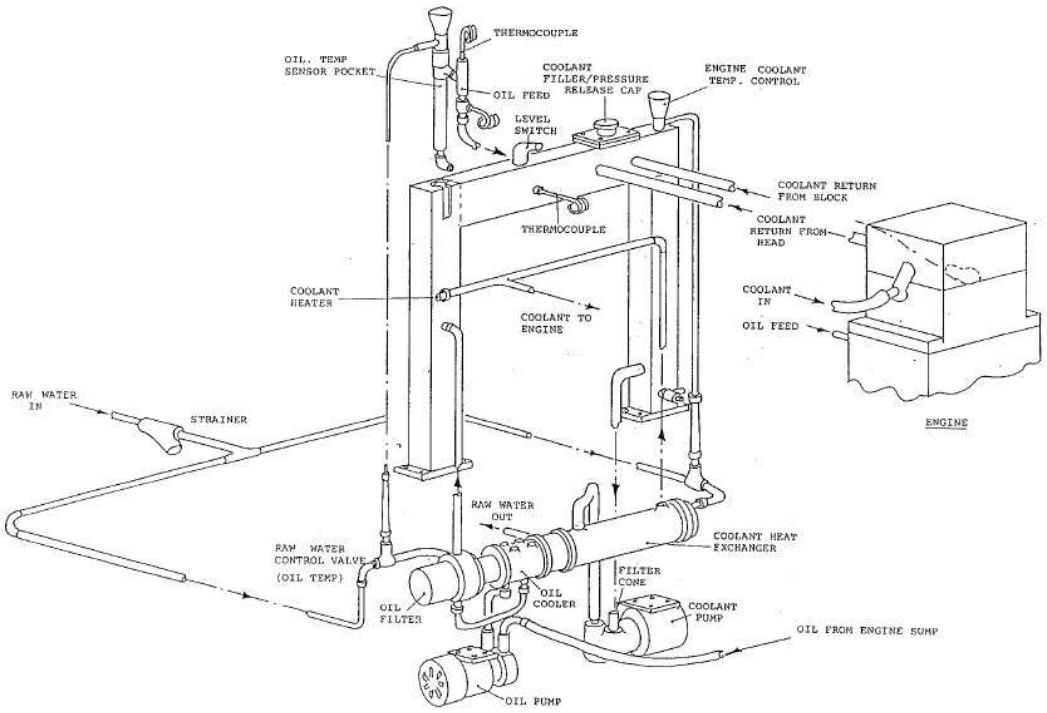

Figure 3.4: Engine test bed lubricating oil and coolant system (Ricardo, 1986)

3.3. Conventional fuel injection

For all direct injection experiments, a servo-hydraulic solenoid valve fuel injector was used (Delphi DFI 1.3), the nozzle of which had six holes, each of 154 μm diameter.

Figure 3.5 highlights the major features of a typical solenoid valve injector. The timing of the fuel injection, the duration of injection and the fuel pressure at the injector were all controlled by a multiprocessor dedicated electronic control system with PC interface (Emtronix EC-GEN-500).

Figure 3.6 shows the Emtronix system as installed in the engine test cell. Signals from two hall effects sensors mounted on the engine flywheel and camshaft were used by the Emtronix system to calculate engine speed and control the injection timing.

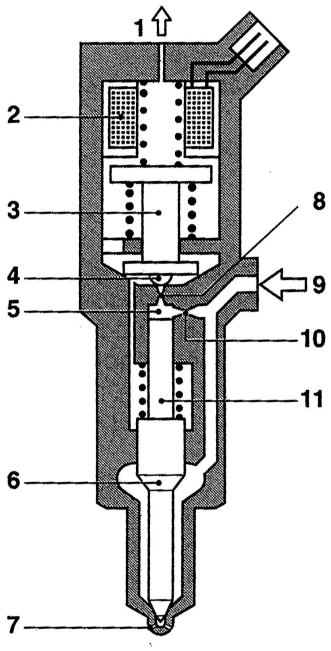

Figure 3.5: Servo-hydraulic solenoid valve fuel injector: 1 Fuel return, 2 Solenoid coil, 3 Solenoid armature, 4 Valve ball, 5 Valve control chamber, 6 Nozzle-needle pressure shoulder, 7 Injector nozzle holes, 8 Outlet restrictor, 9 High pressure port, 10 Inlet restrictor, 11 Valve Plunger (BOSCH, 2004)

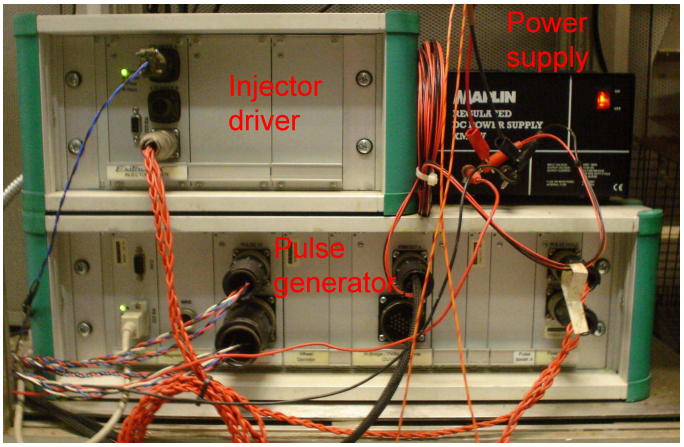

Figure 3.6: Emtronix injection control unit

3.4. Direct injection common rail system

To provide fuel injection at high pressure pressure the engine was equipped with a common rail system similar to those found on many modern compression ignition engines. Figure 3.7 shows a schematic of this system.

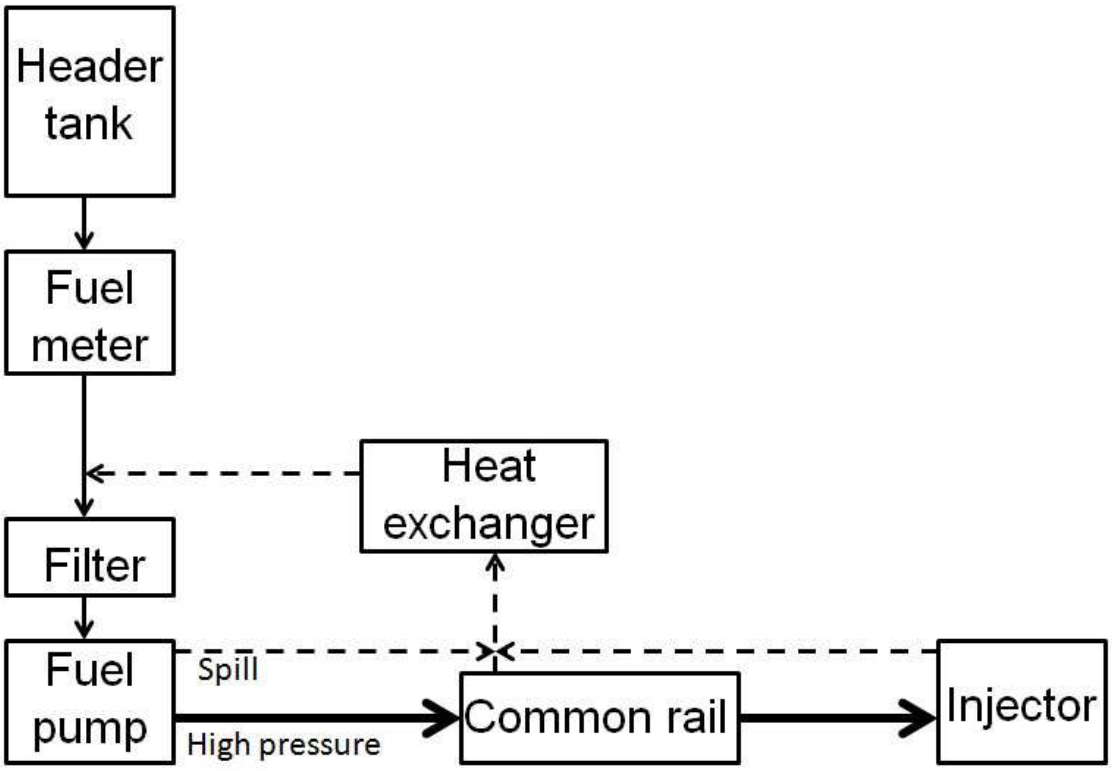

Figure 3.7: Schematic of common rail injection system

A small header tank ($\approx$ 2 l) fed fossil diesel fuel (by gravity) to a crank-shaft driven, self-lubricating fuel pump (Bosch CP3). Between the tank and the pump was an inline fuel filter and a positive displacement fuel meter for determination of fuel flow-rates. Pressure out from the pump was unregulated and fed directly to the common rail (Bosch CRS2) where a solenoid valve was used to set the desired injection pressure by bleeding fuel from the common rail back to the pump inlet. A pressure sensor mounted on the common rail was used in conjunction with a solenoid valve to control the fuel pressure within the common rail. The closed loop system operating this solenoid valve used a control signal sent from the Emtronix unit. The Emtronix unit raised the PWM duty cycle so as to keep the pressure in the common rail at the level set by the user. Low pressure spill fuel from the fuel pump, common rail and injector was cooled by a counter-flow heat exchanger with chilled water as the cooling fluid. Spill fuel was then fed back into the fuel supply circuit downstream of the fuel meter (but upstream of the fuel pump) so that the fuel measured was equivalent to the volume of fuel fed to the injector only.

3.5. Ultra-low volume fuel system

The remit of this project was to investigate how the molecular structure of future renewable fuels impacted on combustion in a compression ignition engine and the subsequent formation of emissions. The methodology generally applied to achieve this aim was to combust a series of structurally near-identical single component fuels in which only the feature of molecular structure which was undergoing investigation was varied. In several cases, the fuels used were not available from a commercial chemical supplier and were obtained from specialist synthesis companies. As a consequence, the cost of the fuel per volume was high. The amount of fuel required to fill the conventional common rail fuel system was several litres, which would therefore have been prohibitively high in terms of cost. Furthermore, many of the fuels tested possessed physical or chemical properties which would have proved highly problematic and detrimental to the functioning of the common rail system; for example, several of the fuels were solid at room temperature, displayed low lubricity or were incompatible with elastomers present in the normal engine fuel circuit. Flushing of the common rail fuel circuit between every combustion experiment would also have been arduous and entailed wastage of large fuel volumes. These issues were first encountered and overcome by Schönborn (2009) whom originated the idea of a special low volume fuel delivery system that could be accurately controlled and utilise a conventional direct injection diesel injector.

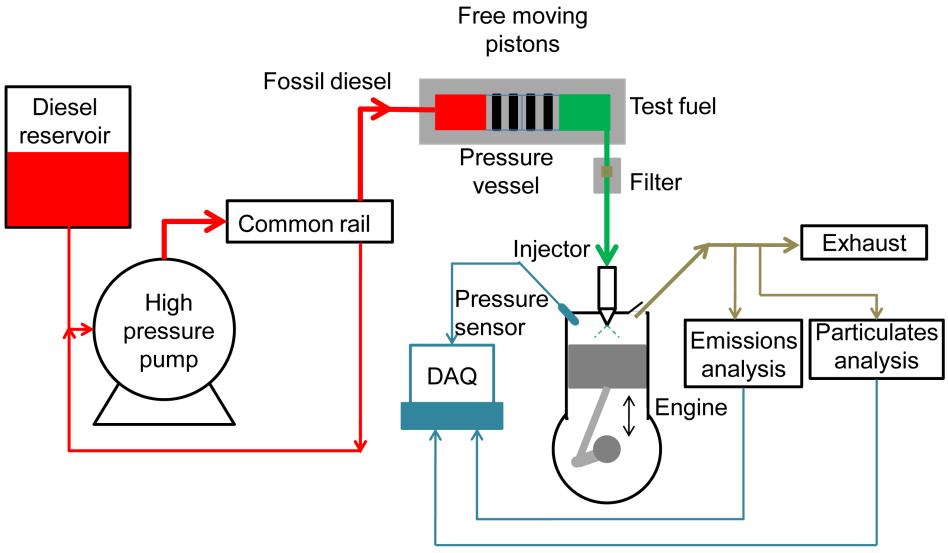

Figure 3.8: Conceptual schematic of the ultra low volume fuel system

The concept proposed and implemented by Schönborn was to utilise fossil diesel fuel as a hydraulic fluid, pressurised by the normal engine common rail system, and then to use this high pressure fossil diesel to generate injection pressure in the test fuel. Figure 3.8 shows the original realisation of this concept which consisted of a stainless steel hydraulic cylinder divided in two by a centrally located free moving piston. One chamber was connected directly to the common rail and thus filled with fossil diesel fuel, while the other chamber was filled with the test fuel ($\approx$ 100 ml) prior to commencing the experiment and fed to the fuel injector. The pressure of the diesel chamber was determined by the common rail pressure and as the piston was entirely free moving, the pressure was also communicated to the test fuel chamber. In this way the test fuel could be injected at the common rail pressures which could be set up to a maximum of 1600 bar. Two o-rings carried by the free moving piston ensured that no mixing of the fossil diesel fuel and the test fuel occurred. Furthermore, between experiments, the system could be easily completely dismantled for cleaning. Using this system the Emtronix control unit could be used to accurately set the injection pressure of the test fuel and also the timing and duration of the injection event.

Figure 3.9: Ultra low volume fuel system Mk I (Schönborn, 2009)

The original design of an ultra low volume fuel system, the components of which are shown in Figure 3.9, provided proof of concept and facilitated a great number of studies. However, during repeated use of the system several issues which limited the effectiveness and efficiency of the design became apparent. Key to the success

of the design was a low level of friction between the free moving piston and cylinder bore so that no pressure drop existed between them. On manufacture, the cylinder bore had been honed to a high quality finish. However, with time, slight skewing of the free piston off the central axis had led to scoring of the cylinder bore resulting in increased friction between the free piston and bore. Figure 3.10 shows the damaged cylinder bore after repeated piston skewing.

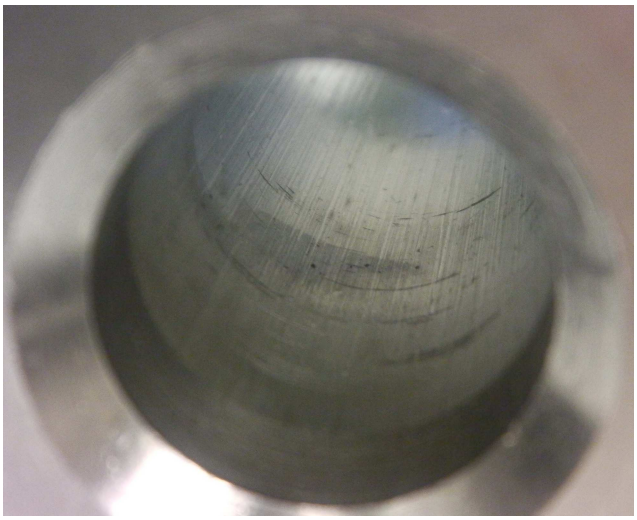

Figure 3.10: Cylinder bore scoring in ultra low volume fuel system Mk I

A new ultra low-volume fuel system was designed and manufactured based on the original concept by Schönborn of utilising a free moving piston within a hydraulic cylinder to transmit pressure from the fossil diesel (as the hydraulic fluid) to the test fuel. Figure 3.11 shows the new design, which addressed not only the issue of the cylinder bore scoring but also added several other improvements which enhanced the usability of the system for the experimenter.

The central innovation of the new design was the simultaneous use of two separate free pistons (each of which was exposed either only to the fossil diesel fuel or test fuel) and the supply of compressed air to within the cylinder to individually manipulate the position of each free piston. Such features were advantageous primarily because they allowed for the piston that was directly in contact with the sample fuel to be ejected from the fuel system for cleaning after each experimental run, while the other piston, that was in contact with only the fossil diesel fuel, would remain in-situ. This meant that only the sample fuel end of the cylinder was dismantled between tests, leaving the fossil diesel fuel piston and circuit intact.

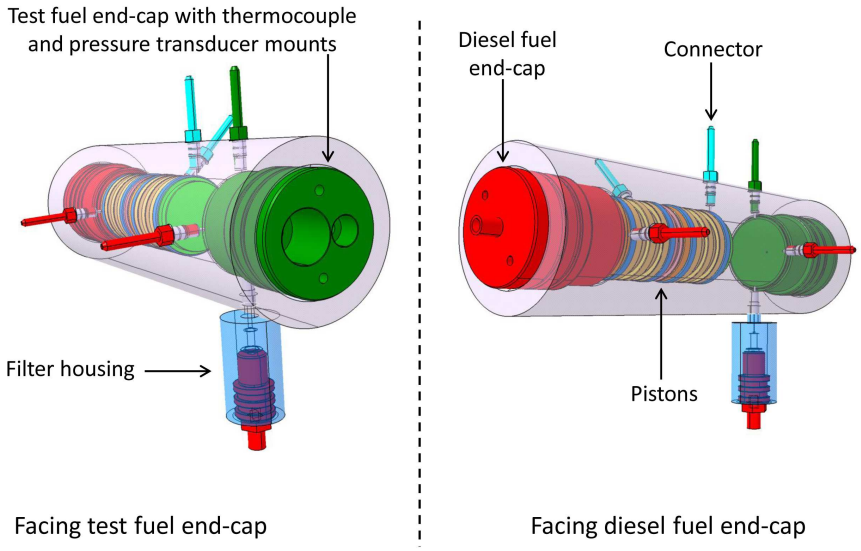

Figure 3.11: CAD design of ultra low volume fuel system Mk II

Figure 3.12 shows the sixteen specially designed and precision manufactured stainless steel components that comprise the fuel system. The main hydraulic cylinder for the fuel system was designed in accordance with British Standard 5500 to withstand the hoop stress generated by a maximum pressure of 2000 bar within the cylinder. Sealing the cylinder at either end were two end caps, each with two radial stretched o-rings around the largest circumference which compressed against an inner bore of the cylinder. Holding the end caps in place against the internal cylinder pressure was an interior depth of thread located between the piston bore and the end cap sealing bore. Two designs of the test fuel side cylinder end cap (end cap A) were used: one blank with no internal features, and a second with an internally fitted thermocouple and piezoresistive pressure transmitter. The thermocouple tip was mounted at a depth of 25 mm from the internal face of end cap A so as to give an indication as to the test fuel temperature with the cylinder. The pressure transmitter communicated with the test fuel chamber via a 1.5 mm diameter hole and sealed with a compressible metal washer.

Figure 3.13 shows the fuel flows in and around the ultra low volume fuel system. Machined into the wall of the fuel system cylinder were six ports for additional flows of fuel and air. Custom connectors sealed into these ports using the same principle as the cylinder end caps, that is, two radial sealing o-rings held in place by a depth of thread. The external end of the connectors was designed to interface directly

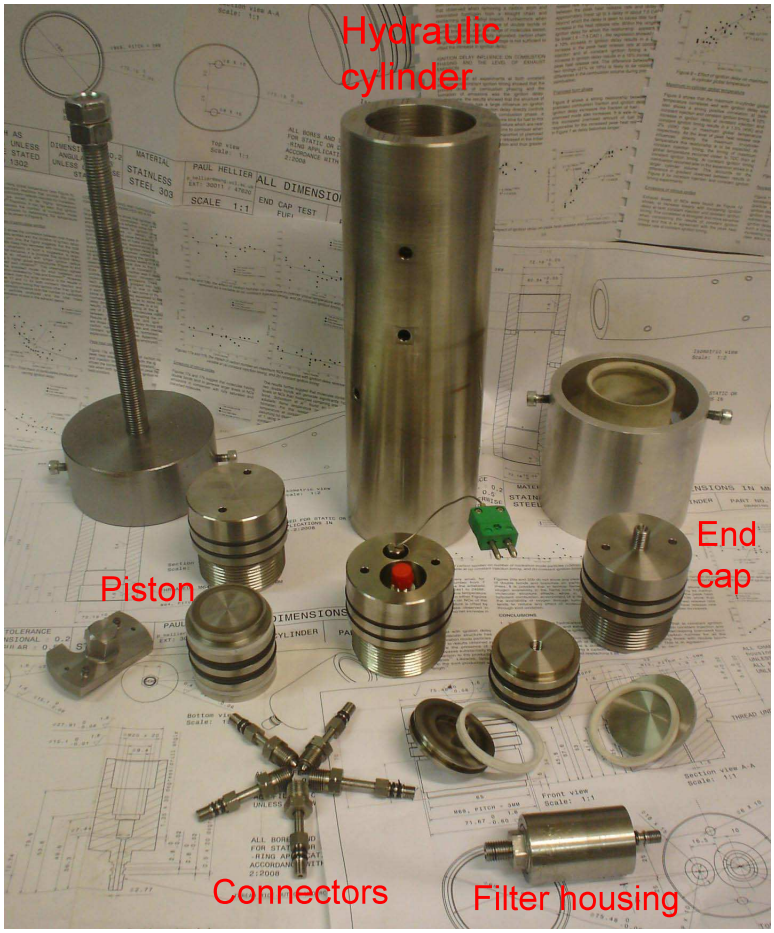

Figure 3.12: Ultra low volume fuel system Mk II components

with high pressure needle valves (Autoclave). A two part filter housing was also manufactured and connected directly into the cylinder test fuel outlet port. The custom filter housing was designed to operate at pressures of up to 2000 bar and it housed a sintered steel filter element (elements of pore size between 1 µm and 50 µm could be purchased). An o-ring stretched over the filter element circumference and, compressed by the filter housing, was used to ensure that all test fuel flow was directed through the filter element. The filter was also sealed against pressure with two radial sealing o-rings and a depth of thread. The filter housing downstream outlet was a high pressure diesel connection (ISO 2974 A 6) which communicated with the fuel injector via a high pressure line and a further high pressure needle valve (8) and "T" junction. The "T" junction allowed for running of the engine on fossil diesel fuel by completely bypassing the ultra low volume fuel system and

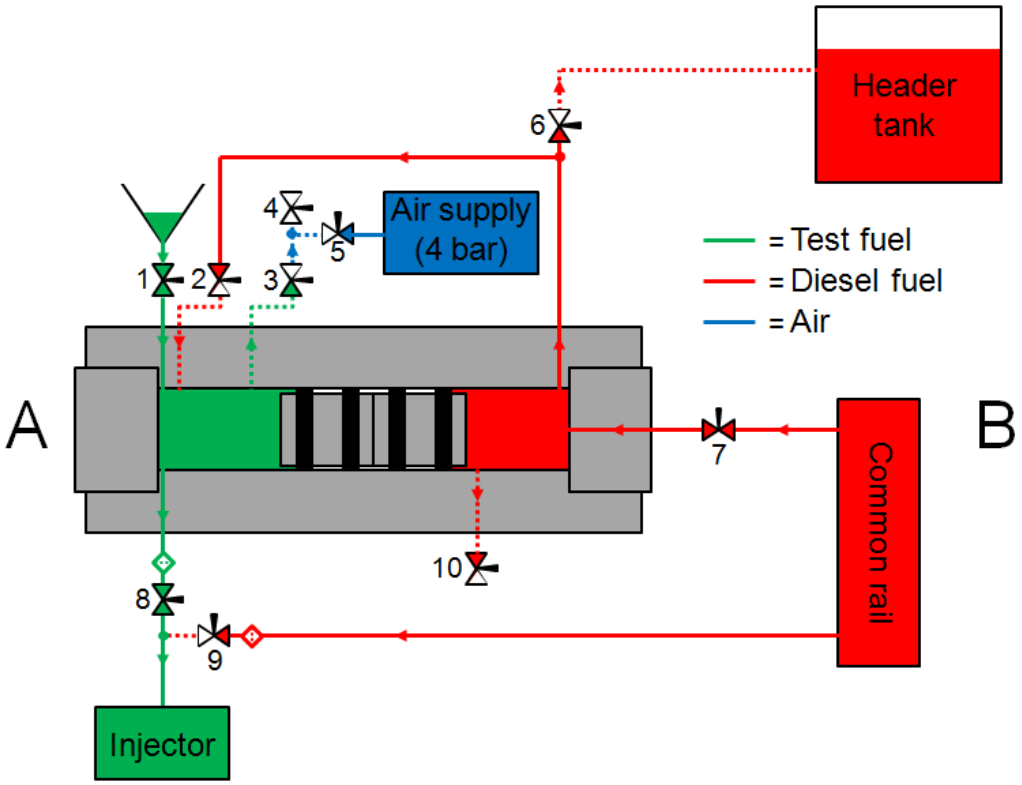

Figure 3.13: Schematic of fuel flow in ultra low volume fuel system Mk II

running fossil diesel fuel direct from the common rail, with a second inline custom high pressure filter housing (identical to the previous description except that both inlet and outlet were fitted with high pressure diesel connections) and a high pressure needle valve (9) to control the flow.

To facilitate the combustion of fuels which were normally solid at room temperature, the outer circumference of the hydraulic cylinder was fitted with three band heaters of 1.55 kW total power. In addition, one further band heater was fitted to the test fuel filter housing, two tape heaters to the high pressure fuel lines and control valves communicating the test fuel to the fuel injector and one tape heater on the fuel line carrying spill from the injector. A three way low pressure valve was in line with the injector spill outlet so that when running with fossil diesel fuel, the spill volume could be directed back to the fuel supply circuit. In the case of the test fuels the spill volume was diverted to a measuring cylinder. The heaters were maintained at a constant temperature by five individual PID controllers so as to ensure that the fuel components were at as uniform a temperature as possible. Figure 3.14 shows the location of the five different thermal controls zones.

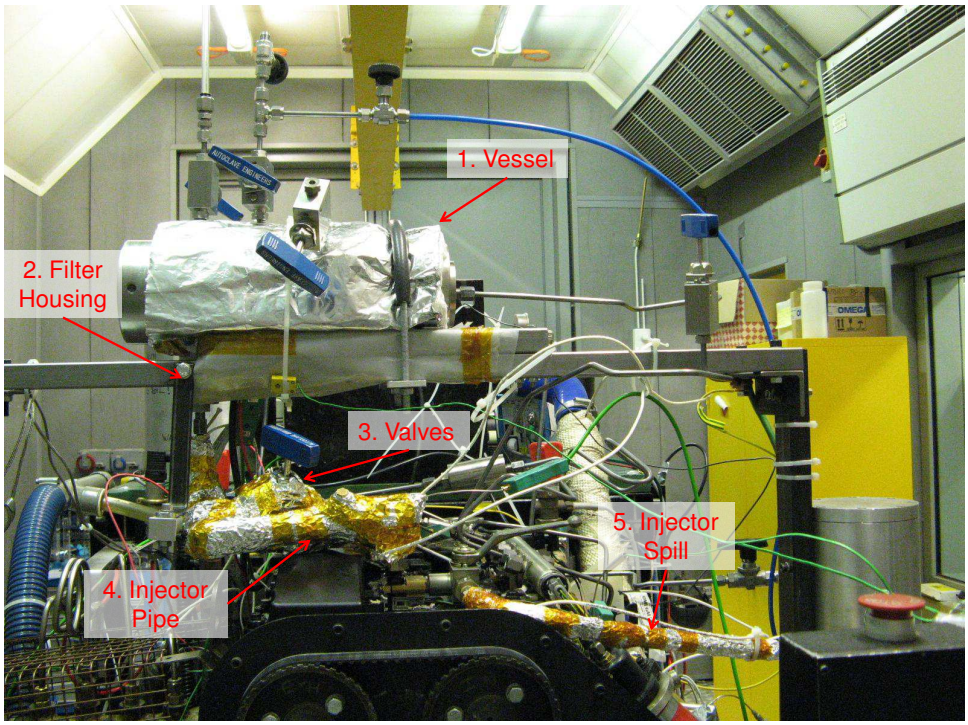

Figure 3.14: Fuel system heating zones

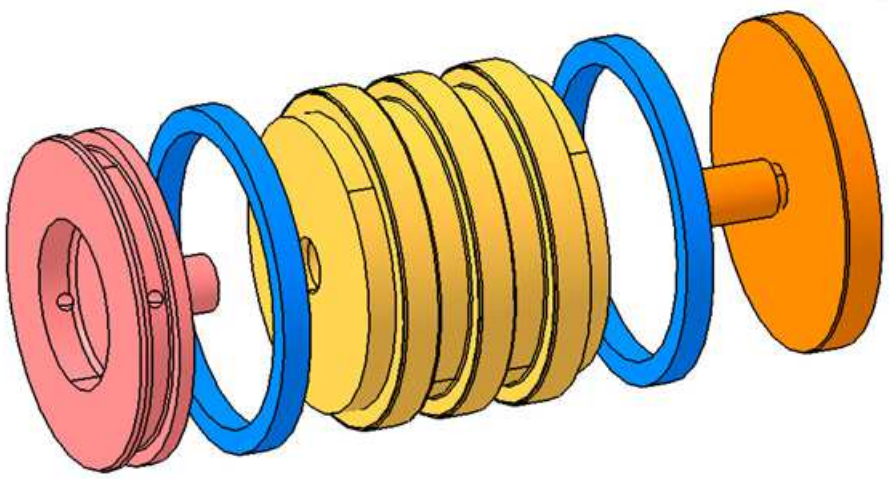

Figure 3.15: CAD design of fuel system piston (diesel fuel side); the blue bands are PTFE spacers

To prevent the occurrence of scoring to the cylinder bore via skewing of the pistons, the improved fuel system was designed with a much smaller clearance between the pistons and cylinder bore than the system of Schönborn (2009). Figure 3.15 shows the design of the two pistons, each of which actually comprised of three individual

components: a body with housing grooves for two dynamic o-rings and two bespoke end caps with threaded studs for insertion at either end of the piston body. This allowed for insertion of a PTFE guide ring at either end of each piston (between the end cap and body, shown in a blue colour in Figure 3.15) designed for an interference fit with the cylinder bore and thus further inhibit any skewing motion by the pistons. A bespoke design of the piston end caps was necessary to facilitate two important functions of the fuel system: flushing of the sample fuel circuit and injector with fossil diesel fuel at the end of every experiment (immediately on exhaustion of the fuel sample), and subsequent separation of the pistons and repositioning of each to either end of the cylinder.

Figure 3.16 shows the various air and fuel flow circuits of the fuel system during a typical combustion experiment. On exhaustion of the test fuel, the end cap of the piston closest to the test fuel (piston A) would be pressed hard against the end of the fuel system cylinder. The piston end cap, therefore, incorporated a small fillet, allowing a small volume of fuel to be present and also a gap that could be flushed with fossil diesel fuel. Test fuels flowed to the fuel injector, via a high pressure filter, from the test fuel chamber (chamber A) within the cylinder, through a small outlet port positioned so as to ensure communication with the clearance volume between the piston A end cap and the cylinder bore. A second port also in communication with this clearance volume connected directly to a high pressure needle valve (2) behind which was fossil diesel fuel (at injection pressure) routed round from the fossil diesel fuel chamber of the system. Therefore, by opening this valve it was possible to allow fossil diesel fuel, at injection pressure, to flow into the small clearance volume present and into the fuel injector (Figure 3.16a). Flushing of the test fuel circuit in this way was conducted after every combustion experiment, and was of particular value when testing fuels normally solid at room temperature.

The bespoke end cap of the fossil diesel side piston (piston B) featured a radial grove on the outside diameter which communicated, via four small holes, with a small hollow on the outward face of the end cap. On completion of a combustion experiment and subsequent flushing of the test fuel circuit with fossil diesel fuel, the two pistons would be directly adjacent to one another, with the bespoke piston B end cap in the middle of this arrangement, in contact with the face of the rear piston A end cap. An inlet port connected to a high pressure valve (3) had been positioned precisely over the radial groove of the end cap. Opening of the high

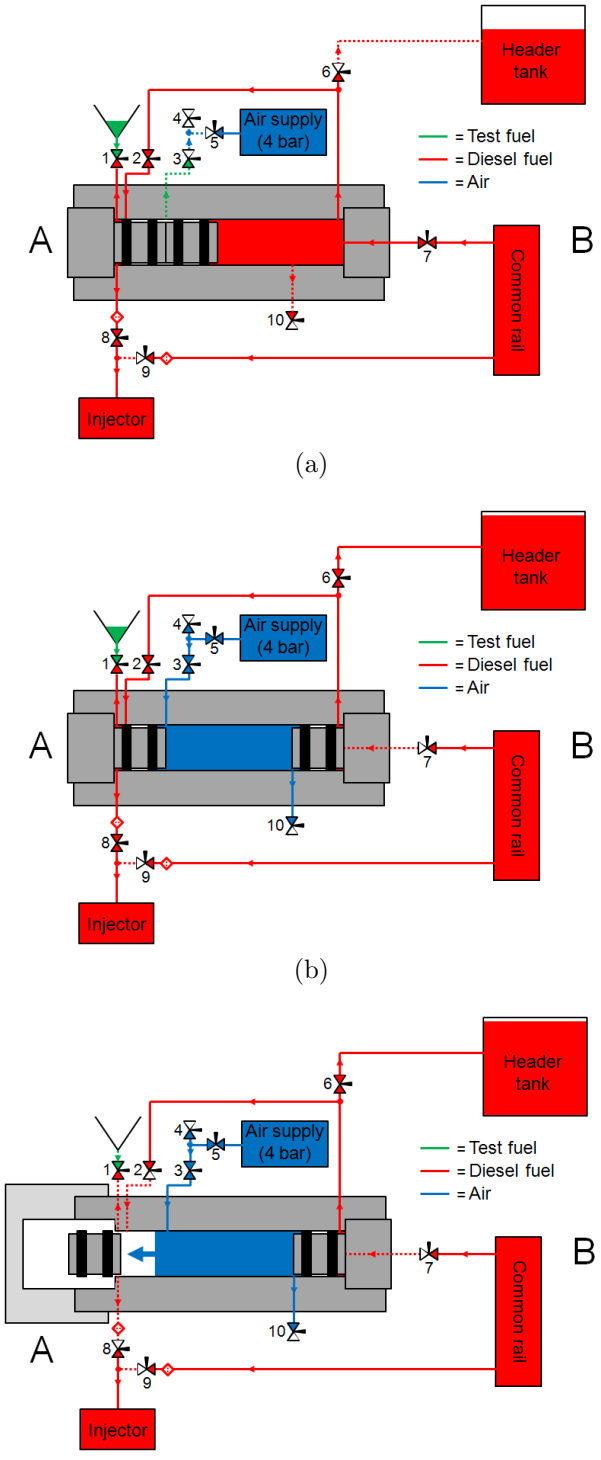

Figure 3.16: Fuel system experimental procedure, (a) fuel sample just exhausted, (b) two pistons separated and (c) sample piston ejected for cleaning

pressure valve (3) allowed flow into the cylinder of compressed air at 4 bar and pressurised the clearance volume between the two pistons (present due to the cavity in the piston B end cap). The build up of pressure in the cavity was sufficient to overcome the friction between piston B and the cylinder bore, thus moving the piston back till in contact with the cylinder fossil diesel fuel end cap (end cap B) (Figure 3.16b). In addition to overcoming the friction generated by the piston o-rings, further resistance was provided by the volume of fossil diesel fuel present in the fossil diesel fuel chamber of the cylinder (chamber B). This was allowed to leave chamber B and return to the fossil diesel fuel header tank by the opening of a further high pressure valve (6).

Figure 3.17: Aluminium external cap

Following this repositioning of the pistons, dismantling of the test fuel circuit would then be carried out. Figure 3.17 shows the aluminium external cap fitted around the cylinder at the test fuel end following unscrewing and removal of end cap A. Compressed air was then fed at 4 bar to the cavity between the two pistons (Figure 3.16c). This accelerated piston A to high velocity and the piston was captured by the aluminium external cap. With piston B positioned directly adjacent to end cap B, the exposed cylinder bore was cleaned thoroughly prior to replacement of piston A.

During cleaning of the piston A, it was required to replace the sealing o-rings, so as to avoid cross contamination of test fuels and also because, as Figure 3.18 shows, the o-rings would exhibit slight scalloping of the outer diameter. This was believed to be due to the extrusion of the piston o-rings into the cylinder ports when one side of the o-ring was exposed to high pressure fuel. However, the use of the two o-rings for sealing per piston meant that such scalloping did not result in any cross contamination between the fossil diesel and test fuels. After cleaning, piston A was

Figure 3.18: Piston o-ring scalloping

reinserted into the cylinder bore and positioned directly adjacent to piston B. With end cap A also cleaned and reinserted, the fuel system would then be filled with a test fuel and a new combustion experiment conducted (Figure 3.13).

3.5.1. Characterisation of the ultra low volume fuel system

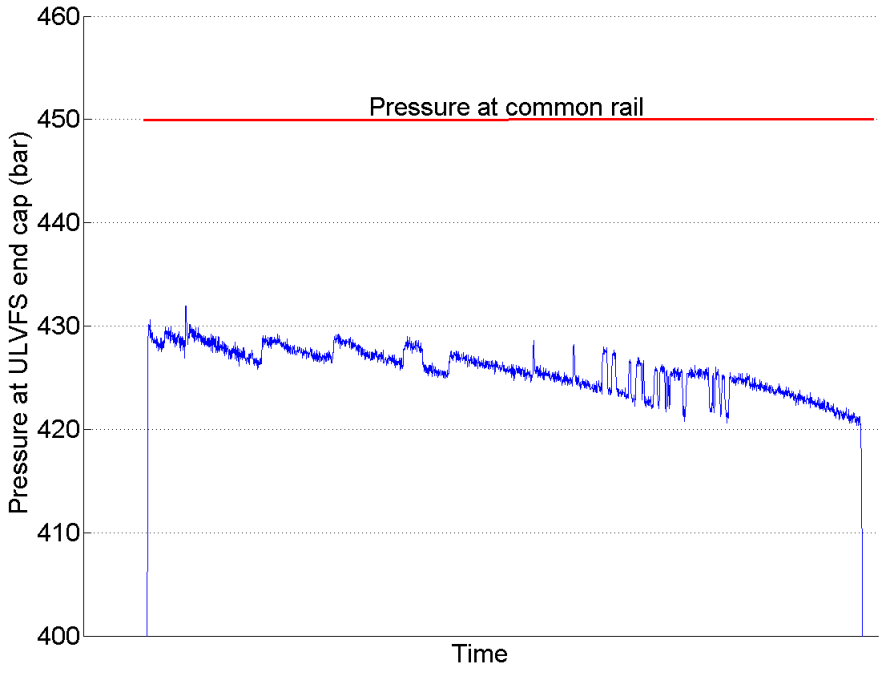

Figure 3.19: Measured ULVFS test fuel pressure during a combustion experiment at 450 bar common rail pressure

Placement of a pressure transducer in end cap A allowed for the effect of the friction between the piston o-rings and cylinder walls on test fuel injection pressure

to be observed. Figure 3.19 shows the measured pressure at end cap A during a combustion experiment with a common rail pressure of 450 bar. Pressures in the test fuel were found to be between 20 - 30 bar lower than those at the common rail, with the injection pressure of the test fuel generally decreasing as the combustion experiment advanced and the volume of the test fuel decreased. Several sharp fluctuations in the test fuel pressure were observed (Figure 3.19) of the order of around 2 - 5 bar and these indicate that (most likely due to the friction presented by the piston o-rings) passage of the pistons through the fuel system bore is a series of short discrete movements.

3.6. Measuring instruments

For analysis of the combustion and emissions characteristics of various test fuels, the primary measurements taken were the in-cylinder pressure and the composition of exhaust gases. The following sections describe in detail the instruments and analysers utilised.

3.6.1. Pressure

Measurements of the in-cylinder pressure were taken with a piezoelectric pressure transducer (Kistler 6056AU38) used in conjunction with a charge amplifier (Kistler type 5011). Calibration of the pressure transducer had been conducted previously by the manufacturer and also as the complete pressure measurement system (transducer, charge amplifier and data acquisition system) by Schönborn (2009).

For each combustion cycle, the in-cylinder pressure was referenced to the intake manifold pressure at intake-stroke bottom-dead-centre (at which point the inlet valve was open). To this end, a piezoresistive pressure transmitter (Druck PTX 7517-3257) was situated in the intake manifold, 160 mm upstream of the intake valves. Two further in-line piezoresistive pressure transmitters (Druck PTX 717-3275), were used to measure pressure in the exhaust and also of the intake air just prior to the air flow meter respectively. The mounting and position of all three pressure transmitters is shown in Appendix B.

3.6.2. Temperature

Temperature measurements were made with K-type thermocouples of 1.5 mm and 3 mm diameter and shielded thermocouple wire. In total 17 thermocouples were deployed: engine oil and coolant water were monitored for safety by the test-bed console, air intake temperature just downstream of the air heater was required by the PID air heater controller and temperature measurements of the heated components of the test circuit were needed by the five PID controllers maintaining constant test fuel temperature. Measurements made by the remaining nine thermocouples were logged by the system. These replicated some of the above measurements and, in addition, made those of fuel, injector, intake air (at the air flow meter and manifold) and ambient temperatures.

3.6.3. Air flow rate

An in-line air flow meter (Romet G40), positioned as previously described (Figure B.3), measured the volumetric flow of air into the engine. In addition, measurements of the intake pressure and temperature, just prior to the air flow meter, allowed for accurate calculation of the mass flow rate of air into the engine.

3.6.4. Fuel flow rate

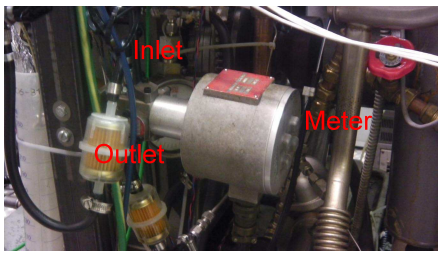

Figure 3.20: Fuel flow meter

Figure 3.20 shows the positive displacement fuel pump (Max machinery 213-310) used for measurements of fuel flow rate, positioned as described in Section 3.4. When combusting test fuels and diverting the injector spill away from the fuel supply circuit, the spill volume could be collected and measured so as to permit accurate determination of the flow rate of only the fuel volume injected into the cylinder. The fuel flow meter had twice been calibrated at the manufactures with an uncertainty in measurements of 0.2 %.

3.7. Exhaust gas composition

(a) (b)

Figure 3.21: (a) Automotive gas analyser rack, and (b) Flame ionisation detector oven for THC measurement

The composition of the engine exhaust gas (as sampled 180 mm downstream of the engine exhaust valve) was determined by individually measuring the concentrations present in the exhaust gas of the following chemical species: CO, CO_2, O_2, THC, NO and NO_x. Figure 3.21a shows the automotive exhaust gas analyser rack (Horiba MEXA 9100 HEGR) which performed these measurements and incorporated individual instruments to analyse concentrations of each of the species above except THC.

Figure 3.21b shows the analyser which made measurements of THC and which was under the control of the analyser rack but housed in a separate unit (Horiba FIA OV-04). Two heated lines (held at a constant temperature of 190 °C) conveyed exhaust gases from the exhaust sampling points to the analysers, with the gas sample taken by the main analyser subject to filtering and condensation of water vapour and gaseous hydrocarbons before entering the individual analysers. Measurements of exhaust gas composition by the analyser rack were recorded on PC via a GPIB output from the rack control unit.

3.7.1. CO and CO_2

The method of non-dispersive infrared absorption was utilised by the CO and CO_2 analyser (Horiba AIA-120) to determine concentrations of each. This relied upon the principle of wavelength-specific absorption of infrared energy by heterogeneous molecules. The degree of absorption by a specific molecule in a gas mixture is proportional to the concentration of that molecule present (assuming mixture pressure and temperature being constant).

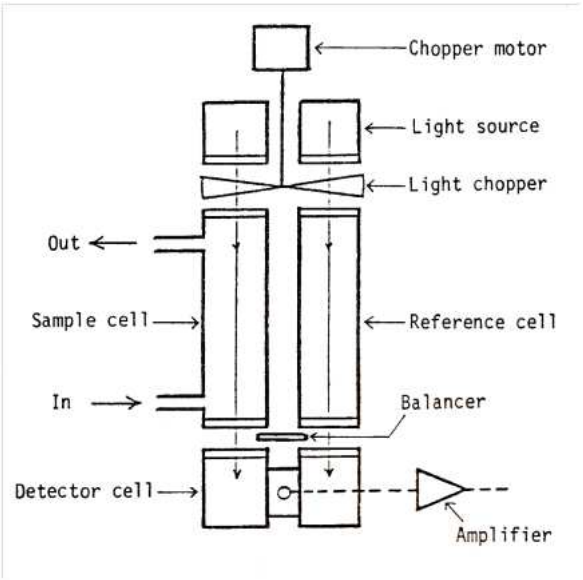

Figure 3.22: CO and CO_2 analyser schematic (Horiba Instruments, 1984)

Figure 3.22 shows a schematic representation of basic single detector system. In such a system, two cells are placed in parallel. Through one of them flows the sample gas and the other contains an infrared-inactive gas as a reference. Modulated by a light chopper, an infrared beam passes through both cells simultaneously then exits and impacts on a detector cell. The intensity of the two infrared beams entering the detector cell is different due to the presence of CO or CO_2 in the sample gas partially absorbing the beam, depending on the CO or CO_2 concentration. The beams cause a metallic membrane within the detector to deflect and a capacitive sensor measures this deflection and produces an electrical output.

Two separate infrared absorption detector systems were employed within the analyser used (Horiba AIA-120) for measurement of CO and CO_2. One system was specially configured to accurately measure low concentrations of CO (< 3000 ppm),

and achieved this high sensitivity through the addition of a second detector cell in series with the first. In such a dual detector system, the first detector features infrared transparent windows so as to allow the beam to exit and enter the adjacent second detector cell (Zhao and Ladammatos, 2001). This arrangement is beneficial; as it allows the first detector to respond primarily to the sample, with only a small portion of the output signal produced by an interferent species (such as CO_2 in the case of CO detection), while the second detector behaves in the inverse manner. A compensated composite signal can then be produced that effectively removes the influence of the intereferent.

The second unit within the analyser was a stacked detector system that simultaneously measured CO_2 levels and higher concentrations of CO (< 3000 ppm). As the absorption wavelengths of CO_2 and CO do not overlap, utilising two separate detector cells allows for concentrations of both to be determined from the same sample when both species are present at similar ranges of concentration. As in the case of a dual detector system, the detector cells are arranged in series, with the detector signals processed by separate amplifier networks for independent output (Horiba Instruments, 1984).

3.7.2. O_2

Figure 3.23 shows in schematic form the magneto-pneumatic analyser (Horiba FMA-125) utilised to determine levels of O_2 present in the sample gas. Oxygen possesses a much higher paramagnetic susceptibility than the other gases present in the exhaust stream and this property is exploited in determining the O_2 concentration present. The sample gas flowed past two pairs of poles which are alternately magnetised by excited coils. Oxygen is drawn to whichever of the poles is currently magnetised and this disrupts the flow of nitrogen from an orifice located within the poles. Thus at any time the flow of N_2 from one orifice will be restricted while the other is not. This pressure differential of the N_2 is converted by the detector (a condenser microphone) to an electrical output equivalent to the concentration of O_2 present (Horiba Instruments, 1984).

3.7.3. THC

Quantification of hydrocarbons present in the exhaust gases was conducted by a hydrogen flame ionisation detector which consisted of a rack controller (Horiba FMA-

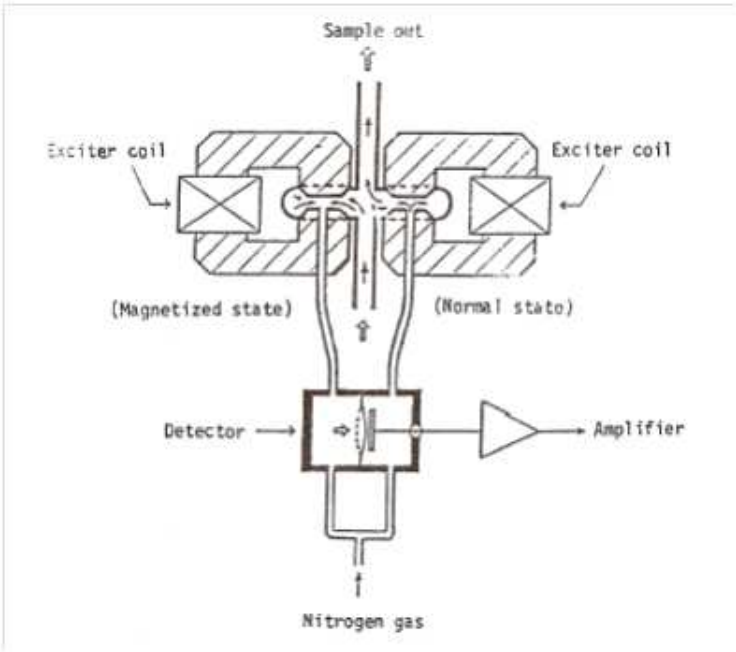

Figure 3.23: O_2 analyser schematic (Horiba Instruments, 1984)

125) and an external heated oven cabinet (Horiba FIA OV-04) held at a constant temperature of 190 °C. Located within the oven unit, a constant hydrogen flame was maintained and through which the sample gas flowed. Any hydrocarbons present in the sample gas would pass through the high temperature flame and undergo break-down of the carbon-carbon bonds and produce ionised current. Two electrodes with a steady direct current voltage applied across them were positioned either side of the flame, and thus the ionisation of hydrocarbons within the sample gas would result in production of a current proportional to the number of carbon atoms ionised (Horiba Instruments, 1984).

3.7.4. NO_x

The NO and NO_x analyser (Horiba CLA-150) utilised the chemilumiscent method of detection for both species. The reaction of NO with ozone (O_3), during which around 10 % of the resultant NO_2 are in an electrically excited state and, when these then immediately revert back to the unexcited state, photons are emitted (Horiba Instruments, 1984):

$$NO + O_3 \rightarrow NO_2^* + O_2 \tag{3.1}$$
$$NO_2^* \rightarrow NO_2 + hv$$

(where h = Planck's constant, v = frequency (hZ) and * denotes the excited state)

The sample gas was mixed with O_3 and then fed to an evacuated reaction chamber where the NO + O_3 reaction took place. A photo multiplier measured the resulting luminescence which was proportional to the amount of NO present.

To measure any NO_2 present in the sample concurrently by the same method, prior to entering the reaction chamber, the whole exhaust sample flowed through a NO_2 converter. Any NO_2 present in the heated converter in the presence of a catalyst, will then dissociate to form NO, i.e.

$$NO_2 + C \rightarrow NO + CO \tag{3.2}$$

The analyser unit (Horiba CLA-150) included a vacuum pump so that the above reactions could take place in the reaction chamber under reduced pressure conditions. This reduced the possibility of collision between excited NO_2^* and other molecules prior to their relaxation and thus any interference due to other species present in the sample (Horiba Instruments, 1984).

3.7.5. Particulates

Figure 3.24 shows the fast particulate spectrometer (Cambustion DMS500) utilised to determine the size distribution of particulates (5 to 1000 nm) in the exhaust gas. Figure 3.25 shows the flow of sample gases through the spectrometer. From the exhaust sampling point, the sample gas was conveyed through stainless steel pipe (of length 320 mm) to a heated cyclone which was kept at constant temperature (80 °C). This cyclone was required to dilute the sample gas with dry compressed air prior to entering the instrument for two reasons: dilute the exhaust gas sample so that the water dew point of the sample gas would be below the ambient operating temperature of the instrument and also reduce the concentration of particulates, thus reducing accumulation of particulates in the instrument and extending cleaning

Figure 3.24: Fast particulate spectrometer (Cambustion DMS500)

intervals. The dilution ratio (air:sample) at the cyclone was maintained at four to five throughout the running of experiments. The cyclone also served to remove any particles present in the exhaust stream greater than 1 μm. To further prevent condensation of water vapour the sample gas flowed from the cyclone to the main instrument via a heated line maintained at constant temperature (5 m length at 80 °C). The compressed air supply to the remote cyclone was also conveyed through the same heated line, albeit along a different path.

On entering the instrument the sample flow was subject to secondary dilution (ratio of 100) through a second heated cyclone (80 °C) positioned in series and downstream of the first cyclone described above. From the second cyclone the sample flowed through a corona discharge charger and into the classifier column (particle sizer), which was maintained constantly at an absolute pressure of 0.25 bar by an external vacuum pump (Figure 3.25).

Figure 3.26 shows the classifier column which consisted of a uniform, cylindrical column of air flowing around a central high voltage electrode and surrounded by a sheath of particle free air (Cambustion, 2010). Twenty-two grounded rings surrounded the sheath flow and repulsion from the central high voltage electrode caused particulates within the sample flow to deflect on to the grounded rings. Charge from the particulates was then transferred to the grounded electrode ring; the magnitude of the charge and the ring position were determined by the electrical mobility of the particles, a function of a particle's charge and size. The aerodynamic drag of a particle can be related to the particle diameter (assuming a spherical form),

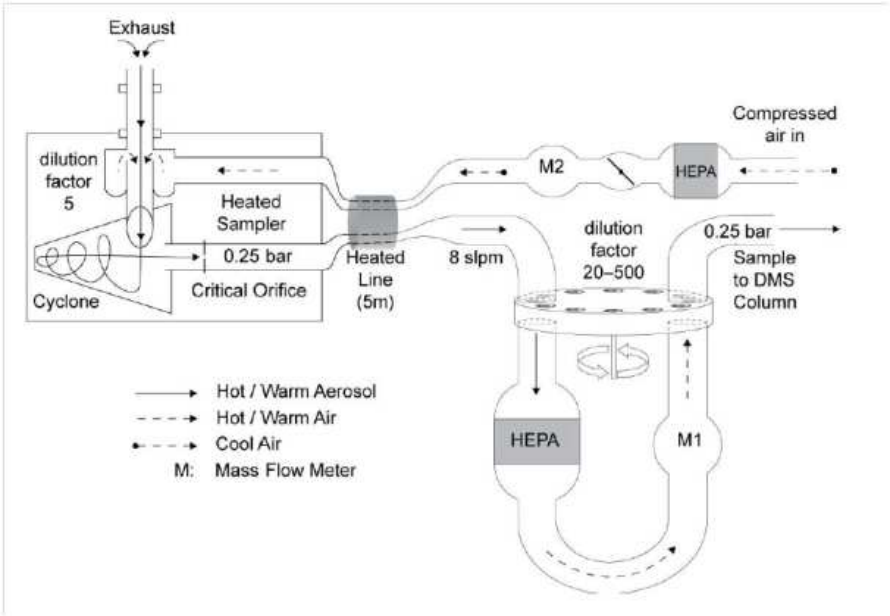

Figure 3.25: Sample flow of DMS500 (Cambustion, 2010)

which will thus will effect particle velocity on entering the classifier. Therefore, it can be seen that the angle of deflection towards the grounded electrode rings will be determined by particle velocity and the magnitude of the particle charge creating attraction between the particle and grounded electrode rings. The PC instrument interface would then translate the charge and ring data into particle number and size data which was displayed graphically in real time and also logged.

3.8. Data acquisition systems

For logging of experimental data three independent non-networked PC's were utilised: one for logging of pressure and temperature data, a second for the logging of exhaust gas composition data (and also as an interface with the injector control system) and a third exclusively for the logging of measurements of particulate size and number.

The PC for pressure and temperature logging was equipped with two internally mounted PCI 16 channel input data acquisition cards, one of which is referred to as high speed and was capable of sampling at 1.25 MS/s with a single analogue to digital converter in conjunction with a multiplexer, while the other is referred to as low speed and had a peak sampling rate of 250 KS/s also with a single analogue to di-

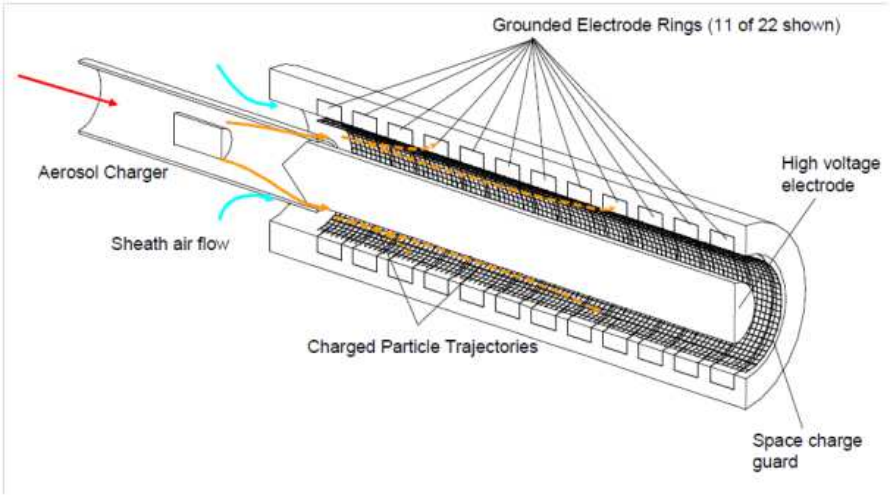

Figure 3.26: DMS500 classifier columnCambustion (2010)

gital converter (National Instruments PCI-6251 and National Instruments PCI-6224 respectively). The high speed card was utilised for sampling the analogue outputs of the in-cylinder, inlet manifold air, exhaust and air intake pressure transmitters and also the engine speed (as outputted from the dyno test-bed control console). The data acquisition software utilised to process and log the incoming signals was developed by the author in a graphical programming environment (National Instruments Labview 8.1), and was an evolution of the software originally developed for the test facility by Schönborn (2009).

Figure 3.27 shows a screenshot of the DAQ program interface. Data was acquired at a resolution of 0.2 CAD and was recorded, stored and processed as one complete engine cycle, with three separate timing signals from the engine utilised to correctly time the data recording procedure. An optical shaft encoder coupled to the crankshaft gave 1800 square-form signals per crankshaft revolution (thus defining the resolution of pressure measurements as 0.2 CAD) and also a square synchronisation pulse once per crankshaft revolution. By processing this synchronisation pulse through an AND logical control gate with a third signal from a camshaft mounted optical sensor a once-per-engine-cycle reference signal was created. This allowed for all high speed measurements to be synchronised according to engine cycle, rather than crankshaft rotation, and thus instantaneous display of the acquired data and real-time processing. Using the engine geometry parameters stored in the data acquisition software, the position of TDC (as determined by the method of entropy

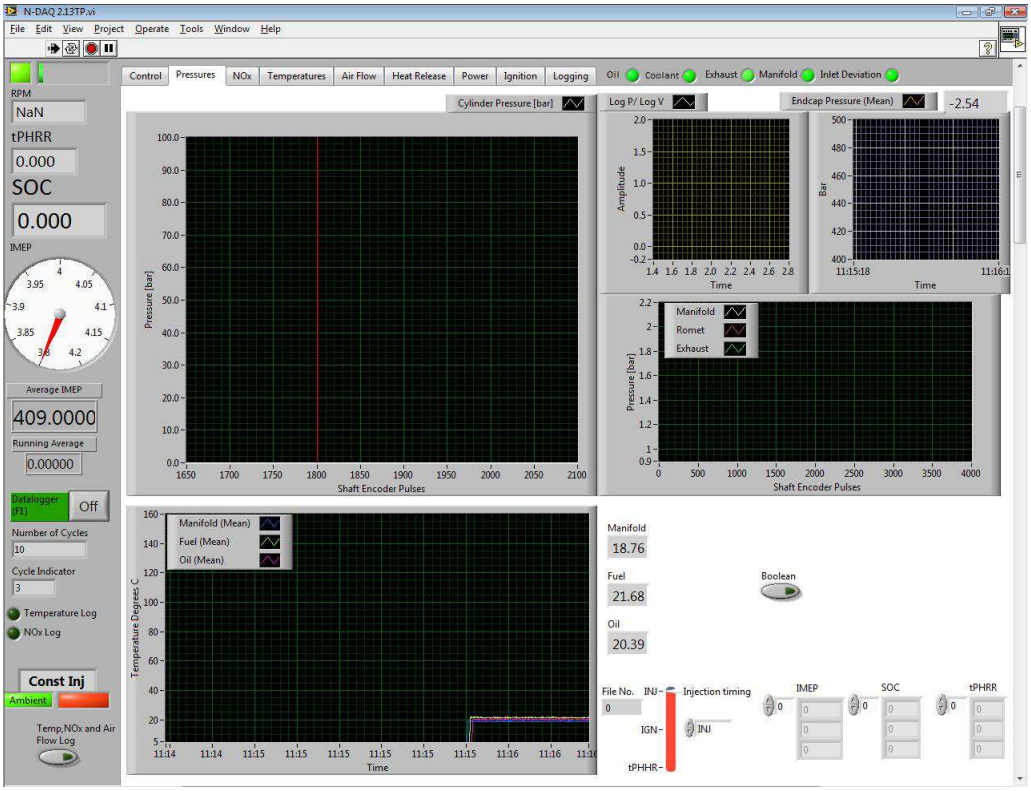

Figure 3.27: In-cylinder pressure DAQ screenshot

developed by Tazerout et al. (1999)) and the shaft encoder timing signals, several combustion variables were calculated in real time so as to exercise better experimental control. These included: indicated mean effective pressure (IMEP), heat release rate, cumulative heat release rate, mass fraction burnt, global in-cylinder temperature, entropy, time of start of combustion and time of peak heat release rate. The data acquisition software displayed and logged (in tabular format in an ASCII format file) the original measurements, the calculated parameters and also data acquired from the low speed card.

The low speed data acquisition card sampled at a rate of 10 samples per second signals from nine thermocouples, the test fuel pressure transmitter, the intake air flow meter and also an analogue output from the exhaust gas NO_x analyser. The analogue output from the NO_x analyser was implemented so as to overcome a partial failure of the analyser's analogue to digital converter, with a feature added to the data acquisition software for calibration of the analogue signal. Signals from the nine thermocouples were averaged with time and displayed in real time with audible

alarms for deviation of temperatures from preset values. The test fuel injection pressure was also displayed in real time for monitoring of the low volume fuel system function, while the signal from the air flow meter was used with measurements of pressure and temperature at the meter for real-time calculation of mass air flow-rates.

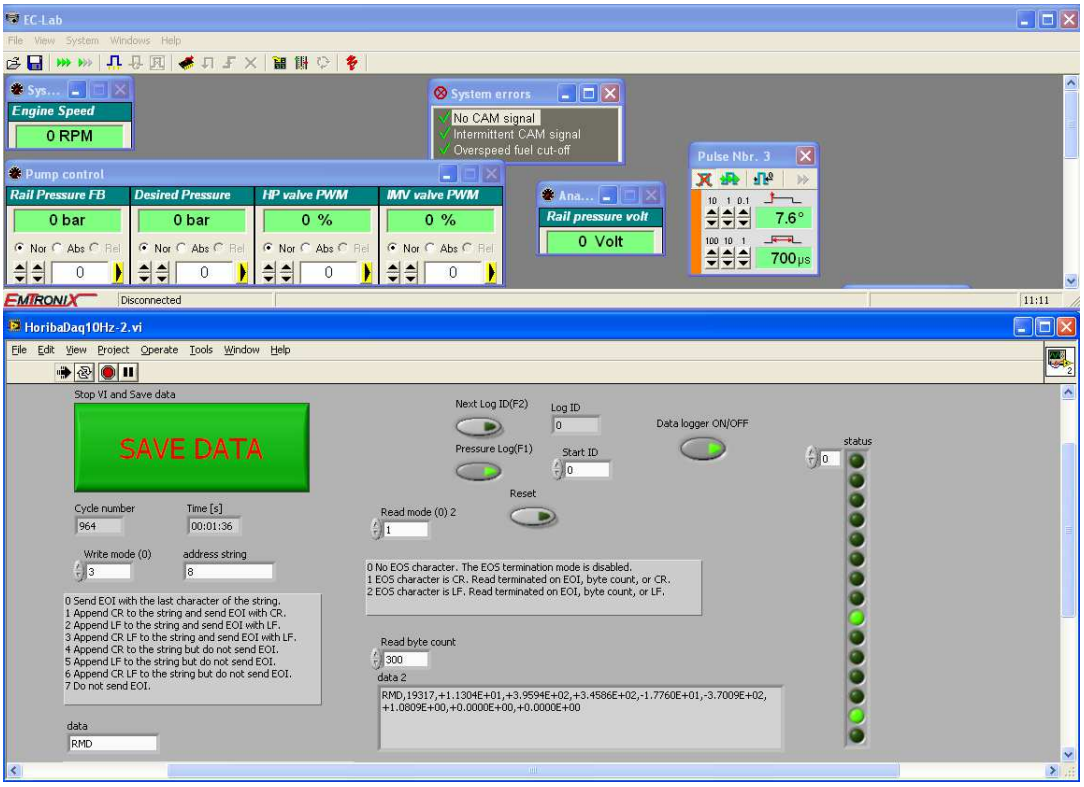

Figure 3.28: Exhaust gas composition logging and injection control interface PC screenshot

The second PC displayed and logged the exhaust gas composition as measured by the gas analyser rack and also hosted an interface for control of injection, timing and pressure (Emtronix EC Lab 7.3i). Figure 3.28 shows a screenshot of the interfaces utilised for both tasks. A GBIP to USB module (National Instruments GPIB-USB-HS) read the data into the PC where it was logged by software developed in the same graphical programming environment (National Instruments Labview), based on original software by Schönborn (2009) and included a time-stamp for correlation with combustion variables logged by the first PC.

The third PC was reserved exclusively for control of the fast particulate spectrometer and logging of the data acquired by the instrument. Both operations

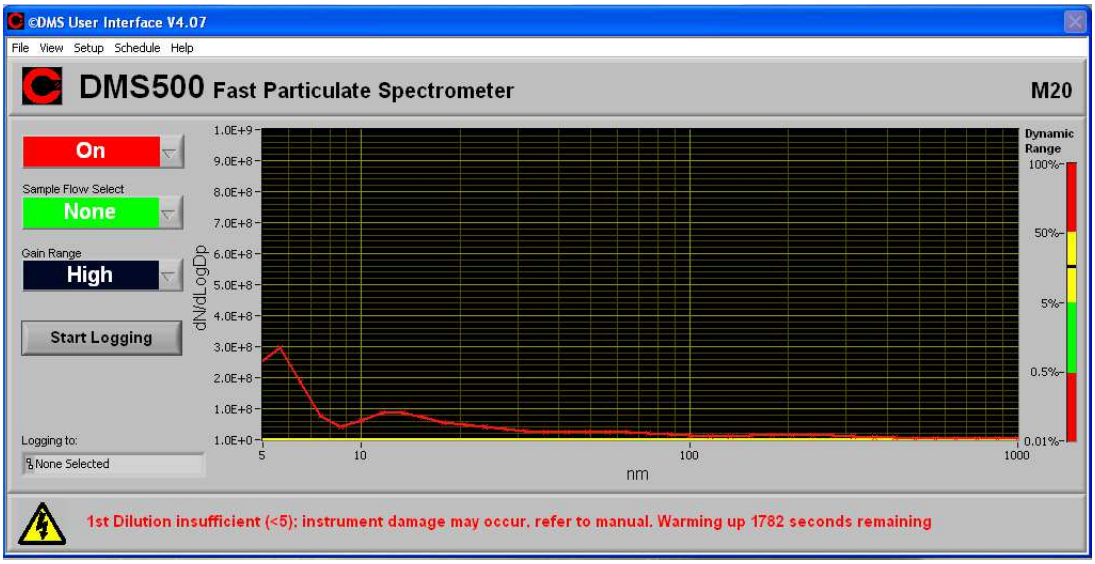

Figure 3.29: Fast particulate spectrometer interface

were performed with the PC user interface supplied by the instrument manufacturer (Cambustion DMS User Interface V2.13, 4.05 and 4.07); Figure 3.29 shows a screenshot of the spectrometer interface.

3.9. Spark ignition engine

A small number of combustion experiments (Chapter 11) were conducted in a normally aspirated Ricardo E6 single cylinder research spark ignition engine. For all tests with the spark ignition engine, fuel was delivered at atmospheric pressure and mixed with air in a carburetor approximately 150 mm upstream of the engine intake valves and subsequently ignited by a spark plug (NGK B7HS) within the cylinder. Further details of the E6 spark ignition engine and control apparatus are given in Table 3.2 and Figure 3.30 shows the engine installation. In-cylinder pressure data from the spark ignition engine was logged utilising a data acquisition system based on that described in Section 3.8.

Table 3.2: Spark ignition engine specification

Engine model	Ricardo E6
Number of cylinders	1
Cylinder bore	76.2 mm
Crankshaft stroke	55.57 mm
Swept volume	506.8 cc
Compression ratio	10.3 : 1
Oil temperature	40 ± 2.5 °C
Water temperature	40 ± 2.5 °C
Fuel delivery system	Single barrel, fixed venture carburetor
Shaft encoder	0.4 CAD resolution

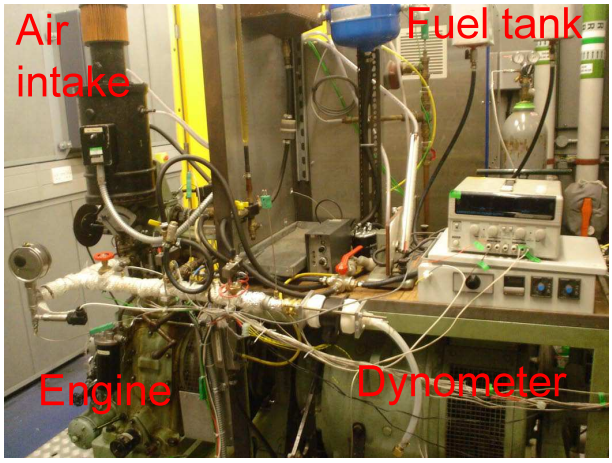

Figure 3.30: Ricardo E6 single cylinder research spark ignition engine

4. Analytical methods

The present chapter describes the analytical methods applied to the experimental data. In particular, mathematical analysis of the cylinder pressure data, which allowed for calculation of heat release rates and in-cylinder global temperatures, and also the definition and identification of several important stages of the combustion process.

4.1. Heat release analysis of in-cylinder pressure data

For all combustion experiments, in-cylinder pressure data was logged as a discrete value at intervals of 0.2 CAD over the entire duration of the four stroke combustion cycle (720 CAD). Appraisal of the raw in-cylinder pressure data, plotted against CAD, can give an indication as to the compression ratio and volumetric efficiency of the engine, the effect of fuel evaporation and the duration of both ignition delay and combustion. However, for more detailed analysis of combustion, it is desirable to consider the heat release rate of a fuel over a range of CAD.

4.1.1. Cylinder volume calculation

In order to calculate heat release rate from in-cylinder pressure data, the cylinder volume (also referred to as the combustion chamber) at each interval of CAD must be known. The total cylinder volume (V) at a given CAD can be calculated according to

$$V = V_{clear} + [A_{bore}(l_{con} + r_{crank} - \sigma)] \tag{4.1}$$

where A_{bore} is the cylinder bore area, r_{crank} is the crank radius, V_{clear} is the clearance volume and σ the instantaneous stroke.

The cylinder bore area (A_{bore}) can be found from

$$A_{bore} = \frac{D_{bore}^2}{4}\pi \tag{4.2}$$

where D_{bore} is the cylinder bore diameter, and the instantaneous stroke position (σ) from

$$\sigma = a\cos(\theta) + \sqrt{l_{con}^2 - a^2\sin^2(\theta)} \tag{4.3}$$

where θ is the crank angle from the TDC position.

4.1.2. Apparent net heat release of combustion

To calculate the heat release of combustion occurring within the combustion chamber, a number of assumptions are made (necessitating the term apparent, as the heat release calculated is an approximation of the actual values which cannot be determined exactly (Heywood, 1981)): the cylinder contents are assumed to be at a uniform instantaneous temperature (T), no mass flow occurs across the system boundaries for the duration of heat release and that for the calculation of net heat release the system is adiabatic. The net heat release (Q_n) is therefore the difference between the gross heat release of the fuel during combustion (Q_{ch}) and the heat transfer from the system to the cylinder walls in accordance with the second law of thermodynamics (Q_{ht}). Therefore, the net heat release rate at any given position in the combustion cycle can be expressed as

$$\frac{dQ_n}{d\theta} = \frac{dQ_{ch}}{d\theta} - \frac{dQ_{ht}}{d\theta} \tag{4.4}$$

In accordance with the first law of thermodynamics, the apparent net heat release rate is equal to the work done on the piston, plus the rate of change of sensible internal energy of the system (U_s), and therefore the apparent net heat heat release rate can also be expressed as

$$\frac{dQ_n}{d\theta} = p\frac{dV}{d\theta} + \frac{dU_s}{d\theta} \tag{4.5}$$

Further assuming that the cylinder contents can be modeled as an ideal gas, i.e.

$$pV = mRT \tag{4.6}$$

then Equation 4.5 may be rewritten as

$$\frac{dQ_n}{d\theta} = p\frac{dV}{d\theta} + mc_v\frac{dT}{d\theta} \tag{4.7}$$

Where R is constant, it follows from the ideal gas law (Equation 4.6) that a change in temperature can be described by changes in pressure and volume, i.e.

$$\frac{dp}{p} + \frac{dV}{V} = \frac{dT}{T} \tag{4.8}$$

With T substituted according to Equation 4.8, the net heat release rate can be expressed as

$$\frac{dQ_n}{d\theta} = (1 + \frac{c_v}{R})p\frac{dV}{d\theta} + \frac{c_v}{R}V\frac{dp}{d\theta} \tag{4.9}$$

Taking the ratio of specific heats (γ) to be

$$\gamma = \frac{c_p}{c_v} \tag{4.10}$$

and the gas constant (R) as

$$R = c_p - c_v \tag{4.11}$$

the net heat release rate can also be expressed as

$$\frac{dQ_n}{d\theta} = \frac{\gamma}{\gamma - 1}p\frac{dV}{d\theta} + \frac{1}{\gamma - 1}V\frac{dp}{d\theta} \tag{4.12}$$

For all combustion experiments presented in this work, this expression (Equation 4.12) was used to calculate the apparent net heat release rate at increments of CAD equivalent to the resolution of the shaft encoder utilised in recording in-cylinder pressure data. The values of $\frac{dp}{d\theta}$ and $\frac{dV}{d\theta}$ used were the difference between the values of P and V at the CAD for which Q_n was calculated (as measured and calculated according to Equation 4.1 respectively) and the values of the same variables at the preceding increment of crank angle:

$$\frac{dp}{d\theta} + \frac{p_n - p_{n-1}}{d\theta} \tag{4.13}$$

$$\frac{dV}{d\theta} + \frac{V_n - V_{n-1}}{d\theta} \tag{4.14}$$

The values of the ratio of specific heats used in Equation 4.12, were those suggested by Heywood (1981), namely $\gamma = 1.35$ during the compression stroke prior to TDC and $\gamma = 1.28$ subsequent to TDC during the expansion stroke.

4.1.3. Ignition delay

The fuel ignition delay was defined as the duration, in crank angle degrees (CAD), between the start of injection (SOI, defined as the time at which the injector actuating signal commences) and the start of combustion (SOC); which was defined as as the time in CAD (after SOI and before the time of peak heat release rate) at which the minimum value of cumulative heat release occurs. For fuels showing clear two stage ignition, a second point of combustion (SOC2) was also identified.

In Figure 4.1, heat release rate (HRR) , cumulative heat release rate, the 1st derivative of heat release rate (dHRR) and d($\tan^{-1}$(dHRR/dCAD)), where dCAD is the 1st derivative of crank angle position , are plotted against the crank angle position. Figure 4.1 also shows the definition of SOC in terms of cumulative heat release rate in the case of a fuel showing clear two stage combustion. The point at which the second stage of combustion commences (SOC2) is also displayed in Figure 4.1; SOC2 is defined as the minimum value of d($\tan^{-1}$(dHRR/dCAD)) between SOC and the time of peak heat release rate where dHRR is positive.

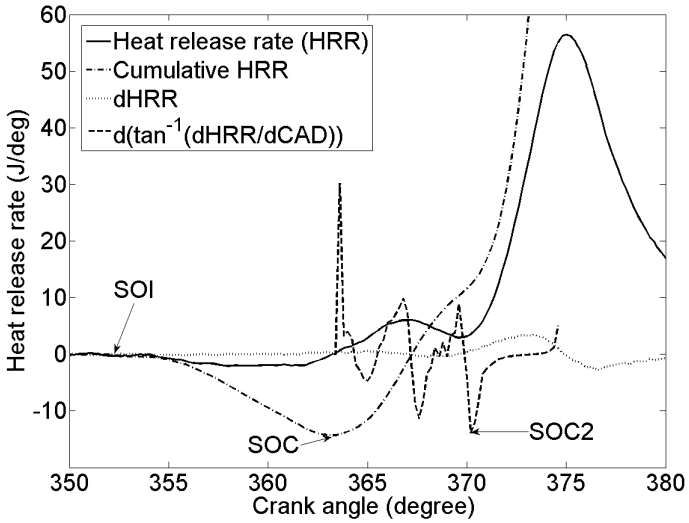

Figure 4.1: Definition of SOC and SOC2 in terms of apparent net heat release rate (HRR), cumulative heat release rate, 1st derivative of heat release rate (dHRR) and d($\tan^{-1}$(dHRR/dCAD)) where dCAD is the 1st derivative of the crank angle position.

4.1.4. Cumulative heat release

For further information regarding the manner in which energy release occurred over the duration of combustion, the accumulated heat release from SOC to each increment of CAD during combustion was calculated. The duration of combustion was defined as the interval between SOC and the first appearance of negative of heat following the occurrence of peak heat release rate. The cumulative heat release was therefore found by integrating the HRR (as found according to Equation 4.12) for the entire duration of combustion.

4.1.5. Premixed burn fraction

Figure 4.2 shows the definition of premixed fraction in terms of apparent net heat release rate, 1st derivative of heat release rate and 2nd derivative of heat release rate (d^2HRR). The extent of the premixed burn fraction was determined by a semi-automated graphical method; following visual inspection of the HRR, dHRR and d^2HRR plot (Figure 4.2), a range of CAD was selected within which the point at which combustion ceased to be predominantly premixed and became mostly diffusion rate controlled was judged to be. The precise point of change over was then taken as

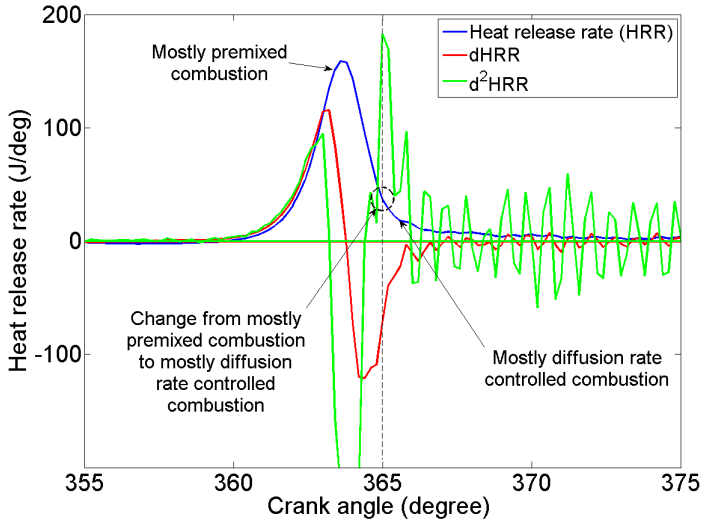

Figure 4.2: Definition of premixed burn fraction in terms of apparent net heat release rate (HRR), 1st derivative of heat release rate (dHRR) and 2nd derivative of heat release rate (d^2HRR)

the CAD at which the maximum value of d^2HRR occurred, and the corresponding value of mass fraction burnt (as calculated from the cumulative heat release defined in Section 4.1.4) at this CAD was taken to be the premixed burn fraction.

4.1.6. In-cylinder global temperature

At any given CAD, the global temperature of the cylinder contents may be calculated by maintaining the same assumptions stated for calculation of apparent net heat release rate (Section 4.1.2). The ideal gas law (Equation 4.6) allows temperature (T) to be calculated from (p), (V) and knowledge of the number of mols of air present (n) and the molar gas constant ($\bar{R}$), in accordance with

$$T = \frac{pV}{n\bar{R}} \tag{4.15}$$

The number of mols of air present was estimated by measurement of the volumetric air flow rate into the cylinder during each cycle (Chapter 3.6.3). No allowance was made for the presence of fuel and combustion product molecules within the combustion chamber; however, as compression ignition combustion is in general lean

and thus the cylinder contents predominantly consist of air, such an assumption is valid.

4.2. Indicated mean effective pressure

Throughout this work, engine output is defined by the indicated mean effective pressure (IMEP), which can be calculated from the net indicated displacement work per cycle (W_i) and the swept volume of the engine (V_d) according to

$$IMEP = \frac{W_i}{V_d} \tag{4.16}$$

The indicated displacement work per cycle (W_i) is found by calculating the integral of pressure with respect to the cylinder volume, i.e.

$$W_i = \int p dV \tag{4.17}$$

The swept volume is found from the cylinder bore area A_{bore} and the piston stroke length $\bar{\sigma}$

$$V_d = A_{bore}\bar{\sigma} \tag{4.18}$$

4.3. Indicated thermal efficiency

The indicated thermal efficiency of the engine η_t was calculated as the ratio of indicated work per cycle to the chemical energy contained within the fuel injected per cycle; that is the lower heating value of the fuel (Q_{HV}), multiplied by the mass of fuel injected (m_f), i.e.

$$\eta_t = \frac{W_i}{Q_{HV} m_f} \tag{4.19}$$

As no direct measurement of the mass of fuel injected per engine cycle was made, this value was instead found from measurements of the exhaust gas composition and

air flow into the engine using the numerical method of atomic balances described in considerable detail in Chapter 4 of the PhD thesis of Alessandro Schönborn (2009).

4.4. Adiabatic flame temperature

The constant pressure adiabatic flame temperature (T_{ad}) can be found from the equivalence of the absolute enthalpy of the reactants (H_{reac}) at the initial temperature and that of the products (H_{prod}) at the adiabatic flame temperature, i.e.

$$H_{reac}(T_i, P) = H_{prod}(T_{ad}, P) \tag{4.20}$$

The calculations were made according to the method prescribed by Turns (2000), assuming no dissociation and an equivalence ratio of 1. The initial temperature was taken as the calculated minimum in-cylinder global temperature between SOI and SOC and values of the enthalpy of formation in a gaseous state for the combustion products and reactants were obtained from literature.

4.5. Representation of experimental error

Throughout this work, where present on figures, the extent of the error bars given are plus and minus one standard deviation from the mean value (which is the point displayed on the plots) taken from repeat experimental runs of the same test fuel within that experimental series. Where in different chapters of this work, different values of combustion characteristics and emissions levels are reported for the same fuel (ie. the reference fossil diesel) at equivalent test conditions, this can be attributed to the maintenance and repairs undertaken on the experimental apparatus; for example, replacement of the fuel injector or servicing and calibration of the particulate spectrometer. For this reason, each of the discrete experimental studies were conducted in as short a period of time as practicably possible, and thus the error bars presented only consider repeat tests of the same fuel performed within that particular series of experiments.

5. Design of combustion experiments

The present chapter describes the general design of the combustion experiments presented in this work, namely the injection timings utilised in tests with the compression ignition engine.

5.1. Reference fossil diesel

Throughout this work, a reference fossil diesel was tested alongside the pure component and binary mixture fuels investigated. This provided a means with which to measure day to day variability in engine performance, and also a constant baseline against which to assess the test fuels under consideration. At all points in this work, reference fossil diesel refers to blend G07/478 provided by BP Global Fuels, the full properties of which are listed in Appendix C.

5.2. Constant injection timing

All of the combustion experiments presented in this work were initially conducted at two injection timings so as to separate the effects of cylinder volume and turbulence on key stages of the combustion process from those of the fuel molecular structure. The first of these, constant injection timing, was designed to subject all fuels to identical conditions on start of injection (SOI, as defined in Section 4.1.3) and during initial fuel and air mixing. Therefore, at constant injection timing, the SOI was held constant at 7.5 CAD BTDC (at which timing the reference fossil diesel was found to combust at approximately TDC), and start of combustion (SOC, as defined in Section 4.1.3) for each fuel varied according to the ignition delay of that fuel.

5.3. Constant ignition timing

The second of the two injection timings at which all fuels were initially tested was designed so that all fuels experienced the same in-cylinder conditions at SOC. As such, at constant ignition timing, the time of SOI was varied so that the SOC of all fuels always occurred at TDC.

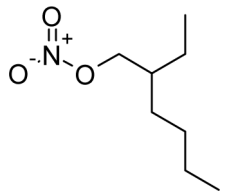

Figure 5.1: Molecular structure of ignition improving additive 2-ethylhexyl nitrate

5.4. Constant duration of ignition delay

After the initial two sets of experiments at constant injection and constant ignition timing were completed, for many of the studies presented in this work, it was desirable to investigate any secondary effects of fuel molecular structure that may have been masked by the duration of ignition delay. Use of regression techniques or design of experiment methods are of limited value because many physical and chemical properties of fuels correlate highly with ignition delay. A useful experimental technique for removing the presence of ignition delay is to use small quantities of ignition improver added to the fuel to equalise the delay.

As such, a third series of experiments was carried out during which the ignition delay of different sample fuels was held constant by adding the radical providing ignition improver 2 ethyl-hexyl nitrate (2 EHN, the molecular structure of which is given in Figure 5.1) in small concentrations to each test fuel, in an iterative process to determine the correct dosage. The experiments at constant ignition delay were conducted at both a fixed SOI of 7.5 CAD BTDC and also at a SOC of TDC. All fuels treated with 2 EHN had ignition delays which differed, at most, only by the resolution of the engine shaft encoder (0.2 CAD).

5.5. Constant IMEP

For all combustion tests, fuels were compared on the basis of equal work output from the engine. Therefore, for each series of combustion experiments, the injection duration was adjusted in the case of every fuel so that the engine IMEP was always an equivalent value for all fuels.

6. The effect of alkyl straight carbon chain length, degree of saturation and the presence of methyl branches

Of the simplest molecules suitable for combustion in compression ignition engines are non-oxygenated acyclic (no aromatic ring structures present) alkanes and alkenes. Such molecules can be produced chemically from biomass and fossil feedstocks via the Fischer Tropsch process (Huber et al., 2006; Naik et al., 2010; Larson and Jin, 1999), and have also found to be directly produced by micro-organisms (Kinderlerer et al., 1988; Dembitsky et al., 2001).

Furthermore, most fuels considered for compression ignition combustion feature alkyl chains (fossil diesel, fatty acid esters), and this chapter attempts to quantify the impact on combustion and emissions of three molecular structural features of alkanes: straight carbon chain length, degree of saturation and the presence of methyl branches. The chapter also investigates how molecule properties other than ignition delay shape the combustion process and the exhaust emissions produced.

6.1. Experimental method

6.1.1. Apparatus

All of the combustion experiments described in the present chapter were performed using the compression ignition engine and ultra low volume fuel system described in Chapter 3.

6.1.2. Fuel molecules investigated

In total, 18 non-oxygenated acyclic hydrocarbons were tested so as to study the influence of three molecular structural features on combustion phasing and emissions production:

1. Straight carbon chain length.
2. Degree of saturation (i.e. Number of double bonds).
3. Carbon chain branching

To assess the effect of increasing straight carbon chain length in a fully saturated, un-branched and non-oxygenated hydrocarbon, eleven *n*-alkanes were tested and were of chain length between *n*-heptane and *n*-docosane as follows: C7, C8, C10, C11, C12, C14, C15, C16, C18, C20 and C22. In order to understand the impact of a double bond within a molecule, four 1-alkenes were tested: 1-octene (C8), 1-decene (C10), 1-dodecene (C12) and 1-tetradecene (C14).

In addition one molecule featuring two double bonds, 1, 7-octadiene (C8), was included to assess the importance of the number of double bonds within a straight carbon chain. So as to study the influence of carbon branches, two molecules were specially synthesised by an organic synthesis company: 8-methylhexadecane (C17) and 2, 6, 10, 14-tetramethylpentadecane (C19). All molecules, other than the synthesised branched molecules, were obtained from a chemical supplier (Sigma Aldrich UK), with assay and other properties of each presented in Table 6.1 and the molecular structures of the fuels shown in Table 6.2.

A fossil derived reference diesel fuel with zero oxygen content was tested at the start and end of every day of experimentation so as to monitor drift and experimental error in the test conditions and analysis equipment. This reference diesel was also flowed through the test sample side of the fuel system and injected into the combustion cylinder between every test fuel so as to flush through any residual of the test sample and reset the injector to the same initial state for every test fuel. After flushing the low volume fuel system, the test sample fuel chamber was dismantled and cleaned thoroughly between every experiment so as to avoid cross-contamination between fuel samples.

In addition to repeat testing of the reference diesel fuel, many of the fuel molecules investigated were tested more than once at the same experimental conditions during different experiment series so as to provide another indicator of any experimental error and system drift, and also allow better overlap of data collected on different test days. The largest source of discrepancy between data collected on different days at identical conditions arose from the need to replace the injector several times during the course of the experiments. The adverse physical properties of the test fuels (e.g. low viscosity) resulted in an average continuous operational lifetime for the injectors of around 4 hours before failing shut due to port erosion within the injector body. The repeat of baseline tests with the reference fossil fuel and repeats

Table 6.1: Properties of alkanes, alkenes and reference fossil diesel

Fuel	Molecular formula	Assay (%)	T_{boil} (°C)[1]	△vapH° (kJ/mol)[1]	Cetane number [2]	Density (kg/m^3)[3]	Kinematic viscosity at 20 °C (mm^2/s)[4]
Reference fossil diesel	-	-	268.9	-	51.7	834.5*	2.672
n-heptane	C_7H_{16}	99	98.4	36.66	54.4	683.8	-
n-octane	C_8H_{18}	98	125.6	41.53	64.1	702.8	-
n-decane	$C_{10}H_{22}$	99	174.1	51.39	76.7	730.1	1.27
n-undecane	$C_{11}H_{24}$	99	194.9	56.43	81.1	740.2	1.602
n-dodecane	$C_{12}H_{26}$	99	215.9	61.51	82.5	749	1.979
n-tetradecane	$C_{14}H_{30}$	99	249.9	71.3	95	762.7	3.05
n-pentadecane	$C_{15}H_{32}$	99	266.9	76.11	96	768.4	3.8
n-hexadecane	$C_{16}H_{34}$	98	280.9	81.38	96	773.3	-
n-octadecane	$C_{18}H_{38}$	99	316.2	54.48[5]	106.3	776.7	-
n-eicosane	$C_{20}H_{42}$	97	343.1	-	110	782.3	-
n-docosane	$C_{22}H_{46}$	99	368.7	-	-	778.2	-
1-octene	C_8H_{16}	98	121.9	40.44	0.8	714.9	-
1, 7-octadiene	C_8H_{14}	97	115.9	32.07[5]	-	-	-
1-decene	$C_{10}H_{20}$	95	166.9	50.44	56.5	740.8	1.06
1-dodecene	$C_{12}H_{24}$	95	213.1	60.78	71.2	758.4	1.661
1-tetradecene	$C_{14}H_{28}$	92	251.1	-	80.3	775	2.503
8-methyl-hexadecane	$C_{17}H_{36}$	98	314.8[5]	53.05[5]	-	-	-
2, 6, 10, 14 -tetra-methyl-pentadecane	$C_{19}H_{40}$	98	166.1	56.34[5]	-	782.7	-

* = data taken at 40 °C, [1] = data from National Institute of Standards and Technology (2010), [2] = data from Murphy et al. (2004), [3] = data from Speight (2005), [4] = data taken from Champion and Meeten (1968) and [5] = data taken from online database (2011)

of tests with the sample fuel enabled both early detection and replacement of a deteriorating injector.

Table 6.2: Alkane and alkene fuel structures

1	Straight carbon chain length	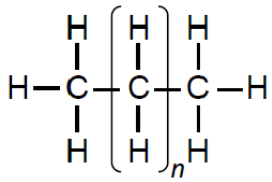 where n = 5 (n - heptane), 6, 8, 9, 10, 12, 13, 14, 16, 18 and 20 (n-docosane)
2	Degree of saturation	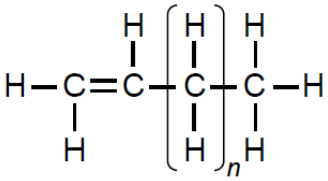 where n = 5 (1-octene), 7 (1-decene), 9 (1-dodecene) and 11 (1-tetradecene) 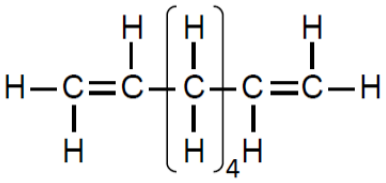 1, 7 octadiene
3	Carbon chain branching	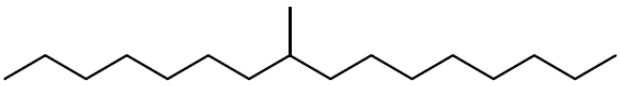 8 methyl - hexadecane 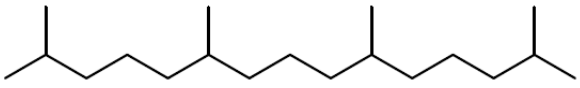 2, 6, 10, 14 tetra-methyl - pentadecane

6.1.3. Experimental conditions

Each of the 18 molecules was initially tested at the two experimental conditions of constant injection and constant ignition timing, as defined in Chapter 5.

After the initial two sets of experiments at constant injection and constant ignition timing were completed, a third series of experiments was carried out during which the ignition delay of different sample fuels was held constant by adding the radical providing ignition improver (2 EHN) in small concentrations of up to 2.9 % (wt/wt) to each test fuel, as described in Chapter 5.4. These experiments at constant delay were conducted at both a fixed SOI of 7.5 CAD and also a fixed time of SOC at TDC.

Where some of the test fuels were solid at room temperature, these were first melted in a PID controlled water bath held at 85 ± 2 °C prior to filling of the low volume fuel system which had been preheated to 85 ± 2 °C and was held at this temperature throughout the subsequent experiment.

All tests, irrespective of inlet air or fuel heating, were conducted at an engine speed of 1200 rpm and at 450 bar fuel injection pressure. The injection duration was adjusted between 708 - 861 µs in the case of every fuel, so that the engine IMEP was always constant at 4 bar for all fuels.

6.2. Results and discussion

All results presented in this work are the average of 100 combustion cycles. Table 6.3 shows the ignition delay and standard deviation of ignition delay for each fuel at both constant injection and constant ignition timing.

6.2.1. The effect of increasing the straight carbon chain length of n-alkanes

Figure 6.1 shows the ignition delay of the n-alkanes at constant injection and constant ignition timing. Experiments conducted at constant injection and constant ignition timing both show a strong correlation between straight carbon chain length of the n-alkanes and the duration of ignition delay (Figure 6.1). With increasing straight carbon chain length the duration of ignition delay decreases. For the experimental conditions tested this impact is largest for the shortest straight chain molecules tested. For example, addition of a carbon atom to a carbon chain length of 7 has more impact on delay than addition of a carbon to a chain length of 14.

Table 6.3: Ignition delay and standard deviation of ignition delay for each fuel

Fuel	Constant injection timing (SOI at 7.5 CAD BTDC)		Constant ignition timing (SOC at TDC)	
	Mean ignition delay (CAD)	1 σ	Mean ignition delay (CAD)	1 σ
Reference fossil diesel	7.4	0.3	7.3	0.3
n-heptane	7.4	0.1	7.5	0.2
n-octane	7	0.4	6.9	0.3
n-decane	6.3	0.0	6.1	0.0
n-undecane	5.8	0.4	5.8	0.2
n-dodecane	5.6	0.3	5.4	0.2
n-tetradecane	5.1	0.3	5	0.3
n-pentadecane	4.8	0.2	4.7	0.1
n-hexadecane	4.9	0.1	4.7	0.0
n-octadecane	4.4	0.1	4.4	0.1
n-eicosane	4.3	0.0	4.3	0.0
n-docosane	4.3	0.0	4.1	0.0
1-octene	9	0.7	8.7	0.4
1, 7 - octadiene*	13	2.8	12.2	0.7
1-decene	7.8	0.4	7.6	0.4
1-dodecene	7	0.4	7	0.2
1-tetradecene	6	0.5	5.9	0.4
8-methyl-hexadecane	5	0.0	4.9	0.0
2, 6, 10. 14-tetra-methyl-pentadecane	6	0.1	5.9	0.0

* = extrapolated to ambient conditions from data taken at an elevated inlet temperature of 135 °C

In Figure 6.1, it can be seen that beyond C18, extension of the chain length to C20 and C22 has only a small influence on ignition delay which is not greater than the resolution of the shaft encoder of 0.2 CAD.

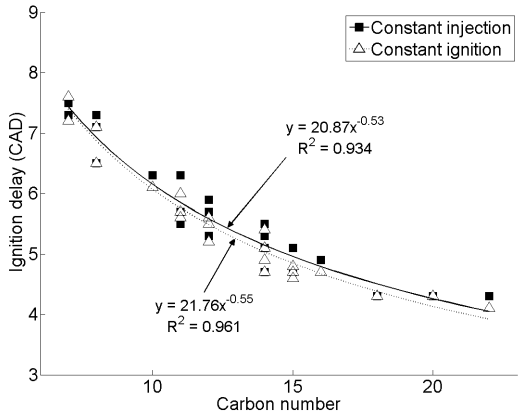

Figure 6.1: Ignition delay of the n-alkanes at constant injection and constant ignition timing

Figure 6.1 also shows a curve fit at constant injection timing corresponding to the expression $y = 20.87x^{-0.53}$ with an R^2 value of 0.93. All figures in this work only show such expressions where the confidence level has been determined as 98 % or higher. The form of the regression equation used $Y = Ax^b$ allows the exponent b to provide a measure of the impact x has on Y (e.g. ignition delay), because $\frac{\frac{dY}{Y}}{\frac{dx}{\bar{x}}} = b$. This means that a 1 % change in x will cause a b % change in Y, and so in Figure 6.1 for every 10 % increase in the carbon length, the ignition delay reduces by 5 %.

This significant trend is contrary to the results of Shen et al. (2009) obtained in shock tubes with premixed mixtures and the kinetic reaction mechanisms of Westbrook et al. (2008), who found no discernable trends in ignition delay with increasing straight carbon chain length. However, these results are in agreement with measurements of cetane numbers for n-alkanes (Knothe et al., 2006; Murphy et al., 2004) and ignition delays observed during engine experiments (Roy, 2005). A key difference between the this study and that of Shen et al. (2009) is that the latter utilised premixed fuel and air.

6.2.2. The impact on ignition delay of reducing the degree of saturation

Figure 6.2 shows the effect of introducing a single double bond to an alkyl chain at various carbon numbers and both constant injection and constant ignition timing. It can be seen from Figure 6.2, that forming double bonds by removing hydrogen atoms from a fully saturated straight chains results in an increase in ignition delay at

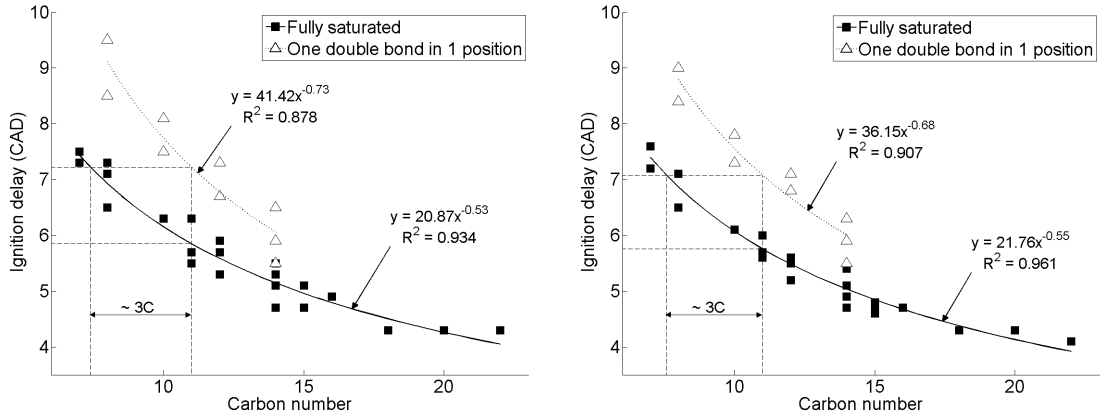

Figure 6.2: Effect of a double bond on ignition delay at varying carbon number at (a) constant injection and (b) constant ignition timing

constant injection and constant ignition timing. At both timing conditions (Figure 6.2), it can be seen that addition of a double bond has approximately the same effect on delay as the removal of 3 carbon atoms from the straight chain of a fully saturated molecule. Figure 6.2 show the exponents for the curves fitted to the double bonded results to be -0.73 for constant injection timing and -0.68 for constant ignition. These values imply that a 10 % increase in chain length of the double bonded molecules will result in a 6.8 - 7.3 % reduction in ignition delay, compared with 5.3 - 5.5 % for the saturated molecules. Therefore, it would appear that the delay is more sensitive to change in chain length when double bonds are included in the molecule.

Figure 6.3 shows the shift in ignition delay with percentage double bonds present at both constant injection and constant ignition timing. Results are shown for five molecules, four of which have one double bond but are of different carbon chain lengths, and one of which, 1, 7-octadiene, has two double bonds. In Figure 6.3, it can be seen that at both constant injection and constant ignition timing the shift in ignition delay correlates highly with the percentage of double bonds present and that the relationship is linear and close to a straight line. At both constant injection and constant ignition timing a 5 % increase in the percentage of double bonds present results in an increase in ignition delay of approximately 0.8 and 0.9 CAD respectively. The trends seen in Figure 6.3 are in agreement with those observed in Figure 6.2. As the relationship between the shift in ignition delay, due to the presence of double

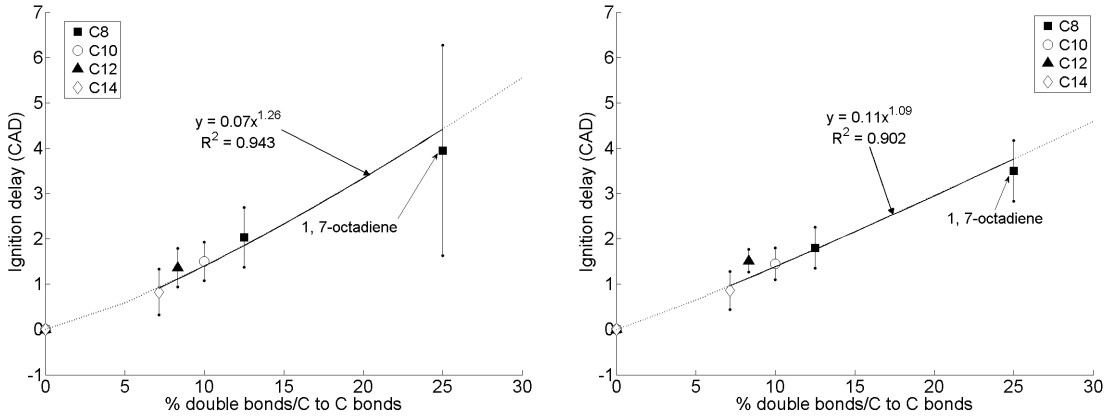

(a) (b)

Figure 6.3: Shift in ignition delay (relative to n-alkane of equivalent carbon chain length) with percentage double bonds present at (a) constant injection and (b) constant ignition timing

bonds, and the percentage double bonds present is linear and with an exponent close to 1 it follows that unsaturated molecules are more sensitive to changes in straight carbon chain length. Addition of a carbon atom to the straight chain length of a molecule containing a double bond reduces the percentage of double bonds present and thus the impact from un-saturation on ignition delay.

Results for 1, 7-octadiene in Figure 6.3 show large error bars implying poor test repeatability. This is caused to an extent by the poor ignition quality of this compound which necessitated inlet air heating to 135 °C for sustained combustion. Two of the other compounds in Figure 6.3 were also tested at this elevated temperature as well as at normal ambient temperature. The two sets of results for these compounds were used to normalise the ignition delay for 1, 7-octadiene to ambient conditions for plotting Figure 6.3.

6.2.3. Effect of branching in a fully saturated molecule on ignition delay

Figure 6.4 shows the effect on ignition delay of introducing branches to a fully saturated molecule at both timing conditions. In order to ascertain the effect of increased branching, two branched molecules were synthesised. The first one was a 17-carbon atom straight chain alkane with just one hydrogen replaced by a CH_3 methyl group (Table 6.2) resulting in 8 methyl-hexadecane. The second was a 19-carbon atom

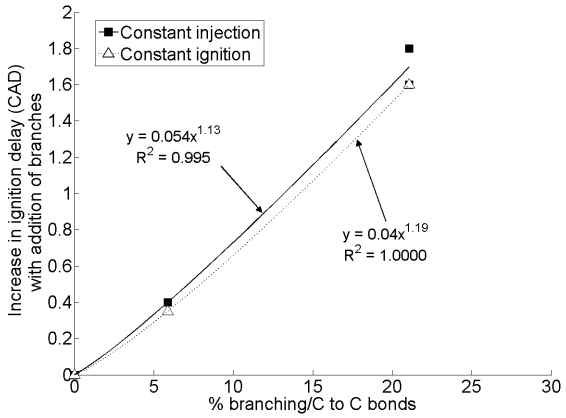

Figure 6.4: Shift in ignition delay with percentage branching present at constant injection and constant ignition timing

alkane compound in which four hydrogen atoms were replaced by four CH_3 methyl groups (Table 6.2) resulting in 2, 6, 10, 16-tetra-methyl-pentadecane. Figure 6.4 describes the impact of branching by plotting the shift in ignition delay (relative to an *n*-alkane with no branches and a straight carbon chain length equivalent to the total number of carbon atoms in the branched molecules) with the introduction of methyl branches against the percentage of carbon bonds which are present as methyl branches over the total number of carbon-to-carbon atoms.

For both constant injection and constant ignition timing the relationship found shows a very strong correlation and a linear trend close to a straight line (Figure 6.4). As with the presence of double bonds, the impact of branching is slightly higher in experiments conducted at constant injection timing relative to constant ignition timing, and this may be due to differing in-cylinder volumes at SOC. For either timing condition, a 5 % increase in the percentage of branched molecules present results in an increase in ignition delay of approximately 0.4 CAD.

6.2.4. Quantification of the impact on ignition delay of various molecular structures

Table 6.4 quantifies the effects of molecular structure on ignition delay. The results in the table were obtained using the regressions in Figures 6.1 to 6.4. Accordingly, Table 6.4 shows the change in ignition delay when each of the three structural properties considered, straight carbon chain length, percentage of double bonds

Table 6.4: Relative impacts of structure on ignition delay, at constant injection and constant ignition timing

Carbon chain length	% Shift in ignition delay (CAD) relative to the base n-alkane						
	% increase	Straight carbon chain length		Double bonds		Branching	
		Constant injection	Constant ignition	Constant injection	Const ignition	Constant injection	Constant ignition
C10	10	-4.93	-5.15	22.69	22.83	11.87	10.85
	20	-9.22	-9.62	54.23	48.6	26.03	24.78
C16	10	-4.93	-5.15	29.11	29.63	15.23	14.08
	20	-9.22	-9.62	69.59	63.06	33.41	32.16

present and percentage of branched carbons present, are increased by 10 and 20 % at a total carbon number of C10 and C16. It can be seen that introducing a double bond into a straight carbon chain results in approximately twice the increase in ignition delay, at both constant injection and constant ignition timing, as that observed when removing a carbon atom and associated hydrogen from a straight chain and reattaching as a methyl branch. Furthermore, when increasing either the presence of double bonds or methyl branches, over the range of molecules tested, increasing the straight, fully saturated, carbon chain length by an equivalent percentage is not sufficient to offset the increase in ignition delay.

6.2.5. Ignition delay influence on combustion phasing and the level of exhaust emissions

The results of all experiments at both constant injection and constant ignition timing showed that the primary driver of combustion phasing and the formation of emissions was the ignition delay. Furthermore, the results showed that the structure of the fuel molecule has a large influence on ignition delay.

Figure 6.5 shows the influence of ignition delay on peak heat release at both constant injection and constant ignition timing. It can be seen that the peak heat release rate reached within a combustion cycle correlates strongly with the duration of ignition delay (Figure 6.5), and that at both constant injection and constant

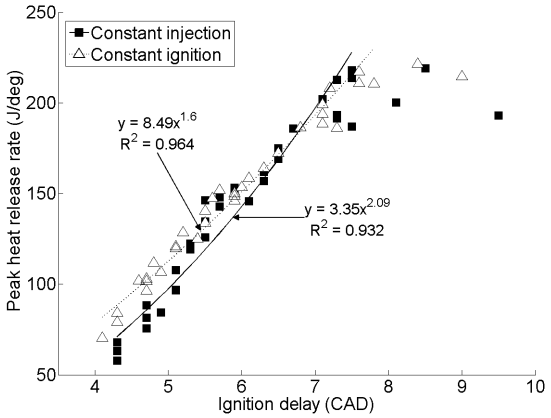

Figure 6.5: Impact of ignition delay on peak heat release

ignition timing, an increase in ignition delay resulted in a higher rate of peak heat release rate. Figure 6.5 suggests that the relationship between the peak heat release rate and delay is approximately linear up to a delay of about 7.5 CAD, beyond which the delay is seen to cause little further increase in the heat release rate. Within the range of ignition delay for which the relationship appears to be linear (4 to 7.5 CAD) , the regression showed that a 10 % increase in ignition delay results in a 21 % increase in the peak heat release rate at constant injection and at constant ignition timing a 10 % increase in ignition delay results in a 16 % increase in peak heat release rate. The difference between the two timings (21 % vs 16 %) is likely to be related to differences in the combustion volume during premixed combustion.

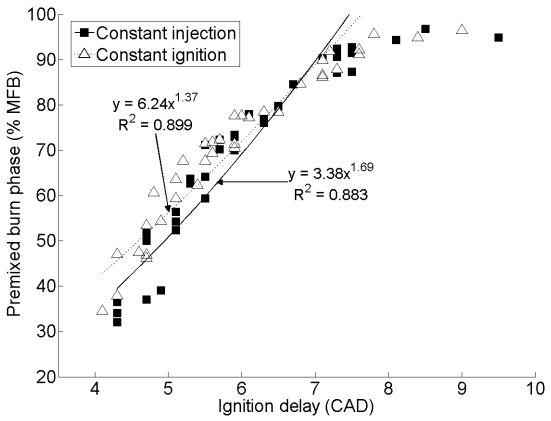

Figure 6.6: Impact of ignition delay on the premixed burn fraction

Figure 6.6 shows the impact of ignition delay on the premixed burn fraction at both timing conditions, with a strong relationship between the two evident. The premixed burn phase is defined as the combustion of fuel which has mixed with air to within the flammability limits during the ignition delay period (Heywood, 1988), and has been derived from the measurements of peak heat release rate (Section 4.1.5). As ignition delay increases the fraction of fuel burnt in premixed mode also increases and it follows that the duration of ignition delay will directly influence the extent of the premixed combustion phase, a longer ignition delay will allow more time for fuel to mix with air and prepare regions of mixture which are near enough to stoichiometric conditions to combust when autoignition occurs. Furthermore, a greater proportion of premixed fuel and air will see more energy released in the initial premixed burn phase of combustion and thus greater cylinder pressures and peak heat release rates reached, as seen in Figure 6.5.

A good fit of both constant injection and constant ignition timing data to a linear relationship was found except at very long ignition delays (< 7.5 CAD). Clearly, as the premixed fraction of the fuel burnt becomes 100 % one could no longer expect the delay to have an influence on premixed fraction burned. The longest injection duration used of 861 μs is equivalent to 6.2 CAD at 1200 rpm. Therefore, allowing for a probable lag in injector response, at approximately 7.5 CAD autoignition is occurring after the end of injection (rather than during injection as is the case for shorter ignition delays). This is possibly one reason why the delay ceases to have an influence on the peak heat release rate in Figure 6.5 for delay greater than 7.5 CAD. Where the linear relationship is valid a 10 % increase in ignition delay results in a 17 % and 14 % increase in the premixed burn fraction, at constant injection and constant ignition timings respectively.

Figure 6.7 shows the effect of ignition delay on maximum in-cylinder global temperature, and shows a strong positive correlation at both constant injection and constant ignition timing. A 10 % increase in ignition delay at constant injection and constant ignition timing results in a 1.5 % (45 K) and 2 % (55 K) rise in maximum global temperature respectively.

An influence of peak heat release (Figure 6.6) on the magnitude of the in-cylinder temperatures reached Figure (6.7) is to be expected, as it follows that higher temperatures will be reached when energy is released more rapidly in a system where heat transfer to the cylinder walls occurs. Furthermore, at constant ignition timing

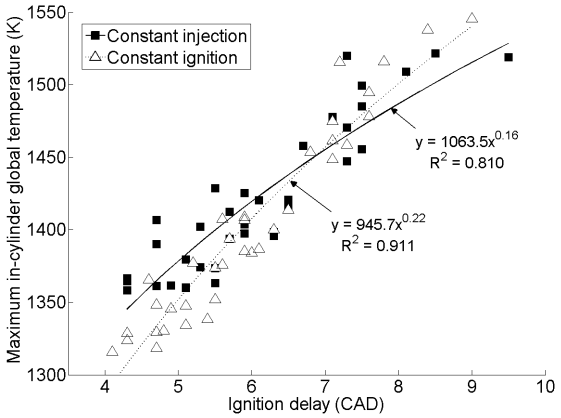

Figure 6.7: Effect of ignition delay on maximum in-cylinder global temperature at constant injection and constant ignition timing

combustion occurred later in the expansion stroke in a larger cylinder volume with more opportunity for heat transfer to the cylinder walls. This accounts for the difference in gradient observed between results in Figure 6.7 for constant injection and constant ignition timing experiments.

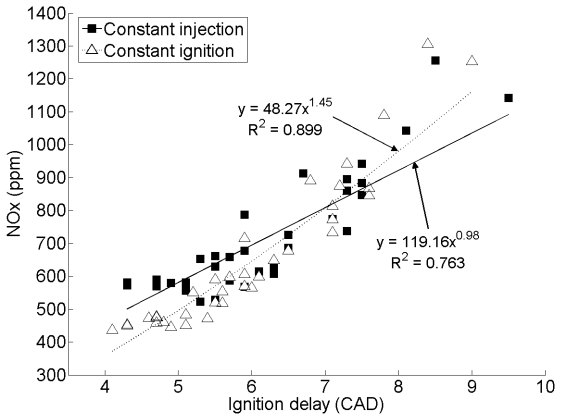

Figure 6.8: Impact of ignition delay on emission of NO_x at constant injection and constant ignition timing

Figure 6.8 shows the influence of ignition delay on exhaust levels of NO_x, which can be seen to increase linearly with increasing ignition delay at both constant injection and constant ignition timing. The correlation is strongest and more sensitive when considering the results of constant ignition timing and this is in agreement with the peak heat release rate at constant ignition timing (Figure 6.5). Figure 6.8 shows

that a 10 % increase in ignition delay at constant ignition timing resulted in a 14 % increase in NO_x emissions, whereas at constant injection timing a 10 % increase in ignition delay resulted in a 10 % increase in NO_x emissions. Thus the exhaust level of NO_x is very sensitive to the maximum global in-cylinder temperature (which is representative of local temperatures) and this is in agreement with the experimental work of Schönborn et al. (2009b) and Mueller et al. (2009).

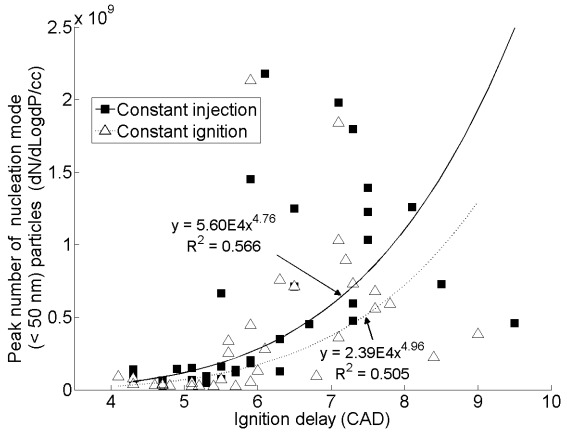

Figure 6.9: Influence of ignition delay on the peak number of nucleation mode (Dp < 50 nm) particles

Figure 6.9 shows the influence of ignition delay on the peak number of nucleation mode particles (Dp < 50 nm) at both constant injection and constant ignition timing. Figure 6.9 is suggestive of a trend of an increasing peak number of nucleation mode particles with increasing ignition delay (though only at an ignition delay of > 5.5 CAD), at both constant injection and constant ignition timing although the scatter in Figure 6.9 is substantial. One possible explanation for the increasing peak number of nucleation particles as the delay rises above 5.5 CAD is that this rise in number is caused by rising global temperature (Figure 6.7). The fuel pyrolysis reactions that provide the poly-aromatic hydrocarbon radicals required for nucleation reactions are known to be highly temperature dependent (Tree and Svensson, 2007). Levels of nucleation mode particles are also known to correlate with levels of un-burnt hydrocarbons in exhaust gases, as nucleation mode particles can arise from incomplete combustion and it has also been speculated that some nucleation mode particles are condensed droplets of un-burnt fuel (Schönborn et al., 2009b).

Figure 6.10 shows the influence of ignition delay on the levels of total hydrocarbons in the exhaust gases at both constant injection and constant ignition timing. While,

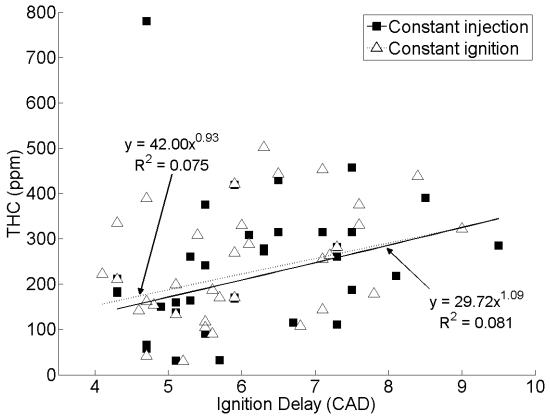

Figure 6.10: Effect of ignition delay on exhaust gas levels of THC at constant injection and constant ignition timing

at both timing conditions, there is a suggestion of increasing levels of hydrocarbons with increasing duration of ignition delay there is a large degree of scatter in results (Figure 6.10). However, when investigated, no direct correlation between levels of hydrocarbons and the peak number of nucleation mode particles (Figure 6.9) was found.

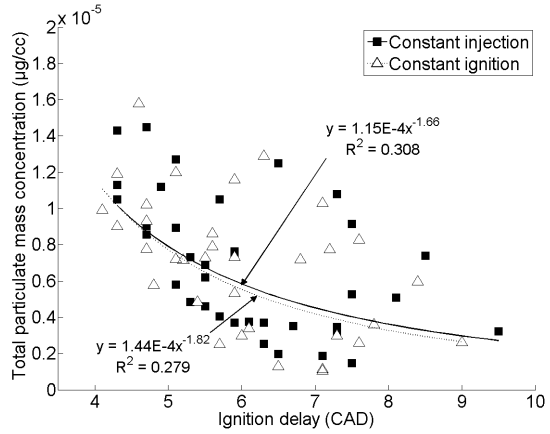

Figure 6.11: Effect of ignition delay on total mass of particulates emitted at constant injection and constant ignition timing

Figure 6.11 shows the correlation between total mass of particulates emitted and the duration of ignition delay to be a poor one; Figure 6.11 suggests that the total particulate mass may decrease with increasing delay but the uncertainty of such a suggestion is large. While not exclusive, it is possible that ignition delay may

be an influence with longer ignition delays leading to higher global temperatures (Figure 6.7) and improved soot oxidation (both due to elevated temperatures and increased fuel air mixing). This observation agrees with the proposed model for soot oxidation and production reviewed by Tree and Svensson (2007). However, it is evident from the large variance of the results in Figures 6.9 and 6.11 for both constant injection and constant ignition timing that factors other than ignition delay strongly influence both the peak number of nucleation mode particles produced and the total mass concentration of soot in the exhaust gases.

6.2.6. Combustion phasing and emissions when ignition delay is removed as a variable

The previous sections show that ignition delay has a large influence on combustion and emissions. A question that remains is whether other influences exist which are overshadowed by ignition delay and thus further experiments were conducted in which the ignition improving additive 2 EHN was utilised. However, equalising the ignition delay of all 18 widely different molecules tested to a single value of delay was not practical due to the large spread observed in the delays at constant injection and constant ignition timing; neither was it desirable, as 2 EHN contains fuel bound nitrogen which may contribute to total NO_x emissions. Therefore the 18 molecules tested were grouped into five sets and each set was equalised to one of five values of constant ignition delay. In fact some of the molecules in each set had their delay equalised to the delay of some of the other sets so as to allow overlap and normalisation of all 18 molecules to a single ignition delay through post processing of the experimental results. Having five sets of molecules minimised the use of 2 EHN while still disrupting the relationship between molecular structure and ignition delay. Results of constant ignition delay timing experiments are those of the five separate and overlapping (by carbon number) trend lines normalised to single constant ignition delay (see Appendix E.1 for an explanation of the methodology employed).

Figure 6.12a shows the effect of carbon number on peak heat release rate when both the ignition delay and injection timing were held constantn (fixed SOI timing). Figure 6.12b shows the corresponding effect on peak heat release rate when both ignition delay and ignition timing were held constant (SOC at TDC timing). It can be seen that removing carbon atoms from the straight carbon chain and reattaching

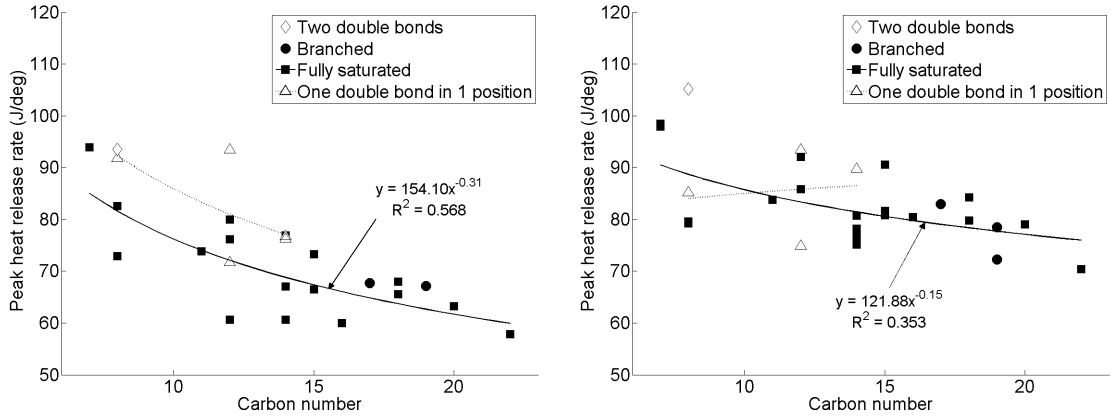

(a) (b)

Figure 6.12: The influence of carbon number on peak heat release rate with ignition delay removed as a variable at (a) fixed SOI timing, and (b) SOC at TDC timing

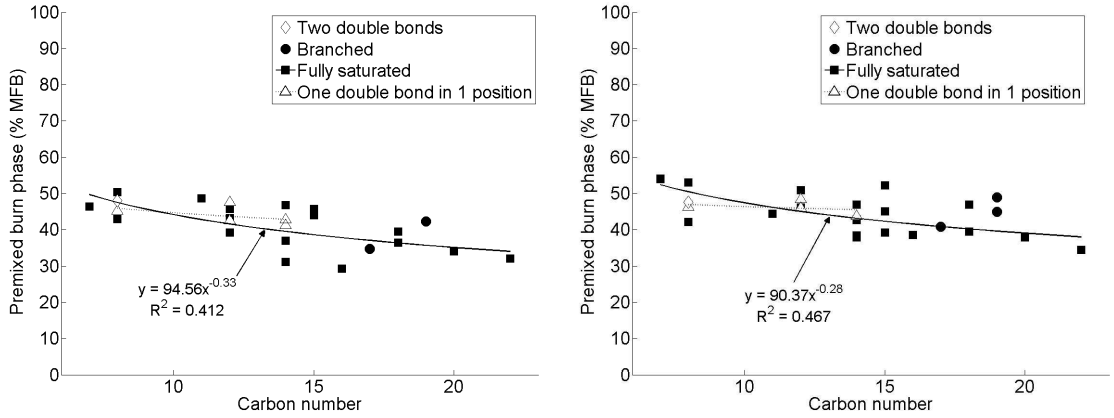

(a) (b)

Figure 6.13: The impact of carbon number on premixed burn fraction with ignition delay removed as a variable at (a) fixed SOI timing, and (b) SOC at TDC timing

as methyl groups does not appear to impact on the peak heat release rate (Figure 6.12). Both Figures 6.12a and 6.12b show a degree of correlation between peak heat release rate and carbon number, with the peak heat release rate becoming lower as the carbon number increases.

Figures 6.13a and 6.13b show that at constant ignition delay, there is a trend at both fixed SOI and SOC at TDC timing of decreasing premixed burn fraction with increasing carbon number for all the molecules tested including those with double bonds and methyl branches. This coincides with the observed decrease in peak heat release rate in Figures 6.12a and 6.12b, and is in agreement with the observed relationship between peak heat release rate and premixed burn fraction with ignition delay present as a variable (Section 6.2.5).

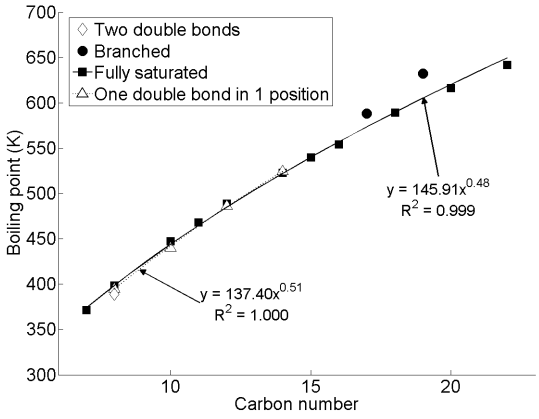

Figure 6.14: Correlation between carbon number and boiling point

Figure 6.14 shows the relationship between carbon number and boiling point, and it can be seen that there is a strong positive correlation which shows no influence of double bonds or from the presence of branches. It is tentatively suggested that this trend of increasing boiling point with carbon chain length may explain the observed decrease in the premixed burn fraction at constant ignition delay timings.

With the delay being held constant, the duration available for the mixing of fuel and air prior to SOC is held constant; however, there is no control on the rate at which the fuel and air mix. Molecules of higher carbon number have higher boiling points and values of enthalpy of vaporisation(Table 6.1) and one can expect them to vaporise more slowly, resulting in a lower premixed burn fraction as seen in Figures 6.13a and 6.13b.

This impact of boiling point and enthalpy in determining the premixed quantity of fuel is not visible when ignition delay is present as a variable because of the large effect of delay itself on the premixed amount of fuel, tending to mask out these secondary influences. It is worth noting at this point that ignition delay correlates highly with boiling point and enthalpy of vaporisation and for this reason it would be

impossible to separate the effect of delay from those of the boiling point and latent heat of vaporisation using regression techniques or design of experiment approach. The only way that the subtle effects of boiling point and enthalpy of vaporisation can be revealed is by actually holding delay constant with small quantities of 2 EHN.

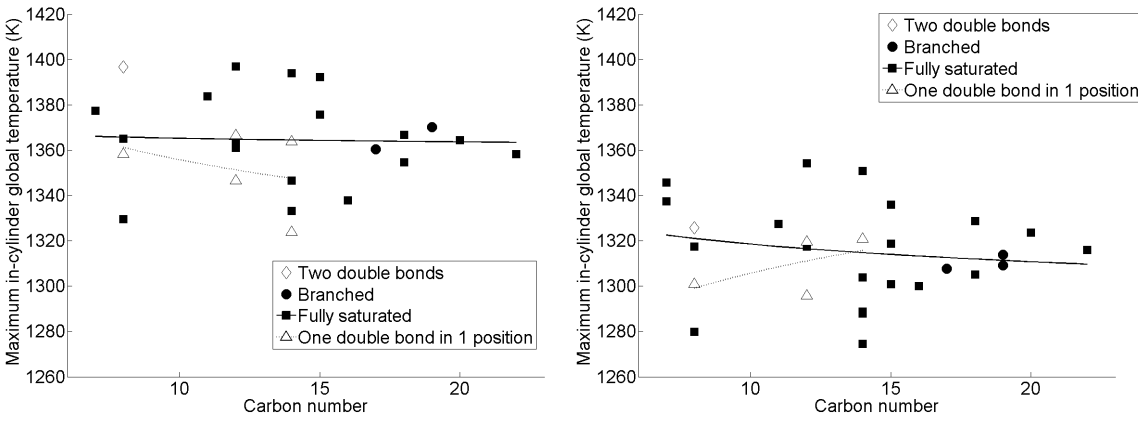

Figure 6.15: The effect of carbon number on maximum in-cylinder global temperature with ignition delay removed as a variable at (a) fixed SOI timing, and (b) SOC at TDC timing

Figures 6.15a and 6.15b show no discernable impact of molecular structure on maximum global temperature at constant ignition delay. A trend similar to that observed in peak heat release (Figure 6.12) might have been expected. However, while ignition delay has been removed as a variable, the variation in in-cylinder volume at time of peak heat release rate has not been removed as a variable and this may impact significantly on the maximum global temperature.

Figures 6.16a and 6.16b show the influence of carbon number on NO_x emissions at both fixed SOI and SOC at TDC timing, and suggest that molecules having double bonds tend to generate larger levels of NO_x emissions in comparison with fully saturated and branched molecules.

The results further suggest that molecules containing two double bonds will generate significantly higher levels of NO_x than molecules containing one double bond. Schönborn et al. (2009b) found an influence of adiabatic flame temperature on levels of NO_x formation. For this reason, the adiabatic flame temperature at constant pressure was calculated according to the method described in Chapter 4.4, for a constant

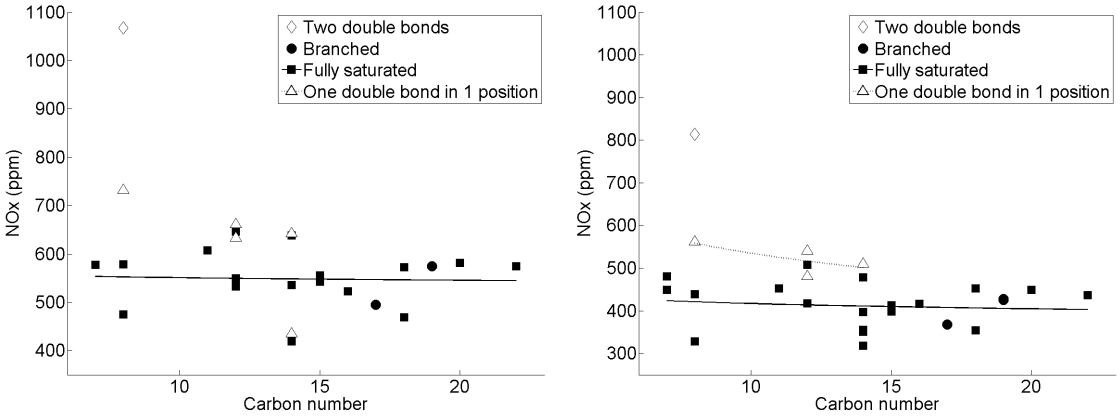

Figure 6.16: The impact of carbon number on NO_X emissions with ignition delay removed as a variable at (a) fixed SOI timing, and (b) SOC at TDC timing

initial temperature of 800 K which is representative of measured maximum global in-cylinder temperatures immediately before SOC.

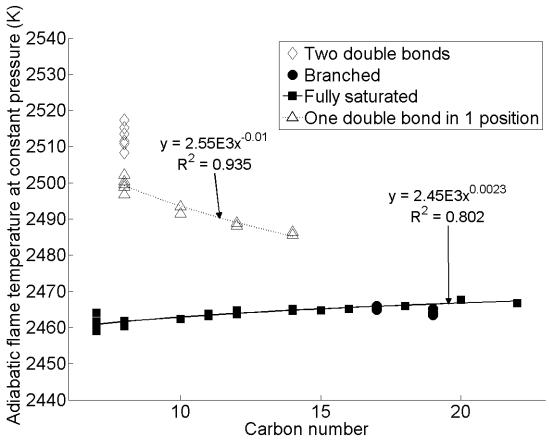

Figure 6.17: Effect of carbon number on the calculated adiabatic flame temperature at constant pressure, for constant initial temperature, where repeat points indicate the influence of 2 EHN

Figure 6.17 shows the effect of carbon number, degree of saturation and presence of branches on adiabatic flame temperature. Figure 6.17 shows strikingly that the presence of a double bond increases the adiabatic flame temperature; furthermore that as the percentage of double bonds increase the adiabatic flame temperature

increases even further. Therefore, it would appear that, at constant ignition delay timing, the increase in NO_x production by unsaturated molecules is attributable to an increased production of NO_x by the thermal mechanism due to a higher flame temperature during combustion.

A second trend in adiabatic flame temperature is apparent in Figure 6.17, namely that of increasing adiabatic flame temperature with increasing straight carbon chain length in fully saturated molecules. This trend is very clear but also very small, for example, an increase in carbon number from 7 (*n*-heptane) to 22 (*n*-docosane) raises the adiabatic flame temperature by only 7 K from 2461 to 2468 K. This trend in slowly rising adiabatic flame temperature is not however reflected in rising NO_x in either Figures 6.16a or 6.16b. It may be that the effect on NO_x of the small rise in adiabatic flame temperature is offset by the lower rates of peak heat release observed in Figures 6.12a and 6.12b and so there is no net increase in thermal NO_x production.

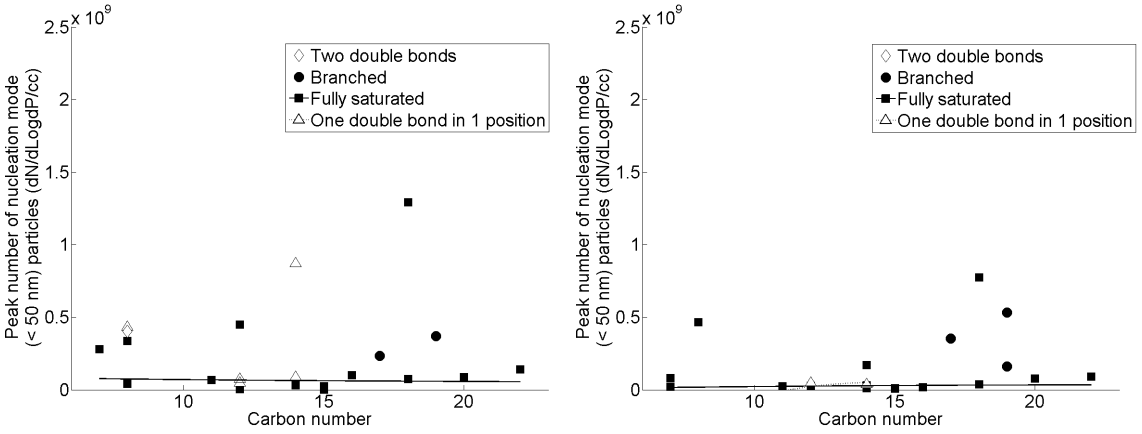

Figure 6.18: The influence of carbon number on the peak number of nucleation mode particles (Dp < 50 nm) with ignition delay removed as a variable at (a) fixed SOI timing, and (b) SOC at TDC timing

Figures 6.18a and 6.18b show the influence of carbon number on the peak number of nucleation mode particles (Dp < 50 nm) with ignition delay removed as a variable at constant ignition delay fixed SOI and SOC at TDC timing. It can be see that with ignition delay removed as a variable, no discernable impacts on the peak number of nucleation mode particles attributable to specific molecular features are present

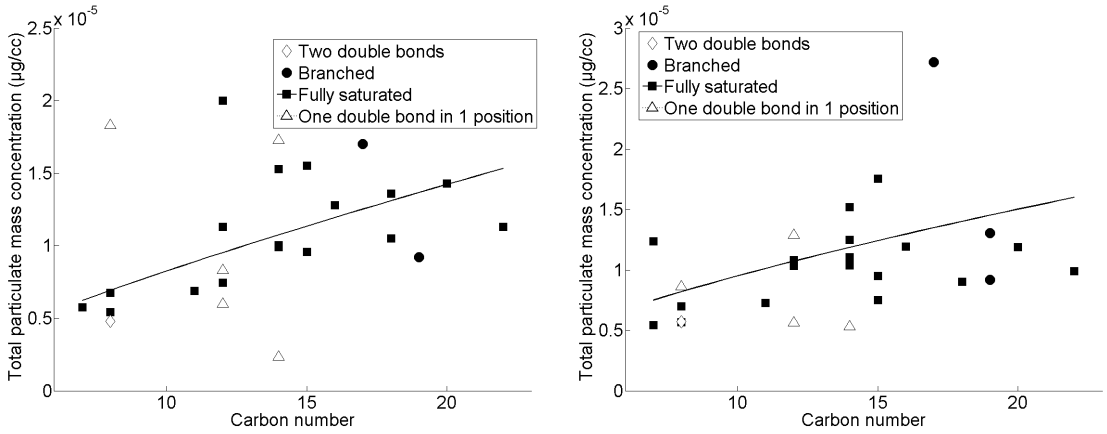

Figure 6.19: The influence of carbon number on total particulate mass produced with ignition delay removed as a variable at (a) fixed SOI timing, and (b) SOC at TDC timing

(Figures 6.18a and 6.18b). Figures 6.19a and 6.19b show that with ignition delay removed as a variable, the total mass of particulates tends to increase with carbon number, although the scatter in both figures is large at both constant injection and constant ignition timing. Both Figures 6.19a and 6.19b do not show any clear influence of double bonds and branches on particulate total mass. These results are contradictory to results obtained in laminar diffusion flames where the presence of a double bond and branches increases substantially the soot production rate in comparison to the production rate for fully saturated alkanes (Ladommatos et al., 1996).

6.3. Conclusions

1. In non-oxygen bearing hydrocarbons, the primary influence on combustion and exhaust emissions of NO_x and particulates is the ignition delay.

2. The following all increase ignition delay: reducing the straight carbon chain length of a molecule; removing hydrogen to introduce a double bond into a molecule; and or removing a carbon atom from the straight chain length and reattaching it as a methyl branch. The impact on ignition delay due to

un-saturation is approximately twice that due to branching (when the same percentage of carbon atoms is involved).

3. Ignition delay is the major factor that determines the extent of fuel and air premixing prior to the start of combustion. In turn the amount of premixed fuel determines both the peak heat release rate and the maximum global temperature reached within the cylinder; both NO_x and soot emissions are highly temperature sensitive. Thus for a longer ignition delay, where more time is available for fuel and air mixing, the rate of peak heat release will be higher and production of thermal NO_x will increase, while oxidation of soot particles will also increase, in general, reducing the total mass of particulates produced.

4. A secondary influence of molecular structure on levels of NO_x formation is the adiabatic flame temperature. Structurally the most significant feature of a molecule in determining the adiabatic flame temperature is the presence of double bonds which increase the flame temperature and thus NO_x formation by the thermal mechanism.

5. With ignition delay removed as a variable, it appears that physical properties such as boiling point may influence the rate at which fuel and air mix and thus the extent of the premixed burn phase and peak heat release rate. As carbon number increases both the boiling point and the enthalpy of vaporisation of a molecule rise irrespective of the presence of double bonds or methyl branches. It is suggested that these properties limit the rate at which fuel and air mix for a given duration of ignition delay, thus causing a reduction in premixed burning with higher carbon number molecules.

7. The importance of double bond position and cis - trans isomerisation

The impact of fuel saturation on compression ignition combustion and emissions has been the subject of numerous studies, the bulk of which have been concerned with the suitability of various saturated fatty acids for FAME production (Benjumea et al., 2010; Fisher et al., 2011; Knothe et al., 1997; McCormick et al., 2001; Schönborn et al., 2009b). Furthermore, the presence of double bonds within non-oxygenated compounds was considered in Chapter 6. While the effect of moving a single double bond within an alkyl chain and the arrangement of that bond has received less attention the following observations have been made: *cis* isomers are of equivalent or higher ignition quality than *trans* isomers of otherwise identical molecular structure (Salooja, 1968; Hughes and Prodhan, 1973), and movement of a single double bond towards the centre of an alkyl chain reduces ignition quality (Tanaka et al., 2003; Vanhove et al., 2005; Zhang et al., 2009).

The current chapter presents the results of engine experiments in which a series of octene isomers were tested. The isomers were chosen to investigate the effect of double bond position and *cis* versus *trans* isomerisation on compression ignition combustion and emissions. Relative to previous studies on this subject, this work is the first to utilise a modern direct injection compression ignition engine and to consider alkenes of longer carbon chain length than heptene.

7.1. Experimental method

7.1.1. Apparatus

All of the combustion experiments described in the present chapter were performed using the compression ignition engine and ultra low volume fuel system described in Chapter 3.

7.1.2. Fuel molecules investigated

Four octene isomers were tested as pure components so as to investigate the effect of the following molecular structural properties on compression ignition combustion and emissions:

(a) The position of a double bond within an un-branched alkene.

(b) *cis* versus *trans* isomerisation in an un-branched alkene, with constant double bond position.

To observe the impact of moving the position of the single double bond towards the centre of the alkyl chain, 1-octene, *trans*-2-octene and *trans*-3-octene were selected. To allow a comparison of *cis* and *trans* isomerisation, *cis*-3-octene was chosen. A further two reference fuels were also tested, *n*-octane and a fossil diesel with zero FAME content. Two of the pure component fuels, *n*-octane and 1-octene, were obtained from a chemical supplier (Sigma Aldrich), while the remaining octene isomers were specially synthesized by an organic synthesis company (further details are given in Appendix D.1). The assay and other properties of each fuel are presented in Table 7.1, while the molecular structure of each is given in Table 7.2.

Table 7.1: Properties of *n*-octane, octene isomers and reference fossil diesel

Fuel	Molecular formula	Assay (%)	T_{boil} (°C)	T_{melt} (°C)	△vapH° (kJ/mol)	Cetane number	Density (kg/m^3)	Dynamic viscosity at 20 °C (mPa.s)	Lower heating value (MJ/Kg)
Reference fossil diesel	-	-	268.9‡	-	-	51.7$^{\bullet}$	834.5$^{\diamond}$	-	43.14†
n-octane	C_8H_{18}	98	125.7[1]	-56.9[2]	41.53[3]	64.1[4]	702.8[5]	0.546[5]	44.79[6]
1-octene	C_8H_{16}	98	121.3[7]	-102.6[7]	40.44[3]	40.8[4]	714.9[5]	0.47[5]	44.56[12]
trans-2-octene	C_8H_{16}	98	124.9[7]	-87.8[7]	34.3[8]	-	718.42[9]	0.48[10]	44.45[11]
cis-3-octene	C_8H_{16}	98	122.7[7]	-137.5[7]	40.78[10]	38.09*	718.88[9]	0.52[10]	44.49[11]
trans-3-octene	C_8H_{16}	98	123.3[7]	-110.1[7]	40.45[10]	33.98*	716.3[9]	0.51[10]	44.46[11]

† = calculated from experimental data obtained by the IP12 method (Institute of Petroleum, 2001), $^{\diamond}$ = experimental data obtained according to ASTM D4052 at 15 °C, $^{\bullet}$ = experimental data obtained according to EN ISO 516, ‡ = experimental data obtained according to EN ISO 3405, * = from IQT of samples used in this study, [1] = data from Hiaki et al. (1995), [2] = data from Ott and Goates (1983), [3] = data from Majer et al. (1985), [4] = data from Murphy et al. (2004), [5] = data from Speight (2005), [6] = data from Prosen and Rossini (1945), [7] = data from Henne and Greenlee (1943), [8] = data from Hopfe (1990), [9] = data from Campbell and Eby (1941), [10] = data from Liessmann et al. (1995), [11] = data from Alberty and Gehrig (1984) and [12] = data from Rockenfeller and Rossini (1961).

Table 7.2: Structures of *n*-octane, octene isomers and fuel additive

n-octane	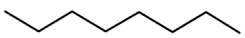
1-octene	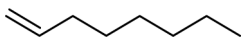
trans-2-octene	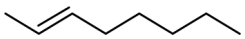
cis-3-octene	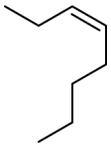
trans-3-octene	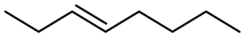
2-ethylhexyl nitrate	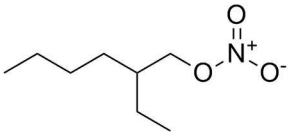

7.1.3. Experimental conditions

Each of the five molecules and reference diesel were initially tested at the two experimental conditions of constant injection and constant ignition timing, as defined in Chapter 5.

After the initial two sets of experiments, at constant injection and constant ignition timing were completed, a third series of experiments was carried out during which the ignition delays of some the different sample fuels were held constant, utilising 2 EHN as described in Chapter 5.

All tests were conducted at an engine speed of 1200 rpm and at 450 bar fuel injection pressure. The experiments presented were conducted in two batches: in the first the injection duration was adjusted in the case of every fuel so that the engine IMEP was always constant at 4.12 bar for all fuels and in the second the injection duration was adjusted for a constant IMEP of 3.96 bar for all fuels. A summary of the engine and test operating conditions is given in Table 7.3.

Table 7.3: Octene isomers engine and test operating conditions

Fuel	2 EHN dosage (ppm)	Engine speed (rpm)	Fuel injection pressure (bar)	IMEP (bar)	Constant injection timing (SOI at 7.5 CAD BTDC)						Constant ignition timing (SOC at TDC)					
					Ignition delay (CAD)		Injection duration (µs)		Indicated thermal efficiency (%)		Ignition delay (CAD)		Injection duration (µs)		Indicated thermal efficiency (%)	
					Mean	1σ	Mean	1σ	Mean	1σ	Mean	1σ	Mean	1σ	Mean	1σ
Reference fossil diesel	0	1200	450	4.04 ± 2 %	6	0.14	701	10	38.81	0.22	5.9	0.06	704	11	38.34	0.16
n-octane	0	1200	450	4.04 ± 2 %	5.6	0.09	726	3	38.81	0.11	5.5	0.05	725	4	38.75	0.09
1-octene	0	1200	450	4.04 ± 2 %	6.8	0.1	729	3	38.61	0.06	6.7	0.15	730	2	38.44	0.07
trans-2-octene	0	1200	450	4.04 ± 2 %	8.7	0	727	6	39.06	0.07	8.8	0.05	737	9	38.58	0.05
cis-3-octene	0	1200	450	4.04 ± 2 %	7.6	-	728	-	38.85	-	7.6	-	729	-	38.35	-
trans-3-octene	0	1200	450	4.04 ± 2 %	8.4	-	731	-	39.28	-	8.2	-	737	-	38.36	-
1-octene	6029	1200	450	4.04 ± 2 %	5.7	-	729	-	-	-	5.5	-	729	-	38.48	-
trans-2-octene	14247	1200	450	4.04 ± 2 %	5.5	-	727	-	38.09	-	5.5	-	728	-	38.28	-

7.2. Results and discussion

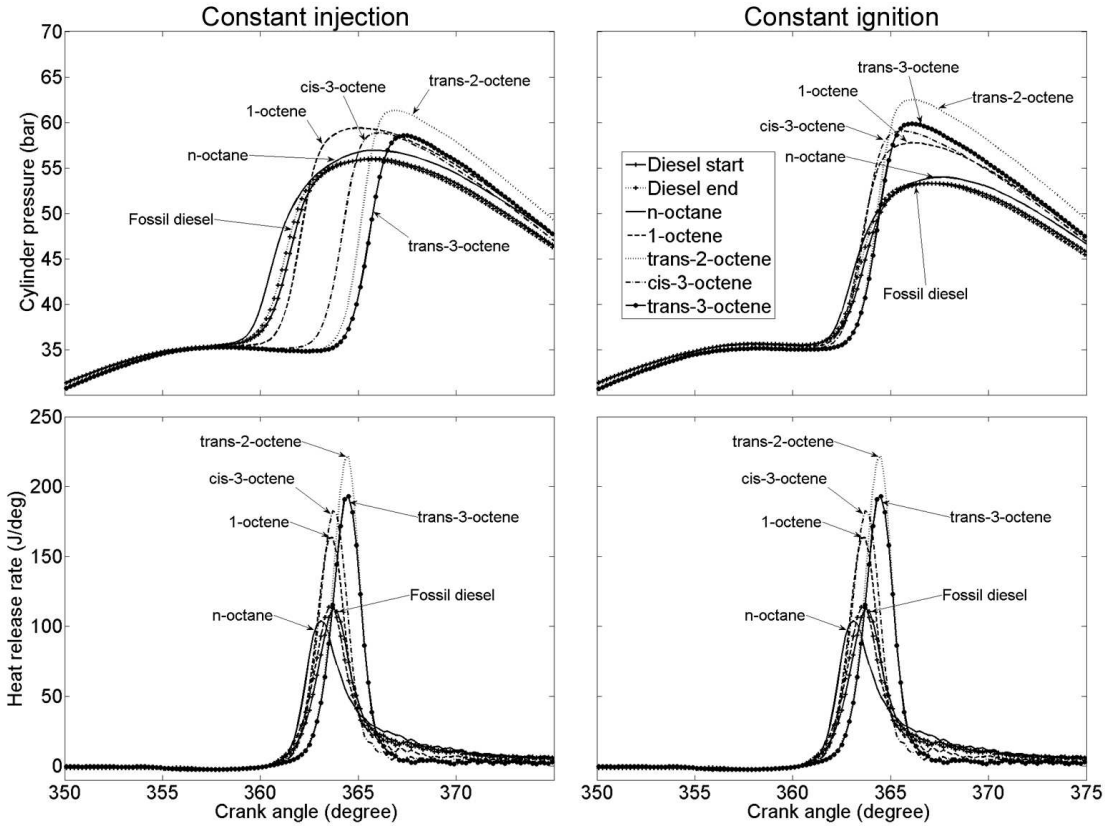

Figure 7.1: In-cylinder pressures and apparent net heat release rates of *n*-octane, octene isomers and reference fossil diesel at constant injection and constant ignition timing

Figure 7.1 shows the in-cylinder pressures and apparent net heat release rates of *n*-octane, the octene isomers and the reference fossil diesel at constant injection and constant ignition timing. Immediately apparent is the increase in ignition delay (as defined in Chapter 4.1.3 as the interval in CAD between SOI and SOC), and the resultant increase in peak in-cylinder pressure and apparent heat release rate, with movement of the double bond in the octene isomers from the 1 position to either the 2 or 3 position (Figure 7.1). At constant ignition timing it can be seen that for *trans*-2-octene and *trans*-3-octene, the heat release rate curves indicate a slower rate of premixed combustion after SOC relative to the other fuels. Also visible is a decrease in the diffusion controlled burn fraction with the introduction of a double bond (*n*-octane to 1-octene) and subsequent movement of the double

bond towards the centre of the molecule, with premixed combustion dominating heat release (Figure 7.1).

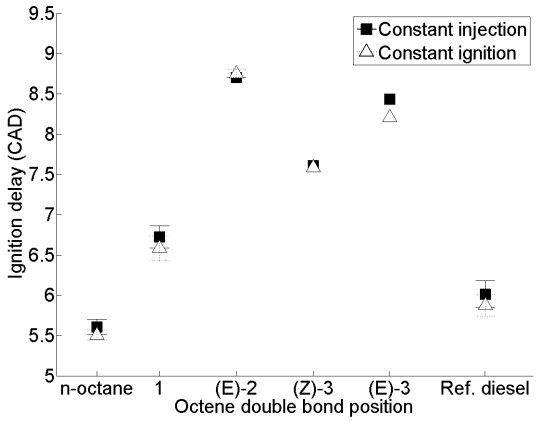

Figure 7.2: Ignition delays of octene isomers, *n*-octane and reference diesel at constant injection and constant ignition timings (normalised for constant IMEP)

Figure 7.2 shows the ignition delays of the octene isomers, n - octane and the reference fossil diesel at constant injection and constant ignition timing and normalised for a constant IMEP of 4.12 bar (the method of normalisation ultised is described in Appendix E.2). From Figure 7.2 it can be seen that moving the double bond position of octene from 1 to 2 results in an increase in ignition delay at both timing conditions, and that this increase is more significant than the introduction of a terminal double bond to *n*-octane to form 1-octene. However, further movement of the double bond towards the centre of the molecule reduces the duration of ignition delay, in the case of both *cis*- and *trans*-3-octene.

The values of ignition delay presented in Figure 7.2 are defined as the interval between SOI and the first appearance of positive apparent heat release for each fuel (SOC). In the heat release rate traces of Figure 7.1, it can be seen, in particular at constant injection timing, that the octene isomers all exhibit a cool flame period after the SOC. At constant ignition timing (Figure 7.1), it can be seen that 1-octene and *cis*-3-octene display approximately equal duration cool flame periods, with *trans*-2-octene and *trans*-3-octene both showing a longer cool flame period. However, at constant injection timing (Figure 7.1), where the ignition delay of *trans*-3-octene was found to be 0.3 CAD less than that of *trans*-2-octene (Figure 7.2), it can be seen that *trans*-3-octene actually displays a longer cool flame period than *trans*-2-

octene. Considering the effect of the double bond configuration, it can be seen that the ignition delay of *cis*-3-octene is somewhat shorter than that of *trans*-3-octene. This is in agreement with the IQT DCN of the same fuel samples (Table 7.1), which were found to be 38.09 and 33.98 respectively.

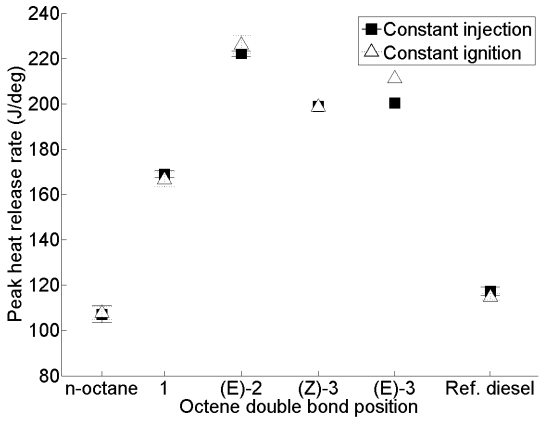

Figure 7.3: Peak apparent heat release rate of octene isomers, *n*-octane and reference diesel at constant injection and constant ignition timings (normalised for constant IMEP)

Figure 7.3 shows the peak apparent heat release rate of the octene isomers, *n*-octane and reference fossil diesel at both timing conditions and with all data normalised to a constant IMEP of 4.12 bar. The peak apparent heat release rates in Figure 7.3 correlate with the ignition delays presented in Figure 7.2, *trans*-2-octene which exhibited the longest ignition delay exhibits the highest peak heat release rate, and *n*-octane which displayed the shortest ignition delay displays the lowest peak heat release rate. This could be expected given that when considering single component fuels with not dissimilar physical properties (Table 7.1), it follows that the most significant limiting factor on the level of premixed fuel and air available at SOC would be the duration of ignition delay as observed in Chapter 6.

Another possible effect of the duration of ignition delay (Figure 7.2) on peak heat release rate (Figure 7.3) is the nature of the in-cylinder environment at SOC. At constant injection timing, those fuels with an ignition delay greater than 7.5 CAD commenced combustion during the expansion stroke, in which trapped end gases are released and increase levels of in-cylinder turbulence. It is therefore tentatively suggested that the higher reactivity of *trans*-2-octene relative to *trans*-3-octene after SOC at constant injection timing (Figure 7.1) can be attributed to the occurrence

of SOC of the former during more turbulent conditions, which are known to increase combustion speeds (Mansson, 1972).

When comparing Figures 7.2 and 7.3, the importance of the timing of peak heat release rate and thus the cylinder volume at which it occurs is also apparent. In Figure 7.3 it can be seen that at constant injection timing, *trans*-3-octene displays a peak heat release rate roughly equivalent to that of *cis*-3-octene, despite the longer ignition delay of the former which at constant ignition timing did result in a higher peak heat release rate. From Figure 7.1, it is apparent that at constant injection timing, the timing of peak heat release rate occurs further into the expansion stroke for *trans*-3-octene and *cis*-3-octene. With more of the cylinder wall exposed it follows that more heat transfer from the cylinder charge would occur, thus lowering the apparent peak heat release rate.

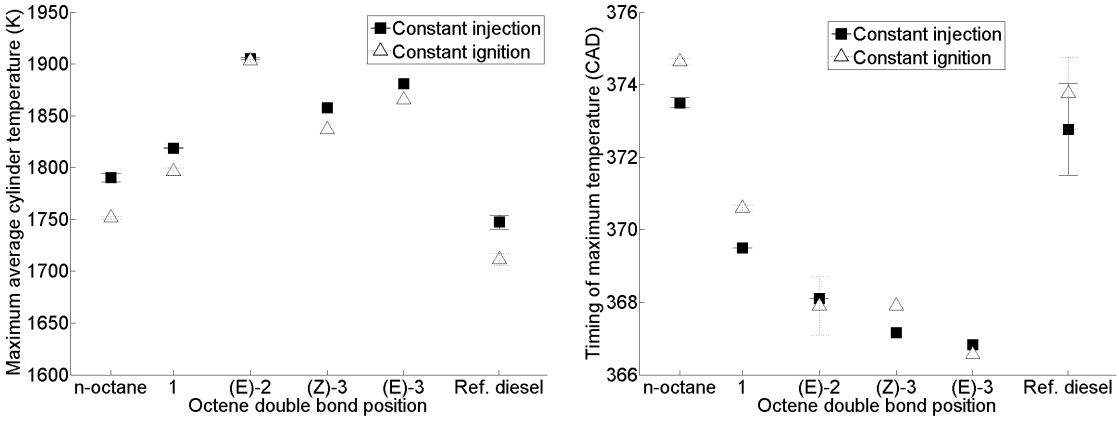

(a) (b)

Figure 7.4: (a) Calculated maximum in-cylinder global temperature and (b) time of occurrence of octene isomers, *n*-octane and reference diesel at constant injection and constant ignition timings (normalised for constant IMEP)

Figures 7.4a and 7.4b show the calculated maximum in-cylinder global temperature and time at which it occurs respectively for each of the fuels at both constant injection and constant ignition timing, and normalised for a constant IMEP of 4.12 bar. The trend apparent in maximum in-cylinder global temperatures (Figure 7.4a) of the single component fuels mirrors that seen in ignition delay (Figure 7.2), with *trans*-2-octene exhibiting the highest temperature and the *n*-octane displaying the lowest. In Figure 7.3, it can be seen that the same molecules also exhibited the

highest and lowest peak heat release rates respectively, and it is sensible to assume that a more concentrated release of the fuel energy (visible through the peak heat release rates and as was seen in Chapter 6) would result in higher in-cylinder temperatures. The calculated values of maximum in-cylinder global temperature for the reference fossil diesel do not fit within this trend, with the fossil diesel displaying a lower maximum in-cylinder temperature than *n*-octane, despite both a longer ignition delay and higher peak heat release rate.

In Figure 7.4b it can be seen that there is an inverse relationship between ignition delay (Figure 7.2) and the time of calculated maximum in-cylinder global temperature, with the maximum in-cylinder global temperature calculated for *n*-octane occurring later than for all the octene isomers. As observed in Chapter 6, ignition delay influences the timing of the maximum in-cylinder global temperatures via the extent of the premixed combustion and heat release rate (Figure 7.1); it follows that a less concentrated release of fuel energy (with a greater fraction of diffusion controlled combustion arising from a shorter ignition delay and reduced time available for fuel and air premixing) will result in a later occurrence of maximum in-cylinder temperature of a lower magnitude (Figure 7.4a). Also clear from Figure 7.4b is the effect of injection timing. Where the fuels exhibited an ignition delay equal to or less than the SOI for constant injection timing of 7.5 CAD BTDC the maximum in-cylinder temperature occurs before that of the same fuel at constant ignition timing.

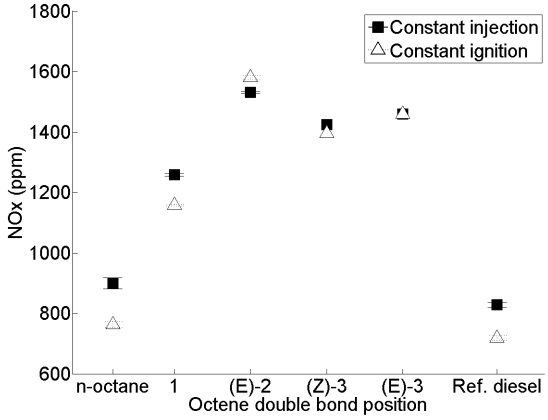

Figure 7.5: Exhaust gas NO_x emissions of octene isomers, *n*-octane and reference diesel at constant injection and constant ignition timings (normalised for constant IMEP)

Figure 7.5 shows the exhaust gas NO_x concentrations of the octene isomers, *n*-octane and the reference fossil diesel at both timing conditions and normalised for a constant IMEP of 4.12 bar. The production of NO_x in diesel combustion is known to be highly thermally sensitive (Ban-Weiss et al., 2007), both to the magnitude of the in-cylinder temperature and the residence time of the cylinder contents at elevated temperatures (Mueller et al., 2009; Schönborn et al., 2009b; Szybist et al., 2005). It is therefore readily apparent that the ignition delay (Figure 7.2) is acting through both the magnitude and time of occurrence of the maximum in-cylinder global temperature (Figures 7.4a and 7.4b) to dictate the extent of NO_x production. Thus the levels of NO_x emitted closely follow the duration of ignition delay, with no influence of the octene isomer double bond position or arrangement visible.

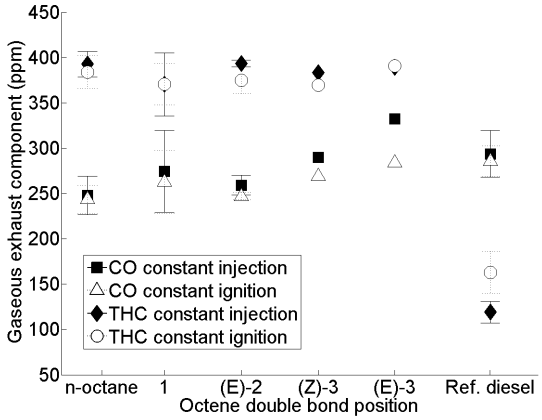

Figure 7.6: Exhaust gas CO and THC emissions of octene isomers, *n*-octane and reference diesel at constant injection and constant ignition timings

Figure 7.6 displays both the CO and THC exhaust emissions of the octene isomers, *n*-octane and reference fossil diesel at constant injection and constant ignition timings. The values were not normalised for a constant IMEP due to the large range of error visible in both measurements of CO and THC. With the extent of error present in Figure 7.6 it is not possible to discern any effect of double bond position; however, there is a clear offset between the single component fuels and the reference fossil diesel. Emissions of both CO and THC are lower for the fossil diesel than the octene isomers and *n*-octane, possibly suggesting that the lower boiling points of the single component fuels (Table 7.1) resulted in a greater level of fuel dilution and incomplete combustion.

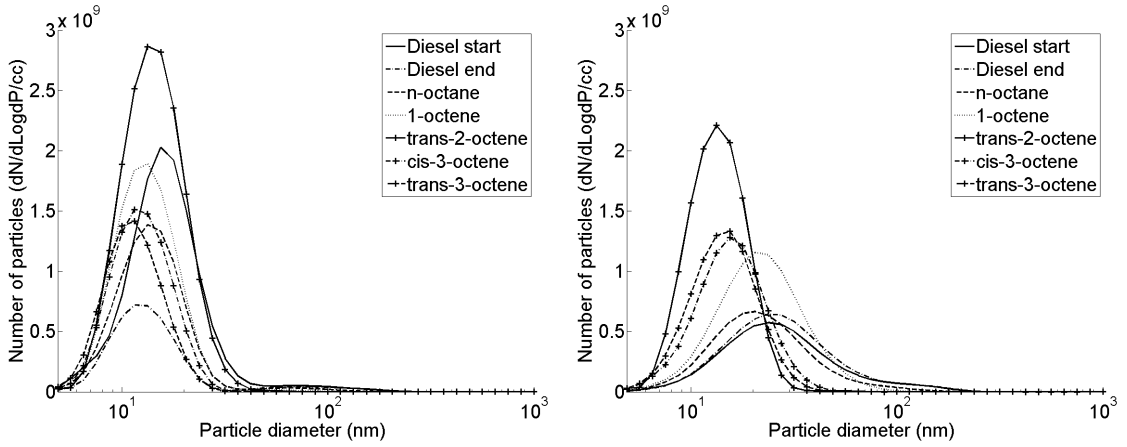

Figure 7.7: Particle emissions of octene isomers, *n*-octane and reference fossil diesel at (a) constant injection and (b) constant ignition timings

Figures 7.7a and 7.7b show the particle emissions of the octene isomers, *n*-octane and reference fossil diesel at constant injection and constant ignition timings respectively, with the peak number of nucleation mode particles (Dp $<$ 50 nm) readily visible. In both Figures 7.7a and 7.7b it can be seen that *trans*-2-octene produced the largest peak in particulate numbers at a particle diameter of approximately 15 nm, followed by *cis*-3-octene, again at approximately 15 nm particle diameter. In both Figures 7.7a and 7.7b it can be seen that the initial introduction of the double bond (*n*-octane to 1-octene) results in a higher peak number of particulates and that the effect of moving the double bond towards the centre of the molecule is not linear or consistent. How much of this possible effect of moving the double bond is an effect of ignition delay is difficult to quantify; the generally lower peaks in particulate numbers (and larger particle diameter) at constant ignition timing (Figure 7.7b) relative to constant injection timing (Figure 7.7a) suggests an influence of both SOI and SOC on nucleation mode particle (Dp $<$ 50 nm) production.

Figure 7.8 shows the total mass of particulates produced by the octene isomers, *n*-octane and reference fossil diesel at constant injection and constant ignition timings. While it would appear that of the octene isomers, *trans*-3-octene emitted the highest level of particulate mass, with the range of error presented in Figure 7.8 it is difficult to discern with any confidence the influence of double bond position or arrangement. However, two effects are clearly apparent: the total mass of particulates produced is

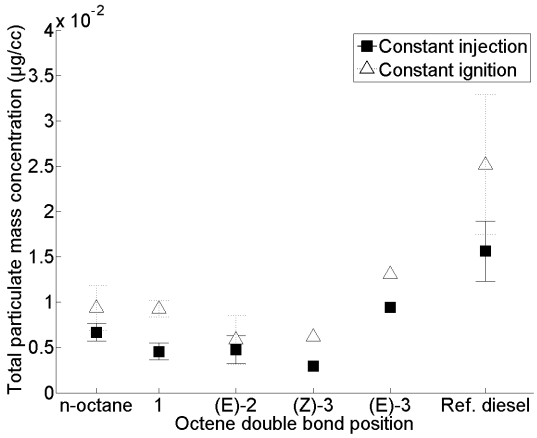

Figure 7.8: Total mass of particulates emitted by octene isomers, *n*-octane and reference diesel at constant injection and constant ignition timings

consistently lower at constant injection timing relative to that produced by the same fuel at constant ignition timing, and secondly the reference fossil diesel produced a greater total mass of particulates than any of the single component fuels. Soot production is known to be thermally sensitive, and in Figure 7.4a maximum in-cylinder global temperatures are consistently higher at constant injection timing, and so it is likely that the trend seen in Figure 7.8 is a reflection of this with the higher temperatures at constant injection timing resulting in higher levels of soot oxidation (Tree and Svensson, 2007) and thus a lower level of particulate mass emitted. The higher level of particulate mass emitted by the fossil diesel (Figure 7.8) would seem to be at least partly attributable to the same thermal soot oxidation mechanism, with Figure 7.4a showing the lowest maximum in-cylinder global temperature for this fuel. The presence of aromatic compounds in the fossil diesel could also be a contributing factor, as such molecules are known to have higher soot propensities (Ladommatos et al., 1996).

7.2.1. Constant ignition delay experiments

The results of engine experiments at constant injection and constant ignition timing revealed that the primary pathway through which the double bond position and arrangement of octene isomers impacts on combustion characteristics and emission levels is the duration of ignition delay. Therefore, where sufficient quantities of the fuels were available, ignition delay was isolated as a variable by the use of

the ignition improving additive 2 EHN. Employing the methodology described in Chapter 5, the correct dosage of 2 EHN was found so that 1-octene and *trans*-2-octene both exhibited the same ignition delay as pure *n*-octane (within 0.2 CAD, the resolution of the shaft encoder utilised in the recording of in-cylinder pressure), with the engine experiments then performed at a fixed SOI of 7.5 CAD BTDC and also an injection timing of 5.5 - 5.7 CAD BTDC so that SOC always occurred at TDC.

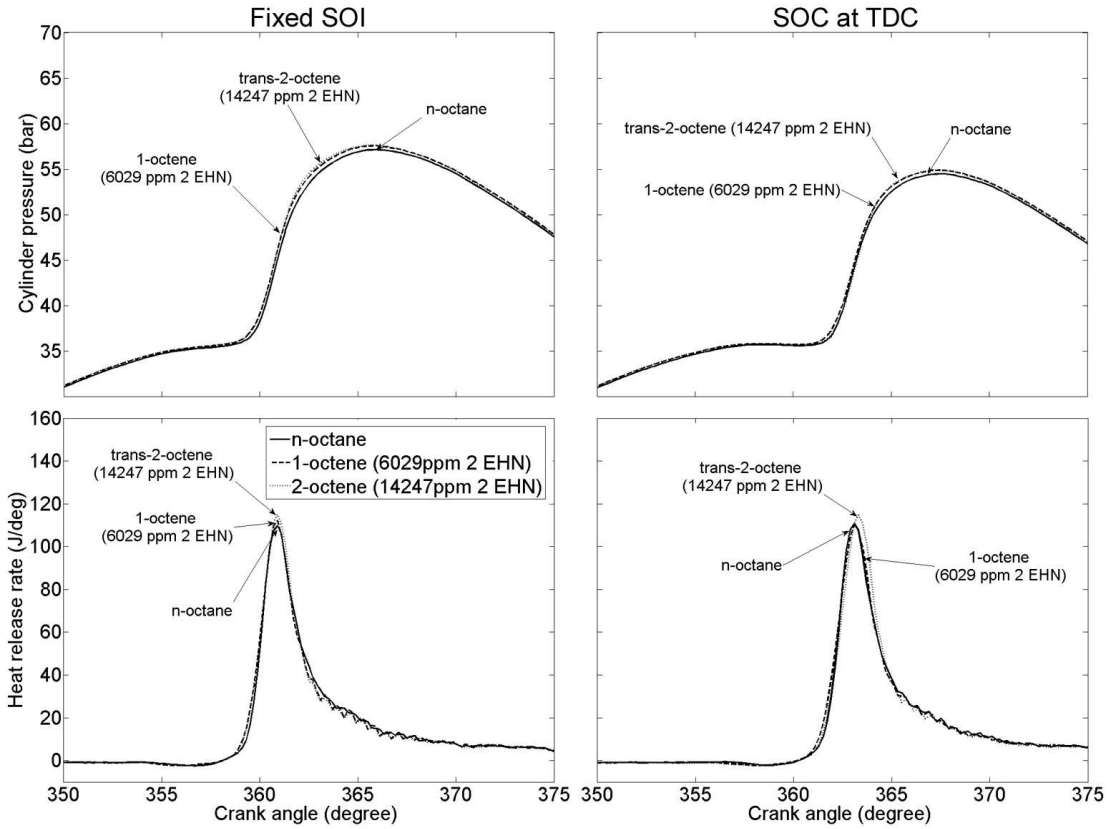

Figure 7.9: In-cylinder pressures and apparent net heat release rates for an IMEP of 4.12 bar of *n*-octane, octene isomers with constant ignition delay and at fixed SOI and SOC at TDC timings

Figure 7.9 shows the in-cylinder pressures and apparent net heat release rates of *n*-octane, 1-octene and *trans*-2-octene at 4.12 bar with constant ignition delay at both fixed SOI and SOC at TDC injection timings. It can be seen that with the ignition delays of 1-octene and *trans*-2-octene equalised to that of *n*-octane, all three exhibit a similar balance of premixed and diffusion mode combustion.

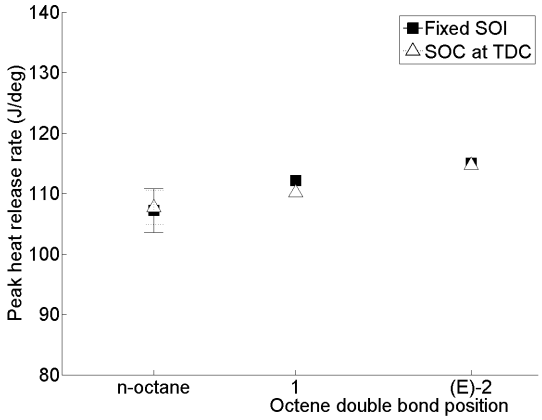

Figure 7.10: Peak apparent heat release rate of *n*-octane, 1-octene and *trans*-2-octene with constant ignition delay and at fixed SOI and SOC at TDC timings

Figure 7.10 shows the peak apparent heat release rate of *n*-octane, 1-octene and *trans*-2-octene with constant ignition delay and at fixed SOI timing and also SOC at TDC timing. Notwithstanding the margin of error presented in Figure 11, there is possibly apparent a suggestion that the introduction of the double bond (*n*-octane to 1-octene) and subsequent movement of the double bond (1-octene to *trans*-2-octene) does result in a higher peak heat release rate at both timing conditions. This is also visible in Figure 7.9, where in addition it can be seen that the time of peak heat release rate occurs slightly later for *trans*-2-octene than 1-octene and *n*-octane, despite the constant duration of ignition delay.

Figures 7.11a and b show the calculated maximum in-cylinder global temperature and the time at which it occurs respectively for *n*-octane, 1-octene and *trans*-2-octene with constant ignition delay and at fixed SOI timing and also SOC at TDC timing. While the shifts in maximum in-cylinder global temperature and the time of at which it occurs are slight with introduction of the double bond and movement of that bond, the apparent trend of an earlier time of maximum in-cylinder global temperature (Figure 7.11b) coinciding with an increasing peak heat release rate (Figure 7.10) is in agreement with the relationship observed between Figure 7.4b and Figure 7.3. The offset in Figures 7.11a and b between data taken at the constant ignition delay timings of fixed SOI and SOC at TDC, is also consistent with the offset observed in Figures 7.4a and b between data taken at constant injection timing and that taken at constant ignition timing.

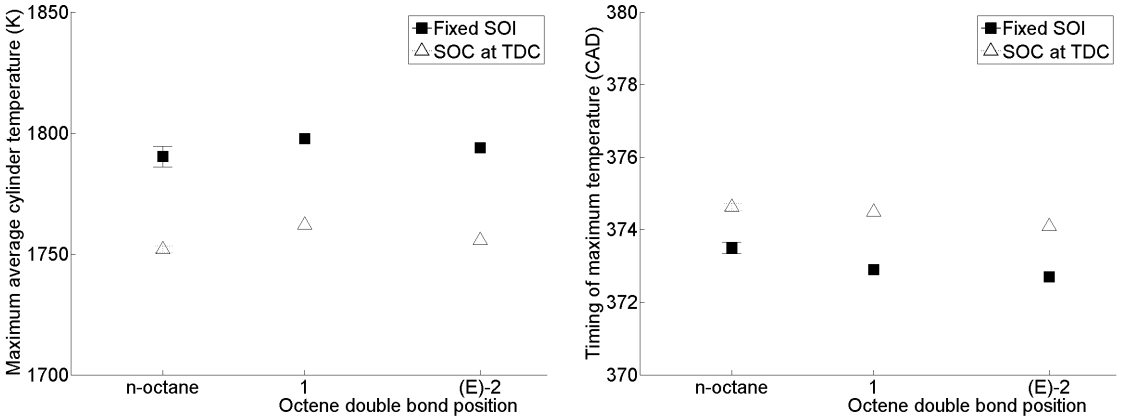

(a) (b)

Figure 7.11: (a) Calculated maximum in-cylinder global temperature and (b) time of occurrence of *n*-octane, 1-octene and *trans*-2-octene with constant ignition delay and at fixed SOI and SOC at TDC timings

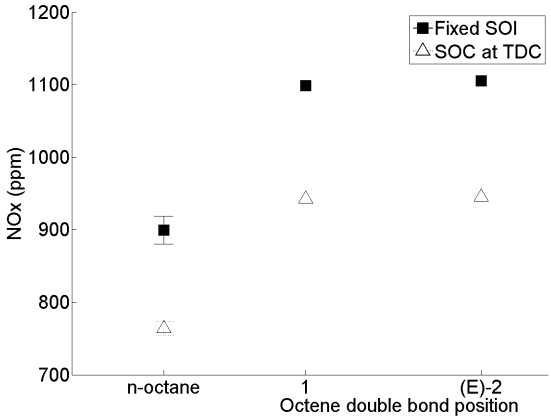

Figure 7.12: NO_x emissions of *n*-octane, 1-octene and *trans*-2-octene with constant ignition delay and at fixed SOI and SOC at TDC timings

Shown in Figure 7.12 are the exhaust gas levels of NO_x for *n*-octane, 1-octene and *trans*-2-octene with constant ignition delay and at fixed SOI timing and also SOC at TDC timing. Immediately apparent at both timings is the increase in NO_x emissions with the introduction of the double bond (*n*-octane to 1-octene), while in Figure 7.11a there is no concurrent increase in the calculated maximum in-cylinder global temperature. As in the previous chapter, this is suggestive of an influence of the adiabatic flame temperatures of the fuels studied.

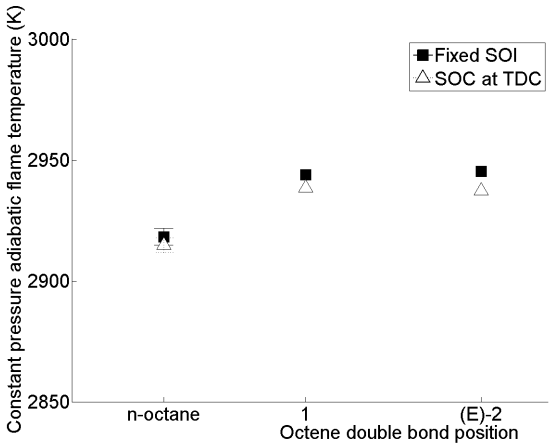

Figure 7.13: Constant pressure adiabatic flame temperatures of *n*-octane, 1-octene and *trans*-2-octene with constant ignition delay and at fixed SOI and SOC at TDC timings

As such, Figure 7.13 shows the calculated constant pressure adiabatic flame temperature of *n*-octane, 1-octene and *trans*-2-octene with constant ignition delay and at fixed SOI timing and also SOC at TDC timing. The adiabatic flame temperature at constant pressure was calculated, assuming no dissociation and an equivalence ratio of 1 using the method described in Section 4.4 for the calculated minimum in-cylinder global temperature between SOI and SOC. The calculations were performed for each of the three molecules using literature values of the enthalpy of formation in a gaseous state (Alberty and Gehrig, 1984; Prosen and Rossini, 1945; Rockenfeller and Rossini, 1961). In Figure 7.13 it can be seen that the adiabatic flame temperature of 1-octene is significantly higher than that of *n*-octane, thus accounting for the shift in NO_x emissions observed (Figure 7.12). It is also clear from Figure 7.13 that movement of the double bond from the 1 to 2 position does not impact on the adiabatic flame temperature of octene. Therefore, with the ignition delay equalised, the results strongly imply that any other influence of double bond position on NO_x production must be subordinate to the adiabatic flame temperature as there is no discernible difference in the level of NO_x emissions from 1-octene and *trans*-2-octene (Figure 7.12). However, it must at this point be highlighted that any observations made from Figure 7.12 are weakened by the use of 2 EHN to equalise ignition delays. The presence of adjacent nitrogen and oxygen atoms within 2 EHN may well result in NO_x formation independent of the thermal oxidation of molecular nitrogen, and could contribute to the total level of NO_x emitted.

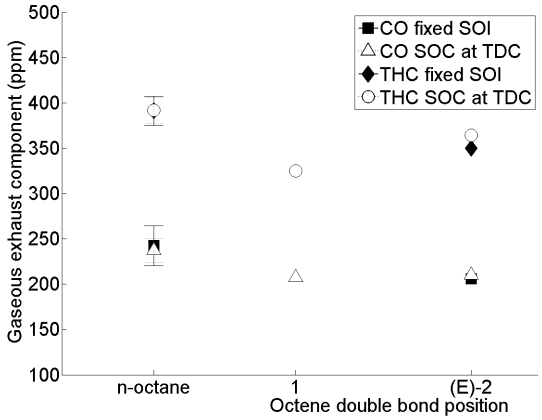

Figure 7.14: Exhaust gas CO and THC of *n*-octane, 1-octene and *trans*-2-octene with constant ignition delay and at fixed SOI and SOC at TDC timings

Figure 7.14 shows the exhaust gas emissions of CO and THC of *n*-octane, 1-octene and *trans*-2-octene with constant ignition delay and at fixed SOI timing and also SOC at TDC timing. It can be seen that at both timing conditions that there is a correlation between emissions of CO and THC, with 1-octene emitting the lowest level of each, *trans*-2-octene emitting slightly higher amounts of both and *n*-octane emitting the highest levels of both pollutants. In Table 7.1 it can be seen that the boiling points of the molecules also follow this trend, with 1-octene having a lower boiling point that *trans*-2-octene and *n*-octane. It is therefore tentatively suggested that this variation in boiling point is leading to differing degrees of incomplete combustion, of which both CO and THC are known products. This may be attributed either to over-dilution of fuel in air or insufficient mixing of fuel with air, the latter of which may possibly be the leading driver of both the CO and THC emissions shown in Figure 7.14 when considering that *n*-octane emitted the highest level of each and possesses the highest boiling point (Table 7.1).

Figures 7.15a and b show the particle emissions of *n*-octane, 1-octene and *trans*-2-octene with constant ignition delay and at fixed SOI timing and also SOC at TDC timing respectively. It can be seen that at both timing conditions, introduction of a double bond (*n*-octane to 1-octene) results in a decrease in the number of nucleation mode particles produced (Dp $<$ 50 nm), while movement of the double bond from the 1 to 2 position significantly increases the number of nucleation mode particles produced. This implies that in Figure 7.8a, where *trans*-2-octene also produced the highest peak in nucleation mode particles that this result cannot be wholly

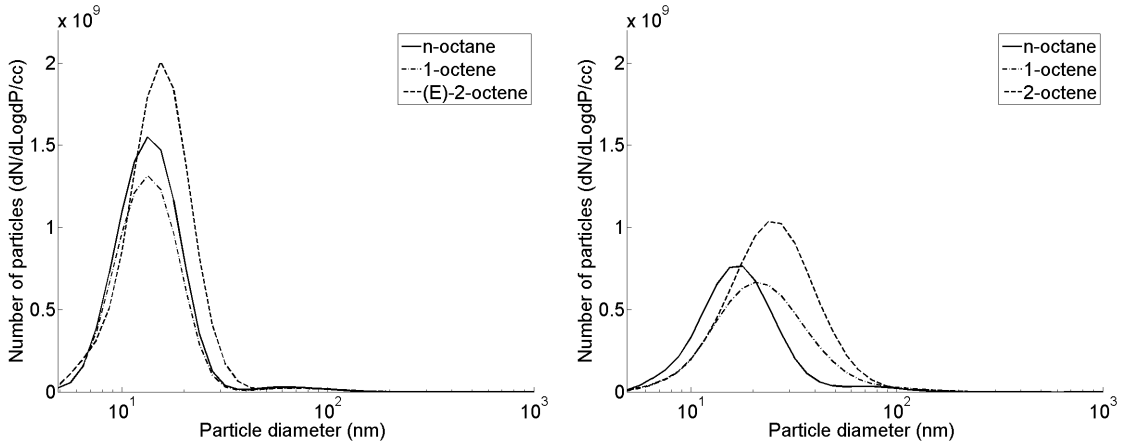

Figure 7.15: Particle emissions of *n*-octane, 1-octene and *trans*-2-octene with constant ignition delay and at (a) fixed SOI and (b) SOC at TDC timings

attributed to the longer ignition delay of *trans*-2-octene, as in Figure 7.15a the same result is seen despite the removal of ignition delay as a variable. Figures 7.15a and b are also consistent with Figures 7.8a and b in that there is a significant offset between tests conducted at different injection timings.

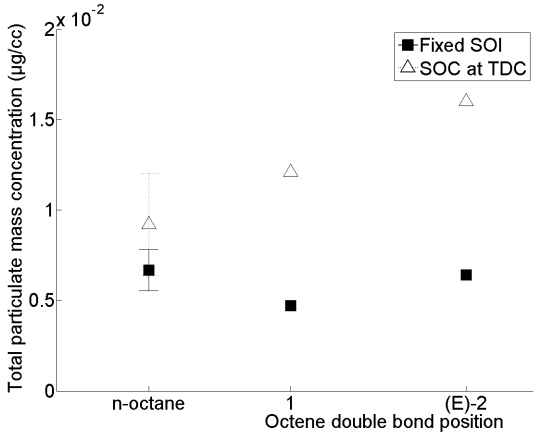

Figure 7.16: Total mass of particulates emitted of *n*-octane, 1-octene and *trans*-2-octene with constant ignition delay and at fixed SOI and SOC at TDC timings

Shown in Figure 7.16 is the total mass of particulates produced by *n*-octane, 1-octene and *trans*-2-octene with constant ignition delay and at fixed SOI timing and also SOC at TDC timing. Despite the range of error present in Figure 7.16, the

offset between data taken at fixed SOI timing and SOC at TDC timing is consistent with the thermal sensitivity of soot formation and the calculated maximum in-cylinder temperatures shown in Figure 7.11a. Figure 7.16 also weakly suggests that movement of the double bond from the 1 to 2 position with SOC at TDC resulted in an increase in the total mass of particulates produced (in addition to the increase in the number of nucleation mode particles observed in Figure 7.16). Therefore it can be tentatively suggested that in Figure 7.8, where *trans*-3-octene produced the highest particulate mass of all the octene isomers, but did not exhibit the longest ignition delay, this is attributable to the double bond position of the molecule.

7.2.2. Effect of *cis-trans* isomerisation on ignition delay

The shorter ignition delay of *cis*-3-octene relative to *trans*-3-octene (Figure 7.2) is in agreement with previous observations of shorter alkene isomers (Salooja, 1968) and of bicyclic compounds (Heyne et al., 2009; Murphy et al., 2004). It is known that for an alkenyl or alkenyl peroxy radical to undergo internal H abstraction and isomerisation across a double bond (a radical branching step at low temperatures (Westbrook, 2000)), the radical must be in the *cis* conformation (Bounaceur et al., 2009; Salooja, 1968). It is therefore suggested that this necessity of the double bond to be in the *cis* arrangement explains the shorter ignition delay of *cis*-3-octene relative to *trans*-3-octene. This is either because in the case of *trans*-3-octene the internal isomerisation of alkenyl and alkenyl peroxy across the double bond cannot take place whatsoever (and isomerisation takes place in only the saturated alkyl chain of the radical), or it first requires a conversion from a *trans* to *cis* arrangement and thus an additional activation energy. In either scenario it can seen that the branching of radicals is reduced and the escalation towards ignition delayed. Furthermore, this implies that for the conditions tested, the isomerisation of alkenyl and alkenyl peroxy across the unsaturated portion of the radical is an important route in the low temperature kinetics of octene isomers where such reactions are possible.

7.2.3. Effect of double bond position on ignition delay

The trend of ignition delay (Figure 7.2), and also the duration of the cool flame period (Figure 7.1), with moving double bond position found in the case of octene isomers is somewhat contrary to previous experimental studies, where moving the

double bond towards the centre of the molecule consistently reduced the overall ignition quality (Hughes and Prodhan, 1973; Salooja, 1968; Tanaka et al., 2003; Vanhove et al., 2005; Zhang et al., 2009). In these studies, where alkene isomers of carbon chain length 4 to 7 were considered, the primary driver of ignition delay was found to be the carbon chain length of the residual alkyl radicals present (as these will follow the low temperature kinetic routes of *n*-alkanes (Westbrook, 2000)). While in Chapter 6 the carbon chain length of *n*-alkanes has previously been found to be a primary driver of ignition delay when following the same experimental method as the current study, it is worth noting that the aforementioned studies of double bond position all utilised premixed fuel and air (Hughes and Prodhan, 1973; Salooja, 1968; Tanaka et al., 2003; Vanhove et al., 2005; Zhang et al., 2009). Therefore, physical properties of the octene isomers which affect fuel and air mixing, such as boiling point, enthalpy of vaporisation and viscosity, may be contributing to the deviation in ignition delay from the trend previously observed. On inspection of the fuel properties listed in Table 7.1, and the order of ignition displayed in Figure 7.2, it can be seen that there is a good correlation between octene boiling point and ignition delay (Figure 7.17).

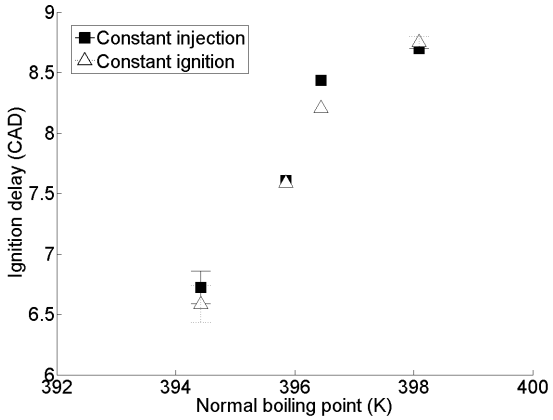

Figure 7.17: Ignition delay of octene isomers at constant injection and constant ignition delay timings (normalised for constant IMEP) against molecule normal boiling point

However, if the hypothesis is made that the boiling point of the octene isomers is significant in determining the relative ignition delays of the molecules, via a limitation on the rate of fuel and air mixing, there are at least two important considerations that weaken the argument presented by the correlation seen in Figure 7.17. Firstly,

the range of boiling points exhibited by the octene isomers is very narrow ($\approx$ 5 K) and furthermore all of the values are significantly below the calculated in-cylinder global temperature at the time of injection ($\approx$ 1000 K). Secondly, if the hypothesis were valid, a correlation between ignition delay (Figure 7.2) and the peak heat release rate (Figure 7.3, which is indicative of the amount of fuel and air premixed prior to SOC as seen in Chapter 6) would be moderated.

With isomer boiling point discredited as a primary influence on ignition delay and no other physical property (Table 7.1) correlating with ignition delay (Figure 7.2), it is suggested that the trend seen in the octene isomers can indeed be attributed to the length of the saturated chain portions. It is plausible that *cis*-3-octene may possess a shorter ignition delay than *trans*-2-octene due to the previously discussed advantage of the *cis*- arrangement (Section 7.2.2) outweighing any disadvantage brought about by the shortening of the longest saturated portion of the isomer by 1 C. However, in the case of *trans*-2-octene and *trans*-3-octene, the reduced ignition delay of the latter relative to the former can only be attributed to the change in double bond position. Previously the isomers of longest carbon chain length studied in the context of double bond position were those of heptene (Tanaka et al., 2003), and Figure 7.18 compares the molecular structures of *trans*-2-heptene, *trans*-3-heptene, *trans*-2-octene and *trans*-3-octene, highlighting the nature of the carbon atoms (and thus C-H bonds) present.

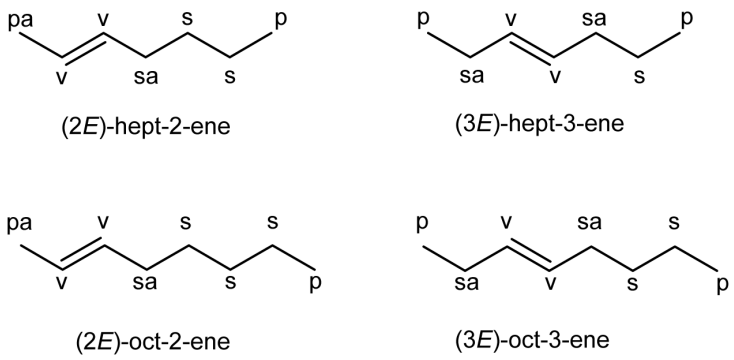

Figure 7.18: Molecular structures of *trans*-2-heptene, *trans*-3-heptene, *trans*-2-octene and *trans*-3-octene, with carbon atoms labelled p (primary), pa (primary allylic), s (secondary), sa (secondary allylic) and v (vinylic)

In both *trans*- heptene and octene, it can be seen that in moving the double bond from positions 2 to 3, the alkyl chain to the left of the double bond increases by one

carbon atom while the alkyl chain to right of the double bond decreases in length by one carbon atom (Figure 7.18). In the heptene isomer this results in a significant net decrease in reactivity (Tanaka et al., 2003), whereas in the octene isomer there appears to be a net increase in reactivity prior to SOC. It is therefore suggested that the shortening of the saturated carbon chain length from 5 to 4 in the case of octene is less detrimental to reactivity than that of a shortening of the saturated chain from 4 to 3 carbon atoms in the case of heptene; in turn this reduction in reactivity could be attributed to two important stages of low temperature branching kinetics. Firstly, the relative greater availability of more easily abstractable and weakly bonded secondary H atoms (Westbrook, 2000); from Figure 7.18 it can be seen that to the right of the double bond, there is a decrease in secondary H atoms from 6 to 4 in heptene and 8 to 6 in the octene isomer. Secondly, the potential of the alkyl chain to the right of the double bond to form six and seven member transition state rings. The ability of alkyl chains to form these rings reduces with decreasing carbon chain length (Westbrook, 2000) and requires that the chain is formed from at least 3 fully saturated carbons (Mehl et al., 2011). In the previous chapter, investigation of C7 - C22 alkanes highlighted a similar effect, that for shorter chain lengths the removal of 1 carbon atom has a greater effect on ignition delay than the same action on a longer *n*-alkane.

7.3. Conclusions

1. Movement of the double bond to form *trans*-2-octene from 1-octene increases the ignition delay of the molecule. Further movement of the double bond to form either *cis* or *trans*-3-octene does not result in a further increase in ignition delay, with both isomers exhibiting a shorter ignition delay than *trans*-2-octene but longer than 1-octene.

2. This is contrary to previous studies involving shorter alkenes (C4 - C7), where a consistent trend of increasing ignition delay was observed with movement of the double bond towards the centre of the molecule. In contrast to shorter alkenes, it is suggested that the slightly longer overall carbon chain length of the octene isomers results in a net increase of low temperature reactivity of the molecule prior to SOC with movement of the double bond from position two to three.

3. *Cis*-3-octene possesses a shorter ignition delay than *trans*-3-octene. This can be attributed to the need for alkenyl and alkenyl peroxy radicals to be in the *cis* arrangement prior to internal isomerisation across the double bond. It also indicates that such reactions do take place in the combustion of octene isomers where possible.

4. The primary influence of the octene isomer structure on combustion phasing and emission is via the duration of the ignition delay. This is especially apparent in the case of NO_x emissions, where the route of ignition delay influence is via the peak heat release and both the magnitude and timing of maximum in-cylinder temperatures.

5. With ignition delay removed as a variable, *trans*-2-octene was found to produce more nucleation mode particles (Dp $<$ 50 nm) than 1-octene. Furthermore, with and without ignition delay present as a variable, the largest mass of particulates was produced by the *trans*-octene with the double bond closest to the middle of the molecule.

6. The adiabatic flame temperatures of 1-octene and *trans*-2-octene were found to be very similar, and so with ignition delay isolated as a variable and the effect of adiabatic flame temperature on NO_x emissions readily apparent, no difference in the NO_x emissions of 1-octene and *trans*-2-octene were detected. This implies that any influence of double bond position on NO_x emissions outside of ignition delay is of lesser importance than adiabatic flame temperature.

8. Influence of the fatty acid ester alcohol moiety

Since the initial development of biodiesel, methanol has been the most widely used alcohol for the process of transesterification, and in 1999 some 90 % of the methanol produced was from natural gas (Ogden et al., 1999) by means of steam reformation. However, if considering a bio-fuel to truly be an alternative to fossil fuels the use of either natural gas or coal (which is another suitable feedstock for methanol production via steam reformation) would be inappropriate.

Alternative alcohols to methanol have been available via production from biomass for some time, and the combustion and emissions characterization of stearic acid esters produced from such alcohols forms the subject of this chapter. Production of *iso*-propanol, butanol and ethanol can be achieved via fermentation of biomass by both yeast and bacteria (Rosillo-Calle and Walter, 2006; Krouwel et al., 1983; Ezeji et al., 2007) and in recent years large petroleum companies have invested in production of butanol from biomass, with several butanol production facilities are under development (www.butamax.com, 2011; www.gevo.com, 2011). Furthermore, acid catalysed methods of transesterification with longer chained alcohols than methanol have reported high yields of fatty acid esters (Graboski and McCormick, 1998; Wahlen et al., 2008).

Previous assessments of the ignition quality of fatty acid esters produced from alcohols other than methanol have either found no discernable or consistent effect of the alcohol moiety (Knothe et al., 1997; Serdari et al., 1999; Lapuerta et al., 2008; Knothe et al., 2003; Kinoshita, 2011), or an increase in ignition quality with alcohol moiety carbon chain length (Schönborn et al., 2009b; Zhang and Boehman, 2010; Zhang et al., 2009). However, several researchers have reported a decrease in NO_x emissions with a concurrent increase in the emissions of CO, THC and particulate matter when increasing the alcohol moiety carbon chain length (Makareviciene and Janulis, 2003; Lapuerta et al., 2008; el Ammouri et al., 1986; Kinoshita, 2011).

This chapter presents the results of engine experiments in which a series of fatty acid esters were tested. The esters were chosen to investigate the effect of fatty acid ester alcohol moiety carbon chain length and branching on compression ignition combustion and emissions.

8.1. Experimental method

8.1.1. Apparatus

All of the combustion experiments described in the present chapter were performed using the compression ignition engine and ultra low volume fuel system described in Chapter 3.

8.1.2. Fuel molecules investigated

A series of eight fatty acid esters were tested to assess the impact on combustion phasing and emissions production of two structural properties specific to the alcohol moiety of fatty acid esters:

(a) Straight carbon chain length in the alcohol moiety.

(b) Carbon chain branching in the alcohol moiety.

To observe the impact of increasing the straight carbon chain length of the alcohol moiety of a fatty acid ester, four esters of stearic acid were tested: methyl stearate (C19), ethyl stearate (C20), *n*-propyl stearate (C21) and *n*-butyl stearate (C22). A further three esters of stearic acid were tested to investigate the effect of carbon chain branching in the alcohol moiety: *iso*-propyl stearate (C21), *iso*-butyl stearate (C22) and *tert*-butyl stearate (C22). While esters of stearic acid are not particularly representative of the vegetable oils commonly utilized in the production of bio-diesel (as they are fully saturated) they were chosen so to reduce the complexity of the chemical synthesis and thus ensure a high degree of purity. One additional fatty acid ester, methyl oleate (C19), a single *n*-alkane (C18) and a reference fossil diesel (with zero FAME content) were also tested so as to allow an understanding of the relative importance of the two properties of alcohol moiety relative to other structural features of fatty acid esters.

Two of the fatty acid esters studied and one *n*-alkane (methyl stearate, ethyl stearate and *n*-octadecane) were obtained from a chemical supplier (Sigma Aldrich UK). All other molecules studied were specially synthesized by an organic synthesis company (further details are given in Appendix D.2), with assay and other properties of each presented in Table 8.1; the molecular structure of each fuel is given in Table 8.2. The reference diesel used was fossil derived and contained no fatty acid esters.

Table 8.1: Properties of fatty acid esters and reference fossil diesel

Fuel	Molecular formula	Assay (%)	T_{boil} (°C)	T_{melt} (°C)	Cetane number$^{\square}$	Density (kg/m^3)	Dynamic viscosity at 20 °C (mPa.s)	Lower heating value (MJ/Kg)
Reference fossil diesel	-	-	268.9‡	-	51.7$^{\bullet}$	834.5$^{\diamond}$	-	43.14†
Methyl oleate	$C_{19}H_{36}O_2$	93.8	327.2*	-20.2[5]	62.3	845.1[1]	2.638[1]	37.42
Methyl stearate	$C_{19}H_{38}O_2$	96	328.7*	37.7[5]	88.9	835.3[1]	3.2252[1]	37.64[2]
Ethyl stearate	$C_{20}H_{40}O_2$	97	338.4*	33.0[5]	86.83	830.3[1]	3.3073[1]	37.79[2, 3]
n-propyl stearate	$C_{21}H_{42}O_2$	98.4	347.7*	28.1[5]	80.4	829.6[4]	4.406[4]	37.72
n-butyl stearate	$C_{22}H_{44}O_2$	98.3	356.5*	25.6[5]	86.3	-	-	38.40
iso-propyl stearate	$C_{21}H_{42}O_2$	98.8	343.0*	28.4[6]	96.5	824.4[4]	4.355[4]	37.96
iso-butyl stearate	$C_{22}H_{44}O_2$	99.3	352.1*	29.8[6]	99.3	-	-	38.06
tert-butyl stearate	$C_{22}H_{44}O_2$	94.7	349.4*	31.9[7]	-	-	-	38.10
n-octadecane	$C_{18}H_{38}$	99	316.2[8]	28.5[9]	106.3	755.8[10]	2.062[11]	43.90[12]

* = 2nd order calculations by the method of Constantinou and Gani (1994), † = calculated from experimental data obtained by the IP12 methodInstitute of Petroleum (2001), $^{\diamond}$ = experimental data obtained according to ASTM D4052 at 15 °C, $^{\bullet}$ = experimental data obtained according to EN ISO 516, ‡ = experimental data obtained according to EN ISO 3405, $^{\square}$ = data from Murphy et al. (2004), [1] = data from Pratas et al. (2010), [2] = data from Maksimuk et al. (2012), [3] = data from Rozenthal (1936), [4] = data from Bonhorst et al. (1948), [5] = data from Knothe (2009), [6] = data from Schlenk (1969), [7] = data from Silbert (1959), [8] = data from National Institute of Standards and Technology (2010), [9] = data from Domanska (1999), [10] = data from American Petroleum Instititute (1946), [11] = data from e. al. Schiessler (1945) and [12] = data from Prosen and Rossini (1945)

Table 8.2: Structures of fatty acid esters and fuel additive

1.	Straight carbon chain length in the alcohol moiety	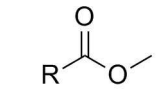 methyl stearate 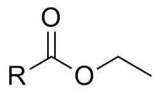 ethyl stearate 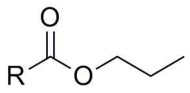 *n*-propyl stearate 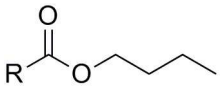 *n*-butyl stearate Where R = 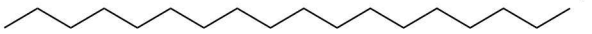 *
2.	Addition of carbon chain methyl branches in the alcohol moiety	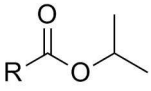 *iso*-propyl stearate 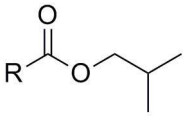 *iso*-butyl stearate 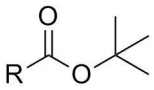 *tert*-butyl stearate
	Importance of alcohol moiety relative to fatty acid saturation	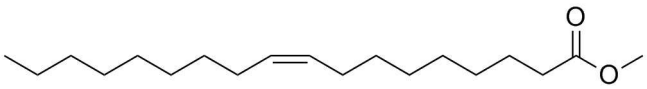 methyl oleate
	Importance of alcohol moiety relative to ester functional group	 *n*-octadecane
	Ignition improving additive	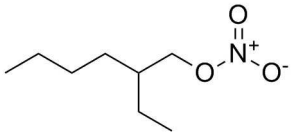 2-ethylhexyl nitrate

8.1.3. Experimental conditions

Each of the eight molecules was tested at the two experimental conditions of constant injection and constant ignition timing, as defined in Chapter 5. After the initial two sets of experiments at constant injection and constant ignition timing were

completed, a third series of experiments was carried out at constant ignition delay timing, utilising the ignition improver 2 EHN and the method described in Chapter 5.

As some fuels were solid at room temperature, all fuels were first heated in a PID controlled water bath held at 85 ± 2 °C prior to filling of the low volume fuel system which had been preheated to 85 ± 2 °C and was held at this temperature throughout the subsequent experiment.

All tests were conducted at an engine speed of 1200 rpm and at 450 bar fuel injection pressure. The injection duration was adjusted in the case of every fuel, so that the engine IMEP was always constant at 4 bar for all fuels. A summary of the engine and test operating conditions is given in Table 8.3.

Table 8.3: Fatty acid esters engine and test operating conditions

Fuel	2 EHN dosage (ppm)	Engine speed (rpm)	Fuel injection pressure (bar)	IMEP (bar)	Constant injection timing (SOI at 7.5 CAD BTDC)						Constant ignition timing (SOC at TDC)					
					Ignition delay (CAD)		Injection duration (µs)		Indicated thermal efficiency (%)		Ignition delay (CAD)		Injection duration (µs)		Indicated thermal efficiency (%)	
					Mean	1σ	Mean	1σ	Mean	1σ	Mean	1σ	Mean	1σ	Mean	1σ
Ref. fossil diesel	0	1200	450	4	6.7	0.14	739	15	34.84	0.45	6.6	0.07	740	15	34.5	0.59
n-octadecane	0	1200	450	4	3.7	0	747	17	35.41	0.61	3.6	0.05	747	17	35.27	0.75
Methyl oleate	0	1200	450	4	6.1	0	820	-	34.29	-	5.9	0	823	-	34.07	-
Methyl stearate	0	1200	450	4	4.4	0.09	816	16	35.16	0.51	4.3	0.08	815	18	35.04	0.48
Ethyl stearate	0	1200	450	4	4.3	-	804	-	35.31	-	4.3	-	801	-	34.68	-
n-propyl stearate	0	1200	450	4	4.5	-	816	-	35.35	-	4.3	-	817	-	34.9	-
n-butyl stearate	0	1200	450	4	4.5	-	843	-	34.9	-	4.4	-	848	-	34.26	-
iso-propyl stearate	0	1200	450	4	4.5	0	847	31	35.26	0.15	4.4	0.1	864	44	34.96	0.46
iso-butyl stearate	0	1200	450	4	4.5	-	820	-	35.53	-	4.3	-	829	-	34.88	-
tert-butyl stearate	0	1200	450	4	4.9	-	862	-	34.82	-	4.7	-	854	-	34.54	-
Ref. fossil diesel	15 322	1200	450	4	4.7	-	725	-	33.74	-	4.4	-	723	-	33.7	-
n-methyl oleate	11 338	1200	450	4	4.5	-	804	-	34.58	-	4.4	-	805	-	34.23	-
n-methyl stearate	3 717	1200	450	4	3.7	-	840	-	35.98	-	3.7	-	838	-	36.21	-
tert-butyl stearate	3 425	1200	450	4	4.3	-	886	-	35.15	-	4.2	-	898	-	34.9	-

8.2. Results and discussion

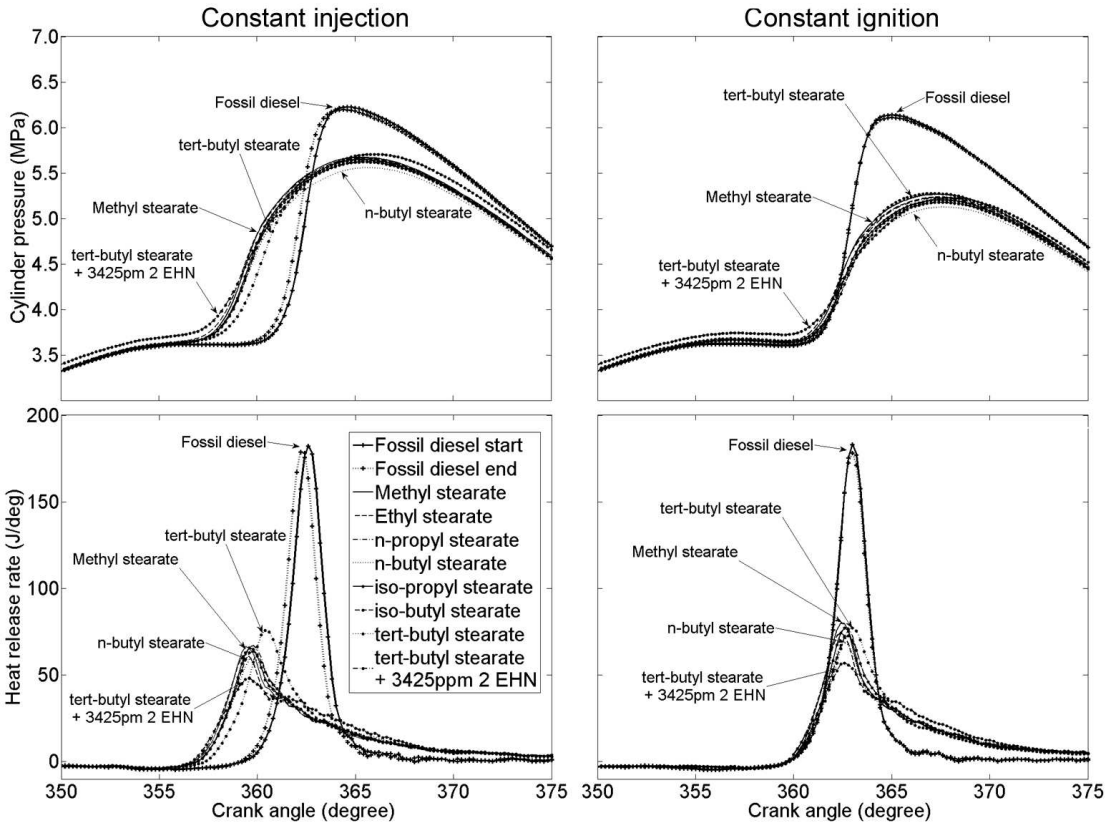

Figure 8.1: In-cylinder pressures and apparent net heat release rates of the stearates and reference fossil diesel at constant injection and constant ignition timing

All of the fatty acid esters in which the alcohol moiety was varied ignited after a shorter ignition delay than the reference fossil diesel, as shown in Figure 8.1. The esters also released a higher proportion of energy during diffusion combustion than the reference fossil diesel, resulting in a much longer duration of combustion (Figure 8.1). This is predominately attributable to the shorter ignition delay of the esters, which relative to the reference fossil fuel limits the extent of fuel and air premixing. Injection durations required for constant IMEP (Table 8.3) were also consistently longer for the fatty acid esters than the reference fossil diesel and this can be clearly attributed to the lower heating values of the esters (Table 8.1). Variation in the heat release rates of the fatty acid esters is apparent from Figure 8.1 and this is discussed in the following sections, with respect to individual structural properties of the alcohol moiety.

8.2.1. Impact of the alcohol moiety straight carbon chain length

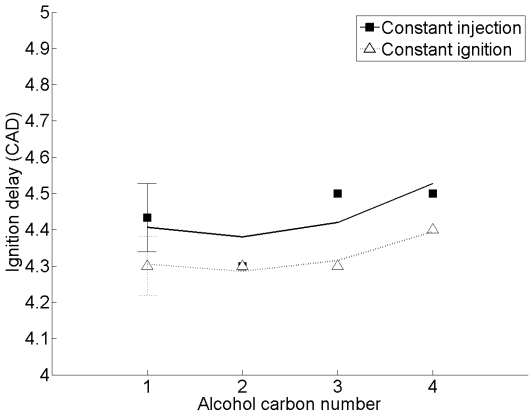

Figure 8.2: Influence of straight carbon chain length of the alcohol moiety in a fatty acid ester on ignition delay

Figure 8.2 shows the impact of the alcohol moiety carbon chain length on the ignition delay at both constant injection and constant ignition timing conditions. It can be seen from Figure 8.2 that the variation found in ignition delay between the molecules of differing alcohol moiety carbon chain length (and also the day to day variation exhibited by n-methyl stearate) is equal, or less than, 0.2 CAD. As the shaft encoder utilized in measuring the in-cylinder pressure (from which the SOC, and thus ignition delay, was determined) has a resolution of 0.2 CAD, it is impossible from Figure 8.2 to discern an impact on ignition quality with varying alcohol moiety carbon chain length. The error bars presented in Figure 8.2 are around 0.2 CAD in total magnitude at both timing conditions suggesting that the largest source of experimental uncertainty in determining the duration of ignition delay is indeed the shaft encoder resolution.

Previously, at the same experimental conditions, a very strong relationship was found between straight carbon chain length in *n*-alkanes and ignition delay (Section 6.2.1). As variation in the alcohol moiety carbon chain length has no discernable impact on the ignition delay, and for all the fatty acid esters tested the fatty acid moiety was a fully saturated straight carbon chain of length 18, it could be concluded that the ignition delay is being controlled solely by the fatty acid moiety. However, it is not possible to rule out a contribution in determining the duration of ignition delay from the alcohol moiety of the fatty acid ester. Figure 6.1 shows that for

an n-alkane of carbon chain length C18, extension of the chain length to C20 and C22 has only a small influence on ignition delay which is not greater than the shaft encoder resolution of 0.2 CAD. If one considers the total carbon number of the fatty acid esters, then methyl stearate and n-butyl stearate have carbon numbers of 19 and 22 respectively. Therefore, whilst clearly a gross oversimplification of the reaction kinetics involved, it is interesting to note that Figure 6.1 does suggest that the difference in ignition delay between these two molecules would be 0.2 CAD or less.

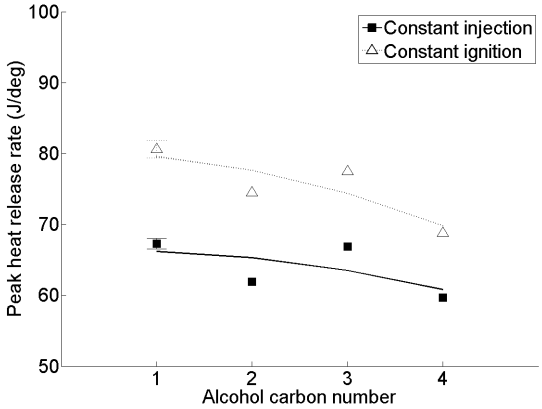

Figure 8.3: Effect of straight carbon chain length of the alcohol moiety in a fatty acid ester on peak heat release rate

Figure 8.3 shows the effect on peak heat release rate of the alcohol moiety carbon chain length at both timing conditions; constant injection and constant ignition. While the trend generally apparent is for decreasing peak heat release rate with increasing alcohol moiety carbon chain length, at both timing conditions n-propyl stearate produced a higher peak heat release rate than ethyl stearate.

The range of error shown by the results in Figure 8.3 is smaller than the difference between the maximum and minimum peak heat release rates recorded at both timing conditions, suggesting that the non-linear trends observed do exist. It is suggested that the trends in peak heat release can be attributed to differing premixed burn fractions, as the two were found to correlate well in the case of non-oxygenated molecules (Chapter 6) and it follows that greater peak heat release rates will be obtained when a greater proportion of fuel and air has been mixed to combustible stoichiometry prior to ignition. Two explanations for differing premixed burn frac-

tions which could account for the trends seen in Figure 8.3 are offered, firstly that of an underlying trend in ignition delay.

To test this theory, use was made of the previously found relationship between the ignition delay and peak heat release rate of acyclic non-oxygenated hydrocarbons (Section 6.2.1). At both constant injection and constant ignition timing, the shift in peak heat release rate corresponding to the uncertainty in measurement of the ignition delay of the fatty acid esters was calculated (the difference in peak heat release for a fuel of ignition delay 4.5 CAD and for a fuel of ignition delay 4.3 CAD) and found to be 7.1 J/deg and 6.7 J/deg for constant injection and constant ignition timing respectively. For both timing conditions these shifts are of roughly the same magnitude as the difference between the highest and lowest peak heat release rates exhibited by the fatty acid esters in Figure 8.3. This lends support to the hypothesis that differences in ignition delay of the fatty acid esters, beyond the resolution of the shaft encoder, account for the trends in peak heat release rate. Under this hypothesis methyl and *n*-propyl stearates possess the longest ignition delays (allowing more time for fuel and air mixing and thus a larger premixed burn fraction resulting in higher peak heat release rates), while *n*-butyl stearate exhibits the shortest ignition delay. This would a suggest a non-linear relationship between the carbon chain length of the alcohol moiety and the ignition quality of the fatty acid ester, as found in cetane measurements by Knothe et al. (1997). The shorter ignition delay of the ethyl ester is also in agreement with the engine studies of Schönborn et al. (2009b) and Zhang and Boehman (2010). However, while there is some support in the literature for this theory, it must be highlighted that this hypothesis assumes that the relationship between ignition delay and peak heat release found in the study of acyclic non-oxygenated hydrocarbons (Chapter 6) remains valid in the case of fatty acid esters.

The second hypothesis offered to which the trends in Figure 8.3 can be attributed, is that a physical property of the esters, such as boiling point, may be sufficiently influential in determining the extent of fuel and air mixing during equivalent periods of ignition delay. However, the linear increase in boiling point with alcohol moiety chain length (Table 8.1) does not correlate well the non-linearity apparent in Figure 8.3.

Figure 8.4 shows a linear decrease in calculated maximum in-cylinder temperature with increasing alcohol moiety carbon chain length, therefore consistent with

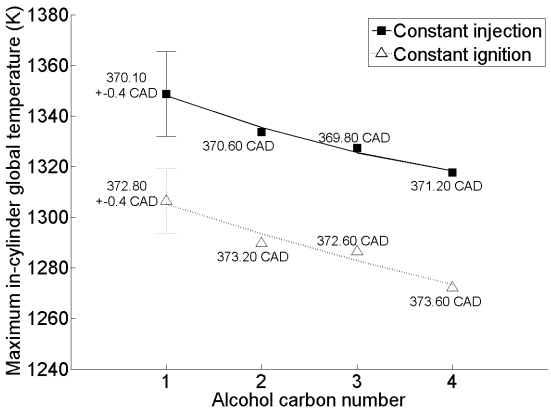

Figure 8.4: Impact of straight carbon chain length of the alcohol moiety in a fatty acid ester on calculated maximum global in-cylinder temperature and time of occurrence

the peak in-cylinder pressures recorded (Figure 8.1). The non-linear relationship between alcohol moiety carbon chain length and peak heat release rate (Figure 8.3) is reflected in the timing of the calculated maximum in-cylinder global temperature (Figure 8.4), those esters which exhibited a higher peak release rate (Figure 8.3) reached the maximum in-cylinder temperature earlier.

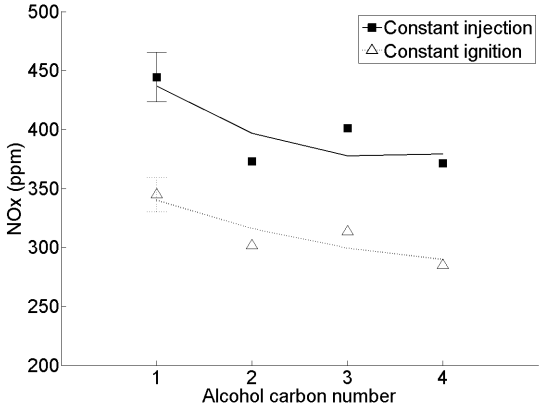

Figure 8.5: Impact of straight carbon chain length of the alcohol moiety in a fatty acid ester on NO_x emissions

Figure 8.5 shows the effect of alcohol moiety carbon chain length on the levels of NO_x in the exhaust gas, at constant injection and constant ignition timing, and shows the methyl and butyl esters to emit the highest and lowest exhaust levels respectively. Formation of NO_x in the combustion of fatty acid esters has been

suggested to be primarily by the thermal (Zeldovich) mechanism (Ban-Weiss et al., 2007). Both the global maximum in-cylinder temperature achieved and the time at which it is reached have been put forward as the primary driver of NO_x formation and the ignition quality is fundamental in determining both of these variables (Mueller et al., 2009; Schönborn et al., 2009b; Szybist et al., 2005). Earlier and faster combustion events increase the duration for which in-cylinder conditions are suitable for NO_x formation. Notwithstanding the error margins presented, a possible interpretation of the trend seen in Figure 8.5 is that both the timing and magnitude of the global maximum in-cylinder temperature are exerting an influence; in particular the non-linearity of the trend in Figure 8.5 may be attributable to the similarly non-linear timing of maximum in-cylinder global temperatures shown in Figure 8.4.

Additionally, when calculating the shifts in NO_x emissions that could be expected from the uncertainty in the ignition delay of the fatty acid esters (utilizing the previously found relationship between NO_x emissions and ignition delay in Chapter 6), these are found to be less than the observed difference in the maximum and minimum NO_x emissions from the fatty acid esters at both constant injection and constant ignition timing (significantly so for constant injection timing where the calculated shift is 23 ppm and the difference between NO_x emissions from n-methyl and *n*-butyl stearate is 56 ppm). In Chapters 6 and 7, with the ignition delay of fuels equalized, the adiabatic flame temperature was found to influence NO_x formation. For this reason, the adiabatic flame temperature at constant pressure was calculated, assuming no dissociation and an equivalence ratio of 1 using the method described in Section 4.4 for the calculated minimum in-cylinder global temperature between SOI and SOC. The enthalpies of formation of all fuels except methyl stearate, ethyl stearate and *n*-octadecane were calculated from the lower heating values of the fuels obtained by the IP12 method (Institute of Petroleum, 2001) and shown in Table 8.1. In the case of methyl stearate and *n*-octadecane the lower heating values presented in Table 8.1 were calculated from the literature values of the enthalpies of formation in a liquid state (Maksimuk et al., 2012; Prosen and Rossini, 1945). The lower heating value of ethyl stearate is calculated from the enthalpy of formation in a solid state (Maksimuk et al., 2012) and the enthalpy of fusion (Rozenthal, 1936).

The results of the adiabatic flame temperature calculations are shown in Figure 8.6. In this case the adiabatic flame temperature does not appear to be a major contributor to the levels of NO_x production, as the molecule with the highest adiabatic

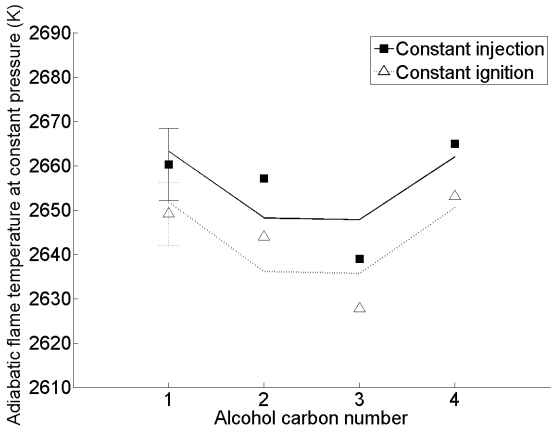

Figure 8.6: Impact of carbon chain length in the alcohol moiety on constant pressure adiabatic flame temperature

flame temperature (*n*-butyl stearate) exhibits the lowest level of exhaust gas NO_x emissions. As the error bars present in Figure 8.6 are of some significance relative to the visible trend and are the result of deviation in the start temperature of the adiabatic flame temperature calculations, the same calculations were repeated for a constant starting temperature and the same trend with increasing alcohol moiety carbon chain length observed.

A further physical property of the esters which could account for the trend apparent in Figure 8.5 is that of oxygen content. As the alcohol moiety carbon chain length increases the percentage oxygen content of the stearates decreases. The effect of this decrease could have two important effects: to reduce the availability of oxygen for NO_x formation and to decrease the level of mixture at stoichiometric conditions suitable for combustion at SOC (Mueller et al., 2009), thus resulting in lower peak heat release rates and maximum in-cylinder temperatures (though the latter seems unlikely given the non-linearity of the trends seen in Figure 8.3).

Figure 8.7 shows the effect of alcohol moiety carbon chain length on exhaust gas emissions of CO, THC and the peak number of nucleation mode particles (Dp $<$ 50 nm). In the case of all three pollutants, the trend is for a peak in the emission level at an alcohol moiety carbon chain length of 2 or 3. However, the range of error for these emissions is high, especially in the case of THC. Therefore, while only very tentative inferences can be made from these results, there does appear to be a correlation between the levels of all three emissions at varying alcohol moiety carbon chain length. Both CO and THC are known products of incomplete combustion (a

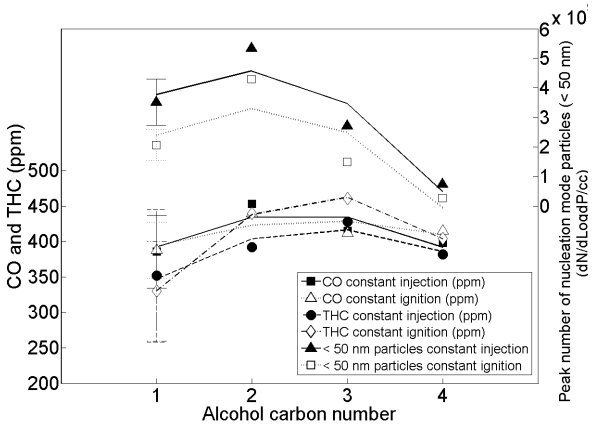

Figure 8.7: The influence of carbon chain length in the alcohol moiety on exhaust emissions of CO, THC and peak number of nucleation mode particles (Dp < 50 nm)

possible effect of both insufficient fuel and air mixing and over-dilution of fuel in air), and it has previously been suggested that a large proportion of nucleation mode particles are in fact droplets of un-burnt fuel (Schönborn et al., 2009b).

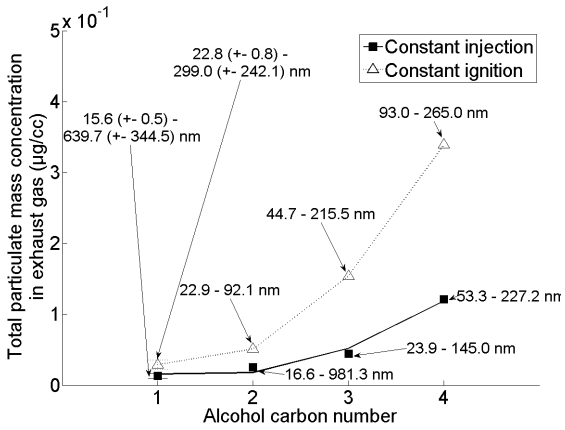

Figure 8.8: Impact of carbon chain length in the alcohol moiety on the total mass of particulates in the exhaust gas, including the particle diameter range in which 5 - 85 % of the total particulate mass is produced

Figure 8.8 shows a trend of increasing total mass of particulates measured in the exhaust gas with increasing alcohol moiety carbon chain length. From the molecules tested the trend appears exponential; at both timing conditions addition of a carbon atom to the straight carbon chain of the alcohol moiety results in at least a doubling of the total mass of particulates produced. This trend appears to be a continuation

of the result found by Schönborn et al. (2009b), where ethyl oleate was found to produce roughly double the mass of particulates of methyl oleate at constant ignition delay timing.

It is possible that the trends seen in Figure 8.8 are, at least in part, the effect of the trends in calculated maximum in-cylinder temperature seen in Figure 8.4. It is apparent that the ester producing the highest mass of particulates, *n*-butyl stearate, also experienced the coolest estimated global in-cylinder temperatures. Rates of soot oxidation are known to be thermally sensitive, with reactions rates increasing with temperature (Tree and Svensson, 2007). However, the strength of the trend would perhaps suggest that other factors are also of importance.

Poorer fuel atomization could be expected to increase the presence of fuel rich zones which are conducive to the production of particulate matter (Tree and Svensson, 2007); the efficiency of fuel atomization is determined by a number of physical properties of the fuel, including boiling point. In Table 8.1 it can be seen that the boiling point of the fatty acid esters increases with alcohol moiety carbon chain length. Increased boiling points may reduce the efficiency of fuel atomization by increasing the energy required for fuel vaporisation, and so the trend in boiling point does correlate well with the trend seen in Figure 8.8. However, it must be iterated that values for the enthalpy of vaporisation are not available for the fatty acid esters and the correlation of boiling point with enthalpy of vaporisation is not guaranteed. Although a value of viscosity was not available for *n*-butyl stearate (Table 8.1), viscosity of the fatty acid esters does increase with alcohol moiety carbon chain length. This could also be expected reduce the efficiency of fuel and air mixing, with the fuel droplet size increasing with viscosity. An influence of increasing fuel melting point reducing the efficiency of fuel atomization (as postulated by Schönborn et al. (2009b)) is not apparent as it can be seen that fuel melting point (Table 8.1) actually decreases with increasing alcohol moiety carbon chain length and the total mass of particulates emitted. Another potential driver of the trend in Figure 8.8 is the decreasing oxygen content of the stearates with increasing alcohol moiety carbon chain length. This would decrease the availability of oxygen for soot oxidation after initial formation (Tree and Svensson, 2007).

An influence of soot radiative heat transfer on the exhaust gas levels of NO_x (Figure 8.5), which has previously been suggested as accounting for an increase in NO_x emissions from fatty acid esters relative to those from fossil diesel (Mueller

et al., 2009; Schönborn et al., 2009b), is possibly apparent when comparing Figure 8.5 with Figure 8.8. However, the non-linearity of the trend in Figure 8.5 is not reflected in Figure 8.8, nor is the exponential increase in particulate mass with increasing alcohol moiety carbon chain length (Figure 8.8) visible when inspecting Figure 8.5.

8.2.2. Effect of carbon chain branching in the alcohol moiety

In order to observe the impact on combustion and emissions of branching in the alcohol moiety of fatty acid esters, combustion characteristics and emissions levels have been plotted on the y axis as a shift relative to the value of the variable exhibited by the fatty acid ester with equivalent alcohol moiety straight carbon chain length. This shift is plotted against the ratio of branched carbon atoms present in the alcohol moiety relative to the straight carbon chain length in the alcohol moiety. For example, *iso*-propyl stearate has an alcohol moiety straight carbon chain length of 2 and one carbon present as a methyl branch in the alcohol moiety. Therefore the percentage branching of *iso*-propyl stearate is 50 % and the y axis values plotted are shifts relative to ethyl stearate (which possesses the same straight alcohol moiety carbon chain length of 2).

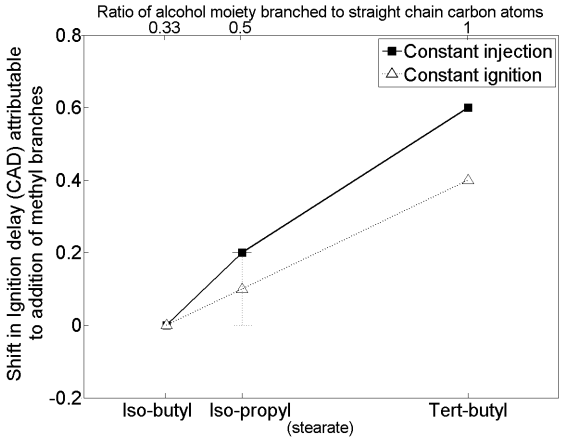

Figure 8.9: Influence of carbon chain branching in the alcohol moiety in a fatty acid ester on ignition delay

Figure 8.9 shows the effect of carbon branching in the alcohol moiety on ignition delay. It can be seen that for *iso*-propyl stearate and *iso*-butyl stearate any shift (relative to n-ethyl stearate and *n*-propyl stearate respectively) is within the shaft

encoder resolution of 0.2 CAD for both constant injection and constant ignition timing. However, the molecule with the highest degree of branching in the alcohol moiety, *tert*-butyl stearate does show a measurable increase in ignition delay (relative to n-ethyl stearate, and thus all the other stearates tested) at both timing conditions. A similar influence of branching on ignition delay has been observed previously in the case of alkanes (Chapter 6), where increasing the degree of branching resulted in a longer ignition delay.

With only one of the branched esters showing a change in ignition quality relative to the un-branched ester of equivalent alcohol moiety straight carbon chain length, the combustion and emissions characteristics of the branched esters are compared with ignition delay removed entirely as a variable. This was achieved as described in Chapter 5 by iteratively adding small quantities of the of the ignition promoting additive (2 EHN) to *tert*-butyl stearate until it exhibited the same duration of ignition delay (within the shaft encoder resolution) as the other stearates tested.

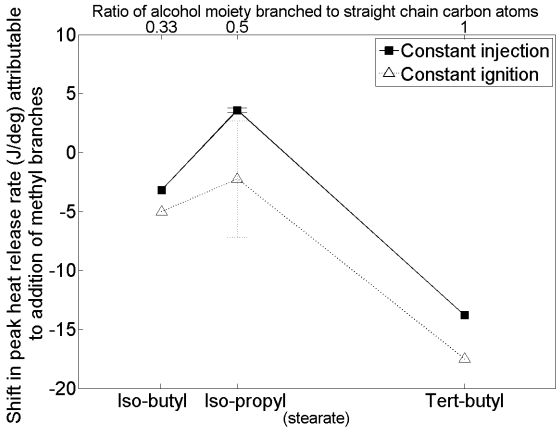

Figure 8.10: Influence of carbon chain branching in the alcohol moiety in a fatty acid ester on peak heat release rate at constant ignition delay

Figure 8.10 shows the carbon chain branching in the alcohol moiety on peak heat release rate at both constant ignition delay timings. From Figure 8.10 it can be seen that the addition of 2 EHN to *tert*-butyl stearate caused the fuel to switch from exhibiting the highest peak heat release rate of the stearates tested to the lowest (the former can be explained by a difference in ignition delay, the second cannot). As *tert*-butyl stearate is the only stearate to have been treated with 2 EHN, it is possible that the presence of the additive is affecting the peak heat release rate through mechanisms other than the change in ignition delay. The slightly higher peak heat

release rate of *iso*-butyl palm ester relative to *n*-butyl palm ester (attributed to a slightly longer ignition delay) reported by Kinoshita (2011) is not apparent when considering the same esters of stearic acid.

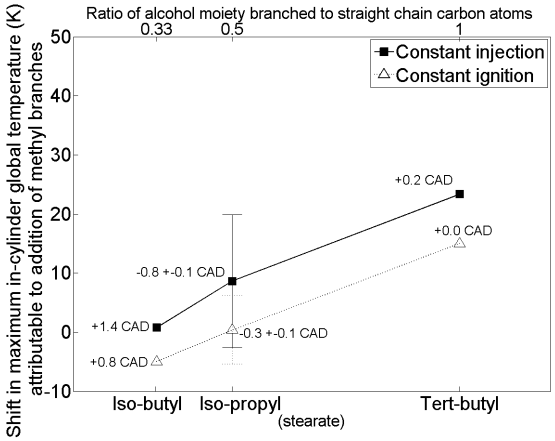

Figure 8.11: Effect of carbon chain branching in the alcohol moiety in a fatty acid ester on the calculated maximum in-cylinder global temperature and time of occurrence at constant ignition delay timings

Figure 8.11 shows a trend of increasingly large positive relative shifts in the calculated maximum in-cylinder global temperature with the increasing ratio of carbon atoms present as methyl branches in the alcohol moiety of a fatty acid ester, at both timing conditions. It also shows that for *iso*-butyl and *iso*-propyl stearate the timing of maximum in-cylinder temperature move later and earlier respectively in comparison to the esters of equivalent alcohol moiety straight carbon chain length. While the large margin of error presented makes it difficult to draw any firm conclusions from these results, it is interesting to note that *tert*-butyl stearate shows a relative increase in maximum in-cylinder temperature despite a decrease in peak heat release rate (Figure 8.10). Decreasing peak heat release rates previously coincided with decreasing maximum in-cylinder temperatures in the study of non-oxygenated molecules (Chapter 6) and there is little shift in the timing of the maximum in-cylinder temperature ($\leq$ 0.2 CAD). Whether this shift in maximum in-cylinder temperature can be attributed to a property of the fuel or the presence of 2 EHN is uncertain.

Figure 8.12 shows the impact of branching in the alcohol moiety on the levels of NO_x exhaust emissions, at both constant ignition delay timings. The trend at both timing conditions is for an increasingly large shift in NO_x levels relative to

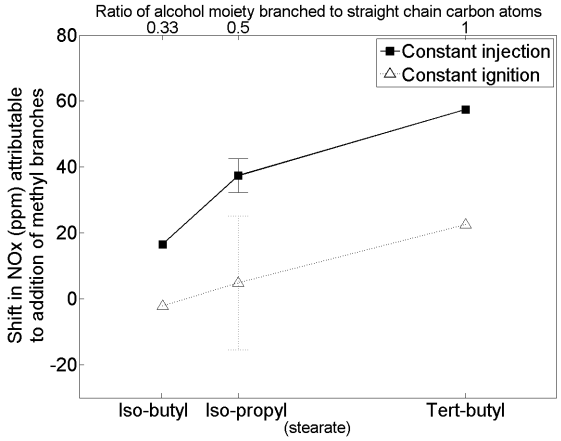

Figure 8.12: Influence of branching in the alcohol moiety on exhaust emissions of NO_x at constant ignition delay timings

the equivalent un-branched fatty acid ester with increasing ratio of branched methyl groups present. When considering the thermally sensitive nature of NO_x production, this is consistent with the trends in maximum in-cylinder global temperature seen in Figure 8.11.

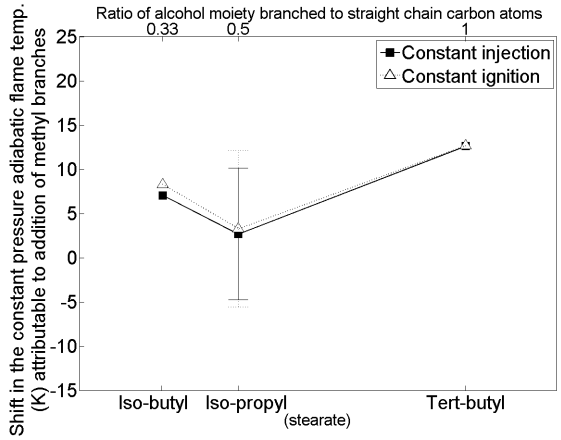

Figure 8.13: Impact of branching in the alcohol moiety on the constant pressure adiabatic flame temperature

Figure 8.13 shows the shift in the constant pressure adiabatic flame temperature attributable to the addition of methyl branches to the straight carbon chain in the alcohol moiety of the fatty acid esters. While all of the branched esters display a relative increase in adiabatic flame temperature, *iso*-butyl stearate displays a greater relative increase than *iso*-propyl stearate. This is not reflected in Figure 8.12 where

iso-propyl stearate shows a greater relative increase in NO_x emissions. Furthermore, the relative shifts in temperature are small (15 K) with a range of error equivalent in magnitude. Therefore, if the adiabatic flame temperature is an influence on NO_x emissions it would appear to be secondary to the maximum in-cylinder global temperature (Figure 8.11).

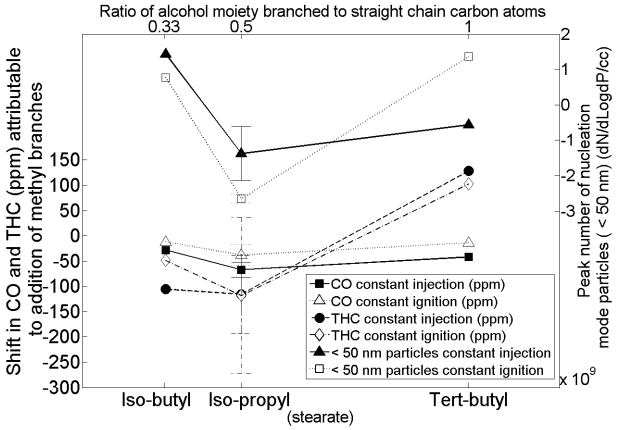

Figure 8.14: The influence of branching in the alcohol moiety on exhaust emissions of CO, THC and peak number of nucleation mode particles (Dp < 50 nm) at constant ignition delay timings.

Figure 8.14 shows the effect of branching in the alcohol moiety of a fatty acid ester on exhaust gas emissions of CO, THC and the peak number of nucleation mode particles. At both timing conditions, the addition of branches appears to reduce CO levels, especially in the case of *iso*-propyl stearate. Emissions of THC are reduced by as much as 100 ppm by the addition of branches, apart from in the case of *tert*-butyl stearate in which they are increased by a similar amount. However, when considering the trends in both CO and THC it must be noted that the range of the results is roughly equal to the range of error under both timing conditions.

Figure 8.14 does, however, show results for peak number of nucleation mode particles that are significantly outside of the experimental variability and which are also outside of the range of error brought about by uncertainty in the ignition delay (as calculated from relationship between peak number of nucleation mode particles and ignition delay determined in Chapter 6). The addition of a methyl branch to the alcohol moiety of *n*-propyl stearate (to form *iso*-butyl stearate) increases the number of nucleation mode particles, while making the same addition to ethyl stearate (to form *iso*-propyl stearate) results in a drop in the number of nucleation

mode particles. At constant injection *tert*-butyl stearate shows a small relative decrease in the peak number of nucleation mode particles, but at constant ignition timing a larger increase in the peak number of nucleation mode particles.

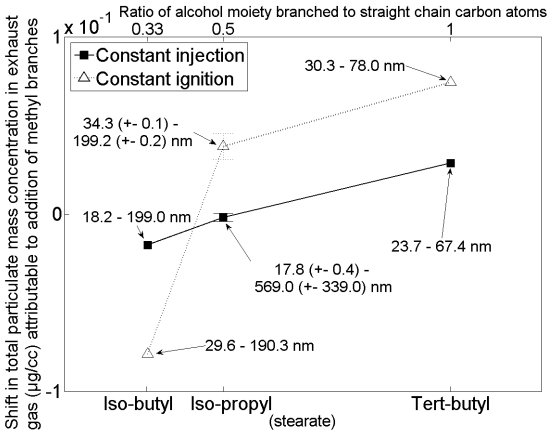

Figure 8.15: The effect of branching in the alcohol moiety on the total mass of particulates in exhaust emissions with ignition delay removed as a variable, including the particle diameter range (absolute) in which 5 - 85 % of the total particulate mass is produced

Shown in Figure 8.15 is the effect of branching in the alcohol moiety on the total mass of particulates produced at both constant ignition delay timings. At constant injection timing, *iso*-butyl stearate shows a slight decrease in the total mass of particulates produced relative to the un-branched fatty acid ester of equivalent alcohol moiety straight carbon chain length. *Iso*-propyl stearate shows little shift in the total mass of particulates, while the most branched molecule, *tert*-butyl stearate, shows an increase in the total mass of particulates produced. The same general trend is apparent in the results of tests conducted at constant ignition timing, though the magnitude of the shifts seen is significantly greater and with *iso*-propyl stearate displaying a relative increase in the total mass of particulates produced. At both constant injection and constant ignition timing the measured day-to-day variability is smaller than the range of results. Revisiting the theories put forward when considering the effect of alcohol moiety carbon chain length on total particulate mass (Figure 8.8), an effect of temperature seems unlikely as the molecule displaying the largest increase in particulate mass also shows an increase in maximum in-cylinder global temperatures.

When comparing Figure 8.15 to Figure 8.8, it can be seen that in Figure 8.8, at both timing conditions, the addition of two carbon atoms to the straight chain length of the alcohol moiety of ethyl stearate to form *n*-butyl stearate results in a larger increase in the total mass of particulates produced than the addition of two methyl branches to form *tert*-butyl stearate (Figure 8.15). It has previously been observed that sooting tendencies tend to increase with both increasing straight carbon chain length and the addition of methyl branches (Ladommatos et al., 1996).

8.2.3. Importance of the alcohol moiety relative to other structural properties of fatty acid esters

Previous studies have looked at extensively at the impact of structural features other than the alcohol moiety of fatty acid esters on combustion and emissions, notably the degree of unsaturation, carbon chain length of the fatty acid moiety and also the presence of the ester functional group through comparison to normal alkanes (Benjumea et al., 2010; Fisher et al., 2011; Knothe et al., 1997; McCormick et al., 2001; Mueller et al., 2009; Schönborn et al., 2009b; Zhang and Boehman, 2010; Zhang et al., 2009). To gauge the importance of alcohol moiety structure on the combustion and emissions of fatty acid esters relative to these better understood structural properties a further series of experiments were conducted at constant injection, constant ignition and constant ignition delay timings. In these the combustion characteristics and exhaust emissions levels of methyl stearate were compared to methyl oleate, *n*-octadecane and a reference fossil diesel with zero fatty acid ester content.

Figure 8.16 shows that the properties of alcohol moiety structure found are, at both constant injection and constant ignition timing, of less significance in determining the duration of ignition delay than the fatty acid moiety degree of saturation and roughly equivalent to the importance of the presence of the ester functional group. The ignition delays exhibited by methyl oleate, *n*-octadecane and the reference diesel relative to methyl stearate are consistent with previous studies (Schönborn et al., 2009b; Zhang and Boehman, 2010).

Figures 8.17 to 8.20 compare the impact of the alcohol moiety with the other features of fatty acid ester molecular structure at constant ignition delay timings. As before, this was achieved by iteratively adding small quantities of the of the ignition promoting additive (2 EHN) until the fuel exhibited the desired ignition

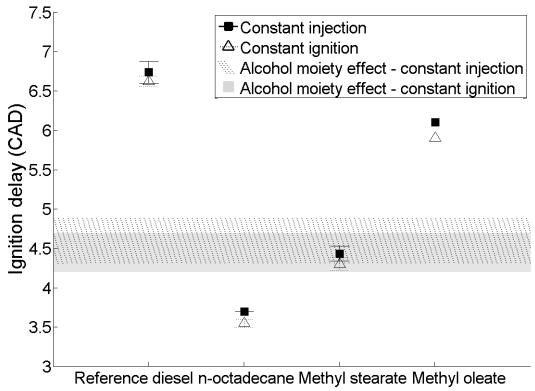

Figure 8.16: Ignition delay of reference fuels and impact of the alcohol moiety at constant injection and constant ignition timing

delay. Equalizing the delays of all four fuels was not practical due to the large spread observed in the delays; neither was it desirable as 2 EHN contains fuel bound nitrogen and oxygen which may contribute to total NO_x emissions. Therefore, the reference fossil diesel and methyl oleate were equalized to the same ignition delay as that of methyl stearate, and then separately, methyl stearate was equalized to the same ignition delay as that of *n*-octadecane. This was done at both constant injection and constant ignition timings, and as such the results are presented as two sets of data acquired at two equalized values of ignition delay for each timing condition.

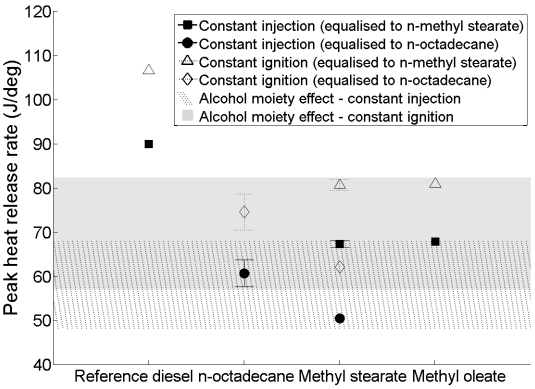

Figure 8.17: Peak heat release rate reference fuels and impact of the alcohol moiety at constant injection and constant ignition constant ignition delay timing

Figure 8.17 shows the peak heat release rates recorded for each of the fuels at constant injection and constant ignition constant ignition delay timing. It can be seen that alterations to the structure of the alcohol moiety are of far greater significance in determining rates of peak heat release than introducing a single double bond to the fatty acid moiety, with no discernable difference in the peak heat release rates of methyl stearate and methyl oleate. *N*-octadecane was found to possess a higher peak release rate than methyl stearate, but the range of variation brought about by the changes in the alcohol moiety is approximately twice this increase.

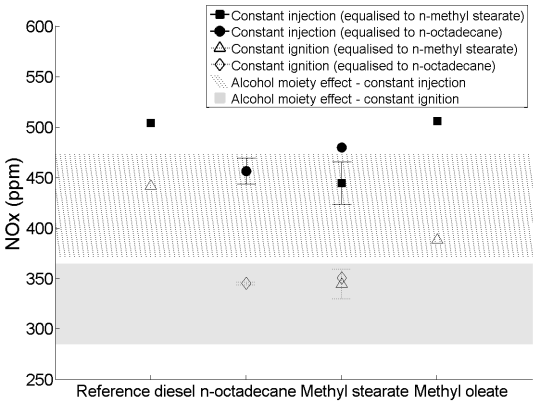

Figure 8.18: NO_x emission levels of reference fuels and impact of the alcohol moiety at constant injection and constant ignition constant ignition delay timing

Figure 8.18 shows the exhaust gas levels of NO_x for each fuel and the variation brought about by changes to the alcohol moiety, at both constant injection and constant ignition constant ignition delay timing. From Figure 8.18 it can be seen that variation of the alcohol moiety (the most influential being the increase in alcohol moiety chain length, Figure 8.5) has approximately twice the impact on NO_x emissions as the change in saturation from methyl stearate to methyl oleate, at both timing conditions. The observed increase in NO_x emissions with the addition of a double bond (methyl stearate to methyl oleate) can be attributed to an increase in adiabatic flame temperature and is in agreement with the previous investigation into the effect of saturation in acyclic chain (Chapter 6) and also the experimental findings of Schönborn et al. (2009b).

In Figures 8.19 and 8.20 the significance of the alcohol moiety structure in the production of nucleation mode particle and the total mass of particulates is presen-

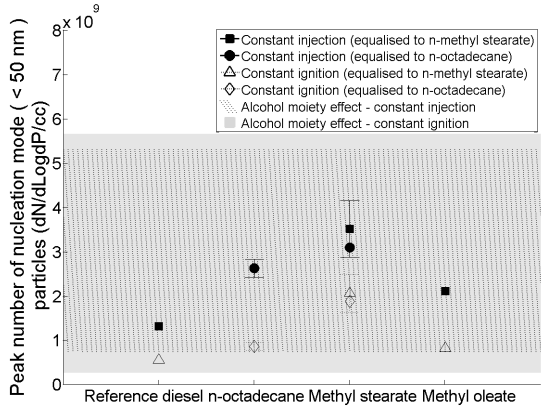

Figure 8.19: Peak number of nucleation mode particles (Dp < 50 nm) of reference fuels and impact of alcohol moiety at constant injection and constant ignition constant ignition delay timing

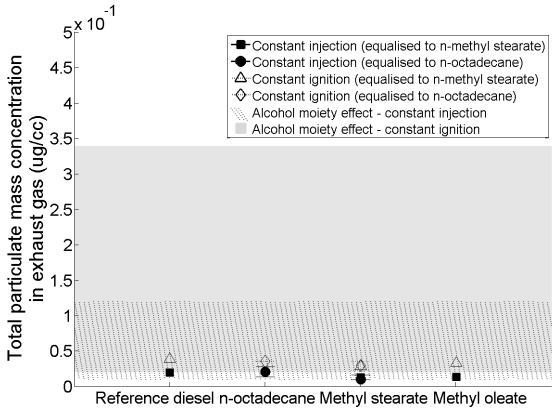

Figure 8.20: Total particulate mass concentration of reference fuels and the impact of the alcohol moiety at constant injection and constant ignition constant ignition delay timing

ted. While Figure 8.19 does show alcohol moiety structure to be a larger influence on the peak number of nucleation mode particles than either the degree of fatty acid saturation or the presence of the ester functional group, far more striking is the impact of the alcohol moiety on the total particulate mass produced. In Figure 8.20 it can be seen that the variation with alcohol moiety in the total mass of particulates produced dwarfs the effect of either fatty acid saturation or ester functional group, and that of the many differences between the reference diesel and the three pure component fuels tested alongside it.

8.2.4. Effect of injection timing

Visible in many of the engine experiment results is a clear offset between those taken at constant injection timing and those taken at constant ignition timing. For example, when considering the effect of carbon chain length in the alcohol moiety, Figure 8.3 shows that at constant ignition timing all fuels displayed a higher peak heat release rate than at constant injection timing. This is likely attributable to differences in physical conditions within the engine cylinder during fuel injection. As all fuels possessed an ignition delay of less than 7.5 CAD, when injection timing was adjusted for SOC at TDC (constant ignition timing) the SOI of every fuel was less than 7.5 CAD. It is suggested that the smaller cylinder volume and higher temperatures thus experienced during the fuel injection increased the level of fuel and air mixing. Therefore, a greater amount of fuel and air was mixed to an ignitable equivalence ratio at SOC and a greater peak heat release rate resulted.

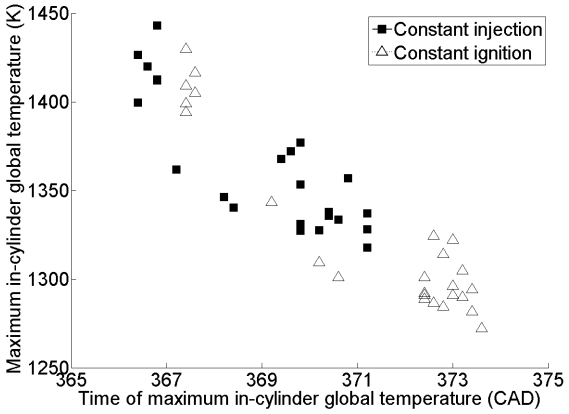

Figure 8.21: Calculated maximum in-cylinder global temperature versus the timing of calculated maximum in-cylinder temperature for all fuels

In Figure 8.4, it can be seen that despite producing higher peak heat release rates, experiments conducted at constant injection timing resulted in lower global maximum in-cylinder temperatures. At constant ignition timing, SOC commences later than at constant injection timing and so the maximum in-cylinder temperature also occurs later into the expansion stroke and thus at greater in-cylinder volumes, this is illustrated by Figure 8.21. The offset between levels of NO_x and also the total mass of particulates at the two timings (Figures 8.5 and 8.8) is therefore clearly the result of the offset seen in Figure 8.4. It is also possible that these results are

highlighting the importance of residence time of gases at elevated temperatures in the production of thermal NO_x, as was suggested by Szybist et al. (2007).

The same effects of injection timing are also readily apparent when considering the effect of the fatty acid functional group and the degree of saturation in the fatty acid moiety. At constant ignition timing, relative to measurements at constant injection timing, peak heat release rates are higher (Figure 8.17), while the global maximum in-cylinder temperatures are lower, as are NO_x emissions (Figure 8.18), and the total mass of particulates is increased (Figure 8.20).

8.2.5. Effect of molecular structure on adiabatic flame temperature

In the case of increasing carbon chain length in the alcohol moiety, it is hard to discern a firm trend in the adiabatic flame temperatures calculated (Figure 8.6). However, it can be seen that *n*-butyl stearate does possess a significantly higher adiabatic flame temperature than the other *n*-alkyl esters. This is also apparent when considering the lower heating value (Table 8.1) of the *n*-butyl stearate relative to the other n-alkyl esters. Increased carbon chain length could be expected to increase the adiabatic flame temperature as the carbon to hydrogen ratio decreases, but the reduced percentage oxygen content of *n*-butyl stearate might also be expected to decrease the adiabatic flame temperature. Considering the branched esters, the two with the highest degree of branching (*iso*-propyl stearate and *tert*-butyl stearate) showed an increase in adiabatic flame temperature relative to the esters of equivalent alcohol moiety straight carbon chain length. Figure 8.22 shows the results of preliminary thermo-gravimetric analysis (TGA) undertaken on some of the esters. The two *n*-alkyl stearates tested (methyl and *n*-butyl stearate) showed one distinct mass loss event, potentially representative of a boiling point, while *tert*-butyl stearate displayed several mass loss events below the expected boiling point (Figure 8.22).

Emran et al. (1999) obtained similar results with TGA of *tert*-butyl ester terminated dendrimers. They find that the magnitude and occurrence temperature of the mass loss events closely correlate with the theoretical amounts of *iso*-butylene that would be produced were the *tert*-butyl moiety to separate from the ester moiety. It is therefore suggested that *tert*-butyl stearate is experiencing the same process of thermal decomposition prior to fuel vaporisation, with the production of isobutylene and the resulting carboxylic acid (stearic). A recent shock tube and kinetic mod-

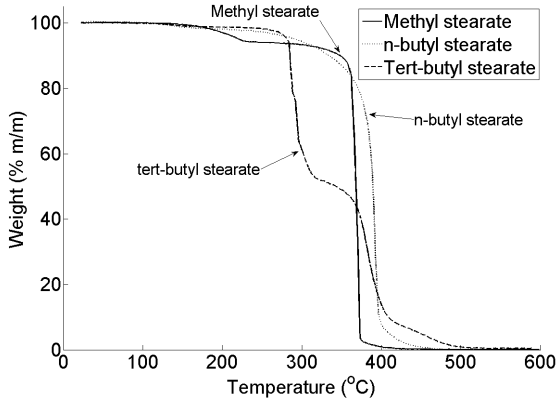

Figure 8.22: Thermo-gravimetric analysis of methyl, *n*-butyl and *tert*-butyl stearate

eling study (Yasunaga et al., 2011) of methyl *tert*-butyl ether and ethyl *tert*-butyl ether found these species to undergo a similar thermal decomposition, with the high temperature reactivity of the ethers inhibited by the formation of iso-butene.

This could explain the decreased ignition quality of *tert*-butyl stearate relative to the other stearates tested. Cetane number measurements of *tert*-butyl stearate are not available, but *iso*-butyl stearate has been reported to possess a cetane number of near 99.3, while stearic acid was found to have a cetane number of 61.7 (Murphy et al., 2004). *Iso*-butylene could also be expected to be of poor ignition quality; the molecule is relatively short and the presence of a double bond and methyl branches were found to further impair ignition quality (Chapter 6).

It is also tentatively suggested that the thermal decomposition of *tert*-butyl stearate is responsible for an elevated adiabatic flame temperature relative to the ester of equivalent alcohol moiety straight carbon chain length. An increase in adiabatic flame temperature is known to occur when introducing a double bond and has been previously observed to be of sufficient importance to influence emissions formation when differences in ignition delay are not present (Chapters 6 and 7, Schönborn et al. (2009b)). Therefore, it is possible that the formation of *iso*-butylene and thus the addition of a further double bond to the reactant mix is having a similar effect. Though purely a speculative suggestion, it could also be that that the thermal degradation of *tert*-butyl stearate is responsible for the discrepancy between Figures 8.10 and 8.11 (*tert*-butyl stearate shows a decrease in peak heat release rate but an increase in in-cylinder maximum temperature).

From the TGA thus conducted it is not possible to draw any firm conclusions as to whether any of the other esters tested are experiencing similar thermal degradation. However, it is apparent that the single mass loss event experienced by n-methyl stearate is of much steeper gradient than that experienced by *n*-butyl stearate. One could therefore speculate that *n*-butyl stearate may be undergoing thermal degradation prior to vaporisation (though of a much lesser extent than *tert*-butyl stearate) and the resulting structure, perhaps with an increased number of double bonds, is responsible for the elevated adiabatic flame temperature seen in Figure 8.8. This could be an observation of the six centered uni-molecular elimination reaction suggested by Zhang et al. (2009). It could also be that such a thermally induced change to the molecular structure is contributing to the increased levels of particulate mass for *n*-butyl stearate seen in Figure 8.8 (as some structural features, such as double bonds, are known to increase sooting levels (Ladommatos et al., 1996)).

8.2.6. Effect of fuel physical properties

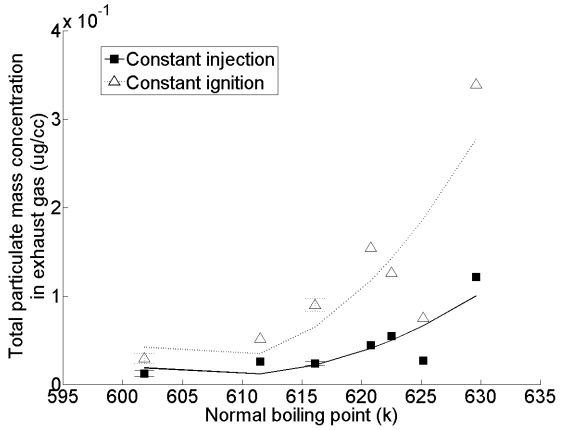

Figure 8.23: Effect of stearate normal boiling point on total mass of particulates in the exhaust gas at constant ignition delay timings

When in Section 8.2.1 considering the effect of fatty acid ester alcohol moiety carbon chain length on the total mass of particulates in the exhaust gas (Figure 8.8), it was suggested that a physical property of the esters may be influencing the fuel atomization and thus levels of soot formation. Therefore, to investigate this hypothesis further Figure 8.23 shows the influence of fuel normal boiling point on the

total mass of particulates produced in the exhaust gas for all the stearates tested at constant ignition delay timings. It can be seen that there is a degree of correlation between boiling point and particulate mass and that the one notable exception to the trend is *tert*-butyl stearate (boiling point 349.4 °C). If the theory outlined in Section 8.2.5, that *tert*-butyl stearate is undergoing severe thermal degradation on injection and prior to soot formation, is correct then this is not particularly surprising. However, it must be noted when considering the degree of correlation present in Figure 8.23 that the values of boiling point plotted are values calculated by a group theory method, not experimental data. The possible influence of other fuel physical properties, such as viscosity or enthalpy of vaporisation, for which experimental data is not readily available but which are likely to correlate well with boiling point must also not be overlooked.

8.2.7. Effect of fuel oxygen content

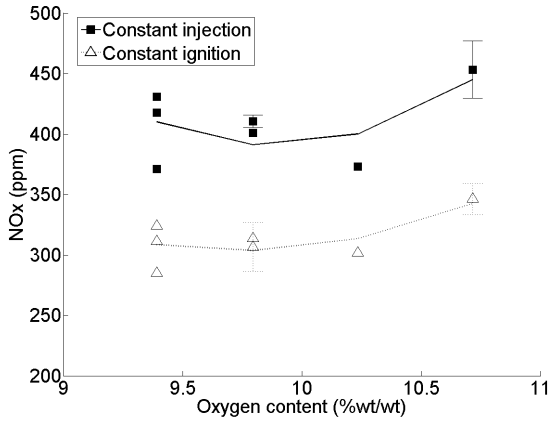

Figure 8.24: The influence of stearate oxygen content on exhaust gas emissions of NO_x at constant ignition delay timings

In Section 8.2.1, when considering the effect of alcohol moiety carbon chain length, oxygen content of the stearates was mooted as a possible influence on emissions of NO_x and particulate mass in the exhaust gas (Figures 8.5 and 8.8). Therefore Figures 8.24 and 8.25 show for all stearates tested, at constant ignition delay timings, the effect of oxygen on the exhaust gas emissions of NO_x and particulate mass respectively. No significant correlation between oxygen content and NO_x emissions can be seen in Figure 8.24, with branching in the alcohol moiety producing differing

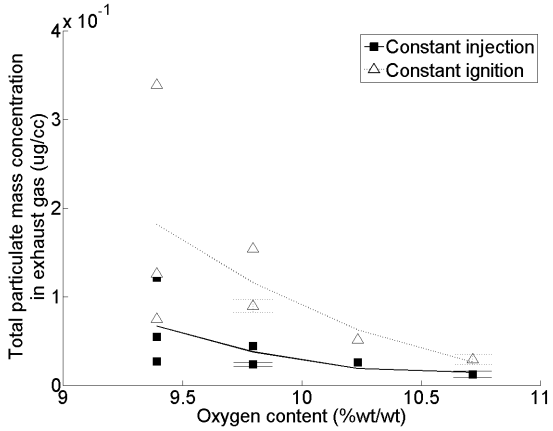

Figure 8.25: The impact of stearate oxygen content on total mass of particulates in the exhaust gas at constant ignition delay timings

NO_x levels even in the case of identical oxygen contents. Similarly, Figure 8.25 shows molecules of identical oxygen content to exhibit varying levels of soot production. In fact, as the degree of correlation in Figure 8.25 is somewhat less than that of Figure 8.23 (where the effect of stearate boiling point on particulate emissions was considered), it could be surmised that while an effect of fuel oxygen content cannot be entirely dismissed, it is of less importance than the fuel boiling point (or correlated thermal property) in determining the levels of particulate mass produced.

8.3. Conclusions

1. In esters of stearic acid, considering the alcohol moiety, an increase in the straight carbon chain length or the addition of methyl branches has no significant impact on the ignition quality of the fuel. Only addition of two methyl branches to the alcohol moiety of a fatty acid ester resulted in a discernable, though slight, increase in ignition delay. Therefore, it would be possible to substitute fatty acid methyl esters with those of longer straight, or branched, alcohols without changes to the diesel combustion strategy.

2. With ignition delay completely removed as a variable, emissions of NO_x reduce with the addition of carbon atoms to the alcohol moiety straight chain carbon length, but increase with the addition of methyl branches to the alcohol moiety. Such changes to the alcohol moiety are at least as significant in determining

exhaust gas levels of NO_x as the addition of one double bond to the fatty acid moiety of an ester.

3. The total mass of particulates in the exhaust gas increases with a longer alcohol moiety carbon chain and to a lesser extent the addition of methyl branches to the alcohol moiety. Both alcohol moiety carbon chain length and branching is of greater importance than the addition of one double bond to the fatty acid moiety or the presence of the ester functional in determining exhaust gas levels of particulate mass.

4. Even with little or no variation in ignition delay between fuels, the primary route by which levels of exhaust NO_x are influenced by molecular structure is through estimated global maximum in-cylinder temperature. NO_x levels decrease with decreasing maximum in-cylinder temperature which is a function of the peak heat release rate of a fuel and the combustion strategy.

5. *Tert*-butyl esters are known to thermally decompose prior to vaporisation. The products of this decomposition are expected to be of lower ignition quality than the original ester and would thus explain the observed increase in ignition delay of *tert*-butyl stearate relative to the other stearates.

In addition, one can advance the following hypotheses:

(a) A trend of ignition delay varying with alcohol carbon number can be deduced from the observed peak heat release rates and does not appear to be wholly attributable to experimental variability. Increasing the alcohol moiety carbon chain length reduces ignition delay, though the trend is non-linear with *n*-propyl stearate possessing a slightly longer ignition delay than ethyl stearate.

(b) The thermal decomposition of *tert*-butyl stearate may also account for an observed increase in adiabatic flame temperature by increasing the number of double bonds present in the reactants. It is also possible that *n*-butyl stearate is undergoing thermal decomposition (although to a lesser extent) and impacting on the production of particulate mass.

(c) A physical property of the stearates, such as boiling point or viscosity, is a primary driver of soot production through influencing fuel atomization and subsequent fuel and air mixing.

(d) An effect of ester oxygen content on NO_x and particulate emissions is possible but is certainly of less importance than the in-cylinder maximum global temperature in the case of NO_x production. Considering soot production, it is likely to be at the highest of tertiary importance with in-cylinder maximum global temperatures and ester physical properties of more significance.

9. The impact of carbonate ester alkyl moiety structure and oxygen content

The development of a liquid fuel that may potentially be produced by reaction of biomass-derived species with atmospheric CO_2 is an attractive proposition that warrants investigation. Carbonate esters may represent such a fuel, as synthesis of such molecules can potentially be achieved by the reaction of CO_2 and alcohols (Chapter 2). While alcohols such as ethanol and butanol have both been found to be suitable drop-in replacements for fossil gasoline, the cetane number of both (Murphy et al., 2004) is too low for direct injection combustion in compression ignition engines as pure components, thus also limiting their use in blends with fossil diesel. Therefore, production of carbonates from such alcohols could potentially result in a fuel of higher compression ignition quality, the manufacture of which includes carbon sequestration.

As reviewed in Chapter 2, di-methyl carbonate (DMC)and di-ethyl carbonate (DEC) have both seen interest as an oxygen bearing fuel additive for compression ignition engines (Zhang et al., 2005; Cheung et al., 2011; European Commission, 2012; Xiaolu et al., 2006; Ren et al., 2008; Bruno et al., 2009). The current chapter investigates the potential of carbonate esters to fuel a modern direct injection compression ignition engine and presents results of experiments which show the influence of carbonate molecular structure on combustion phasing, heat release rates and exhaust emissions. Eight carbonate, and carbonate related, molecules were chosen so as to investigate the effect of alkyl chain length, branching in the alkyl chain and molecule oxygen content.

9.1. Experimental method

9.1.1. Apparatus

All of the combustion experiments described in the present chapter were performed using the compression ignition engine and the ultra low volume fuel system described in Chapter 3. For all the tests, air was aspirated into the combustion chamber at atmospheric pressure and a PID-controlled air intake heater, located 200 mm upstream of the inlet manifold, was utilised to heat the intake air (at atmospheric pressure) to a temperature of 130 $\pm$ 2.5 °C at the entrance to the inlet manifold.

9.1.2. Fuel molecules investigated

Six carbonates, one ketone and one ester were tested so as to investigate the effect of the following molecular structural properties on compression ignition combustion and emissions:

(a) The alkyl chain length of symmetrical carbonate esters.

(b) Branching in the alkyl chains of symmetrical carbonate esters with constant alkyl chain carbon number.

(c) Reducing the oxygen content of an oxygenate while keeping all other structural features constant.

To observe the effect of increasing the carbon chain length of symmetrical carbonates, di-methyl carbonate (DMC) , di-ethyl carbonate (DEC) and di-*n*-butyl carbonate (DnBC) were chosen. A further three carbonates were selected to investigate the impact of branching in the alkyl chains of carbonates: di-1-methyl propyl carbonate (D1MPC) , di-2-methyl propyl carbonate (D2MPC) and di-tert-butyl carbonate (DTBC) . One fatty acid ester, butyl valerate, and one ketone, 5-nonanone, were also tested to assess the influence of oxygen content. All of the molecules were blended with *n*-decane as the majority would not combust as single component fuels, despite attempts with considerable modification to the normal running conditions of the engine (1 bar inlet boost pressure and heating of the inlet air to 160 °C). A reference fossil diesel with zero FAME content was also tested.

Four of the carbonates, DnBC, D1MPC, D2MPC and DtBC, were specially synthesized by an organic synthesis company (further details are given in Appendix D.3), with the remaining fuel molecules and *n*-decane obtained from a chemical supplier (Sigma Aldrich). The assay and other properties of each fuel are presented in Table 9.1, while the molecular structure of each is given in Table 9.2.

9.1.3. Experimental conditions

Each of the fuel molecules (blended with 30 % *n*-decane) and reference diesel were initially tested at two experimental conditions: constant fuel injection timing and constant start of ignition timingas defined in Chapter 5. After the two sets of experiments at constant injection and constant ignition timing were completed, a

third series of experiments was carried out at constant ignition delay timing, utilising the ignition improver 2 EHN and the method described in Chapter 5.

A further series of experiments were conducted in which di-methyl carbonate and di-ethyl carbonate were blended with *n*-decane in varying proportions. These were conducted at constant injection and constant ignition timing only.

All tests were conducted at an engine speed of 1200 rpm and at 450 bar fuel injection pressure. The injection duration was adjusted in the case of every fuel so that the engine IMEP was always constant at 4.00 bar for all fuels. Fuels which were solid at room temperature were preheated to 60 °C in a temperature controlled water bath. A summary of the engine and test operating conditions is given in Tables 9.3 and 9.4.

Table 9.1: Properties of carbonate esters and reference fossil diesel

Fuel	Molecular formula	Assay (%)	T_{boil} (°C)	T_{melt} (°C)	△vapH° (kJ/mol)	△vapH° (kJ/kg)	Density (kg/m^3)	Dynamic viscosity at 20 °C (mPa.s)	Lower heating value (MJ/Kg)
Reference fossil diesel	-	-	268.9‡	-	-	-	834.5◇	-	43.14†
di-methyl carbonate	$C_3H_6O_3$	99	90.4[1]	-5.6[2]	37.7[3]	418.5	1063[4]	0.579[4]	14.51[3]
di-ethyl carbonate	$C_5H_{10}O_3$	99	127.0[5]	-75.2[6]	43.6[5]	369.1	969[4]	0.749[4]	22.17[7]
di-*n*-butyl carbonate	$C_9H_{18}O_3$	98	207.0[8]	-	62.5[9]	358.7	923.9[10]	1.763*[11]	-
di-1-methyl-propyl carbonate	$C_9H_{18}O_3$	98	179.0[12]	-	-	-	921[13]	-	-
di-2-methyl-propyl carbonate	$C_9H_{18}O_3$	98	190.0[14]	-	-	-	906.8[15]	1.832*[11]	-
di-tert-butyl carbonate	$C_9H_{18}O_3$	98	161.0[16]	37.0[16]	65.4[17]	375.6	-	-	-
Butyl valerate	$C_9H_{18}O_2$	98	187.0[18]	-92.8[19]	53.0[20]	334.9	871.1[23]	1.348*[18]	-
5-nonanone	$C_9H_{18}O$	97	188.0[3]	-5.9[21]	53.3[22]	374.7	821[22]	-	37.61[22]
n-decane	$C_{10}H_{22}$	99	174.0[24]	-29.6[25]	51.4[24]	361.2	729.8[26]	0.913[27]	44.50[17]

† = calculated from experimental data obtained by the IP12 methodInstitute of Petroleum (2001), ◇ = experimental data obtained according to ASTM D4052 at 15 °C, ‡ = experimental data obtained according to EN ISO 3405, [1] = data from Comelli and Francesconi (1997), [2] = data from Biltz et al. (1930), [3] = data from Steele et al. (1997), [4] = data from Arbad et al. (2005), [5] = data from Mansson (1972), [6] = data from Yakovenko et al. (2011), [7] = data from Thomsen (1905), [8] = data from Wright (1961), [9] = data from Kozlova et al. (2008), [10] = data from Gurvich (1966), [11] = data from Bowden and Butler (1939), [12] = data from Bayer (1901), [13] = data from Pastushenko (1983), [14] = data from Lecat (1943), [15] = data from Nefedov (1972), [16] = data from Bigley and Wren (1972), [17] = data from Verevkin et al. (2008), [18] = data from Gill and Dexter (1934), [19] = data from Lievens (1924), [20] = data from Schjanberg (1937), [21] = data from Timmermans (1927), [22] = data from Harrop et al. (1970), [23] = data from Turowa-Poljak (1964), [24] = data from Lefkowitz et al. (2012), [25] = data from Kulkarni et al. (1974), [26] = data from Xiang et al. (2007) and [27] = data from Feitosa et al. (2009).

Table 9.2: Carbonate ester molecular structures

di-methyl carbonate (DMC)	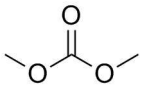
di-ethyl carbonate (DEC)	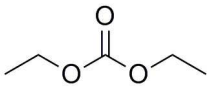
di-*n*-butyl carbonate (DnBC)	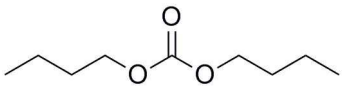
di-1-methyl-propyl carbonate (D1MPC)	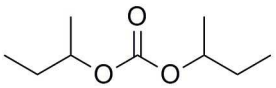
di-2-methyl-propyl carbonate (D2MPC)	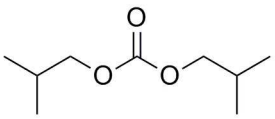
di-tert-butyl carbonate (DTBC)	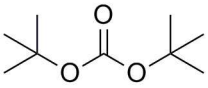
Butyl valerate	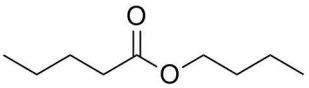
5-nonanone	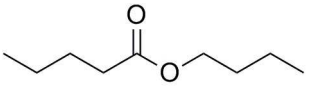
n-decane	

Table 9.3: Engine and test operating conditions of carbonates with 30 % (wt/wt) *n*-decane

Fuel	2 EHN dosage (ppm)	Engine speed (rpm)	Fuel injection pressure (bar)	IMEP (bar)	Constant injection timing (SOI at 7.5 CAD BTDC)				Constant ignition timing (SOC at TDC)			
					Ignition delay (CAD)		Injection duration (µs)		Ignition delay (CAD)		Injection duration (µs)	
					Mean	1σ	Mean	1σ	Mean	1σ	Mean	1σ
Reference fossil diesel	0	1200	450	4	5.1	0.1	746	11	4.9	0.2	750	11
di-methyl carbonate	0	1200	450	4	8.8	0.2	1244	13	8.5	0.5	1280	25
di-ethyl carbonate	0	1200	450	4	10	0.1	1016	9	9.9	0.1	1048	7
di-*n*-butyl carbonate	0	1200	450	4	7.4	0.2	860	12	7.3	0.1	871	16
di-1-methyl-propyl carbonate	0	1200	450	4	8.6	0.1	837	3	8.6	0.1	853	3
di-2-methyl-propyl carbonate	0	1200	450	4	8.7	0	852	3	8.8	0.1	865	4
di-tert-butyl carbonate	0	1200	450	4	9.1	0.2	845	1	9.1	0.1	860	3
Butyl valerate	0	1200	450	4	6.9	0	820	5	6.9	0	827	7
5-nonanone	0	1200	450	4	6.1	0	769	7	6	0	828	40
di-methyl carbonate	3894	1200	450	4	7.1	0	1258	8	7.1	0	1275	0
di-ethyl carbonate	11576	1200	450	4	7.2	0.1	1039	2	7.3	0	1048	0
di-*n*-butyl carbonate	4236	1200	450	4	6	0.1	873	13	6.1	0.1	887	3
di-1-methyl-propyl carbonate	7018	1200	450	4	7.3	0	884	0	7.3	0	890	0
di-2-methyl-propyl carbonate	8533	1200	450	4	7.1	0	895	0	7.1	0	903	0
di-tert-butyl carbonate	10066	1200	450	4	7.5	0	886	0	7.3	0	895	0
Butyl valerate	3034	1200	450	4	5.9	0	828	0	5.8	0	829	0

Table 9.4: Engine and test operating conditions of carbonates with varying *n*-decane proportion

Fuel	% Carbonate (wt/wt)	Engine speed (rpm)	Fuel injection pressure (bar)	IMEP (bar)	Constant injection timing (SOI at 7.5 CAD BTDC)				Constant ignition timing (SOC at TDC)			
					Ignition delay (CAD)		Injection duration (µs)		Ignition delay (CAD)		Injection duration (µs)	
					Mean	1σ	Mean	1σ	Mean	1σ	Mean	1σ
Reference fossil diesel	0	1200	450	4	5.3	0.2	731	8	5.1	0.3	735	9
n-decane	0	1200	450	4	4.2	0.3	728	13	4	0.4	733	8
di-methyl carbonate	27.5	1200	450	4	4.9	0	801	0	4.7	0	803	0
di-methyl carbonate	51.1	1200	450	4	5.9	0	972	0	5.8	0	971	0
di-methyl carbonate	44	1200	450	4	5.3	0	900	0	5.1	0	898	0
di-methyl carbonate	60.7	1200	450	4	5.9	0	977	0	5.7	0	984	0
di-methyl carbonate	70.1	1200	450	4	8.9	0	1117	0	9	0	1145	0
di-methyl carbonate	75.4	1200	450	4	10.8	0.1	1179	4	10.7	0.2	1220	8
di-methyl carbonate	84.8	1200	450	4	DNC	-	-	-	14.2	0	1412	0
di-ethyl carbonate	25	1200	450	4	4.5	0	802	0	4.3	0	802	0
di-ethyl carbonate	50	1200	450	4	5.7	0	905	0	5.7	0	908	0
di-ethyl carbonate	70	1200	450	4	9.9	0	1020	0	9.9	0	1060	0
di-ethyl carbonate	80	1200	450	4	DNC	-	-	-	16.9	0	1153	0

9.2. Results and discussion

9.2.1. Carbonate alkyl moiety length

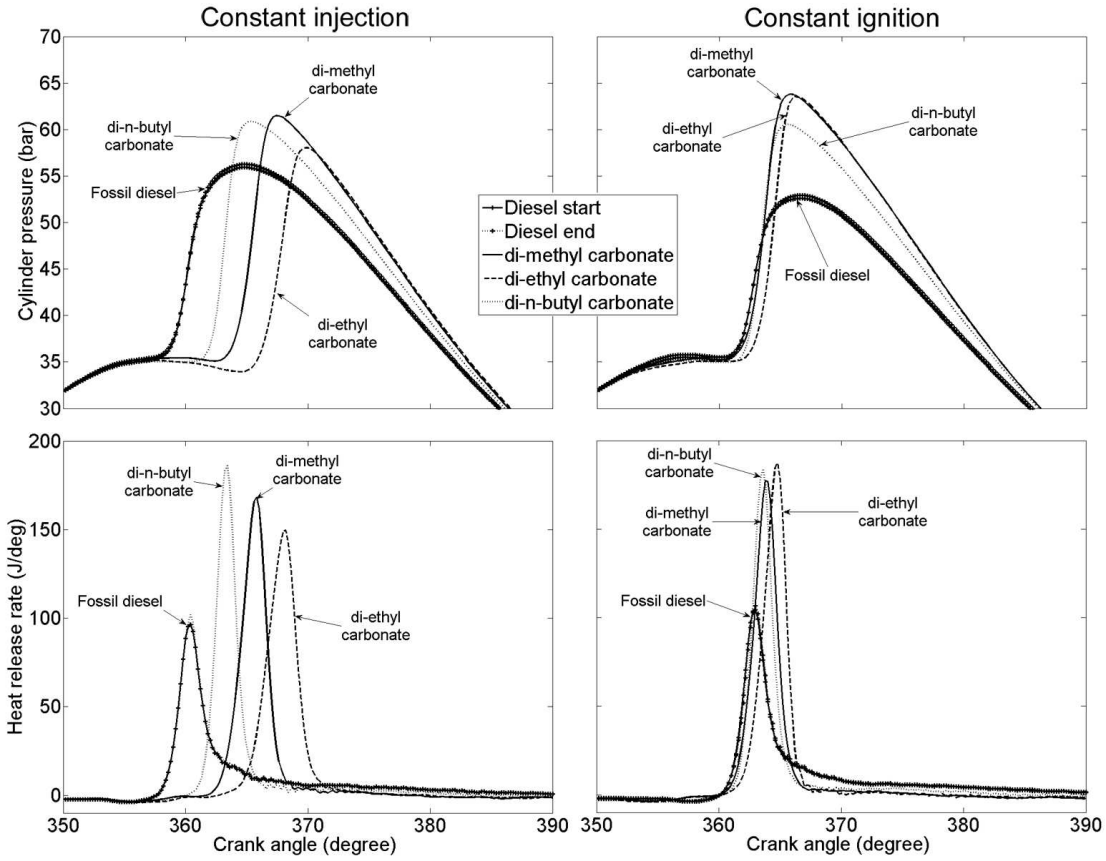

Figure 9.1: In-cylinder pressures and apparent net heat release rates of di-methyl carbonate, di-ethyl carbonate, di-*n*-butyl carbonate and reference fossil diesel at constant injection and constant ignition timing

Figure 9.1 shows the in-cylinder pressures and apparent net heat release rates of di-methyl carbonate (DMC), di-ethyl carbonate (DEC) and di-*n*-butyl carbonate (DnBC), each blended with 30 % (wt/wt) *n*-decane, at constant injection and constant ignition timing. It can be seen from Figure 9.1 that in the case of all fuels, the majority of heat release occurred during premixed combustion, signified by the rapid rise and subsequent fall of heat release rates following ignition. It is evident from Figure 9.1 that, as might be expected, the carbonate of longest alkyl chain length (DnBC) is of higher ignition quality than the shorter alkyl carbonates chained (DMC and DEC) and displays the shortest ignition delay.

A further series of experiments was conducted where the ignition delay of the carbonates was removed as a variable by the use of the ignition improving additive 2 EHN, as described in Chapter 5. These engine experiments were then performed at a fixed SOI of 7.5 CAD BTDC and also an injection timing of 7.1 to 7.3 CAD BTDC so that SOC always occurred at TDC.

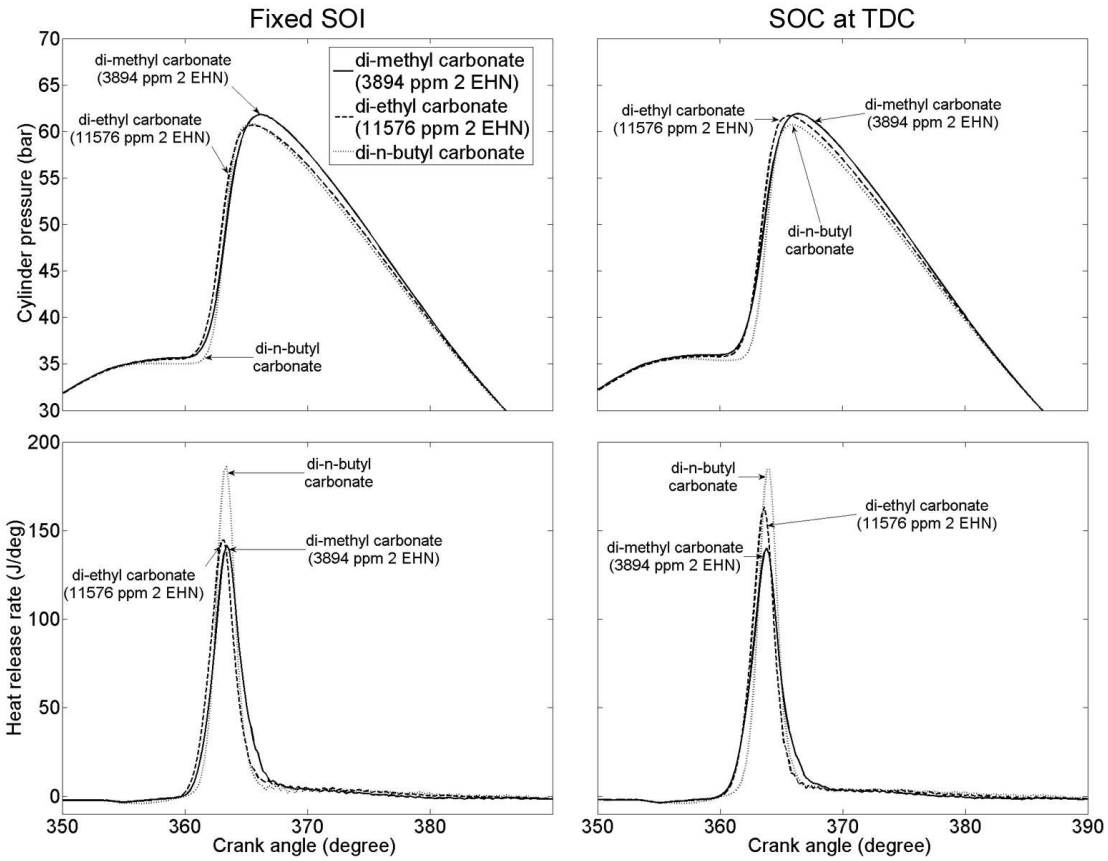

Figure 9.2: In-cylinder pressures and apparent net heat release rates of di-methyl carbonate, di-ethyl carbonate and di-*n*-butyl carbonate at constant ignition delay timings of fixed SOI and SOC at TDC

Figure 9.2 shows the in-cylinder pressures and apparent net heat release rate of DMC, DEC and DnBC blends with 30 % *n*-decane at constant ignition delay timings of fixed SOI and SOC at TDC. It can be seen that the use of 2 EHN has resulted in all three carbonates now exhibiting a similar duration of ignition delay and combustion, although some variation in their peak heat release rates achieved persisted (Figure 9.2).

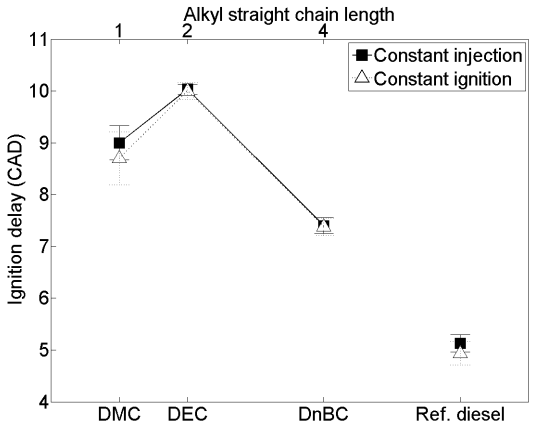

Figure 9.3: Ignition delays of di-methyl carbonate (DMC), di-ethyl carbonate (DEC) and di-*n*-butyl carbonate (DnBC) with 30 % *n*-decane and reference fossil diesel at constant injection and constant ignition timings

Figure 9.3 shows the ignition delays (as defined in Chapter 5) of DMC, DEC and DnBC blended with 30 % *n*-decane and the reference fossil diesel at constant injection and constant ignition timings. The shorter ignition delay of DnBC (Figure 9.3) relative to the two carbonates of shorter alkyl chain length (DMC and DEC) is consistent with the study of *n*-alkanes in Chapter 6 where increasing the straight alkyl chain length reduced ignition delay times. However, this study did not consider *n*-alkanes shorter than *n*-heptane.

Glaude et al. (2005) in simulating the low temperature kinetics of DMC in an opposed flow and non-premixed flame found that the route of oxygenate breakdown leading to production of CO_2 (Equation 2.9, p 44) dominated. In premixed flames of *n*-heptane, Chen et al. (2012) found that the majority of CO_2 formed on addition of DMC to the flame could be attributed to Equation 2.9. Investigating the combustion of dibutyl maleate in a direct injection compression ignition engine, Buchholz et al. (2004) also found that direct production of CO_2 from the two ROC$^{\bullet}$=O groups present (Equation 2.9) overwhelmed formation of CO (Equation 2.10) by a ratio of 9:1. Therefore assuming that under the experimental conditions in the current study Equation 2.9 is the dominant pathway of DMC decomposition (via initial H abstraction by H or OH radicals (Glaude et al., 2005)), then it is suggested that

the decomposition of DMC results in production of CO_2, an alkyl radical and an alkyoxy radical, i.e.

$$CH_3OCOOCH_3 \leftrightarrow CH_2O^{\bullet} + CH_3^{\bullet} + CO_2 \tag{9.1}$$

Kinetic modelling specific to the decomposition of DEC or DnBC has not yet been reported, and to propose such mechanisms is beyond the scope of this study. However, it is tentatively suggested that the decomposition of DEC and DnBC is likely to result in radicals possessing ethyl and butyl chains respectively. The shorter ignition delay of DnBC relative to the shorter alkyl chain (Figure 9.3) can therefore likely be attributed to the potential of butyl chains, unlike ethyl chains and methyl groups, to form six member transition rings that allow oxidized alkyl chains to undergo internal isomerisation and is a key step in the low temperature branching reactions of alkyl chains (Westbrook, 2000; Zdor et al., 2011). Considering the reactivity of ethyl chains relative to methyl groups, measurements of cetane number (Murphy et al., 2004) and calculation of reaction rates (Abou-Rachid et al., 2003) of methanol and ethanol would suggest that the ethyl chain is more reactive, contrary to the longer ignition delay of DEC relative to DMC observed (Figure 9.3). The potential of cross reactions between the straight alkyl chain carbonates and the *n*-decane present is explored in Section 9.2.4.

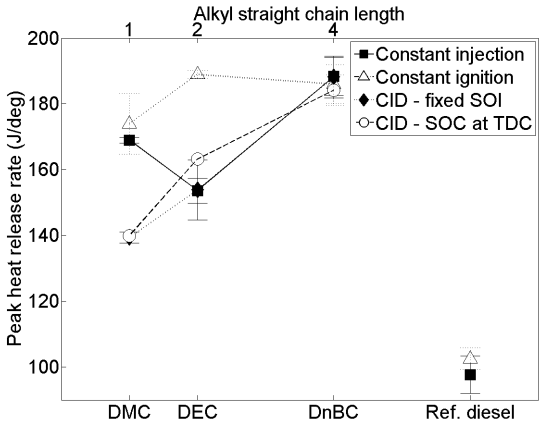

Figure 9.4: Apparent net peak heat release rates of di-methyl carbonate (DMC), di-ethyl carbonate (DEC) and di-*n*-butyl carbonate (DnBC) with 30 % *n*-decane and reference fossil diesel at constant injection, constant ignition and constant ignition delay timings

Figure 9.4 shows the apparent net peak heat release rate of DMC, DEC and DnBC with 30 % (wt/wt) *n*-decane and the reference fossil diesel at constant injection and constant ignition timings, and also constant ignition delay timings of fixed SOI and SOC at TDC. Notwithstanding the extent of experimental error shown in Figure 9.4, it can be seen that all of the carbonates displayed a higher peak heat release rate than the reference fossil diesel, in agreement with previous studies of DMC and fossil diesel blends (Cheung et al., 2011; Zhang et al., 2005). At constant injection and constant ignition timing, the disparity between the peak heat release rates displayed by DEC at the two timing conditions (Figure 9.4) can be attributed to the time at which peak heat release occurs. In Figure 9.1, it can be seen that at constant injection timing, the apparent peak heat release rate of DEC occurs significantly later into the expansion stroke than at constant ignition timing. A seen in Chapter 8, it follows that further into the expansion stroke, at greater cylinder volumes, there is increased potential for heat transfer to the cylinder walls and thus the peak heat release of DEC at constant injection timing is significantly lower than at constant ignition where peak heat release rate occurs closer to TDC (Figure 9.1).

Previously, in Chapter 6, a strong correlation was found between the duration of ignition delay and the peak heat release rate, where a longer ignition delay allowed more time for fuel and air mixing prior to SOC, resulting in more fuel and air mixture at combustible stoichiometry at SOC and thus a larger premixed burn fraction. However, the peak heat release rates of the carbonates (Figure 9.4) do not fit this relationship, with the carbonate displaying the shortest ignition delay (Figure 9.3), DnBC, also exhibiting the highest peak heat release rate. Cheung et al. (2011) suggested that the high latent heat of vaporisation of DMC relative to fossil diesel results in localised cooling of the in-cylinder charge. In Table 9.1, it can be seen that when considered on a mass basis, the latent heat of vaporisation of the straight alkyl chain carbonates decreases with alkyl chain length, and it is therefore suggested that levels of localised cooling results also decrease with increasing alkyl chain length.

Figures 9.5a and b show the calculated maximum in-cylinder global temperature and time of occurrence of DMC, DEC and DnBC with 30 % (wt/wt) *n*-decane and the reference fossil diesel at constant injection and constant ignition timings, and also constant ignition delay timings of fixed SOI and SOC at TDC. No clear impact of peak heat release rate (Figure 9.4) on the maximum in-cylinder temperature is

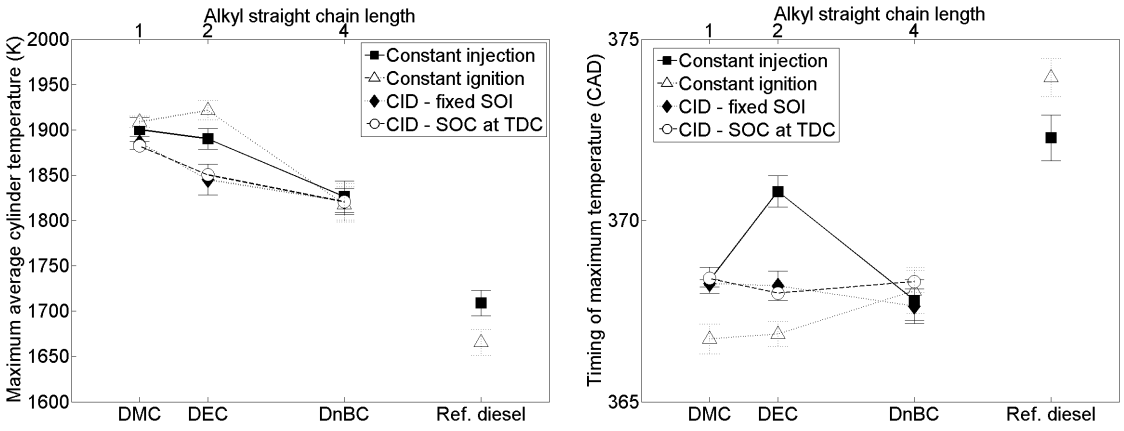

(a) (b)

Figure 9.5: (a) Calculated maximum in-cylinder global temperature and (b) time of occurrence of di-methyl carbonate (DMC), di-ethyl carbonate (DEC) and di-*n*-butyl carbonate (DnBC) with 30 % *n*-decane and reference fossil diesel at constant injection, constant ignition and constant ignition delay timings

visible (Figure 9.5a). However, considering the time of maximum in-cylinder global temperature (Figure 9.5b), the effect of injection timing is apparent; at constant injection timing DMC and DEC show a later time of occurrence than at constant ignition, consistent with the time of peak heat release rate at each timing condition (Figure 9.1).

Figure 9.6 shows the exhaust NO_x emissions of DMC, DEC and DnBC blended with 30 % *n*-decane and the reference fossil diesel at constant injection and constant ignition timings, and the constant ignition delay timings of fixed SOI and SOC and TDC. Rates of NO_x production increase with temperature and so NO_x emissions from compression ignition combustion are sensitive to both the magnitude of the in-cylinder temperature and the residence time of the cylinder contents at elevated temperatures (Mueller et al., 2009; Schönborn et al., 2009b; Szybist et al., 2005). An influence of both factors is apparent in the NO_x emissions of the straight alkyl chain carbonates: DnBC exhibits the lowest maximum in-cylinder temperature (Figures 9.5a) and emitted the lowest level of NO_x (Figure 9.6), while at constant injection timing the maximum in-cylinder temperature of DMC and DEC occurs later than at constant ignition timing and at the former timing both carbonates also emitted lower levels of NO_x. With ignition delay equalised, the NO_x emissions of DEC are similar

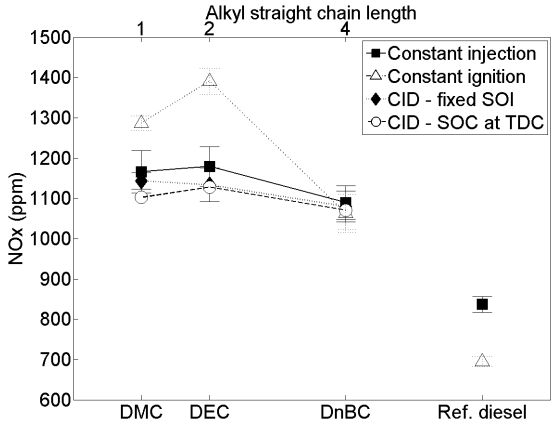

Figure 9.6: NO_x emissions of di-methyl carbonate (DMC), di-ethyl carbonate (DEC) and di-*n*-butyl carbonate (DnBC) with 30 % *n*-decane and reference fossil diesel at constant injection, constant ignition and constant ignition delay timings

to those of DMC (Figure 9.6), despite a lower maximum in-cylinder temperature (Figure 9.5a) occurring at a similar time (Figure 9.5b) and suggests an influence of peak heat release rate (Figure 9.4), which DEC exhibited a higher magnitude of relative to DMC.

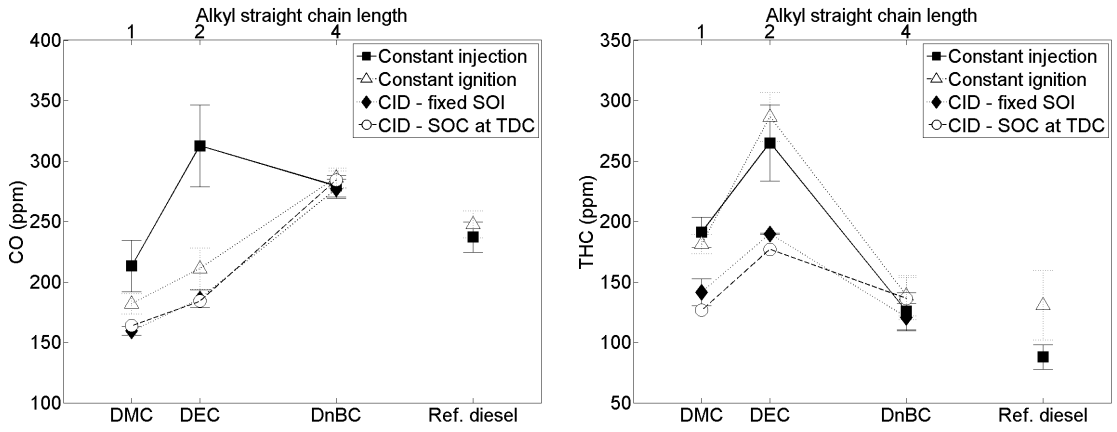

(a) (b)

Figure 9.7: (a) CO and (b) THC emissions of di-methyl carbonate (DMC), di-ethyl carbonate (DEC) and di-*n*-butyl carbonate (DnBC) with 30 % *n*-decane and reference fossil diesel at constant injection, constant ignition and constant ignition delay timings

Figures 9.7a and b show the CO and THC emissions of DMC, DEC and DnBC with 30 % *n*-decane and the reference fossil diesel at constant injection, constant ignition and the constant ignition delay timings of fixed SOI and SOC at TDC. Both CO and THC are known products of incomplete combustion, arising under fuel rich and fuel lean conditions respectively. DEC at constant injection timing exhibits the latest time of maximum in-cylinder temperature (Figure 9.5b) of the carbonates and also the highest CO emissions (Figure 9.7a); with peak temperatures occurring later into the expansion stroke it follows that a greater degree of the cylinder charge will undergo incomplete combustion. Previous studies of carbonate and fossil diesel blends have attributed the decrease in CO emissions of such blends relative to fossil diesel to the provision of oxygen in fuel rich zones (Ren et al., 2008). Similarly, it can be seen in Figure 9.7a that, in general, emissions of CO decrease with the level of fuel bound oxygen present. Therefore, it is hypothesised that the apparent increase in the degree of incomplete combustion with carbonate alkyl chain length can explain the decrease in maximum in-cylinder temperature (Figure 9.5a) with increasing carbonate alkyl chain length.

Apparent in Figure 9.7b is an effect of ignition delay; when the duration of DMC and DEC ignition delay have been reduced utilising 2 EHN, the levels of THC emitted are lower. This decrease in THC emissions with reduced ignition delay potentially suggests that over-dilution of the fuels in air is occurring and resulting in emission of THC. However, consistently higher emissions of THC by DEC (Figure 9.7b) relative to the other straight alkyl chain carbonates at the same timing conditions would seem to suggest that a physical property of DEC is also influencing the degree of fuel over-dilution. However, of the physical properties that might be expected to affect the efficiency of fuel and air mixing (boiling point, density and viscosity (Wu et al., 2006)), the properties of DEC lie between those of DMC and DnBC (Table 9.1), except in the case of density where DMC is denser than both DEC and DnBC.

Figures 9.8a and b show the particulate emissions of DMC, DEC and DnBC with 30 % *n*-decane at constant injection and constant ignition timing. With both timings, the increase in the chain length correlates well with an increase in particulate matter (Figures 9.8a and b). An influence of the timing condition is also apparent in the emission of nucleation mode particles, with constant ignition at TDC showing

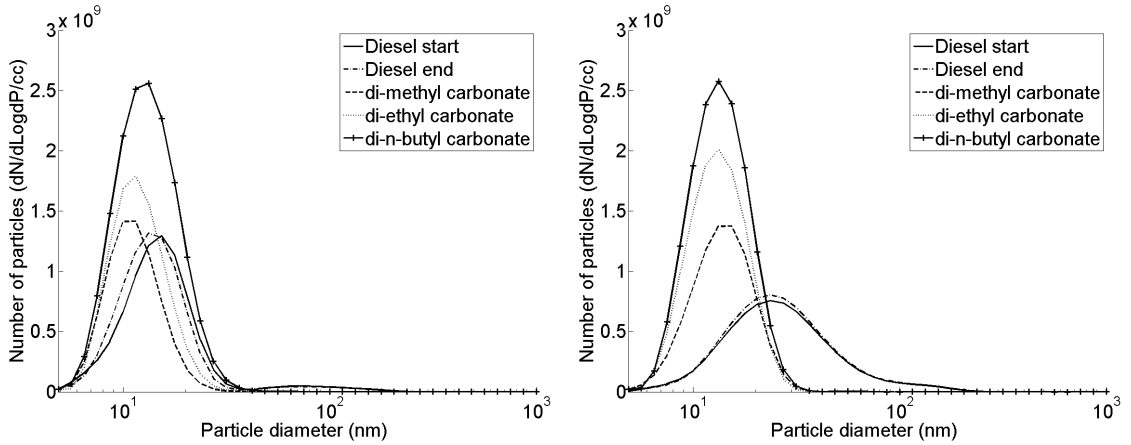

Figure 9.8: Particulate emissions of di-methyl carbonate (DMC), di-ethyl carbonate (DEC) and di-*n*-butyl carbonate (DnBC) with 30 % *n*-decane and reference fossil diesel at (a) constant injection and (b) constant ignition timing

a decrease in the number particles and a shift in their size to larger diameters (from $\approx$ 10 nm to about 15 - 20 nm).

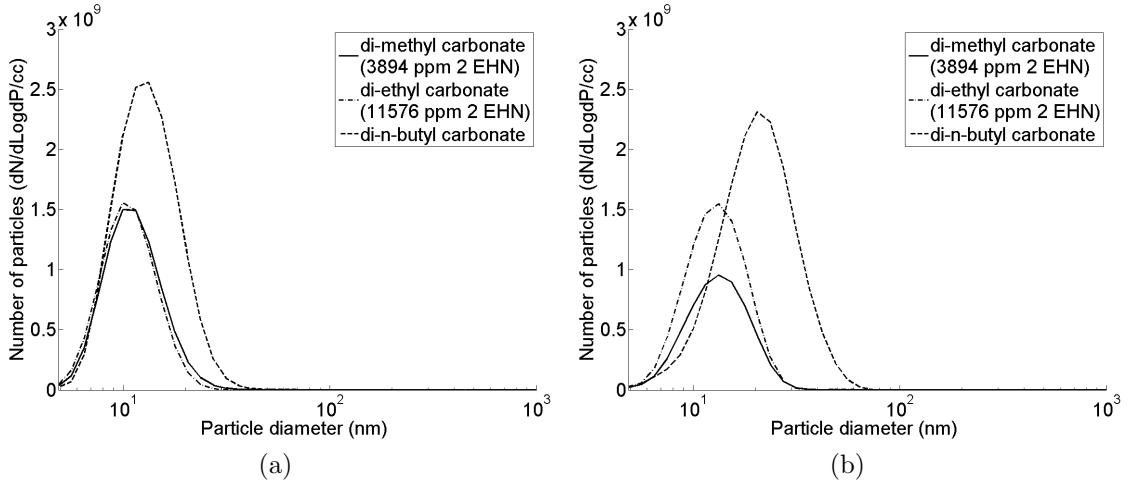

Figure 9.9: Particulate emissions of di-methyl carbonate (DMC), di-ethyl carbonate (DEC) and di-*n*-butyl carbonate (DnBC) with 30 % *n*-decane and reference fossil diesel at constant ignition delay (a) fixed SOI and (b) SOC at TDC timing

Figures 9.9a and b show the particulate emissions of DMC, DEC and DnBC blended with 30 % (wt/wt) *n*-decane at the constant ignition delay timings of fixed SOI and SOC at TDC. At SOC at TDC timing (Figure 9.9b), the same trend of increasing peak number of nucleation mode particles with increasing carbonate straight alkyl chain length observed with differences in ignition delay present (Figures 9.8a and b) is still apparent.

The increasing peak in nucleation mode emissions of the carbonates with increasing alkyl chain length, irrespective of the duration of ignition delay, also coincides with an increasing boiling point of the molecules (Table 9.1). It has previously been speculated that a significant proportion of nucleation mode particles are in fact condensed droplets of un-burnt fuel (Schönborn et al., 2009b). Therefore, it is suggested that the majority of the nucleation mode emissions of the straight chain carbonates are in fact droplets of condensed fuel, as DnBC possesses the highest boiling point (thus the vapour of which is most likely to condense) and emits the highest levels of nucleation mode particles.

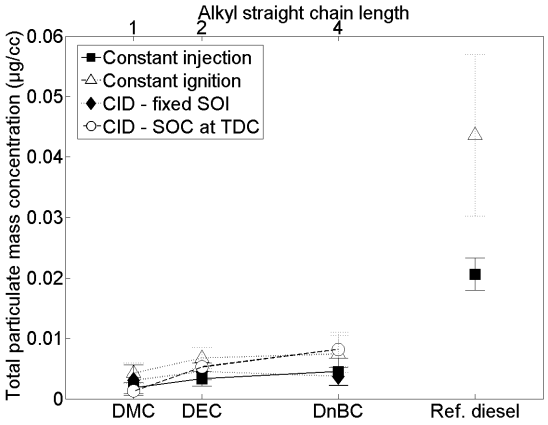

Figure 9.10: Total particulate mass emitted by di-methyl carbonate (DMC), di-ethyl carbonate (DEC) and di-*n*-butyl carbonate (DnBC) with 30 % *n*-decane and reference fossil diesel at constant injection, constant ignition and constant ignition delay timings

Figure 9.10 shows the total particulate emissions of DMC, DEC and DnBC blended with 30 % *n*-decane and the reference fossil diesel at constant injection, constant ignition and both constant ignition delay timings. It is known that rates of soot oxidation increase with temperature (Tree and Svensson, 2007); however, there is no readily apparent correlation between the total mass of particulates emitted (Figure

9.10) and the maximum in-cylinder temperature reached or the time which it occurs (Figures 9.5a and b). Rates of soot oxidation are also influenced by the availability of oxygen, with levels of soot produced observed to decrease with increasing fuel oxygen content (Tree and Svensson, 2007). Thus the significantly higher emission of particulate mass by the reference fossil diesel relative to all of the carbonates (Figure 9.10) can primarily be attributed to the zero oxygen content of the reference fossil diesel and is in agreement with previous studies where addition of carbonates to fossil diesel reduced particulate emissions (Cheung et al., 2011; Ren et al., 2008; Zhang et al., 2005). The observed trend of increasing total particulate mass with increasing carbonate straight alkyl chain length can be explained by the concurrent increasing level of fuel bound oxygen (Table 9.1); it is also known that longer alkyl and alkane molecules tend to produce more soot (Ladommatos et al., 1996).

9.2.2. Carbonate alkyl moiety branching

This section of the current chapter deals with branching of the carbonate ester alkyl moiety. Figure 9.11 shows the in-cylinder pressures and apparent net heat release rates of di*n*-*n*-butyl carbonate (DnBC), di-1-methyl-propyl carbonate (D1MPC), di-2-methyl-propyl carbonate (D2MPC) and di-tert butyl carbonate (DTBC) blends with 30 % (wt/wt) *n*-decane and the reference fossil diesel at constant injection and constant ignition timing. It is apparent at constant ignition timing (Figure 9.11), that while during running of these experiments injection timing was adjusted so that all fuels showed initial heat release (SOC) at TDC, D1MPC and DTBC both display a 2nd period of ignition delay prior to peak heat release rates.

As in Section 9.2.1, a further series of experiments were conducted where the ignition delay of the branched alkyl moiety carbonates was equalised to that of DnBC by the use of the ignition improving additive 2 EHN. Figure 9.12 shows the in-cylinder pressures and apparent net heat release rates of DnBC, D1MPC, D2MPC and DTBC blends with 30 % (wt/wt) *n*-decane at the constant ignition delay timings of fixed SOI and SOC at TDC. With the initial duration of ignition delay equalised (SOI to SOC), D1MPC and DTBC no longer exhibit a period of 2nd ignition delay (Figure 9.12), though variation in the magnitude of peak heat release of the carbonates is still apparent.

Figures 9.13a and b show the duration of initial ignition delay (SOI to SOC) and also 2nd ignition delay of DnBC, D1MPC, D2MPC and DTBC blended with 30 %

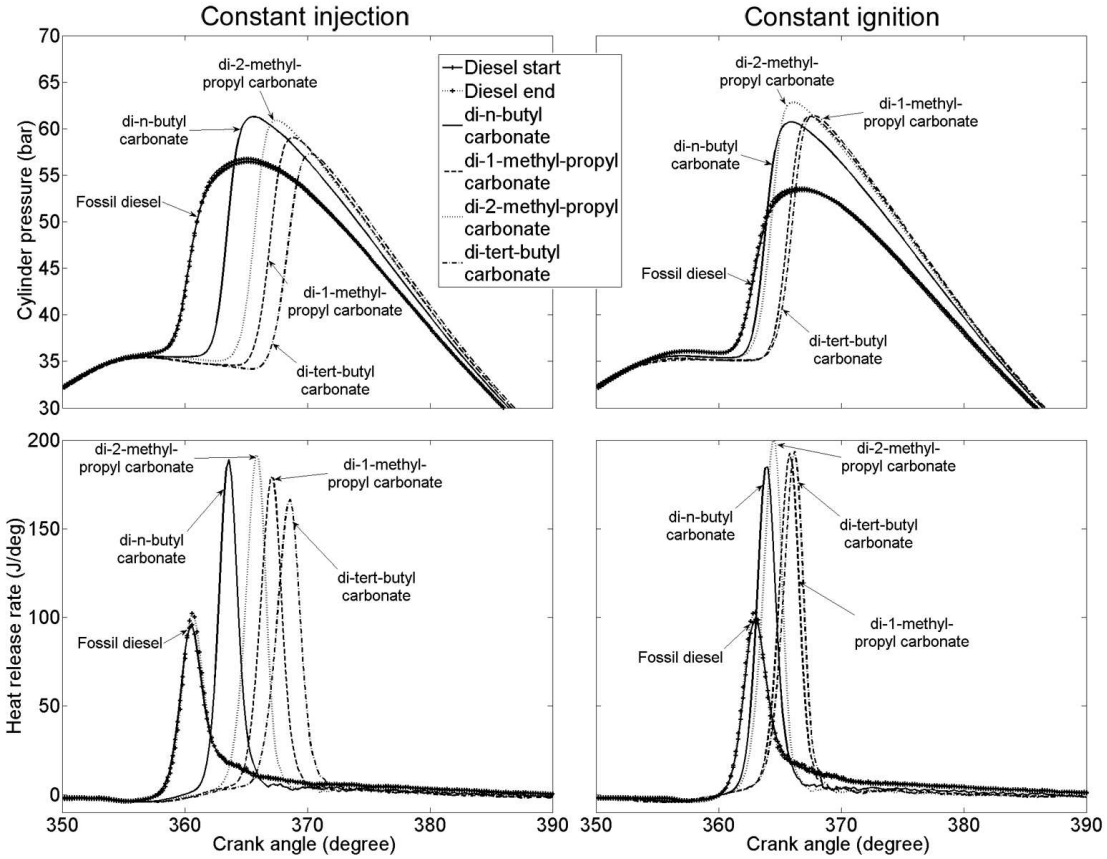

Figure 9.11: In-cylinder pressures and apparent net heat release rates of DnBC, D1MPC, D2MPC and DTBC with 30 % (wt/wt) *n*-decane and reference fossil diesel at constant injection and constant ignition timing

n-decane and the reference fossil diesel at constant injection and constant ignition timing. The values of 2nd ignition delay presented in Figure 9.13b are defined as the interval between initial fuel ignition (SOC) and the point at which a second phase of heat release commences (SOC2 as defined in Chapter 4). The increase in ignition delay with an increasing degree of branching in the butyl moiety of the carbonates (Figure 9.13a), is consistent with Chapter 6 where increasing the percentage of branches present in a fully saturated alkane resulted in longer ignition delays. This can be attributed to an increase in the presence of primary C-H bonds (abstraction of H atoms from which is more difficult than that from the secondary C-H bonds present in straight alkyl chains) and a reduction in the number of transition rings that can be formed (Westbrook, 2000).

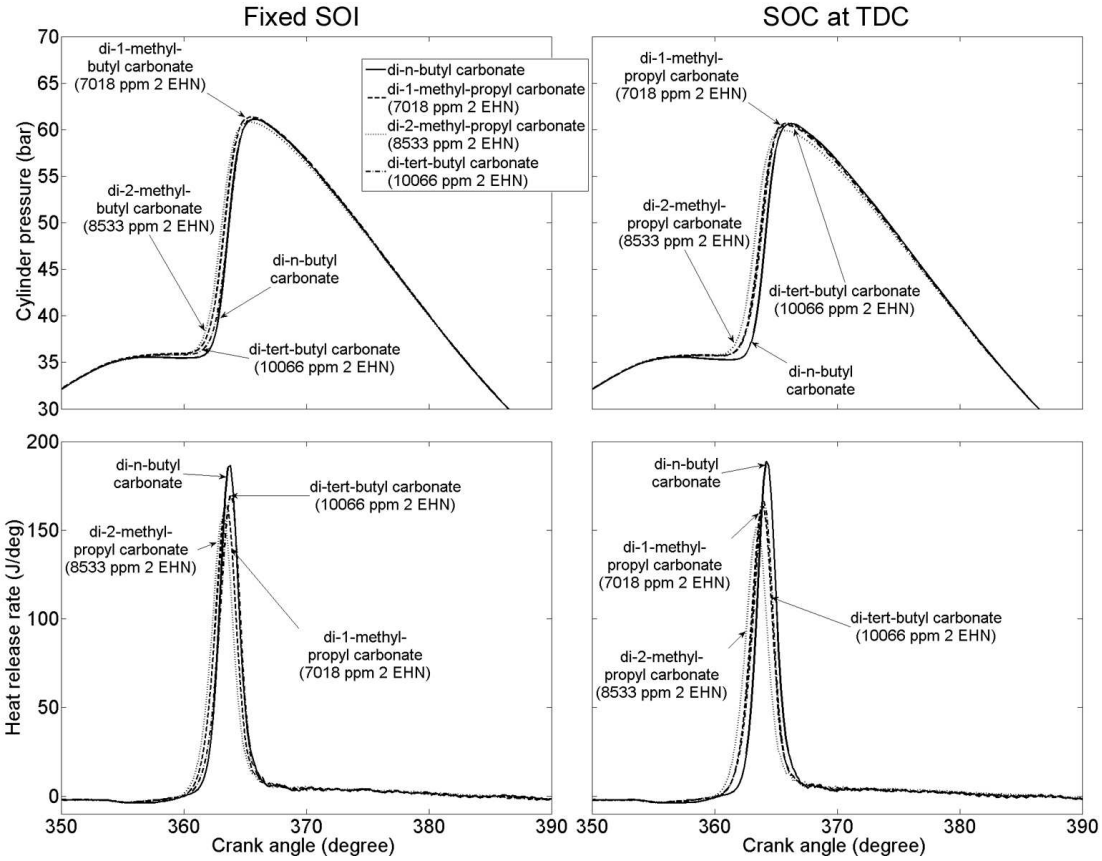

Figure 9.12: In-cylinder pressures and apparent net heat release rates of DnBC, D1MPC, D2MPC and DTBC with 30 % (wt/wt) *n*-decane at constant ignition delay timings of fixed SOI and SOC at TDC

While the initial ignition delay of DTBC (Figure 9.13a) is less than that of DEC (Figure 9.3), DTBC shows a significant duration of 2nd ignition delay (Figure 9.13b), which was not readily apparent in the case of the straight alkyl moiety carbonates (Figure 9.1). Of the single branched carbonates, D1MPC also exhibits a significant duration of 2nd ignition delay (Figure 9.13b) while D2MPC does not, despite both displaying a similar duration of initial ignition delay (Figure 9.13a). It is suggested that this effect of alkyl branch position can be attributed to the preferential abstraction of H atoms from carbons bonded to an oxygen atom (relative to secondary carbon atoms) (Zhang and Boehman, 2010). In the case of D1MPC the carbon bonded to an oxygen has only one H available for abstraction (due to the methyl branch bonded to this atom), whereas in the case of D2MPC there are two H atoms available for abstraction from this carbon. Therefore, it can be seen the

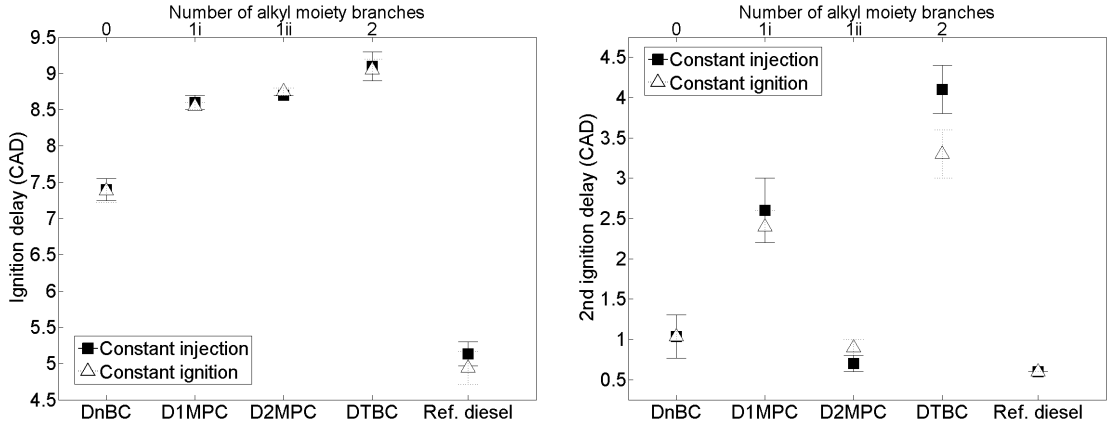

(a) (b)

Figure 9.13: Duration of (a) ignition delay and (b) 2nd ignition delay of di-*n*-butyl carbonate (DnBC), di-1-methyl-propyl carbonate (D1MPC), di-2-methyl-propyl carbonate (D2MPC) and di-tert-butyl carbonate (DTBC) with 30 % *n*-decane and reference fossil diesel at constant injection and constant ignition timings

single branch present in D1MPC will have a greater inhibiting effect on the rates of low temperature branching reactions than the single branch present in D2MPC.

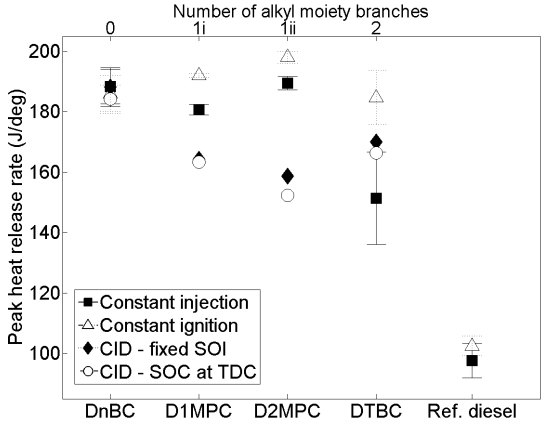

Figure 9.14: Apparent net peak heat release rates of di-*n*-butyl carbonate (DnBC), di-1-methyl-propyl carbonate (D1MPC), di-2-methyl-propyl carbonate (D2MPC) and di-tert-butyl carbonate (DTBC) with 30 % *n*-decane and reference fossil diesel at constant injection, constant ignition and constant ignition delay timings

Figure 9.14 shows the apparent net peak heat release rate of DnBC, D1MPC, D2MPC and DTBC blends with 30 % *n*-decane and the reference fossil diesel at constant injection and constant ignition timing and both constant ignition delay timings. The same effect of cylinder volume as described in Section 9.2.1 plausibly explains the lower peak heat release rates of DTBC and D1MPC relative to DnBC and D2MPC, despite significantly longer ignition delays (Figures 9.13a and b).

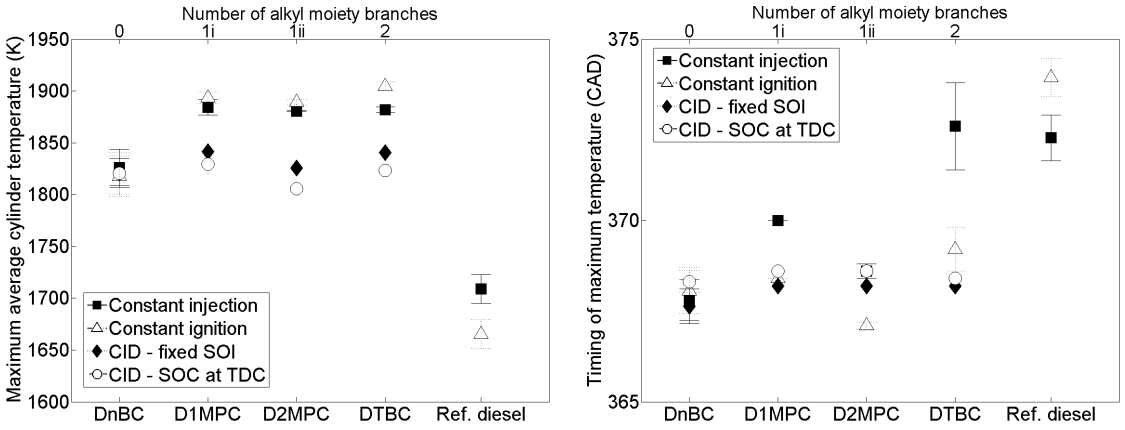

(a) (b)

Figure 9.15: (a) Calculated maximum in-cylinder global temperature and (b) time of occurrence of di-*n*-butyl carbonate (DnBC), di-1-methyl-propyl carbonate (D1MPC), di-2-methyl-propyl carbonate (D2MPC) and di-tert-butyl carbonate (DTBC) with 30 % *n*-decane and reference fossil diesel at constant injection, constant ignition and constant ignition delay timings

Figures 9.15a and b show the magnitude and time of occurrence of the calculated maximum in-cylinder global temperature of DnBC, D1MPC, D2MPC and DTBC blends with 30 % *n*-decane at constant injection, constant ignition and constant ignition delay timings. The late time of maximum in-cylinder temperature of the reference fossil diesel relative to the carbonates (Figure 9.15b) despite a shorter ignition delay (Figures 9.13a and b), can be attributed to a significantly lower peak heat release (Figure 9.14).

Figure 9.16 shows the NO_x emissions of DnBC, D1MPC, D2MPC and DTBC, blended with 30 % (wt/wt) *n*-decane, and the reference fossil diesel at constant injection, constant ignition timings and the constant ignition delay timings of fixed SOI and SOC at TDC. At all injection timings the levels of NO_x emitted by the

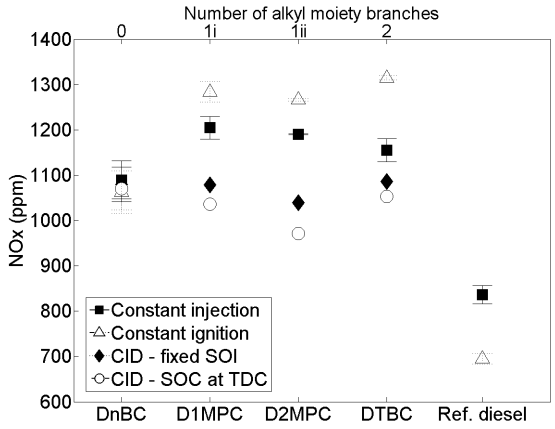

Figure 9.16: NO_x emissions of di-*n*-butyl carbonate (DnBC), di-1-methyl-propyl carbonate (D1MPC), di-2-methyl-propyl carbonate (D2MPC) and di-tert-butyl carbonate (DTBC) with 30 % *n*-decane and reference fossil diesel at constant injection, constant ignition and constant ignition delay timings

carbonates and reference fossil diesel (Figure 9.16) mirror precisely the maximum in-cylinder temperature reached (Figure 9.15a); except in the case of DTBC at constant injection timing where a latter time of maximum in-cylinder temperature (Figure 9.15b) results in a lower level of NO_x than might be expected.

Figures 9.17a and b show the CO and THC emissions of DnBC, D1MPC, D2MPC and DTBC with 30 % *n*-decane and the reference fossil diesel at constant injection, constant ignition and both constant ignition delay timings. At a shorter duration of ignition delay (Figure 9.13), the three branched carbonates produced lower levels of CO (Figure 9.17a); at a shorter ignition delay it could be expected that a lesser degree of fuel dilution in air would have taken place and zones of fuel rich mixture would be more prevalent. This would suggest that formation of CO by the branched carbonates can be primarily attributed to insufficient temperatures (as opposed to insufficient levels of oxygen) for complete combustion. This is further supported by the large range of experimental error shown by DTBC at constant injection timing (Figure 9.17a) as it correlates well with the range of error present in both the time of maximum in-cylinder global temperature (Figure 9.15b) and the peak heat release rate (Figure 9.14). While the range of experimental error presented in Figure 9.17 is significant, there is apparent a possible influence of ignition delay and probable fuel over-dilution; DTBC possessed the longest ignition delays of all the carbonates

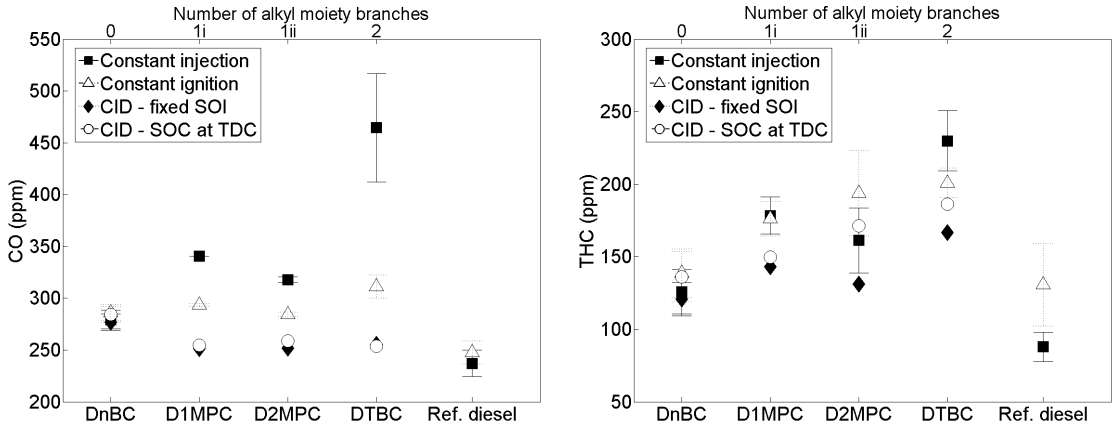

(a) (b)

Figure 9.17: (a) CO and (b) THC emissions of di-*n*-butyl carbonate (DnBC), di-1-methyl-propyl carbonate (D1MPC), di-2-methyl-propyl carbonate (D2MPC) and di-tert-butyl carbonate (DTBC) with 30 % *n*-decane and reference fossil diesel at constant injection, constant ignition and constant ignition delay timings

at constant injection and constant ignition timing (Figures 9.3a and b) and also produces the highest levels of THC.

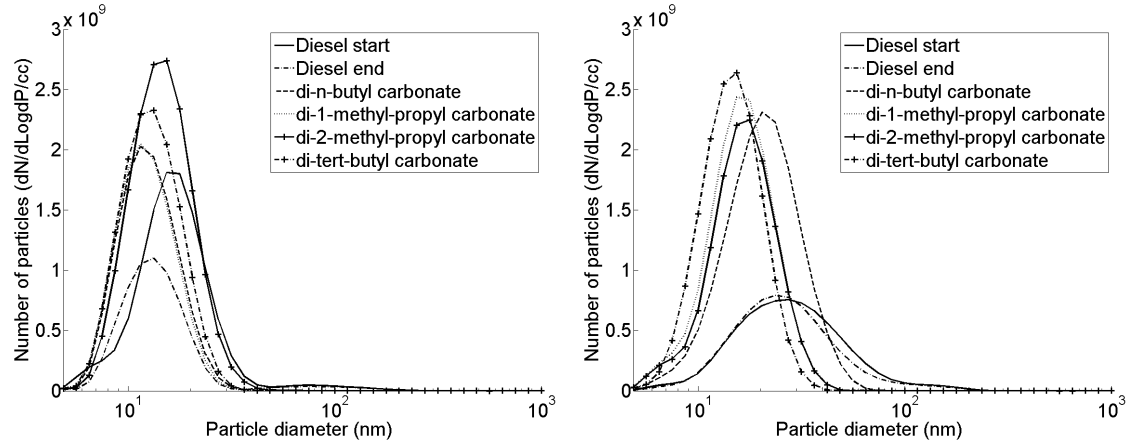

(a) (b)

Figure 9.18: Particulate emissions of di-*n*-butyl carbonate (DnBC), di-1-methyl-propyl carbonate (D1MPC), di-2-methyl-propyl carbonate (D2MPC) and di-tert-butyl carbonate (DTBC) with 30 % *n*-decane and reference fossil diesel at (a) constant injection and (b) constant ignition

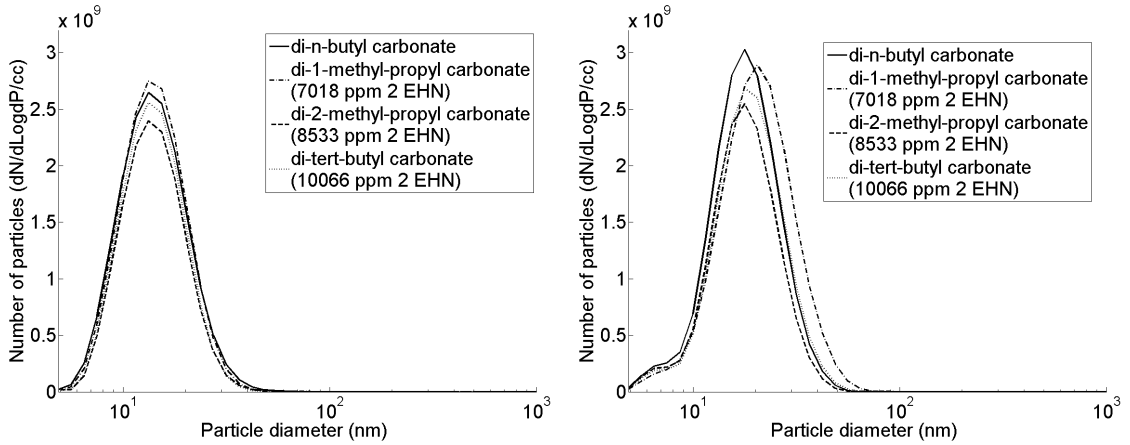

Figure 9.19: Particulate emissions of di-*n*-butyl carbonate (DnBC), di-1-methyl-propyl carbonate (D1MPC), di-2-methyl-propyl carbonate (D2MPC) and di-tert-butyl carbonate (DTBC) with 30 % *n*-decane and reference fossil diesel at constant ignition delay (a) fixed SOI and (b) SOC at TDC timing

Figures 9.18a and b show the particulate emissions of DnBC, D1MPC, D2MPC and DTBC blended with 30 % (wt/wt) *n*-decane and the reference fossil diesel at constant injection and constant ignition timing. Figures 9.19a and b show the particulate emissions of DnBC, D1MPC, D2MPC and DTBC blendes with 30 % (wt/wt) *n*-decane at constant ignition timings of fixed SOI and SOC at TDC. Contrary to the straight alkyl chain carbonates (Figures 9.9a and b), no clear evidence of an effect of carbonate fuel boiling point (Table 9.1) on the production of nucleation mode particles is visible in the case of the branched alkyl moiety carbonates at any of the timing conditions (Figures 9.18a and b and 9.19a and b).

Figure 9.20 shows the total particulate mass emitted by DnBC, D1MPC, D2mPC and DTBC blended with 30 % (wt/wt) *n*-decane and the reference fossil diesel at constant injection, constant ignition and both constant ignition delay timings. As with the straight alkyl chain carbonates (Figure 9.10), an effect of injection timing, via influence on in-cylinder thermal conditions (Figures 9.15a and b), is apparent and especially so at constant ignition delay timings. With the margin of error present in Figure 9.20, any effect of increasing the level or position of branching in the alkyl moiety in the carbonates is difficult to discern, though there is no suggestion

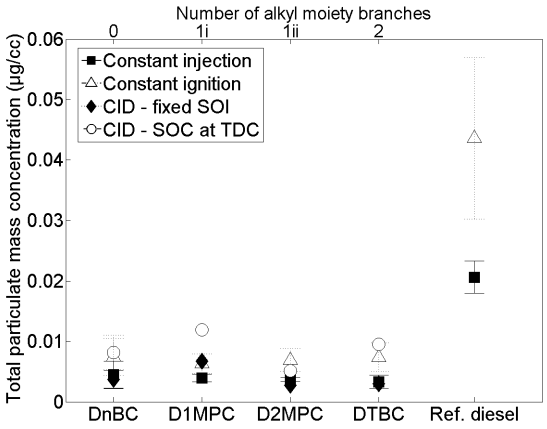

Figure 9.20: Total particulate mass emissions of di-*n*-butyl carbonate (DnBC), di-1-methyl-propyl carbonate (D1MPC), di-2-methyl-propyl carbonate (D2MPC) and di-tert-butyl carbonate (DTBC) with 30 % *n*-decane and reference fossil diesel at constant injection, constant ignition and constant ignition delay timings

that increased branching is resulting in increased soot levels as has been previously observed (Ladommatos et al., 1996).

9.2.3. Molecular oxygen content

This section of Chapter 9 considers the effect of oxygen content within otherwise structurally similar molecules. Figure 9.21 shows the in-cylinder pressures and apparent net heat release rates of di-*n*-butyl carbonate, butyl valerate and 5-nonannone blended with 30 % (wt/wt) *n*-decane and the reference fossil diesel at constant injection and constant ignition timing. As with the straight alkyl chain and branched alkyl chain carbonates (Figures 9.1 and 9.11), the heat release of butyl valerate and 5-nonanone is predominantly during premixed combustion (Figure 9.21). In addition to the tests of DnBC, butyl valerate and 5-nonanone blended with 30 % (wt/wt), an attempt was made to combust the oxygenates at the same conditions, but as single component fuels. However, without the presence of *n*-decane, only 5-nonanone was found to combust in a steady manner.

As in Sections 9.2.1 and 9.2.2, a further series of experiments were conducted in which through use of 2 EHN the ignition delays of DnBC and butyl valerate were matched to that of 5-nonanone, and performed at injection timings of fixed SOI of 7.5 CAD BTDC and also an SOI of 5.8 - 6.1 CAD BTDC for constant SOC at TDC.

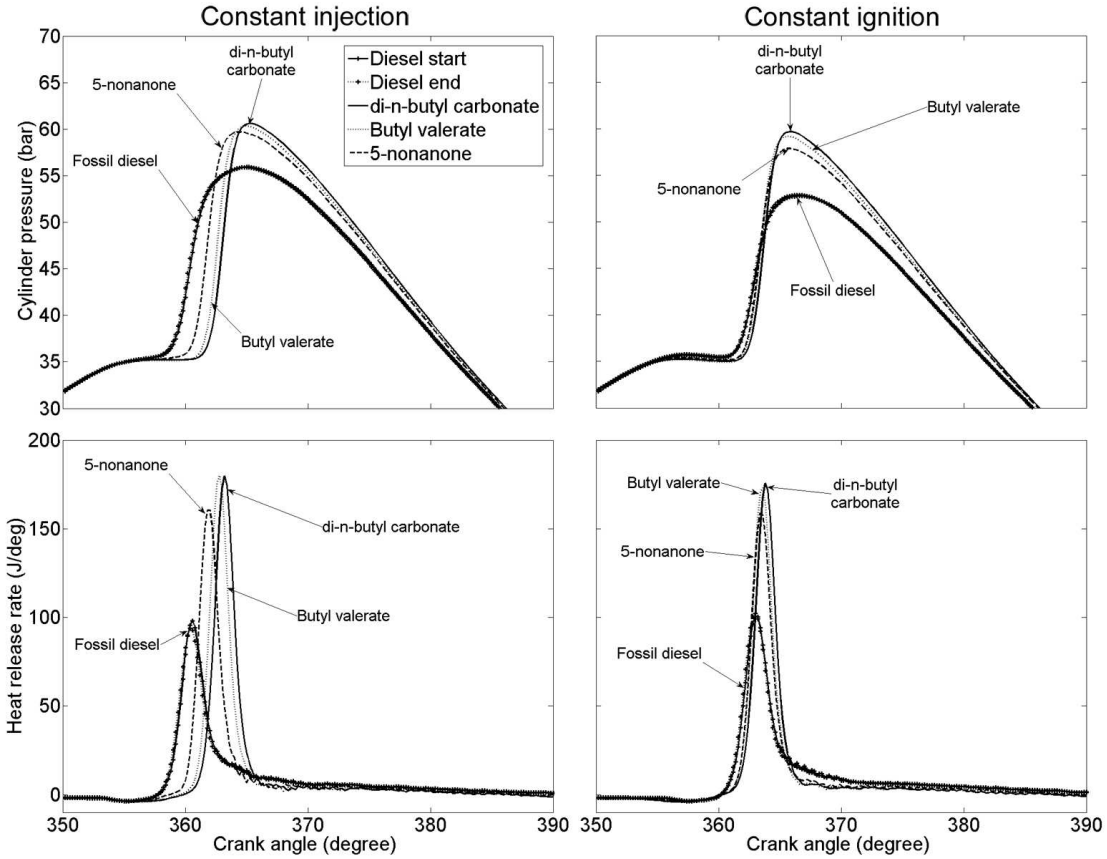

Figure 9.21: In-cylinder pressures and apparent net heat release rates of di-*n*-butyl carbonate, butyl valerate and 5-nonanone with 30 % (wt/wt) *n*-decane and reference fossil diesel at constant injection and constant ignition timing

Figure 9.22 shows the in-cylinder pressures and apparent net heat release rates of DnBC, butyl valerate and 5-nonanone with 30 % (wt/wt) *n*-decane at the constant ignition delay timings of fixed SOI and SOC at TDC. At both timings (Figure 9.22), it can be seen that despite an equivalent SOC for all of the oxygenates, rates of heat release rate increase more slowly for 5-nonanone than either DnBC or butyl valerate. It should be noted that of the three oxygenates, at constant ignition delay timings only 5-nonanone has not been treated with the radical providing additive 2 EHN. However, it is also possible that this is attributable to the reduced level of fuel bound oxygen in fuel rich areas (relative to butyl valerate and DnBC), the availability of which was observed to increase rates of combustion in blends of DMC with fossil diesel (Cheung et al., 2011; Zhang et al., 2005).

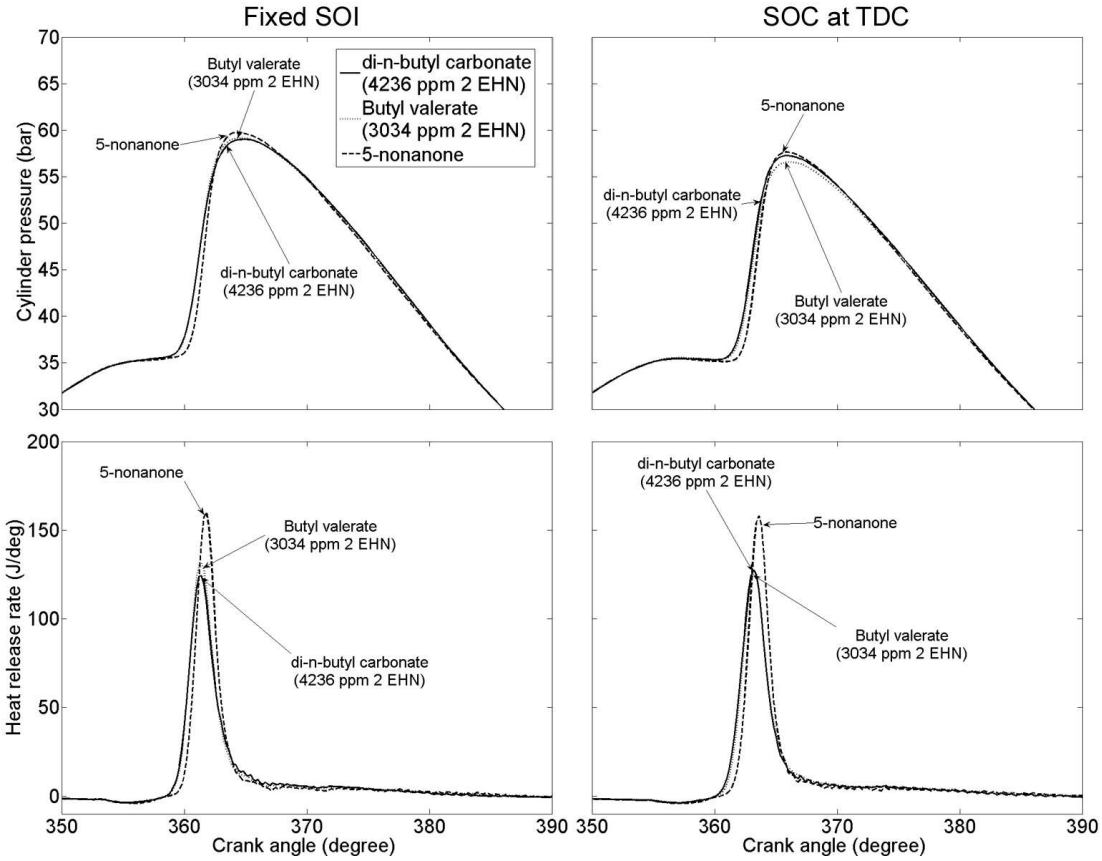

Figure 9.22: In-cylinder pressures and apparent net heat release rates of di-*n*-butyl carbonate, butyl valerate and 5-nonanone with 30 % (wt/wt) *n*-decane and reference fossil diesel at constant ignition delay timings of fixed SOI and SOC at TDC

Figure 9.23 shows the ignition delay (SOI to SOC) of DnBC, butyl valerate and 5-nonanone blends with 30 % (wt/wt) *n*-decane and the reference fossil diesel at constant injection and constant ignition timing. The higher ignition quality of the ketone relative to the ester (Figure 9.23) is in agreement with cetane number measurements of 2-heptanone and methyl caproate (Murphy et al., 2004), whose relationship (in terms of molecular structure) to one another, is identical to that of 5-nonanone to butyl valerate. Assuming that DnBC and butyl valerate both initially decompose at low temperatures according to Equations 2.9 and 2.10, and that the ratios of CO_2 formation according to Equation 2.9 and the formation of CO according to Equation 2.10 are similar in the case of both fuel molecules, it can be seen that the decomposition of DnBC will result in a greater number of alkyoxy radicals relative to that of butyl valerate. It is therefore hypothesised that this greater num-

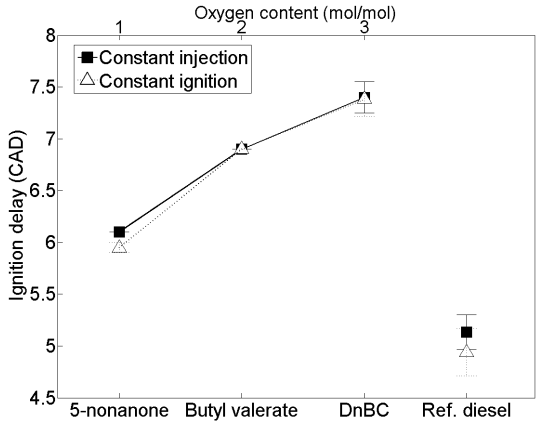

Figure 9.23: Duration of ignition delay of di-*n*-butyl carbonate (DnBC), butyl valerate and 5-nonanone with 30 % *n*-decane and reference fossil diesel at constant injection and constant ignition timings

ber of alkyoxy radicals results in the longer ignition delay of DnBC relative to butyl valerate, as the presence of an oxygen atom attached to alkyl chain can reduce the rate of transition ring reactions (Zhang and Boehman, 2012), which are required for the primary pathway of alkyl chain low temperature radical branching (Westbrook, 2000). Should 5-nonanone be decomposing according to Equation 2.10, then it can be see that none of the resulting radicals would include oxygen, thus accounting for the shorter ignition of the ketone relative to both DnBC and butyl valerate.

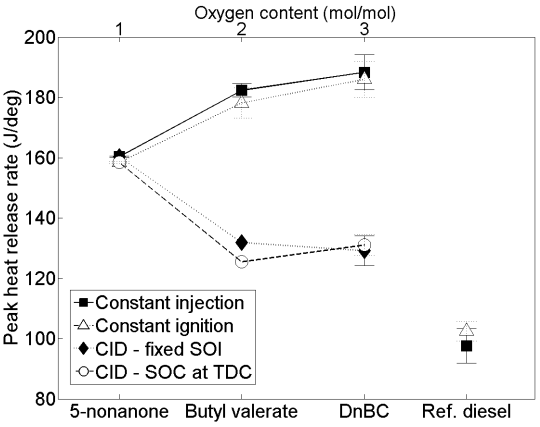

Figure 9.24: Apparent net peak heat release rates of di-*n*-butyl carbonate (DnBC), butyl valerate and 5-nonanone with 30 % *n*-decane and reference fossil diesel at constant injection, constant ignition and constant ignition delay timings

Figure 9.24 shows the apparent neat peak heat release rates of DnBC, butyl valerate and 5-nonanone blends with 30 % *n*-decane at constant injection, constant ignition and constant ignition delay timings of fixed SOI and SOC at TDC. The higher peak heat release of 5-nonanone relative to DnBC and butyl valerate at constant ignition delay timings would seem to suggest that the rate of fuel and air mixing in the case of 5-nonanone is faster than that of DnBC and butyl valerate, despite the presence of less molar oxygen. It is suggested that this is perhaps indicative of the limits of 2 EHN in achieving equal durations of ignition delay between differing fuels.

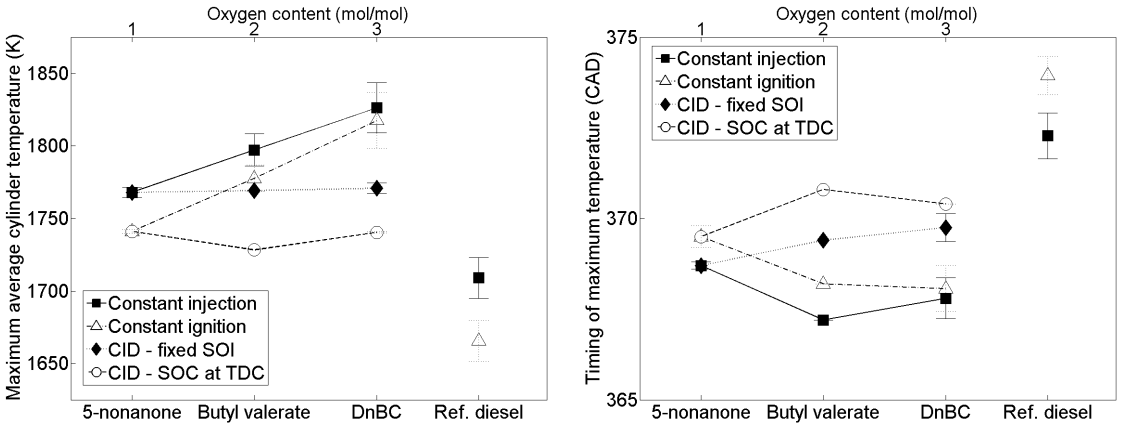

(a) (b)

Figure 9.25: (a) Calculated maximum in-cylinder global temperature and (b) time of occurrence of di-*n*-butyl carbonate (DnBC), butyl valerate and 5-nonanone with 30 % *n*-decane and reference fossil diesel at constant injection, constant ignition and constant ignition delay timings

Figures 9.25a and b show the magnitude and time of occurrence of the maximum in-cylinder global temperature of DnBC, butyl valerate and 5-nonanone blended with 30 % *n*-decane at constant injection, constant ignition and constant ignition delay timings. At constant ignition delay timings, the maximum in-cylinder global temperatures reached (Figure 9.25a), do not mirror the peak heat release rates exhibited (Figure 9.24) and can likely be attributed to the times of maximum in-cylinder temperature of butyl valerate and DnBC occurring closer to TDC than that of 5-nonanone at constant ignition delay timings (Figure 9.25b).

Figure 9.26 shows the exhaust gas levels of NO_x of DnBC, butyl valerate and 5-nonanone blends with 30 % *n*-decane and the reference fossil diesel at constant

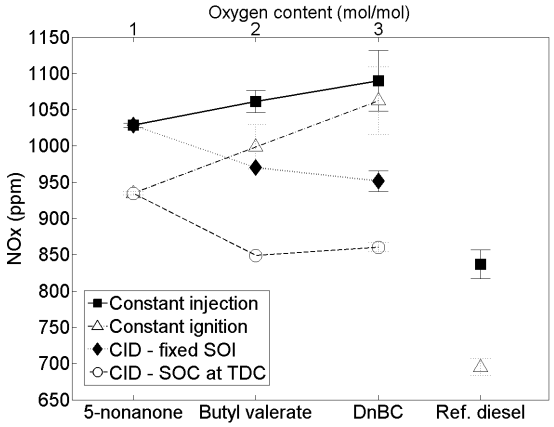

Figure 9.26: NO_x emissions of di-*n*-butyl carbonate (DnBC), butyl valerate and 5-nonanone with 30 % *n*-decane and reference fossil diesel at constant injection, constant ignition and constant ignition delay timings

injection, constant ignition and constant ignition delay timings of fixed SOI and SOC at TDC. The higher emissions of NO_x by 5-nonanone, relative to the carbonate and ester, at constant ignition delay timings (Figure 9.25) show a greater influence of peak heat release rate (Figure 9.24) than either the magnitude or timing of maximum in-cylinder temperature (Figures 9.25a and b).

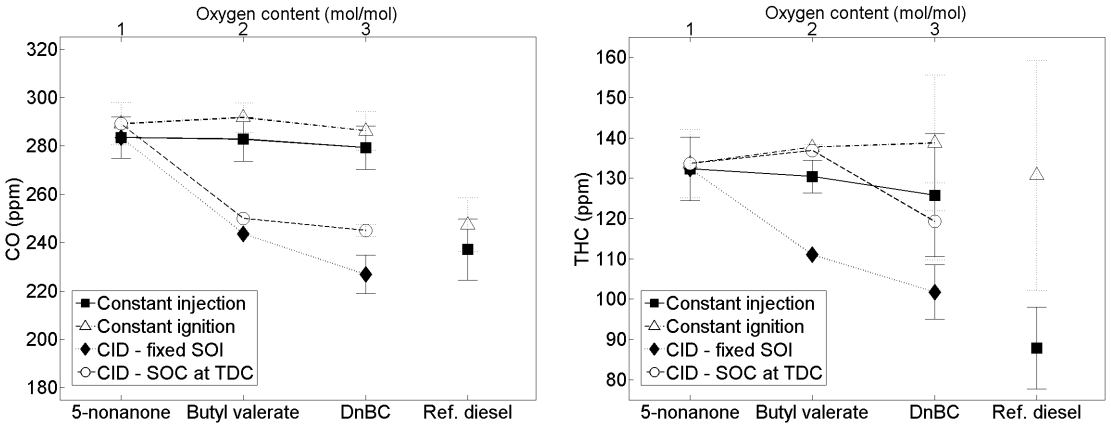

(a) (b)

Figure 9.27: (a) CO and (b) THC emissions of di-*n*-butyl carbonate (DnBC), butyl valerate and 5-nonanone with 30 % *n*-decane and reference fossil diesel at constant injection, constant ignition and constant ignition delay timings

Figures 9.27a and b show the exhaust gas levels of CO and THC of DnBC, butyl valerate and 5-nonanone blends with 30 % n-decane and the reference fossil diesel at constant injection, constant ignition and constant ignition delay timings. It is suggested that at constant ignition delay timings, levels of CO emitted reduce due to the increased availability of molar oxygen and thus higher levels of complete combustion (Figure 9.27a). However, were the molar oxygen content of oxygenates the primary driver of CO emissions it could perhaps be expected that at constant injection and constant ignition timing CO levels would also decrease with increasing fuel oxygen content. An effect of maximum in-cylinder temperatures (Figure 9.25a) is also visible on CO formation, with tests at constant injection timing (where temperatures were higher consistently) emitting lower levels of CO than at constant ignition timing. With ignition delay isolated, emissions of THC are lowest for the oxygenate with the highest molar oxygen content (Figure 9.27b), but the range of error present prevents further interpretation.

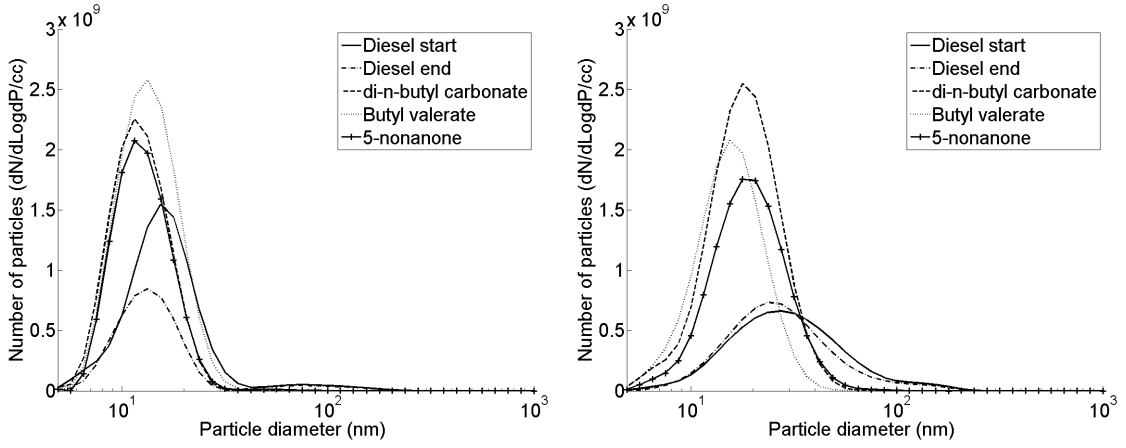

Figure 9.28: Particulate emissions of di-n-butyl carbonate (DnBC), butyl valerate and 5-nonanone with 30 % n-decane and reference fossil diesel at (a) constant injection and (b) constant ignition timings

Figures 9.28a and b show the particulate emissions of DnBC, butyl valerate and 5-nonanone blended with 30 % (wt/wt) and the reference fossil diesel at constant injection and constant ignition timings. No effect of oxygenate boiling point (Table 9.1) on the peak number of nucleation mode particles produced is apparent, nor can a clear influence of ignition delay be inferred from comparison of the oxygenate

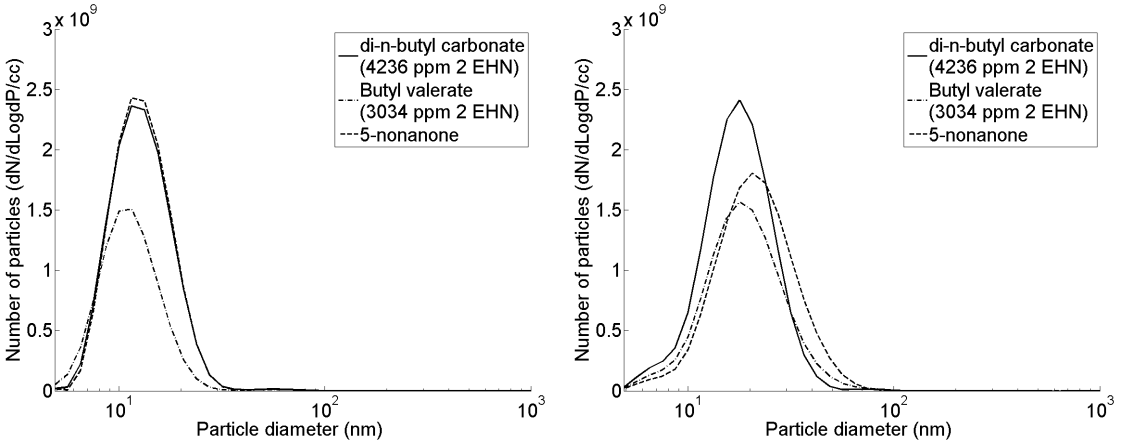

Figure 9.29: Particulate emissions of di-*n*-butyl carbonate (DnBC), butyl valerate and 5-nonanone with 30 % *n*-decane and reference fossil diesel at (a) constant injection and (b) constant ignition timings

particulate emissions with (Figures 9.29a and b) and without (Figures 9.28a and b) ignition delay equalized.

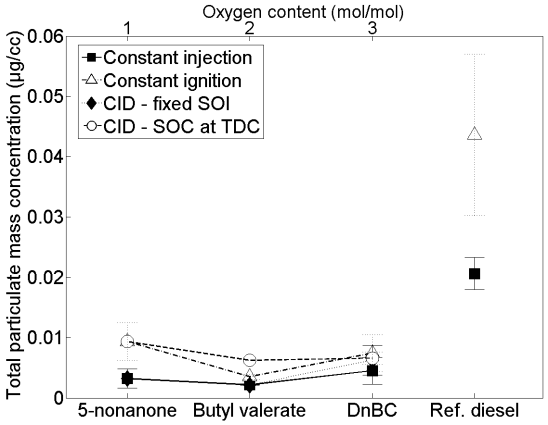

Figure 9.30: Total particulate mass emitted by di-*n*-butyl carbonate (DnBC), butyl valerate and 5-nonanone with 30 % *n*-decane and reference fossil diesel at constant injection, constant ignition and constant ignition delay timings

Figure 9.30 shows the total particulate mass emitted by DnBC, butyl valerate and 5-nonanone blends with 30 % (wt/wt) *n*-decane and the reference fossil diesel at constant injection, constant ignition and both constant ignition timings. No

effect of molar oxygenate content on the total mass of particulates can be discerned beyond the level of experimental error present (Figure 9.30).

9.2.4. Binary mixtures of carbonates with n-decane in varying proportions

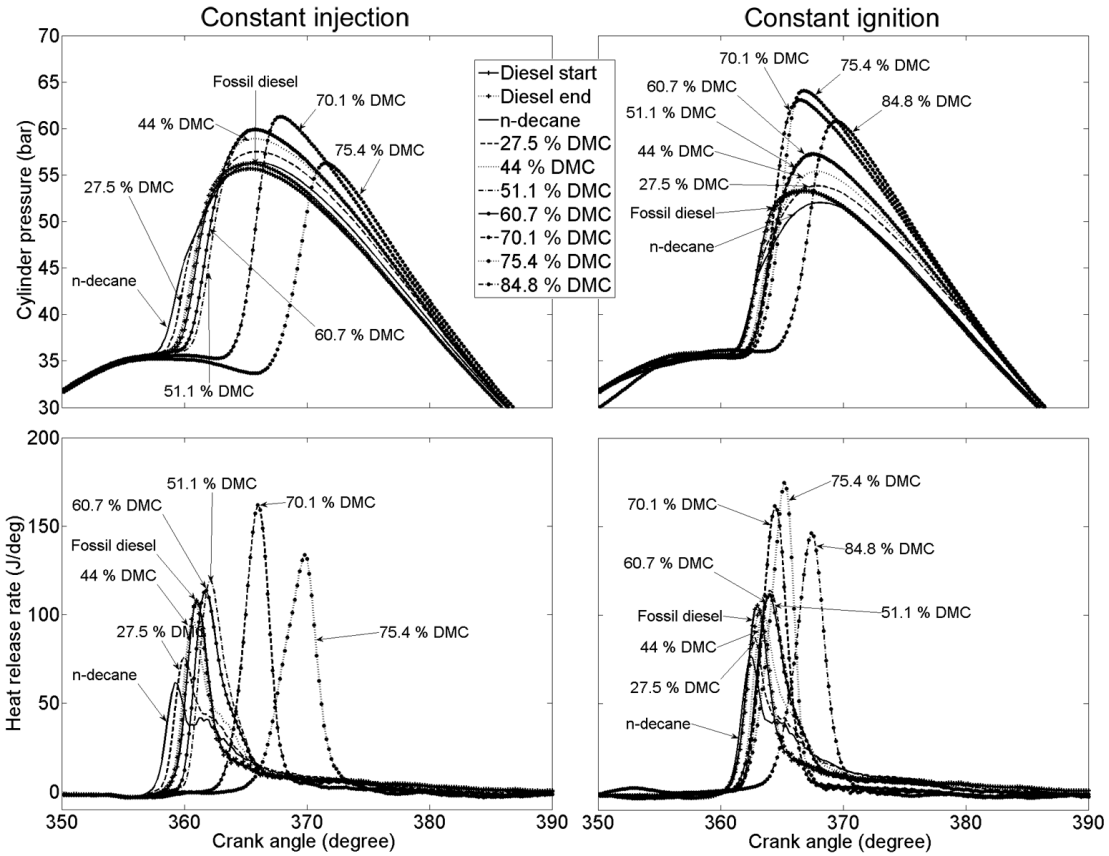

Figure 9.31: In-cylinder pressures and apparent net heat release rates of binary mixtures of di-methyl carbonate (DMC) and n-decane and reference fossil diesel at constant injection and constant ignition timing

This section of Chapter 9 considers binary mixtures of DMC and DEC with n-decane in varying proportions. Figure 9.31 shows the in-cylinder pressure and apparent net heat release rate of the binary mixtures of DMC and n-decane, and the reference fossil diesel, at constant injection and constant ignition timing. It can be seen that pure n-decane exhibits a significant level of diffusion rate controlled combustion at both timing conditions (Figure 9.31), but as the level of DMC present in the blends increases, the fraction of diffusion controlled combustion diminishes consistent with observation of blends of DMC with fossil diesel (Cheung et al., 2011;

Zhang et al., 2005). In the case of the blends containing 70.1 and 75.4 % DMC, nearly all energy release occurs during premixed combustion, and two ignition stages prior to the bulk of heat release are apparent (Figure 9.31).

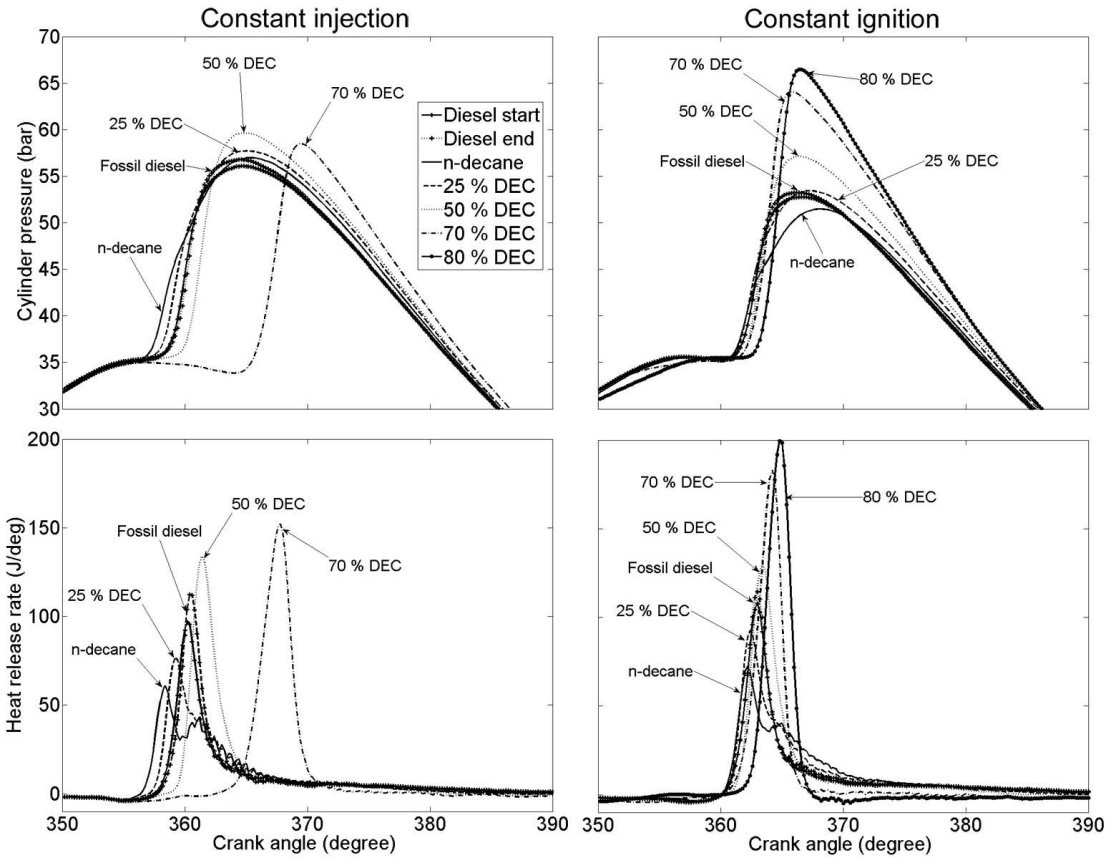

Figure 9.32: In-cylinder pressures and apparent net heat release rates of binary mixtures of di-ethyl carbonate (DEC) and *n*-decane and reference fossil diesel at constant injection and constant ignition timing

Figure 9.32 shows the in-cylinder pressures and apparent net heat release rates of the binary mixtures of DEC and *n*-decane, and the reference fossil diesel, at constant injection and constant ignition timing. As was also the case in the blends of DMC with *n*-decane (Figure 9.31), the magnitude of the premixed burn fraction increases with the level of carbonate present (Figure 9.32), and the binary mixtures containing the highest levels of carbonate (70 and 80 % DEC) display two stage ignition prior to the main heat release event.

Figure 9.33 shows the shift in ignition delays of the binary mixtures of DMC and DEC with *n*-decane and the reference fossil diesel relative to pure *n*-decane at con-

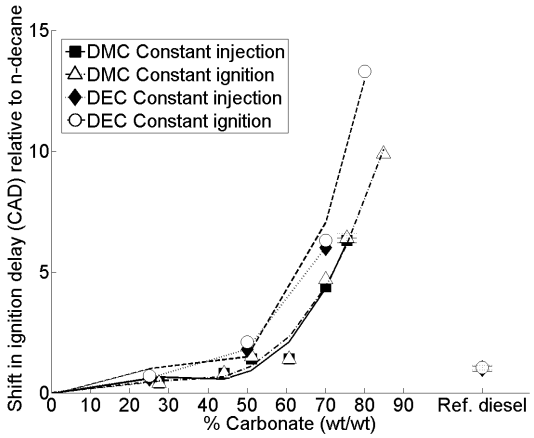

Figure 9.33: Shift in ignition delays relative to n-decane of binary mixtures of dimethyl carbonate (DMC) and n-decane, and di-ethyl carbonate (DEC) and n-decane, and the reference fossil diesel at constant injection and constant ignition timing

stant injection and constant ignition timing. Figures 9.33 - 9.38 present values of the combustion and emissions characteristics of the carbonate mixtures as a shift in that value relative to that exhibited by pure n-decane. For example where pure n-decane displayed an ignition delay of 4.2 CAD at constant injection timing, while the binary mixture containing 60.7 % DMC displayed an ignition delay of 5.9 CAD. Therefore, in Figure 9.33, the shift in ignition delay at constant injection timing of the blend containing 60.7 % is 1.7 CAD. As was observed in Section 9.2.1 (Figure 9.3), blends of DEC display a longer ignition delay than those of equivalent DMC content (Figure 9.33). Sensitivity to in-cylinder thermal conditions in the low temperature reactivity of the mixtures is also apparent; mixtures containing 84.8 and 80 % of DMC and DEC respectively could only be induced at constant ignition timing where injection timing had been advanced (Figure 9.33).

It is suggested that up to a carbonate level of 50 % (wt/wt), the reaction kinetics of n-decane dominate those of the mixtures as a whole, and thus the difference in ignition delay of those blends containing DMC and those containing DEC is not especially pronounced (Figure 9.33). The observed increase in ignition delay with a carbonate content up to 50 % (wt/wt), despite n-decane remaining the major constituent of the blends, is perhaps suggestive of interactions between those radicals produced by n-decane and those produced by the carbonates. At a carbonate level greater than 50 % (wt/wt), it is suggested that any such cross reactions would

result in an insufficient level of radicals available for the low temperature branching reactions of *n*-decane that would otherwise take place, and thus the observed dramatic increase in ignition delay occurs (Figure 9.33). It is very tentatively put forward that such cross reactions may explain the higher reactivity of DMC relative to DEC (Figures 9.3 and 9.33); namely that ethyl radicals may provide more sites for radical addition than methyl groups, and that any innate higher reactivity of the ethyl radicals is insufficient to offset the greater radical depletion of *n*-decane derived radicals than in the case of the DMC blend of identical carbonate content.

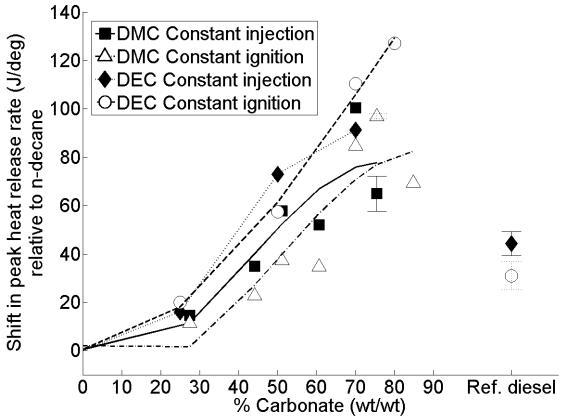

Figure 9.34: Shift in apparent net peak heat release rates relative to *n*-decane of binary mixtures of di-methyl carbonate (DMC) and *n*-decane, and di-ethyl carbonate (DEC) and *n*-decane, and the reference fossil diesel at constant injection and constant ignition timing

Figure 9.34 shows the shift in apparent net peak heat release rate of the binary mixtures of DMC and DEC with *n*-decane, and the reference fossil diesel, relative to pure *n*-decane at constant injection and constant ignition timing. The more uniform gradient of increasing peak heat release rate with increasing levels of either carbonate (Figure 9.34), relative to that of ignition delay (Figure 9.33), potentially indicates that the physical properties of the carbonates which might impact on the efficiency of fuel and air mixing are also of significance in determining the peak heat release rate of the carbonate blends. DMC and DEC possess a lower viscosity and boiling point than *n*-decane (Table 9.1), both of which could be expected to result in smaller fuel droplets (Wu et al., 2006) and faster rates of vaporization respectively, thus increasing the efficiency of fuel and air mixing prior to SOC and the magnitude of the premixed burn fraction. Additionally, it may be that the increasing provision

of oxygen in fuel rich areas with increasing carbonate content is accelerating rates of combustion, as has been observed in blends of carbonates and fossil diesel (Cheung et al., 2011; Ren et al., 2008; Zhang et al., 2005).

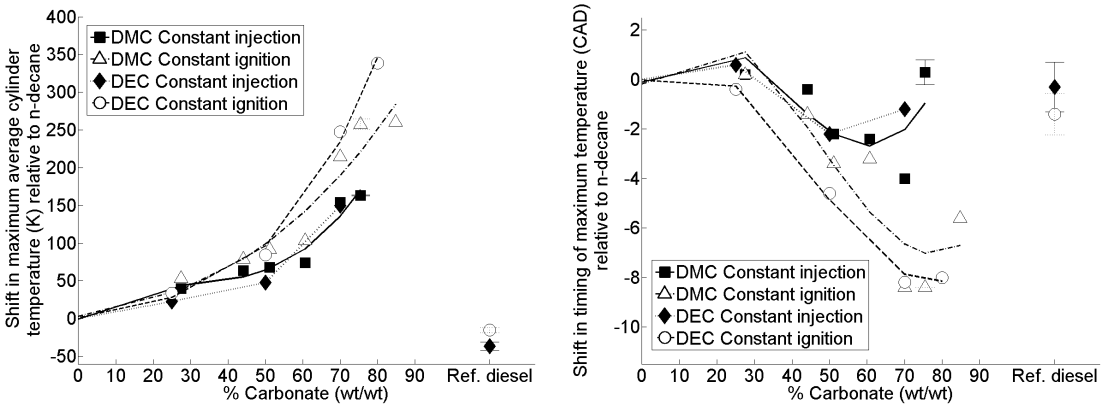

(a) (b)

Figure 9.35: Shift in (a) calculated maximum in-cylinder global temperature and (b) time of occurrence relative to *n*-decane of binary mixtures of dimethyl carbonate (DMC) and *n*-decane, and di-ethyl carbonate (DEC) and *n*-decane, and the reference fossil diesel at constant injection and constant ignition timing

Figures 9.35a and b shows the shift in calculated maximum in-cylinder global temperate and time of occurrence relative to *n*-decane, of the binary mixtures of DMC and DEC with *n*-decane, and also the reference fossil diesel, at constant injection and constant ignition timings. The magnitude of maximum in-cylinder temperature (Figure 9.35a) shows a greater sensitivity to injection timing than the species of carbonate present in the blend; for example, at 70 % carbonate the maximum in-cylinder temperatures displayed by both DMC and DEC are indistinguishable from one another at constant injection timing, while both blends exhibit a significantly higher maximum in-cylinder temperature at constant ignition timing. The occurrence of SOC later into the expansion stroke at constant injection timing (Figures 9.31 and 9.32) offsets the higher peak heat release rate with increasing carbonate content (Figure 9.34), resulting in a later time of maximum in-cylinder temperature (Figure 9.35b).

Figure 9.36 shows the shift in emissions of NO_x relative to *n*-decane of the binary mixtures of DMC and DEC with *n*-decane, and the reference fossil diesel, at constant

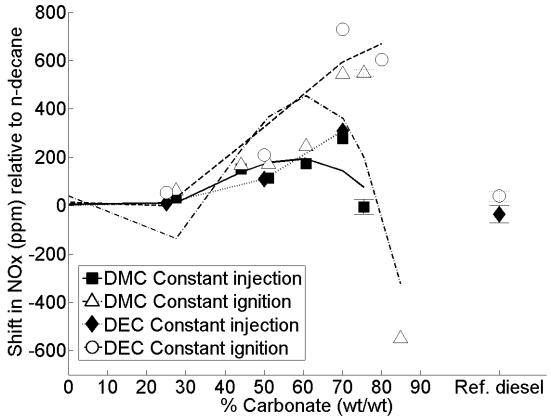

Figure 9.36: Shift in NO_x emissions relative to *n*-decane of binary mixtures of di-methyl carbonate (DMC) and *n*-decane, and di-ethyl carbonate (DEC) and *n*-decane, and the reference fossil diesel at constant injection and constant ignition timing

injection and constant ignition. The importance of the time available for NO_x formation at elevated temperatures is highlighted. While the maximum in-cylinder temperatures of the blends consistently increased with carbonate content (Figure 9.35a), maximum in-cylinder temperatures occur later for those blends with a DMC content higher than 70 % (wt/wt) at constant injection timing (Figure 9.35b).

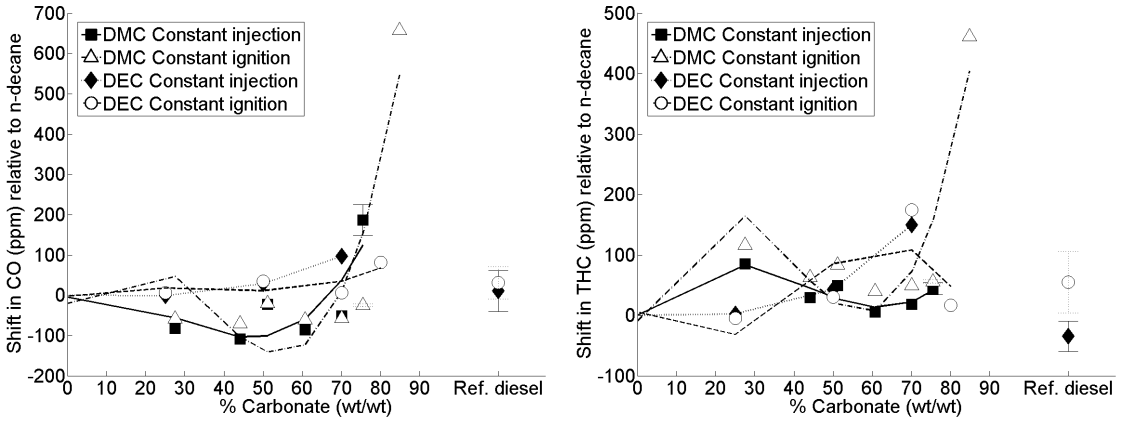

(a) (b)

Figure 9.37: Shift in (a) CO and (b) THC emissions relative to *n*-decane of binary mixtures of di-methyl carbonate (DMC) and *n*-decane, and di-ethyl carbonate (DEC) and *n*-decane, and the reference fossil diesel at constant injection and constant ignition timing

Figures 9.37a and b show the shift in CO and THC emissions relative to those of pure n-decane of the binary mixtures of DMC and DEC with n-decane, and the reference fossil diesel, at constant injection and constant ignition timing. The reduction in CO emissions with increasing carbonate content (Figure 9.37a) is possibly attributable to both the provision of additional fuel bound oxygen (which is greater in the case of DMC relative to DEC) and increasing maximum in-cylinder temperatures (Figure 9.35a), both which could be expected to increase the degree of complete combustion taking place. Emissions of CO and THC for the DMC blend of highest carbonate content are significantly higher than that of pure n-decane and all other binary mixtures (Figures 9.37a and b) and suggestive of greatly increased levels of incomplete combustion. This is potentially attributable to lower local in-cylinder temperatures, as suggested by peak heat release rates (Figure 9.34), and a greater degree of fuel over-dilution due to a longer ignition delay (Figure 9.33).

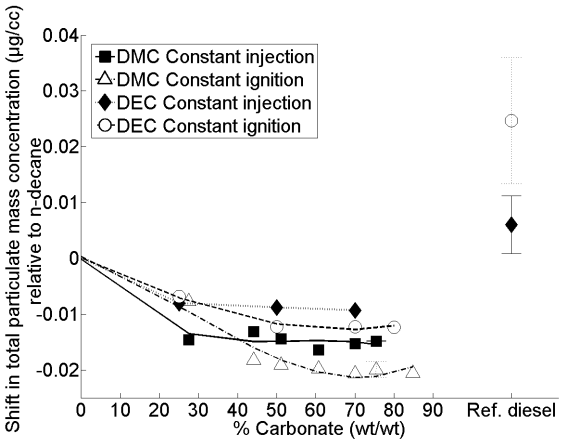

Figure 9.38: Shift in total particulate mass concentration emitted relative to n-decane of binary mixtures of di-methyl carbonate (DMC) and n-decane, and di-ethyl carbonate (DEC) and n-decane, and the reference fossil diesel at constant injection and constant ignition timing

Figure 9.38 shows the shift in total particulate mass concentration emitted relative to n-decane of the binary mixtures of DMC and DEC with n-decane, and the reference fossil diesel, at constant injection and constant ignition timing. Both increased carbonate oxygen content and higher maximum in-cylinder temperatures could be expected to reduce particulate mass emissions via increased soot oxidation rates (Tree and Svensson, 2007), and an influence of both is readily apparent. When con-

sidering particulate emissions by particulate number, no effect of carbonate content was readily apparent.

9.3. Conclusions

1. Symmetrical carbonate esters, comprising of butyl chains or shorter, are not suitable single component fuels for compression ignition engines. However, as binary fuels with a minor component of higher ignition quality, such carbonate esters do combust in a steady manner.

2. Reducing the total alkyl chain length of a carbonate ester, either by reduction in the total carbon content or the introduction of methyl branching in the alkyl chains, increases the ignition delay of the carbonate when blended with 30 % (wt/wt) *n*-decane. This indicates that the low temperature reactivity of carbonate alkyl chains is important in determining the overall reactivity of the molecule. Furthermore, a single methyl branch bonded to a carbon that is bonded to an oxygen has a more detrimental effect on ignition quality than the same methyl branch bonded to a secondary carbon atom.

3. Reducing the oxygen content of a molecule, while keeping the alkyl chain structures constant (carbonate ester to fatty acid ester to ketone), progressively increases the ignition quality in compression ignition combustion. This is suggestive of an inhibiting influence of carbon to oxygen atoms on the low temperature branching reactions of alkyl chains.

4. Di-methyl carbonate possesses a shorter ignition delay than di-ethyl carbonate in blends with equivalent *n*-decane content (wt/wt). This is especially pronounced at a carbonate content of greater than 50 % (wt/wt), suggestive of cross reactions between radicals produced by the decomposition of *n*-decane and those from the decomposition of the carbonates.

5. Peak heat release rates correlate with the duration of ignition delay, except in the case of the straight alkyl chain carbonates where an increasing latent heat of vaporization with decreasing alkyl chain length slows rates of heat release rate. Where di-methyl carbonate and di-ethyl carbonate were blended in varying proportions with *n*-decane, peak heat release rates show an influence

of the physical properties of the carbonate in addition to the duration of ignition delay.

6. Emissions of NO_x are primarily driven by in-cylinder thermal conditions, increasing with maximum in-cylinder temperatures and the residence time of the cylinder charge at elevated temperatures. Emissions of CO and THC are primarily driven by the duration of ignition delay, via the resultant level of fuel in air dilution and degree of incomplete combustion present. In the case of all the molecules of differing oxygen content or alkyl chain length, emissions of CO decrease with increasing oxygen content.

7. All of the carbonates emitted lower levels of particulate mass than the reference fossil diesel. Furthermore, increasing the mass of oxygen present, either by decrease of the alkyl chain length or increasing the carbonate content in the blend, reduces the mass of particulates emitted and is indicative of soot oxidation by fuel bound oxygen.

10. Interactions of binary mixtures of toluene/n-heptane and 1-octene/n-octane

Studying binary fuel mixtures has long been of interest in combustion research and, in particular, mixtures containing toluene have received much attention. As an aromatic compound, toluene is representative of the many such compounds found in fossil fuels and also potential fuels from biomass (Melero et al., 2009; Ross et al., 2010). Fuels suitable for compression ignition combustion nearly always require components that possess long alkyl chains in order to be of significant ignition quality, and several studies have investigated the interactions of toluene with n-heptane in differing proportions and at varying conditions. Such studies have exclusively utilised premixed fuel and air (with the aim of better understanding HCCI and knock in SI engines) and have found the presence of toluene to both suppress low temperature reactivity and increases the duration of ignition delay (Herzler et al., 2007; Hartmann et al., 2011; Tanaka et al., 2003; Andrae et al., 2005; Di Sante, 2012). Furthermore, this decrease in ignition quality has been attributed to consumption of radical species by toluene, inhibiting the low temperature reactivity of n-heptane (Andrae et al., 2005; Hartmann et al., 2011). Emissions of particulates from binary mixtures of toluene and n-heptane have been reported to increase with toluene content (Xiao et al., 2000).

Alkenes are another prominent component of compression ignition fuels. Despite the similarity of alkenes and alkanes in that they both possess long alkyl chains which will dominate reactivity, there has been little direct study on the binary mixtures of such fuels. Cullis et al. (1969) investigated the ignition of n-heptane and 1-heptene mixtures in oxygen, and found that at below 600 K, 1-heptene did have an inhibiting effect on the reactivity of n-heptane. When considering a mixture of 1-hexene and iso-octane in a RCM, Vanhove et al. (2006) found no evidence of cross reactions between the two fuel components.

The current chapter presents results of experiments with a modern direct injection compression ignition engine in which binary mixtures of toluene/n-heptane and 1-octene/n-octane were tested so as to investigate the effects of varying the proportions of the mixtures on combustion phasing and exhaust emissions.

10.1. Experimental method

10.1.1. Apparatus

All of the combustion experiments described in the present chapter were performed using the compression ignition engine and the ultra low volume fuel system described in Chapter 3.

10.1.2. Binary mixtures investigated

Binary mixtures comprising of two pairs of single molecules were tested in varying proportions to observe the following:

(a) The interaction of an aromatic compound with an n-alkane of equal carbon number.

(b) The interaction of a 1-alkene with an n-alkane of equal carbon number.

To investigate the interaction between an aromatic and an n-alkane, toluene and n-heptane were selected. To observe the synergy between a 1-alkene and n-alkane, 1-octene and n-octane were chosen. All four of the pure component fuels were obtained from a chemical supplier (Sigma Aldrich). In addition, a fossil diesel fuel with zero FAME content was tested as a reference fuel. The assay and other properties of each fuel are presented in Table 10.2, while the molecular structure of each is given in Table 10.1.

10.1.3. Experimental conditions

Each of the binary mixtures and the reference diesel tested was initially tested at the two experimental conditions of constant injection and constant ignition timing, as defined in Chapter 5. After the two sets of experiments at constant injection and constant ignition timing were completed, a third series of experiments was carried out at constant ignition delay timing, utilising the ignition improver 2 EHN and the method described in Chapter 5.

All tests were conducted at an engine speed of 1200 rpm and at 450 bar fuel injection pressure. The injection duration was adjusted in the case of every fuel so that the engine IMEP was always constant at 4 bar for all fuels. Summaries of the engine and test operating conditions during the toluene and n-heptane mixtures

Table 10.1: Structures of binary fuel components and fuel additive

Toluene	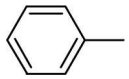
n-heptane	
1-octene	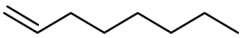
n-octane	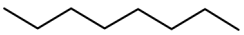
2-ethylhexyl nitrate	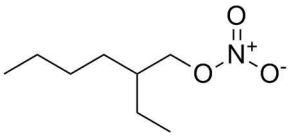

tests and also the 1-octene and *n*-octane mixture tests are given in Tables 10.3 and 10.4.

Table 10.2: Properties of binary mixture components and reference fossil diesel

Fuel	Molecular formula	Assay (%)	T_{boil} (°C)	T_{melt} (°C)	△vapH° (kJ/mol)	Cetane number$^{\square}$	Density (kg/m^3)	Dynamic viscosity at 20 °C (mPa.s)	Lower heating value (MJ/Kg)
Reference fossil diesel	-	-	268.9‡	-	-	51.7$^{\bullet}$	834.5$^{\diamond}$	-	43.14†
Toluene	C_7H_8	99.8	111[1]	-95.6[2]	33.4[3]	7.4	866.75[4]	0.60[4]	40.60[5]
n-heptane	C_7H_{16}	99	98.4[6]	-90.6[7]	32.17[8]	54.4	684.06[9]	0.41[10]	44.50[11]
1-octene	C_8H_{16}	98	121.3[12]	-102.6[12]	40.44[13]	40.8	714.9[14]	0.47[14]	44.56[15]
n-octane	C_8H_{18}	98	125.7[16]	-56.9[17]	41.53[13]	64.1	702.8[14]	0.546[14]	44.79[18]

† = calculated from experimental data obtained by the IP12 methodInstitute of Petroleum (2001), $^{\diamond}$ = experimental data obtained according to ASTM D4052 at 15 °C, $^{\bullet}$ = experimental data obtained according to EN ISO 516, ‡ = experimental data obtained according to EN ISO 3405, * = DCN from IQT of samples used in this study, $^{\square}$ = data from Murphy et al. (2004), [1] = data from Aizawa and Kato (1991), [2] = data from Murthy et al. (1993), [3] = data from Natarajan and Viswanath (1985), [4] = data from Silva et al. (2009), [5] = data from Heywood (1988), [6] = data from Tu et al. (2001), [7] = data from Brown and Ziegler (1979), [8] = data from Pitzer (1940), [9] = data from Alonso et al. (2011), [10] = data from Jimenez et al. (1998), [11] = data from Lu et al. (2007), [12] = data from Henne and Greenlee (1943), [13] = data from Majer et al. (1985), [14] = data from Speight (2005), [15] = data from Prosen and Rossini (1945), [16] = data from Hiaki et al. (1995), [17] = data from Ott and Goates (1983) and [18] = data from Rockenfeller and Rossini (1961).

Table 10.3: Toluene and *n*-heptane mixtures engine and test operating conditions

% toluene (wt/wt)	2 EHN dosage (ppm)	Engine speed (rpm)	Fuel injection pressure (bar)	IMEP (bar)	Constant injection timing (SOI at 7.5 CAD BTDC)						Constant ignition timing (SOC at TDC)					
					Ignition delay (CAD)		Injection duration (µs)		Indicated thermal efficiency (%)		Ignition delay (CAD)		Injection duration (µs)		Indicated thermal efficiency (%)	
					Mean	1σ	Mean	1σ	Mean	1σ	Mean	1σ	Mean	1σ	Mean	1σ
Ref. fossil diesel	0	1200	450	4	7.5	0.1	613	10	43.16	0.49	7.5	0.1	614	7	43.05	0.4
0	0	1200	450	4	7.1	-	655	-	42.67	-	7.4	-	657	0	42.9	-
5	0	1200	450	4	7.3	-	644	-	42.95	-	7.5	-	646	0	43.08	-
10.1	0	1200	450	4	7.5	-	658	-	42.75	-	7.5	-	658	0	42.65	-
25	0	1200	450	4	8.1	-	650	-	42.84	-	8.1	-	648	0	42.96	-
35	0	1200	450	4	8.7	-	642	-	43.28	-	8.8	-	630	0	43.22	-
35.1	0	1200	450	4	8.9	-	628	-	44.09	-	8.9	-	631	0	43.67	-
40	0	1200	450	4	9.3	-	638	-	43.21	-	9	-	638	0	43.19	-
46.3	0	1200	450	4	9.9	-	658	-	41.93	-	9.6	-	632	0	43.62	-
50	0	1200	450	4	10.7	-	717	-	39.31	-	9.9	-	664	0	42.38	-
52.2	0	1200	450	4	DNC	-	-	-	-	-	10.5	-	681	0	39.97	-
0	616	1200	450	4	6.3	0	635	6	43.85	0.08	6.4	0	637	5	43.8	0.06
10	2063	1200	450	4	6.3	-	622	-	43.74	-	6.2	-	618	0	43.91	-
19.8	5514	1200	450	4	6.1	-	622	-	43.67	-	6.2	-	620	0	43.68	-
30.9	7876	1200	450	4	6.1	-	620	-	43.77	-	6.2	-	617	0	43.78	-
40	10780	1200	450	4	6.3	-	639	-	43.65	-	6.4	-	638	0	43.58	-

Table 10.4: 1-octene and *n*-octane mixtures engine and test operating conditions

% 1-octene (wt/wt)	2 EHN dosage (ppm)	Engine speed (rpm)	Fuel injection pressure (bar)	IMEP (bar)	Constant injection timing (SOI at 7.5 CAD BTDC)						Constant ignition timing (SOC at TDC)					
					Ignition delay (CAD)		Injection duration (µs)		Indicated thermal efficiency (%)		Ignition delay (CAD)		Injection duration (µs)		Indicated thermal efficiency (%)	
					Mean	1σ	Mean	1σ	Mean	1σ	Mean	1σ	Mean	1σ	Mean	1σ
Ref. fossil diesel	0	1200	450	4	7.1	0.1	617	2	42.7	0.24	7.2	0	619	3	42.4	0.16
0	0	1200	450	4	6.5	-	615	-	42.12	-	6.5	-	618	-	42.01	-
10	0	1200	450	4	6.5	-	616	-	42.27	-	6.7	-	621	-	42.3	-
25	0	1200	450	4	6.9	-	617	-	42.3	-	6.8	-	619	-	42.05	-
50	0	1200	450	4	7.3	-	619	-	41.84	-	7.4	-	621	-	42.14	-
63.1	0	1200	450	4	7.3	-	617	-	42.09	-	7.4	-	620	-	42	-
75	0	1200	450	4	7.5	-	615	-	42.15	-	7.7	-	620	-	42.28	-
87.5	0	1200	450	4	7.7	-	618	-	42.59	-	7.8	-	621	-	42.13	-
95	0	1200	450	4	7.9	-	617	-	42.31	-	8	-	623	-	42.41	-
100	0	1200	450	4	8.1	-	617	-	42.24	-	8.1	-	618	-	42.08	-
0	441	1200	450	4	5.9	-	619	-	41.9	-	5.9	-	619	-	42.12	-
50	8589.5	1200	450	4	5.7	0	619	1	41.89	0.04	5.8	-	620	-	41.95	-
100	12169	1200	450	4	6.1	0	620	0	41.79	0.09	6	0.1	620	0	41.87	0.03

10.2. Results and discussion

10.2.1. Toluene/n-heptane binary mixtures

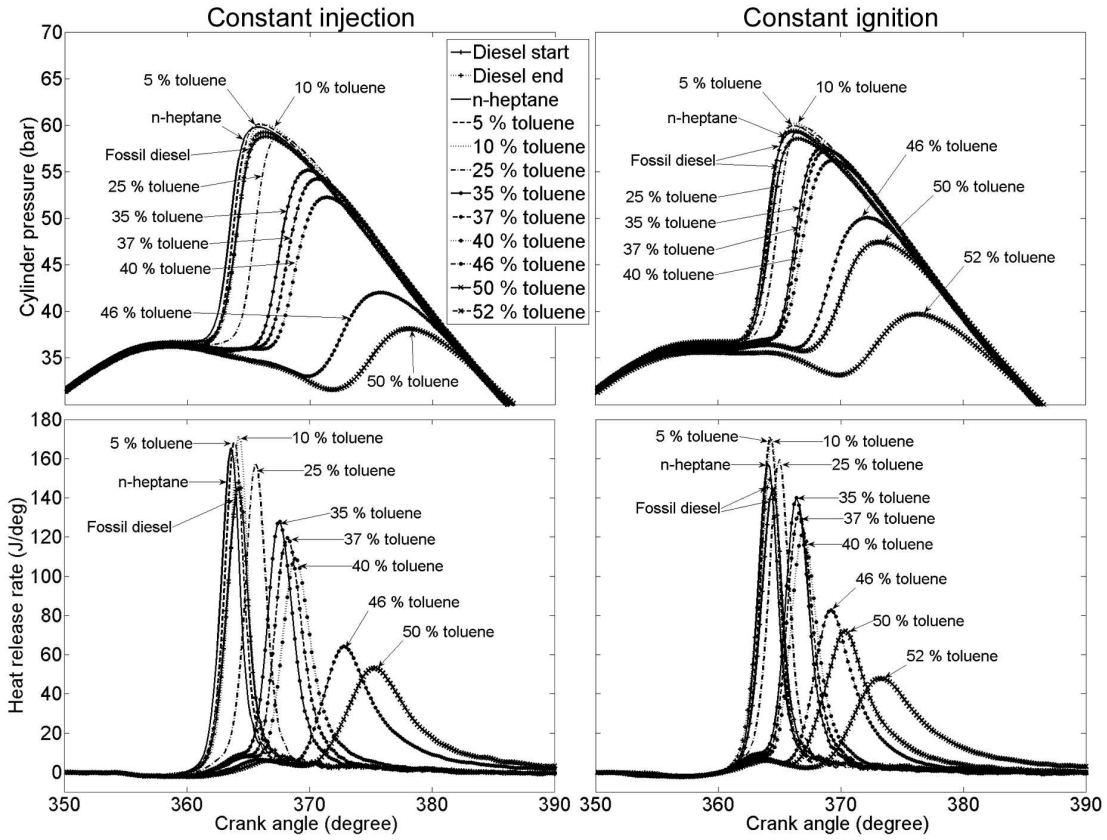

Figure 10.1: In-cylinder pressures and apparent net heat release rates of toluene/n-heptane mixtures and reference fossil diesel at constant injection and constant ignition timing

Figure 10.1 shows the in-cylinder pressures and apparent net heat release rates of the toluene/n-heptane binary fuel mixtures and reference fossil diesel at both constant injection and constant ignition timing. Apparent from Figure 10.1 is that under both timing conditions, for the reference fossil diesel and toluene/n-heptane blends of up to 40 % toluene, the majority of heat release occurs during premixed combustion. Also visible in Figure 10.1, at both timing conditions, is the presence of two stage ignition for all toluene/n-heptane blends containing 25 % or more toluene. The interval between the two ignition stages increases with the level of toluene present, resulting in the bulk of heat release rate occurring later into the expansion stroke for those blends containing more than 40 % toluene. A binary

mixture containing 52 % toluene was found to combust in a steady manner only at constant ignition timing (Figure 10.1), at constant injection timing the same blend did not ignite during every cycle, with any combustion that did occur commencing very late into the expansion stroke.

A further series of experiments were conducted where the ignition delay of the toluene/*n*-heptane binary mixtures was isolated as a variable by the use of the ignition improving additive 2 EHN as described in Chapter 5. These engine experiments were then performed at a fixed SOI of 7.5 CAD BTDC and also an injection timing of 6.2 to 6.4 CAD BTDC so that SOC always occurred at TDC.

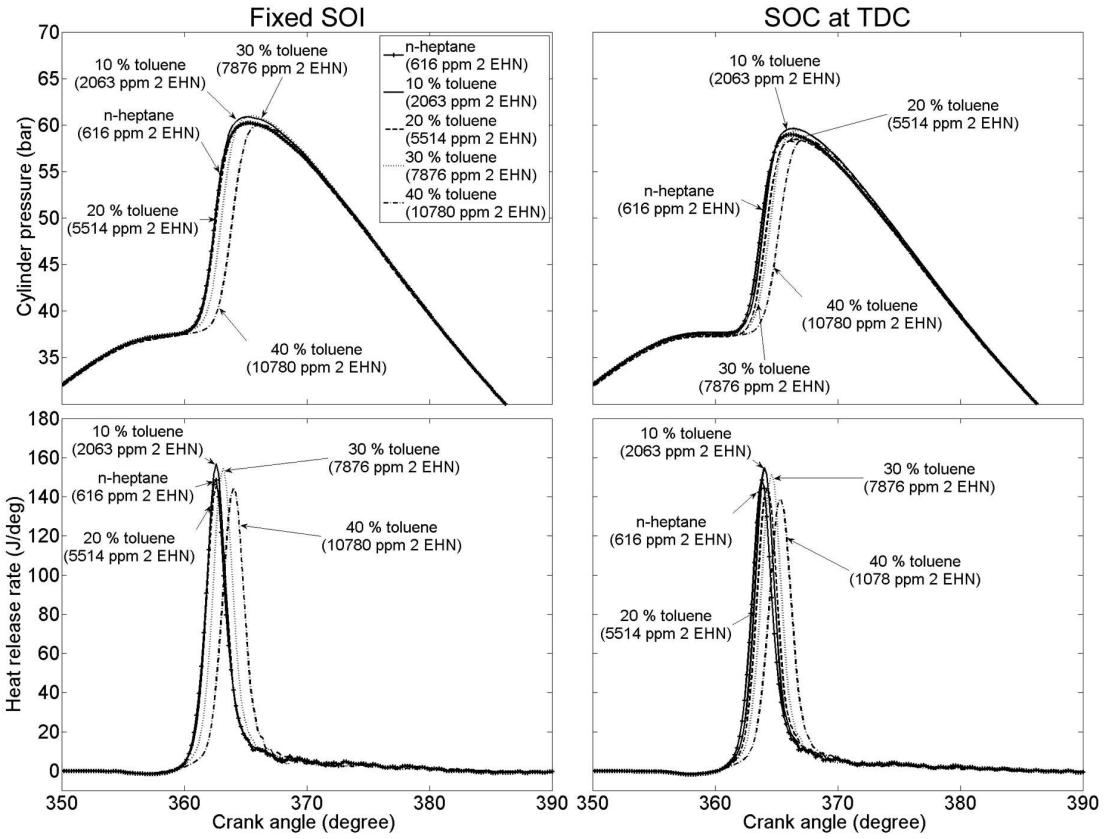

Figure 10.2: In-cylinder pressures and apparent net heat release rates of toluene/*n*-heptane mixtures and reference fossil diesel at constant ignition delay fixed SOI and SOC at TDC timing

Figure 10.2 shows the in-cylinder pressures and apparent net heat release rates of three toluene/*n*-heptane blends at constant ignition delay timings of fixed SOI and SOC at TDC. Despite the use of 2 EHN to equalize the duration of ignition delay, it can be seen that due to the two stage ignition delay observed in Figure 10.1, the

peak heat release rate of the 40 % toluene blend still occurs later into the expansion stroke (Figure 10.2). This is also true to a lesser extent of the 30 % toluene mixture (Figure 10.2). As in Figure 10.1, it can be seen that the majority of heat release for all mixtures occurs during premixed combustion (Figure 10.2).

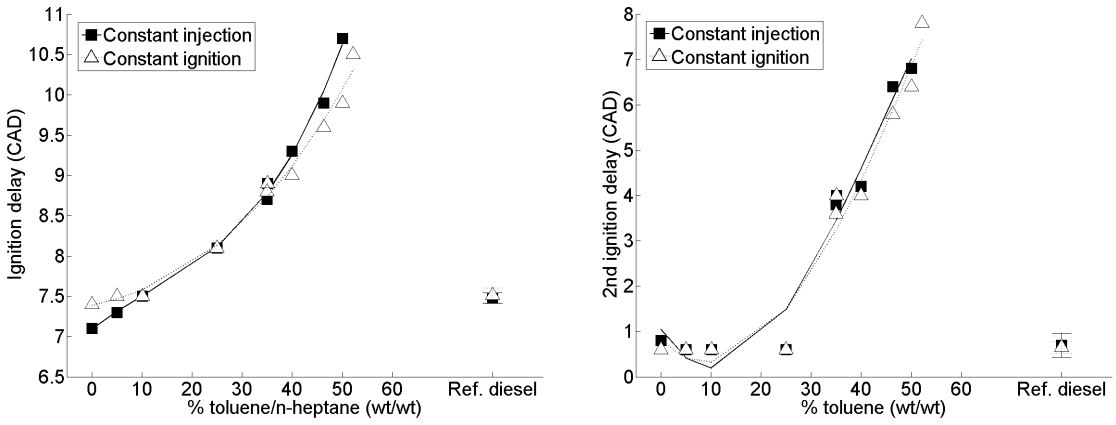

(a) (b)

Figure 10.3: Duration of ignition delay (a) and 2nd ignition delay (b) of toluene/*n*-heptane mixtures and reference fossil diesel at constant injection and constant ignition timing

Figures 10.3a and b show the duration of ignition delay and 2nd ignition delay of the toluene/*n*-heptane binary mixtures at constant injection and constant ignition timing. The values of ignition delay presented in Figure 10.3a are defined as the interval between SOI and the first appearance of positive apparent heat release for each fuel (SOC). The values of 2nd ignition delay presented in Figure 10.3b are defined as the interval between initial fuel ignition (SOC) and the point at which a second phase of heat release commences (SOC2 as defined in Section 4.1.3).

Figure 10.3a shows that increasing the percentage of toluene present in the toluene/*n*-heptane binary mixtures from 0 to 30 % results in an almost linear increase in the duration of ignition delay at both timing conditions. Beyond 35 % toluene, the relationship is no longer close to linear and the effect on ignition delay of further increasing the level of toluene present is much greater. An increase in the level of toluene from 10 - 20 % results in an increase in ignition delay of approximately 0.5 CAD, whereas a similar 10 % increase in the level of toluene from 40 - 50 % results in a 2 CAD increase in ignition delay (Figure 10.3a). Furthermore, the binary mix-

tures would no longer combust in a steady manner without misfiring at toluene levels beyond 50 and 52 % at constant injection and constant ignition timing respectively. The ignition retarding effect of toluene is in agreement with previous experimental results of toluene/*n*-heptane binary mixtures from shock tubes (Hartmann et al., 2011; Herzler et al., 2007), rapid compression machines (Di Sante, 2012; Tanaka et al., 2003; Vanhove et al., 2006) and HCCI (Andrae et al., 2005) and CFR (Xiao et al., 2000) engines.

In Figure 10.3b, it can be seen that at both injection timings the duration of 2nd ignition delay was less than 1 CAD for those toluene/*n*-heptane mixtures containing less than 25 % toluene. At 35 % toluene the duration of 2nd ignition delay has increased significantly to approximately 4 CAD, and at 50 % toluene it rose to approximately 7 CAD (Figure 10.3b). The potential mechanisms by which the presence of toluene affects the mixture reactivity, and thus the duration of both stages of ignition delay, are discussed in some detail in Section 10.2.3.

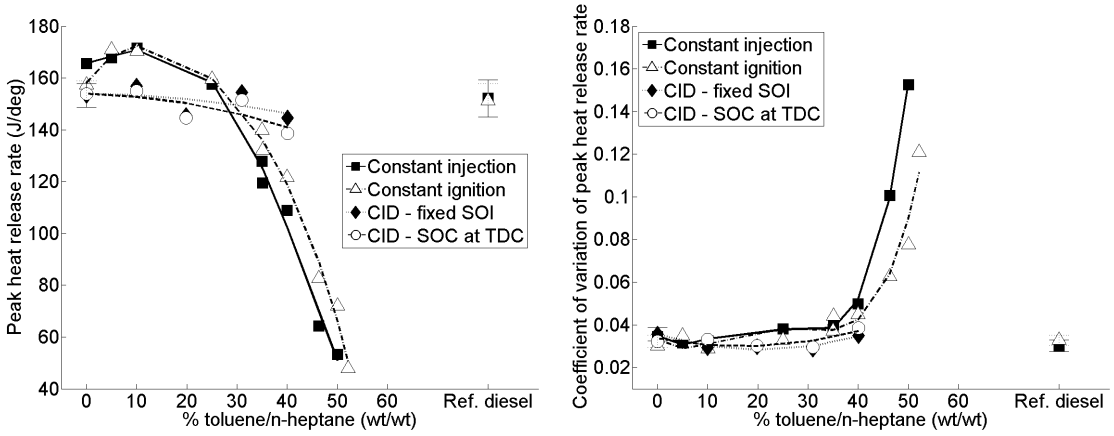

(a) (b)

Figure 10.4: (a) Peak apparent net heat release rates and (b) coefficient of variation of peak heat release rates of toluene/*n*-heptane mixtures and reference fossil diesel at constant injection, constant ignition and constant ignition delay timings

Figures 10.4a and b shows the peak apparent net heat release rates, and coefficient of variation (COV) thereof, of the toluene/*n*-heptane and reference fossil diesel at constant injection, constant ignition and the constant ignition delay timings of fixed SOI and SOC at TDC. At constant injection and constant ignition timings, increasing the level of toluene present in the mixture from 0 - 10 % results in a

slight increase in the peak heat release rate of approximately 160 - 170 J/deg (Figure 10.4a). Further raising the percentage of toluene in the blend sees an increasing reduction in the peak heat release rate down to approximately 50 J/deg. The initial increase in peak heat release rate (between 0 and 10 % toluene) can be explained by the concurrent increase in ignition delay (Figure 10.4a). In Chapter 6, it was clearly observed that an increased duration of ignition delay allows more time for fuel and air mixing prior to ignition and that this larger premixed burn fraction results in a higher peak heat release rate.

For those mixtures containing more than 25 % toluene, the breakdown in this relationship (Figures 10.3a and 10.4a), can be attributed to a visibly later time of peak heat release which is especially apparent at constant injection timing (Figure 10.1). Furthermore, for mixtures containing 35 % toluene and above (Figure 10.1), it can be seen that this is due to the presence of two stage ignition (Figure 10.3b). Concurrently, blends containing greater than 40 % toluene show a significant increase in the COV of peak heat release rate (Figure 10.4b). It follows that with heat release occurring further into the expansion stroke, more of the cylinder wall is exposed and so more heat transfer from the cylinder charge would occur, thus lowering the apparent peak heat release rate and also increasing cycle to cycle variability. Figure 10.4a shows that with the effect of ignition delay isolated, at both constant ignition delay (CID) fixed SOI and SOC at TDC timing, no change in peak heat release rate with increasing levels of toluene is visible beyond the range of experimental error. However, when considering the heat release traces presented in Figure 10.2, the mixture containing 40 % toluene does appear to be subject to a longer 2^{nd} ignition delay and lower peak heat release rate.

Figures 10.5a and b show the calculated maximum in-cylinder global temperature and time of occurrence of the toluene/*n*-heptane mixtures and reference fossil diesel at constant injection, constant ignition and CID timings of fixed SOI and SOC at TDC. At all injection timings, with and without ignition delay isolated, for blends containing up to 40 % toluene the calculated maximum in-cylinder temperature and the time at which it occurs are relatively constant showing no apparent effect of the increasing level of toluene present (Figures 10.5a and b). As the level of toluene exceeds 40 %, maximum in-cylinder temperatures fall rapidly (Figure 10.5a) and the temperatures are reached much further into the expansion stroke (Figure 10.5b). A positive correlation with peak heat release rate could be expected (as a more

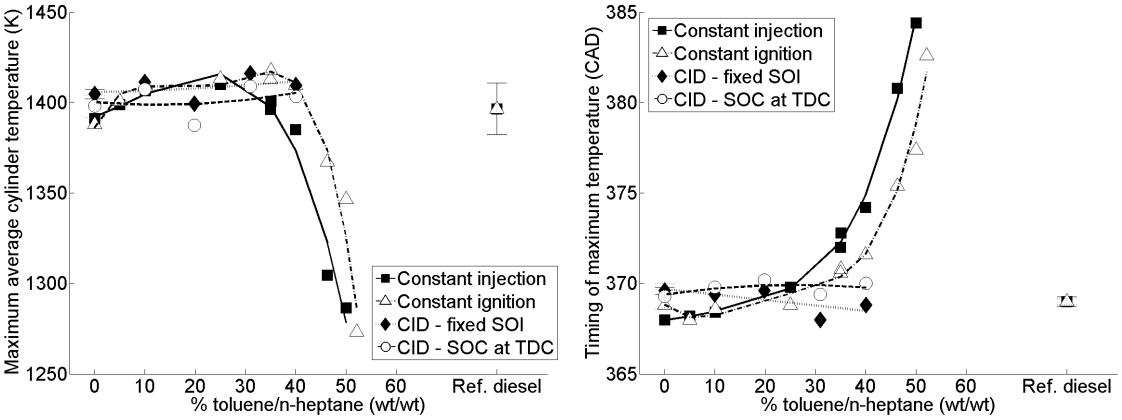

(a) (b)

Figure 10.5: (a) Calculated maximum in-cylinder global temperature and (b) time of occurrence of toluene/*n*-heptane mixtures and reference fossil diesel at constant injection, constant ignition and constant ignition delay timings

intense release of energy will result in higher temperatures and as was observed in Chapter 6) and is apparent to a certain a degree, with the lowest peak heat release rates resulting in the lowest maximum in-cylinder temperatures (Figures 10.4a and 10.5a).

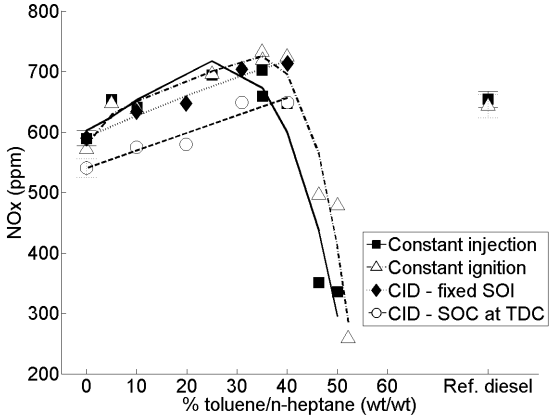

Figure 10.6: Exhaust gas NO_x emissions of toluene/*n*-heptane mixtures and reference fossil diesel at constant injection, constant ignition and constant ignition delay timings

Figure 10.6 shows the exhaust gas NO_x emissions of the toluene/*n*-heptane mixtures and reference fossil diesel at constant injection, constant ignition and both

CID timings. At constant injection and constant ignition timing, levels of NO_x emitted increase with the level of toluene present up to 40 % (Figure 10.6). Beyond 40 % toluene present in the blend, NO_x emissions reduce drastically, mirroring both the decrease and later occurrence of the maximum in-cylinder temperature (Figures 10.5a and b). This could be anticipated as the production of NO_x in compression ignition combustion is known to be highly thermally sensitive (Ban-Weiss et al., 2007), both to the magnitude of the in-cylinder temperature and the residence time of the cylinder contents at elevated temperatures (Mueller et al., 2009; Schönborn et al., 2009b; Szybist et al., 2005). However, where NO_x levels are increasing between 0 - 40 % toluene (Figure 10.6), there is no concurrent increase in the maximum in-cylinder temperature (Figure 10.5a), nor does it occur earlier and increase the residence time of gases at conditions suitable for NO_x production (Figure 10.5b). Furthermore, with ignition delay isolated at CID timings, a similar increase in NO_x emissions with between 0 - 40 % toluene present in the mixtures occurs (Figure 10.6), again with no indication that in-cylinder thermal conditions have become more conducive to NO_x production (Figure 10.5a and b). The increase in NO_x emissions at constant injection and constant ignition timing, up to a toluene content of 40 %, is in agreement with the CFR engine study of Xiao et al. (2000), while the similar increase at constant ignition delay timings is not.

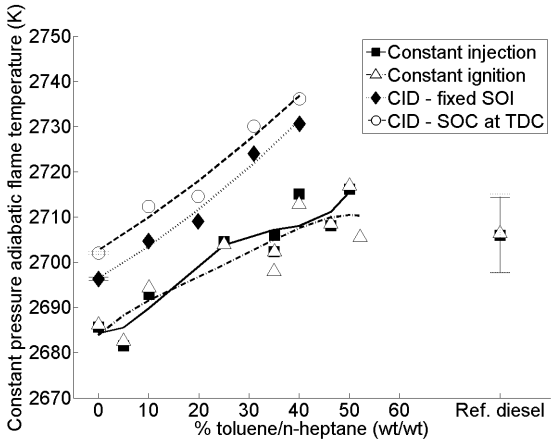

Figure 10.7: Constant pressure adiabatic flame temperatures of toluene/*n*-heptane mixtures and reference fossil diesel at constant injection, constant ignition and constant ignition delay timings

Figure 10.7 shows the constant pressure adiabatic flame temperatures of the toluene/*n*-heptane mixture and reference fossil diesel at constant injection, con-

stant ignition and both CID timings. The adiabatic flame temperature at constant pressure was calculated, assuming no dissociation and an equivalence ratio of 1 using the method described in Chapter 4.4 for the calculated minimum in-cylinder global temperature between SOI and SOC. The calculations were performed for the binary mixtures using literature values of the enthalpy of formation of toluene and *n*-heptane in a gaseous state (Prosen and Rossini, 1945; Battin-Leclerc, 2008). It can be seen in Figure 10.7, that as the percentage of highly unsaturated toluene increases in the blend, the constant pressure adiabatic flame temperature does so as well. It is therefore suggested that the increasing adiabatic flame temperature (Figure 10.7) is the primary driver of the increase in NO_x emissions at all timing conditions for mixtures containing 0 - 40 % toluene (Figure 10.6). The adiabatic flame temperature continues to increase with mixtures containing more than 40 % toluene (Figure 10.7); however, this is not sufficient to offset the changes in combustion phasing and in-cylinder thermal conditions that dramatically reduce the level of NO_x produced (Figure 10.6).

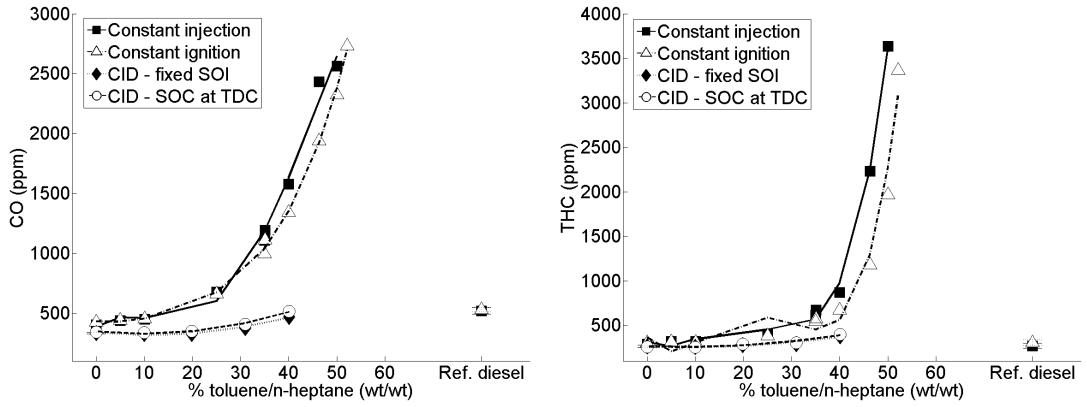

Figure 10.8: (a) CO and (b) THC emissions of toluene/*n*-heptane mixtures and reference fossil diesel at constant injection, constant ignition and constant ignition delay timings

Figures 10.8a and b show the exhaust gas emissions of CO and THC of the toluene/*n*-heptane mixtures and reference fossil diesel at constant injection, constant ignition and CID timings. At constant injection and constant ignition timing, both CO and THC emissions increase with the level of toluene present in the binary mixtures (Figures 10.8a and b), and for the latter the increase becomes exponential

at around 40 % toluene (Figure 10.8b), coinciding with the dramatic decrease in maximum in-cylinder temperatures (Figure 10.5a). CO and THC are known to be products of incomplete combustion, and indicate the increasing existence of both fuel rich and fuel lean regions within the cylinder contents as the level of toluene in the fuel blend and the duration of ignition delay and 2nd ignition delay increases (Figures 10.3a and b). Toluene has a higher density, viscosity and boiling point than n-heptane (Table 10.2), and so it is suggested that these factors produce increasingly poor fuel and air mixing as the level of toluene in the blend increases. Meanwhile, the increasing duration of ignition delay (Figure 10.3a) allows for greater fuel over-dilution. At CID timings, with ignition delay equalised, emissions of CO and THC continue to show an increase with the percentage of toluene present in the mixture (Figures 10.8a and b), albeit much less steeply. This implies that while combustion phasing and in-cylinder conditions are the primary driver in determining the exhaust level emissions of CO and THC, there is indeed a secondary influence of the properties of toluene relative to those of n-heptane.

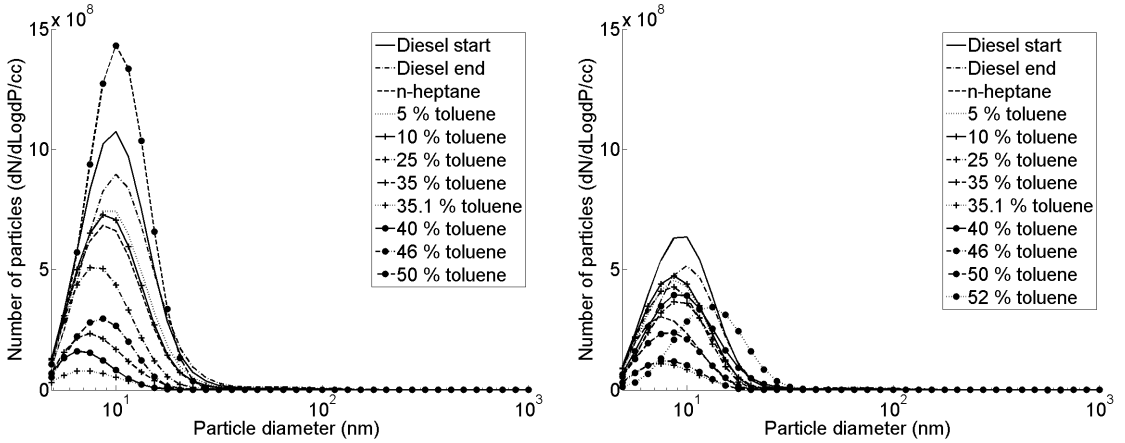

(a) (b)

Figure 10.9: Particle emissions of toluene/n-heptane mixtures and reference fossil diesel at (a) constant injection and (b) constant ignition timings

Figures 10.9a and b show the particle emissions of the toluene/n-heptane binary mixtures and reference fossil diesel at constant injection and constant ignition timings. At constant injection timing (Figure 10.9a), it can be seen that the greatest number of nucleation mode particles (Dp $<$ 50 nm) is produced by the blend containing 50 % toluene, and that the least amount is produced by that containing 35.1

% toluene. At constant ignition timing (Figure 10.9b), the reference fossil diesel produced the greatest amount of nucleation mode particles, with the least number produced by the binary mixture containing 35.1 % toluene. At neither timing condition is a linear influence of the percentage toluene apparent in the peak number of nucleation mode particles produced. However, an effect of combustion phasing is apparent, where at constant ignition timing (Figure 10.9b) SOC and heat release occur close to TDC for all blends that do not show a significant 2nd ignition delay (Figure 10.1), there is a smaller spread in the peak number of nucleation mode particles than at constant injection timing (Figure 10.9a) where SOC of the blends are less similar.

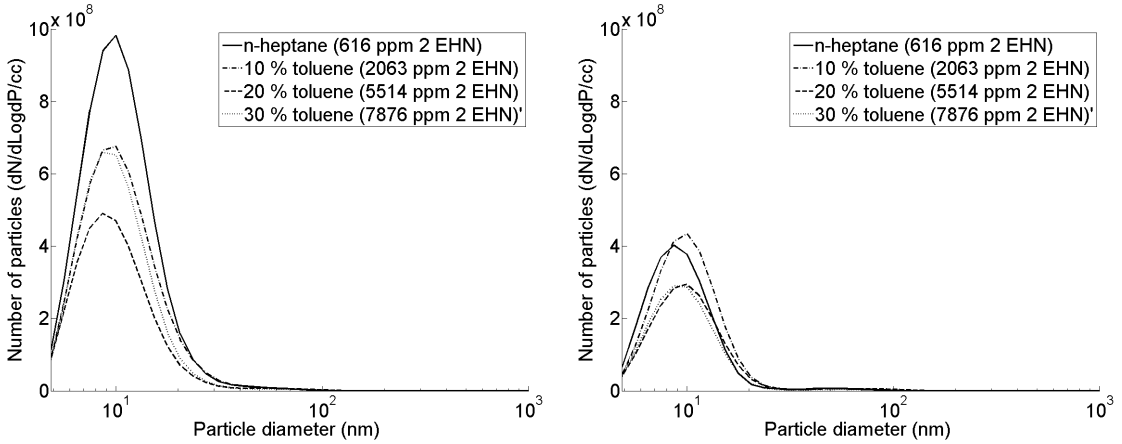

Figure 10.10: Particle emissions of toluene/*n*-heptane mixtures and reference fossil diesel at constant ignition delay timings, (a) fixed SOI and (b) SOC at TDC

Figures 10.10a and b show the particle emissions of the toluene/*n*-heptane binary mixtures at fixed SOI and SOC at TDC constant ignition delay timing conditions. No linear effect of the level of toluene on the peak number of nucleation mode particles can be observed at either timing condition (Figures 10.10a and b), though the effect of combustion phasing where ignition delay was not equalised is still apparent (Figures 10.9a and b). This implies that the influence of combustion phasing on the production of nucleation mode particles produced is via the in-cylinder conditions at which fuel and air mixing, SOC and heat release occur, rather than the duration of ignition delay.

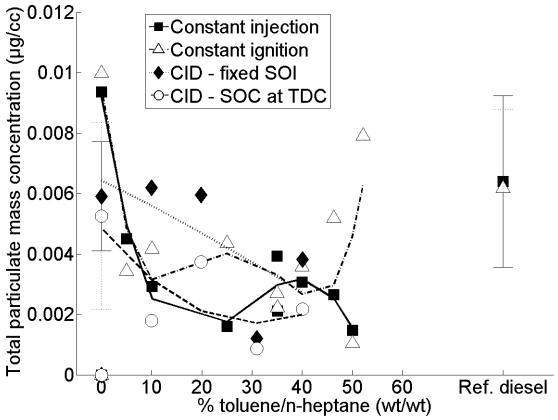

Figure 10.11: Exhaust gas total particulate mass emissions of toluene/*n*-heptane mixtures and reference fossil diesel at constant injection, constant ignition and constant ignition delay timings

Figure 10.11 shows the total particulate mass emitted by the toluene/*n*-heptane mixtures and reference fossil diesel at constant injection, constant ignition and both constant ignition delay timings. With the range of error present (Figure 10.11), is not possible to identify any effect of the percentage toluene present in the binary mixtures on the total particulate produced at any timing condition. Toluene is known to have a higher sooting tendency than *n*-heptane in both premixed and laminar diffusion flames (Alexiou and Williams, 1995; Ladommatos et al., 1996) and has previously been observed to increase smoke emissions in binary mixtures of *n*-heptane and up to 20 % (wt/wt) toluene (Xiao et al., 2000). The lack of any trend reflecting this in Figure 10.11 would suggest that any such influence of toluene is secondary to the combustion phasing and test to test variability at these experimental conditions.

10.2.2. 1-octene/*n*-octane binary mixtures

Figure 10.12 shows the in-cylinder pressures and apparent net heat release rates of the 1-octene/*n*-octane binary mixtures at constant injection and constant ignition timings. It can be seen that regardless of the level of 1-octene present in the blend, the vast majority of heat release occurs during premixed combustion, and that none of the mixtures exhibit appreciable two-stage ignition (Figure 10.12). This is in contrast to the binary mixtures of toluene/*n*-heptane (Figure 10.1), but is to be expected when considering the closer values of cetane numbers for the components

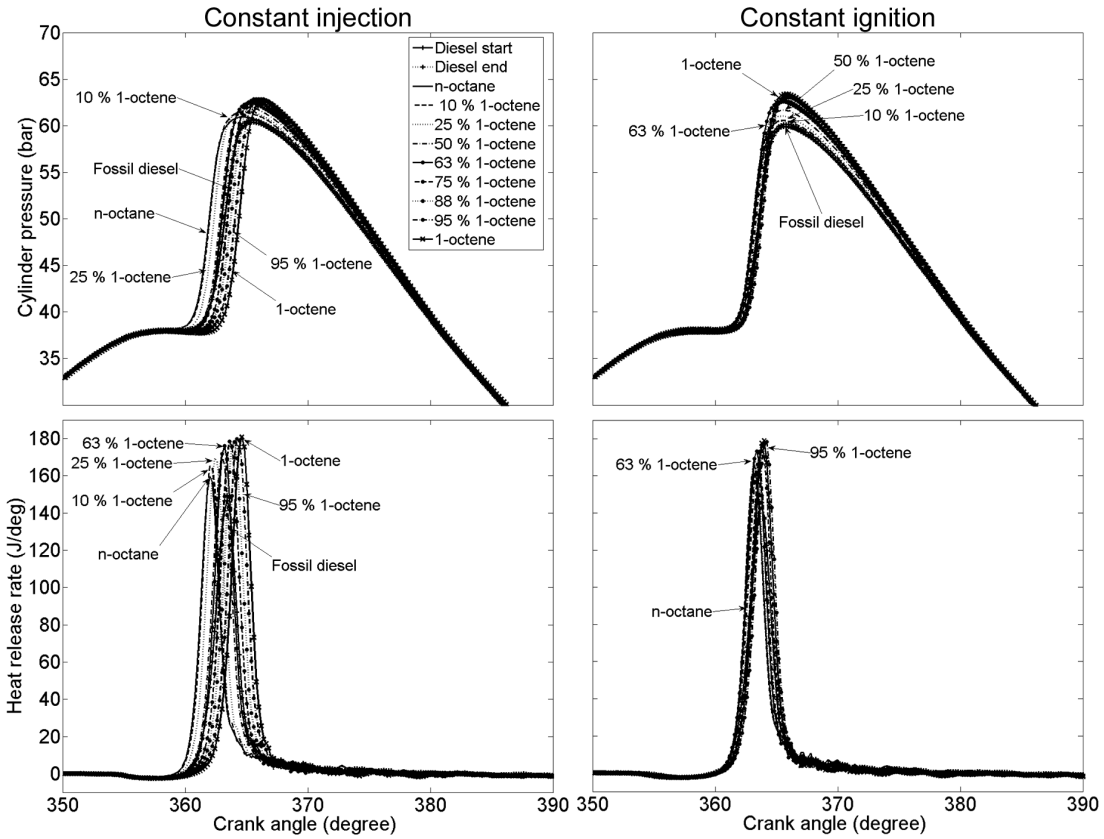

Figure 10.12: In-cylinder pressures and apparent net heat release rates of 1-octene/*n*-octane mixtures and reference fossil diesel at constant injection and constant ignition timing

of the 1-octene/*n*-octane mixtures compared to those for the toluene/*n*-heptane mixtures (Table 10.2).

Employing the same methodology as applied in the case of the toluene/*n*-heptane binary mixtures (Section 10.2.1), a further series of experiments were conducted where the ignition delay of the 1-octene/*n*-octane binary mixtures was isolated as a variable by the use of the ignition improving additive 2 EHN. As such, Figure 10.13 shows the in-cylinder pressure and apparent net heat release rates of the 1-octene/*n*-octane binary mixtures at the constant ignition delay timings of fixed SOI and SOC at TDC. With the initial ignition delay periods equalised, a 2nd ignition delay stage is suggested by the later time of peak heat release as the level of 1-octene present in the blend increases, resulting in a later occurrence of peak heat release rate (Figure 10.13). A similar observation was made of the toluene/*n*-heptane mixtures in which 2 EHN had been used to equalise the duration of the initial ignition delay period

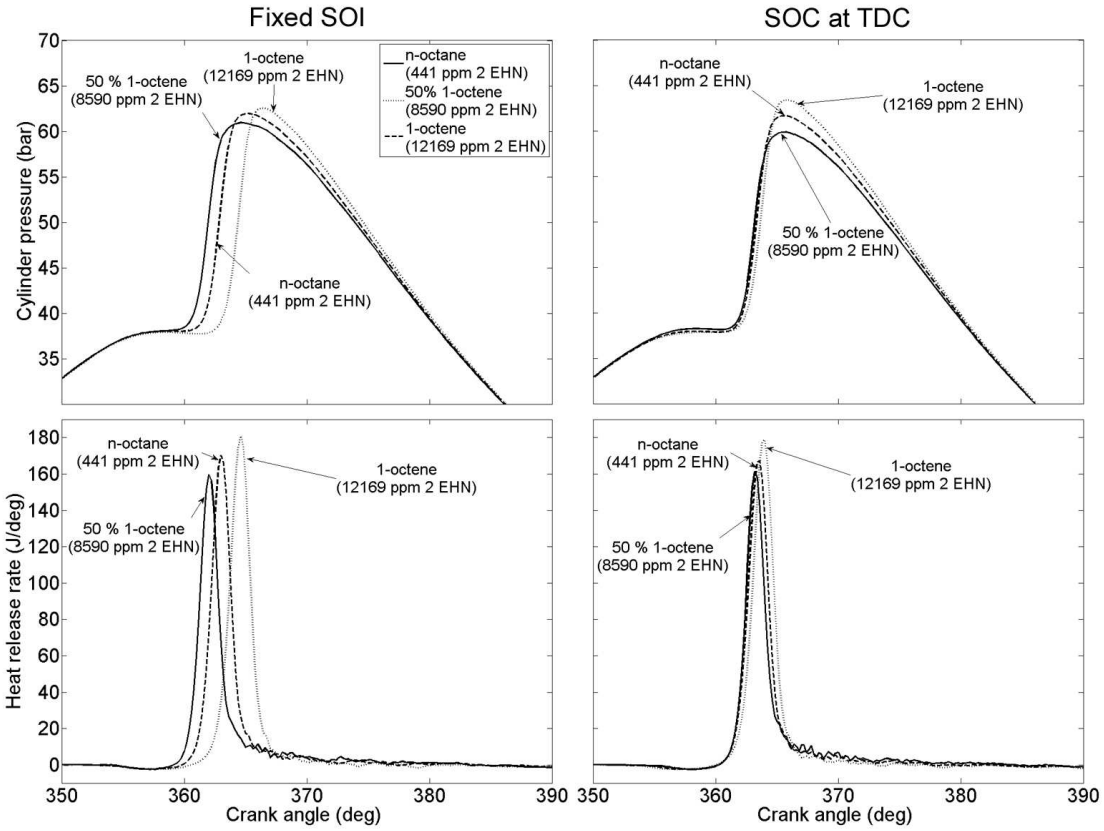

Figure 10.13: In-cylinder pressures and apparent net heat release rates of 1-octene/*n*-octane mixtures and reference fossil diesel at constant ignition delay fixed SOI and SOC at TDC timing

(Figure 10.2), and suggests that the pool of ignition advancing radicals provided by the 2 EHN are consumed during the 1st ignition delay period and are no longer available during the 2nd ignition delay period.

Figures 10.14a and b show the duration of ignition delay and 2nd ignition delay of the 1-octene/*n*-octane binary mixtures and reference fossil diesel at constant injection and constant ignition timing. Increasing the percentage of 1-octene present in the blends results in an approximately linear increase in ignition delay at both timing conditions (Figure 10.14a), though between 80 - 100 % 1-octene the gradient of increase does appear to be slightly steeper. This is possibly suggestive of a disproportionate ignition enhancing influence of small quantities of *n*-octane where the majority of the mixture is 1-octene. No variation in the duration of the 2nd ignition delay outside the resolution of the shaft encoder (0.2 CAD) is visible in measurements of in-cylinder pressure (Figure 10.14b). Discussion as to the influ-

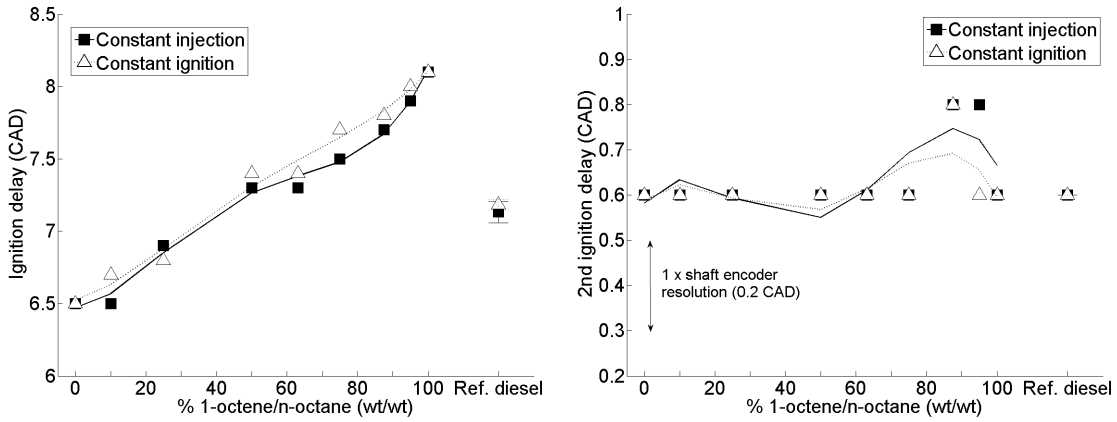

(a) (b)

Figure 10.14: (a) Duration of ignition delay and (b) 2nd ignition delay of 1-octene/*n*-octane mixtures and reference fossil diesel at constant injection and constant ignition timing

ence of 1-octene on the reactivity of 1-octene/*n*-octane mixtures is made in Section 10.2.4, and contrasted with the potential interactions between toluene and *n*-heptane discussed in Section 10.2.3.

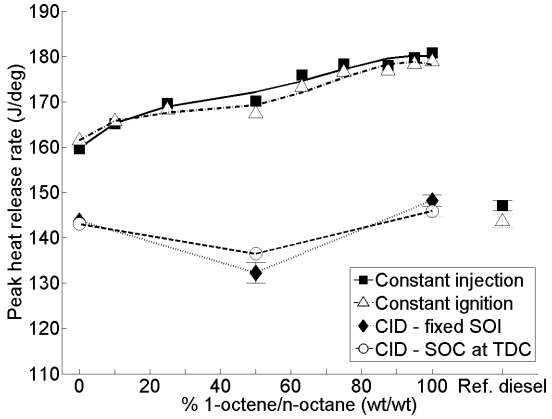

Figure 10.15: Peak apparent net heat release rates of 1-octene/*n*-octane mixtures and reference fossil diesel at constant injection, constant ignition and constant ignition delay timings

Figure 10.15 shows the peak apparent net heat release rates of the 1-octene/*n*-octane binary mixtures and reference fossil diesel at constant injection, constant ignition and the constant ignition delay timings of fixed SOI and SOC at TDC. At

both constant injection and constant ignition timings there is a clear linear trend of increasing peak heat release rates with the level of 1-octene present in the blends (Figure 10.14). This is consistent with the observed trend in ignition delay (Figure 10.14a), and the relatively small range in ignition delay (6.5 - 8.1 CAD) means there is no breakdown in the relationship between ignition delay and peak heat release rate as seen in the case of the toluene/*n*-heptane mixtures (Figures 10.3a and 10.4a) as the majority of heat release for all blends occurs near TDC. For this reason there is also no significant difference between tests conducted at constant injection timing and those at constant ignition timing (Figure 10.15). With the effect of ignition delay removed (Figure 10.15), at both fixed SOI and SOC at TDC, the mixture containing 50 % 1-octene displayed a lower peak heat release rate than either *n*-octane or 1-octene (Figure 10.15). However, this trend is in agreement with that which could be expected when considering that the method of equalizing ignition delay was not able to do so at an accuracy greater than ± the shaft encoder resolution of 0.2 CAD (Table 10.4).

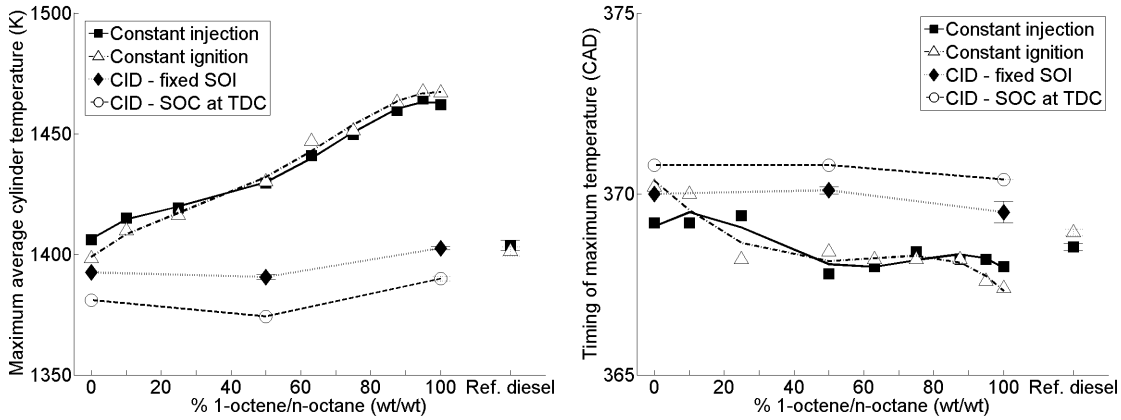

(a) (b)

Figure 10.16: (a) Calculated maximum in-cylinder global temperature and (b) time of occurrence of maximum in-cylinder temperature for 1-octene/*n*-octane mixtures and reference fossil diesel at constant injection, constant ignition and constant ignition delay timings

Figures 10.16a and b show the calculated maximum in-cylinder global temperature and time of occurrence of the 1-octene/*n*-octane binary mixtures and reference fossil diesel at constant injection, constant ignition and both constant ignition delay timings. Increasing the level of 1-octene present in the binary mixtures results in a

higher maximum in-cylinder temperature (Figure 10.16a) which also occurs earlier into the expansion stroke (Figure 10.16b). This correlates well with the peak heat release rates of the binary mixtures (Figure 10.15), those mixtures which displayed the highest peak heat release rate reach higher maximum in-cylinder temperatures more quickly than those mixtures which displayed lower peak heat release rates (Figures 10.16a and b). It follows that a more concentrated release of energy, owing to longer ignition delay and greater premixed combustion, will result in higher and earlier temperatures when combustion is occurring near TDC where changes in cylinder volume are minimal. At constant ignition delay timings (Figure 18b), the maximum in-cylinder temperature again mirrors the peak heat release rate (Figure 10.15) and so the slightly higher in-cylinder temperature reached by 1-octene can likely be attributed to the small residual differences in ignition delay (Table 10.4). There is, however, a notable offset between tests conducted fixed SOI and those at SOC at TDC timing, with the latter condition consistently producing higher temperatures (Figure 10.16a) despite similar levels of peak heat release rate (Figure 10.14). There is also a consistent offset between the two timing conditions when considering the timing of maximum in-cylinder temperature (Figure 10.16b) and the earlier occurrence of the maximum in-cylinder temperature at SOC at TDC timing explains the higher temperatures reached.

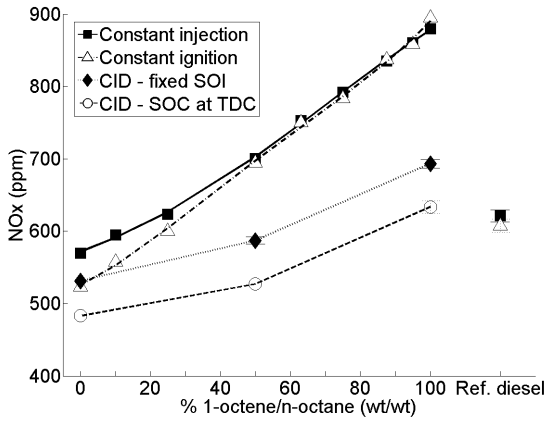

Figure 10.17: Exhaust gas NO_x emissions of 1-octene/*n*-octane mixtures and reference fossil diesel at constant injection, constant ignition and constant ignition delay timings

Shown in Figure 10.17 are the exhaust gas NO_x emissions of the 1-octene/*n*-octane binary mixtures and reference fossil diesel at constant injection, constant ignition

and the constant ignition delay timings of fixed SOI and SOC at TDC. At constant injection and constant ignition timing, with an increasing percentage of 1-octene present in the blends, levels of NO_x also increase linearly (Figure 10.17). Clearly apparent is a strong correlation between the level of NO_x emitted and the in-cylinder thermal conditions, the highest levels of NO_x were emitted by pure 1-octene which also displayed the highest maximum in-cylinder temperature (Figure 10.16a). At constant ignition delay timings, there is also a linear increase in NO_x emissions with increasing 1-octene content (Figure 10.17), despite the mixture containing 50 % 1-octene displaying a lower maximum in-cylinder temperature (Figure 10.16a), occurring at approximately the same time (Figure 10.16b), as that consisting of just *n*-octane. This suggests an effect of 1-octene on the level of NO_x emitted outside of that of affecting the duration of ignition delay and subsequently the peak heat release rate and thereby maximum in-cylinder temperature reached. Furthermore, close inspection of Figure 10.16a shows that at constant injection and constant ignition timings, between 90 - 100 % 1-octene there is no increase in maximum in-cylinder temperature but NO_x levels continue to increase (Figure 10.17). This could plausibly be due to the timing of maximum in-cylinder temperature (Figure 10.16b), which does advance with the increase of 90 - 100 % 1-octene in the mixtures resulting in a higher residence time for gases at elevated temperatures suitable for NO_x production. However, none of the non-linearity apparent in the time of maximum in-cylinder temperature (Figure 10.16b) is apparent in the levels of NO_x emitted (Figure 10.17).

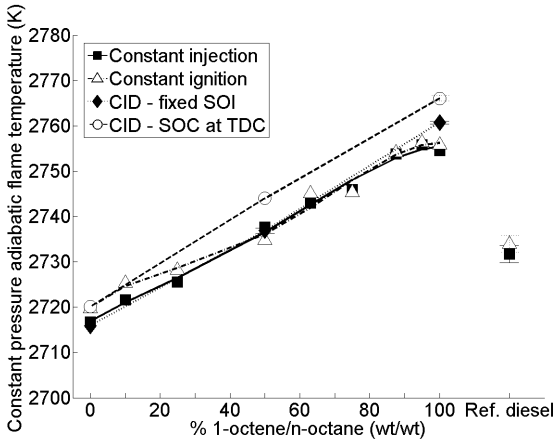

Figure 10.18: Constant pressure adiabatic flame temperatures of 1-octene/*n*-octane mixtures and reference fossil diesel at constant injection, constant ignition and constant ignition delay timings

Figure 10.18 shows the constant pressure adiabatic flame temperatures of the 1-octene/*n*-octane binary mixtures and reference fossil diesel at all timing conditions. The constant pressure adiabatic flame temperatures of the 1-octene/*n*-octane blends were calculated according to the same method as employed in the calculation of the adiabatic flame temperatures of the toluene/*n*-heptane mixtures (Section 10.2.1), with values for the enthalpy of formation of 1-octene and *n*-octane obtained from literature (Prosen and Rossini, 1945; Rockenfeller and Rossini, 1961). It can be seen that there is a linear increase in the adiabatic flame temperature with the level of 1-octene present (Figure 10.18), and so it is suggested that this is contributing to the trend of increasing NO_x emissions (Figure 10.17). This is in agreement with Chapter 7 where the higher adiabatic flame temperature of 1-octene relative to *n*-octane was been identified as generating higher NO_x emissions where ignition delays were equalised.

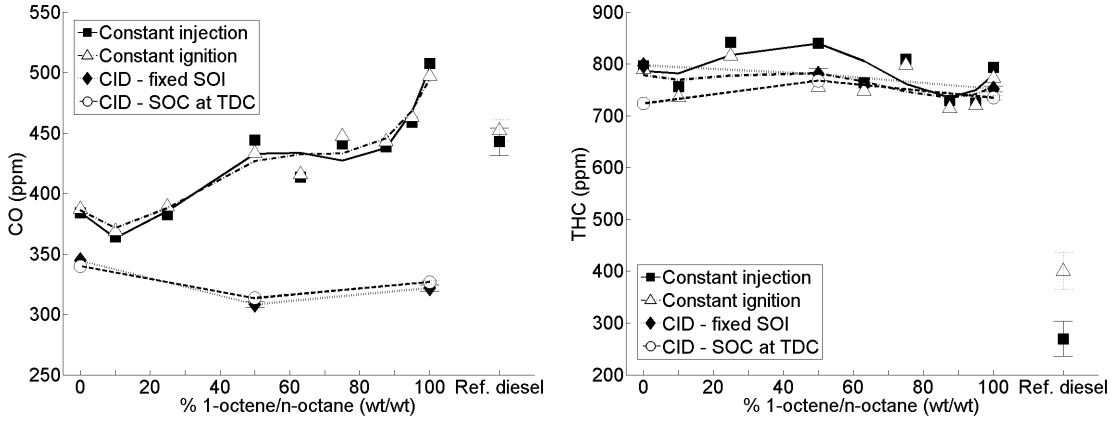

(a) (b)

Figure 10.19: (a) CO and (b) THC emissions of 1-octene/*n*-octane mixtures and reference fossil diesel at constant injection, constant ignition and constant ignition delay timings

Figure 10.19a and b show the exhaust gas emissions of CO and THC of the 1-octene/*n*-octane binary mixtures and reference fossil diesel at constant injection, constant ignition and both constant ignition delay timings. At constant injection and constant ignition timing, increasing the level of 1-octene in the mixture results in an increase in CO levels (Figure 10.19a) but has no clear influence on the emission of THC (Figure 10.19b). At fixed SOI and SOC at TDC timing, where the duration of

ignition delay has been equalized, there is no apparent influence of 1-octene levels on the emission of either CO or THC (Figures 10.19a and b). This would imply that the increase in CO emissions observed at constant injection and constant ignition timing (Figure 10.19a) is more likely attributable to the effect of 1-octene on combustion phasing than any physical property (Table 10.2).

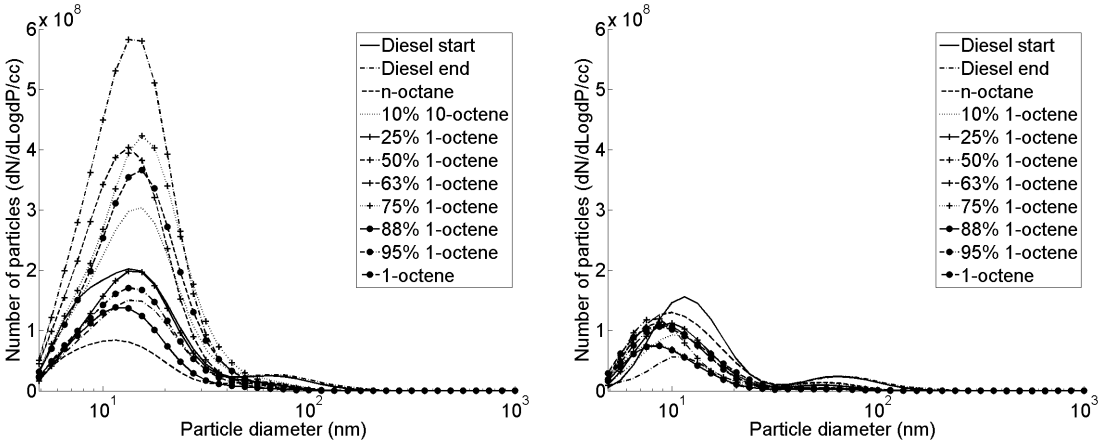

Figure 10.20: Particle emissions of 1-octene/*n*-octane mixtures and reference fossil diesel at (a) constant injection and (b) constant ignition timings

Figures 10.20a and b show the particle emissions of the 1-octene/*n*-octane mixtures and reference fossil diesel at constant injection and constant ignition timings. The highest peak number of nucleation mode particles (Dp < 50 nm) are produced by the binary mixture containing 63 % 1-octene and the fossil diesel at constant injection and constant ignition timing respectively (Figures 10.20a and b). No effect of 1-octene levels on the production of nucleation mode particles can be readily discerned, but it is of interest to note that at both timing conditions the reference fossil diesel produces substantially more particles in the 50 - 100 nm range than any of the 1-octene/*n*-octane binary mixtures. As was also apparent in the case of the toluene/*n*-heptane mixtures (Figures 10.9a and b) there is a smaller range of peak number of nucleation mode particles present at constant ignition timing (Figure 10.20b) than at constant injection timing (Figure 10.20a).

Shown in Figures 10.21a and b are the particle emissions of the 1-octene/*n*-octane binary mixtures, at both constant ignition delay timings. At constant ignition delay fixed SOI timing (Figure 10.21a), *n*-octane produces a much higher peak in the

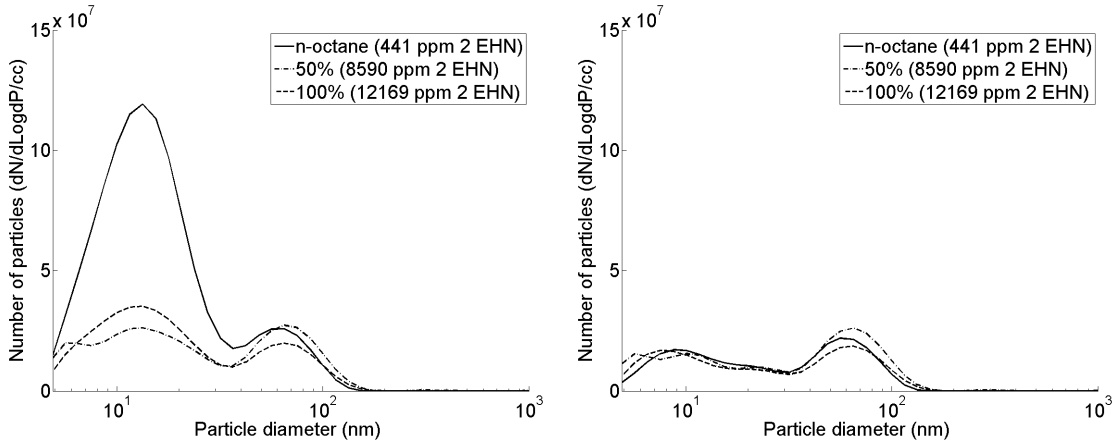

Figure 10.21: Particle emissions of 1-octene/*n*-octane mixtures at constant ignition delay timings, (a) fixed SOI and (b) SOC at TDC

number of nucleation mode particles (Dp < 50 nm) than either 1-octene or the mixture containing 50 % 1 - octene. However, at SOC at TDC timing (Figure 10.21b), all three mixtures produce very similar levels of nucleation mode particles.

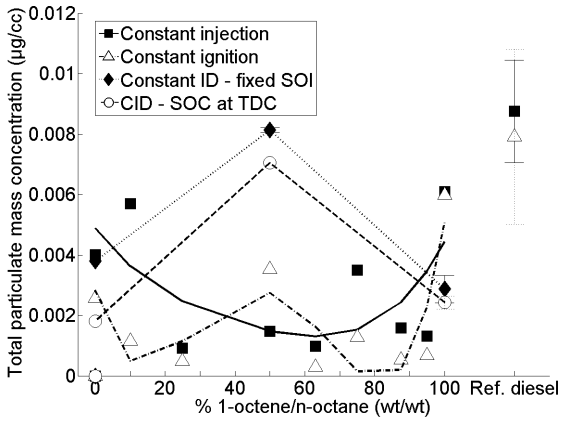

Figure 10.22: Exhaust gas total particulate mass emissions of 1-octene/*n*-octane mixtures and reference fossil diesel at constant injection, constant ignition and constant ignition delay timings

Figure 10.22 shows the total mass of particulates emitted by the 1-octene/*n*-octane binary mixtures and reference fossil diesel at all timing conditions. At constant injection and constant ignition timing, the range of error presented does not make it possible to draw any conclusions as to the effect of 1-octene in the mixtures, and

furthermore no clear trends are readily apparent (Figure 10.22). However, at both constant ignition delay timings, the mixture containing 50 % 1 - octene produced significantly more particulate mass than either *n*-octane or 1-octene (Figure 10.22). This is plausibly due to the thermal sensitivity of soot oxidation, (the rates of which increase with temperature (Tree and Svensson, 2007)) as the 50 % 1-octene mixture displayed a lower peak heat release rate than either pure *n*-octane or 1-octene (Figure 10.15).

10.2.3. Effect of toluene content on toluene/*n*-heptane binary mixture reactivity

The effect of increasing toluene content in a binary mixture with *n*-heptane is consistent with results of previous studies (Andrae et al., 2005; Di Sante, 2012; Hartmann et al., 2011; Herzler et al., 2007; Vanhove et al., 2006) in so much as that the mixture reactivity is decreased and the duration of ignition delay increased (Figures 10.1, 10.3a and b). However, developing an understanding as to how toluene is impacting on the ignition process in the current study is not straightforward as the experimental conditions are somewhat different to the previous studies mentioned. Perhaps most significantly, the binary mixtures were directly injected at high pressures (450 bar) into the cylinder near TDC (and thus into a highly turbulent environment) with no premixing of fuel and air possible. In the case of the studies conducted on high pressure shock tubes and rapid compression machines the fuel mixtures were evaporated and in some cases allowed to mix with the charge air for ten minutes prior to compression. Therefore, before considering the influence of toluene on the low temperature reaction chemistry of *n*-heptane, it is sensible to explore any possible effect of the physical properties of toluene on the efficiency of fuel and air mixing.

As suggested in Section 10.2.1, the higher density, viscosity and boiling point of toluene relative to *n*-heptane are likely to reduce the efficiency of fuel and air mixing (Table 10.2). Figure 10.23 shows the variation with injection pressure of mean droplet diameter of pure toluene, a toluene/*n*-heptane binary mixture of 50 % toluene and *n*-heptane from a single hole injector measured with an optical droplet sizing system (Malvern). While the measurements presented in Figure 10.23 were conducted at much lower injection pressures than the engine experiments (110 vs. 450 bar), it can be seen that the droplet size of the 50 % toluene mixture lies between

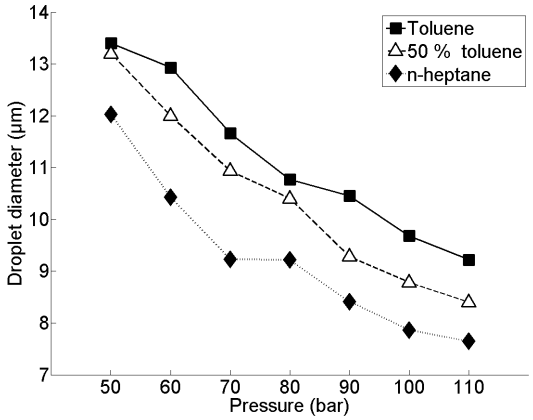

Figure 10.23: Variation with injection pressure of mean droplet diameter of toluene, 50 % toluene binary mixture and *n*-heptane; data courtesy of M. Magi

that of pure toluene and *n*-heptane at all pressures. Therefore, it can be assumed that the physical properties of the binary mixtures corresponds proportionally to those of the components, thus increasing the percentage of toluene in the mixture would have reduced the efficiency of fuel and air mixing. If these changes in physical properties were significantly affecting the fuel and air mixing then an indication might be provided by the toluene/*n*-heptane mixtures in which ignition delay was equalized (Figure 10.2). Peak heat release rate has been previously observed to correspond well with the extent of the premixed fraction (Chapter 6), and where the duration of ignition delays are equal, it follows that the premixed burn fraction will be dictated by the efficiency of fuel and air mixing prior to SOC. Therefore, with physical properties becoming less favorable for air and fuel mixing, with increasing percentage of toluene (equal duration of ignition delay), the observed peak heat release rate could be expected to decrease (Figure 10.4a). While Figure 10.4a does hint at such a trend, the extent of the error bars is relatively substantial and the lower peak heat release rate of the blend containing 40 % toluene can be attributed to a later time of occurrence. Therefore, while an effect of changing physical properties is a potential influence on the mixture reactivity, the likely importance (if any) of such properties relative to other factors is minimal. Vanhove et al. (2006) did suggest that the ignition inhibiting influence of toluene on *n*-heptane could not be attributed to chemical effects, however, the compression pressure of the RCM study on which this assertion is based was significantly lower than that for the current study (4 vs. 37 bar).

Toluene, as a single component and unlike *n*-heptane, has been observed to exhibit no low temperature reactivity that results in heat release (Griffiths et al., 1993). However, Figures 10.1 and 10.3b would seem to suggest that addition of toluene results in an increasingly significant 2nd ignition delay period that is not present at all in the case of pure *n*-heptane and binary mixtures containing less than 25 % toluene. Previous studies have reported that addition of toluene diminishes the presence of the NTC and distinct two stage ignition (Hartmann et al., 2011; Herzler et al., 2007). However, in the current study, in-cylinder conditions are such that two distinct phases of ignition delay of pure *n*-heptane are not apparent (Figure 10.1 and 10.3b); this was also observed in the RCM measurements of Di Sante (2012) at compression temperatures in excess of 800 K. This is not unexpected as for *n*-alkanes the region of NTC is generally considered to end at approximately 750 K (Pilling, 1997); at the SOI for all tests of the toluene/*n*-heptane mixtures, the calculated in-cylinder global temperature was 775 K or greater.

As such the 2nd ignition delay visible for mixtures containing more than 25 % toluene is unlikely to be attributable the NTC of the *n*-heptane present (Figures 10.1 and 10.3b). Considering now those mixtures with 25 % or less toluene, the effect of toluene is to increase the ignition delay period but not induce a 2nd ignition delay. At low temperatures, toluene can be oxidised via the abstraction of a H from the methyl group by O_2, or preferentially non-selective OH radicals (Andrae et al., 2005; Vanhove et al., 2006):

$$C_2H_5CH_3 + O_2 \rightarrow C_2H_5CH_2{}^* + HO_2 \tag{10.1}$$

$$C_2H_5CH_3 + OH^* \rightarrow C_2H_5CH_2{}^* + H_2O \tag{10.2}$$

In the binary mixtures considered, the only source of OH radicals is those produced by H abstraction from *n*-heptane by O_2

$$C_7H_{16} + O_2 \rightarrow C_7H_{15}O^* + OH^* \tag{10.3}$$

which is the first step in the radical branching process of internal isomerisation and peroxidation that governs the ignition chemistry of long alkyl chains (Westbrook, 2000).

The benzyl radicals that are formed in Equations 10.1 and 10.2 are thermally stable below 1000 K and cannot be oxidised further by O_2 (Pilling, 1997). Therefore, as previously suggested (Andrae et al., 2005; Vanhove et al., 2006), it can be seen that toluene will delay the SOC by consuming radicals that otherwise would be utilised in the radical propagating reactions of *n*-heptane. This is confirmed by the use of the radical providing additive 2 EHN to equalise the ignition delay of binary mixtures containing differing proportions of toluene (Figure 10.2). A second possible mechanism by which toluene may be acting as an inhibitor of radical branching during ignition delay is the physical presence of the non-reactive molecules within the fuel mixture. It is tentatively suggested that in addition to consuming radicals, the toluene molecules act as a diluent of the more reactive *n*-heptane molecules and thus reduce rates of reaction.

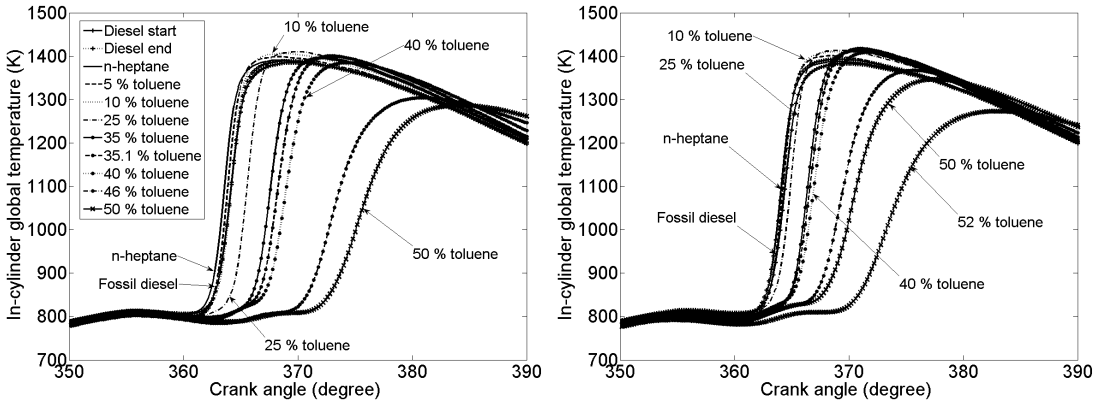

(a) (b)

Figure 10.24: Calculated in-cylinder global temperatures of toluene/*n*-heptane mixtures and reference fossil diesel at (a) constant injection and (b) constant ignition timing

Figure 10.24a and b show the calculated in-cylinder global temperature profiles of the toluene/*n*-heptane binary mixtures at constant injection and constant ignition timing. At both timing conditions it can be seen that for all mixtures temperatures do not rise significantly above 800 K until sometime after SOC, when a substantial amount of heat release has occurred (Figure 10.1). Therefore, it would seem that for

those binary mixtures that do exhibit a 2nd ignition delay, thermal conditions are broadly the same as during the first period of ignition delay and so the initial reactions of the fuel components according to Equations 10.1 - 10.3 are likely to remain valid. As such, the following hypothesis is put forward regarding the presence of a 2nd ignition delay for those binary mixtures containing greater than 25 % toluene.

At the point of SOC, local temperatures will have reached 900 - 1000 K and H_2O_2, formed by the radical branching reactions initiated by Equation 10.3, will decompose and release large numbers of OH radicals, resulting in rapid branching reactions and ignition (Westbrook, 2000). For the mixtures containing up to 25 % toluene, the ensuing heat release from the local SOC is sufficient to initiate ignition throughout the charge. In the case of the mixtures containing more than 25 % toluene, after ignition and consumption of a portion of the charge a further period of time is required during which a further build up of radical numbers must be occurring. The presence of toluene may prevent the escalation of ignition by removing OH from the radical pool produced by the decomposition of H_2O_2. Additionally, where ignition could be expected to spread to other areas of the fuel and mixture as stoichiometry allows (Dec, 1997), toluene may have prevented the build-up of sufficient radicals for this despite an increase in local temperature provided by the initial period of heat release (Figure 10.1). During the 2nd ignition delay period, radical branching reactions involving *n*-heptane (Equation 10.3) and radical stabilizing reactions involving toluene (Equations 10.1 and 10.2) continue. Fuel and air mixing would also continue and, given that a degree of premixing has already occurred during the initial period of ignition delay, it could be expected that more of the fuel and air mixture would be at ideal stoichiometry for combustion at SOC2; it is also likely that local temperatures are somewhat higher as a result of the first heat release period. Thus this 2nd point of ignition is able to propagate throughout the cylinder charge. It is also possible during the 2nd ignition delay and SOC2 that the radical stabilising effect of toluene is potentially somewhat diminished as some toluene molecules will have been oxidised to thermally stable benzyl radicals during the 1st period of ignition delay.

It can be seen that the 2nd ignition delay period (Figure 10.2b) increases as the toluene content of the binary mixture rises from 35 - 50 %, and it follows that this can be attributed to the fewer number of *n*-heptane molecules available to produce radicals and more toluene to consume those that are produced. Ignition cannot

occur at all for mixtures containing more than 52 % toluene (at the conditions tested), indicating that at this proportion of toluene there is insufficient build up of radicals and local temperatures for any ignition to take place, regardless of the degree of fuel and air premixing.

10.2.4. Effect of 1-octene on low temperature behavior of 1-octene/n-octane binary mixtures

In contrast to the binary mixtures of toluene and n-heptane, those of 1-octene and n-octane show a reasonably linear relationship between ignition delay and the mixture composition (Figure 10.14a). As the ignition delay is proportional to the 1-octene content, it is suggested that the longer ignition delays of the binary mixtures relative to n-octane can be attributed to the lower ignition quality of 1-octene (Table 10.2). In Chapter 6, in which several alkanes and alkenes (including n-octane, 1-octene and 1, 7 - octadiene) were compared as pure fuel components, it was found that the ignition delay of an alkene relative to that of n-alkane of equivalent carbon chain length correlated highly with the percentage of double bonds present within the alkene. A similar relationship can be observed in the current study when considering that as the level of 1-octene increases in the binary mixtures, the proportion of double bonds does so also.

This implies that the addition of the 1-octene to the binary mixture does not result in significant interactions between those molecules and the n-octane within the mixture. This is not a surprising result as the low temperature reactivity of alkenes is considered to be dominated by the saturated portions of the molecule (Bounaceur et al., 2009; Mehl et al., 2008), which will follow the same low temperature branching pathways as n-alkanes.

10.3. Conclusions

1. Increasing the percentage of toluene present in a binary mixture with n-heptane significantly reduces the ignition quality of a blend. Furthermore, at the conditions tested, n-heptane displayed one stage ignition but addition of more than 25 % (wt/wt) of toluene resulted in two distinct ignition stages. Where the level of toluene present exceeded 50 %, no ignition occurred whatsoever.

2. Where the toluene/*n*-heptane mixtures show only one stage of ignition delay and this increases in duration with the percentage of toluene present, this can be attributed to the radical stabilizing behavior of toluene. This effect can be offset by the radical providing additive 2 EHN.

3. Where two stages of ignition delay were apparent in the combustion of the toluene/*n*-heptane binary mixtures, the failure of the initial ignition to propagate throughout the cylinder charge can also be attributed to the consumption of radicals by toluene. It is suggested that the 2^{nd} point of ignition is able to propagate throughout the charge as the second period of ignition delay allows for more fuel and air mixture to reach combustible stoichiometry.

4. Increasing the content of 1-octene present in a binary mixture with *n*-octane results in a proportional increase in ignition delay.

5. Exhaust emissions produced by the binary mixtures of toluene/*n*-heptane and 1-octene/*n*-octane show a significant influence of the in-cylinder thermal conditions as dictated by the duration of ignition delay.

6. With the ignition delay of the binary mixtures removed as a variable, an increase in toluene or 1-octene content results in higher NO_x levels and can be attributed to a simultaneous rise in adiabatic flame temperature.

11. Characterisation of terpenes with a view to their biological production in cyanobacteria

The advent of genetically engineered micro-organisms is an exciting opportunity to explore novel and sustainable methods of bio-fuel production (Lu et al., 2011; Peralta-Yahya et al., 2012). While the introduction of novel biosynthesis pathways into micro-organisms is a field still very much in its infancy, un-modified micro-organisms have already seen considerable utilisation in industrial applications (Rude and Schirmer, 2009). Recently, the use of algal lipids for the production of bio-diesel via transesterification of fatty acids with an alcohol is attracting significant interest (Demirbas and Demirbas, 2011; Krohn et al., 2011; Um and Kim, 2009; Yang et al., 2011a), with favourable comparisons to other lipid sources (Ahmad et al., 2011; Chisti, 2007). However, while the feedstock is renewable, the production of algal bio-diesel via lipid extraction and transesterification does not yet represent a low-carbon route to replace fossil fuels. It is also, at present, generally considered economically non-viable without either government subsidy or the a decline in global oil resources and a concurrent escalation in the price of crude fossil oil (Campbell et al., 2011; Gallagher, 2011; Lee, 2011). This economic non-viability can in part be attributed to the large energy cost associated with the harvesting and drying of algal cells that grow in aqueous media at densities typically less than 10 g/L (Delrue et al., 2012) and is currently considered to be a major limitation of biochemical production from photosynthetic organisms (Atsumi et al., 2009). Therefore, the possibility of engineering a photosynthetic organism in such a way so as to negate this prohibitive energy cost is highly attractive.

Figure 11.1 shows the terpenoid (or isoprenoid) pathways available in the cyanobacteria *Synechocystis* sp PCC6803 with introduction of one more biosynthesis enzymes. As can be seen in Figure 11.1, a variety of terpenes could potentially be produced from five-carbon isoprene units as building blocks (Vranova et al., 2012). Amongst the simplest of these terpenes, and requiring only a single synthase enzyme, is geraniol, a hydrophobic C10 terpene (Figure 11.1). Further engineering of a cyanobacteria, such as *Synechocystis*, can cause the secretion of any hydrocarbons produced within the cell membrane (Dunlop et al., 2011), and so in the case of the a hydrophobic molecule, harvesting of the hydrocarbon could potentially be greatly simplified relative to extraction of lipids from within a cell.

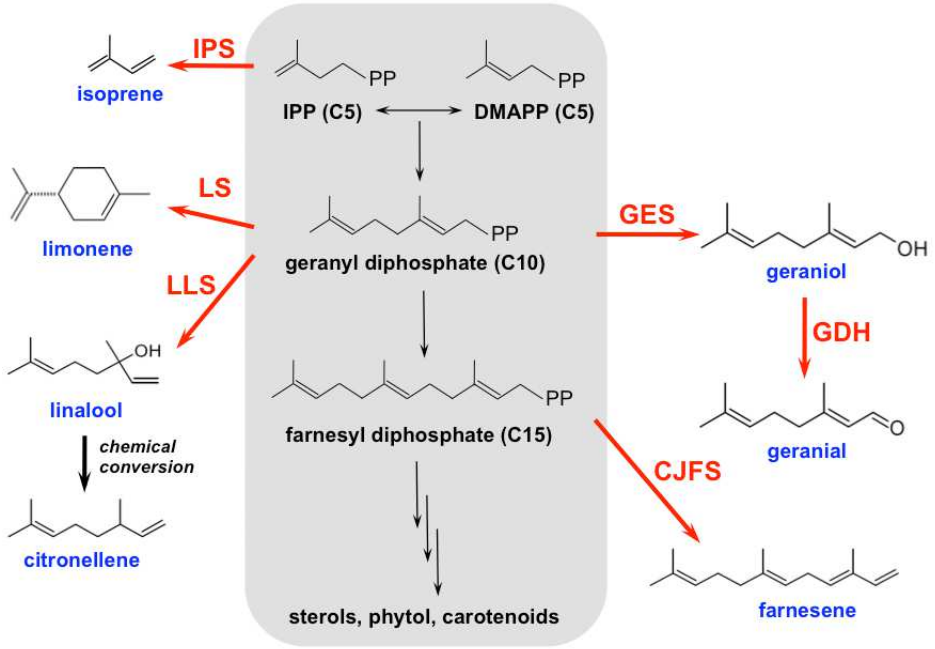

Figure 11.1: The isoprenoid pathway (highlighted in grey) and examples of possible pathways (red) that could be introduced to produce novel hydrocarbons (blue). IPS: isoprene synthase; LS: limonene synthase; LLS linalool synthase; GES: geraniol synthase; GDH: geraniol dehydrogenase; CJFS: (E)-β-farnesene synthase. Courtesy of S. Purton and L. Al-Haj.

However, unlike lipids, terpenes and especially monoprenoids have to date received little attention as potential fuels for either compression or spark ignition engines. Tracy et al. (2009) hydrogenated the monoterpenes myrcene and limonene and blended the products with fossil diesel at 5 - 10 %. All of the blends met the minimum standards of ASTM D975, though in the case of the hydrogenated products of myrcene (comprising 84.5 % 2,6-dimethyloctane), the viscosity of the blends was higher than that for the fossil diesel. Peralta-Yahya et al. (2011) produced the monocyclic sesquiterpene bisabolene by metabolic engineering of *E. coli* and also the yeast *S. cerevisiae*. The sesquiterpene was hydrogenated to form bisabolene, and was determined by IQT to possess a cetane number of between 41.9 and 52.6. Anand et al. (2010) investigated the combustion and emissions production of a turpentine oil (consisting of at least 40 % pinene) in a direct injection compression ignition engine and found the turpentine oil to have a cetane number of 38. At a fixed injection timing of 23 BTDC they found emissions of NO_x, CO and THC all to decrease up to

a blend level of 50 % turpentine oil in diesel, concurrent with the movement of peak heat release earlier into the compression stroke. Combustion of pure turpentine oil was somewhat less steady than the fossil diesel, as indicated by greater variation in the peak cylinder pressure.

This chapter presents the results of an investigation into the potential of cyanobacterial produced terpene bio-fuels, specifically geraniol and several other terpenes that represent a change to the molecular structure of geraniol. This consists of experiments assessing terpene combustion characteristics and emissions production in compression ignition and spark ignition engines as single components and blends with fossil fuels.

11.1. Experimental methods

11.1.1. Apparatus

The majority of the combustion experiments described in the present chapter were performed using the compression ignition engine described in Chapter 3, Section 3.2, and utilising the ultra low volume fuel system described in Chapter 3, Section 3.5. Additional experiments were conducted in the Ricardo E6 spark ignition engine described in Chapter 3, Section 3.9.

11.1.2. Fuel molecules investigated

The C10 compound, geraniol which could be produced in *Synechocystis* using a single enzyme (Figure 11.1) and a further eleven others, were tested in the compression ignition engine as single component fuels. The eleven molecules possessed molecular structures, in most cases, not dissimilar to geraniol and were thus chosen as they could potentially either be produced instead of geraniol via additional enzymes added to the pathway (Figure 11.1), or post-processed from geraniol by chemical or physical methods. Furthermore, the eleven molecules were chosen to provide an insight as to how the following changes to molecular structure would impact on combustion phasing and emissions production:

(a) *Cis* vs *trans* isomerisation of geraniol (geraniol and nerol).

(b) Increasing the degree of saturation while keeping all other aspects of molecular structure constant (geraniol, citronellol and 3,7 - dimethyl - 1 - octanol).

(c) Movement of the OH within an monoprenoid (geraniol and linalool).

(d) Replacement of the OH group of an monoprenoid with other oxygen containing functional groups (geraniol, geranyl acetate, geranial, citral dimethyl acetal and (-)-β-citronellene).

(e) Comparison of an monoprenoid and cyclic compound with identical carbon and oxygen content (geraniol and l-menthol).

(f) Increasing the carbon chain length of sesquiterpenes (farnesene and squalene).

Alongside the twelve single component fuels, a reference fossil diesel with zero FAME content and a reference fossil gasoline with zero alcohol content were also tested. All of the pure component fuels were obtained from a chemical supplier (Sigma Aldrich). The assay and other properties of each fuel are presented in Table 11.1, while the molecular structure of each is given in Table 11.2.

11.1.3. Experimental conditions

Compression ignition engine experiments Each of the 12 molecules and reference diesel were tested at the two experimental conditions of constant injection and constant ignition timing, as defined in Chapter 5.

All single component fuels (including the reference diesel) were first heated in a PID controlled water bath held at 60 °C prior to filling of the low volume fuel system which had been preheated to 63 ± 4 °C and was held at this temperature throughout the subsequent experiment. Inlet air for all experiments was heated to 133.5 ± 2.4 C.

All tests of single components fuels were conducted at an engine speed of 1200 rpm and at 700 bar fuel injection pressure. The injection duration was adjusted in the case of every fuel so that the engine IMEP was always constant at 4.00 bar for all fuels, with a summary of the engine and test operating conditions given in Table 11.3.

A further series of experiments was undertaken in which two of the molecules, farnesene and geranial, were blended in varying proportions with the reference fossil diesel. These experiments were performed at the same conditions of constant injection and constant ignition timing, but with no preheating of the fuel blends and with the low volume fuel system allowed to remain at ambient room temperature ($\approx$ 25

°C). Inlet air for these experiments was not heated. The tests with the fuel blends were also conducted at an engine speed of 1200 rpm, but at a lower fuel injection pressure of 450 bar. The injection duration was adjusted in the case of every fuel so that the engine IMEP was always constant at 4.00 bar for all blends. A summary of the engine and test operating conditions for these experiments is given in Table 11.4.

Spark ignition engine experiments. Following tests conducted in the compression ignition engine, three of the terpenes were tested as potential gasoline substitutes in the spark ignition engine. Geraniol, linalool and citronellene were blended in varying proportions with a reference fossil unleaded gasoline (RON 95), with the tests conducted at spark timings of 26 and 30 CAD BTDC.

All tests were conducted at an engine speed of 1200 rpm with wide-open throttle (WOT) and with the carburetor set so that for all fuels the lambda value was always constant at a value of 1.00 $\pm$ 0.02. A summary of the engine and test operating conditions for these experiments is given in Table 11.5.

Table 11.1: Terpene fuel properties

Fuel	Molecular formula	Assay (%)	T_{boil} (°C)	T_{melt} (°C)	△vapH° (kJ/mol)	Density at 20 °C (kg/m^3)	Dynamic viscosity at 19.7 °C (mPa.s)	Dynamic viscosity at 59.7 °C (mPa.s)
Ref. fossil diesel	-	-	269‡	-	-	834.5^{+}	3.42	1.75
Geraniol	$C_{10}H_{18}O$	≥ 97	229.9 to 231[1, 2]	-15[3]	-	880.1[1]	8.28	2.85
Nerol	$C_{10}H_{18}O$	≥97	226.2[1]	-	-	876[1]	7.19	2.52
Citronellol	$C_{10}H_{20}O$	≥95	224.9[2]	-	-	855.1[4]	11.50	3.30
3, 7 - dimethyl - 1 - octanol	$C_{10}H_{22}O$	≥98	-	-	66.15[5]	830.8 [19]	15.33	3.82
Linalool	$C_{10}H_{18}O$	≥97	198[6]	-	-	862.4 to 872[7, 8]	4.47*[8]	1.84
Geranyl acetate	$C_{10}H_{20}O_2$	≥98	-	-	-	915[9]	3.03	1.63
Geranial (citral - A)	$C_{10}H_{16}O$	≥95	225 to 227[10]	-	-	886.8[10]	2.65	1.48
Citral dimethyl acetal	$C_{10}H_{22}O_2$	≥90	-	-	-	-	2.41	1.37
(-)-β-Citronellene	$C_{10}H_{18}$	≥90	158.85[11]	-	-	760.1[12]	1.00	0.84
L-Menthol	$C_{10}H_{20}O$	≥99	214.6[13]	42.5[14]	-	913.1[15]	-	6.17
Farnesene (mixture of isomers)	$C_{15}H_{24}$	-	-	-	-	841[16]	3.29	1.70
Squalene	$C_{30}H_{50}$	≥98	-	-5.2 to -4.8[17]	-	857.7[18]	15.50	5.49

$^{+}$ = experimental data obtained according to ASTM D4052 at 15 C, ‡= experimental data obtained according to EN ISO 3405, * = data at 25 C. Values of viscosity were measured at temperatures of 19.7 C and 59.7 C using a stand-alone rheometer (Brookfield LVDV - III +U), [1] = data from Greenlee and Wiley (1962), [2] = data from Tufeu et al. (1993), [3] = data from Jacobsen (1871), [4] = data from Naves and Tullen (1961), [5] = data from Serpinskii (1954), [6] = data from Iwai et al. (1994), [7] = data from Deng et al. (2002), [8] = data from Francesconi et al. (2001), [9] = data from Rummens (1965), [10] = data from Stiehl (1898), [11] = data from Pines et al. (1954), [12] = data from Longinow (1929), [13] = data from Huggett (1941), [14] = data from Yang et al. (2011b), [15] = data from Read and Grubb (1934), [16] = data from Ruzicka (1923), [17] = data from Ernst et al. (1976), [18] = data from Tsujino (1953)and [19] = data from Naves (1947).

Table 11.2: Terpene molecular structures

Geraniol	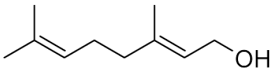
Nerol	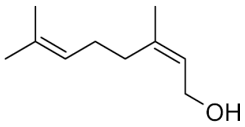
Citronellol	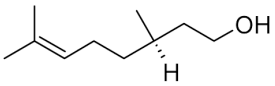
3, 7 - dimethyl - 1 - octanol	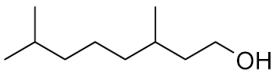
Linalool	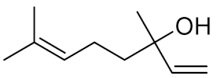
Geranyl acetate	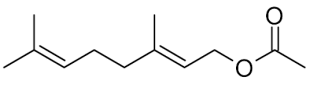
Geranial (citral - A)	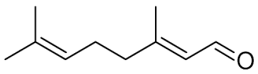
Citral dimethyl acetal	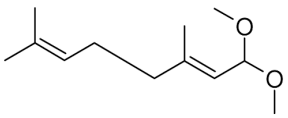
(-)-β-Citronellene	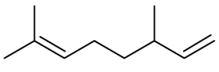
L-Menthol	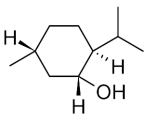
Farnesene (mixture of isomers)	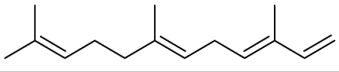
Squalene (mixture of isomers)	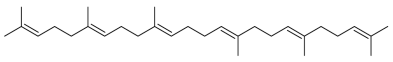

Table 11.3: Single component terpene fuels compression ignition engine test operating conditions

Fuel	Engine speed (rpm)	Fuel injection pressure (bar)	IMEP (bar)	Constant injection timing (SOI at 7.5 CAD BTDC)				Constant ignition timing (SOC at TDC)			
				Ignition delay (CAD)		Injection duration (µs)		Ignition delay (CAD)		Injection duration (µs)	
				Mean	1σ	Mean	1σ	Mean	1σ	Mean	1σ
Reference fossil diesel	1200	700	4	5.0	0.1	589	13	4.8	0.2	590	14
Geraniol	1200	700	4	9.5	0.2	597	15	8.5	0.2	600	14
Nerol	1200	700	4	8.1	-	583	-	7.7	-	591	-
Citronellol	1200	700	4	8.5	-	618	-	8.7	-	624	-
3, 7 - dimethyl - 1 - octanol	1200	700	4	7.9	-	596	-	7.8	-	603	-
Linalool	1200	700	4	DNC	-	-	-	DNC	-	-	-
Geranyl acetate	1200	700	4	8.4	0.1	637	5	8.2	0.1	642	5
Geranial (citral - A)	1200	700	4	5.5	-	598	-	5.1	-	601	-
Citral dimethyl acetal	1200	700	4	7.9	-	647	-	7.7	-	654	-
(-)-β-Citronellene	1200	700	4	DNC	-	-	-	13.6	-	596	-
L-Menthol	1200	700	4	DNC	-	-	-	9.3	-	596	-
Farnesene (mixture of isomers)	1200	700	4	6.5	-	566	-	6.4	-	571	-
Squalene	1200	700	4	6.7	-	598	-	6.7	-	591	-

Table 11.4: Terpene and reference diesel blends compression ignition engine test operating conditions

% terpene in reference diesel (wt/wt)	Engine speed (rpm)	Fuel injection pressure (bar)	IMEP (bar)	Constant injection timing (SOI at 7.5 CAD BTDC)				Constant ignition timing (SOC at TDC)			
				Ignition delay (CAD)		Injection duration (μs)		Ignition delay (CAD)		Injection duration (μs)	
				Mean	1σ	Mean	1σ	Mean	1σ	Mean	1σ
0	1200	450	4.09 ± 2 %	7.5	0.4	685	53	7.5	0.4	686	53
Farnesene											
5	1200	450	4.09	8.1	-	736	-	8	-	736	-
10.1	1200	450	4.09	8.5	-	735	-	8.3	-	737	-
20.3	1200	450	4.09	8.9	-	736	-	8.7	-	741	-
40	1200	450	4.09	10.1	-	737	-	9.9	-	735	-
51.2	1200	450	4.09	11.1	-	778	-	10.7	-	742	-
59.9	1200	450	4.09	DNC	-	-	-	10.9	-	751	-
Geranial											
7.8	1200	450	4.09	7.5	-	636	-	7.4	-	639	-
10	1200	450	4.09	7.5	-	640	-	7.6	-	642	-
20.3	1200	450	4.09	7.9	-	635	-	8	-	635	-
40	1200	450	4.09	8.9	-	644	-	9	-	647	-
50	1200	450	4.09	9.9	-	658	-	9.7	-	652	-
60	1200	450	4.09	10.1	-	677	-	10.1	-	655	-

Table 11.5: Terpene and reference gasoline blends spark ignition engine test operating conditions.

% terpene in reference gasoline (wt/wt)		Engine speed (rpm)	Lambda value (λ) $\pm$ 0.02	Throttle position	Spark timing (CAD BTDC)	IMEP (bar)		Knock frequency	
						Mean	1σ	Mean	1σ
0		1200	1.00	WOT	26	10.48	0.11	3.8	1.44
Geraniol	25.9	1200	1.00	WOT	26	DNC	-	DNC	-
	40.4	1200	1.00	WOT	26	DNC	-	DNC	-
	54.3	1200	1.00	WOT	26	DNC	-	DNC	-
Citronellene	28.8	1200	1.00	WOT	26	10.24	0.04	1.81	0.19
	45.2	1200	1.00	WOT	26	10.47	0.33	1.77	0.16
0		1200	1.00	WOT	30	10.17	-	23.17	-
Linalool	10.7	1200	1.00	WOT	30	10.81	-	1	-
	37.5	1200	1.00	WOT	30	10.4	-	16.67	-
	64.8	1200	1.00	WOT	30	10.49	-	2	-

11.2. Results and discussion

11.2.1. Compression ignition single component fuels

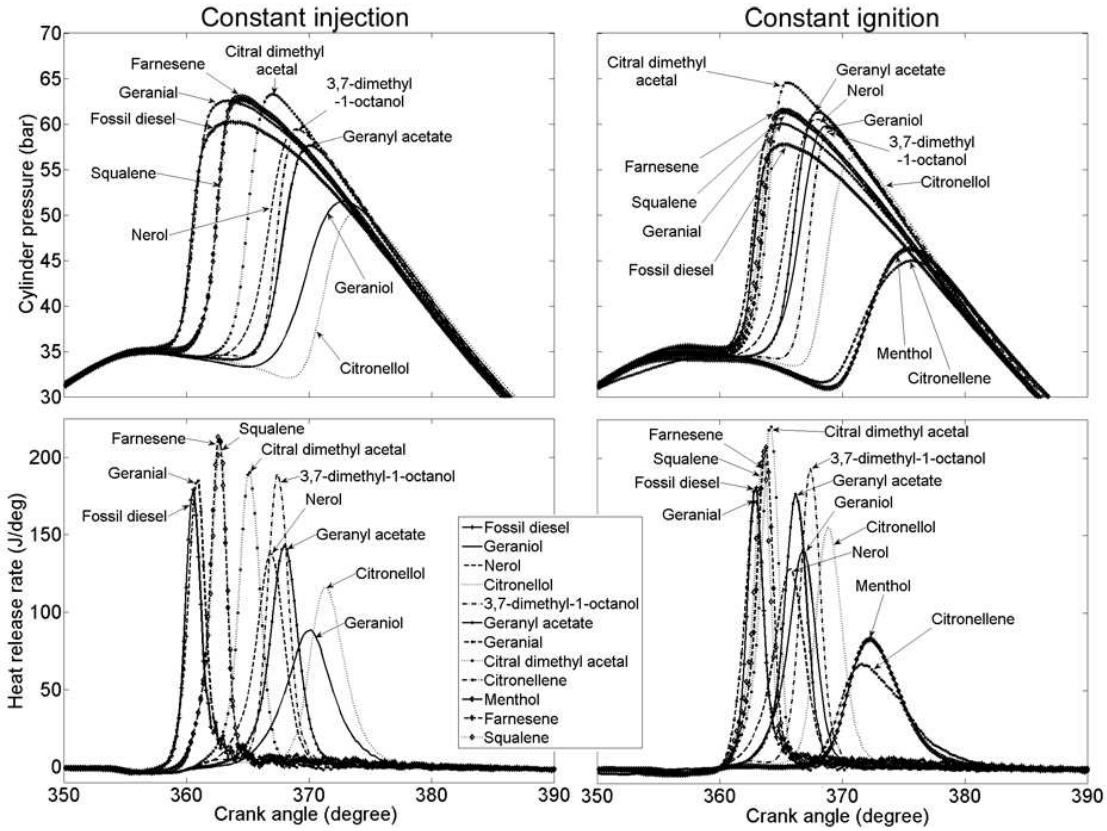

Figure 11.2: In-cylinder pressures and apparent net heat release rates of the terpenes and reference fossil diesel at constant injection and constant ignition timing

Figure 11.2 shows the in-cylinder pressures and apparent net heat release rates of the terpenes and reference fossil diesel at constant injection and constant ignition timing. Linalool could not be induced to combust at either timing condition, while the remaining 11 single component fuels did combust at one or more of the timing conditions. The poor ignition quality of linalool is consistent with a previous study in which 2-decanol was found to exhibit a longer ignition delay than 1-decanol (Schönborn et al., 2007). While the terpenes exhibited a wide range of ignition delays, for all of the fuels (including the reference fossil diesel) the majority of heat release occurred during premixed combustion. Also visible in Figure 11.2 is that several of the fuels exhibited significant cool flame combustion prior to peak heat

release rates occurring. This is most prominent at constant ignition timing where menthol and citronellene in particular show limited heat release at TDC, but the bulk of heat release does not then commence for approximately another seven CAD.

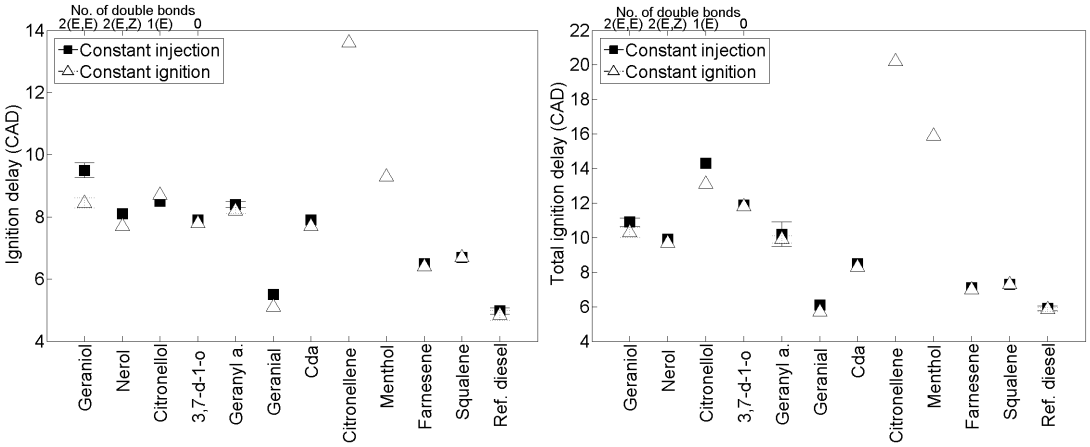

Figure 11.3: (a) Initial ignition delay (SOI to SOC) and (b) total ignition delay (SOI to SOC2) of the terpenes and reference fossil diesel at constant injection and constant ignition timing.

Figures 11.3a and b show the duration of the initial ignition delay period and the total duration of ignition delay of the terpenes and reference fossil diesel at constant injection and constant ignition timing. The values of initial ignition delay presented in Figure 11.3a are defined as the interval between SOI and the first appearance of positive apparent heat release for each fuel (SOC). The values of total ignition delay presented in Figure 11.3b are defined as the interval between SOI and the point at which a second phase of heat release commences (SOC2 as defined in Chapter 4.1.3).

The low temperature reactions of molecules containing alkyl chains are well understood (Westbrook, 2000) and the effects of molecular structure on the rates of radical branching steps are apparent when considering the ignition delays of the terpenes. Geraniol displayed a greater initial ignition delay than the reference fossil diesel (Figure 11.3a), while nerol exhibited a slightly shorter initial ignition delay than geraniol (Figure 11.3a); this higher reactivity of the *cis* isomer is consistent with the results of Chapter 7 and other studies of *cis* and *trans* isomers (Heyne et al., 2009; Murphy et al., 2004; Salooja, 1968). It also suggests that isomerisation across the double bond of nerol in the *cis* arrangement is an important radical

branching step, as it is known that such reactions can only occur with the double bond in the *cis* arrangement (Bounaceur et al., 2009; Salooja, 1968). The significant difference ($\approx$ 1 CAD) in the duration of initial ignition delay of geraniol at the two timing conditions (Figure 11.3a), is greater than for all other molecules tested and suggests a particular sensitivity of the low temperature kinetics of geraniol to in-cylinder conditions.

Reducing the number of double bonds present in the molecular structure, from two in geraniol to one in citronellol and none in 3, 7 dimethyl - 1 - octanol (3,7-d-1-o) , results in a linear decrease in initial ignition delay with increasing saturation at constant injection timing and a reduced ignition delay for only 3,7-d-1-o at constant ignition timing (Figure 11.3a). The effect of increasing ignition quality with higher levels of saturation has observed previously in both straight alkyl chains (Chapter 6) and fatty acid esters (Schönborn et al., 2009b) and correlates with the ability of the molecule to undergo two important stages of low temperature radical branching. Namely, there is an increased availability of easily abstracted and weakly bonded secondary H atoms and there is increased potential of the alkyl chain to undergo internal isomerisation (Westbrook, 2000), via the formation of six and seven member transition state rings (where the chain is formed of at least three saturated carbons (Mehl et al., 2011)). However, when considering the total duration of ignition delay (Figure 11.3b), citronellol and 3,7-d-1-o both possess a longer total duration of ignition delay than geraniol despite a shorter duration of initial ignition delay (Figure 11.3a). This implies that while in the case of citronellol and 3,7-d-1-o sufficient build up of radicals at low temperatures to initiate heat release occurs more quickly than geraniol, a longer 2nd period of ignition delay (SOC to SOC2) is required before a second autoignition event occurs and is able to propagate throughout the cylinder charge. It is tentatively put forward that this may be an effect of the viscosity of the terpenes, which is likely to influence the fuel droplet size and thus the efficiency of fuel and air mixing. In Table 11.1 it can be seen that at the test conditions of 60 °C, geraniol possesses a value of dynamic viscosity of 2.82 mPa.S, citronellol 3.30 mPa.S and 3,7-d-1-o 3.82 mPa.S. Therefore it is suggested that a longer 2nd ignition delay period is required for citronellol and 3,7-d-1-o relative to geraniol as the rates of fuel and air mixing of the former are impeded by a higher fuel viscosity, and thus a critical amount of fuel and air mixture at suitable stoichiometry for ignition to escalate is arrived at more slowly. The longer total ignition delay of citronellol

relative to 3,7-d-1-o (Figure 5b), despite a lower viscosity (Table 11.1), would seem to indicate that if the hypothesis is correct, then the importance of viscosity is no greater than that of the influence of molecular structure (Table 11.2) on low temperature reactivity.

Of the molecules which represent a change to the functional group of geraniol, geranial exhibits an ignition delay closest to that of the reference fossil diesel (with no significant 2^{nd} ignition delay period), while citronellene possessed the longest initial and total ignition delay of any of the fuels tested (Figures 11.3a and b) and could only be induced to combust at constant ignition timing (Figure 11.2). Furthermore, while fuels were considered to have not combusted (DNC) in the case of any misfire cycles, the combustion of citronellene was observed to be highly unsteady during engine tests. The shorter ignition delay of geranial relative to geraniol is consistent with cetane number measurements of the aldehyde octanal, which was found to possess a higher cetane number than the equivalent alcohol, octanol (Murphy et al., 2004). Aldehydes are known intermediates in the low temperature reactions of alcohols (Salooja, 1965) and the high reactivity of such species can be attributed to the relative ease with which peroxy radicals may be formed, with only a single H atom to be abstracted and no addition of O required (Pilling, 1997).

Geranyl acetate (Geranyl a.) and citral dimethyl acetal (Cda) possess a similar initial ignition delay that is shorter than that of geraniol but similar to that possessed by nerol (Figure 11.3a). Geranyl a. also displayed a similar total duration of ignition delay similar to nerol (Figure 11.3b) but that of Cda is slightly shorter. As previously discussed, an effect of viscosity on determining the duration of 2^{nd} ignition delay is possible, with Cda possessing a lower viscosity than both geranyl a. and nerol (Table 11.1). However, nerol possesses a viscosity significantly greater than geranyl a. and displays a similar total ignition delay (Figure 11.3b). The poor ignition quality of citronellene (Figure 11.3a) relative to these molecules and the others of equal carbon number highlights the importance of the oxygenated functional groups relative to the unsaturated and branched alkyl moiety. Cetane number measurements of fully saturated and un-branched alcohols show them to possess approximately the same cetane number as un-branched 1-alkenes of equivalent carbon chain length and lower than that of *n*-alkanes of equivalent carbon chain length (Murphy et al., 2004). Therefore, it could be expected that an alcohol such as geraniol would be of lower ignition quality than the equivalent alkene, citronellene, whereas the opposite is true

(Figures 11.2 and 11.3a). As citronellene possesses both the lowest viscosity (Table 11.1) and longest 2nd ignition delay period (Figure 11.3b) of all the fuels tested, it would seem that any possible influence of fuel viscosity in determining the time of SOC2 is secondary to low temperature reactivity.

Farnesene and squalene were of similar ignition quality to one another and exhibited an initial ignition delay (Figure 11.3a) and also a total duration of ignition delay of farnesene and squalene (Figure 11.3b) only slightly greater than that of the reference fossil diesel and geranial. Citronellene, despite an overall shorter carbon chain length, possess a longest saturated alky chain equal in length to that possessed by the farnesene and squalene. Therefore, the shorter ignition delay of farnesene and squalene relative to citronellene suggests that reactions involving the unsaturated portions of the alkenes are significant low temperature branching routes. The only cyclic molecule tested, l-menthol, could not be induced to combust at constant injection timing (Figure 11.2) and at constant ignition timing exhibited an ignition delay slightly greater than that exhibited by geraniol (Figure 11.3a) and the longest total duration of ignition delay of all molecules except citronellene (Figure 11.3b).

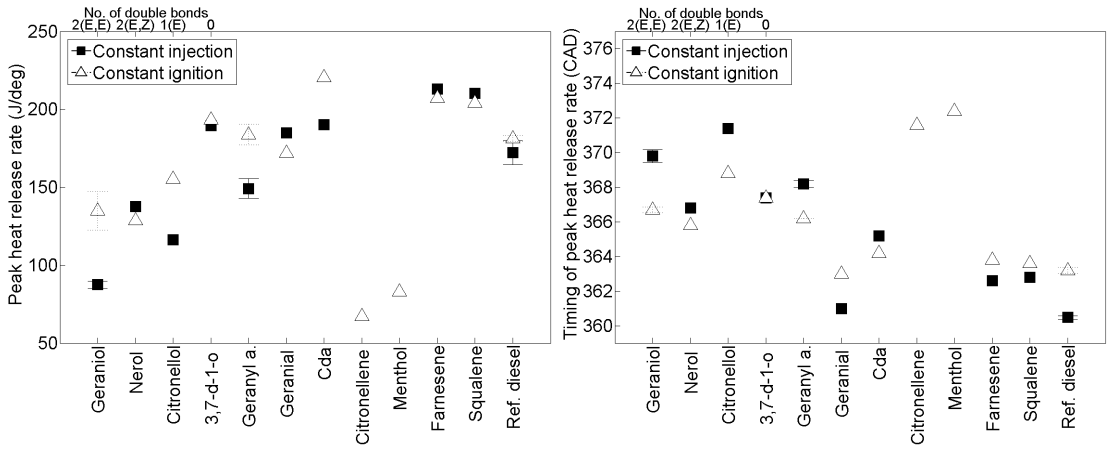

Figure 11.4: (a) Peak apparent heat release rate and (b) time of peak apparent heat release rate of the terpenes and reference fossil diesel at constant injection and constant ignition timing

Figures 11.4a and b show the peak apparent heat release rate and time of peak apparent heat release rate of the terpenes and reference fossil diesel at both timing conditions. For those molecules that exhibited a total ignition delay (Figure 11.3b)

less than 8 CAD, there is a clear trend of increasing peak heat release rate (Figure 11.4b) with increasing duration of total ignition. This can be attributed to the longer duration available for fuel and air mixing prior to SOC2 resulting in more combustible fuel air mixture available at ignition and this higher peak heat release rate. This is consistent with the study of *n*-alkanes and alkenes in Chapter 6 where a very strong correlation between the duration of ignition delay, the extent of the premixed burn fraction and the peak heat release rate was found.

For those molecules which exhibited a longer ignition delay than 8 CAD, the inverse relationship between ignition delay and peak heat release rate becomes apparent; that is, the longer the duration of total ignition delay (Figure 11.3b) and thus the later the time of peak heat release rate (Figure 11.4b), the lower was the magnitude of peak heat release rate (Figure 11.4a). This is especially apparent in the case of citronellene and menthol which display the lowest peak heat release rates (Figure 11.4a) of all the fuels tested despite possessing the longest durations of total ignition delay (Figure 11.3b). It follows that with the time of peak heat release rate (Figure 11.4b) for these molecules occurring later into the expansion stroke, a greater degree of heat transfer to the cylinder walls could be expected and thus result in lower values of apparent heat release rate (where heat transfer has not been accounted for). Similarly, Cda displays a higher peak heat release than those molecules with a longer ignition delay by virtue of a time of peak heat release rate closer to TDC (Figure 11.4b). This effect of cylinder volume at the time of peak heat release rate can also account for the differing peak heat release rates observed for tests conducted at constant ignition timing relative to those conducted at constant injection timing (Figure 11.4a) and is consistent with observations made in Chapters 7, 8 and 9 .

Figures 11.5a and b show the calculated maximum in-cylinder global temperature and the time of occurrence of the terpenes and reference fossil diesel at both timing conditions. It could be expected that those fuels that exhibited the highest peak heat release rates would also show the highest global maximum in-cylinder temperatures. However, such an influence is only visible for those fuels with a total ignition delay (Figure 11.3b) less than 8 CAD, citronellene, menthol and also Cda, which exhibits both the highest peak heat release rate (Figure 11.4a, constant ignition timing only) and maximum in-cylinder temperature (Figure 11.5a). Geraniol, nerol, citronellol, and geranyl a. all show a higher maximum in-cylinder temperat-

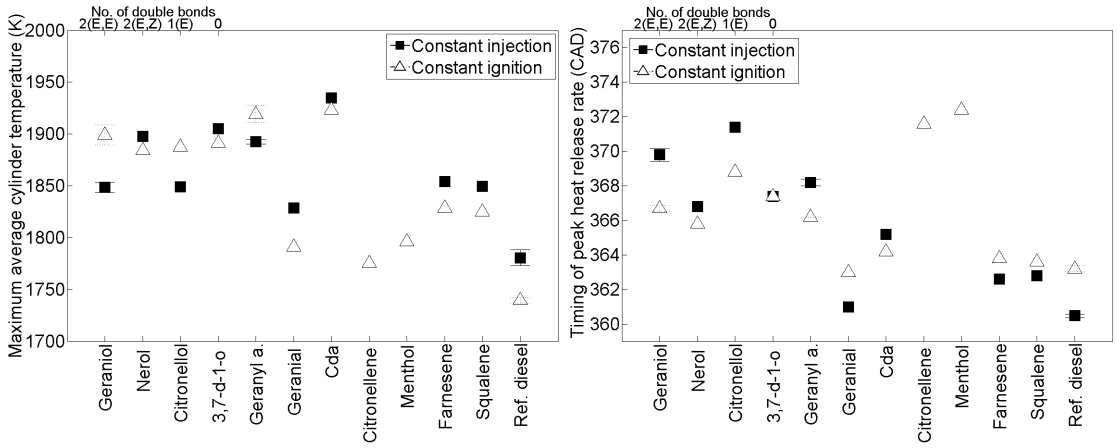

Figure 11.5: (a) Calculated maximum in-cylinder global temperature and (b) time of occurrence of the terpenes and reference fossil diesel at constant injection and constant ignition timing

ure (Figure 11.5a) than geranial, farnesene and squalene despite possessing similar or lower peak heat release rates (Figure 11.3b). Nor does the time of maximum in-cylinder global temperature (Figure 11.5b) mirror the time of peak heat release rate (Figure 11.4b) as closely as might be expected. However, there is a consistent effect of injection timing; at constant injection timing geraniol displayed both a lower peak heat release rate (Figure 6a) and maximum in-cylinder temperature (Figure 11.5a) that occur later into the expansion stroke (Figures 11.4b and 11.5b), than at constant ignition timing. It is suggested that this lack of a clear trend in maximum in-cylinder temperature highlights the sensitivity of in-cylinder thermal conditions to the volume at which they occur, as differences in cylinder volume will be more significant for those fuels which displayed a total ignition delay of less than 8 CAD (Figure 11.3b) where SOC and SOC2 occur further away from TDC.

Figure 11.6 shows the NO_x exhaust levels of the terpenes and reference fossil diesel at both timing conditions. At constant injection timing, all of the fuels except geraniol and citronellol produced higher NO_x emissions than the reference diesel, while at constant ignition timing all of the fuels except citronellene and menthol emitted higher levels of NO_x than the reference diesel (Figure 11.6). The production of NO_x in diesel combustion is known to be highly thermally sensitive (Ban-Weiss et al., 2007), both to the magnitude of the in-cylinder temperature and the residence time

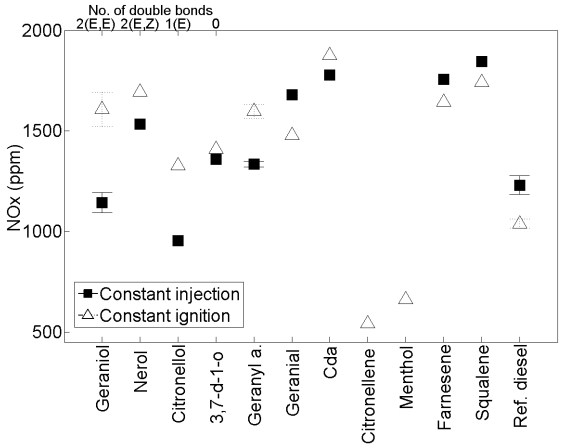

Figure 11.6: Exhaust NO_x emissions of the terpenes and reference fossil diesel at constant injection and constant ignition timing

of the cylinder contents at elevated temperatures (Mueller et al., 2009; Schönborn et al., 2009b; Szybist et al., 2005). An influence of both is apparent in the levels of NO_x emitted, for example the lowest NO_x levels were emitted by citronellene and menthol (Figure 11.6), despite both exhibiting a higher maximum in-cylinder global temperature than the reference fossil diesel (Figure 11.5a). This can therefore most likely be attributed to the timing of the maximum in-cylinder temperature (Figure 11.5b), which is significantly later for both citronellene and menthol, thus resulting in a shorter duration of time at which the cylinder contents are at a sufficiently high temperature for NO_x production. The same two mechanisms appear to also be responsible for the differing levels of NO_x emitted at the two timing conditions for some fuels. For example, geraniol produced significantly higher levels of NO_x at constant ignition timing relative to constant injection timing; the calculated maximum in-cylinder temperature at constant injection timing was lower and occurred later. The importance of peak heat release in determining NO_x emissions is also apparent; both farnesene and squalene emit similar levels of NO_x as citral dimethyl acetal despite a lower maximum in-cylinder temperature (Figure 11.5a) occurring only slightly earlier, but do exhibit a similar peak heat release rate (Figure 11.4a). This is perhaps indicative of the limitations of calculated maximum in-cylinder global temperature in understanding conditions within local combustion zones.

Figures 11.7a and b show the exhaust gas levels of CO and THC of the terpenes and reference fossil diesel at both timing conditions. The highest levels of CO and THC were both emitted by citronellene and menthol (Figures 11.7a and b), which

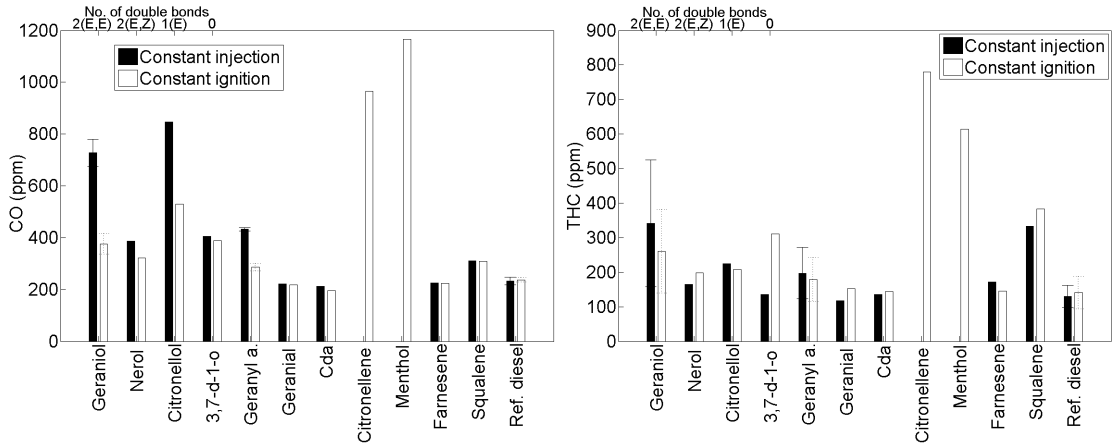

Figure 11.7: (a) CO and (b) THC emissions of the terpenes and reference fossil diesel at constant injection and constant ignition timing

suggests the presence of both fuel rich and fuel lean regions during combustion. Geraniol and citronellol both produced significantly more CO at constant injection timing (Figure 11.7a), at which condition both fuels also exhibited a lower maxium in-cylinder temperature (Figure 11.5a) and thus suggests that lower temperatures resulted in a greater degree of incomplete combustion. At both timing conditions squalene emitted higher levels of THC than farnesene (Figure 11.7b) despite both fuels exhibiting broadly similar combustion characteristics; however, the range of error presented in Figure 11.7b is also significant.

Figures 11.8a and b show the particulate number distribution of the terpenes and reference fossil at both timing conditions. At constant injection timing the most significant peak in nucleation mode particles (Dp $<$ 50 nm) is displayed by the reference fossil diesel (Figure 11.8a) with the terpenes exhibiting considerably smaller peaks in the same size range (1E9 vs 2.7E9). At constant ignition timing the peak in nucleation mode particles displayed by several of the terpenes increased, while that displayed by the reference fossil diesel decreased (Figure 11.8b). Of the oxygenated molecules tested, at both timing conditions, geraniol and nerol displayed the lowest peaks in nucleation mode particles (Figure 11.8a and b).

Considering larger accumulation mode particles (Dp $>$ 50 nm), these were produced in far greater abundance by squalene than any other fuel at both timing conditions (Figures 11.8a and b). Squalene possesses the highest viscosity of all the

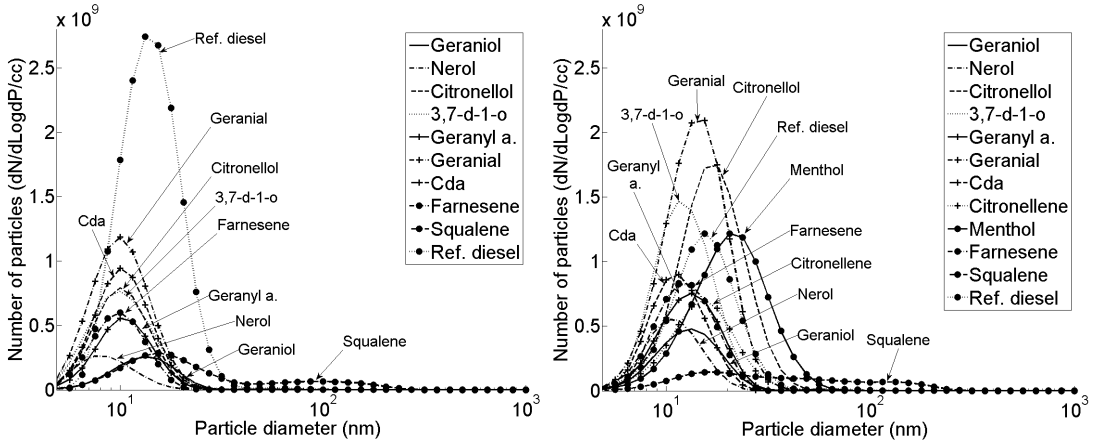

(a) (b)

Figure 11.8: Particulate emissions of the terpenes and reference fossil diesel at (a) constant injection timing and (b) constant ignition timing

fuels tested (Table 11.1) by a considerable margin to the next most viscous, 3,7-d-1-o (6.17 to 3.82 mPa.s) and thus fuel droplets of squalene prior to combustion and during mixing with air are likely to be larger than those of the other fuels. It is suggested that this results in the high production of accumulation mode particles observed by increasing the presence of fuel rich zones (with larger droplet sizes impeding fuel and air mixing) which are conducive to the production of soot (Tree and Svensson, 2007), and may also explain the higher emissions of CO and THC of squalene relative to farnesene (Figures 11.7a and b).

Figure 11.9 shows the total mass of particulates emitted by the terpenes and reference fossil diesel. At both timing conditions, squalene produced a significantly greater total mass of particulates than any of the other fuels tested (Figure 11.9). This can be attributed to the higher number of accumulation mode particles produced by squalene relative to the other fuels (Figures 11.8a and b). After squalene, menthol and citral dimethyl acetal emitted the next highest mass concentrations of soot; this could be expected from the former as cyclic structures are know for a higher propensity to form soot (Ladommatos et al., 1996) but less so the later, the high oxygen content and calculated maximum in-cylinder global temperature of which could both be expected to increase soot oxidation (Tree and Svensson, 2007). All of the other terpenes tested produced an equivalent or lower amount of soot

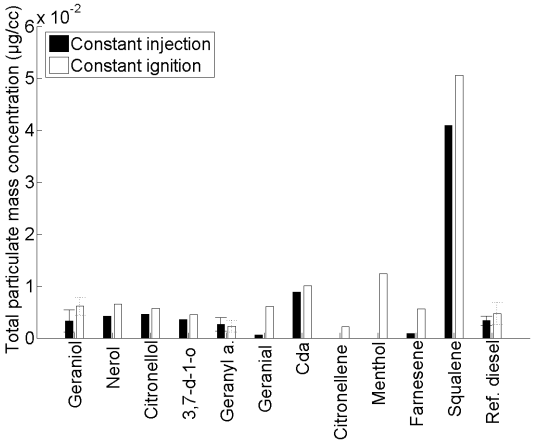

Figure 11.9: Total mass of particulates emitted in the exhaust gas of the terpenes and reference fossil diesel at constant injection and constant ignition timing

than geraniol (Figure 11.9), however the range of error encountered makes further characterization somewhat difficult.

11.2.2. Compression ignition terpene and reference fossil diesel blends

Testing of the terpenes as pure components (Section 11.2.1) revealed geranial and farnesene to be the most promising in terms of both combustion characteristics and production of emissions. Therefore, a further series of experiments was conducted in which both geranial and farnesene were blended with the reference fossil diesel in varying proportions and tested in the engine at less extreme operating conditions (Section 11.1.3). Figures 11.10 and 11.11 show the in-cylinder pressures and apparent hear release rates of both the farnesene and geranial blends with reference fossil diesel at constant injection and constant ignition timing. Both terpenes could not be induced to combust at the experimental conditions (Section 11.1.3 and Table 11.4) at blend levels greater than 60 % with the reference fossil diesel, at either timing conditions. Apparent, from both Figures 11.10 and 11.11, is a reduction in the premixed burn fraction and a more pronounced period of 2$^{\text{nd}}$ ignition delay (with a latter time of peak heat release rate) when either terpene is blended with the reference fossil diesel in concentrations greater than 20 %. It is interesting to note that both geranial and farnesene combusted as single components with a similar, or not significantly longer, ignition delay than the reference fossil diesel under the conditions of elevated fuel and inlet air temperature and higher injection pressure

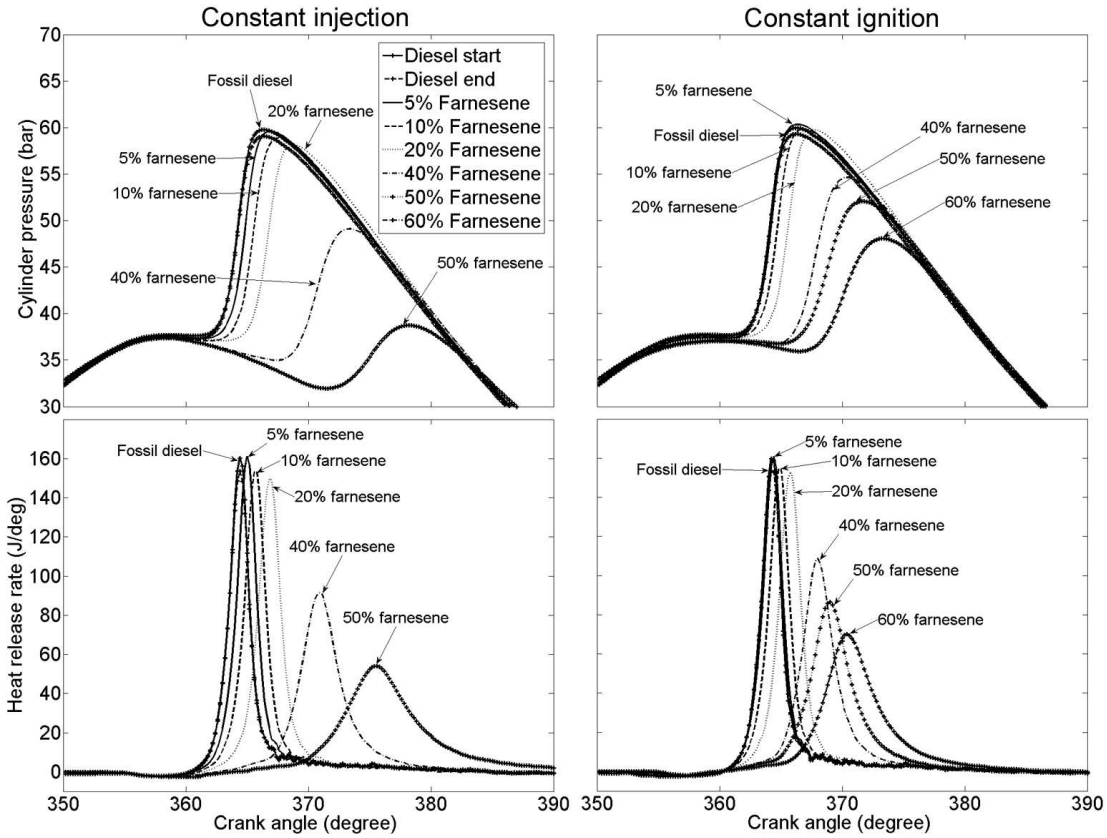

Figure 11.10: In-cylinder pressures and apparent net heat release rates of the farnesene and reference fossil diesel blends at constant injection and constant ignition timing

(Section 11.1.3 and Table 11.3). Geranial and farnesene possess a lower viscosity than the reference fossil diesel at both 20 °C and 60 °C (Table 11.1), so it would seem unlikely that the greater reactivity of the terpenes can be attributed to a change in physical properties and the efficiency of fuel and air mixing. Therefore, it would seem that for pure geranial and farnesene, the extra kinetic and thermal energy provided by the elevated air and fuel temperatures and injection pressure activates radical branching routes that are not available at the lower energy input conditions used in the tests of the terpenes as blends with reference fossil diesel. For the reference fossil diesel, while ignition delay is reduced at the elevated temperature and injection pressure conditions (Tables 11.3 and 11.4) the change in reactivity is much less pronounced.

Figures 11.12a and b show the initial ignition delay (SOI to SOC) and coefficient of variation in ignition delay of the terpene and reference fossil diesel blends at

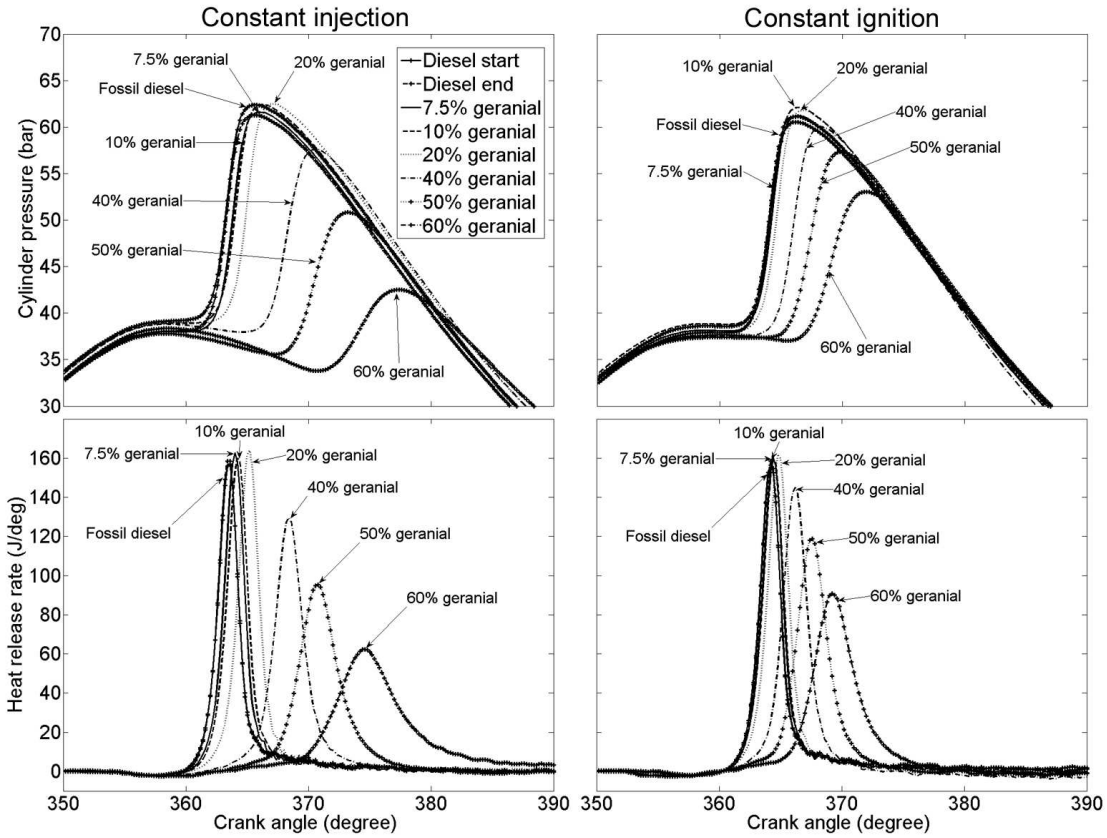

Figure 11.11: In-cylinder pressures and apparent net heat release rates of the geranial and reference fossil diesel blends at constant injection and constant ignition timing

both timings. There is a near linear increase in the initial ignition delay of the blends with the increasing terpene component (Figure 11.12a), while the stability of combustion (as indicated by the coefficient of variation in ignition delay) decreases appreciably for blends of greater than 40 % terpene (Figure 11.12b) and coincides with visibly much longer periods of 2nd ignition delay (Figures 11.10 and 11.11). While at constant ignition timing, the effect of both geranial and farnesene on ignition delay was similar, at constant injection timing the geranial blends with fossil diesel generally had a slightly shorter ignition delay than those comprising of farnesene and the fossil diesel in the same proportions (Figure 11.12a).

Figures 11.13a and b show the peak apparent heat release rate and the calculated maximum in-cylinder global temperature of the terpene and reference fossil diesel blends at both timings. The increase of either terpene in the blend results in both a decrease in the peak heat release rate (Figure 11.13a) and the calculated maximum

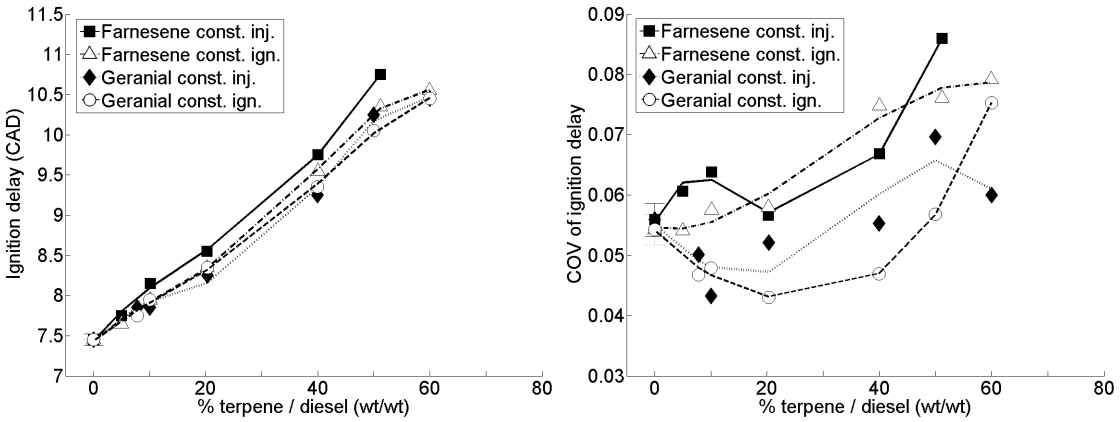

(a) (b)

Figure 11.12: (a) Ignition delay and (b) coefficient of variation in ignition delay of the terpene and reference fossil diesel blends at constant injection and constant ignition timing

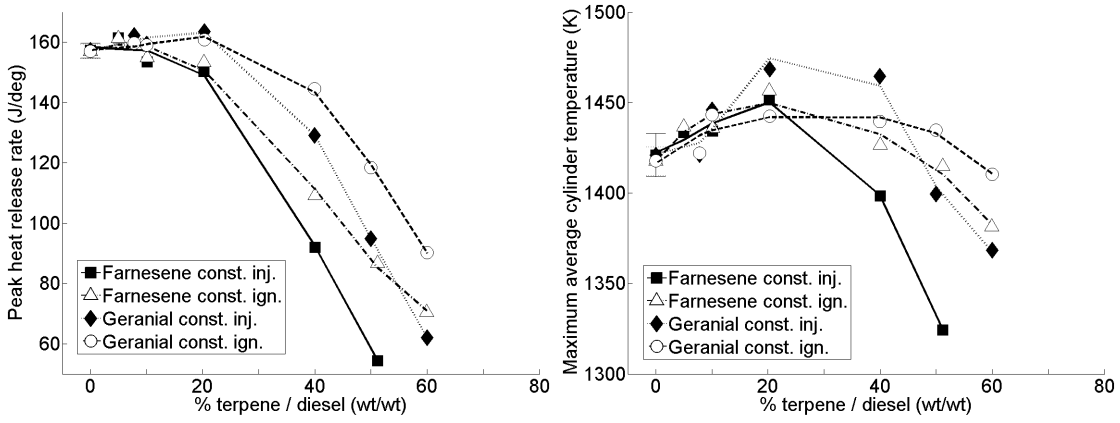

(a) (b)

Figure 11.13: (a) Peak apparent heat release rate and (b) calculated maximum in-cylinder global temperature of the terpene and reference fossil diesel blends at constant injection and constant ignition timing

in-cylinder temperature (Figure 11.13b). Both trends are significant only after the terpene is present at 20 % or greater (Figures 11.13a and b) and the occurrence of peak heat release rate significantly further into the expansion stroke was observed (Figures 11.10 and 11.11). A correlation with ignition delay is readily apparent; blends of farnesene with fossil diesel at constant injection timing, which possessed the

longest relative ignition delays for equivalent terpene content (Figure 11.12a), show the steepest decrease in both peak heat release rate (Figure 11.13a) and maximum in-cylinder global temperature (Figure 11.13b).

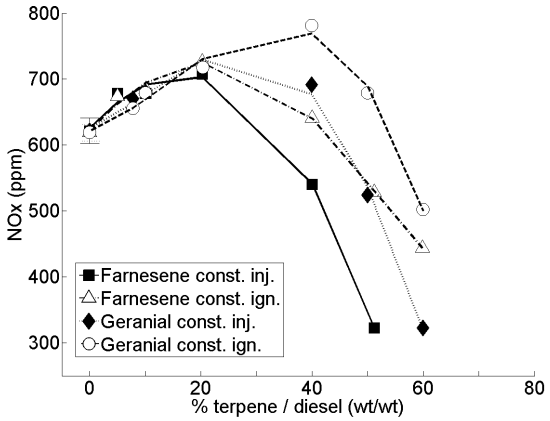

Figure 11.14: NO_x emissions of the terpene and reference fossil diesel blends at constant injection and constant ignition timing

Figure 11.14 shows the exhaust gas levels of NO_x for the terpene and reference fossil blends at both timing conditions. A strong correlation between the levels of NO_x emitted (Figure 11.14) and the magnitude and time of occurrence of maximum in-cylinder temperature reached (Figures 11.13a and b) is readily apparent. Any influence of fuel oxygen content would appear to be secondary to the in-cylinder thermal conditions and is not visible as the increasing availability of oxygen might be expected to result in increasing NO_x emissions with terpene content, whereas the opposite is true.

Figures 11.15a and b show the CO and THC emissions of the terpene and reference fossil diesel blends at both timing conditions. Exhaust gas levels of CO and THC increase with the level of terpene present in the fuel blend, though levels of both are consistently higher at constant injection timing relative to constant ignition timing (Figures 11.15a and b). The farnesene blends produced higher CO emissions (Figure 11.15a) than those of geranial at both timing conditions, but only produced higher emissions of THC in the case of the blend containing 50 % farnesene at constant injection timing. As was observed in the combustion of citronellene and menthol (Figures 11.7a and b), the concurrent emission of high levels of THC and CO indicates the presence of both fuel lean and fuel rich areas within the cylinder charge (Figures 11.15a and b). An influence of in-cylinder thermal conditions via the peak

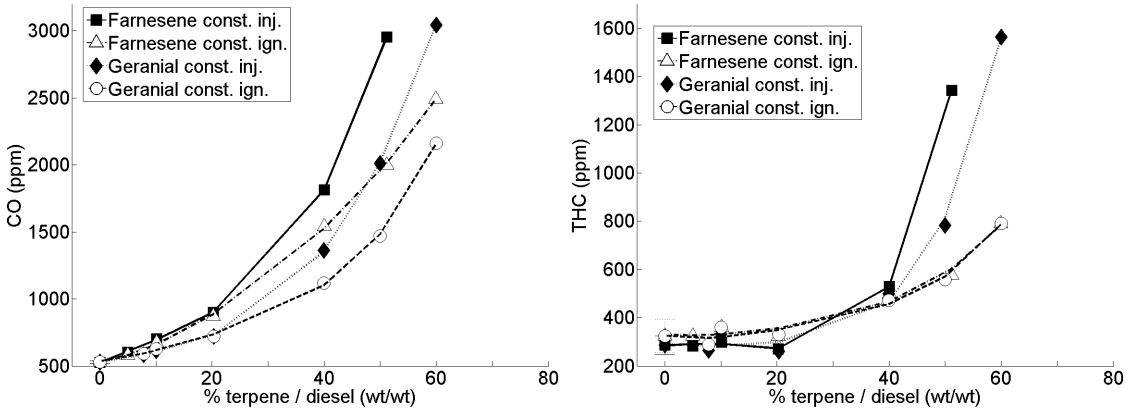

(a) (b)

Figure 11.15: CO (a) and THC (b) emissions of the terpene and reference fossil diesel blends at constant injection and constant ignition timing

heat release rate (Figure 11.13a) is readily apparent in the levels of CO emitted (Figure 11.15a). The blends of farnesene at constant injection timing display the lowest peak heat release rates (Figure 11.13a) and the highest emissions of CO (Figure 11.15a) for a given terpene content, while blends of geranial at constant ignition timing show both the highest peak heat release rates and lowest CO emissions for a given terpene content.

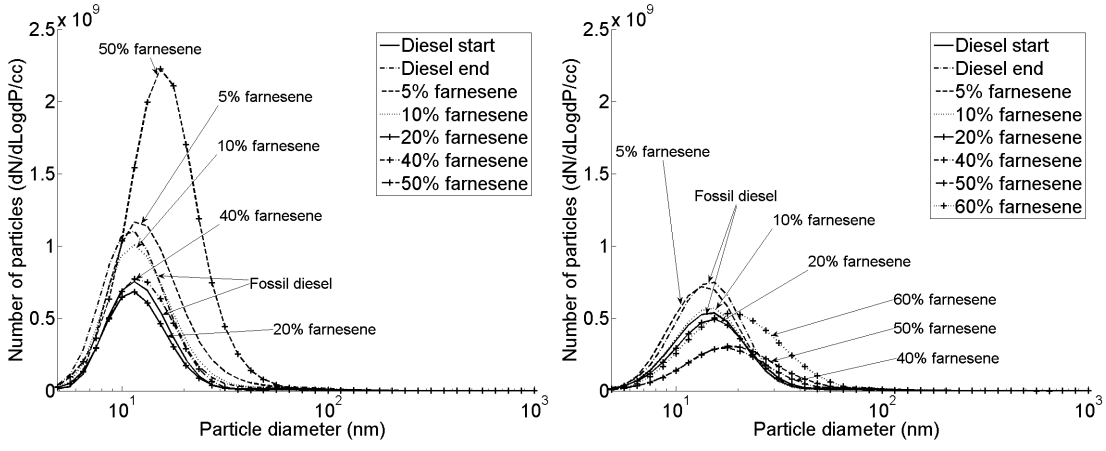

(a) (b)

Figure 11.16: Particulate emissions of farnesene and reference fossil diesel blends at (a) constant injection timing and (b) constant ignition timing

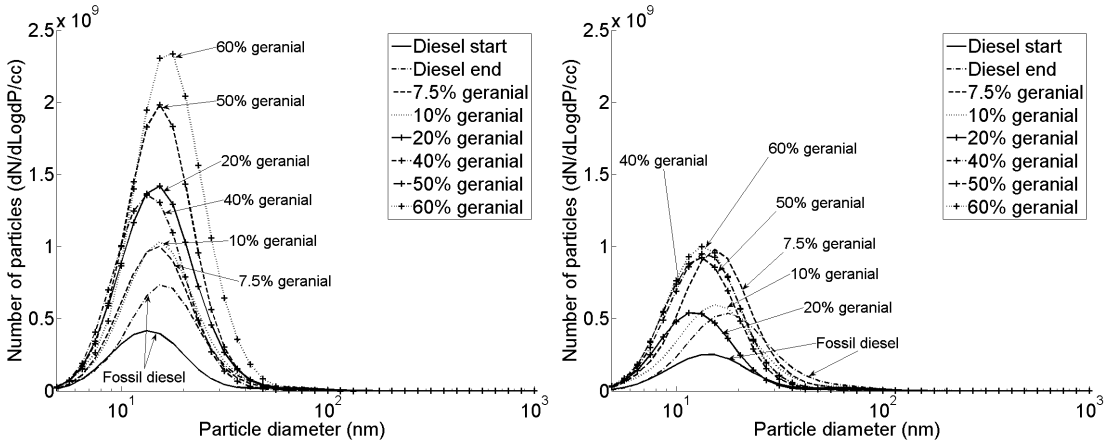

Figure 11.17: Particulate emissions of geranial and reference fossil diesel blends at (a) constant injection timing and (b) constant ignition timing

Figures 11.16a and b, and 11.17a and b, show the particulate emissions of the farnesene and geranial blends with reference fossil diesel at both timing conditions. At constant injection timing, for both blends of farnesene and geranial, the blends with the highest terpene content produced the largest peak in nucleation mode particles (Figures 11.16a and 11.17a). In the case of the geranial blends, there is a suggestion from Figure 11.17a that the peak number of nucleation mode particles produced decreases with the geranial content of the fuel blend. This is not apparent in the case of the farnesene blends (Figure 11.16a). At constant ignition timing (Figures 11.16b and 11.17b), the peak levels of nucleation mode particles produced by the highest terpene content blends are lower relative to the peaks observed at constant injection timing (Figures 11.16a and 11.17a). Furthermore the range of peaks produced is narrowed with the experimental error (as indicated by repeat data of pure fossil diesel) remaining similar. The high levels of THC displayed by those blends with the highest terpene content (Figure 17b), potentially suggest that a portion of the nucleation mode particles measured are in fact droplets of un-burnt fuel.

Figure 11.18 shows the total mass of particulates produced by the terpene and reference fossil diesel blends at both timing conditions. It is not possible to discern any particular influence of the level of terpene present on the production with the range of error present in Figure 11.18. However, it is tentatively suggested that this

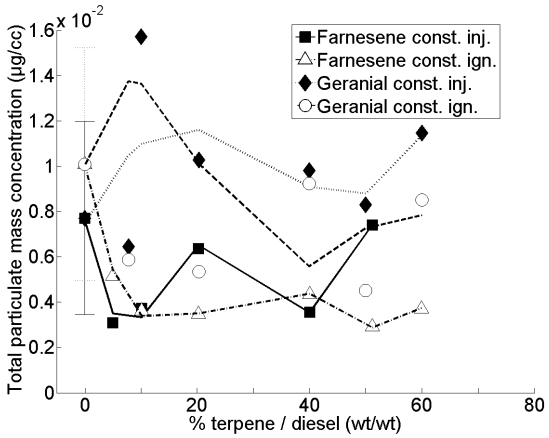

Figure 11.18: Total mass of particulates emitted in the exhaust gas of the terpene and reference fossil diesel blends at constant injection and constant ignition timing

is itself a useful observation as no significant increase in soot production was noted with the highest concentration terpene blends despite lower temperatures (Figure 11.13b) and possible fuel rich conditions (Figure 11.15a) which might normally be considered conducive to the formation of soot particles (Tree and Svensson, 2007).

11.2.3. Spark ignition engine terpene and reference gasoline blends

A further series of experiments was conducted in a spark ignition engine to assess the performance of citronellene and linalool which, by virtue of being exceptionally poor compression ignition fuels, would potentially prove better suited to spark ignition. Geraniol was also to be assessed but found not to be readily soluble with fossil gasoline, and mixtures of both would not remain stable for sufficient periods of time in which to conduct the engine experiments. Citronellene and linalool were, however, found to be soluble and stable in fossil gasoline up to a content of 45 and 65 % (wt/wt) respectively.

Figures 11.19a and b show the average IMEP (mean of 300 cycles) and knock frequency (% cycles) for the terpene and fossil gasoline blends. With the range of error presented, it is difficult to discern a clear effect of adding either terpene on the average IMEP (Figure 11.19a). However, it is of interest to note that in the case of the blend of 45 % citronellene with fossil gasoline the magnitude of this error is significantly larger than that of pure fossil gasoline or the blend of 29 % citronellene, suggestive of less steady combustion. Notwithstanding the extent of

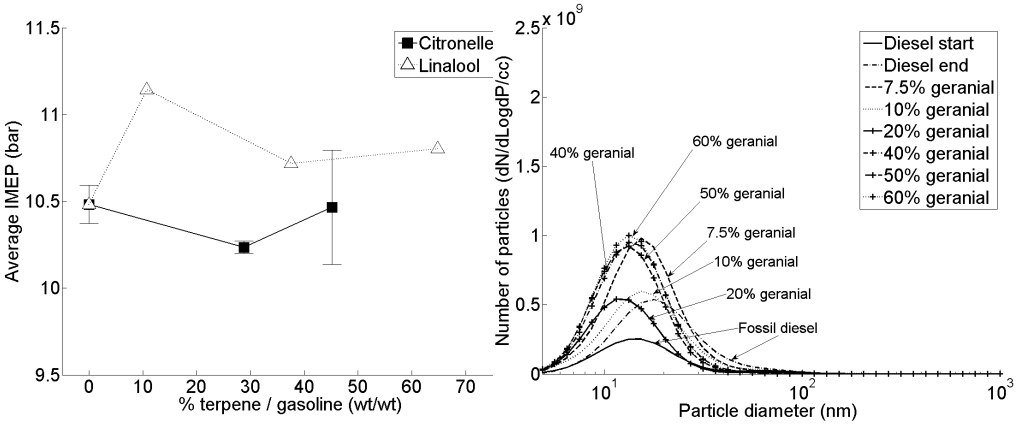

(a) (b)

Figure 11.19: (a) Average IMEP and (b) knock frequency of terpene and fossil gasoline blends

error presented, there is a suggestion that the addition of linalool to fossil gasoline increased IMEP, whereas the addition of citronellene did not (Figure 11.19a). In Figure 11.19b, it can be seen that increasing the level of either terpene in the blend with fossil gasoline reduced the propensity to knock; though a significant level of cycle-to-cycle variation is visible. This is not unexpected; as pure components, both terpenes proved to be poor diesel fuels (Table 11.3 and Figure 11.2) and as such proved themselves resistant to auto-ignition.

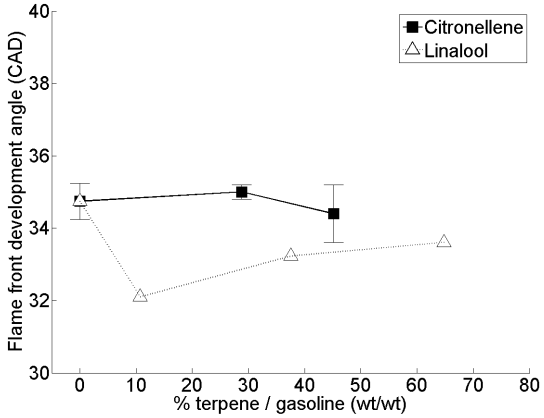

Figure 11.20: Flame front development angles (0 - 10 % mass fraction burnt) of terpene and fossil gasoline blends

Figure 11.20 shows the flame front development angles (0 - 10 % mass fraction burnt) for the terpene and fossil gasoline blends. For all blends the flame front development angle is between 32 - 36 CAD and with all tests conducted at spark timing of 26 CAD BTDC Table 11.5 shows that combustion occured near TDC for all blends. In the case of the citronellene and fossil gasoline blends no significant impact of terpene content of the flame front development angle can be observed, though as when considering the average IMEP (Figure 11.19a) combustion of the mixture containing 29 % citronellene would appear more steady than that containing 45 % citronellene as indicated by the size of the respective error bars (Figure 11.20). Addition of linalool to gasoline would appear to decrease the flame front development angle (Figure 11.20), most severely for the blend containing 10 % linalool and progressively less so as the linalool content is increased to 65 %. This mirrors the trend apparent in IMEP (Figure 11.19a) in which the blend containing 10 % linalool displayed the highest IMEP of all blends tested.

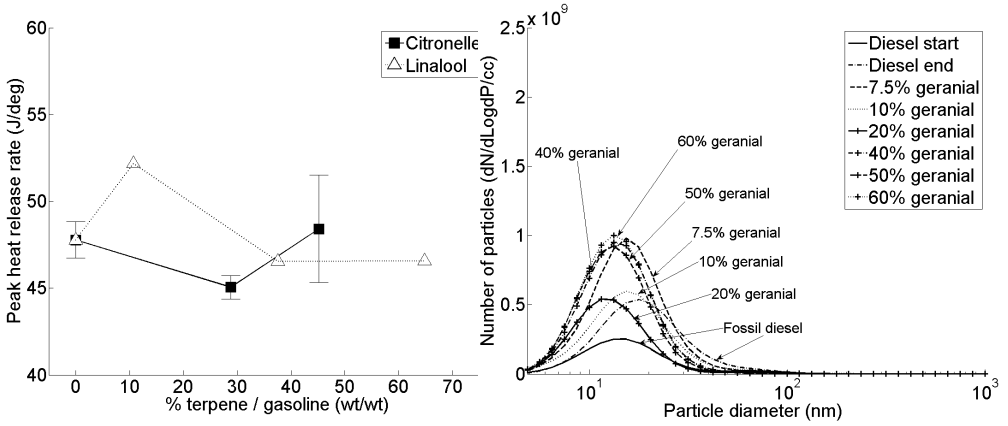

(a) (b)

Figure 11.21: (a) Peak apparent heat release rate and (b) time of occurrence peak apparent heat release rate of terpene and fossil gasoline blends

Figures 11.21a and b shows the peak heat release rate and time of occurrence for the terpene and fossil gasoline blends. Peak heat release rates (Figure 11.21a) show a correlation with average IMEP (Figure 11.19a), which is to be expected when combustion of all blends is occurring near TDC and at similar cylinder volumes. The timing of peak heat release rate (Figure 11.21b) correlates well the flame front development angle (Figure 11.20) and suggests that combustion of all the terpene and fossil gasoline blends commences at a similar rate once the flame front has

propagated throughout the cylinder charge. It is difficult to discern a clear effect of increasing the content of citronellene on either peak heat release rate (Figure 11.21a) or the time at which it occurs (Figure 11.21b), however, the relative size of the error bars presented again indicates the combustion of the mixture containing 45 % citronellene to be somewhat less steady than that containing 29 % of the same terpene. Addition of 10 % linalool to the reference fossil gasoline would appear to increase combustion rates, with both a higher peak heat release rate (Figure 11.21a) than pure fossil gasoline and earlier time of occurrence (Figure 11.21b). However, further addition of linalool results in no significant net change in either peak heat release or its timing relative to pure fossil gasoline. The higher peak heat release rate of the 10 % linalool blend (Figure 11.21a) is in agreement with the observed higher IMEP of the same blends (Figure 11.19a), and is suggestive of a non-linear effect on combustion of increasing the level of linalool present; however, the absence of error bars for this mixture should be noted.

11.3. Conclusions

1. Geraniol is a poor compression ignition fuel due to a long ignition delay. Of the changes that could be made to the molecular structure to improve the combustion and emission characteristics of the molecule, most beneficial was removal of a single H atom from the alcohol moiety of geraniol to form the aldehyde, geranial. Complete removal of the alcohol moiety and increasing the length of the alkenyl moiety, while maintaining a constant level of carbon branching and unsaturation, to form farnesene and squalene, also resulted in a molecule of higher ignition quality.

2. Increasing the saturation of the alkenyl moiety of geraniol, and changing the configuration of a double bond in the alkyl moiety from *trans* to *cis*, suggested that the initial ignition delay of the terpenes when tested as single component fuels is dictated by the well understood low temperature reactions of alkyl and alkenyl radicals. However, a large influence of the various oxygenated functional groups of the terpenes on the reactivity of the alkenyl moiety was also apparent as the terpene that resembled solely the alkenyl moiety of geraniol, citronellene, exhibited the longest ignition delay of all the terpenes tested.

3. As single component fuels, the emissions characteristics of the terpenes are primarily driven by the duration of ignition delay and combustion phasing. However, in the case of squalene, a significantly higher viscosity than the other terpenes resulted in much higher emissions of particulate mass. This indicates an influence of fuel viscosity on the efficiency of fuel and air mixing via the fuel droplet size.

4. Blended with fossil diesel fuel, geranial and farnesene had no significant impact on combustion phasing up to a terpene content of 20 %. At higher levels, the presence of either terpene resulted in a significantly longer duration of ignition delay and at a level of 60 % terpene neither terpene and fossil diesel blend would combust. This suggests that the higher energy input experimental conditions employed in the tests of the terpenes as single fuel components activated low temperature radical branching routes not viable at the lower energy input experimental conditions employed when blending the geranial and farnesene with fossil diesel.

5. Geraniol was found not to be soluble with fossil gasoline. Citronellene and linalool, which were both found to be very poor compression ignition fuels, did however mix well with gasoline and blends of up to 45 and 65 % respectively were found to combust in a steady manner in a spark ignition engine.

12. The influence of natural vegetable oil composition

In the early 1980's, concern as to the security of supply of fossil fuels saw the use of vegetable oils as a replacement investigated, especially in the context of agricultural usage (Cruz et al., 1981; Pryde, 1983), and the current chapter re-assesses the use of non-transesterified oils in the context of modern combustion technology. While the structure of the fatty acids that make up the triglycerides, and the level of each triglyceride species present, varies from oil to oil, it is the long alkyl chain present in the fatty acids that make the oils suitable for compression ignition combustion. However, the use of vegetable oils was found to compromise the durability of compression ignition engines, in particular by increased injector nozzle coking, piston ring sticking and dilution of the engine lubrication oil (Pryde, 1983; Ryan et al., 1984).

Ryan et al. (1984) studied the combustion of several vegetable oils, at various stages of refinement, in a heated and pressurised constant volume chamber and also in direct and indirect compression ignition engines. All of the oils were heated from 40 to 145 °C so as to reduce the viscosity of oils to a level similar to that of a reference fossil diesel. It was expected that reducing fuel viscosity would increase fuel atomization on injection, and also decrease the penetration rate of the spray (rate of spray tip travel from the injector nozzle) with a concurrent increase in the cone angle of the spray. However, heating of the oils, while reducing viscosity, actually increased the penetration rate and decreased the cone angle. In combustion tests, the direct injection engine was found to both suffer more of the durability issues relative to the indirect injection engine and a greater sensitivity to the composition of the vegetable oils.

Transesterification of vegetables oils to fatty acid esters was found to diminish many of the durability issues encountered in the use of vegetables oils (Graboski and McCormick, 1998; Harrington, 1986). Nevertheless, use of straight vegetable oils, neat and blended with fossil diesel, has persisted (Altin et al., 2001b; Basinger et al., 2010; Karaosmanoglu et al., 2000; Laza and Bereczky, 2011; Nwafor, 2004; Nwafor and Rice, 1996; Rakopoulos et al., 2010, 2011; Valente et al., 2010; Wang et al., 2006). There have been several reviews (Misra and Murthy, 2010; Ramadhas et al., 2004; Sidibq et al., 2010) on the use of vegetable oils, which have repeatedly highlighted

the dependence of engine durability, combustion phasing and emissions production on fuel temperature and the subsequent physical properties of the vegetable oil. Recently, there have been several studies which have sought to characterise the effect of heating on straight vegetable oils (Esteban et al., 2012a). Franco and Nguyen (2011) measured the dynamic viscosity of six vegetable oils, and found that at all temperatures (20 to 80 °C) the viscosity decreased with a decreasing degree of saturation of the fatty acid alkyl chains. The same observation was made by Santos et al. (2005) who found a better correlation between viscosity and the level of alkyl chains containing more than two double bonds (polyunsaturates) than those containing only one double bond.

Deshmukh et al. (2012) undertook optical spray characterisation of two vegetable oils of differing viscosity (pongamia and jatropha), utilising a single hole solenoid valve injector at an injection pressure of 1600 bar. For the spray characterisation, both oils were heated to 60 °C, and at a lower temperature of 40 °C, the pongamia and jatropha oils had exhibited dynamic viscosities of 37 and 30 mPa.s respectively. Measurement of the injection delay was made (defined as the interval between commencement of injector actuating signal and the first appearance of fuel at the injector tip) and found to be of longer duration for the oil of higher viscosity (pongamia). Furthermore, the more viscous oil exhibited greater injection to injection variability in the duration of injection delay. This was attributed to the greater degree of resistance presented by the more viscous oil to the opening of the injector needle. Pongamia oil also exhibited a lower penetration rate relative to the less viscous jatropha oil, and it was suggested that the higher viscosity of the former reduced the momentum of the spray during injection.

Pinzi et al. (2011) investigated the effect of vegetable oil fatty acid composition on the physical properties of the fatty acid methyl esters of the same vegetable oil. They found that the lower heating value, cetane number and kinematic viscosity of the fatty acid esters increased with the carbon chain length of the vegetable oil fatty acid alkyl chain and decreased with decreasing saturation. While the alkyl carbon chain length influenced most the lower heating value of the fatty acid esters, cetane number was most affected by the degree of saturation. Mehta and Anand (2009) investigated the effect of fatty acid composition on vegetable oil lower heating value, and found a similar influence of alkyl chain carbon length and degree of saturation

on lower heating value, with an increase in both properties raising the lower heating value of the vegetable oil.

This chapter presents results of combustion experiments with five edible vegetable oils, and one non-edible from micro-algae, in a single cylinder direct injection compression ignition engine. Combustion characteristics and emission levels are compared to a reference fossil diesel and the influence of the vegetable oil chemical and physical properties investigated.

12.1. Experimental method

12.1.1. Apparatus

All of the combustion experiments described in the present chapter were performed using the compression ignition engine described and ultra low volume fuel system described in Chapter 3.

12.1.2. Fuel molecules investigated

Seven neat vegetable oils were tested so as to investigate the effect of natural oil fatty acid composition on compression ignition combustion and emissions: sunflower, soya, rapeseed, palm, groundnut, corn and algal. All of the vegetable oils were obtained as commercially available edible oils, except the algal oil which was produced and harvested from the micro-algae species *Chlorella protothecoides*.

A reference fossil diesel with zero FAME content was also tested. The fatty acid composition of each oil is presented in Table 12.1, the fatty acid molecular structures are shown in Table 12.2 and the physical properties of each fuel are given in Table 12.3.

12.1.3. Experimental conditions

Each of the six vegetable oils and reference diesel were tested at the two experimental conditions of constant injection and constant ignition timing, as defined in Chapter 5.

For all engine tests, fuels were first heated in a PID controlled water bath held at 60 °C prior to filling of the low volume fuel system which had been preheated to 60 ± 2 °C and was held at this temperature throughout the subsequent experiment.

Table 12.1: Vegetable oil fatty acid composition (Bannister et al., 2011)

Source oil	Fatty acid							
	C8:0 - C14:0	C16:0 (*palmitic*)	C16:1 (*palmit-oleic*)	C18:0 (*stearic*)	C18:1 (*oleic*)	C18:2 (*linoleic*)	C18:3 (*linolenic*)	Other
Algal†	0	51.0	0	2.0	39.0	7.0	0	1.0
Corn	0 - 0.6	8.6 - 16.5	0 - 0.4	1 - 3.3	20 - 42.2	39.4 - 62.5	0.5 - 1.5	0.5 - 2.1
Groundnut	0	6 - 14	0	2 - 6	36.4 - 67.1	13 - 43	0	0
Palm	0 - 2	40 - 47	0 - 0.6	3 - 6	36 - 44	6 - 12	0 - 0.5	0 - 0.1
Rapeseed	0 - 0.2	3.3 - 6.0	0 - 3.0	4 - 6	52 - 65	18 - 25	10 - 11	0 - 7.4
Soybean	0 - 0.2	8 - 13.3	0 - 0.2	3 - 5	18 - 26	49 - 57	6 - 9	0.3 - 2.4
Sunflower	0 - 0.3	5.6 - 7.6	0 - 0.3	3 - 6	14 - 40	48 - 74	0 - 0.2	0 - 2.4

† = experimental data courtesy of T. Yusaf.

All tests were conducted at an engine speed of 1200 rpm and at 450 bar fuel injection pressure. The injection duration was adjusted in the case of every fuel so that the engine IMEP was always constant at 4.00 bar for all fuels. A summary of the engine and test operating conditions is given in Table 12.4.

Table 12.2: Fatty acid molecular structure

C16:0 (*palmitic*)	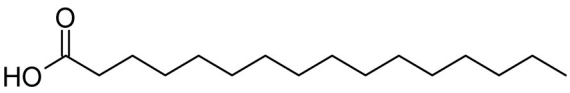
C16:1 (*palmitoleic*)	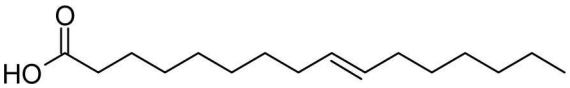
C18:0 (*stearic*)	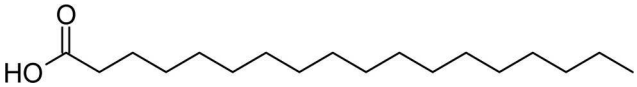
C18:1 (*oleic*)	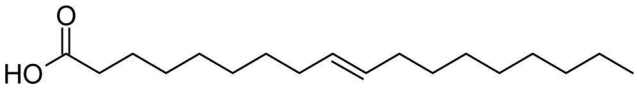
C18:2 (*linoleic*)	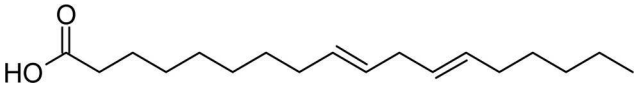
C18:3 (*linolenic*)	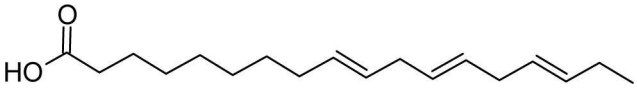

Table 12.3: Vegetable oil and reference diesel physical properties

Fuel	Flash point (°C)[1]	Cetane number[1]	Density at 20 °C (kg/m^3)[2]	Dynamic viscosity at 19.7 °C (mPa.s)	Dynamic viscosity at 59.7 °C (mPa.s)	Lower heating value (MJ/Kg)[1]	Surface tension (mN/m) at 60 °C
Reference fossil diesel	66.5‡	51.7	834.5$^{\diamond}$	3.41	1.72	43.14†	-
Algal	220$^{\bullet}$	-	912.0$^{\bullet}$*	79.87	18.7	35.8$^{\bullet}$	21.04$^{\square}$
Corn	277	37.6	916.7	66.57	16.7	39.5	30
Groundnut	271	41.8	902.6[1]	86.7	19.87	39.8	-
Palm	330.0[4]	42.0[5]	910[6]	87.67	19.4	36.54[5]	30.7
Rapeseed	246	37.6	914.5	73.97	18	39.7	28
Soybean	254	37.9	918.5	71.9	17.6	39.6	30.7
Sunflower	274	37.1	916.9	69.5	17.2	39.6	30.5

‡ = experimental data obtained according to EN ISO 2719, $^{\diamond}$ = experimental data obtained according to ASTM D4052 at 15 °C, † = calculated from experimental data obtained by the IP12 method (Institute of Petroleum, 2001), $^{\bullet}$ = experimental data courtesy of T. Yusaf, * = data obtained at 25 °C and $^{\square}$ = data obtained at 26.8 °C. Values of viscosity were measured at temperatures of 19.7 °C and 59.7 °C using a stand-alone rheometer (Brookfield LVDV - III +U), [1] = data from Barnwal and Sharma (2005), [2] = data from Esteban et al. (2012b), [3] = data from Esteban et al. (2012a), [4] = data from Suwarno et al. (2003), [5] = data from de Almeida et al. (2002) and [6] = data from Abollq et al. (2009).

Table 12.4: Vegetable oil engine and test operating conditions

Fuel	Engine speed (rpm)	Fuel injection pressure (bar)	IMEP (bar)	Constant injection timing (SOI at 7.5 CAD BTDC)						Constant ignition timing (SOC at TDC)					
				Ignition delay (CAD)		Injection duration (µs)		Indicated thermal efficiency (%)		Ignition delay (CAD)		Injection duration (µs)		Indicated thermal efficiency (%)	
				Mean	1σ	Mean	1σ	Mean	1σ	Mean	1σ	Mean	1σ	Mean	1σ
Ref. fossil diesel	1200	450	4	7.2	0.2	602	5	42.97	0.4	7.1	0.1	604	4	42.81	0.43
Algal	1200	450	4	6.9	-	737	-	41.1	0	6.8	-	743	-	40.21	-
Corn	1200	450	4	7.7	-	752	-	37.07	0	7.5	-	754	-	36.88	-
Groundnut	1200	450	4	7.1	-	746	-	36.5	0	7.1	-	743	-	36.28	-
Palm	1200	450	4	6.9	-	747	-	39.94	0	6.8	-	747	-	39.44	-
Rapeseed	1200	450	4	7.7	0	764	12	36.87	0.3	7.7	0.1	759	8	36.59	0.26
Soybean	1200	450	4	7.7	0.4	760	13	37.21	0.43	7.6	0.3	761	14	36.92	0.15
Sunflower	1200	450	4	7.5	0.4	756	20	37.27	0.45	7.6	0.5	750	18	36.53	0.35

12.2. Results and discussion

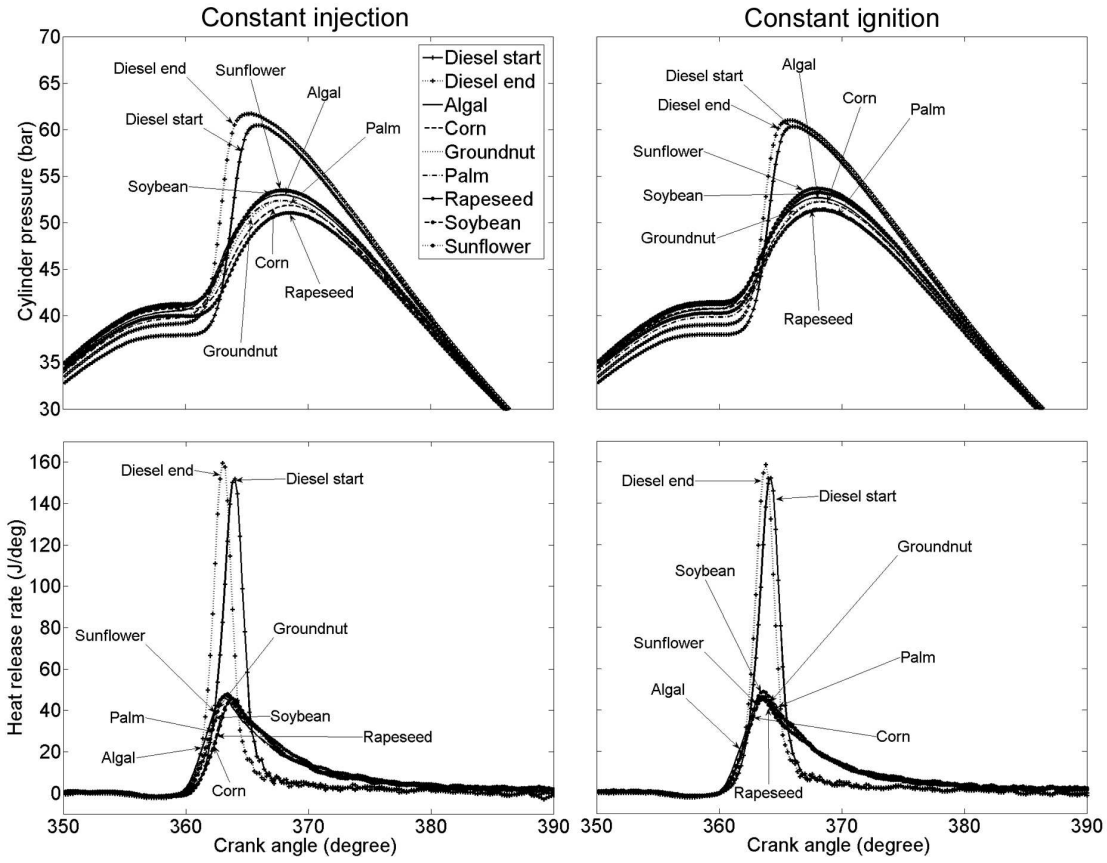

Figure 12.1: In-cylinder pressures and apparent net heat release rates of the vegetable oils and reference fossil diesel at constant injection and constant ignition timing

Figure 12.1 shows the in-cylinder pressures and apparent net heat release rates of the vegetable oils and reference fossil diesel at constant injection and constant ignition timing. Apparent at both timing conditions, is the significantly higher peak in-cylinder pressures and heat release rate of the reference fossil diesel relative to the oils (Figure 12.1). Furthermore, it can be seen that in the case of the reference fossil diesel the majority of heat release occurs during premixed combustion, whereas all of the oils show a more pronounced period of diffusion controlled combustion (Figure 12.1). Also apparent in Figure 12.1, is a variation between all fuels in the in-cylinder pressure prior to SOC. The offset between diesel start and diesel end suggests that the variation in in-cylinder pressure is not attributable to fuel vaporisation after SOI, and has not been observed in previous tests with different fuels (Chapters 6 to

11). Therefore, it is hypothesised that injection and combustion of the oils resulted in a change to the effective compression ratio of the engine, possibly by reduction of blowby due to fuel wall-wetting and formation of fuel deposits on the piston rings, as been observed in other engine tests with straight vegetable oils (Pryde, 1983; Ryan et al., 1984).

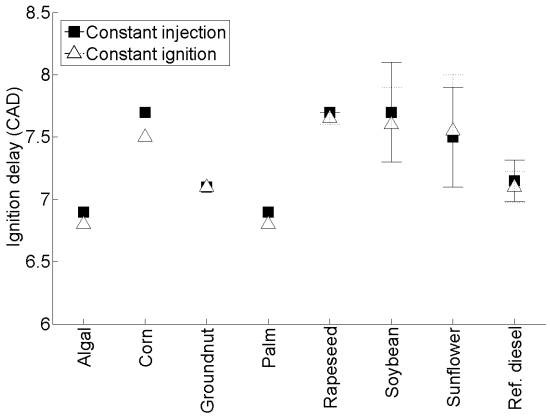

Figure 12.2: Ignition delay (SOI to SOC) of the vegetable oils and reference fossil diesel at constant injection and constant ignition timing

Figure 12.2 shows the duration of ignition delay of the vegetable oils and reference fossil diesel at both constant injection and constant ignition timings. Notwithstanding the extent of the error bars present in Figure 12.2, at both timing conditions, three of the vegetable oils, algal, groundnut and palm, displayed an ignition delay slightly shorter ($\approx$ 0.2 CAD) than the reference fossil diesel. The remaining four vegetable oils, corn, rapeseed, soybean and sunflower, exhibited a longer ignition delay ($\approx$ 0.5 CAD) than the reference fossil diesel at both timing conditions. All of the vegetable oils (except the algal oil for which comparable values are not available) possess a lower cetane number than the reference fossil diesel (Table 12.3) so it might have been expected that all of the vegetable oils would have displayed a longer ignition delay than the reference fossil diesel. However, considering only the vegetable oils, the two oils of highest cetane number (Table 12.3), groundnut and palm, both display a shorter ignition delay (Figure 12.2) than all the oils (other than the algal oil for which no cetane number is available).

Figures 12.3a and b show the peak apparent net heat release rate of the vegetable oils and reference fossil diesel at constant injection and constant ignition timing. In Figure 12.3a, it can be seen that at both timing conditions the reference fossil diesel

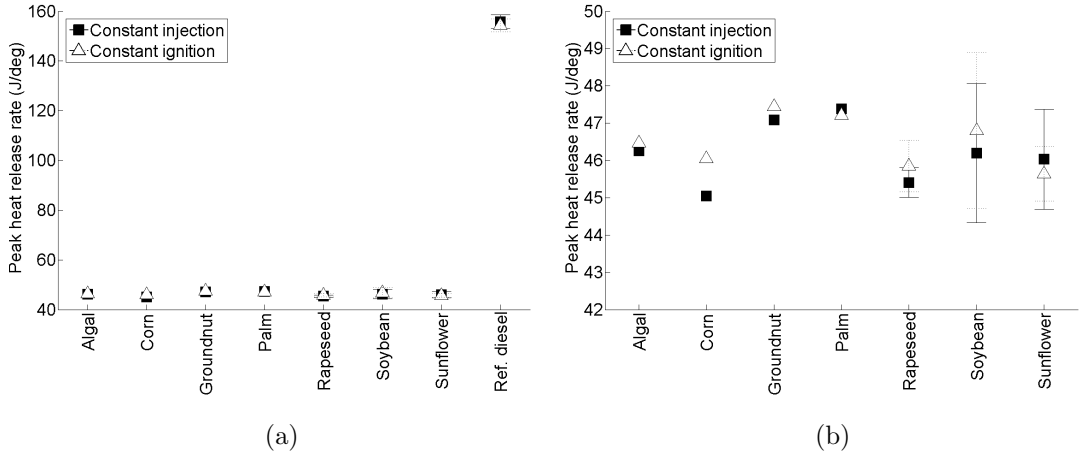

Figure 12.3: Peak apparent heat release rate of (a) the vegetable oils and reference fossil diesel, and (b) the vegetable oils only, at constant injection and constant ignition timing

exhibits a significantly higher peak heat release rate than any of the vegetable oils. In Chapter 6, where single component alkane and alkene fuels were considered, a strong correlation was found between the duration of ignition delay and the peak heat release rate. It was observed that an increasing duration of ignition delay allowed more time for fuel and air mixing prior to SOC, resulting in a larger premixed combustion fraction and a higher peak heat release rate. No such relationship is visible when considering the peak heat release rate of the vegetable oils relative to the reference fossil diesel (Figure 12.3a), with the latter displaying a duration of ignition delay (Figure 12.2) within the range of those exhibited by the vegetable oils. In Figure 12.3b, notwithstanding the extent of the error bars present, considering the peak heat release rates of the vegetable oils relative to one another, no clear relationship between duration of ignition delay (Figure 12.2) and the peak heat release rates can be seen (Figure 12.3b). This, and the much higher peak heat release rates of the reference fossil diesel relative to the vegetable oils (Figure 12.3a), would suggest that in the case of the vegetable oils, duration of ignition delay is not the limiting factor on the rate of fuel and air mixing. Therefore, the influence of vegetable oil physical properties, such as boiling point and viscosity, on combustion phasing is explored in Section 12.2.1.

Figures 12.4a and b show the calculated maximum in-cylinder global temperature and time of occurrence of the vegetable oils and reference fossil diesel at constant

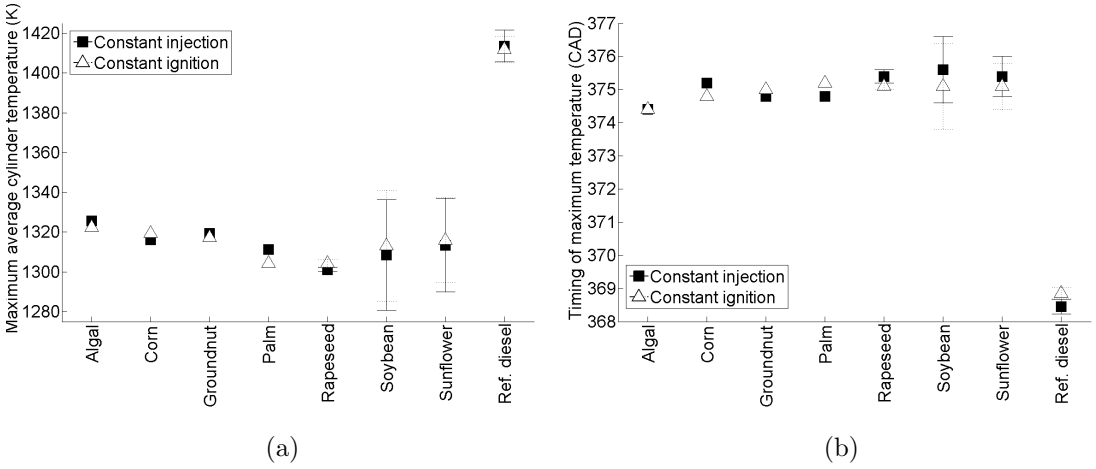

Figure 12.4: (a) Calculated maximum in-cylinder global temperature and (b) time of occurrence of maximum global temperature of the vegetable oils and reference fossil diesel at constant injection and constant ignition timing

injection and constant ignition timing. At both timing conditions, it can be seen that the reference fossil diesel exhibited a significantly higher maximum in-cylinder global temperature than all of the vegetable oils (Figure 12.4a). This correlates with the higher peak heat release rate of the reference fossil diesel relative to the vegetable oils (Figure 12.3a), and it follows that a more concentrated release of energy near TDC (Figure 12.1), with lower levels of heat transfer to the cylinder walls, would result in a higher magnitude of maximum in-cylinder temperature (Figure 12.4a). Considering the magnitude of maximum in-cylinder temperature of the vegetable oils relative to one another (Figure 12.4a), an effect of peak heat release is not readily apparent (Figure 12.3b).

In Figure 12.4b, it can be seen that at both timing conditions, the reference fossil diesel reached the maximum in-cylinder temperature earlier than all of the vegetable oils. This can be attributed to the lower heat release rates of the vegetables oils (Figure 12.3a), and a greater proportion of energy release during the diffusion controlled combustion phase (Figure 12.1).

Figures 12.5a and b show the NO_x emissions of the vegetable oils and reference fossil diesel at constant injection and constant ignition timing. At both timing conditions, it can be seen that the reference fossil diesel emitted significantly higher levels of NO_x than all of the vegetable oils (Figure 12.5a). Production of NO_x in compression ignition engines is primarily by the thermal oxidation of nitrogen, the

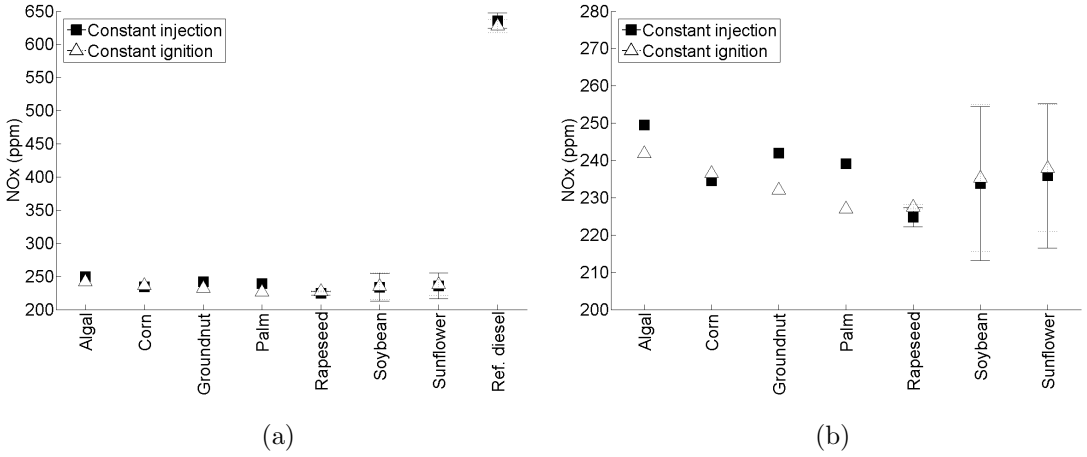

Figure 12.5: NO_x emissions of (a) the vegetable oils and reference fossil diesel, and (b) the vegetable oils only, at constant injection and constant ignition timing

reaction rate of which increases with increasing in-cylinder temperatures and the residence time of the cylinder contents at elevated temperatures (Mueller et al., 2009; Schönborn et al., 2009b; Szybist et al., 2005). Thus the high NO_x emissions of the reference fossil diesel (Figure 12.5a) are in agreement with the observed larger magnitude (Figure 12.4a) and earlier time of maximum in-cylinder temperature (Figure 12.4b) of the reference fossil diesel relative to the vegetable oils. Considering only the NO_x emissions of the vegetable oils (Figure 12.5b), an influence of the in-cylinder thermal conditions is also apparent. The algal and rapeseed oils emitted the highest and lowest levels of NO_x respectively (Figure 12.5b), and also displayed the highest and lowest maximum in-cylinder temperatures respectively (Figure 12.4a). The lower NO_x emissions of the vegetables oils relative to the reference fossil diesel have been previously reported in engine tests of vegetable oils (Wang et al., 2006).

Figures 12.6a and b show the CO and THC emissions of the vegetable oils and reference fossil diesel at both constant injection and constant ignition timing. At both timing conditions, all of the vegetable oils emit significantly higher levels of both CO (Figure 12.6a) and THC (Figure 12.6b) than the reference fossil diesel. Both CO and THC are known products of incomplete combustion, the levels of which could be expected to be higher at the lower maximum in-cylinder temperatures displayed by the vegetable oils relative to the reference fossil diesel (Figure 12.4a). An effect of injection timing is apparent in the emissions of CO and THC (Figures 12.6a and

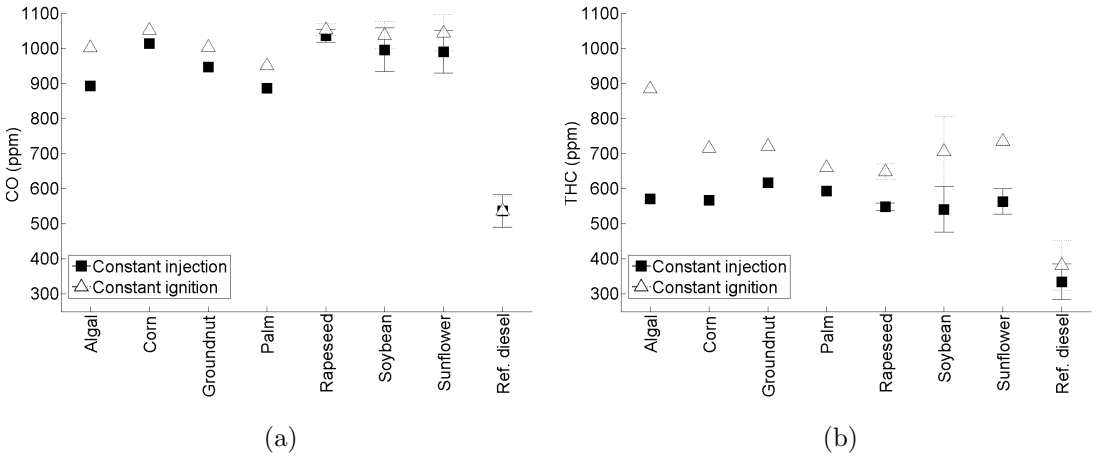

Figure 12.6: (a) CO and (b) THC emissions of the vegetable oils and reference fossil diesel at constant injection and constant ignition timing

b), with levels of both higher for all of the vegetable oils at constant ignition timing. As there is no comparable trend of maximum in-cylinder temperature with injection timing, this would suggest a significant sensitivity of the vegetable oil and air mixing to the cylinder volume and turbulence conditions near TDC. This sensitivity is most apparent in the THC emissions of the vegetable oils (Figure 12.6a); the largest offsets with injection timing are exhibited by the algal and palm oils, which displayed the shortest ignition delays of the oils (Figure 12.1) and thus experienced the greatest shifts in combustion phasing at constant ignition timing relative to constant injection timing. It is hypothesised that the higher levels of both CO and THC (Figures 12.6a and b) at constant ignition timing might be attributable to a greater level of piston fuel impingement at this timing, where a SOI closer to TDC would reduce the distance between the injector nozzle and piston bowl. The higher CO emissions of the vegetable oils relative to the reference fossil diesel (Figure 12.6a) are similar to those reported by Altin et al. (2001a) in engine testing of vegetable oils heated to 80 °C.

Figures 12.7a and b show the particulate emissions of the vegetable oils and reference fossil diesel at constant injection and constant ignition timing. Immediately apparent, at both timing conditions (Figures 12.7a and b), is the lower number of ultrafine particles (Dp $<$ 10 nm) but higher numbers of both nucleation mode (Dp $<$ 50 nm) particles and accumulation mode particles emitted by the vegetable oils relative to the reference fossil diesel. This is likely to be due to the higher viscosity

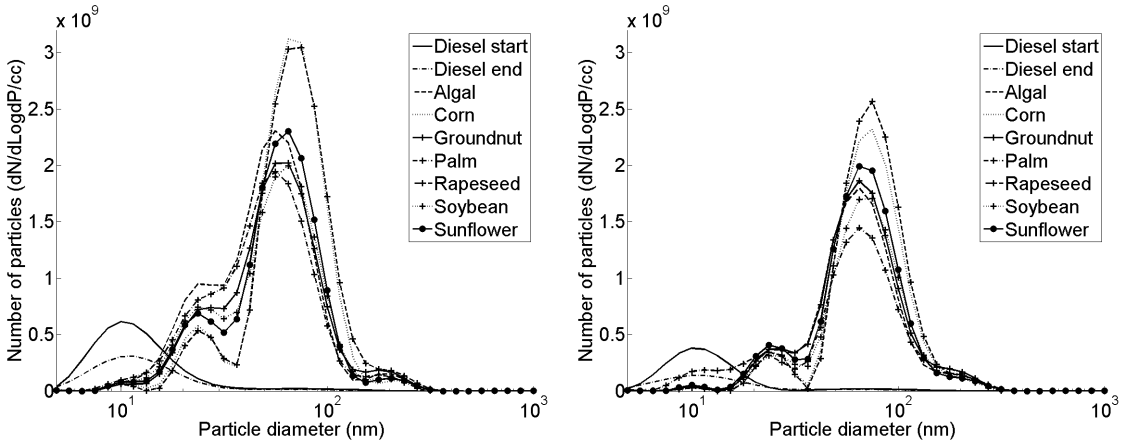

Figure 12.7: Particulate emissions of the vegetable oils and reference fossil diesel at (a) constant injection and (b) constant ignition timing

of the vegetable oils compared to the reference fossil diesel, which could be expected to adversely affect fuel atomisation, creating fuel rich zones required for particulate production (Tree and Svensson, 2007). At both timings (Figures 12.7a and b), the highest peaks in particulate number are produced by the corn and rapeseed oils, while the palm and soybean oils consistently produce the lowest peaks. An effect of injection timing, is however apparent, with peak numbers of both nucleation and accumulation mode particles lower for all vegetable oils lower at constant ignition timing (Figure 12.7b) than at constant injection timing (Figure 12.7a).

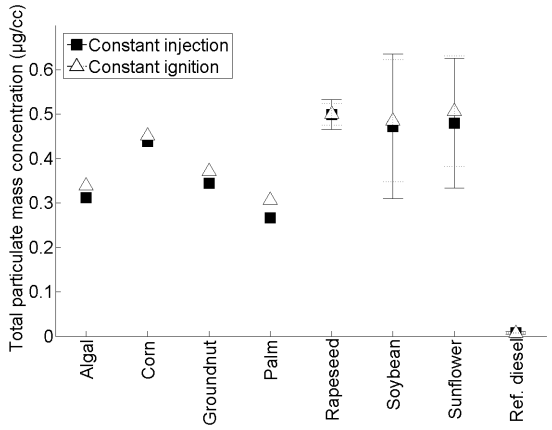

Figure 12.8: Total particulate mass emitted by the vegetable oils and reference fossil diesel at constant injection and constant ignition timing

Figure 12.8 shows the total particulate mass emitted by the vegetable oils and reference fossil diesel at both timing conditions. The emission of particulate mass by the reference fossil diesel (Figure 12.8) is an order of magnitude lower than that of all the vegetable oils, and can be attributed to the significant production of large accumulation mode particles by the vegetable oils (Figures 12.7a and b). At both timing conditions (Figure 12.8), the lowest particulate mass is emitted by the palm oil and the highest by the rapeseed and sunflower oils, and when considering only the vegetables oils it can be seen that emissions of particulate mass increase with duration of ignition delay (Figure 12.2). Exhaust emission of soot is known to be sensitive to in-cylinder temperatures (Tree and Svensson, 2007), as rates of soot oxidation increase with temperature. However, no clear effect of ignition delay (Figure 12.2) was visible on either the magnitude or time of occurrence of maximum in-cylinder temperature of the vegetable oils (Figures 12.4a and b). Furthermore, in the case of the vegetable oils, and as was observed in emissions of CO and THC (Figures 12.6a and b), cylinder geometry at SOI may be a significant factor as emissions of total particulate mass are higher for all vegetable oils at constant ignition timing (Figure 12.8), despite no obvious correlation with in-cylinder thermal conditions (Figures 12.4a and b).

12.2.1. Effect of vegetable oil fatty acid composition on low temperature reactivity

As described in Chapter 2, many studies of both fatty acids and fatty acid esters have shown the structure of the alkyl chain of the fatty acid to be important in determining the ignition quality of the molecule as a whole (Benjumea et al., 2010; Fisher et al., 2011; Graboski and McCormick, 1998; Knothe et al., 1997; McCormick et al., 2001; Mueller et al., 2009; Salamanca et al., 2012; Schönborn et al., 2009b; Zhang and Boehman, 2010; Zhang et al., 2009).

Figure 12.9 shows the ignition delay of the vegetable oils as a function of the carbon to hydrogen (C:H) ratio at both constant injection and constant ignition timing. Figure 12.9 also shows a curve fit at constant injection timing corresponding to the expression $y = 24.79x^{1.94}$ with an R^2 value of 0.826. The C:H ratio for each vegetable oil was determined by assuming individual fatty acid content to be the mean of the range of values presented for each fatty acid in Table 12.1. In Figure 12.9, it can be seen that at both timing conditions, increasing the vegetable oil C:H

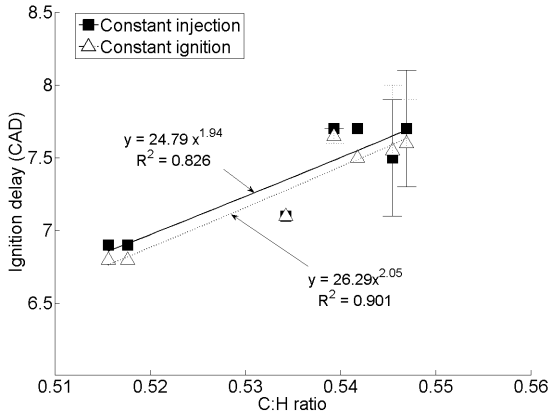

Figure 12.9: Ignition delay of the vegetable oils as a function of carbon to hydrogen (C:H) ratio at constant injection and constant ignition timing

ratio increases the duration of ignition delay. Shortening the fatty acid alkyl chain length, or the introduction of further double bonds to the fatty acid alkyl chain, would both increase the C:H ratio which has been observed in the case of the fatty acid esters to increase the duration of ignition delay (Schönborn et al., 2009b).

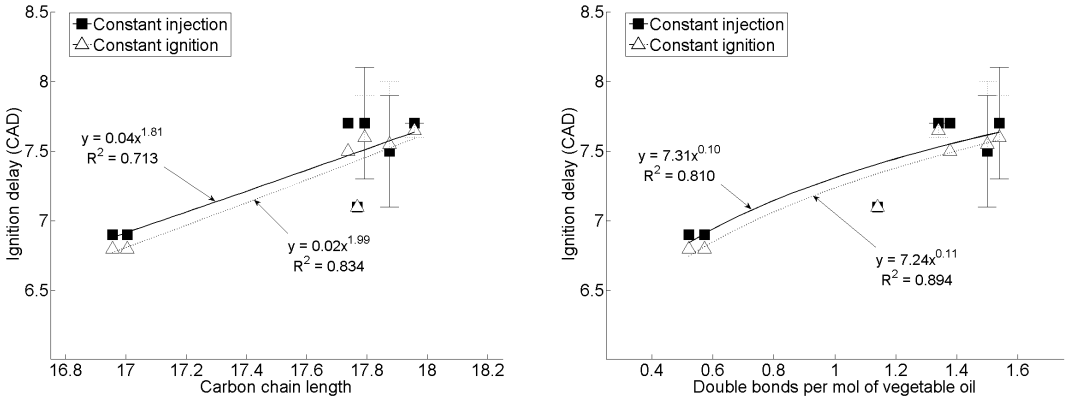

(a) (b)

Figure 12.10: Ignition delay of the vegetable oils as a function of (a) carbon chain length and (b) number of double bonds at constant injection and constant ignition timing

Figures 12.10a and b show the ignition delay of the vegetable oils as a function of average vegetable oil carbon chain length and number of double bonds. It can be seen that increasing carbon chain length (Figure 12.10a) and number of

double bonds (Figure 12.10b) both correlate with an increasing duration of ignition delay. Increasing the number of double bonds in an alkyl chain, has previously been observed to increase the duration of ignition delay in both un-branched alkanes (Chapter 6) and fatty acid esters (Schönborn et al., 2009b), while an increase in the total number of double bonds present has also been observed to decrease the cetane number of vegetable oils (Mehta and Anand, 2009). Thus the correlation between ignition delay and number of double bonds in Figure 12.10b is in agreement with these previous observations and can be attributed to the influence of double bonds within alkyl chains on the low temperature reactivity of such structures. During the ignition delay period of compression ignition combustion, escalation of temperatures and propagation of radical species towards SOC is primarily driven by the oxidation and isomerisation of alkyl chains (Westbrook, 2000). Internal isomerisation of an alkyl chain requires the formation of a six or seven member transition state ring, and such rings can only be formed by a chain of at least three fully saturated carbon atoms (Mehl et al., 2011; Westbrook, 2000). Therefore, it follows that an increased presence of double bonds will reduce rates of low temperature branching reactions and thus increase the duration of ignition delay.

The observed relationship between chain length and ignition delay (Figure 12.10a), is however, the inverse of what might be expected. Previous studies have found that where other features of molecular structure have been held constant, increasing the straight alkyl chain length reduces ignition delay (Chapter 6 and Schönborn et al. (2009b)), due to the availability of more easily abstractable secondary H atoms that increase rates of low temperature branching reactions (Westbrook, 2000). However, in the case of the vegetable oils, and as can be seen in Table 12.1, in general increasing alkyl chain length coincides with an increasing number of double bonds. For example, the algal and palm oils, which exhibited the shortest duration of ignition delay (Figure 12.2), have a high content of saturated palmitic acid (C16:0) and oleic acid, whereas the sunflower and soybean oils, which exhibited the longest duration of ignition delay (Figure 12.2), are nearly exclusively made up of oleic and linoleic acids (C18:1 and C18:2). Therefore, the trend in Figure 12.10a is in fact also representative of the number of double bonds present, suggesting that the presence of double bonds in the fatty acids has more of an impact on ignition delay than average carbon chain length and is in agreement with the observations of Mehta and Anand (2009). The lower R^2 values of the correlation of carbon chain

length to ignition delay relative to that of number of double bonds to ignition delay (0.713 and 0.834 compared to 0.810 and 0.894), is therefore perhaps suggestive of the expected counter-influence of carbon chain length; that is given an equal degree of saturation, increasing carbon chain length would decrease ignition delay. A more accurate determination as to the influence of vegetable oil alkyl chain length might be ascertained by considering only the saturated alkyl chain length, however, such analysis was considered unreliable without more detailed analysis of the vegetable oil composition.

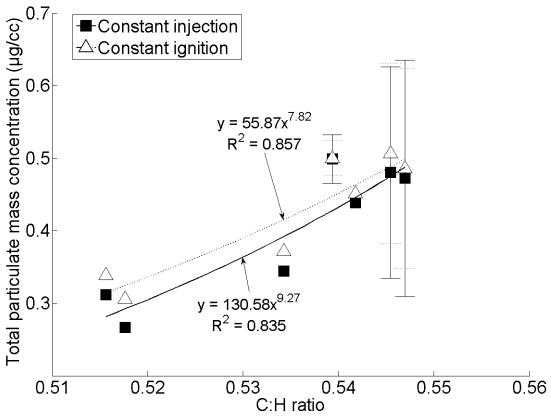

Figure 12.11: Total particulate mass emitted by the vegetable oils as a function of carbon to hydrogen ratio at constant injection and constant ignition timing

Figure 12.11 shows the total particulate mass emitted by the vegetable oils as a function of the carbon to hydrogen ratio at both constant injection and constant ignition timing. It can be seen from Figure 12.11, as either the alkyl chain length or degree of saturation decreases, the level of particulates emitted increase. This is to be expected given the observed correlation between C:H ratio and the duration ignition delay (Figure 12.9), and the concurrent increase in particulate emissions (Figure 12.8) with duration of ignition delay (Figure 12.2). However, this effect of ignition delay (Figure 12.2) cannot be attributed to in-cylinder thermal conditions (Figures 12.4a and b) and thus levels of soot oxidation. Therefore, it is suggested that the increasing number of double bonds present with increasing C:H ratio is resulting in greater levels of initial soot production; the presence of double bonds is known to increase the sooting tendency of a molecule (Ladommatos et al., 1996).

12.2.2. Effect of vegetable oil fatty acid physical properties

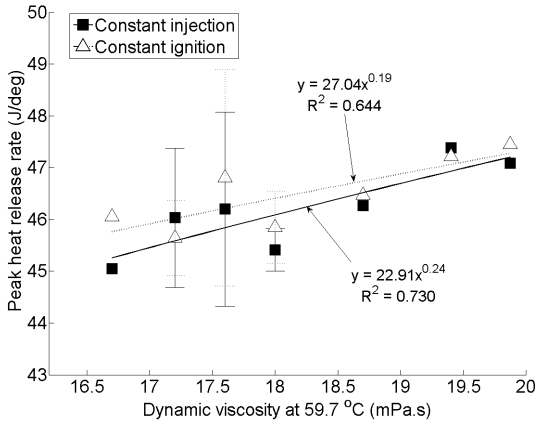

Figure 12.12: Apparent peak heat release rate of the vegetable oils as a function of dynamic viscosity at 59.7 °C at constant injection and constant ignition timing

Figure 12.12 shows the apparent net peak heat release of the vegetable oils as a function of dynamic viscosity at 59.7 °C at both constant injection and constant ignition timing. Increasing dynamic viscosity correlates with increasing peak heat release rate (Figure 12.12) at both injection timings, though the correlation is stronger at constant injection timing (R^2 of 0.730 relative to 0.644). This is somewhat counter-intuitive, in general it could be expected that an increase in fuel viscosity would result in larger droplet sizes upon atomisation, and thus reducing rates of fuel vaporisation and subsequent mixing of air. The peak heat release of the fuels, via the premixed burn fraction, can be considered to be a function of the time available for fuel and air mixing (fuel ignition delay) and the rate at which it occurs. Increased viscosity could therefore be expected to reduce peak heat release rate by both reducing the rate of fuel and air mixing and the duration of ignition delay; increased alkyl chain length and degree of saturation both increase viscosity (Pinzi et al., 2011) and reduce ignition delay (Section 12.2). The reduced rates of fuel and air mixing may account for the significantly lower peak heat release rate of the vegetable oils relative to the reference fossil diesel (Figures 12.1 and 12.4a), where the viscosity of reference fossil diesel is an order of magnitude lower than that of the vegetable oils (Table 12.3). However, the absence of such a trend in Figure 12.12, would therefore suggest that above a threshold viscosity, the duration of ig-

nition delay is not of primary importance in determining the peak heat release rate and that, furthermore, the oil droplet size is not the primary impact of viscosity on the rate of vegetable oil and air mixing at the conditions presented.

Possible relationships between other physical properties that may influence fuel droplet size and fuel air mixing were investigated (density and surface tensions); however, the correlations found were weak relative to that displayed by viscosity and peak heat release rate ($R^2 < 0.513$ relative to $R^2 > 0.644$). Ryan et al. (1984) and Deshmukh et al. (2012) both observed that increasing vegetable oil viscosity reduced the spray penetration rate, and it is suggested that this phenomenon may account for the reduction in peak heat release rate with decreasing viscosity observed in Figure 12.12. Namely, it is hypothesised that in the case of all the vegetable oils a degree of fuel impingement on the piston bowl and cylinder walls is occurring and that this reduces the rate of fuel and air mixing. Therefore, where an increase in vegetable oil viscosity reduces the spray penetration rate, the incidence of fuel impingement on the piston bowl and cylinder walls will decrease also. Subsequently, the efficiency of fuel and air mixing is improved (due to a reduced level of fuel impingement), and the extent of the premixed burn fraction and the peak heat release rate increases. Such a hypothesis is supported by the stronger correlation of peak heat release rate at constant injection timing than at constant ignition timing (Figure 12.12), as at the former condition all fuels would be subject to the same initial dynamic cylinder geometry. It is also tentatively suggested that this may partially account for the extent of cycle to cycle variability exhibited by the sunflower and soybean oils (Figures 12.4b and 12.12), as a greater degree of fuel impingement may increase the sensitivity of combustion phasing to cylinder wall heat transfer.

An influence of fuel impingement on the significantly higher peak heat release rate displayed by the reference fossil diesel relative to the vegetable oils (Figure 12.3a) is also suggested. Assuming that a degree of fuel impingement also occurs in tests with the reference fossil diesel, it can be seen that the higher boiling points of the vegetable oils relative to the reference fossil diesel (as indicated by the relative flash points in Table 12.3) will exacerbate the negative impact of fuel impingement on fuel and air mixing. With higher boiling points, the vegetable oils will require higher local temperatures than the reference fossil diesel for vaporisation of fuel present on the cylinder walls, and so it could be expected that the impinged vegetable oils will be available for combustion somewhat later than the impinged reference fossil diesel.

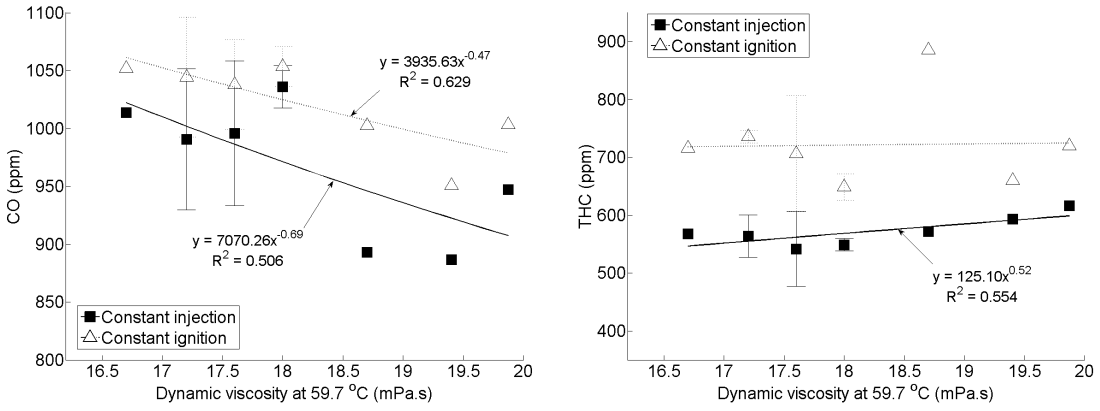

(a) (b)

Figure 12.13: (a) CO and (b) THC emissions of the vegetable oils as a function of dynamic viscosity at 59.7 °C at constant injection and constant ignition timing

Figures 12.13a and b show the CO and THC emissions of the vegetables oils as a function of dynamic viscosity at 59.7 °C at both constant injection and constant ignition timing. At both timing conditions, levels of CO emitted increase with decreasing viscosity (Figure 12.13a), with the trend stronger at constant ignition timing, with the correlation described by an R^2 of 0.620 relative to that of 0.506 at constant injection timing. At constant injection timing, levels of THC increase with increasing dynamic viscosity (Figure 12.13b), while it is not possible to clearly discern a trend at constant ignition timing. The increase in CO emissions with decreasing vegetable viscosity (Figure 12.13a) supports the hypothesis that levels of fuel impingement increase with decreasing viscosity, as an increase in cylinder wall and piston bowl fuel impingement would likely result in a greater degree of incomplete combustion via both lower global peak heat release rates (Figure 12.12) and local temperatures.

Figure 12.14 shows the total particulate mass emitted by the vegetable oils as a function of dynamic viscosity at 59.7 °C at both constant injection and constant ignition timing. Notwithstanding the range of error shown (Figure 12.14), it can be seen that reducing viscosity increases the total particulate mass produced at both timing conditions. While the R^2 values of the relationships found between total particulate mass and dynamic viscosity (Figure 12.14, $R^2 = 0.588$ and 0.595 at constant injection and constant ignition timing respectively) are somewhat lower than

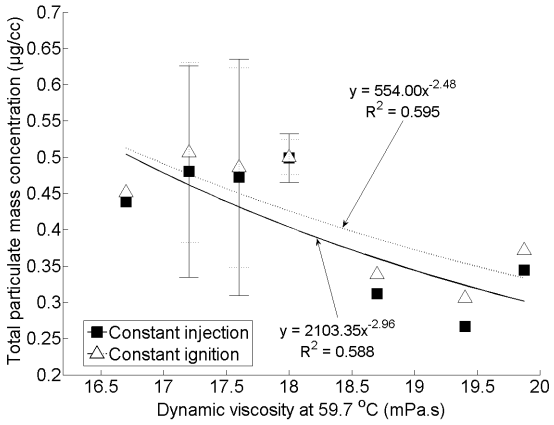

Figure 12.14: Total particulate mass emitted by the vegetable oils as a function of dynamic viscosity at 59.7 °C at constant injection and constant ignition timing

those with C:H ratio (Figure 12.11, $R^2 = 0.857$ and 0.835 at constant injection and constant ignition timing respectively), they are higher than the value of R^2 found when investigating the relationship between dynamic viscosity and C:H ratio ($R^2 = 0.454$). Therefore, while secondary to the C:H ratio of the vegetable oils, an influence of viscosity on soot production is plausible. With regards to the suggestion that decreasing vegetable oil increases fuel impingement, concurrent lower peak heat release rates and local temperatures may both reduce rates of soot oxidation, and thus increase particulate emissions. However, in general, soot emissions are found to increase under fuel rich conditions (Tree and Svensson, 2007), which might be expected to be more prevalent where fuel droplet sizes are potentially larger due to increased fuel viscosity. Therefore, the presence of a correlation between increasing particulate matter and decreasing fuel viscosity, would suggest that the effect of vegetable oil cylinder wall and piston bowl impingement is of more significance than vegetable oil droplet size. It is hypothesised that by the time the vaporisation of fuel impinged on the cylinder wall during the expansion stroke, after local temperatures have been raised sufficiently by the combustion of fuel not impinged, in-cylinder temperatures may remain hot enough for the formation of soot but not for subsequent oxidation of particulate matter. Therefore, it follows that reduced vegetable oil viscosity, resulting in an increased level of fuel cylinder wall impingement, will see an increase in the level of fuel present at these cooler in-cylinder conditions with a subsequent increase in exhaust gas levels of particulate matter.

12.3. Conclusions

1. At a fuel temperature of 60 °C, in a direct injection compression ignition delay engine, six vegetable oils were found to exhibit durations of ignition delay similar to that of a reference fossil diesel. However, the peak heat release exhibited by vegetable oils was significantly lower than that of the reference fossil diesel.

2. The ignition delay of the vegetable oils was found to correlate well with the carbon to hydrogen ratio of the constituent fatty acids, indicating that the ignition delay of the vegetable oils was dictated by the molecular structure and thus low temperature reactivity of the fatty acid alkyl chains. Furthermore, with regards to the duration of ignition delay, the number of double bonds present was found to be of more importance than changes to the average fatty acid carbon chain length.

3. The significantly lower peak heat release rate of the vegetable oils relative to the reference fossil diesel can be attributed to the substantially higher viscosities of the former impacting on the efficiency of fuel and air mixing during the ignition delay period. Reduced efficiency of fuel and air mixing reduces the extent of the premixed burn fraction, and thus the peak heat release rate. However, considering only the vegetable oils, decreasing viscosity correlated with reduced peak heat release rate. It was hypothesised that decreasing vegetable oil viscosity increased fuel cylinder wall and piston bowl impingement, negatively affecting the efficiency of fuel and air mixing.

4. All of the vegetable oils emitted significantly lower levels of NO_x than the reference fossil diesel. This is in agreement with observed peak heat release rates, and thereby reduced production of NO_x by the thermal mechanism.

5. Emissions of CO and THC were higher for all of the vegetable oils relative to the reference fossil diesel, and showed a clear effect of injection timing. Furthermore, increasing levels of CO were found to correlate with decreasing vegetable oil viscosity. This trend and the observed offset in emissions of CO and THC with injection timing, were both in agreement with the hypothesised increase in fuel impingement with decreasing vegetable oil viscosity.

6. Relative to the reference fossil diesel, particulate emissions of the vegetable oils were much higher and can be attributed to higher viscosities of the oils reducing in-cylinder temperatures, and thus rates of soot oxidation, and also reducing the efficiency of fuel atomisation and increasing the presence of fuel rich zones within the cylinder charge. However, considering only the vegetable oils, increasing levels of particulate mass correlated with increasing oil C:H ratio and to a lesser extent decreasing oil viscosity. This suggests the presence of double bonds and the effects of fuel impingement to be of more importance in determining soot levels than local fuel air stoichiometry.

13. Conclusions and recommendations for future work

13.1. Summary and conclusions

This chapter summarises the major findings of the literature review and experimental studies conducted in this work. Furthermore, claims as to the originality of this work are stated, and recommendations for future work made.

13.1.1. Literature review

From the literature review presented in Chapter 2 the following conclusions can be drawn:

1. Advanced methods of transesterification, and utilisation of micro-organisms for conversion of biomass to liquid hydrocarbons, are expanding the range of molecules potentially available (beyond fatty acid methyl esters) as future fuels for compression ignition engines.

2. Compression ignition combustion follows a sequence of overlapping phases, ignition delay is the first of these and is influenced by the low temperature reactions of the fuel molecules. Exhaust emission levels of NOx and soot are both sensitive to in-cylinder conditions and thus combustion phasing.

3. Where fuel molecules possess long alkyl chains, these have been observed to be the primary driver of fuel ignition quality. However, fuel molecular structure can also impact on emission levels via molar oxygen content and the adiabatic flame temperature.

13.1.2. Influence of molecular structure on ignition delay in direct injection compression ignition combustion

The following points summarise the effects of single component fuel molecular structure on the duration of ignition delay:

1. In the case of n-alkanes and straight chain mono-unsaturated alkenes of carbon chain length equal to, or greater than, seven, increasing the straight carbon chain length results in a linear decrease in the duration of ignition delay. However, in the case of the fatty acid ester alcohol moiety, no linear effect

of increasing the alkyl chain length from one to four was observed (methyl stearate to *n*-butyl stearate).

2. Addition of one or more methyl branches to an *n*-alkane increases the duration of ignition delay. In the esters of stearic acid, the presence of a single methyl branch in the alcohol moiety had no discernable effect on the duration of ignition delay, but a slight increase was observed with two such branches present (tert-butyl stearate).

3. In acyclic non-oxygenates and terpenoids, the introduction of double bonds increases the duration of ignition delay, and considered on a bond number basis is approximately twice as influential as the presence of methyl branches. In isomers of octene, movement of a single double bond from the one to two position increases the duration of ignition delay, but contrary to previous studies of shorter chained isomers, further movement of the double bond to the three position (in either the *cis* or *trans* configuration) does not result in a further increase ignition delay. Furthermore, where double bonds are in the *cis* configuration, ignition delay is reduced relative to the same molecule but with double bonds in the *trans* arrangement.

4. Where the alkyl moiety of a molecule possess a high degree of methyl branches or unsaturation, the presence of an attached oxygenated moiety reduces the duration of ignition delay. Furthermore, small changes to the oxygenated moiety (such as removal of a single H atom) can significantly reduce further the duration of ignition delay.

Regarding fuel mixtures of the two or more components, the following observations of the impact of molecular structure on ignition delay have been made:

1. In the case of carbonate esters blended with 30 % (wt/wt) *n*-decane, reducing the total alkyl chain length, either by reduction in the total carbon content or the introduction of methyl branching in the alkyl chains, generally increases the ignition delay. However, di-methyl carbonate displays a shorter ignition delay than di-ethyl carbonate in blends with equivalent *n*-decane content. Maintaining constant alkyl moiety structure while reducing the molar oxygen content decreased the duration of ignition delay.

2. Considering acyclic molecules, increasing the percentage of the lower ignition quality molecule (1-octene) in a binary mixture with a higher ignition quality molecule (*n*-octane) proportionally increases the duration of ignition delay. In a binary mixture of an aromatic (toluene) and an equivalent carbon number and higher ignition quality *n*-alkane (*n*-octane), the relationship between the presence of the aromatic and ignition delay is not linear, with the duration of ignition delay increasing exponentially beyond a critical aromatic content.

3. The ignition delay of natural fatty acid mixtures correlates and increases with increases in the cumulative carbon:hydrogen ratio. Furthermore, of the two changes to molecular structure effect the carbon to hydrogen ratio (the degree of unsaturation and the alkyl chain length), the presence of double bonds was found to be more significant.

13.1.3. Influence of molecular structure on low temperature reaction rates

From the observations summarised in Section 13.1.2, the following conclusions as to the impact of fuel molecular structure on low temperature reaction kinetics (during the ignition delay period) can be deduced:

1. In direct injection compression ignition combustion, the duration of ignition delay correlates with rates of alkyl chain hydrogen abstraction from the fuel and subsequent internal isomerisation. Where changes to alkyl chain lengths, and the number of carbon branches and double bonds result in an increase in the mean carbon to hydrogen bond strength in the fuel molecule, rates of low temperature radical branching reactions decrease and durations of ignition delay increase.

2. When the position of a double bond within an alkyl chain alters, rates of low temperature reactions are dominated by the net reactivity of the residual saturated portions of the alkyl chain. Furthermore, where a fuel experiences thermal decomposition prior to vaporisation, the subsequent low temperature reactivity of the fuel is dictated by the products of the thermal decomposition.

3. The shorter ignition delay of molecules possessing double bonds in the *cis* arrangement relative to those with double bonds in the *trans* configuration, but otherwise identical molecular structure, suggests that reactions in which

internal isomerisation across double bonds take place also contribute to low temperature reactivity.

4. In symmetrical straight alkyl chain esters, the presence of carbon to oxygen bonds inhibits the reactivity of the alkyl chains. However, in the case of terpene molecules, where the alkyl moiety is branched and unsaturated, the presence of oxygenated functional groups enhances the reactivity of the alkyl moiety. The degree to which the reactivity of the alkyl moiety is improved is dependent on the structure of the oxygenated functional group, and also the operating conditions of the engine.

5. In binary mixtures of acyclic molecules, where the components differ only by the presence of a single double bond, there is no indication of cross reactions between the fuel molecules. However, cross reactions between the aromatic molecule toluene and *n*-heptane do occur, with the radical stabilizing behavior of toluene inhibiting the rates of low temperature branching reactions of *n*-heptane. Furthermore, this can result in two stages of ignition delay where the failure of the initial ignition event to propagate throughout the cylinder charge can also be attributed to the consumption of radicals by toluene.

6. Cross reactions between radicals produced by the decomposition of *n*-decane and those from the decomposition of carbonate esters are also likely and may account for the shorter ignition delay of di-methyl carbonate relative to di-ethyl carbonate.

13.1.4. Impact of fuel physical properties on combustion phasing

Combustion phasing was found to be primarily driven by the duration of ignition delay, and the level of fuel and air mixed to combustible stoichiometry at the start of combustion. In general, the extent of fuel and air mixing was limited by the time available for the fuel and mixing (the ignition delay period), and effects of fuel physical properties on the rate of fuel and air mixing were not visible. However, where ignition delays were equalised, or physical properties differed substantially from those of the reference fossil diesel, effects of fuel physical properties on combustion phasing were visible.

1. Considering acyclic non-oxygenates of carbon to chain length 7 to 22, with ignition delay removed as a variable, an influence of both boiling point and enthalpy of vaporisation on the magnitude of peak heat release rate is possible, with both properties potentially limiting the extent of fuel and air premixing during a constant duration of ignition delay.

2. In the case of the straight alkyl chain carbonate esters, an increasing latent heat of vaporization with decreasing alkyl chain length was observed to reduce rates of heat release rate.

3. Significant increases in fuel viscosity ($\approx$ 15 mPa.s) reduce peak heat releases, irrespective of relative durations of ignition delay, attributable to an effect of viscosity on fuel and air mixing. However, considering only fuels of elevated viscosity ($>$ 15 mPa.s), further increases in fuel viscosity correlate with increased peak heat release rates, potentially attributable to a decreased level of fuel cylinder wall and piston bowl impingement.

13.1.5. Effect of molecular structure on formation and emissions of gaseous species and particulates

While the primary driver of NO_x formation was found to be the thermal conditions to which the cylinder charge was subject, effects of molecular structure on levels of gaseous emissons and particulates outside of determining such conditions (primarily via the duration of ignition delay) were also observed:

1. A secondary influence of molecular structure on rates of thermal NO_x formation (relative to the duration of ignition delay) is the adiabatic flame temperature. Most significant in determining the adiabatic flame temperature is the presence of double bonds, and increasing either the number of double bonds within a molecule or increasing the overall number of double bonds in a fuel mixture increases the flame temperature and susequently NO_x emissions.

2. Emissions of CO and THC are sensitive to in-cylinder thermal conditions and geometry at the time of autoignition. Furthermore, in the case of the carbonate esters, levels of CO decreased with increasing fuel bound oxygen, suggesting that both reaction temperature and the availability of oxygen contribute to levels of incomplete combustion.

3. Local stoichiometry conditions are important in determining levels of particulate emitted. Where increased fuel viscosity resulted in increased particulate emissions, the abundance of fuel rich mixture zones conducive to soot formation could also be expected to increase via a reduction in the efficiency of fuel and air mixing. Such an effect was visible in the case of fatty acid esters with varying alcohol moiety, terpenes and vegetable oils (relative to the reference fossil diesel).

4. Increasing the presence of oxygen, either on a molar basis, or by increasing the oxygenate content within a fuel mixture, reduces levels of particulate matter emitted in the case of carbonate esters blended with *n*-decane. This can be attributed to an increase in combustion temperatures and soot oxidation with the greater availability of fuel bound oxygen.

5. In the isomers of octene, irrespective of in-cylinder thermal conditions, the largest mass of particulates was produced by the *trans*-octene with the double bond closest to the middle of the molecule.

6. Particulate emissions of high viscosity vegetable oils (16 to 20 mPa.s) show a more significant influence of the presence of double bonds and the effects of fuel impingement than local fuel air stoichiometry.

13.1.6. Summary of conclusions

The experimental studies presented in this work have shown that minor alterations to the molecular structure of potential fuels for compression ignition engines can greatly effect to the degree to which they are fit for purpose. The low temperature reactivity of a fuel, which controls the duration of ignition delay, is dependent on the molecular structure of a fuel and, where present, is dominated by the reactivity of alkyl chains. In binary fuel mixtures, both the reactivity of the individual components and kinetic synergy between the components determine the overall mixture low temperature reactivity. The duration of ignition delay is the dominant route by which the molecular structure of fuels impacts on levels of NOx formation, while levels of particulates emitted are influenced by the presence of fuel bound oxygen and physical properties that effect fuel and air mixing. This understanding of the influence of molecular structure and how it may be manipulated to improve combustion characteristics and reduce emissions of pollutants, shows that the range of

viable fuel molecules for compression ignition combustion can be widened to include those from potentially more sustainable sources than those currently in use.

13.2. Claims of originality

It is believed that the system developed for testing low volumes of fuels in a direct injection compression ignition engine is entirely novel. The major advantage of this system has been the ability to test potential fuel molecules as single components, where they would otherwise require blending with a second fuel component. Utilising high assay fuels, this has allowed for observations of effects on combustion and emissions directly attributable to the fuel molecular structure.

A significant percentage of the molecules investigated in this work had not previously been considered as fuels or blend components for compression ignition engines. In some cases this can be attributed to physical properties of the fuels, such as high melting point or low lubricity, that would make them unsuitable for use in conventional direct injection fuel systems. In other instances, the pure component fuels were produced by specialist synthesis and could not have been economically obtained in large enough quantities to test without the low volume fuel system. Collaboration with UCL Structural Molecular Biologists inspired the testing of a range of terpenes that otherwise would not have been considered. Furthermore, this collaboration will see the direct utilisation of the results of Chapter 11 in directing the genetic modification of micro-organisms for production of fuel molecules.

To date, this work has resulted in the publication of three peer-reviewed journal papers:

- P. Hellier, N. Ladommatos, R. Allan, S. Filip and J. Rogerson, "The importance of double bond position and *cis trans* isomerisation in diesel combustion and emissions", Fuel, Volume 105, March 2013, Pages 477-489. http://dx.doi.org/10.1016/j.fuel.2012.08.007
- P. Hellier, N. Ladommatos, R. Allan, M. Payne and J. Rogerson, "The Influence of Fatty Acid Ester Alcohol Moiety Molecular Structure on Diesel Combustion and Emissions", Energy and Fuels, 2012, 26 (3), pp 19121927. http://dx.doi.org/10.1021/ef2017545

- P. Hellier, N. Ladommatos, R. Allan, M. Payne and J. Rogerson, "The Impact of Saturated and Unsaturated Fuel Molecules on Diesel Combustion and Exhaust Emissions", SAE Int. J. Fuels Lubr. 5(1):106-122, 2012. http://dx.doi.org/10.4271/2011-01-1922

In addition, a further four journal papers based on this work are currently under preparation.

13.3. Recommendations for future work

While this work has explored several features of molecular structure and has identified clearly the relationship between ignition delay, combustion phasing and emissions production, further understanding on the impact of molecular structure on low temperature reactivity is required. In the study of octene isomers (Chapter 7), movement of a single double bond towards the centre of the molecule did not result in a linear increase in ignition delay; this was contrary to studies of shorter alkyl chained molecules. Therefore, it would be of interest to investigate the effect of double bond position in alkenes longer than octene, so as ascertain whether this behaviour is typical of all longer alkyl chain molecules.

In Chapter 11, the reactivity of two of the terpene fuels was found to be highly sensitive to the engine operating conditions; both combusted as single component fuels at elevated injection pressures and elevated fuel and air temperatures, but in blends with fossil diesel, at reduced injection pressure and ambient fuel conditions, could not be induced to combust when present at a level greater than 50 % (wt/wt). Investigating which of the changes in engine operating conditions was primarily responsible for the decrease in ignition quality may cast light on the low temperature reactivity of such molecules, and ultimately suggest compression ignition combustion strategies that extends the range of suitable fuels. Alternatively, it may be possible to induce the combustion of the terpenes at conventional operating conditions through synergy with a second fuel component.

The study of carbonate esters in Chapter 9 considered only three molecules possessing straight alkyl chains and failed to discover a consistent influence of alkyl chain length. However, as all of the symmetrical carbonate esters were unsuitable as single component fuels, it might be of interest to investigate asymmetrical carbonates esters as this would allow for the presence of a longer alkyl chain length, while

maintaining a similar molecular mass. As was observed in Chapter 8 in the case of fatty acid esters, it might be expected that where one alkyl chain is significantly longer than the other it will dictate the low temperature reactivity of the molecule.

An element of compression ignition combustion not considered in this work is the effect of fuel molecular structure on high temperature reaction kinetics subsequent to the start of combustion. If possible, manipulation of combustion rates via the fuel molecular structure may allow for optimising combustion phasing to both increase the efficiency of energy release and reduce in emission levels.

A. Characterisation of inlet air heater

For several of the studies described in this work (Chapters 6, 7, 9 and 11), the engine air inlet was heated above the ambient air temperature, as described in Chapter 3. However, as the air heater employed was maintained at constant temperature by a PID pulse-width modulator (PWM) controller, it was important to investigate the possibility of any engine cycle to cycle variation in air inlet temperature induced by the duration of the PWM duty cycle ($\approx$ 1 s).

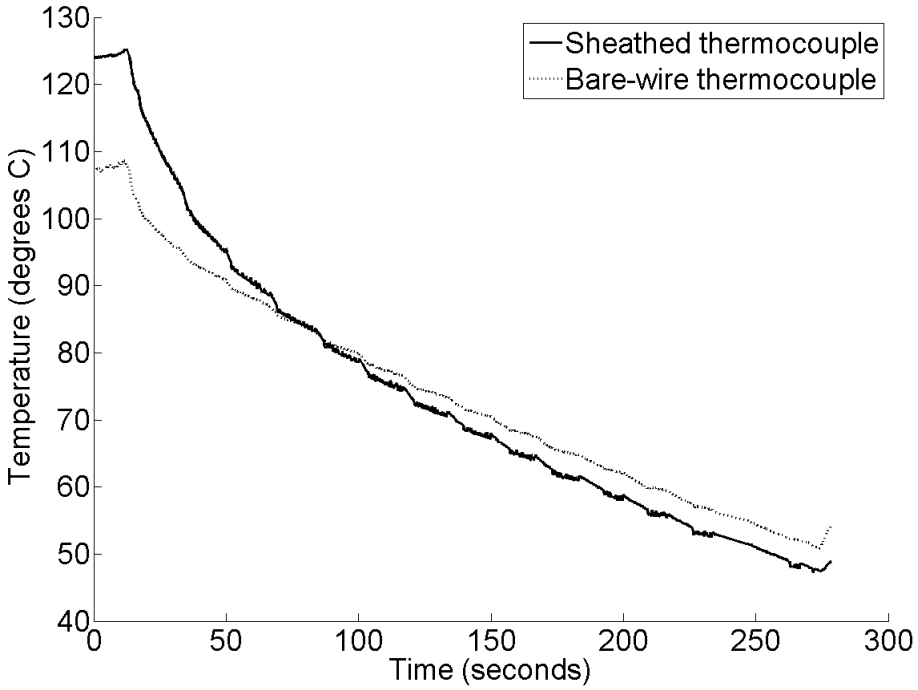

Figure A.1: Cooling curves of thermocouples at the engine inlet manifold post air inlet heating

Figure A.1 shows the cooling curves of two K-type thermocouples situated in the engine inlet manifold on cessation of air inlet heating, and with the engine motored by the dynometer at a speed of 1200 rpm. The sheathed thermocouple employed had a a tip diameter of 1.5 mm and was thus of slower response than the bare-wire thermocouple, which had an effective tip diameter less than 1 mm. In Figure A.1, it can be seen that while the sheathed thermocouple is initially at a higher temperature than the bare-wire thermocouple (attributable to differing mounting positions within the inlet manifold), on cessation of air inlet heating, the

sheathed thermocouple cools more quickly than the bare-wire thermocouple. As it could be expected that the bare-wire thermocouple would respond more quickly to a rapid change in temperature than the sheathed thermocouple, this indicates that the cooling rates displayed in Figure A.1 are the genuine cooling rates of air flow through the inlet manifold, and not influenced by the thermocouple response rate. Therefore, it can be seen that the thermal inertia of the air inlet manifold is sufficient to prevent any influence of the PWM duty cycle on cycle to cycle variation in the air inlet temperature.

B. Pressure measurement mounting points

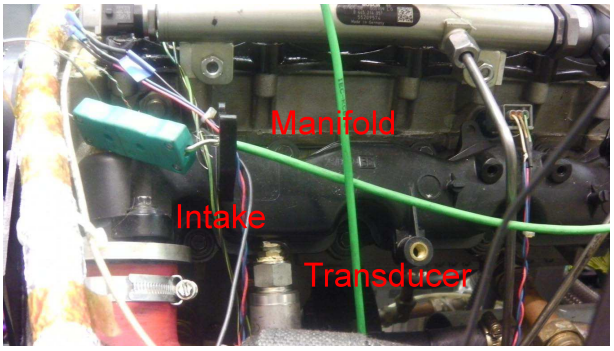

Figure B.1: Mounting and position of inlet air pressure transducer

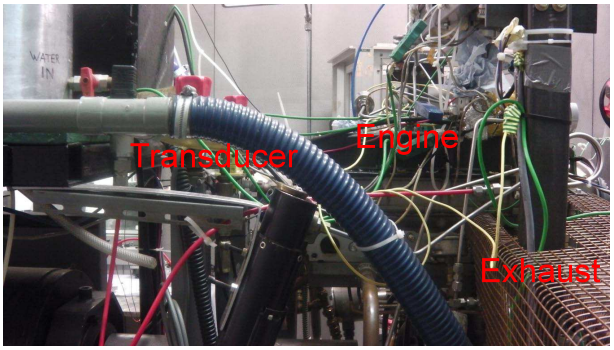

Figure B.2: Mounting and position of exhaust gas pressure transducer

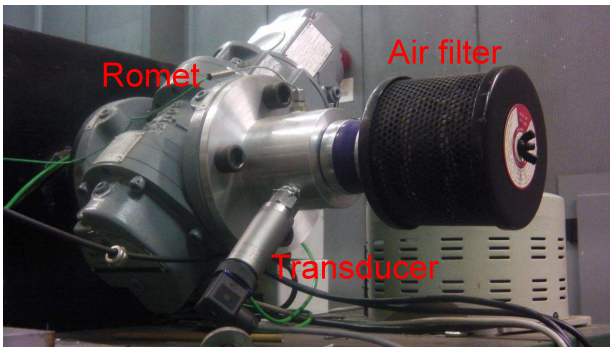

Figure B.3: Mounting and position of intake air pressure prior to the air flow meter

Figure B.1 shows the mounting of the pressure transmitter at the intake manifold. Figures B.2 and B.3 show the mountings of two further in-line piezoresistive pressure transmitters (Druck PTX 717-3275), which were used to measure pressure in the exhaust and also of the intake air just prior to the air flow meter respectively.

C. Reference fossil diesel properties

Table C.1: Reference fossil diesel properties

Test	Unit	Method	Result
Density at 15 °C	kg/L	ASTM D4052	0.8345
Gross Calorific Value	MJ/kg	IP 12	46.00
Nett Calorific Value	MJ/kg	Calculated from IP 12	43.14
Carbon	% (m/m)	ASTM D5291	86.30
Hydrogen	% (m/m)	ASTM D5291	13.50
Oxygen	% (m/m)	ASTM D5291	0.06
Sulphur Content	mg/kg	IP 373	5.4
Appearance		Visual	Clear & Bright
Colour		Visual	Yellow
Water and Sediment, % (v/v)		Visual	None Visible
Cetane Number		EN ISO 5165	51.7
Density at 15 °C	kg/m^3	EN ISO 12185	834.4
Cetane Index		EN ISO 4264	53.0
Cold Filter Plugging Point	°C	EN 116	-15
Cloud Point	°C	IP 219	-8
Monocyclic Aromatics	% (m/m)	EN 12916	22.5
Dicyclic Aromatics	% (m/m)	EN 12916	3.6
Tri+ -Aromatics	% (m/m)	EN 12916	0.2
Polycyclic Aromatics	% (m/m)	EN 12916	3.8
Total Aromatics	% (m/m)	EN 12916	26.3
Flash Point	°C	EN ISO 2719	66.5
Micro Carbon Residue on 10% Res	% (m/m)	EN ISO 10370	< 0.01
Ash Content at 775 °C	% (m/m)	EN ISO 6245	< 0.001
Total Contamination	mg/kg	EN 12662	5
Copper Corrosion 3 hrs.at 50 °C		EN ISO 2160	1
Oxidation Stability	g/m^3	EN ISO 12205	< 1.0
Lubricity	microns	EN ISO 12156-1	343
I.B.P.	°C	EN ISO 3405	179.9
10% v rec. at	°C	EN ISO 3405	212.2
50% v rec. at	°C	EN ISO 3405	268.7
90% v rec. at	°C	EN ISO 3405	324.3
95% v rec. at	°C	EN ISO 3405	338.5
F.B.P.	°C	EN ISO 3405	356.2
% v rec. at 250 °C	% (v/v)	EN ISO 3405	34.1
% v rec. at 340 °C	% (v/v)	EN ISO 3405	95.5
% v rec. at 350 °C	% (v/v)	EN ISO 3405	97.4
Recovery	% (v/v)	EN ISO 3405	99.3
Residue	% (v/v)	EN ISO 3405	0.5
Loss	% (v/v)	EN ISO 3405	0.2
Kinematic Viscosity at 40 °C	mm^2/s	EN ISO 3104	2.672
F.A.M.E.	% (v/v)	EN 14078	< 0.5
Sulphur Content	mg/kg	IP 373-2	5.4
Water	mg/kg	ASTM D1744	54

D. Synthetic molecule details

D.1. Octene isomers

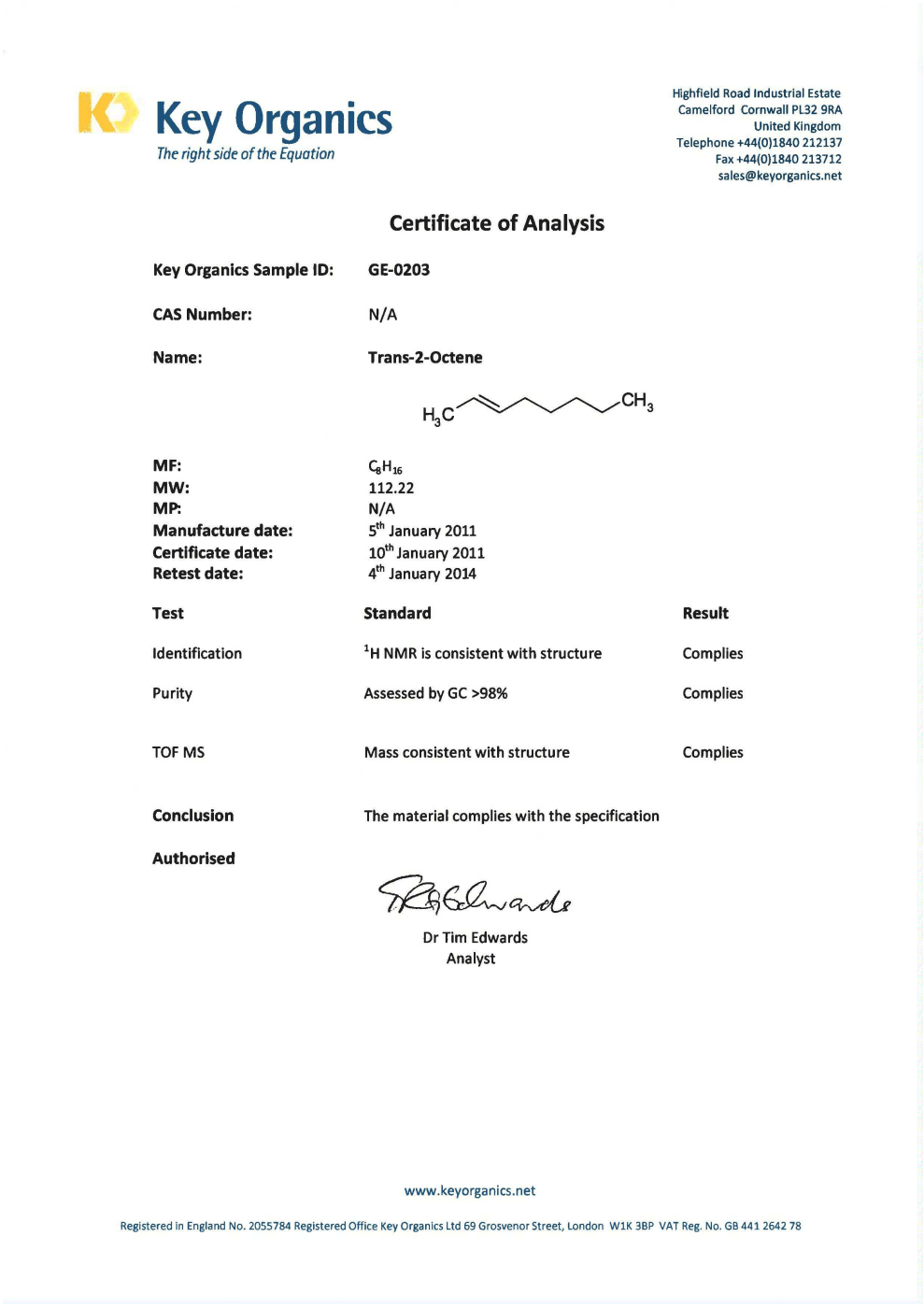

Key Organics
The right side of the Equation

Highfield Road Industrial Estate
Camelford Cornwall PL32 9RA
United Kingdom
Telephone +44(0)1840 212137
Fax +44(0)1840 213712
sales@keyorganics.net

Certificate of Analysis

Key Organics Sample ID:	**GE-0203**
CAS Number:	N/A
Name:	**Trans-2-Octene**
MF:	C_8H_{16}
MW:	112.22
MP:	N/A
Manufacture date:	5th January 2011
Certificate date:	10th January 2011
Retest date:	4th January 2014

Test	**Standard**	**Result**
Identification	^{1}H NMR is consistent with structure	Complies
Purity	Assessed by GC >98%	Complies
TOF MS	Mass consistent with structure	Complies

Conclusion The material complies with the specification

Authorised

Dr Tim Edwards
Analyst

www.keyorganics.net

Registered in England No. 2055784 Registered Office Key Organics Ltd 69 Grosvenor Street, London W1K 3BP VAT Reg. No. GB 441 2642 78

Figure D.1: *Trans*-2-octene

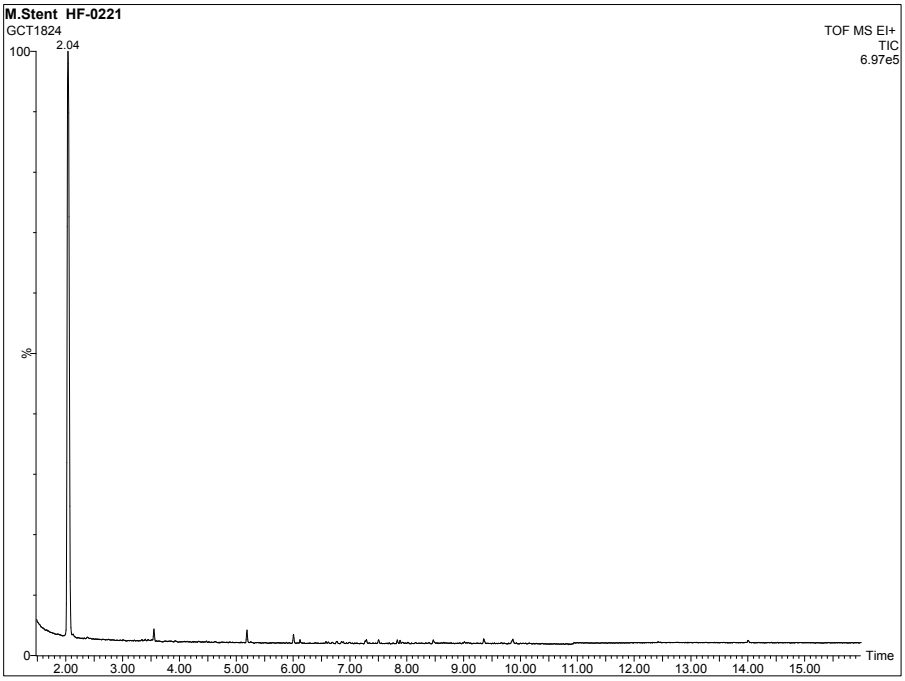

(a)

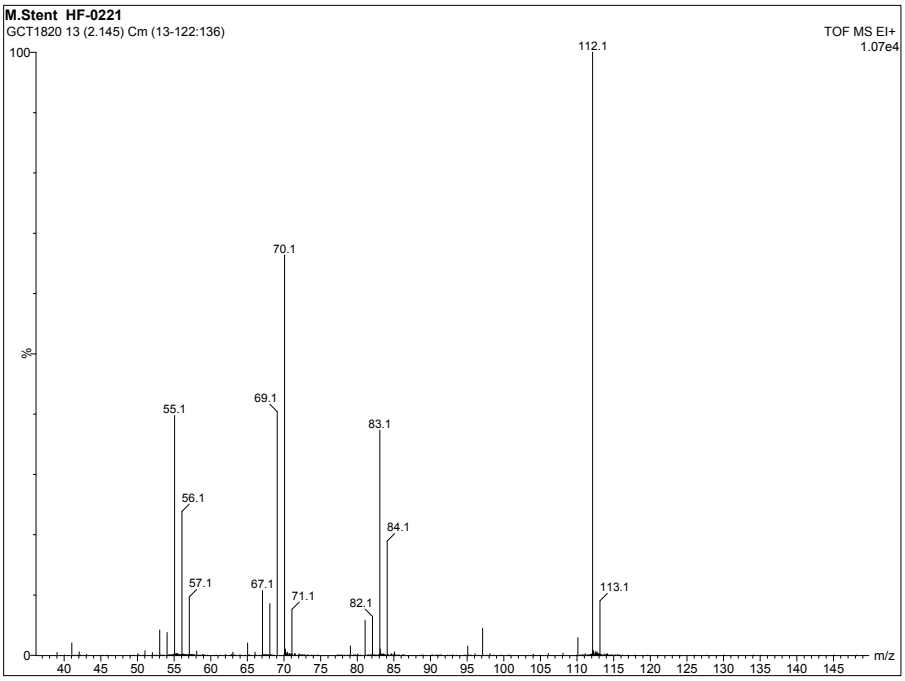

(b)

Figure D.2: *Cis*-3-octene analysis (a) gc (b) gcms

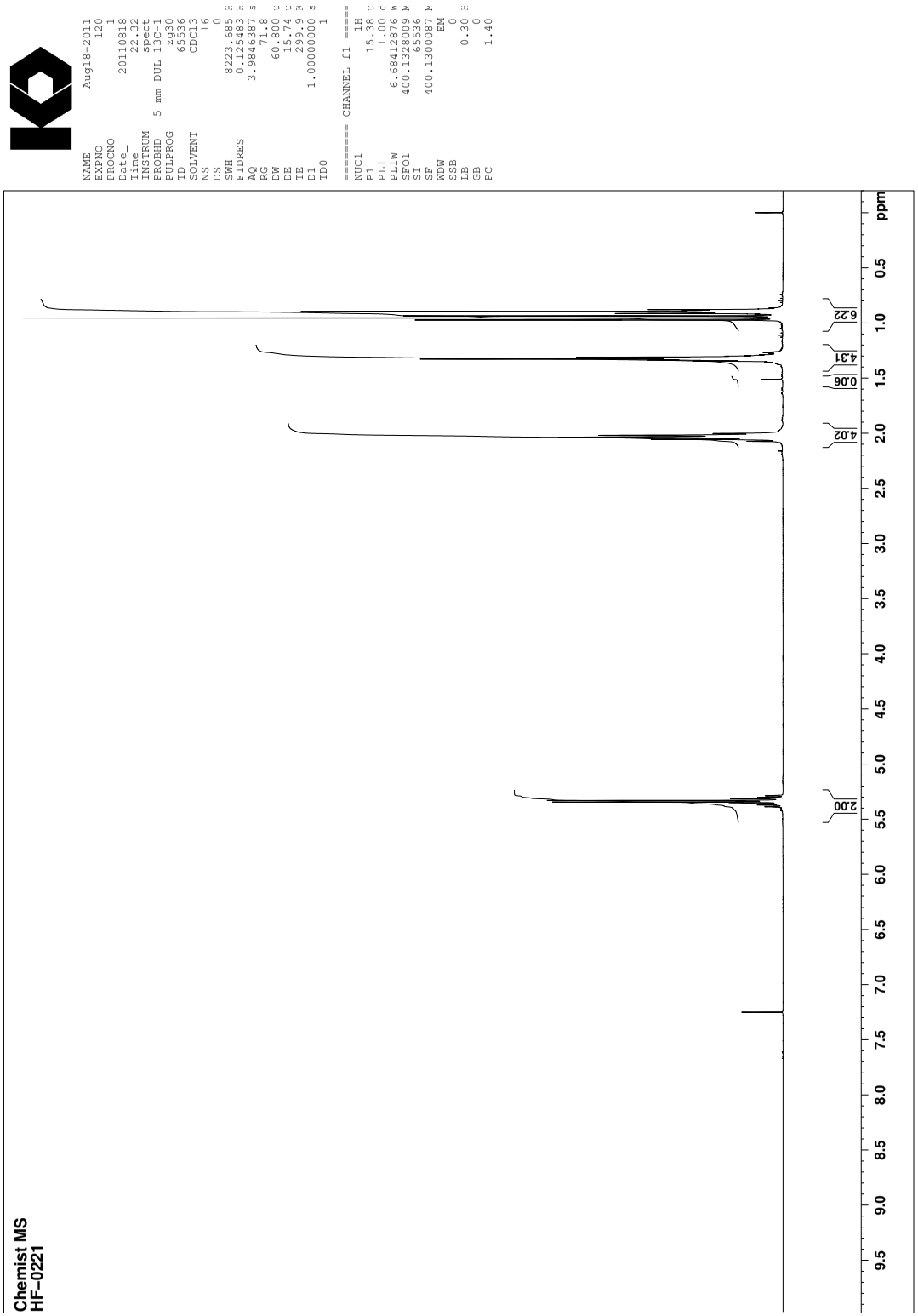

Figure D.3: *Cis*-3-octene 1 H NMR ananlysis

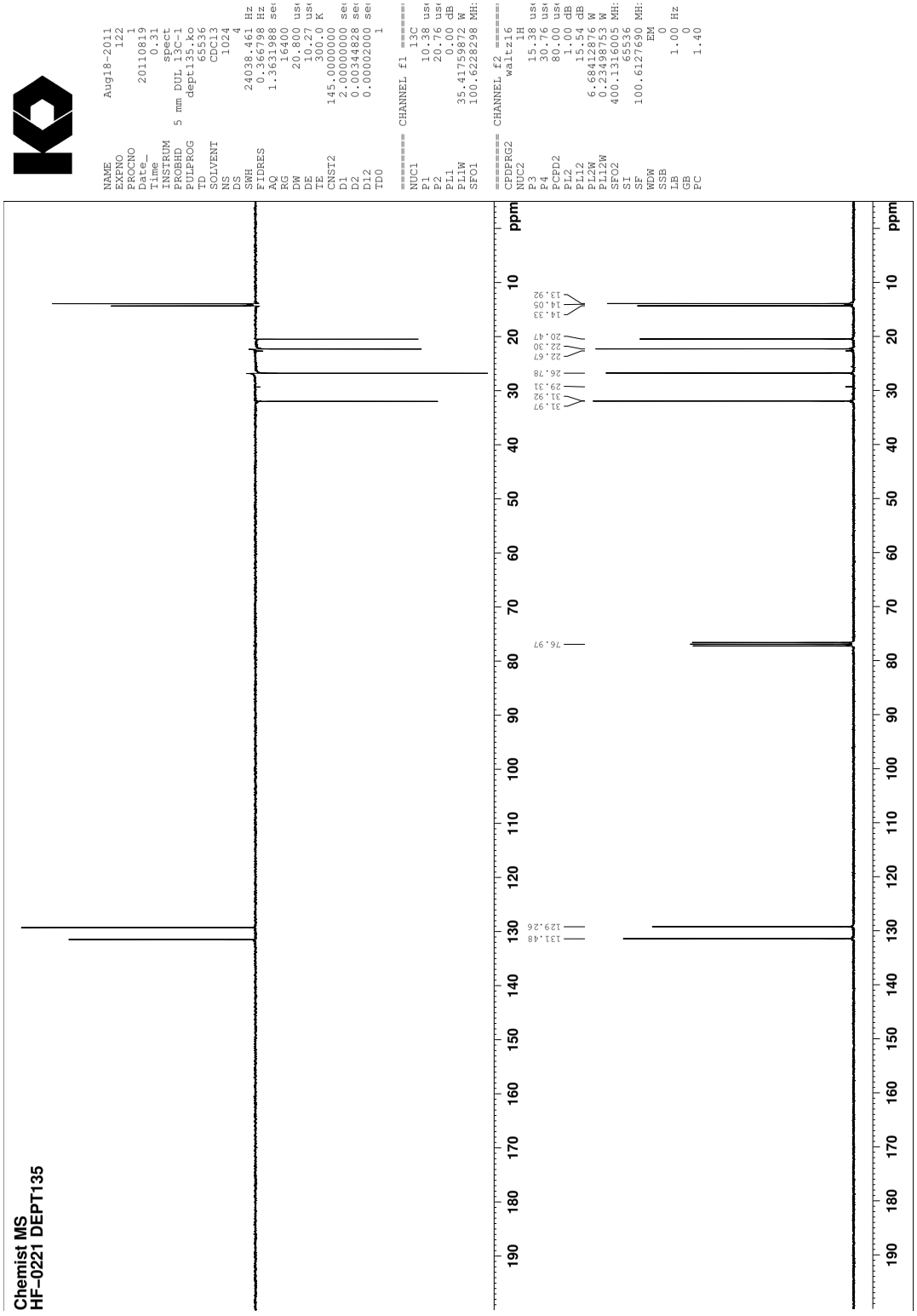

Figure D.4: *Cis*-3-octene 13 C NMR analysis

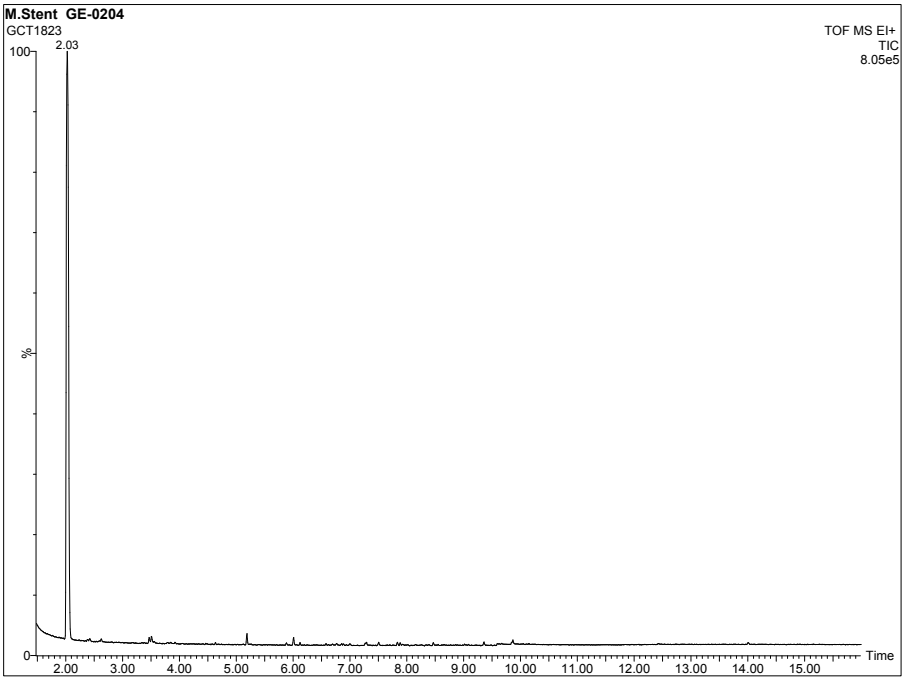

(a)

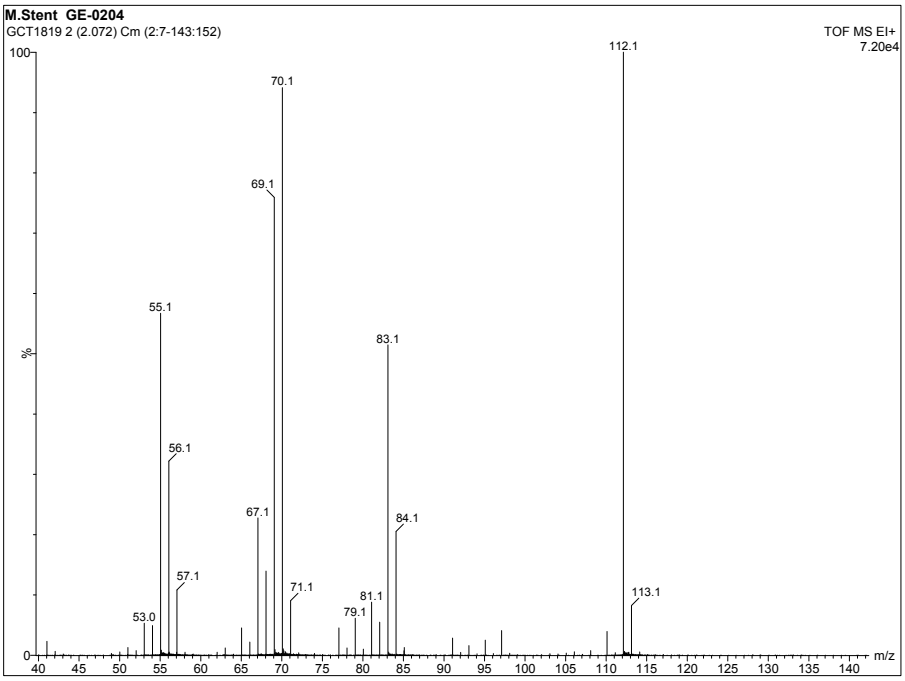

(b)

Figure D.5: *Trans*-3-octene analysis (a) gc (b) gcms

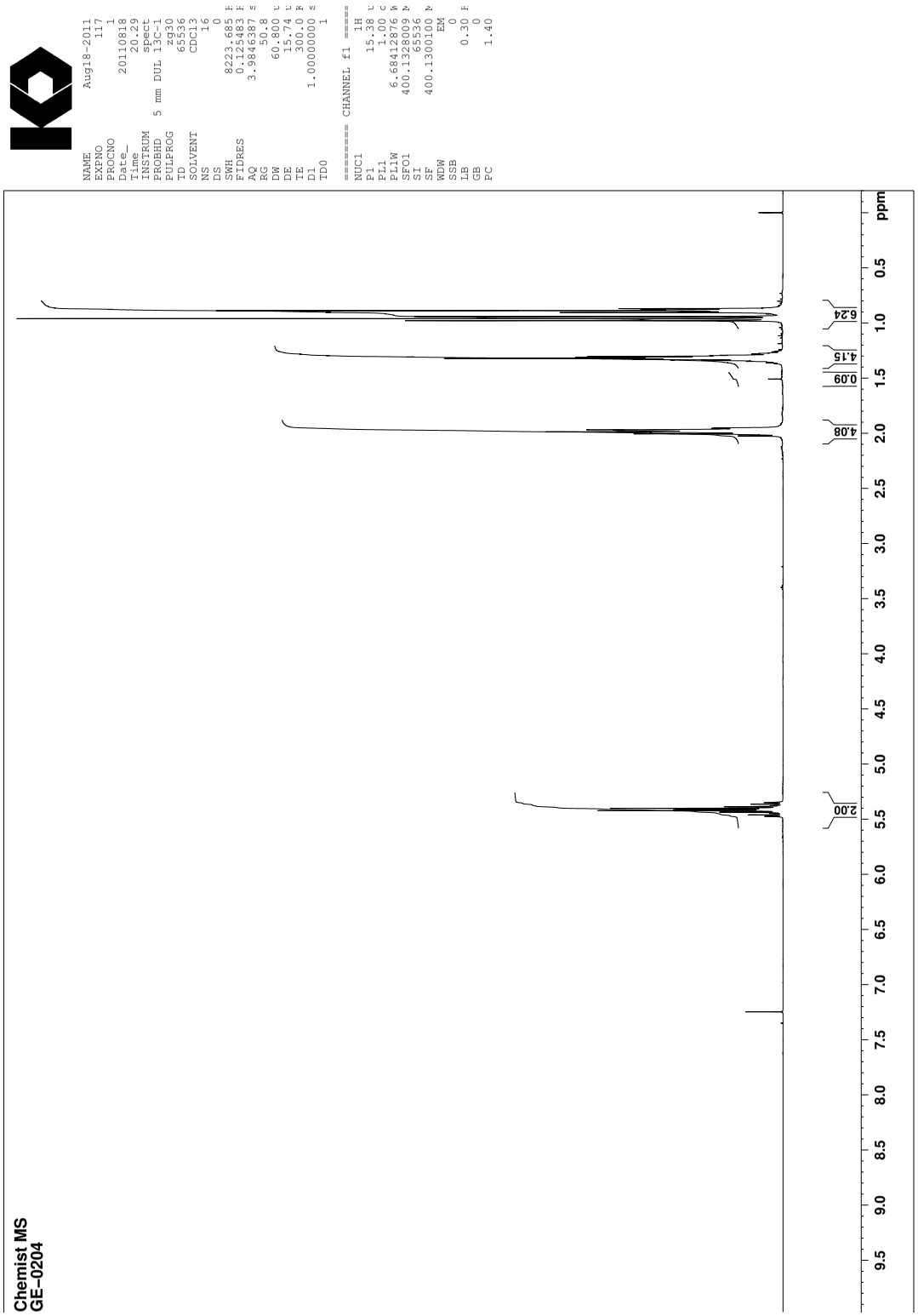

Figure D.6: *Trans*-3-octene 1 H NMR ananlysis

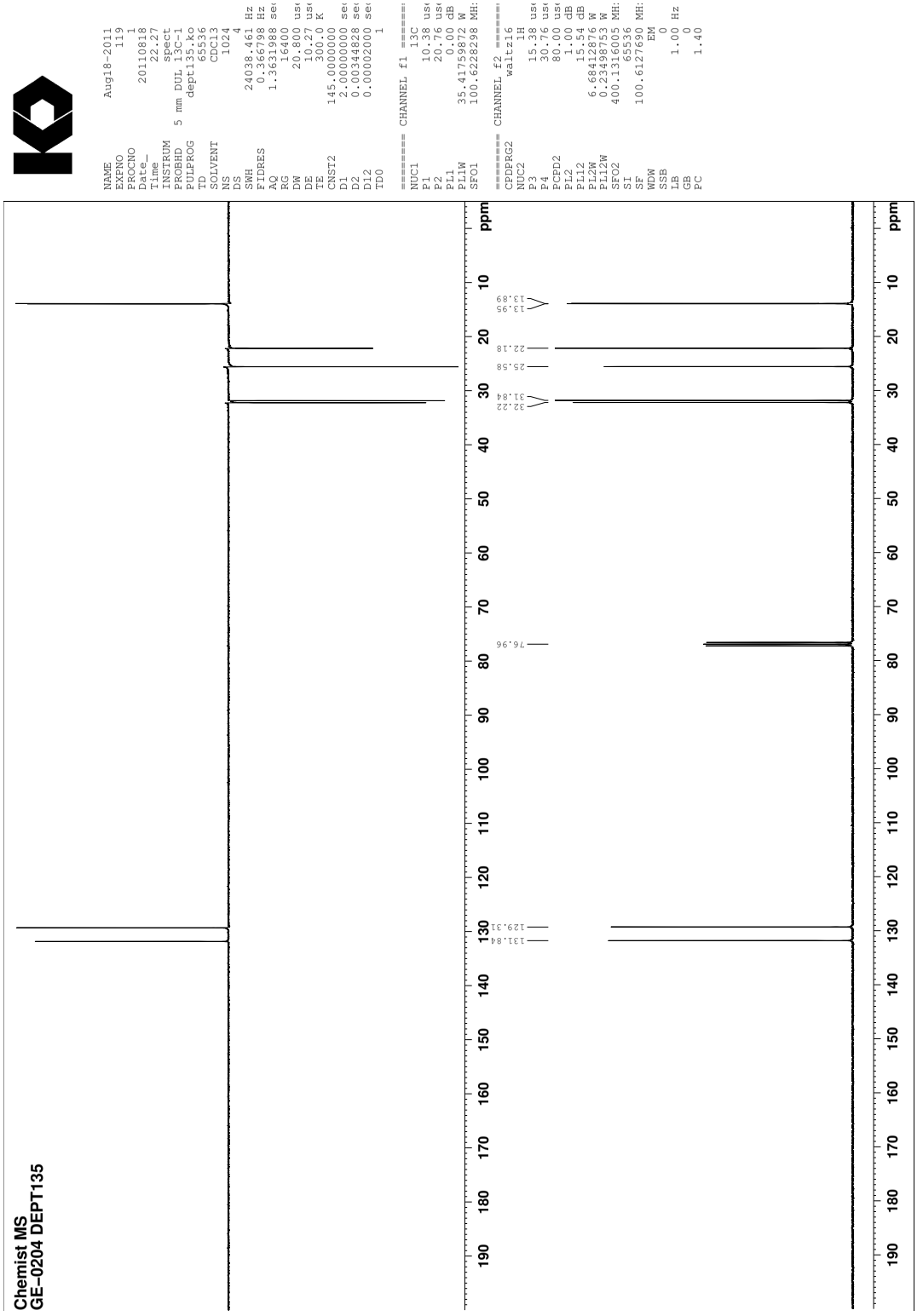

Figure D.7: *Trans*-3-octene 13 C NMR analysis

D.2. Fatty acid esters

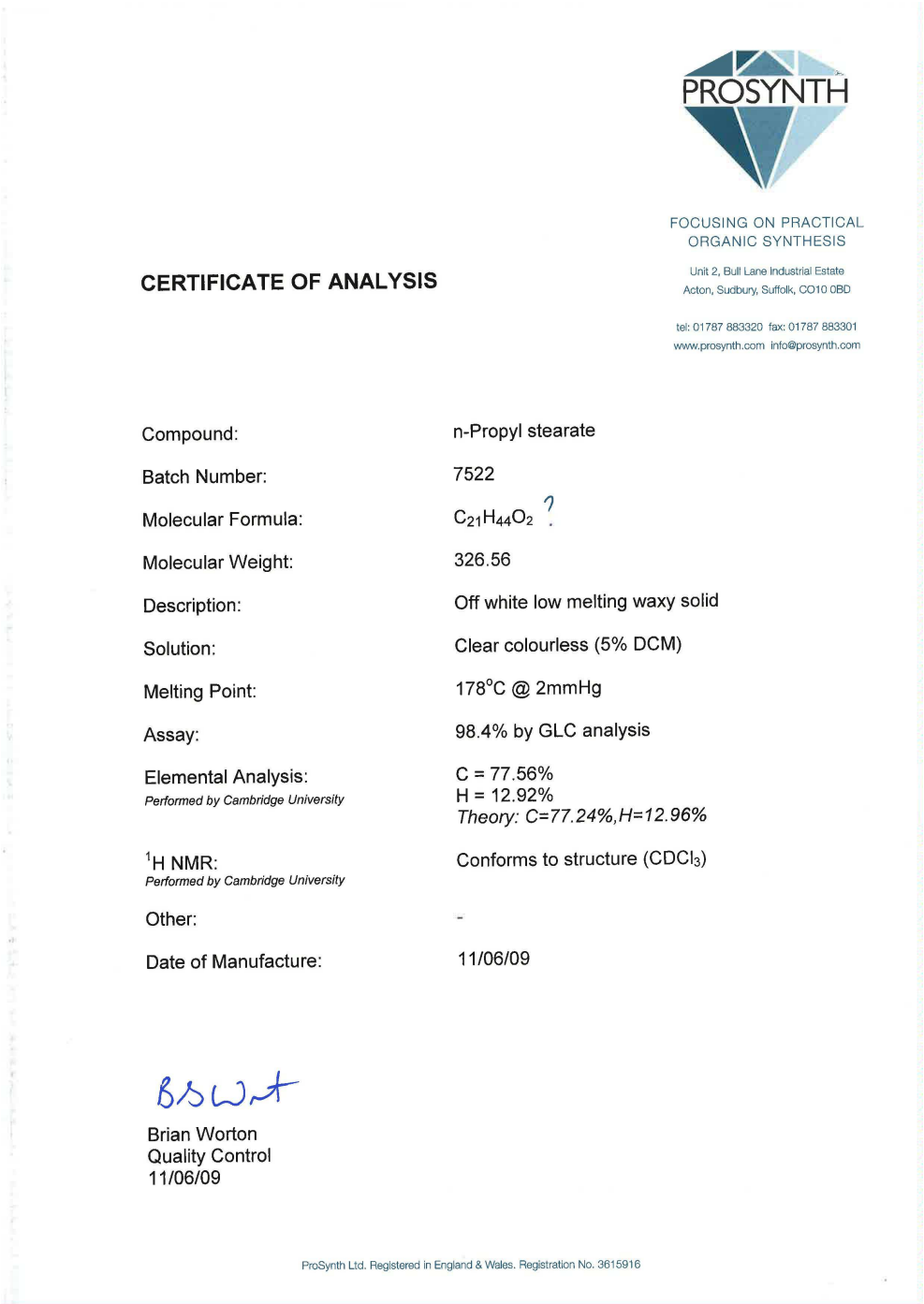

PROSYNTH

FOCUSING ON PRACTICAL ORGANIC SYNTHESIS

Unit 2, Bull Lane Industrial Estate
Acton, Sudbury, Suffolk, CO10 0BD

tel: 01787 883320 fax: 01787 883301
www.prosynth.com info@prosynth.com

CERTIFICATE OF ANALYSIS

Compound:	n-Propyl stearate
Batch Number:	7522
Molecular Formula:	$C_{21}H_{44}O_2$?
Molecular Weight:	326.56
Description:	Off white low melting waxy solid
Solution:	Clear colourless (5% DCM)
Melting Point:	178°C @ 2mmHg
Assay:	98.4% by GLC analysis
Elemental Analysis: *Performed by Cambridge University*	C = 77.56% H = 12.92% *Theory: C=77.24%,H=12.96%*
^{1}H NMR: *Performed by Cambridge University*	Conforms to structure ($CDCl_3$)
Other:	-
Date of Manufacture:	11/06/09

BSWnt

Brian Worton
Quality Control
11/06/09

ProSynth Ltd. Registered in England & Wales. Registration No. 3615916

Figure D.8: *n*-propyl stearate

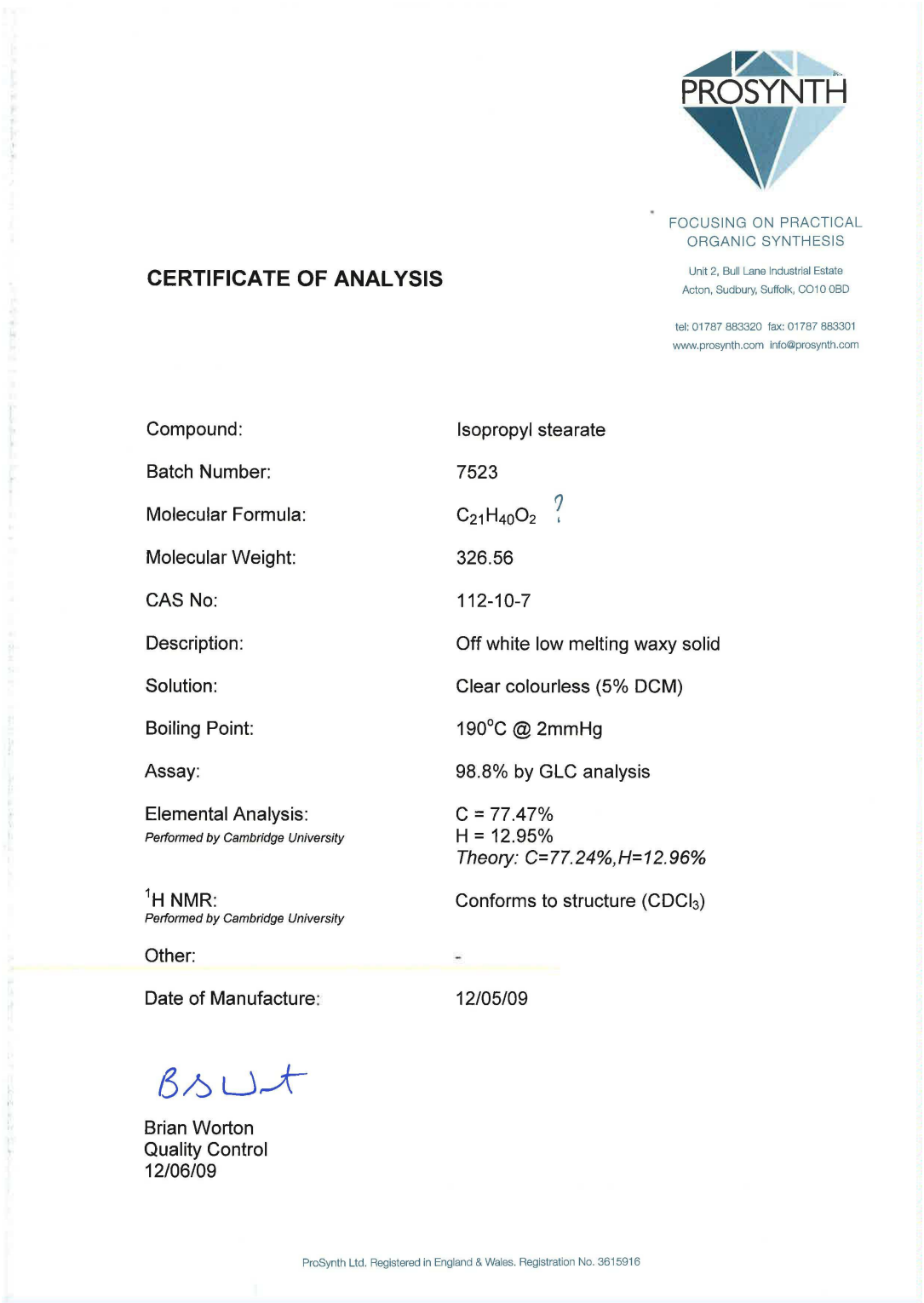

PROSYNTH

FOCUSING ON PRACTICAL ORGANIC SYNTHESIS

Unit 2, Bull Lane Industrial Estate
Acton, Sudbury, Suffolk, CO10 0BD

tel: 01787 883320 fax: 01787 883301
www.prosynth.com info@prosynth.com

CERTIFICATE OF ANALYSIS

Compound:	Isopropyl stearate
Batch Number:	7523
Molecular Formula:	$C_{21}H_{40}O_2$?
Molecular Weight:	326.56
CAS No:	112-10-7
Description:	Off white low melting waxy solid
Solution:	Clear colourless (5% DCM)
Boiling Point:	190°C @ 2mmHg
Assay:	98.8% by GLC analysis
Elemental Analysis: *Performed by Cambridge University*	C = 77.47% H = 12.95% *Theory: C=77.24%,H=12.96%*
^{1}H NMR: *Performed by Cambridge University*	Conforms to structure ($CDCl_3$)
Other:	-
Date of Manufacture:	12/05/09

BSWt

Brian Worton
Quality Control
12/06/09

ProSynth Ltd. Registered in England & Wales. Registration No. 3615916

Figure D.9: *iso*-propyl stearate

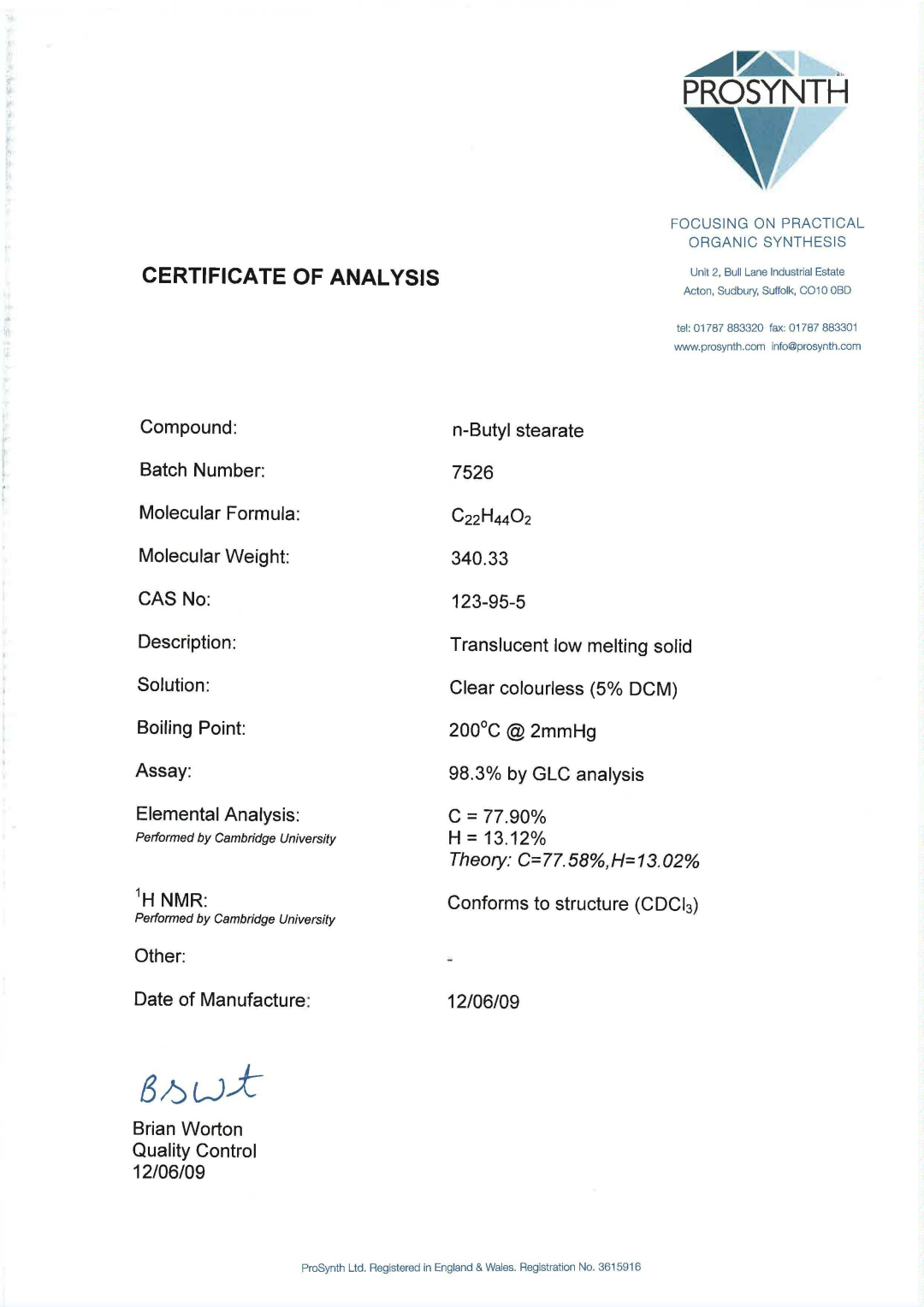

PROSYNTH

FOCUSING ON PRACTICAL ORGANIC SYNTHESIS

Unit 2, Bull Lane Industrial Estate
Acton, Sudbury, Suffolk, CO10 0BD

tel: 01787 883320 fax: 01787 883301
www.prosynth.com info@prosynth.com

CERTIFICATE OF ANALYSIS

Compound:	n-Butyl stearate
Batch Number:	7526
Molecular Formula:	$C_{22}H_{44}O_2$
Molecular Weight:	340.33
CAS No:	123-95-5
Description:	Translucent low melting solid
Solution:	Clear colourless (5% DCM)
Boiling Point:	200°C @ 2mmHg
Assay:	98.3% by GLC analysis
Elemental Analysis: *Performed by Cambridge University*	C = 77.90% H = 13.12% *Theory: C=77.58%,H=13.02%*
^{1}H NMR: *Performed by Cambridge University*	Conforms to structure ($CDCl_3$)
Other:	-
Date of Manufacture:	12/06/09

BSWt

Brian Worton
Quality Control
12/06/09

ProSynth Ltd. Registered in England & Wales. Registration No. 3615916

Figure D.10: *n*-butyl stearate

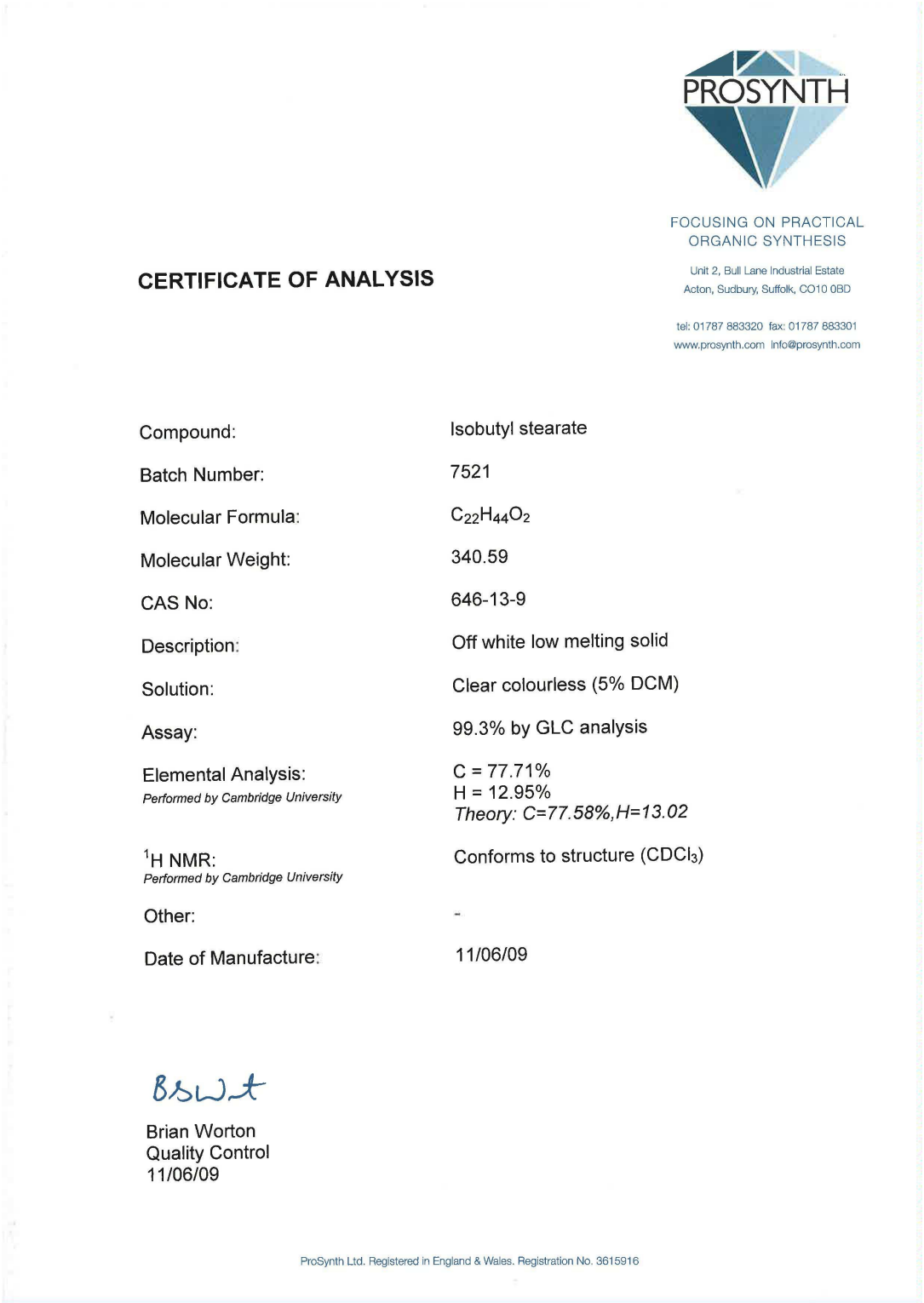

PROSYNTH

FOCUSING ON PRACTICAL ORGANIC SYNTHESIS

Unit 2, Bull Lane Industrial Estate
Acton, Sudbury, Suffolk, CO10 0BD

tel: 01787 883320 fax: 01787 883301
www.prosynth.com info@prosynth.com

CERTIFICATE OF ANALYSIS

Compound:	Isobutyl stearate
Batch Number:	7521
Molecular Formula:	$C_{22}H_{44}O_2$
Molecular Weight:	340.59
CAS No:	646-13-9
Description:	Off white low melting solid
Solution:	Clear colourless (5% DCM)
Assay:	99.3% by GLC analysis
Elemental Analysis: *Performed by Cambridge University*	C = 77.71% H = 12.95% *Theory: C=77.58%,H=13.02*
^{1}H NMR: *Performed by Cambridge University*	Conforms to structure ($CDCl_3$)
Other:	-
Date of Manufacture:	11/06/09

BSWt

Brian Worton
Quality Control
11/06/09

ProSynth Ltd. Registered in England & Wales. Registration No. 3615916

Figure D.11: *iso*-butyl stearate

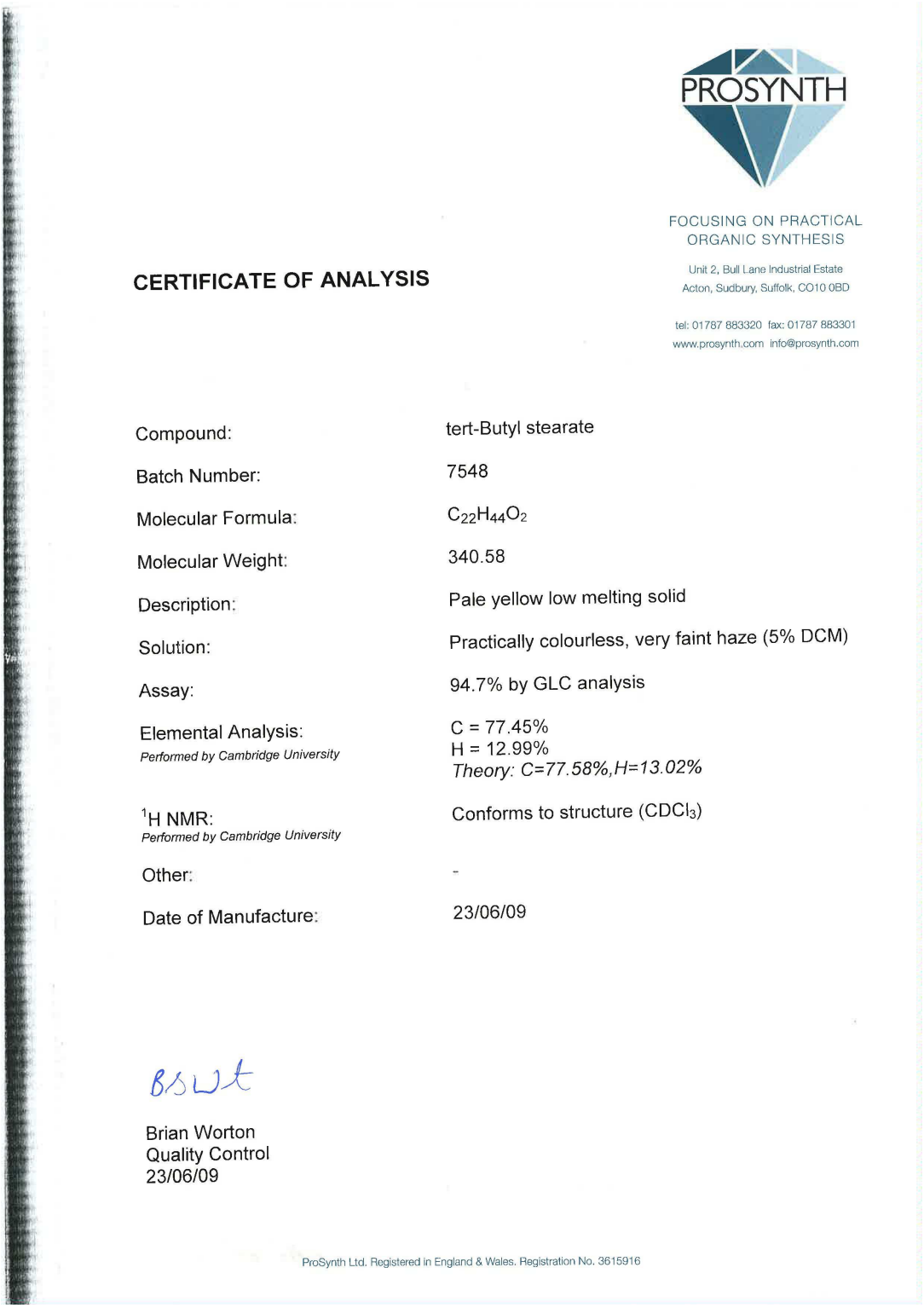

PROSYNTH

FOCUSING ON PRACTICAL ORGANIC SYNTHESIS

Unit 2, Bull Lane Industrial Estate
Acton, Sudbury, Suffolk, CO10 0BD

tel: 01787 883320 fax: 01787 883301
www.prosynth.com info@prosynth.com

CERTIFICATE OF ANALYSIS

Compound:	tert-Butyl stearate
Batch Number:	7548
Molecular Formula:	$C_{22}H_{44}O_2$
Molecular Weight:	340.58
Description:	Pale yellow low melting solid
Solution:	Practically colourless, very faint haze (5% DCM)
Assay:	94.7% by GLC analysis
Elemental Analysis: *Performed by Cambridge University*	C = 77.45% H = 12.99% *Theory: C=77.58%,H=13.02%*
^{1}H NMR: *Performed by Cambridge University*	Conforms to structure ($CDCl_3$)
Other:	-
Date of Manufacture:	23/06/09

BSWt

Brian Worton
Quality Control
23/06/09

ProSynth Ltd. Registered in England & Wales. Registration No. 3615916

Figure D.12: *tert*-butyl stearate

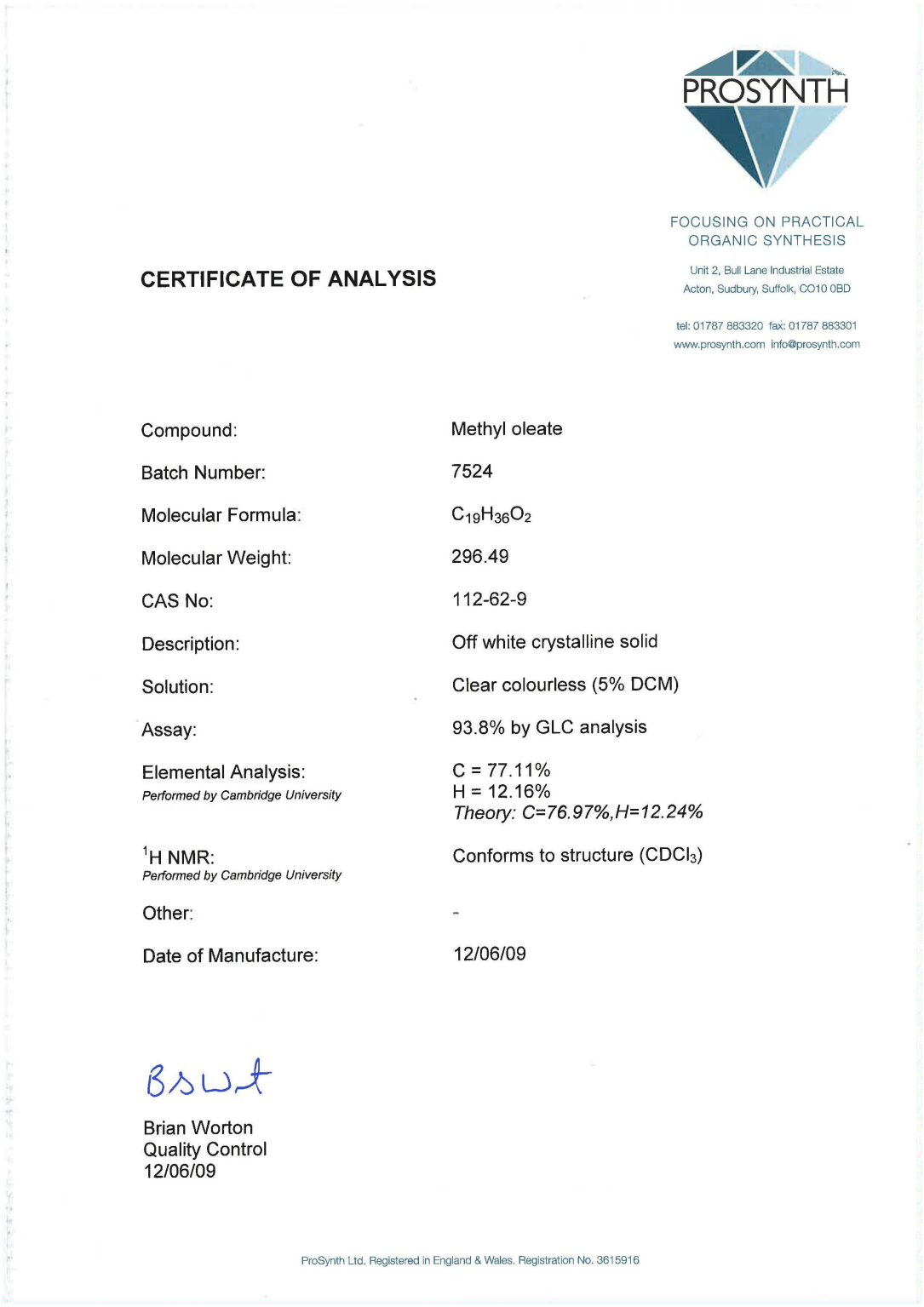

PROSYNTH

FOCUSING ON PRACTICAL ORGANIC SYNTHESIS

Unit 2, Bull Lane Industrial Estate
Acton, Sudbury, Suffolk, CO10 0BD

tel: 01787 883320 fax: 01787 883301
www.prosynth.com info@prosynth.com

CERTIFICATE OF ANALYSIS

Compound:	Methyl oleate
Batch Number:	7524
Molecular Formula:	$C_{19}H_{36}O_2$
Molecular Weight:	296.49
CAS No:	112-62-9
Description:	Off white crystalline solid
Solution:	Clear colourless (5% DCM)
Assay:	93.8% by GLC analysis
Elemental Analysis: *Performed by Cambridge University*	C = 77.11% H = 12.16% *Theory: C=76.97%,H=12.24%*
^{1}H NMR: *Performed by Cambridge University*	Conforms to structure ($CDCl_3$)
Other:	-
Date of Manufacture:	12/06/09

BSWT

Brian Worton
Quality Control
12/06/09

ProSynth Ltd. Registered in England & Wales. Registration No. 3615916

Figure D.13: methyl oleate

Table D.1: Synthesised ester measured properties

Test	Gross Calorific Value	Nett Calorific Value	Hydrogen	Sulphur Content	Nitrogen	Oxygen
Method	IP 12	Calculated from IP 12	ASTM D5291	IP 490	ASTM D5762	Elemental Analysis
Units	MJ/kg	MJ/kg	% (m/m)	mg/kg	mg/kg	% (m/m)
tert-butyl stearate	40.88	38.10	13.10	139	940	8.9
iso-butyl stearate	40.10	38.06	13.36	8.4	6.5	9.0
iso-butyl stearate	40.78	37.96	13.28	12.5	2.8	9.6
methyl oleate	40.06	37.42	12.38	3.3	7.3	10.4
n-butyl stearate	41.06	38.40	12.41	18.6	7.4	9.2
n-propyl stearate	40.54	37.72	13.29	23.6	-	-

Analysis performed by Intertek.

D.3. Carbonate esters

Key Organics
The right side of the Equation

Highfield Road Industrial Estate
Camelford Cornwall PL32 9RA
United Kingdom
Telephone +44(0)1840 212137
Fax +44(0)1840 213712
sales@keyorganics.net

Certificate of Analysis

Key Organics Sample ID:	**ME-0237**
CAS Number:	N/A
Name:	**Di-*n*-butyl carbonate**

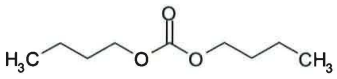

MF:	$C_9H_{18}O_3$
MW:	174.24
MP:	N/A
Manufacture date:	23rd November 2010
Certificate date:	10th January 2011
Retest date:	22nd November 2013

Test	**Standard**	**Result**
Identification	^{1}H NMR is consistent with structure	Complies
Purity	Assessed by GC >98%	Complies
TOF MS	Mass consistent with structure	Complies

Conclusion The material complies with the specification

Authorised

Dr Tim Edwards
Analyst

Registered in England No. 2055784 Registered Office Key Organics Ltd 69 Grosvenor Street, London W1K 3BP VAT Reg. No. GB 441 2642 78

Figure D.14: di-*n*-butyl carbonate

Key Organics
The right side of the Equation

Highfield Road Industrial Estate
Camelford Cornwall PL32 9RA
United Kingdom
Telephone +44(0)1840 212137
Fax +44(0)1840 213712
sales@keyorganics.net

Certificate of Analysis

Key Organics Sample ID: **ME-0714**

CAS Number: N/A

Name: **Di-*sec* butyl carbonate**

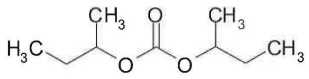

MF: $C_9H_{18}O_3$
MW: 174.24
MP: N/A
Manufacture date: 6th January 2011
Certificate date: 10th January 2011
Retest date: 5th January 2014

Test	Standard	Result
Identification	^{1}H NMR is consistent with structure	Complies
Purity	Assessed by GC >98%	Complies
TOF MS	Mass consistent with structure	Complies

Conclusion The material complies with the specification

Authorised

Dr Tim Edwards
Analyst

Figure D.15: di-1-methyl-propyl carbonate

Key Organics
The right side of the Equation

Highfield Road Industrial Estate
Camelford Cornwall PL32 9RA
United Kingdom
Telephone +44(0)1840 212137
Fax +44(0)1840 213712
sales@keyorganics.net

Certificate of Analysis

Key Organics Sample ID: **ME-0713**

CAS Number: N/A

Name: **Di-isobutyl carbonate**

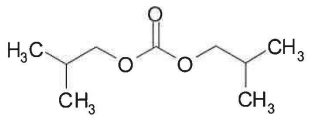

MF: $C_9H_{18}O_3$
MW: 174.24
MP: N/A
Manufacture date: 6th January 2011
Certificate date: 10th January 2011
Retest date: 5th January 2014

Test	Standard	Result
Identification	^{1}H NMR is consistent with structure	Complies
Purity	Assessed by GC >98%	Complies
TOF MS	Mass consistent with structure	Complies

Conclusion The material complies with the specification

Authorised

Dr Tim Edwards
Analyst

Registered in England No. 2055784 Registered Office Key Organics Ltd 69 Grosvenor Street, London W1K 3BP VAT Reg. No. GB 441 2642 78

Figure D.16: di-2-methyl-propyl carbonate

Key Organics
The right side of the Equation

Highfield Road Industrial Estate
Camelford Cornwall PL32 9RA
United Kingdom
Telephone +44(0)1840 212137
Fax +44(0)1840 213712
sales@keyorganics.net

Certificate of Analysis

Key Organics Sample ID:	**ME-0712**
CAS Number:	N/A
Name:	**Di-*tert*-butyl carbonate**

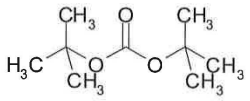

MF:	$C_9H_{18}O_3$
MW:	174.24
MP:	39 – 40°C
Manufacture date:	6th January 2011
Certificate date:	10th January 2011
Retest date:	5th January 2014

Test	**Standard**	**Result**
Identification	^{1}H NMR is consistent with structure	Complies
Purity	Assessed by GC >98%	Complies
TOF MS	Mass consistent with structure	Complies

Conclusion The material complies with the specification

Authorised

Dr Tim Edwards
Analyst

Figure D.17: di-tert-butyl carbonate

E. Data normalisation methods

E.1. Normalisation of data to constant ignition delay

The experiments in Chapter 6 in which ignition delay was removed as a variable produced five sets of results, at five values of constant ignition delay. An overlap existed between all adjacent sets of data; for every value of constant ignition delay at least one of the molecules tested at this ignition delay had also been tested at one, or more, of the other values of constant ignition delay. This was achieved by varying the dose of the ignition improver, 2 EHN, added.

Using the regression relationships of form $Y = Ax^b$ found between ignition delay and combustion and emission parameters in Figures 6.5 to 6.10, results from the five values of constant ignition delay were normalised to a single value of constant ignition delay. This was achieved by removing from the results the value which could be attributed to the difference in ignition delay.

For example, to normalise an experimental value of Y taken at ignition delay x (Y_{expx}) to ignition delay z (Y_{expz}):

$$Y_{expz} = Y_{expx} - ((A.x^b) - (A.z^b))$$

E.2. Normalisation of data to constant IMEP

In conducting the combustion experiments described in Chapter 7, quantities of *trans*-2-octene, *cis*-3-octene and *trans*-3-octene were extremely limited as they were specially synthesised and required to meet a high assay for the purpose of the experiments. Thus the study of these isomers was carried out in two experimental runs, several months apart. While every effort was made to maintain constant experimental conditions, a small error in the TDC calibration (0.4 CAD) of in-cylinder pressure DAQ resulted in the two experimental runs (one consisting of the reference fossil diesel, *n*-octane, 1-octene and *trans*-2-octene, and the second consisting of the reference fossil diesel, *n*-octane, 1-octene, *cis*-3-octene and *trans*-3-octene) being conducted at slightly different load conditions.

However, as the reference fossil diesel, *n*-octane and 1-octene were available in sufficient quantities to be tested on both occasions, it was possible to define a linear relationship (of the form $y = m.x + c$) between the ignition delays of *n*-octane, 1-

octene and the fossil diesel at an IMEP of 4.12 bar (y) and 3.96 bar (x). Therefore, utilising this linear relationship, Figure 7.2 shows the ignition delays of the octene isomers, n - octane and the reference fossil diesel with data obtained during tests ran at 3.96 bar IMEP normalised for a load condition of 4.12 bar IMEP.

Data for the reference fossil diesel was omitted from the dataset utilised in obtaining the linear relationship to perform the normalisation for Figures 7.3 to 7.5. This data was excluded as when the engine experiments at an IMEP of 3.96 bar were performed, the reference diesel displayed a greater shift in ignition delay than the pure component fuels that were tested during both experimental runs, 0.5 CAD and 0.1 CAD for the diesel and pure component fuels respectively (Table 7.3). As ignition delay is known to be a primary driver of combustion phasing and emissions production, including the reference diesel data when deriving relationships for the normalisation of these variables would have distorted the aim of compensating for the differing load conditions of the experimental runs.

References

Allen E. Aaronson and Richard A. Matula. Diesel odor and the formation of aromatic hydrocarbons during the heterogeneous combustion of pure cetane in a single-cylinder diesel engine. *Symposium (International) on Combustion*, 13(1):471–481, 1971.

Sorahi Abedinifar, Keikhosro Karimi, Morteza Khanahmadi, and Mohammad J. Taherzadeh. Ethanol production by mucor indicus and rhizopus oryzae from rice straw by separate hydrolysis and fermentation. *Biomass and Bioenergy*, 33(5): 828–833, 2009.

Abollq Abollq, Kouakou Loukou, and Planche Henri. The density and cloud point of diesel oil mixtures with the straight vegetable oils (svo): Palm, cabbage palm, cotton, groundnut, copra and sunflower. *Biomass and Bioenergy*, 33(12):1653–1659, 2009.

Hakima Abou-Rachid, Karim E. Marrouni, and Serge Kaliaguine. Dft studies of the hydrogen abstraction from primary alcohols by o_2 in relation with cetane number data. *Journal of Molecular Structure: THEOCHEM*, 631(1G3):241–250, 2003.

A. L. Ahmad, N. H. M. Yasin, C. J. C. Derek, and J. K. Lim. Microalgae as a sustainable energy source for biodiesel production: A review. *Renewable and Sustainable Energy Reviews*, 15(1):584–593, 2011.

Kazunori Aizawa and Masahiro Kato. Vapor-liquid equilibrium determination by total pressure measurements for three binary systems made of 1,2-dimethoxyethane with toluene, methylcyclohexane, or (trifluoromethyl)benzene. *J. Chem. Eng. Data*, 36(2):159–161, Jul 1991.

Robert A. Alberty and Catherine A. Gehrig. Standard chemical thermodynamic properties of alkane isomer groups. *Journal of Physical and Chemical Reference Data*, 13(4):1173–1197, 1984.

A. Alexiou and A. Williams. Soot formation in shock-tube pyrolysis of toluene-n-heptane and toluene-iso-octane mixtures. *Fuel*, 74(2):153–158, 1995.

Enrique Alonso, Hernando Guerrero, Diego Montano, Carlos Lafuente, and H. Artigas. Thermophysical study of the n-hexane or n-heptane with 1-chloropropane systems. *Thermochimica Acta*, 525(1 to 2):71–77, 2011.

Recep Altin, Selim Cetinkaya, and Huseyin S. Yucesu. The potential of using vegetable oil fuels as fuel for diesel engines. *Energy Conversion and Management*, 42(5):529–538, 2001a.

Recep Altin, Selim Cetinkaya, and Huseyin S. Yucesu. The potential of using vegetable oil fuels as fuel for diesel engines. *Energy Conversion and Management*, 42(5):529–538, 2001b.

American Petroleum Instititute. Vol.26 iii, p.269. *Chemical Abstracts*, 1946.

B. P. Anand, C. G. Saravanan, and C. A. Srinivasan. Performance and exhaust emission of turpentine oil powered direct injection diesel engine. *Renewable Energy*, 35(6):1179–1184, 2010.

J. C. G. Andrae, P. Björnbom, R. F. Cracknell, and G. T. Kalghatgi. Autoignition of toluene reference fuels at high pressures modeled with detailed chemical kinetics. *Combustion and Flame*, 149(1G2):2–24, 2007.

Johan Andrae, David Johansson, Pehr Bjrnbom, Per Risberg, and Gautam Kalghatgi. Co-oxidation in the auto-ignition of primary reference fuels and n-heptane/toluene blends. *Combustion and Flame*, 140(4):267–286, 2005.

Balasaheb R. Arbad, Machhindra K. Lande, Nilesh N. Wankhede, and Dnyaneshwar S. Wankhede. Viscosities, ultrasonic velocities at (288.15 and 298.15) k, and refractive indices at (298.15) k of binary mixtures of 2,4,6-trimethyl-1,3,5-trioxane with dimethyl carbonate, diethyl carbonate, and propylene carbonate. *J. Chem. Eng. Data*, 51(1):68–72, Sep 2005.

Constantine Arcoumanis, Choongsik Bae, Roy Crookes, and Eiji Kinoshita. The potential of di-methyl ether (dme) as an alternative fuel for compression-ignition engines: A review. *Fuel*, 87(7):1014–1030, 2008.

J. Arregle, V. Bermdez, J. R. Serrano, and E. Fuentes. Procedure for engine transient cycle emissions testing in real time. *Experimental Thermal and Fluid Science*, 30 (5):485–496, 2006.

Alessia Arteconi, Alessandro Mazzarini, and Giovanni Di Nicola. Emissions from ethers and organic carbonate fuel additives: A review. *Water, Air, & Soil Pollution*, 221(1):405–423, 2011.

Shota Atsumi, Wendy Higashide, and James C. Liao. Direct photosynthetic recycling of carbon dioxide to isobutyraldehyde. *Nat Biotech*, 27(12):1177–1180, 2009.

Wilfrid Bach. Impact of increasing atmospheric co_2 concentrations on global climate: Potential consequences and corrective measures. *Environment International*, 2(4-6):215–228, 1979.

O. Badr and S. D. Probert. Environmental impacts of atmospheric nitrous oxide. *Applied Energy*, 44(3):197–231, 1993.

Akhil Bajaj, Purva Lohan, Prabhat N. Jha, and Rajesh Mehrotra. Biodiesel production through lipase catalyzed transesterification: An overview. *Journal of Molecular Catalysis B: Enzymatic*, 62(1):9–14, 2010.

George A. Ban-Weiss, J. Y. Chen, Bruce A. Buchholz, and Robert W. Dibble. A numerical investigation into the anomalous slight no_x increase when burning biodiesel; a new (old) theory. *Fuel Processing Technology*, 88(7):659–667, 2007.

C. D. Bannister, C. J. Chuck, M. Bounds, and J. G. Hawley. Oxidative stability of biodiesel fuel. *Proceedings of the Institution of Mechanical Engineers, Part D: Journal of Automobile Engineering*, 225(1):99–114, 2011.

B. K. Barnwal and M. P. Sharma. Prospects of biodiesel production from vegetable oils in india. *Renewable and Sustainable Energy Reviews*, 9(4):363–378, 2005.

M. Basinger, T. Reding, C. Williams, K. S. Lackner, and V. Modi. Compression ignition engine modifications for straight plant oil fueling in remote contexts: Modification design and short-run testing. *Fuel*, 89(10):2925–2938, 2010.

Simone Bastianoni, Fazio Coppola, Enzo Tiezzi, Andrea Colacevich, Francesca Borghini, and Silvano Focardi. Biofuel potential production from the orbetello lagoon macroalgae: A comparison with sunflower feedstock. *Biomass and Bioenergy*, 32(7):619–628, 2008.

F. Battin-Leclerc. Detailed chemical kinetic models for the low-temperature combustion of hydrocarbons with application to gasoline and diesel fuel surrogates. *Progress in Energy and Combustion Science*, 34(4):440–498, 2008.

Bayer. *Chem. Zentralbl*, 72(1):1302, 1901.

Pedro Benjumea, John R. Agudelo, and Andre . F. Agudelo. Effect of the degree of unsaturation of biodiesel fuels on engine performance, combustion characteristics, and emissions. *Energy Fuels*, 25(1):77–85, 2010.

Raghu Betha and Rajasekhar Balasubramanian. Emissions of particulate-bound elements from stationary diesel engine: Characterization and risk assessment. *Atmospheric Environment*, 45(30):5273 – 5281, 2011.

D. B. Bigley and C. M. Wren. Carbonate pyrolysis. part iii. the gas-phase pyrolysis of some unsymmetrical and t-alkyl carbonates. *J. Chem. Soc. , Perkin Trans. 2*, (15):2359–2361, 1972.

W. Biltz, W. Fischer, and E. Wunnenberg. Molecular and atomic volumes. the volume requirements of crystalline organic compounds and low temperatures. *Z. Phys. Chem.*, Abt. A(151):13–55, 1930.

Joseph B. Binder, Michel J. Gray, James F. White, Z. C. Zhang, and Johnathan E. Holladay. Reactions of lignin model compounds in ionic liquids. *Biomass and Bioenergy*, 33(9):1122–1130, 2009.

G. Black, H. J. Curran, S. Pichon, J. M. Simmie, and V. Zhukov. Bio-butanol: Combustion properties and detailed chemical kinetic model. *Combustion and Flame*, 157(2):363–373, 2010.

Carl W. Bonhorst, Paul M. Althouse, and Howard O. Triebold. Esters of naturally occurring fatty acids - physical properties of methyl, propyl, and isopropyl esters of c6 to c18 saturated fatty acids. *Industrial & Engineering Chemistry*, 40(12): 2379–2384, Feb 1948.

M. E. Borges and L. Diaz. Recent developments on heterogeneous catalysts for biodiesel production by oil esterification and transesterification reactions: A review. *Renewable and Sustainable Energy Reviews*, 16(5):2839–2849, 2012.

BOSCH. *Automotive Handbook*. Wiley-Blackwell, 6th edition, 2004.

R. Bounaceur, V. Warth, B. Sirjean, P. A. Glaude, R. Fournet, and F. Battin-Leclerc. Influence of the position of the double bond on the autoignition of linear alkenes at low temperature. *Proceedings of the Combustion Institute*, 32(1):387–394, 2009.

Sydney T. Bowden and Emil T. Butler. 13. intermolecular forces in liquid systems. part ii. viscosity, surface tension, and parachor relationships in binary systems. *J. Chem. Soc.*, pages 79–83, 1939.

Craig T. Bowman. Kinetics of pollutant formation and destruction in combustion. *Progress in Energy and Combustion Science*, 1(1):33–45, 1975.

G. N. Brown and Waldemar T. Ziegler. Temperature dependence of excess thermodynamic properties of ethanol + n-heptane and 2-propanol + n-heptane solutions. *J. Chem. Eng. Data*, 24(4):319–330, Jul 1979.

Thomas J. Bruno, Arron Wolk, Alexander Naydich, and Marcia L. Huber. Composition-explicit distillation curves for mixtures of diesel fuel with dimethyl carbonate and diethyl carbonate. *Energy Fuels*, 23(8):3989–3997, 2009.

Bruce A. Buchholz, Charles J. Mueller, Ansis Upatnieks, Glen C. Martin, William J. Pitz, and Charles K. Westbrook. Using carbon-14 isotope tracing to investigate molecular structure effects of the oxygenate dibutyl maleate on soot emissions from a di diesel engine. *SAE Technical Paper Series*, pages 2004–01–1849, 2004.

Cambustion. CAMBUSTION DMS500 Mk II transient engine particulate analyser, 2010. http://www.cambustion.com , Last Update 15.10.2002, Downloaded on the 12.06.2010.

Kenneth N. Campbell and Lawrence T. Eby. The reduction of multiple carbon - carbon bonds. iii. further studies on the preparation of olefins from acetylenes1,2. *Journal of the American Chemical Society*, 63(10):2683–2685, Mar 1941.

Peter K. Campbell, Tom Beer, and David Batten. Life cycle assessment of biodiesel production from microalgae in ponds. *Bioresource Technology*, 102(1):50–56, 2011.

Keri B. Cantrell, Thomas Ducey, Kyoung S. Ro, and Patrick G. Hunt. Livestock waste-to-bioenergy generation opportunities. *Bioresource Technology*, 99 (17):7941–7953, 2008.

J. V. Champion and G. H. Meeten. Flow birefringence in simple liquids. *Trans. Faraday Soc.*, 64:238–247, 1968.

Gen Chen, Wu Yu, Jin Fu, Jun Mo, Zuohua Huang, Jiuzhong Yang, Zhandong Wang, Hanfeng Jin, and Fei Qi. Experimental and modeling study of the effects of adding oxygenated fuels to premixed n-heptane flames. *Combustion and Flame*, 159(7):2324–2335, 2012.

C. S. Cheung, Ruijun Zhu, and Zuohua Huang. Investigation on the gaseous and particulate emissions of a compression ignition engine fueled with diesel-dimethyl carbonate blends. *Science of The Total Environment*, 409(3):523–529, 2011.

Yusuf Chisti. Biodiesel from microalgae. *Biotechnology Advances*, 25(3):294–306, Jun 2007.

H. K. Ciezki and G. Adomeit. Shock-tube investigation of self-ignition of n-heptane-air mixtures under engine relevant conditions. *Combustion and Flame*, 93(4): 421–433, 1993.

Fabio Comelli and Romolo Francesconi. Isothermal vaporgliquid equilibria measurements, excess molar enthalpies, and excess molar volumes of dimethyl carbonate + methanol, + ethanol, and + propan-1-ol at 313.15 k. *J. Chem. Eng. Data*, 42 (4):705–709, Sep 1997.

Leonidas Constantinou and Rafiqul Gani. New group contribution method for estimating properties of pure compounds. *AIChE J.*, 40(10):1697–1710, 1994.

J. M. Cruz, A. S. Ogunlowo, W. J. Chancellor, and J. R. Goss. Vegetable oils as fuels for diesel engines. *Resources and Conservation*, 6(1):69–74, 1981.

C. F. Cullis, A. Fish, and J. F. Gibson. The spontaneous ignition of mixture of n-heptane and 1-heptene in oxygen. *Proceedings of the Royal Society of London. Series A, Mathematical and Physical Sciences*, 311(1505):253–266, 1969.

Silvio C. A. de Almeida, Carlos R. Belchior, Marcos V. G. Nascimento, Leonardo d. Vieira, and Guilherme Fleury. Performance of a diesel generator fuelled with palm oil. *Fuel*, 81(16):2097–2102, 2002.

John. E. Dec. A conceptual model of di diesel injection based on laser-sheet imaging. *SAE Technical Paper Series*, page 970873, 1997.

F. Delrue, P. A. Setier, C. Sahut, L. Cournac, A. Roubaud, G. Peltier, and A. K. Froment. An economic, sustainability, and energetic model of biodiesel production from microalgae. *Bioresource Technology*, 111(0):191–200, 2012.

V. M. Dembitsky, I. Dor, I. Shkrob, and M. Aki. Branched alkanes and other apolar compounds produced by the cyanobacterium microcoleus vaginatus from the negev desert. *Russian Journal of Bioorganic Chemistry*, 27(2):110–119, 2001.

Ayhan Demirbas and M. Fatih Demirbas. Importance of algae oil as a source of biodiesel. *Energy Conversion and Management*, 52(1):163–170, 2011.

Dongshun Deng, Haoran Li, and Shijun Han. Isobaric (vapour+liquid) equilibria of (linalool+1-propanol) and (linalool+1-butanol). *The Journal of Chemical Thermodynamics*, 34(9):1431–1437, 2002.

D. Deshmukh, A. Madan Mohan, T. N. C. Anand, and R. V. Ravikrishna. Spray characterization of straight vegetable oils at high injection pressures. *Fuel*, 97(0): 879–883, 2012.

Di Sante. Measurements of the auto-ignition of n-heptane/toluene mixtures using a rapid compression machine. *Combustion and Flame*, 159(1):55–63, 2012.

Domanska. Phase equilibria and volumetric properties in binary mixtures containing branched chain ethers (methyl 1,1-dimethylethyl ether or ethyl 1,1-dimethylethyl ether or methyl 1,1-dimethylpropyl ether or ethyl 1,1-dimethylpropyl ether). *J. Chem. Eng. Data*, 44(5):974, 1999.

Daniel C. Ducat, Jeffrey C. Way, and Pamela A. Silver. Engineering cyanobacteria to generate high-value products. *Trends in Biotechnology*, 29(2):95–103, 2011.

Mary J. Dunlop, Zain Y. Dossani, Heather L. Szmidt, Hou C. Chu, Taek S. Lee, Jay D. Keasling, Masood Z. Hadi, and Aindrila Mukhopadhyay. Engineering microbial biofuel tolerance and export using efflux pumps. *Mol Syst Biol*, 7, 2011.

Brian C. Dunn, Catherine Guenneau, Steven A. Hilton, Jorg Pahnke, Edward M. Eyring, Jacek Dworzanski, Henk L. C. Meuzelaar, J. Z. Hu, Mark S. Solum, and Ronald J. Pugmire. Production of diethyl carbonate from ethanol and carbon monoxide over a heterogeneous catalyst. *Energy Fuels*, 16(1):177–181, Oct 2001.

T. P. Durrett, C. Benning, and J. Ohlrogge. Plant triacylglycerols as feedstocks for the production of biofuels. *The Plant Journal*, 54(4):593–607, 2008.

R. W. e. al. Schiessler. Doc. 4597. *Amer. Doc. Inst*, 1945.

Ghassan Matta el Ammouri, Rachid Janati-Idrissi, Jean M. Rambourg, Henri Petitdemange, and R. Gay. Acetone butanol fermentation by a clostridium acetobutylicum mutant with high solvent productivity. *Biomass*, 10(2):109–119, 1986.

Shayla K. Emran, George R. Newkome, Claus D. Weis, and Julie P. Harmon. Molecular relaxations in ester-terminated, amide-based dendrimers. *J. Polym. Sci. B Polym. Phys.*, 37(16):2025–2038, 1999.

Josef Ernst, William S. Sheldrick, and Jurgen H. Fuhrhop. Die kristallstruktur des squalens. *Angewandte Chemie*, 88(24):851–851, 1976.

Bernat Esteban, Jordi R. Riba, Grau Baquero, Rita Puig, and Antoni Rius. Characterization of the surface tension of vegetable oils to be used as fuel in diesel engines. *Fuel*, 102(0):231–238, 2012a.

Bernat Esteban, Jordi R. Riba, Grau Baquero, Antoni Rius, and Rita Puig. Temperature dependence of density and viscosity of vegetable oils. *Biomass and Bioenergy*, 42(0):164–171, 2012b.

European Biodiesel Board. 2009-2010: Eu biodiesel industry restrained growth in challenging times. Report, 2010.

European Commission. amending directive 98/70/ec relating to the quality of petrol and diesel fuels and amending directive 2009/28/ec on the promotion of the use of energy from renewable sources. Report, 2012.

European Union. Euro 5 and euro 6 standards: reduction of pollutant emissions from light vehicles. Online Source, 2010.

Thaddeus C. Ezeji, Nasib Qureshi, and Hans P. Blaschek. Bioproduction of butanol from biomass: from genes to bioreactors. *Current Opinion in Biotechnology*, 18 (3):220–227, 2007.

G. M. Faeth. Current status of droplet and liquid combustion. *Progress in Energy and Combustion Science*, 3(4):191–224, 1977.

Filipe X. Feitosa, Ana C. Caetano, Tamires B. Cidade, and Hosiberto B. de Sant-GAna. Viscosity and density of binary mixtures of ethyl alcohol with n-alkanes (c6, c8, and c10). *J. Chem. Eng. Data*, 54(10):2957–2963, Sep 2009.

C. P. Fenimore. Formation of nitric oxide in premixed hydrocarbon flames. *Symposium (International) on Combustion*, 13(1):373–380, 1971.

C. P. Fenimore. Formation of nitric oxide from fuel nitrogen in ethylene flames. *Combustion and Flame*, 19(2):289–296, 1972.

Bethany C. Fisher, Anthony J. Marchese, John Volckens, Taehyoung Lee, and Jeffrey L. Collet. Measurement of gaseous and particulate emissions from algae-based fatty acid methyl esters. *SAE Technical Paper Series*, 2011.

Romolo Francesconi, Carlo Castellari, and Fabio Comelli. Densities, viscosities, refractive indices, and excess molar enthalpies of methyl tert-butyl ether + components of pine resins and essential oils at 298.15 k. *J. Chem. Eng. Data*, 46(6): 1520–1525, Jun 2001.

Z. Franco and Q. D. Nguyen. Flow properties of vegetable oil-diesel fuel blends. *Fuel*, 90(2):838–843, 2011.

Alessio Frassoldati, Alberto Cuoci, Tiziano Faravelli, Ulrich Niemann, Eliseo Ranzi, Reinhard Seiser, and Kalyanasundaram Seshadri. An experimental and kinetic modeling study of n-propanol and iso-propanol combustion. *Combustion and Flame*, 157(1):2–16, 2010.

Brian J. Gallagher. The economics of producing biodiesel from algae. *Renewable Energy*, 36(1):158–162, 2011.

Jeroen Geuens, Jennifer M. Kremsner, Bernd A. Nebel, Sigurd Schober, Roger A. Dommisse, Martin Mittelbach, Serge Tavernier, C. O. Kappe, and Bert U. W.

Maes. Microwave-assisted catalyst-free transesterification of triglycerides with 1-butanol under supercritical conditions. *Energy Fuels*, 22(1):643–645, 2008.

Augustus H. Gill and Forest P. Dexter. Viscosity of esters of saturated alphatic acids - relation to the synthesis of fine lubricating oils. *Industrial & Engineering Chemistry*, 26(8):881–881, Sep 1934.

Pierre A. Glaude, William J. Pitz, and Murray J. Thomson. Chemical kinetic modeling of dimethyl carbonate in an opposed-flow diffusion flame. *Proceedings of the Combustion Institute*, 30(1):1111–1118, 2005.

UK Government. The renewable transport fuel obligations order 2007. Statute, 2007.

Michael S. Graboski and Robert L. McCormick. Combustion of fat and vegetable oil derived fuels in diesel engines. *Progress in Energy and Combustion Science*, 24 (2):125–164, 1998.

Kenneth W. Greenlee and Vincent G. Wiley. Geometry of olefins and diolefins. i1. *The Journal of Organic Chemistry*, 27(7):2304–2307, May 1962.

J. F. Griffiths, P. A. Halford-Maw, and D. J. Rose. Fundamental features of hydrocarbon autoignition in a rapid compression machine. *Combustion and Flame*, 95 (3):291–306, 1993.

Gurvich. *Journal of applied chemistry of the USSR [0021-888X]*, 39(2):351, 1966.

Kevin J. Harrington. Chemical and physical properties of vegetable oil esters and their effect on diesel fuel performance. *Biomass*, 9(1):1–17, 1986.

D. Harrop, A. J. Head, and G. B. Lewis. Thermodynamic properties of organic oxygen compounds 22. enthalpies of combustion of some aliphatic ketones. *The Journal of Chemical Thermodynamics*, 2(2):203–210, 1970.

M. Hartmann, I. Gushterova, M. Fikri, C. Schulz, R. Schie+l, and U. Maas. Autoignition of toluene-doped n-heptane and iso-octane/air mixtures: High-pressure shock-tube experiments and kinetics modeling. *Combustion and Flame*, 158(1): 172–178, 2011.

Albert L. Henne and Kenneth W. Greenlee. Hydrogenation of the triple bond1. *Journal of the American Chemical Society*, 65(10):2020–2023, Apr 1943.

J. Herzler, M. Fikri, K. Hitzbleck, R. Starke, C. Schulz, P. Roth, and G. T. Kalghatgi. Shock-tube study of the autoignition of n-heptane/toluene/air mixtures at intermediate temperatures and high pressures. *Combustion and Flame*, 149(1G2):25–31, 2007.

Joshua S. Heyne, Andre . L. Boehman, and Steven Kirby. Autoignition studies of trans- and cis-decalin in an ignition quality tester (iqt) and the development of a high thermal stability unifuel/single battlefield fuel. *Energy Fuels*, 23(12): 5879–5885, 2009.

John B. Heywood. Automotive engines and fuels: A review of future options. *Progress in Energy and Combustion Science*, 7(3):155–184, 1981.

John B. Heywood. *Internal Combustion Engine Fundementals*. McGraw-Hill Book Company, international edition, 1988.

Toshihiko Hiaki, Kenji Takahashi, Tomoya Tsuji, Masaru Hongo, and Kazuo Kojima. Vapor-liquid equilibria of ethanol + octane at 343.15 k and 1-propanol + octane at 358.15 k. *J. Chem. Eng. Data*, 40(1):271–273, Apr 1995.

Seth R. Hoffman and John Abraham. A comparative study of n-heptane, methyl decanoate, and dimethyl ether combustion characteristics under homogeneous-charge compression-ignition engine conditions. *Fuel*, 88(6):1099–1108, 2009.

D Hopfe. *Data Compilation of FIZ CHEMIE, Germany*. 1990.

Horiba Instruments. *MEXA 9100HEGR instructions manual*. Horiba Instruments, Kyoto, Japan, 1984.

George W. Huber, Sara Iborra, and Avelino Corma. Synthesis of transportation fuels from biomass: Chemistry, catalysts, and engineering. *Chemical Reviews*, 106(9):4044–4098, 2006.

Walter E. Huggett. Levo-piperitone. *J. Chem. Technol. Biotechnol.*, 60(3):67–68, 1941.

R. Hughes and A. S. Prodhan. The combustion of the n-pentenes in the cool flame region. *Combustion and Flame*, 20(3):297–301, 1973.

Shin i. Fujita, Bhalchandra M. Bhanage, Yutaka Ikushima, and Masahiko Arai. Synthesis of dimethyl carbonate from carbon dioxide and methanol in the presence of methyl iodide and base catalysts under mild conditions: effect of reaction conditions and reaction mechanism. *Green Chemistry*, 3(2):87–91, 2001.

Institute of Petroleum. Ip 12: Determination of specific energy. Generic, 2001.

International Energy Agency. Co_2 emissions from fuel combustion *highlights*. Technical report, International Energy Agency, 2012.

Yoshio Iwai, Noriaki Hosotani, Tatsuo Morotomi, Yoshio Koga, and Yasuhiko Arai. High-pressure vapor-liquid equilibria for carbon dioxide + linalool. *J. Chem. Eng. Data*, 39(4):900–902, Jun 1994.

Oscar Jacobsen. Untersuchung der fleischflussigkeit von phocaena communis. *Justus Liebigs Annalen der Chemie*, 157(2):227–232, 1871.

E. Jimenez, C. Franjo, L. Segade, J. L. Legido, and M. I. P. Andrade. Viscosities and densities for the 1-propanol + *n*-heptane system at several temperatures. *Journal of Solution Chemistry*, 27(6):569–579, 1998.

Michael B. Johnson and Zhiyou Wen. Production of biodiesel fuel from the microalga schizochytrium limacinum by direct transesterification of algal biomass. *Energy Fuels*, 23(10):5179–5183, 2009.

Rajabathar Jothiramalingam and Ming K. Wang. Review of recent developments in solid acid, base, and enzyme catalysts (heterogeneous) for biodiesel production via transesterification. *Ind. Eng. Chem. Res.*, 48(13):6162–6172, Jan 2009.

F. Karaosmanoglu, G. Kurt, and T. zaktas. Long term ci engine test of sunflower oil. *Renewable Energy*, 19(1-2):219–221, 2000.

Tomaz Katrasnik, Ferdinand Trenc, and Samuel R. Opresnik. A new criterion to determine the start of combustion in diesel engines. *Journal of Engineering for Gas Turbines and Power*, 128(4):928–933, 2006.

Riita Keiski. Sustainable energy biofuels and biorefinery concept. Slide, 2009.

Judith L. Kinderlerer, Paul V. Hatton, Amanda J. Chapman, and Malcolm E. Rose. Essential oil produced by chrysosporium xerophilum in coconut. *Phytochemistry*, 27(9):2761–2763, 1988.

Eiji Kinoshita. Combustion characteristics of a di diesel engine with palm oil butyl and isobutyl esters. *JSAE Powertrains, Fuels and Lubricants Meeting*, (2011-01-1937):460–466, 2011.

Knothe. A comprehensive evaluation of the melting points of fatty acids and esters determined by differential scanning calorimetry. *Journal of the American Oil Chemists' Society*, 86(9):843, 2009.

Gerhard Knothe, M. Bagby, and Thomas W. Ryan. Cetane numbers of fatty compounds: Influence of compound structure of various potential cetane improvers. *SAE Technical Paper Series*, (971681), 1997.

Gerhard Knothe, Andrew C. Matheaus, and Thomas W. Ryan. Cetane numbers of branched and straight-chain fatty esters determined in an ignition quality tester. *Fuel*, 82(8):971–975, 2003.

Gerhard Knothe, Christopher A. Sharp, and Thomas W. Ryan. Exhaust emissions of biodiesel, petrodiesel, neat methyl esters, and alkanes in a new technology engine. *Energy Fuels*, 20(1):403–408, 2006.

Svetlana A. Kozlova, Vladimir N. Emel'yanenko, Miglena Georgieva, Sergey P. Verevkin, Yury Chernyak, Benjamin SchSffner, and Armin Brner. Vapour pressure and enthalpy of vaporization of aliphatic dialkyl carbonates. *The Journal of Chemical Thermodynamics*, 40(7):1136–1140, 2008.

Brian J. Krohn, Clayton V. McNeff, Bingwen Yan, and Daniel Nowlan. Production of algae-based biodiesel using the continuous catalytic mcgyan- process. *Bioresource Technology*, 102(1):94–100, 2011.

P. G. Krouwel, W. J. Groot, N. W. F. Kossen, and W. F. M. van der Laan. Continuous isopropanol-butanol-ethanol fermentation by immobilized clostridium beijerinckii cells in a packed bed fermenter. *Enzyme and Microbial Technology*, 5(1): 46–54, 1983.

Ajit A. Kulkarni, Kraemer D. Luks, and James P. Kohn. Phase-equilibriums behavior of systems carbon dioxide-2-methylnaphthalene and carbon dioxide-n-decane-2-methylnaphthalene. *J. Chem. Eng. Data*, 19(4):349–354, Sep 1974.

Nicos Ladommatos, Paul Rubenstein, and Paul Bennett. Some effects of molecular structure of single hydrocarbons on sooting tendency. *Fuel*, 75(2):114–124, 1996.

Man K. Lam, Keat T. Lee, and Abdul R. Mohamed. Homogeneous, heterogeneous and enzymatic catalysis for transesterification of high free fatty acid oil (waste cooking oil) to biodiesel: A review. *Biotechnology Advances*, 28(4):500–518, Aug 2010.

Magin Lapuerta, Jose M. Herreros, Lisbeth L. Lyons, Reyes Garcia-Contreras, and Yolanda Briceno. Effect of the alcohol type used in the production of waste cooking oil biodiesel on diesel performance and emissions. *Fuel*, 87(15-16):3161–3169, 2008.

Magin Lapuerta, Octavio Armas, and Reyes Garcia-Contreras. Effect of ethanol on blending stability and diesel engine emissions. *Energy Fuels*, 23(9):4343–4354, 2009.

E. D. Larson and H. Jin. Biomass conversion to fischer - tropsch liquids: Preliminary energy balances. Elsiever Science, Ltd, 1999.

George A. Lavoie, John B. Heywood, and James C. Keck. Experimental and theoretical study of nitric oxide formation in internal combustion engines. *Combustion Science and Technology*, 1(4):313–326, 1970.

T. Laza and Bereczky. Basic fuel properties of rapeseed oil-higher alcohols blends. *Fuel*, 90(2):803–810, 2011.

M. Lecat. Azeotropes of ethyl urethane and other azeotropes. *C. R. Hebd. Seances Acad. Sci*, pages 217–273, 1943.

D. H. Lee. Algal biodiesel economy and competition among bio-fuels. *Bioresource Technology*, 102(1):43–49, 2011.

Joseph K. Lefkowitz, Joshua S. Heyne, Sang H. Won, Stephen Dooley, Hwan H. Kim, Francis M. Haas, Saeed Jahangirian, Frederick L. Dryer, and Yiguang Ju.

A chemical kinetic study of tertiary-butanol in a flow reactor and a counterflow diffusion flame. *Combustion and Flame*, 159(3):968–978, 2012.

Dennis Y. C. Leung, Xuan Wu, and M. K. H. Leung. A review on biodiesel production using catalyzed transesterification. *Applied Energy*, 87(4):1083–1095, 2010.

Rongsong Li, Zhi Ning, Jeffery Cui, Bhavraj Khalsa, Lisong Ai, Wakako Takabe, Tyler Beebe, Rohit Majumdar, Constantinos Sioutas, and Tzung Hsiai. Ultrafine particles from diesel engines induce vascular oxidative stress via jnk activation. *Free Radical Biology and Medicine*, 46(6):775 – 782, 2009.

G Liessmann, W Schmidt, and S Reiffarth. *Data compilation of the Saechsische Olefinwerke Boehlen, Germany*. 1995.

Lievens. *Bulletin des Socits chimiques belges [0037-9646]*, 33:127, 1924.

Cherng Y. Lin and Kuo H. Wang. Diesel engine performance and emission characteristics using three-phase emulsions as fuel. *Fuel*, 83(4-5):537–545, 2004.

Longinow. *Chem. Zentralbl*, 100:2631, 1929.

Jing Lu, Con Sheahan, and Pengcheng Fu. Metabolic engineering of algae for fourth generation biofuels production. *Energy Environ. Sci.*, 4(7):2451–2466, 2011.

Xingcai Lu, Libin Ji, Linlin Zu, Yuchun Hou, Cheng Huang, and Zhen Huang. Experimental study and chemical analysis of n-heptane homogeneous charge compression ignition combustion with port injection of reaction inhibitors. *Combustion and Flame*, 149(3):261–270, 2007.

Fangrui Ma and Milford A. Hanna. Biodiesel production: a review. *Bioresource Technology*, 70(1):1–15, 1999.

Vladimir Majer, V. Svoboda, H. V. Kehiaian, International Union of Pure, and Applied Chemistry. *Enthalpies of vaporization of organic compounds : a critical review and data compilation*. Blackwell Scientific, Oxford, 1985.

V. Makareviciene and P. Janulis. Environmental effect of rapeseed oil ethyl ester. *Renewable Energy*, 28(15):2395–2403, 2003.

Yu Maksimuk, Z. Antonova, and V. FesGko. Standard enthalpies of combustion and formation for fatty acid esters in the condensed state. *Russian Journal of Physical Chemistry A, Focus on Chemistry*, 86(2):170–174, 2012.

Margret Mansson. Enthalpies of combustion and formation of ethyl propionate and diethyl carbonate. *The Journal of Chemical Thermodynamics*, 4(6):865–871, 1972.

Robert L. McCormick, Michael S. Graboski, Teresa L. Alleman, Andrew M. Herring, and K. S. Tyson. Impact of biodiesel source material and chemical structure on emissions of criteria pollutants from a heavy-duty engine. *Environmental Science & Technology*, 35(9):1742–1747, 2001.

L. C. Meher, D. Vidya Sagar, and S. N. Naik. Technical aspects of biodiesel production by transesterification–a review. *Renewable and Sustainable Energy Reviews*, 10(3):248–268, 2006.

M. Mehl, W. J. Pitz, C. K. Westbrook, K. Yasunaga, C. Conroy, and H. J. Curran. Autoignition behavior of unsaturated hydrocarbons in the low and high temperature regions. In *Proceedings of the Combustion Institute*, volume 33, pages 201–208, 2011.

Marco Mehl, Guillaume Vanhove, William J. Pitz, and Eliseo Ranzi. Oxidation and combustion of the n-hexene isomers: A wide range kinetic modeling study. *Combustion and Flame*, 155(4):756–772, 2008.

Pramod S. Mehta and K. Anand. Estimation of a lower heating value of vegetable oil and biodiesel fuel. *Energy Fuels*, 23(8):3893–3898, 2009.

Juan A. Melero, M. M. Clavero, Guillermo Calleja, Alicia Garcia, Rube . Miravalles, and Tamara Galindo. Production of biofuels via the catalytic cracking of mixtures of crude vegetable oils and nonedible animal fats with vacuum gas oil. *Energy Fuels*, 2009.

James A. Miller and Craig T. Bowman. Mechanism and modeling of nitrogen chemistry in combustion. *Progress in Energy and Combustion Science*, 15(4):287–338, 1989.

R. Minetti, A. Roubaud, E. Therssen, M. Ribaucour, and L. R. Sochet. The chemistry of pre-ignition of n-pentane and 1-pentene. *Combustion and Flame*, 118(1-2): 213–220, 1999.

R. D. Misra and M. S. Murthy. Straight vegetable oils usage in a compression ignition engine: A review. *Renewable and Sustainable Energy Reviews*, 14(9):3005–3013, 2010.

Charles J. Mueller, Andre L. Boehman, and Glen C. Martin. An experimental investigation of the origin of increased no_x emissions when fueling a heavy-duty compression-ignition engine with soy biodiesel. *SAE Technical Paper Series*, pages 2009–01–1792, 2009.

Michael J. Murphy, Joshua D. Taylor, and Robert L. McCormick. Compendium of experimental cetane number data. *NREL/SR 540-36805*, 2004.

S. S. N. Murthy, Gangasharan, and S. K. Nayak. Novel differential scanning calorimetric studies of supercooled organic liquids. *J. Chem. Soc. , Faraday Trans.*, 89 (3):509–514, 1993.

S. N. Naik, Vaibhav V. Goud, Prasant K. Rout, and Ajay K. Dalai. Production of first and second generation biofuels: A comprehensive review. *Renewable and Sustainable Energy Reviews*, 14(2):578–597, 2010.

Govindarajan Natarajan and Dabir S. Viswanath. Enthalpy of vaporization and vapor pressure of benzene, toluene, p-xylene, and tetralin between 1 and 16 bar. *J. Chem. Eng. Data*, 30(2):137–140, Jul 1985.

National Institute of Standards and Technology. Nist chemistry webbook. Online Source, Feb 2010.

Y. R. Naves. Etudes sur les matieres vegetales volatiles. xliv. presence de nerolidol dans les huiles essentielles de papilionacees. (2eme communication). *HCA*, 30(1): 278–286, 1947.

Yves R. Naves and Paul Tullen. Etudes sur les les matieres vegetales volatiles clxxix. syntheses des cis- et trans-[methyl-2-propane-1]-yl-2-methyl-4-tetrahydropyrannes. *HCA*, 44(7):1867–1872, 1961.

Nefedov. *Bulletin of the Academy of Sciences of the USSR, Division of Chemical Sciences [0568-5230]*, 21:1575, 1972.

Noel De Nevers. *Air pollution control engineering*. McGraw-Hill, Inc., 1st edition, 1995.

O. M. I. Nwafor. Emission characteristics of diesel engine running on vegetable oil with elevated fuel inlet temperature. *Biomass and Bioenergy*, 27(5):507–511, 2004.

O. M. I. Nwafor and G. Rice. Performance of rapeseed oil blends in a diesel engine. *Applied Energy*, 54(4):345–354, 1996.

Hideyuki Ogawa, Taku Ibuki, Takayuki Minematsu, and Noboru Miyamoto. Diesel combustion and emissions of decalin as a high productivity gas-to-liquid fuel. *Energy Fuels*, 21(3):1517–1521, 2007.

Joan M. Ogden, Margaret M. Steinbugler, and Thomas G. Kreutz. A comparison of hydrogen, methanol and gasoline as fuels for fuel cell vehicles: implications for vehicle design and infrastructure development. *Journal of Power Sources*, 79(2): 143–168, 1999.

Chemeo online database. Chemeo online database. Online Source, Nov 2011.

J. Bevan Ott and J. Rex Goates. (solid + liquid) phase equilibria in binary mixtures containing benzene, a cycloalkane, an n-alkane, or tetrachloromethane an equation for representing (solid + liquid) phase equilibria. *The Journal of Chemical Thermodynamics*, 15(3):267–278, 1983.

Martin H. Oyevaar, Bill W. To, Michael F. Doherty, and Michael F. Malone. Process for continuous production of carbonate esters. Patent, 2000.

Michael A. Pacheco and Christopher L. Marshall. Review of dimethyl carbonate (dmc) manufacture and its characteristics as a fuel additive. *Energy Fuels*, 11(1): 2–29, Oct 1997.

Giancarlo Paret, Gianni Donnati, and Maurizio Ghirardini. Process for producing dimethyl carbonate and apparatus suitable for such purpose. Patent, 1996.

Pastushenko. Production of dialkyl carbonates from esters of orthoformic acid. *Journal of applied chemistry of the USSR [0021-888X]*, 56(10):2328, 1983.

P. P. Peralta-Yahya, M. Ouellet, R. Chan, A. Mukhopadhyay, J. D. Keasling, and T. S. Lee. Identification and microbial production of a terpene-based advanced biofuel. *Nat Commun.*, 2:483, 2011.

Pamela P. Peralta-Yahya, Fuzhong Zhang, Stephen B. del Cardayre, and Jay D. Keasling. Microbial engineering for the production of advanced biofuels. *Nature*, 488(7411):320–328, 2012.

Michael J. Pilling. *Low-temperature combustion and autoignition*, volume 35 of *Comprehensive chemical kinetics*. Elsevier, 1997.

Herman Pines, N. E. Hoffman, and V. N. Ipatieff. Studies in the terpene series. xx.1 the thermal isomerization of pinane at atmospheric pressure. *Journal of the American Chemical Society*, 76(17):4412–4416, Jun 1954.

S. Pinzi, I. L. Garcia, F. J. Lopez-Gimenez, M. D. Luque de Castro, G. Dorado, and M. P. Dorado. The ideal vegetable oil-based biodiesel composition: A review of social, economical and technical implications. *Energy Fuels*, 0(0), 2000.

S. Pinzi, D. Leiva, G. Arzamendi, L. M. Gandia, and M. P. Dorado. Multiple response optimization of vegetable oils fatty acid composition to improve biodiesel physical properties. *Bioresource Technology*, 102(15):7280–7288, 2011.

Kenneth S. Pitzer. The thermodynamics of n-heptane and 2,2,4-trimethylpentane, including heat capacities, heats of fusion and vaporization and entropies. *Journal of the American Chemical Society*, 62(5):1224–1227, Jul 1940.

Srinivasa K. Prabhu, Rohit K. Bhat, David L. Miller, and Nicholas P. Cernansky. 1-pentene oxidation and its interaction with nitric oxide in the low and negative temperature coefficient regions. *Combustion and Flame*, 104(4):377–390, 1996.

Maria J. Pratas, Samuel Freitas, Mariana B. Oliveira, Si . C. Monteiro, Alvaro S. Lima, and Joa . A. P. Coutinho. Densities and viscosities of fatty acid methyl and ethyl esters. *J. Chem. Eng. Data*, 55(9):3983–3990, Feb 2010.

E. W. Prosen and F. D. Rossini. Heats of combustion and formation of the paraffin hydrocarbons at 25 c. *Journal of Research of the National Bureau of Standards*, 38:263–267, 1945.

E. Pryde. Vegetable oils as diesel fuels: Overview. *Journal of the American Oil Chemists' Society*, 60(8):1557–1558, 1983.

C. D. Rakopoulos, D. C. Rakopoulos, E. G. Giakoumis, and A. M. Dimaratos. Investigation of the combustion of neat cottonseed oil or its neat bio-diesel in a hsdi diesel engine by experimental heat release and statistical analyses. *Fuel*, 89 (12):3814–3826, 2010.

D. C. Rakopoulos, C. D. Rakopoulos, E. G. Giakoumis, A. M. Dimaratos, and M. A. Founti. Comparative environmental behavior of bus engine operating on blends of diesel fuel with four straight vegetable oils of greek origin: Sunflower, cottonseed, corn and olive. *Fuel*, 90(11):3439–3446, 2011.

A. S. Ramadhas, S. Jayaraj, and C. Muraleedharan. Use of vegetable oils as i.c. engine fuelsga review. *Renewable Energy*, 29(5):727–742, 2004.

John Read and William J. Grubb. 76. researches in the menthone series. part xii. isolation and characterisation of the neoisomenthols. *J. Chem. Soc.*, pages 313–317, 1934.

Yi Ren, Wang, and Huang. Densities, surface tensions, and viscosities of diesel-oxygenate mixtures at the temperature 301.15 k. *Energy Fuels*, 21(3):1628–1630, Oct 2007.

Yi Ren, Zuohua Huang, Haiyan Miao, Yage Di, Deming Jiang, Ke Zeng, Bing Liu, and Xibin Wang. Combustion and emissions of a di diesel engine fuelled with diesel-oxygenate blends. *Fuel*, 87(12):2691–2697, 2008.

Ricardo. *The Ricardo/Cussons Standard Hydra Engine and Test Bed, Details of the Engine, Test Bed, and Control System*, 8th edition, October 1986.

John D. Rockenfeller and Frederick D. Rossini. Heats of combustion, isomerization, and formation of selected c7, c8 and c10 mono+olefin hydrocarbons1. *The Journal of Physical Chemistry*, 65(2):267–272, 1961.

Nam S. Roh, Brian C. Dunn, Edward M. Eyring, Ronald J. Pugmire, and Henk L. C. Meuzelaar. Production of diethyl carbonate from ethanol and carbon monoxide over a heterogeneous catalytic flow reactor. *Fuel Processing Technology*, 83(1G3): 27–38, 2003.

Frank Rosillo-Calle and Arnaldo Walter. Global market for bioethanol: historical trends and future prospects. *Energy for Sustainable Development*, 10(1):20–32, 2006.

A. B. Ross, P. Biller, M. L. Kubacki, H. Li, A. Lea-Langton, and J. M. Jones. Hydrothermal processing of microalgae using alkali and organic acids. *Fuel*, 89 (9):2234–2243, 2010.

M. Roy. Effect of n-heptane and n-decane on exhaust odour in direct injection diesel engines. *Proceedings of the Institution of Mechanical Engineers, Part D: Journal of Automobile Engineering*, 219(4):565–571, 2005.

Rozenthal. *Bulletin des Societes chimiques belges*, 45:621, 1936.

Mathew A. Rude and Andreas Schirmer. New microbial fuels: a biotech perspective. *Current Opinion in Microbiology*, 12(3):274–281, 2009.

Anne M. Ruffing. Engineered cyanobacteria: Teaching an old bug new tricks. *Bioengineered*, 2(3):136–149, 2011.

Rummens. *Recl. Trav. Chim. Pays-Bas*, 84:1003, 1965.

L. Ruzicka. Hohere terpenverbindungen ix. uber die totalsynthese des d, l-nerolidols und des farnesols. *HCA*, 6(1):492–502, 1923.

T. Ryan, L. Dodge, and T. Callahan. The effects of vegetable oil properties on injection and combustion in two different diesel engines. *Journal of the American Oil Chemists' Society*, 61(10):1610–1619, 1984.

Maurin Salamanca, Fanor Mondragon, Jhon R. Agudelo, Pedro Benjumea, and Alexander Santamaria. Variations in the chemical composition and morphology of soot induced by the unsaturation degree of biodiesel and a biodiesel blend. *Combustion and Flame*, 159(3):1100–1108, 2012.

K. C. Salooja. The role of aldehydes in combustion: Studies of the combustion characteristics of aldehydes and of their influence on hydrocarbon combustion processes. *Combustion and Flame*, 9(4):373–382, 1965.

K. C. Salooja. Combustion studies of olefins and of their influence on hydrocarbon combustion processes. *Combustion and Flame*, 12(5):401–410, 1968.

J. C. O. Santos, I. M. G. Santos, and A. G. Souza. Effect of heating and cooling on rheological parameters of edible vegetable oils. *Journal of Food Engineering*, 67 (4):401–405, 2005.

Cenk Sayin. Engine performance and exhaust gas emissions of methanol and ethanol-diesel blends. *Fuel*, 89(11):3410–3415, 2010.

E. Schjanberg. Die verbrennungswarmen und die refraktionsdaten einiger pentensaureeste. *Z. Phys. Chem.*, (178):274–281, 1937.

Schlenk. *Justus Liebigs Annalen der Chemie*, 727:1, 1969.

Matthew J. Scholz, Mark R. Riley, and Joel L. Cuello. Acid hydrolysis and fermentation of microalgal starches to ethanol by the yeast saccharomyces cerevisiae. *Biomass and Bioenergy*, 48(0):59–65, 2013.

Alessandro Schönborn. *Influence of the molecular structure of biofuels on combustion in a compression ignition engine*. PhD thesis, Univeristy College London, Torrington Place, London, United Kingdom, 2009.

Alessandro Schönborn, Nicos Ladommatos, John Williams, Robert Allan, and John Rogerson. Effects on diesel combustion of the molecular structure of potential synthetic bio-fuel molecules. *SAE Technical Paper Series*, pages 2007–24–0125, 2007.

Alessandro Schönborn, Nicos Ladommatos, and Choongsik Bae. Diffusion- and homogeneous-charge combustion of volatile ethers in a compression ignition engine. *Energy Fuels*, 23(12):5865–5878, 2009a.

Alessandro Schönborn, Nicos Ladommatos, John Williams, Robert Allan, and John Rogerson. The influence of molecular structure of fatty acid monoalkyl esters on diesel combustion. *Combustion and Flame*, 156(7):1396–1412, 2009b.

A. W. Schwab, M. O. Bagby, and B. Freedman. Preparation and properties of diesel fuels from vegetable oils. *Fuel*, 66(10):1372–1378, 1987.

Aikaterini Serdari, Euripides Lois, and Stamoulis Stournas. Impact of esters of mono- and dicarboxylic acids on diesel fuel quality. *Ind. Eng. Chem. Res.*, 38(9): 3543–3548, Sep 1999.

Serpinskii. *Zhurnal Fizicheskoi Khimii*, 28:1969, 1954.

Abbas A. Shaikh and Swaminathan Sivaram. Organic carbonates. *Chemical Reviews*, 96(3):951–976, Oct 1996.

E. G. Shay. Diesel fuel from vegetable oils: Status and opportunities. *Biomass and Bioenergy*, 4(4):227–242, 1993.

Hsi P. Shen, Justin Steinberg, Jeremy Vanderover, and Matthew A. Oehlschlaeger. A shock tube study of the ignition of n-heptane, n-decane, n-dodecane, and n-tetradecane at elevated pressures. *Energy Fuels*, 23(5):2482–2489, 2009.

S. S. Sidibq, J. Blin, G. Vaitilingom, and Y. Azoumah. Use of crude filtered vegetable oil as a fuel in diesel engines state of the art: Literature review. *Renewable and Sustainable Energy Reviews*, In Press, Corrected Proof, 2010.

Silbert. *Journal of the American Chemical Society*, 81:3244, 1959.

Amanda A. Silva, Rodrigo A. Reis, and Ma . L. L. Paredes. Density and viscosity of decalin, cyclohexane, and toluene binary mixtures at (283.15, 293.15, 303.15, 313.15, and 323.15) k. *J. Chem. Eng. Data*, 54(7):2067–2072, Jul 2009.

S. P. Singh and Dipti Singh. Biodiesel production through the use of different sources and characterization of oils and their esters as the substitute of diesel: A review. *Renewable and Sustainable Energy Reviews*, 14(1):200–216, 2010.

Ruizhi Song, Ke Li, Yang Feng, and Shenghua Liu. Performance and emission characteristics of dme engine with high ratio of egr. *Energy Fuels*, 23(11):5460–5466, 2009.

James G. Speight. *Lange's Handbook of Chemistry*. McGraw-Hill, 16th edition, 2005.

W. V. Steele, R. D. Chirico, S. E. Knipmeyer, A. Nguyen, and N. K. Smith. Thermodynamic properties and ideal-gas enthalpies of formation for dicyclohexyl sulfide, diethylenetriamine, di-n-octyl sulfide, dimethyl carbonate, piperazine, hexachloroprop-1-ene, tetrakis(dimethylamino)ethylene, n,ng-bis-(2-hydroxyethyl)ethylenediamine, and 1,2,4-triazolo[1,5-a]pyrimidine. *J. Chem. Eng. Data*, 42(6):1037–1052, Sep 1997.

W. Stiehl. Beitrage zur kenntniss des lemongrasols. *J. Prakt. Chem.*, 58(1):51–101, 1898.

Suwarno, F. Sitinjak, I. Suhariadi, and L. Imsak. Study on the characteristics of palm oil and it's derivatives as liquid insulating materials. In *Properties and Applications of Dielectric Materials, 2003. Proceedings of the 7th International Conference on*, volume 2, pages 495–498, 2003.

James P. Szybist, Andrq L. Boehman, Joshua D. Taylor, and Robert L. McCormick. Evaluation of formulation strategies to eliminate the biodiesel nox effect. *Fuel Processing Technology*, 86(10):1109–1126, 2005.

James P. Szybist, Juhun Song, Mahabubul Alam, and Andrq L. Boehman. Biodiesel combustion, emissions and emission control. *Fuel Processing Technology*, 88(7): 679–691, 2007.

Shigeyuki Tanaka, Ferran Ayala, James C. Keck, and John B. Heywood. Two-stage ignition in hcci combustion and hcci control by fuels and additives. *Combustion and Flame*, 132(1-2):219–239, 2003.

M. Tazerout, O. Le Corre, and S. Rousseau. Tdc determination in ic engines based on the thermodynamic analysis of the temperature-entropy diagram. *SAE TECHNICAL PAPER SERIES*, (1999-01-1489), 1999.

Thomsen. Stoechiometrie und verwandtschaftslehre. *Zeitschrift fuer Physikalische Chemie*, 52:343, 1905.

Jie S. Tian, Cheng X. Miao, Jin Q. Wang, Fei Cai, Ya Du, Yuan Zhao, and Liang N. He. Efficient synthesis of dimethyl carbonate from methanol, propylene oxide and co2 catalyzed by recyclable inorganic base/phosphonium halide-functionalized polyethylene glycol. *Green Chemistry*, 9(6):566–571, 2007.

J. Timmermans. The melting point of organic substances. *Bull. Soc. Chim. Belg.*, (36):502, 1927.

Noah I. Tracy, Daichuan Chen, Daniel W. Crunkleton, and Geoffrey L. Price. Hydrogenated monoterpenes as diesel fuel additives. *Fuel*, 88(11):2238–2240, 2009.

Transport Statistics. Uk transport greenhouse gas emissions. Technical report, Department for Transport, 2011.

Dale R. Tree and Kenth I. Svensson. Soot processes in compression ignition engines. *Progress in Energy and Combustion Science*, 33(3):272–309, 2007.

Kikuchi Tsujino. *Nippon Nogei Kagaku Kaishi*, 27:437, 1953.

Chein H. Tu, Hung Y. Hsian, Yi T. Chou, and Wen F. Wang. Vaporgliquid equilibria of methanol, ethanol, propan-2-ol, and 2-methylpropan-2-ol with a five-component hydrocarbon mixture at 101.3 kpa. *J. Chem. Eng. Data*, 46(5):1239–1243, Jul 2001.

Roland Tufeu, Pascale Subra, and Christine Plateaux. Contribution to the experimental determination of the phase diagrams of some (carbon dioxide+a terpene) mixtures. *The Journal of Chemical Thermodynamics*, 25(10):1219–1228, 1993.

Stephen Turns. *An introduction to combustion: Concepts and Applications*. McGraw Hill, 2nd edition, 2000.

Turowa-Poljak. *Journal of general chemistry of the USSR [0022-1279]*, 34:2654, 1964.

Byung H. Um and Young S. Kim. Review: A chance for korea to advance algal-biodiesel technology. *Journal of Industrial and Engineering Chemistry*, 15(1):1–7, 2009.

Osmano S. Valente, Mbrcio J. da Silva, Vanya M. D. Pasa, Carlos R. P. Belchior, and Josq R. Sodrq. Fuel consumption and emissions from a diesel power generator fuelled with castor oil and soybean biodiesel. *Fuel*, 89(12):3637–3642, 2010.

G. Vanhove, M. Ribaucour, and R. Minetti. On the influence of the position of the double bond on the low-temperature chemistry of hexenes. *Proceedings of the Combustion Institute*, 30(1):1065–1072, 2005.

G. Vanhove, G. Petit, and R. Minetti. Experimental study of the kinetic interactions in the low-temperature autoignition of hydrocarbon binary mixtures and a surrogate fuel. *Combustion and Flame*, 145(3):521–532, 2006.

K. Verbiezen, A. J. Donkerbroek, R. J. H. Klein-Douwel, A. P. van Vliet, P. J. M. Frijters, X. L. J. Seykens, R. S. G. Baert, W. L. Meerts, N. J. Dam, and J. J. ter Meulen. Diesel combustion: In-cylinder no concentrations in relation to injection timing. *Combustion and Flame*, 151(1-2):333–346, 2007.

Sergey P. Verevkin, Vladimir N. EmelGyanenko, and Svetlana A. Kozlova. Organic carbonates: Experiment and ab initio calculations for prediction of thermochemical properties. *The Journal of Physical Chemistry A*, 112(42):10667–10673, 2008.

Gemma Vicente, L. F. Bautista, Rosala Rodrguez, F. J. Gutiqrrez, Irantzu Sbdaba, Rosa M. Ruiz-Vbzquez, Santiago Torres-Martnez, and Victoriano Garre. Biodiesel production from biomass of an oleaginous fungus. *Biochemical Engineering Journal*, 48(1):22–27, 2009.

Gemma Vicente, L. F. Bautista, Francisco J. Gutierrez, Rosali . Rodriguez, Virginia Martinez, Rosa A. Rodriguez-Frometa, Rosa M. Ruiz-Vazquez, Santiago Torres-Martinez, and Victoriano Garre. Direct transformation of fungal biomass from submerged cultures into biodiesel. *Energy Fuels*, 2010.

E. Vranova, D. Coman, and W. Gruissem. Structure and dynamics of the isoprenoid pathway network. *Mol Plant*, 5(2):318–333, 2012.

Amish P. Vyas, Jaswant L. Verma, and N. Subrahmanyam. A review on fame production processes. *Fuel*, 89(1):1–9, 2010.

Bradley D. Wahlen, Brett M. Barney, and Lance C. Seefeldt. Synthesis of biodiesel from mixed feedstocks and longer chain alcohols using an acid-catalyzed method. *Energy Fuels*, 22(6):4223–4228, 2008.

Y. D. Wang, T. Al-Shemmeri, P. Eames, J. McMullan, N. Hewitt, Y. Huang, and S. Rezvani. An experimental investigation of the performance and gaseous exhaust emissions of a diesel engine using blends of a vegetable oil. *Applied Thermal Engineering*, 26(14G15):1684–1691, 2006.

C. K. Westbrook, W. J. Pitz, O. Herbinet, H. J. Curran, and B. E. Solsona. A comprehensive detailed chemical kinetic reaction mechanism for combustion of n-alkane hydrocarbons from n-octane to n-hexadecane. *Combustion and Flame*, 2008.

Charles K. Westbrook. Chemical kinetics of hydrocarbon ignition in practical combustion systems. *Proceedings of the Combustion Institute*, 28(2):1563–1577, 2000.

Franklin J. Wright. Influence of temperature on viscosity of nonassociated liquids. *J. Chem. Eng. Data*, 6(3):454–456, Sep 1961.

Libin Wu, Shipeng Guo, Chao Wang, and Zhengyu Yang. Production of alkanes (c7-c29) from different part of poplar tree via direct deoxy-liquefaction. *Bioresource Technology*, 100(6):2069–2076, 2009.

Zhijun Wu, Zhiyong Zhu, and Zhen Huang. An experimental study on the spray structure of oxygenated fuel using laser-based visualization and particle image velocimetry. *Fuel*, 85(10G11):1458–1464, Aug 2006.

Donald J. Wuebbles and Atul K. Jain. Concerns about climate change and the role of fossil fuel use. *Fuel Processing Technology*, 71(1-3):99–119, 2001.

www.butamax.com. Online Source, 2011.

www.gevo.com. Online Source, 2011.

www.hybridcars.com. Clean diesel to represent over 12 percent of global light-duty sales by 2018. Online article, 2012.

Yongsheng Xiang, Xueqin An, and Weiguo Shen. Three-liquid-phase equilibria for the quaternary system water + tert-butanol + n-decane + n-undecane in the tricritical region. *J. Chem. Eng. Data*, 52(3):1113–1117, Sep 2007.

Z. Xiao, N. Ladommatos, and H. Zhao. The effect of aromatic hydrocarbons and oxygenates on diesel engine emissions. *Proceedings of the Institution of Mechanical Engineers, Part D: Journal of Automobile Engineering*, 214(3):307–332, 2000.

Li Xiaolu, Chen Hongyan, Zhu Zhiyong, and Huang Zhen. Study of combustion and emission characteristics of a diesel engine operated with dimethyl carbonate. *Energy Conversion and Management*, 47(11-12):1438–1448, 2006.

Andrey A. Yakovenko, Jose H. Gallegos, Mikhail Y. Antipin, Artem Masunov, and Tatiana V. Timofeeva. Crystal morphology as an evidence of supramolecular organization in adducts of 1,2-bis(chloromercurio)tetrafluorobenzene with organic esters. *Crystal Growth & Design*, 11(9):3964–3978, Sep 2011.

Jia Yang, Ming Xu, Xuezhi Zhang, Qiang Hu, Milton Sommerfeld, and Yongsheng Chen. Life-cycle analysis on biodiesel production from microalgae: Water footprint and nutrients balance. *Bioresource Technology*, 102(1):159–165, 2011a.

Jianhai Yang, Liyan Dai, Xiaozhong Wang, and Yingqi Chen. Di-p-nitrobenzyl azodicarboxylate (dnad): an alternative azo-reagent for the mitsunobu reaction. *Tetrahedron*, 67(7):1456–1462, 2011b.

K. Yasunaga, J. M. Simmie, H. J. Curran, T. Koike, O. Takahashi, Y. Kuraguchi, and Y. Hidaka. Detailed chemical kinetic mechanisms of ethyl methyl, methyl tert-butyl and ethyl tert-butyl ethers: The importance of uni-molecular elimination reactions. *Combustion and Flame*, 158(6):1032–1036, 2011.

Yongwook Yu, Sungmo Kang, Yongmo Kim, and Kwan S. Lee. Numerical study on spray combustion processes in n-heptane and dimethyl ether fueled diesel engines. *Energy Fuels*, 23(10):4917–4930, 2009.

Judi Zdor, Craig A. Taatjes, and Ravi X. Fernandes. Kinetics of elementary reactions in low-temperature autoignition chemistry. *Progress in Energy and Combustion Science*, 37(4):371–421, 2011.

Antonio Zecca and Luca Chiari. Fossil-fuel constraints on global warming. *Energy Policy*, 38(1):1–3, 2010.

Ya. B. Zeldovich, P. Ya. Sadavnikov, and D. A. Frank-Kamentskii. Oxidation of nitrogen in combustion. Report, 1947.

G. D. Zhang, H. Liu, X. X. Xia, W. G. Zhang, and J. H. Fang. Effects of dimethyl carbonate fuel additive on diesel engine performances. *Proceedings of the Institution of Mechanical Engineers, Part D: Journal of Automobile Engineering*, 219 (7):897–903, 2005.

Yu Zhang and André L. Boehman. Experimental study of the autoignition of c8h16o2 ethyl and methyl esters in a motored engine. *Combustion and Flame*, 157(3):546–555, 2010.

Yu Zhang and André L. Boehman. Autoignition of binary fuel blends of n-heptane and c7 esters in a motored engine. *Combustion and Flame*, 159(4):1619–1630, 2012.

Yu Zhang, Yi Yang, and André L. Boehman. Premixed ignition behavior of c9 fatty acid esters: A motored engine study. *Combustion and Flame*, 156(6):1202–1213, 2009.

Hua Zhao and Nicos Ladammatos. *Engine combustion instrumentation and diagnostics*. SAE International, 2001. ISBN 0-7680-0665-1.

Dajian Zhu, Fuming Mei, Lijuan Chen, Wanling Mo, Tao Li, and Guangxing Li. An efficient catalyst co(salophen) for synthesis of diethyl carbonate by oxidative carbonylation of ethanol. *Fuel*, 90(6):2098–2102, 2011.